The Volcanic and Sedimentary Evolution of the Faeroe Plateau Lava Group, Faeroe Islands and Faeroe-Shetland Basin, NE Atlantic

By

SIMON RICHARD PASSEY

B.Sc. (Hons.)(Oxford Brookes), F.G.S.

Thesis submitted for the degree of Doctor of Philosophy

Division of Earth Sciences
University of Glasgow

February 2004

Abstract

The Faeroe Plateau Lava Group (FPLG) of the Faeroe Islands, NE Atlantic, has been re-examined in order to understand its stratigraphy, structure, environment of eruption and evolution, for both the volcanic and the associated sedimentary lithologies. The FPLG has an exposed and drilled stratigraphic thickness of *ca.* 6.5 km on the Faeroe Islands and is separated into five formations.

The Lower Basalt Formation (LBF) is *ca.* 4.5 km thick and is dominated by subaerial tabular-classic facies lava flows, with average thicknesses of *ca.* 25 m. These were erupted at high effusion rates, travelled significant distances rapidly, and each flow was emplaced in a matter of weeks to a few months. The recognition of the Stapin Vent, Suðuroy, indicates that small point source vents contributed pyroclastic material to the land surface, with the major fissure eruptions most likely located to the west of the Faeroe Islands. The exposed *ca.* 900 m of the LBF is predominantly composed of prismatically jointed lava flows, which were emplaced into relatively dry environments. Weathering of the lava flow tops in the upper *ca.* 100 m of the LBF resulted in the formation of significant palaeosols (reddened boles), which implies hiatuses in the volcanic activity of up to 140 kyrs. During these hiatuses, terrestrial environments (fluviatile, lacustrine and swamps) were established and partial erosion of the lava topography ensued. The resulting sedimentary/epiclastic lithologies consist of volcaniclastic conglomerates through to mudstones and coals. The volcaniclastic rocks are composed of reworked palagonitised basaltic tephra and lithoclasts of basalt lava and pre-existing volcaniclastic rocks. The damming of river channels by lavas and the association of columnar jointed flows with fluviatile/lacustrine strata implies that columnar jointing is directly related to lavas that were erupted into wet environments.

Geochemical analysis of the volcanic interval in Well 214/4-1, Faeroe-Shetland Basin, has enabled a correlation to the Lower Basalt Formation of the Faeroe Islands, *ca.* 240 km to the W. The volcanic interval consists of a *ca.* 450 m thick sequence of hyaloclastites, which are overlain by a *ca.* 50 m thick subaerial lava sequence. This volcanic interval is interpreted to have formed at a palaeoshoreline environment, where subaerial lavas flowed from the land surface into a substantial body of water at least 450 m deep (i.e. the Faeroe-Shetland Basin at that time), resulting in the quenching and fragmentation of magma to produce the hyaloclastites. Well 214/4-1 is <50 km to the SE of the Faeroe-Shetland Escarpment, which has previously been interpreted as a hyaloclastite delta, thus implying that there are a number of unrecognised hyaloclastite units within the Faeroe-Shetland

Basin and that the coastline was steadily encroaching W/NW, towards the Faeroe Islands during the volcanic interval.

The overlying *ca.* 10 m thick Coal-bearing Formation (CBF) represents a significant hiatus in the volcanic activity at the end of LBF times. Erosion and subsidence of the lava field led to the development of an expansive lacustrine environment, which resulted in the accumulation of plant material and associated detritus and chemical sediments, mainly ironstones, and the formation of mineable coal seams. Petrographic and geochemical analysis of siderite spherules within the ironstone beds from two localities on Suðuroy have helped to define margin- and centre- of-lake environments, at least 10 km apart. Contemporaneous fluviatile lithologies in West Suðuroy are composed of reworked palagonitised tephra, basalt lava clasts and plant material.

Renewed volcanism marked an abrupt change from the inter-eruption facies of the CBF to the aggrading syn-eruption facies of the Volcaniclastic Sandstone Formation (VSF). The VSF is at least 30 m thick and comprises the initial deposition of laterally extensive, olivine-phyric, vitric tuffs, >8 m thick. This input of volcanic debris to the land surface swamped the CBF fluviatile systems and, possibly combined with high rainfall, produced sheet floods, which resulted in mass flow deposits. The destabilisation of the land surface by the destruction of vegetation by pyroclastic activity also may have aided in the mobilisation of volcanic debris. The resulting volcaniclastic debris and hyperconcentrated flow deposits are characterised by tabular geometries, consisting of volcaniclastic mudstones through to conglomerates, that are poorly sorted and matrix supported. These units are dominated by reworked palagonitised basaltic tephra and minor amounts of basalt.

The *ca.* 1.4 km thick Middle Basalt Formation (MBF) consists of *ca.* 20 m thick subaerial compound-braided facies lava flows made up of thinner flow units, <0.5 to 2 m in thickness. The MBF lavas were erupted at lower effusion rates than those of the Lower and Upper basalt formations. The flow units of the MBF are either S-type (spongy) or, more commonly, P-type (pipe-bearing) pahoehoe lava that was emplaced passively by an inflation (endogenous) mechanism through efficient lava tube networks. Calculations based upon the thicknesses of P-type flow crusts, suggest that the flow units were active for periods of a few hours up to a few days, and that the compound lava flows were emplaced over periods of months to years. The relatively rare interlava lithologies deposited during hiatuses in the MBF volcanism consist of fluviatile volcaniclastic sandstones and siltstones, commonly contained within channel structures. The sandstones

are composed of reworked palagonitised basaltic tephra and plant material, indicating that the surrounding land surface was vegetated. A re-examination of some of the vents defined by Rasmussen & Noe-Nygaard (1970b), for example, Sundsmunnin, Viðoy, suggests that many of them are, in fact, epiclastic conglomeratic deposits and, consequently, no MBF vents are recognised.

The boundary between the Middle and Upper basalt formations is not represented by a simple major hiatus akin to the CBF, although a thin (*ca.* 10 m thick) volcaniclastic debris flow, represented by exposures *ca.* 34 km apart, is recognised. This sedimentary unit is a volcaniclastic conglomerate that is poorly sorted, matrix supported, and has a homogeneous clast population dominated by plagioclase-phyric basalt. These data imply that during early UBF times there was an influx of pyroclastic debris onto the land surface, which was mobilised by surface water and/or high rainfall, producing sheet flood deposits.

The Upper Basalt Formation (UBF) is *ca.* 900 m thick, although a few hundred metres have been removed by erosion. The UBF is dominated by subaerially erupted, prismatically jointed, tabular-classic lava flows, with average thicknesses between 8 and 11 m. Akin to the LBF, these lavas were emplaced rapidly, in weeks to a few months, from high effusion rate eruptions. The identification of a small vent, dominated by upward-terminating minor intrusions associated with highly brecciated country rock material, at Húsið millum Gjáir on Viðoy, may represent a localised feeder to UBF flows. Hiatuses in the volcanism during UBF times saw the development of fluviatile and lacustrine environments, together with palaeosol surfaces which were commonly vegetated, with the rare preservation of tree moulds within the basal parts of lava flows. The interlava lithologies consist of volcaniclastic sandstones and siltstones composed predominantly of reworked palagonitised basaltic tephra. Some of the lavas that flowed over these strata were brecciated and subsequently agglutinated, implying that they were emplaced into wet environments.

Acknowledgements

I would firstly like to thank the Natural Environment Research Council (NERC) and Statoil (UK) Ltd. for providing financial support, through a CASE studentship (GT/04/99/ES/94), for this project. I would like to add a special thank you to David Ellis and Ragnar Poulsen, both of Statoil, for their help in organising accommodation and car hire on the Faeroe Islands, through which I was able to stay in the bridal suite of the Klaksvíkar Sjómansheim and the Queen suite of the Hotel Tórshavn – the most luxurious fieldwork accommodation I have ever had. I am grateful to Atlantic Airways for allowing me to bring back 50 kg of rocks in one go and for just marking it as heavy and not charging me for excess baggage. For the use of the samples collected from Well 214/4-1 I am greatly appreciative of Statoil and ExxonMobil and I am indebted to the person who had the foresight to undertake a sidewall core run.

A big thank you goes to my supervisor, Dr. Brian Bell, for guiding me through the last four years and having the patience to untangle my English! Thank you. I am also indebted to Dr. Colin Braithwaite for pointing me in the right direction in unravelling the secrets of the ironstone beds of the Coal-bearing Formation and for the positive feedback received on that chapter. I would also like to thank Dr. Martin Lee for his time and help in using the microprobe in obtaining the geochemical analyses of the siderite spherules: without him it would not have been accomplished. A special thank you goes to Dr. Dave Jolley of the University of Sheffield, for accompanying me in the field and for examining some of my samples for palynoflora assemblages.

Within the Division of Earth Sciences my thanks go to John Gilleece for the preparation of the numerous thin section slides used in this study and a special thank you goes to Kenny Roberts for his help with all things computer related and especially for recovering my hard drive, when it had given up the ghost – THANK YOU – I hope you enjoyed the whisky? I am greatly appreciative of William (Bill) Higgison for his help in powdering the samples from Well 214/4-1 for analysis at the University of Edinburgh and a grateful thank you goes to Prof. Godfrey Fitton and Doreen James for undertaking the XRF analyses. I am also grateful to Dr. Lotte Larsen of the Geological Survey of Denmark and Greenland, in helping me with her Mg # equation.

Thanks go to the remaining members of staff within the division who gave kind words of encouragement and advice throughout the project. Special thanks go to Drs. Alan Owen &

Maggie Cusack for being in charge of the postgraduates and for putting up with our many demands – I am still surprised the onsite bar never happened! My acknowledgements would not be complete without thanking Dr. Jeff Harris for not only his endless words of encouragement and his stories, but above all for his willingness to stimulate my grey matter through the enjoyment of some lovely wines. I would also like to thank Jeff for entrusting me with the use of the departmental minibus and landrover.

To my fellow postgraduates I bid a fond farewell and thank them for putting up with my witterings and extremely bad jokes. I would like to thank all those who accompanied me to the Research Club, a home away from home, where many scientific discussions were had, especially on comparing real ales to the qualities (?) of Tennents lager! I thank Glasgow Zoo for allowing the lions to regularly roam the underground, which enabled Big Dave to have an excuse to stay out longer! I thank Davie for all the good memories, which I can just about remember, from the Durham, UCL and Edinburgh VMSG conferences; and the Ardnamurchan fieldtrip – I am glad it was you that broke your shoulder bone that night! Above all though I thank Davie for being Davie. To Big Dave for his many funny stories, too colourful to mention here. I am grateful to Stew for sitting at the desk next to me and for realising when I needed dragging away. I thank Will, or not, for introducing me to cigars and being down right ridiculous and Jill for letting him out. Caroline, I thank you for the chats and I will always remember the banana episode! I thank Cristina for bringing a serious element to the group and for letting me know that I was not the only one suffering during the writing-up stage. I also thank JJ for being *classique*. An extremely special thank you goes to Kathy, for listening to my many moanings, putting up with me during the difficult times and for letting me stay at her place when I was in town. I am also indebted to her for reading this thesis and for using her wonderful American vocabulary. I would also like to apologise to her for taking the mick out of her dead things (trilobites).

To my friends from back home and Oxford Brookes I thank Jules, Luke, Phil, Tony, Justine and Trofi for your words of encouragement and the many drinks you have bought me over the years. I will pay you back soon....

I must thank my parents, Chris & Dick, for their unwavering support throughout my many years of study: this inadequate gesture does not come close to how grateful I am. Hopefully, I will be able to get you that cottage with the roses around the door one day soon. I love you both. I must also thank my immediate family, Nan, Cyril, Deb, Neil, Ben & Jack for their emotional support. I love you all.

Dedication

For my brother, Alan James Passey

(1979-2000)

Quotation

I would never die for my beliefs because I might be wrong.

Bertrand Russell (1872-1970)

Declaration

The material presented in this thesis summarises the results of 4 years of research carried out in the Division of Earth Sciences, University of Glasgow under the supervision of Dr B. R. Bell. This study is based on my own independent research and any previously published or unpublished results of other researchers used in this thesis have been given full acknowledgement in the text.

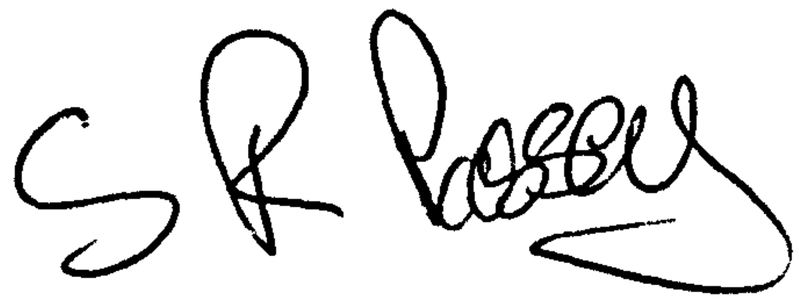

Simon R. Passey

February 2004

Abbreviations

API:	**American Petroleum Institute**
CBF:	**Coal-bearing Formation**
CFBs:	**Continental Flood Basalts**
CRBG:	**Columbia River Basalt Group**
FPLG:	**Faeroe Plateau Lava Group**
FSB:	**Faeroe-Shetland Basin**
FSE:	**Faeroe-Shetland Escarpment**
HCl:	**Hydrochloric Acid**
HVS:	**Horizontal Vesicle Sheet**
HVZ:	**Horizontal Vesicle Zone**
LBF:	**Lower Basalt Formation**
MBF:	**Middle Basalt Formation**
SEM:	**Scanning Electron Microscope**
UBF:	**Upper Basalt Formation**
VSF:	**Volcaniclastic Sandstone Formation**

Table of Contents

List of Figures

1 INTRODUCTION

2 TERMINOLOGY

3 LOWER BASALT FORMATION

4 COAL-BEARING FORMATION

5 VOLCANICLASTIC SANDSTONE FORMATION

6 MIDDLE BASALT FORMATION

7 UPPER BASALT FORMATION

8 FAEROE-SHETLAND BASIN

List of Tables

1 Introduction

1.1 Background

Hydrocarbon exploration over the past three decades has increasingly targeted rift basins on continental margins such as the NE Atlantic margin (Brooks & Glennie 1987; Parker 1993; Fleet & Boldy 1999) and offshore Namibia (Jerram *et al.* 1999). These basins are typically dominated by a range of volcanic facies from Continental Flood Basalts (CFBs) to volcaniclastic deposits (Mathisen & McPherson 1991; Jerram 2002). As a consequence, hydrocarbon exploration has been impeded by the presence of these vast thicknesses of flood basalts, which disrupt seismic responses, known as the sub-basalt imaging problem, that make it difficult to recognise trap structures potentially containing reservoirs of hydrocarbons (Kiørboe & Petersen 1995; Richardson *et al.* 1999; Planke *et al.* 2000; Jerram 2002; White *et al.* 2003). Traditional studies of CFBs have concentrated primarily on their geochemistry (Waagstein 1977; Wood 1979; Hald & Waagstein 1984; Waagstein 1988; Saunders *et al.* 1997; Kerr 1999; Larsen *et al.* 1999; Chambers & Fitton 2000; Holm *et al.* 2001) and geochronology (Tarling 1970; Abrahamsen *et al.* 1984; Hitchen & Ritchie 1993; Sharma 1994; Sinton *et al.* 1998; Tegner *et al.* 1998; Waagstein *et al.* 2001; Riisager *et al.* 2002a; Waagstein *et al.* 2002). However, with the interest, in part, from the petroleum industry, investigations have moved towards understanding their evolution, in particular in terms of environment of eruption (Williamson & Bell 1994; Self *et al.* 1996; Self *et al.* 1997; Lyle & Preston 1998; Jerram *et al.* 1999; Lyle 2000; Jerram 2002).

CFBs occur throughout the geologic past and include, for example, the Siberian Traps (*ca.* 251-249 Ma), the Paraná-Etendeka Flood Basalt Province (*ca.* 134-129 Ma), the Deccan Traps (*ca.* 66 Ma), the North Atlantic Igneous Province (*ca.* 62-58 Ma), and the Columbia River Basalt Group (*ca.* 16.5-14.5 Ma) (Walker 1993; Ernst & Buchan 2001). These flood basalts have no modern analogues, which has made it difficult to understand their complex internal and external architectures (Jerram 2002). However, comparisons of flow architectures of the Columbia River Basalt Group with flows erupted in the last 60 years on Hawai`i have led to a better understanding of the processes involved in the formation of vast thicknesses of basalt lava flows (Self *et al.* 1996). This, coupled with advances in seismic volcanostratigraphy (Planke *et al.* 2000; Planke 2001), the interpretation of facies architecture from seismic data, has aided in the interpretation of environment of eruption directly from the facies architecture observed in lava flows. The terminology used in describing facies architecture is discussed in Section 2.1.

Interlava lithologies occur inbetween lava flows within CFB provinces and help in the understanding the facies architecture observed in the overlying lava flow(s), for example, the development of columnar jointing in flows is closely associated with the presence of fluviatile and lacustrine sediments (Lyle & Preston 1998; Lyle 2000). The interlava lithologies can be derived by either pyroclastic or epiclastic processes in a wide range of environments (Fisher & Schmincke 1984; Cas & Wright 1987; Fisher & Smith 1991; Smith 1991; McPhie *et al.* 1993; Orton 1996). Pyroclastic deposits are more rarely preserved in the rock record because they are rapidly reworked by surface processes (Fisher & Schmincke 1984; Suthren 1985; Cas & Wright 1987; Fisher & Smith 1991; Smith 1991; Orton 1996). However, these processes differ from those of non-volcanic areas, for example, volcaniclastic debris flows travel far greater distances than their non-volcanic counterparts (Smith & Lowe 1991). Furthermore, pyroclastic activity rapidly adds volcanic debris to the surrounding land surface, which is usually quickly reworked and swamps pre-existing alluvial environments (e.g. fluvial and lacustrine) (Smith 1987a; b; 1991; Haughton 1993; Bahk & Chough 1996; Nakayama & Yoshikawa 1997).

This abrupt input of large volumes of volcanic debris can see, for example, a swift transformation from meandering stable fluvial channels to rapidly aggrading braided channels (Smith 1987a; b; 1991; Haughton 1993; Bahk & Chough 1996; Nakayama & Yoshikawa 1997), which are commonly associated with the development of lahars (volcaniclastic debris and hyperconcentrated flows) (Janda *et al.* 1981; Lowe *et al.* 1986; Naranjo *et al.* 1986; Cas & Wright 1987; Smith & Lowe 1991; Orton 1996; Lirer *et al.* 2001). The resulting lahar and flood deposits are interpreted as having formed during syn-eruption periods, whereas, inter-eruption depositional processes lead to the formation of 'normal' fluvial, lacustrine and palaeosol lithofacies (Smith 1988; Besly & Collinson 1991; Smith 1991; Wilkins *et al.* 1994; Bahk & Chough 1996; Bell *et al.* 1996; Orton 1996; Widdowson *et al.* 1997; Retallack 2001). The interplay between these syn- and inter-eruption depositional processes is complex due to the role of aggradation and basin subsidence (Smith 1988; 1991; Bahk & Chough 1996; Orton 1996). Therefore, a clear understanding of the processes involved in the formation of volcaniclastic facies will aid in the interpretation of the environment of eruption and deposition of lava flows and interlava lithologies, respectively. The terminology used in describing volcaniclastic lithologies in this study is outlined in Section 2.2.

1.2 Objectives

Since the publication, over 30 years ago, of the 'Geology of the Faeroe Islands' by Rasmussen & Noe-Nygaard (1969; 1970b) advances in our understanding of the volcanic processes occurring in the formation of flood basalts has aided in the understanding of their evolution through time, their emplacement mechanisms and their environments of eruption (e.g. Jerram 2002). In those 30 years, work on the Faeroe Islands has focused on the petrography (Hald & Waagstein 1984; Waagstein & Hald 1984; Waagstein *et al.* 1984), geochemistry (Waagstein 1977; Jensen 1978; 1979; Wood 1979; Jensen 1982; Gariépy *et al.* 1983; Hald & Waagstein 1983; 1984; Jensen 1985; Waagstein 1988; Larsen *et al.* 1999) and geochronology (Koul & Chadderton 1980; Koul *et al.* 1983; Waagstein 1988; Sharma 1994; Waagstein *et al.* 2001; Riisager *et al.* 2002a; b; Waagstein *et al.* 2002) of the lavas of the Faeroe Plateau Lava Group with little attention being given to their emplacement mechanisms and evolution of environments of eruption through time. Their associated interlava lithologies have been poorly represented in the literature with only minor investigations into their mineralogy (Sabine 1971; Parra *et al.* 1987), palaeomagnetism (Løvlie 1975; Løvlie & Kvingedal 1975; Løvlie 1976) and palynology (Jolley 1997; Ellis *et al.* 2002), especially the Coal-bearing Formation (Lund 1983; 1989; Jolley 1997). The locations of minor interlava lithologies have been reported by Rasmussen & Noe-Nygaard (1969; 1970b), but their petrography and modes of formation have received little attention and under current volcaniclastic classification schemes many of the lithologies need to be re-examined.

Therefore, the overall objective of this study, through a new investigation of lava flow facies architecture and the lithological and genetic classification of interlava lithologies, is to understand the environment of eruption and deposition throughout the evolution of the Faeroe Plateau Lava Group of the Faeroe Islands (Fig. 1.1) and Faeroe-Shetland Basin, NE Atlantic. This was approached by comparing field observations of lava flows and associated lithologies of the Faeroe Islands to other CFB provinces and the basalt lavas erupted on Hawai`i. Interlava lithologies were examined in order to determine whether they were emplaced by pyroclastic or epiclastic processes. Once this had been accomplished, characteristics of the lithologies were compared to pyroclastic and epiclastic rocks of other volcanic settings to try and accurately determine the processes involved in their transportation and the environment of deposition. As an adjunct to the main study, igneous material acquired from Well 214/4-1, Faeroe-Shetland Basin (Fig. 1.2), was petrographically examined and geochemically analysed, in an attempt to correlate the

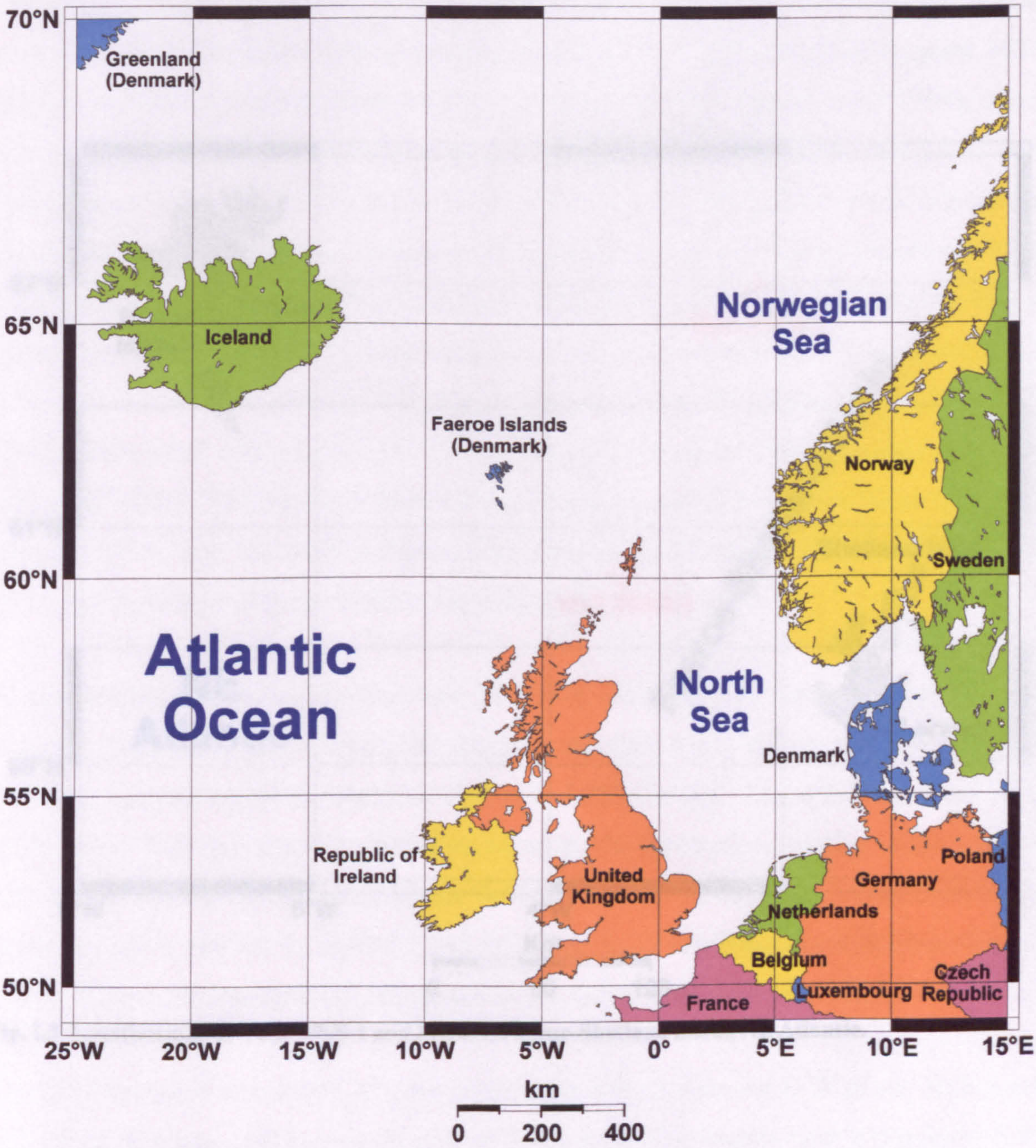

Fig. 1.1. Location map of the Faeroe Islands.

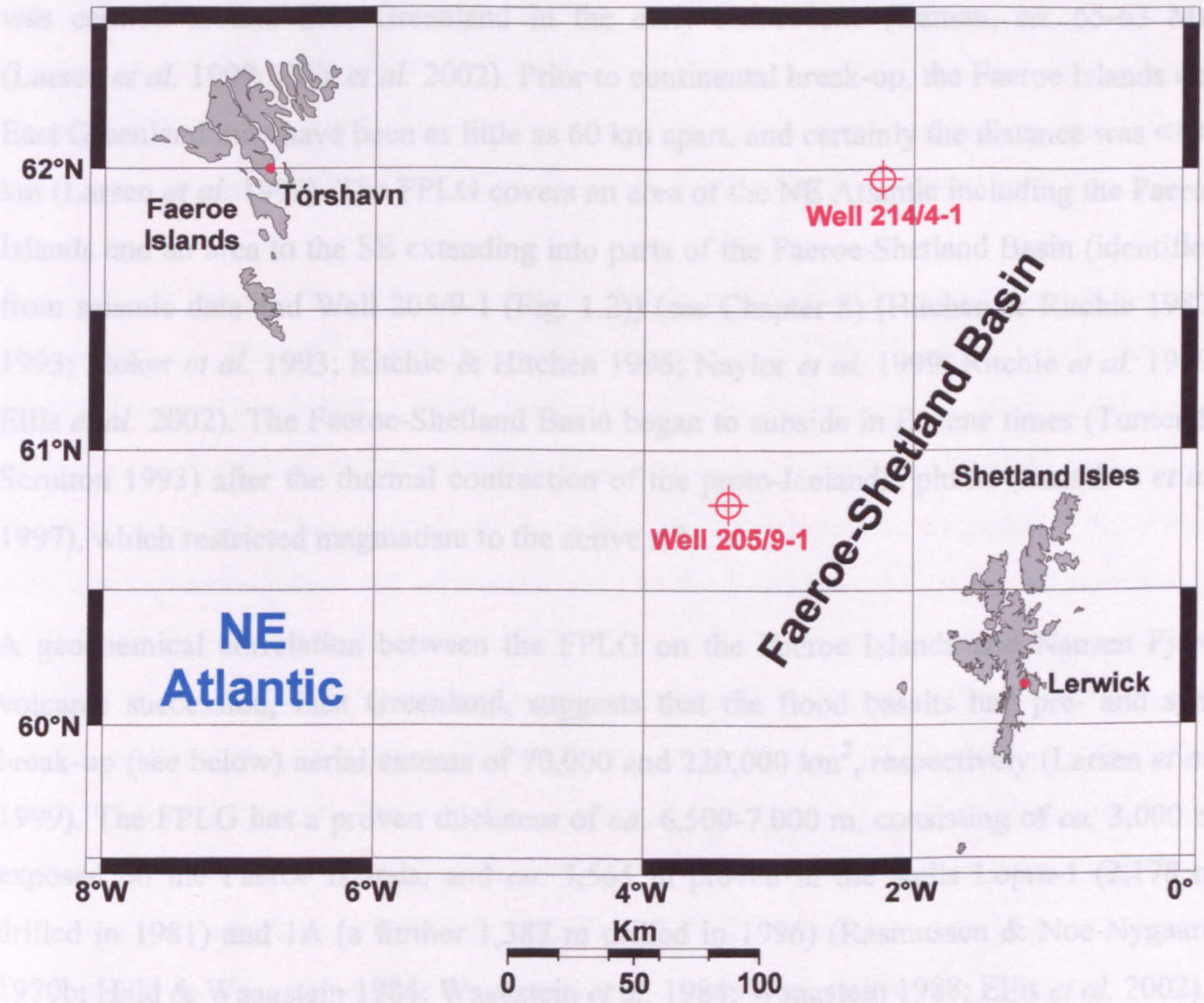

Fig. 1.2. Location map of wells 205/9-1 and 214/4-1, Faeroe-Shetland Basin, NE Atlantic.

offshore material to the volcanic succession encountered on the Faeroe Islands and to understand the mode of emplacement of the igneous-bearing lithologies.

1.3 Faeroe Plateau Lava Group

The Palaeogene Faeroe Plateau Lava Group (FPLG), part of the North Atlantic Igneous Province, comprises extensive flood basalt lavas and associated subaqueous lithologies such as hyaloclastite deltas that were erupted east of the rift fissure (Noe-Nygaard 1974; Waagstein 1988; Ritchie & Hitchen 1996; Larsen *et al.* 1999; Ritchie *et al.* 1999), which was centred around East Greenland in the early Palaeocene (Danian, *ca.* 65-63 Ma) (Larsen *et al.* 1999; Ellis *et al.* 2002). Prior to continental break-up, the Faeroe Islands and East Greenland may have been as little as 60 km apart, and certainly the distance was <100 km (Larsen *et al.* 1999). The FPLG covers an area of the NE Atlantic including the Faeroe Islands and an area to the SE extending into parts of the Faeroe-Shetland Basin (identified from seismic data and Well 205/9-1 (Fig. 1.2)) (see Chapter 8) (Hitchen & Ritchie 1987; 1993; Stoker *et al.* 1993; Ritchie & Hitchen 1996; Naylor *et al.* 1999; Ritchie *et al.* 1999; Ellis *et al.* 2002). The Faeroe-Shetland Basin began to subside in Eocene times (Turner & Scrutton 1993) after the thermal contraction of the proto-Icelandic plume (Saunders *et al.* 1997), which restricted magmatism to the active rift.

A geochemical correlation between the FPLG on the Faeroe Islands and Nansen Fjord volcanic succession, East Greenland, suggests that the flood basalts had pre- and syn-break-up (see below) aerial extents of 70,000 and 220,000 km^2, respectively (Larsen *et al.* 1999). The FPLG has a proven thickness of *ca.* 6,500-7,000 m, consisting of *ca.* 3,000 m exposed on the Faeroe Islands, and *ca.* 3,565 m proven in the wells Lopra-1 (2,178 m drilled in 1981) and 1A (a further 1,387 m drilled in 1996) (Rasmussen & Noe-Nygaard 1970b; Hald & Waagstein 1984; Waagstein *et al.* 1984; Waagstein 1988; Ellis *et al.* 2002).

The Faeroe Islands consist of 18 main islands covering a distance E-W of *ca.* 80 km and N-S of *ca.* 115 km, with an overall area of 1,400 km^2. The islands have a dominant NW-SE trend and are located *ca.* 280 km NW of Scotland and *ca.* 400 km SE of Iceland (Fig. 1.1). The landscape of the Faeroe Islands has been sculpted by glacial action producing mountainous terrain, with Slættaratindur, at a height of 882 m, being the highest peak on the islands. The Faeroe Islands and its insular shelf form the Faeroe Block (Waagstein 1988), which along with the Rockall Plateau are believed to be continental (Bott *et al.* 1974; Roberts 1975; Gariépy *et al.* 1983; Hald & Waagstein 1983) and make up the Faeroe Rise microcontinent (Bott & Watts 1971; Roberts *et al.* 1983).

It is on the Faeroe Islands that the FPLG is subdivided into five formations based on lithology and facies architecture (basalt formations) (Rasmussen & Noe-Nygaard 1969; 1970a; b; Noe-Nygaard 1974; Waagstein 1977; 1988; Rasmussen & Noe-Nygaard 1990). Figures 1.3 to 1.5 summarise the distribution and stratigraphic relationships of the FPLG formations of the Faeroe Islands. The three basalt formations, Lower (LBF), Middle (MBF) and Upper (UBF) are quite clearly separated on geochemical plots of TiO_2/FeO^T vs. FeO^T/MgO and TiO_2/FeO^T vs. Mg # (Figs. 1.6 & 1.7) (Waagstein 1988; Larsen *et al.* 1999) and the geochemistry of these formations shall be discussed in more detail in the relevant chapters: 3, 6, and 7, respectively. The pre-break-up succession is composed of the LBF and the syn-break-up succession consists of the Middle and Upper basalt formations (Larsen *et al.* 1999). The Coal-bearing Formation (CBF) inbetween the Lower Basalt and Volcaniclastic Sandstone formations represents a major hiatus in the volcanic activity, no significant hiatus is observed between the Middle and Upper Basalt formations.

Age data for the FPLG are at present very poorly constrained by radiometric techniques (Waagstein *et al.* 2002), although, in particular, the CBF is well constrained by biostratigraphy (Lund 1983; 1989; Jolley 1997). The upper section of the LBF has a palynoflora assemblage contained within interlava coals yielding an age of 57.5-60.56 Ma (Ellis *et al.* 2002). This assemblage is similar to the palynoflora assemblage recovered from the sediments below and within the lavas of Well 205/9-1, indicating that the lavas in Well 205/9-1 are comparable to the LBF (Ellis *et al.* 2002). The palynoflora assemblage of the CBF is comparable to the assemblages encountered in offshore wells from the base of the F2 subdivision of the Flett Formation (i.e. Ypresian (*ca.* 57 Ma)) (Fig. 1.8) (Jolley 1997; Naylor *et al.* 1999). Figure 1.8 is a correlation of the volcanic rocks within the North Atlantic Igneous Province alongside the most up to date isotopic age data, nannofossil zones and magnetochrons. The LBF has a R-N-R-N-R palaeomagnetic signature, whereas the Middle and Upper basalt formations have a reversed signature (Waagstein 1988). Ritchie *et al.* (1999) suggested that the Lower Basalt Formation was erupted during magnetochrons C27R-C26N, with a few flows in C25R and that the Middle and Upper basalt formations were erupted during C24R. However, Riisager *et al.* (2002a) suggested that the exposed part of the LBF was erupted later during magnetochrons C26N-C24R, although they agreed that the Middle and Upper basalt formations were erupted during C24R (Fig. 1.8).

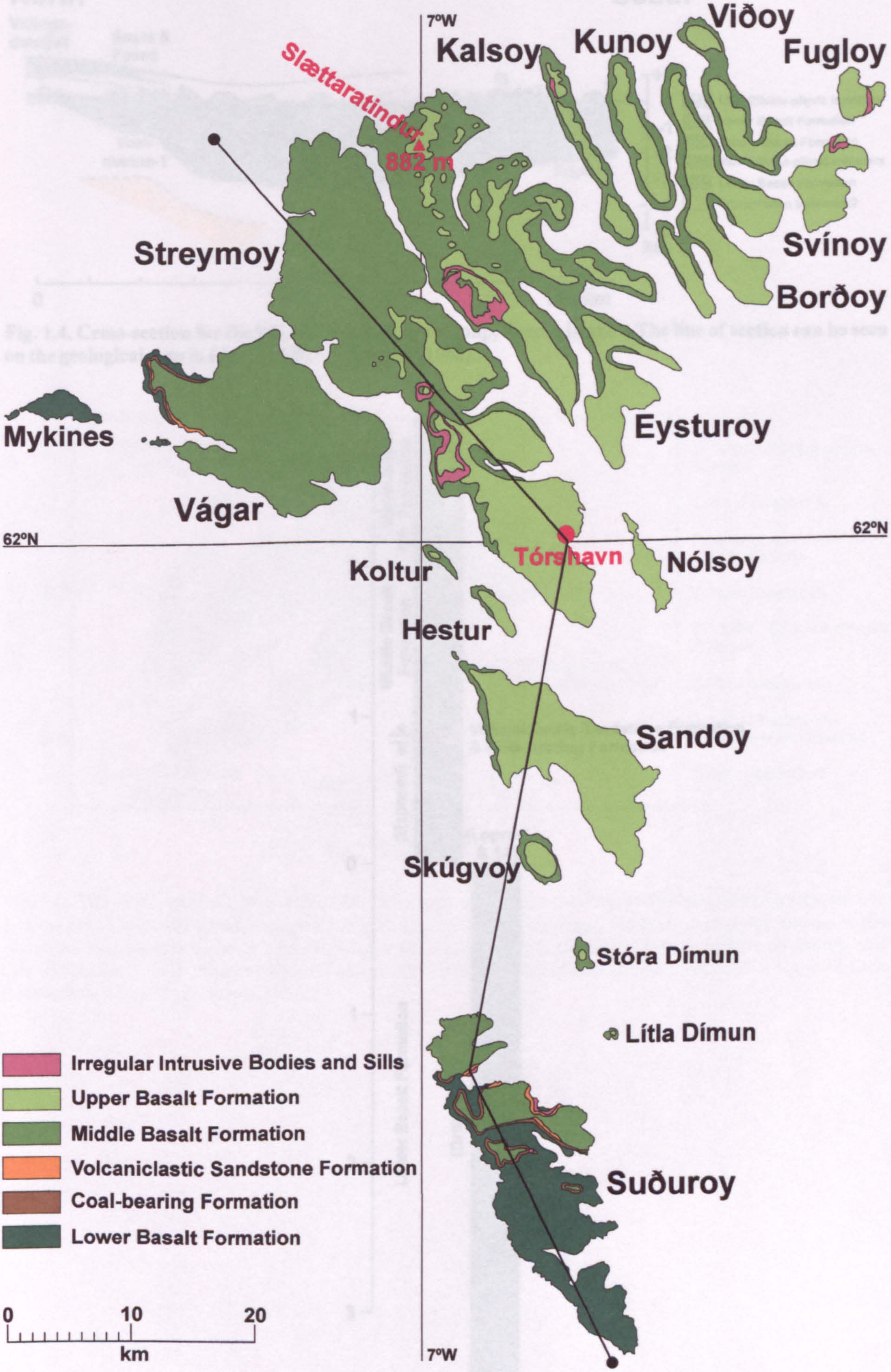

Fig. 1.3. Geological map of the Faeroe Plateau Lava Group, Faeroe Islands. The black line marks the position of the cross-section given in Fig. 1.4. After Rasmussen & Noe-Nygaard (1969; 1970a; b).

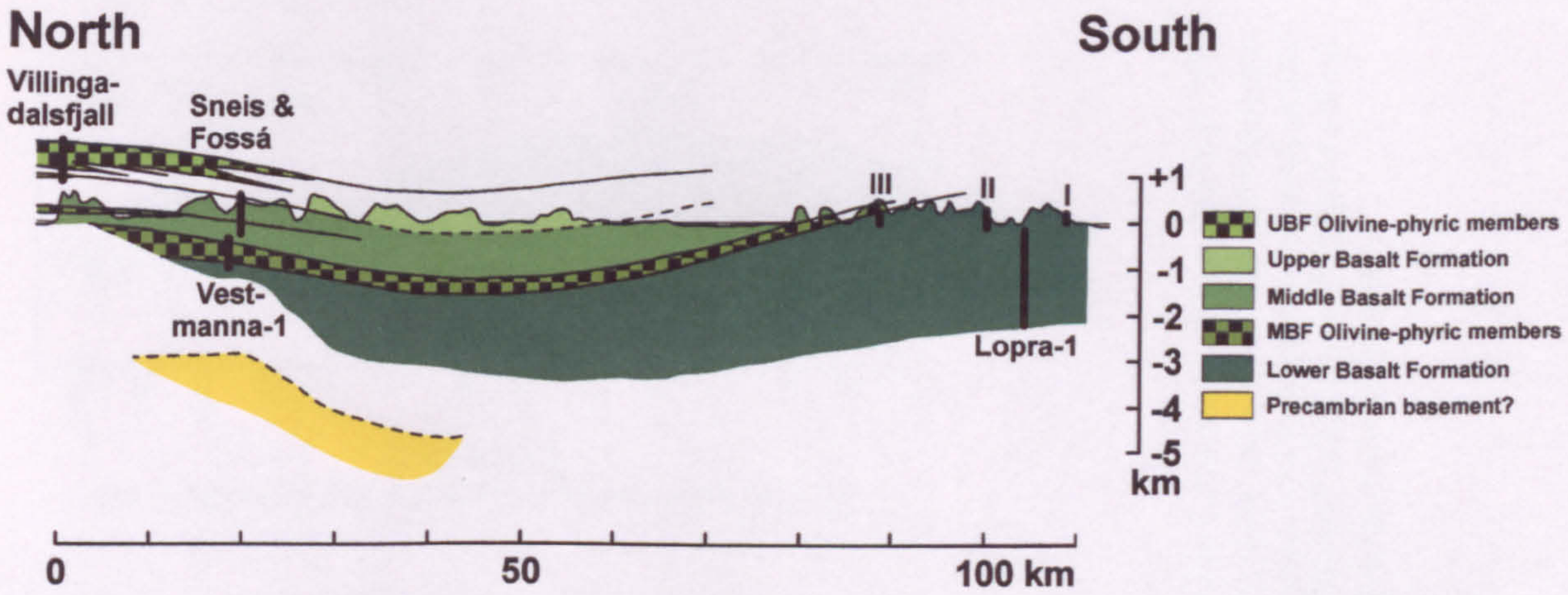

Fig. 1.4. Cross-section for the Faeroe Plateau Lava Group, Faeroe Islands. The line of section can be seen on the geological map in Fig. 1.3. After Waagstein (1988).

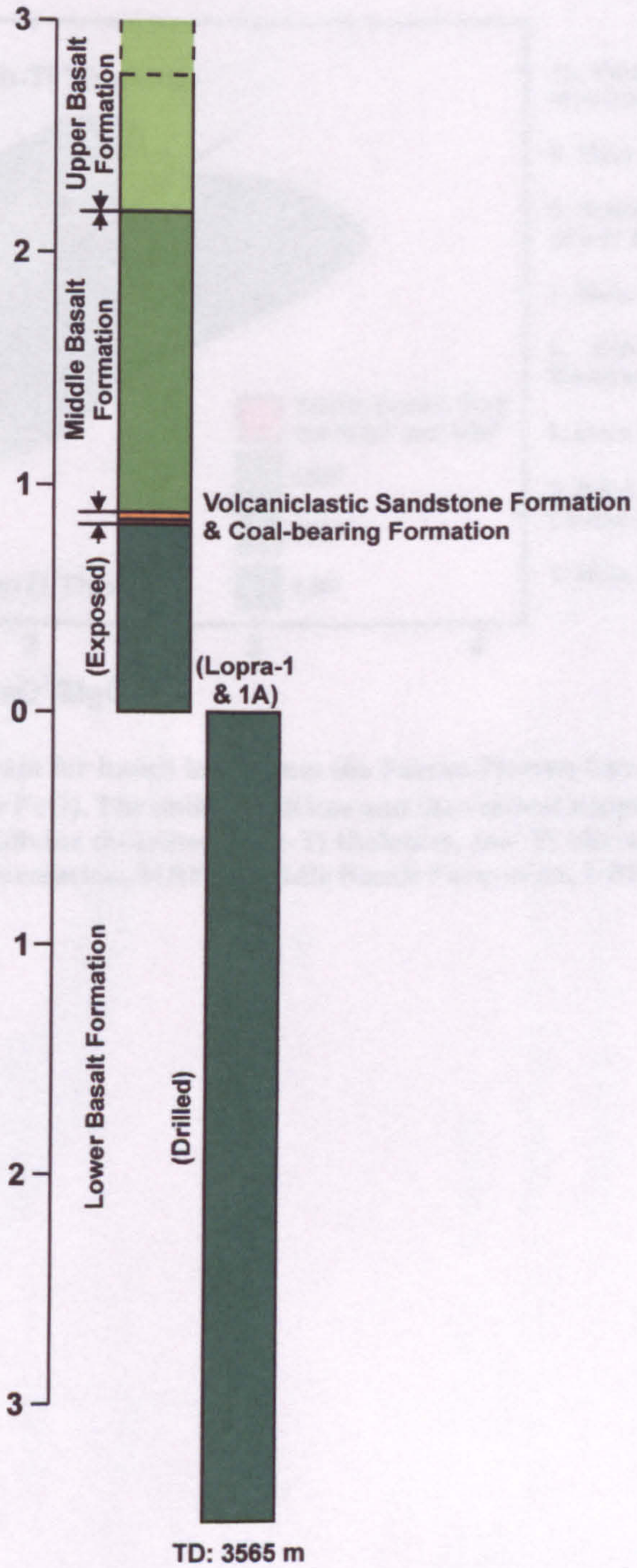

Fig. 1.5. Stratigraphic column for the Faeroe Plateau Lava Group, Faeroe Islands. After Ellis *et al.* (2002).

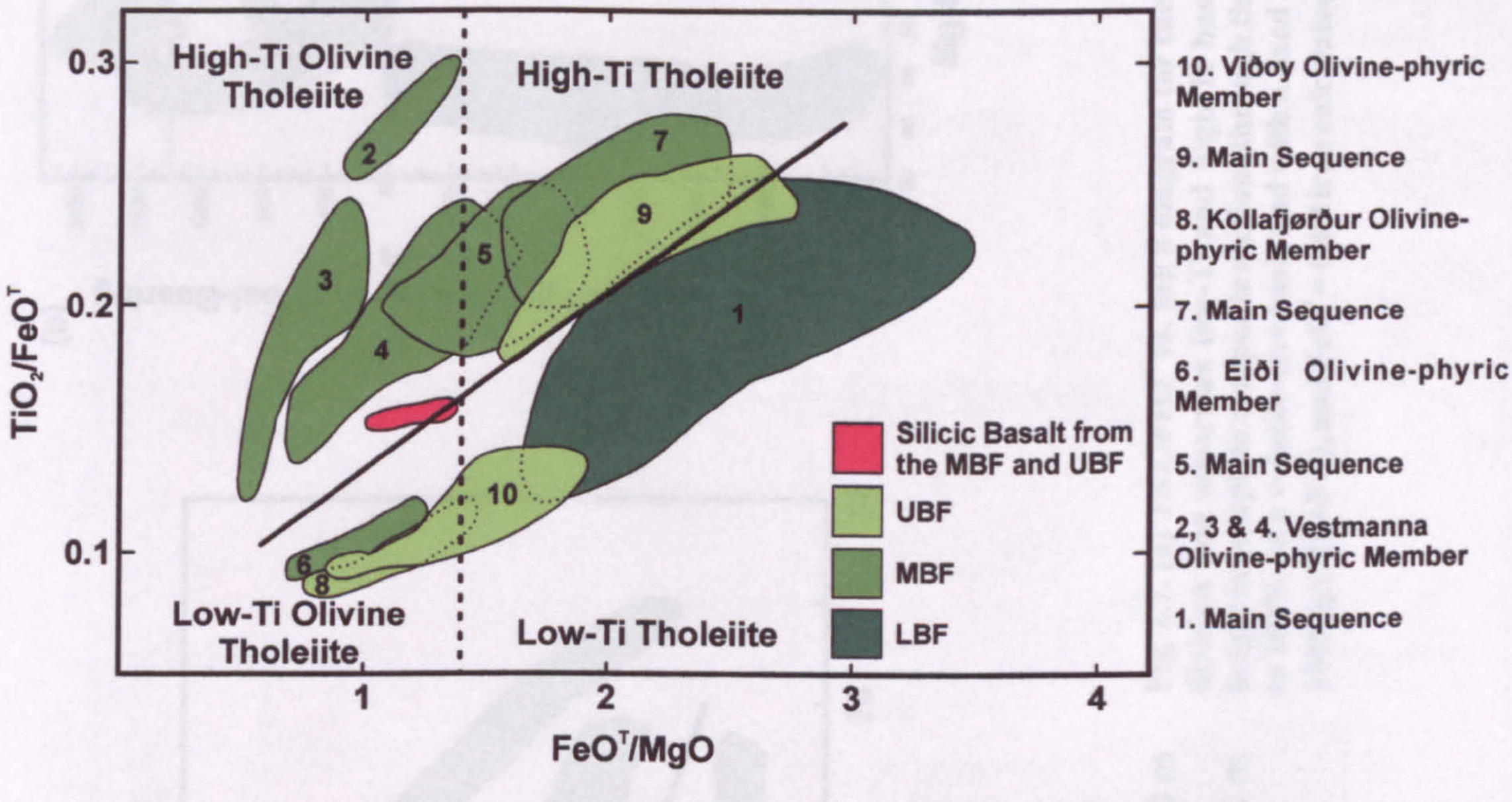

Fig. 1.6. TiO_2/FeO^T vs. FeO^T/MgO diagram for basalt lavas from the Faeroe Plateau Lava Group, Faeroe Islands (FeO^T = total iron recalculated as FeO). The oblique full line and the vertical stippled line mark the proposed boundaries between high-Ti olivine tholeiites, high-Ti tholeiites, low-Ti olivine tholeiites, and low-Ti tholeiites. LBF = Lower Basalt Formation, MBF = Middle Basalt Formation, UBF = Upper Basalt Formation. After Waagstein (1988).

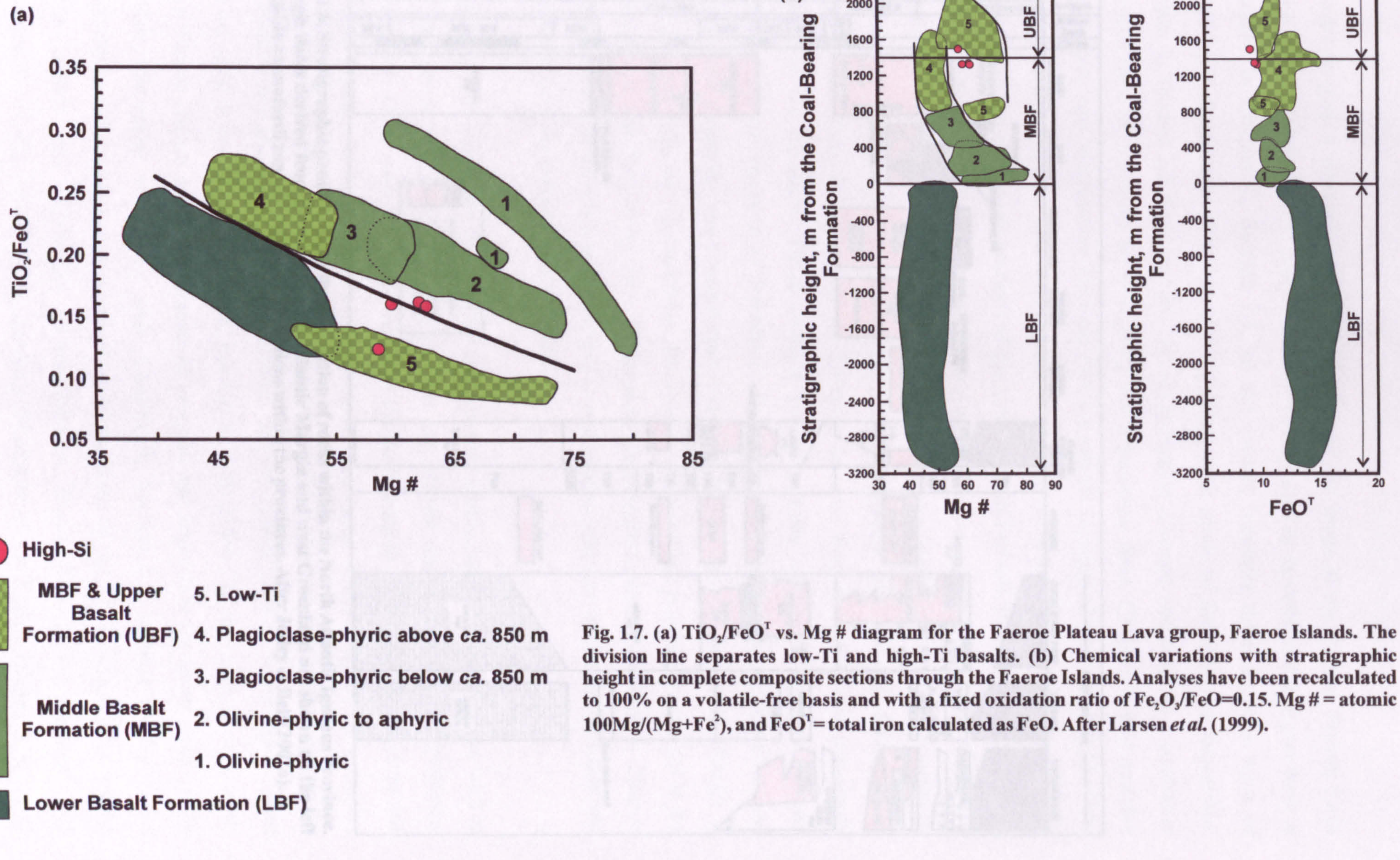

Fig. 1.7. (a) TiO_2/FeO^T vs. Mg # diagram for the Faeroe Plateau Lava group, Faeroe Islands. The division line separates low-Ti and high-Ti basalts. (b) Chemical variations with stratigraphic height in complete composite sections through the Faeroe Islands. Analyses have been recalculated to 100% on a volatile-free basis and with a fixed oxidation ratio of $Fe_2O_3/FeO=0.15$. Mg # = atomic $100Mg/(Mg+Fe^2)$, and FeO^T = total iron calculated as FeO. After Larsen *et al.* (1999).

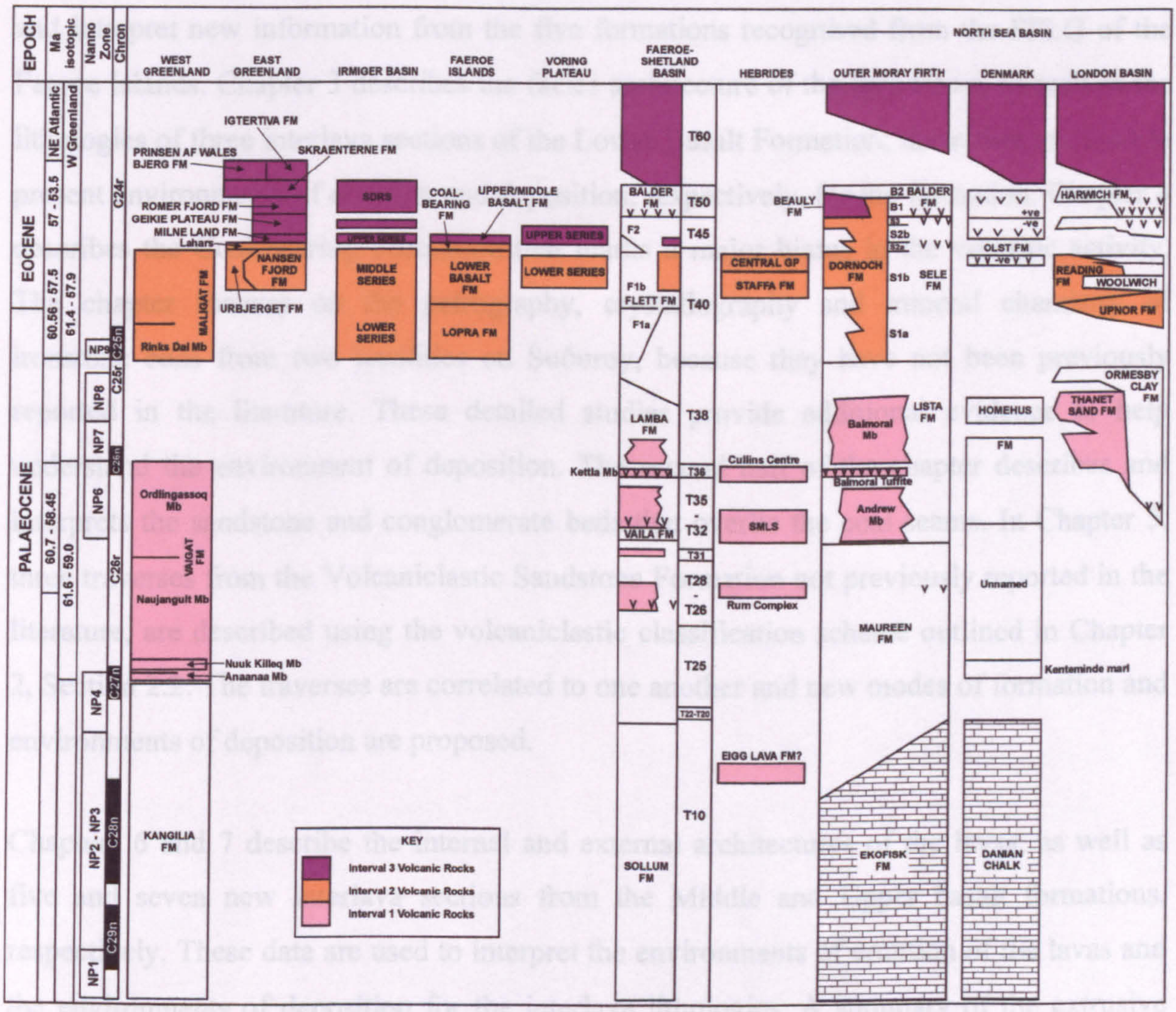

Fig. 1.8. Stratigraphic panel showing the correlation of rocks within the North Atlantic Igneous Province. Isotopic dates derived from rocks in the NE Atlantic Margin and west Greenland are shown on the left alongside nannofossil zones identified from sections within the provinces. After Jolley & Bell (2002a).

1.4 Thesis Outline

In order to give a comprehensive examination of the lavas of the Faeroe Plateau Lava Group (FPLG) of the Faeroe Islands the terminology used to describe and interpret them is presented in Chapter 2, Section 2.1. In the current literature there are two ways of classifying volcaniclastic lithologies, using either their mode of formation or deposition. Chapter 2, Section 2.2 discusses the two classification schemes and outlines a consistent approach used in this thesis for describing and interpreting them. Chapters 3 to 7 describe and interpret new information from the five formations recognised from the FPLG of the Faeroe Islands. Chapter 3 describes the facies architecture of the lava flows, as well as the lithologies of three interlava sections of the Lower Basalt Formation; these data are used to present environments of eruption and deposition, respectively, for the formation. Chapter 4 describes the Coal-bearing Formation that marks a major hiatus in the volcanic activity. The chapter focuses on the petrography, crystallography and mineral chemistry of ironstone beds from two localities on Suðuroy, because they have not been previously reported in the literature. These detailed studies provide additional evidence to help understand the environment of deposition. The second half of the chapter describes and interprets the sandstone and conglomerate beds that overlie the coal seams. In Chapter 5, three traverses from the Volcaniclastic Sandstone Formation not previously reported in the literature, are described using the volcaniclastic classification scheme outlined in Chapter 2, Section 2.2. The traverses are correlated to one another and new modes of formation and environments of deposition are proposed.

Chapters 6 and 7 describe the internal and external architectures of the lavas, as well as five and seven new interlava sections from the Middle and Upper basalt formations, respectively. These data are used to interpret the environments of eruption of the lavas and the environments of deposition for the interlava lithologies. A summary of the extrusive and intrusive volcanic rocks of the Faeroe-Shetland Basin is given in Chapter 8 before the petrography and geochemistry of the volcanic interval of Well 214/4-1 is presented. These data are used to correlate the volcanic interval of Well 214/4-1 to the volcanic succession of the Faeroe Islands and environments of eruption and deposition are determined for the volcanic lithologies within the well. Chapter 9, Section 9.1 summarises the facies architectures and environments of eruption of the lavas of the FPLG investigated on the Faeroe Islands and within the Faeroe-Shetland Basin. Section 9.2 discusses the environments of deposition for the interlava lithologies of the Faeroe Islands in terms of

inter- and syn-eruption facies. Section 9.3 collates all of the information gleaned from the present study and proposes an evolution of the Faeroe Plateau Lava Group.

2 Terminology

This chapter sets out the terminology used in the thesis for describing different types of basaltic lava flows. Focus then turns to the emplacement mechanisms, vesicle patterns and prismatic and columnar jointing of Continental Flood Basalt lavas and the features associated with them. A brief summary of the characteristics of Basaltic Plains Volcanism is also given. The second half of the chapter discusses the problems involved in describing volcaniclastic lithologies, particularly on whether the emphasis of the classification scheme should be based on the volcanic origin of the fragments or the mode of deposition. The chapter presents a consistent approach to the lithological and genetic volcaniclastic classification schemes used in this thesis. Lastly, a description of how the colour names and numerical designations used throughout the thesis is given.

2.1 Lava Flows

Lava flows are coherent masses of magma that are erupted in a single continuous outpouring at the Earth's surface during essentially non-explosive effusive volcanic activity (Cas & Wright 1987; McPhie *et al.* 1993). Lava flows are differentiated into two broad groups: low viscosity and high viscosity types (Walker 1970; 1973). The viscosity of the lava is dependant on a number of factors, although volatile and silica contents are the dominant controlling agents (Walker 1970; 1973). As volatile and silica contents increase so does the viscosity of the lava. As a consequence, high viscosity lavas are associated with andesitic, dacitic and rhyolitic compositions, whereas low viscosity lavas are commonly basaltic in composition (Walker 1970; 1973). The resultant geometry or aspect ratio (average thickness/horizontal extent) of the lava flow is a consequence of the viscosity and the rate of effusion during eruption of the lava (Walker 1970; 1973). Basaltic lavas are commonly thin, laterally extensive and have high volumes compared to more silicic types (Fig. 2.1). The effect of viscosity and effusion rate during the eruption of a lava flow has led to the distinction between two geometric lava flow types: simple lava flows and compound lava flows (Walker 1970; 1973) (Fig. 2.2). A simple lava flow is made up of one flow unit (an individual package of lava that is surrounded by a chilled crust), whereas a compound lava flow is composed of numerous flow units (Walker 1970). Walker (1973) suggested that the length of the lava flow is controlled by the rate of effusion: the higher the rate the more far-reaching the flow, whereas viscosity is important in determining thickness of flow, i.e. the higher the viscosity the greater the thickness. Simple lavas are considered by Walker (1973) to have been produced by high effusion

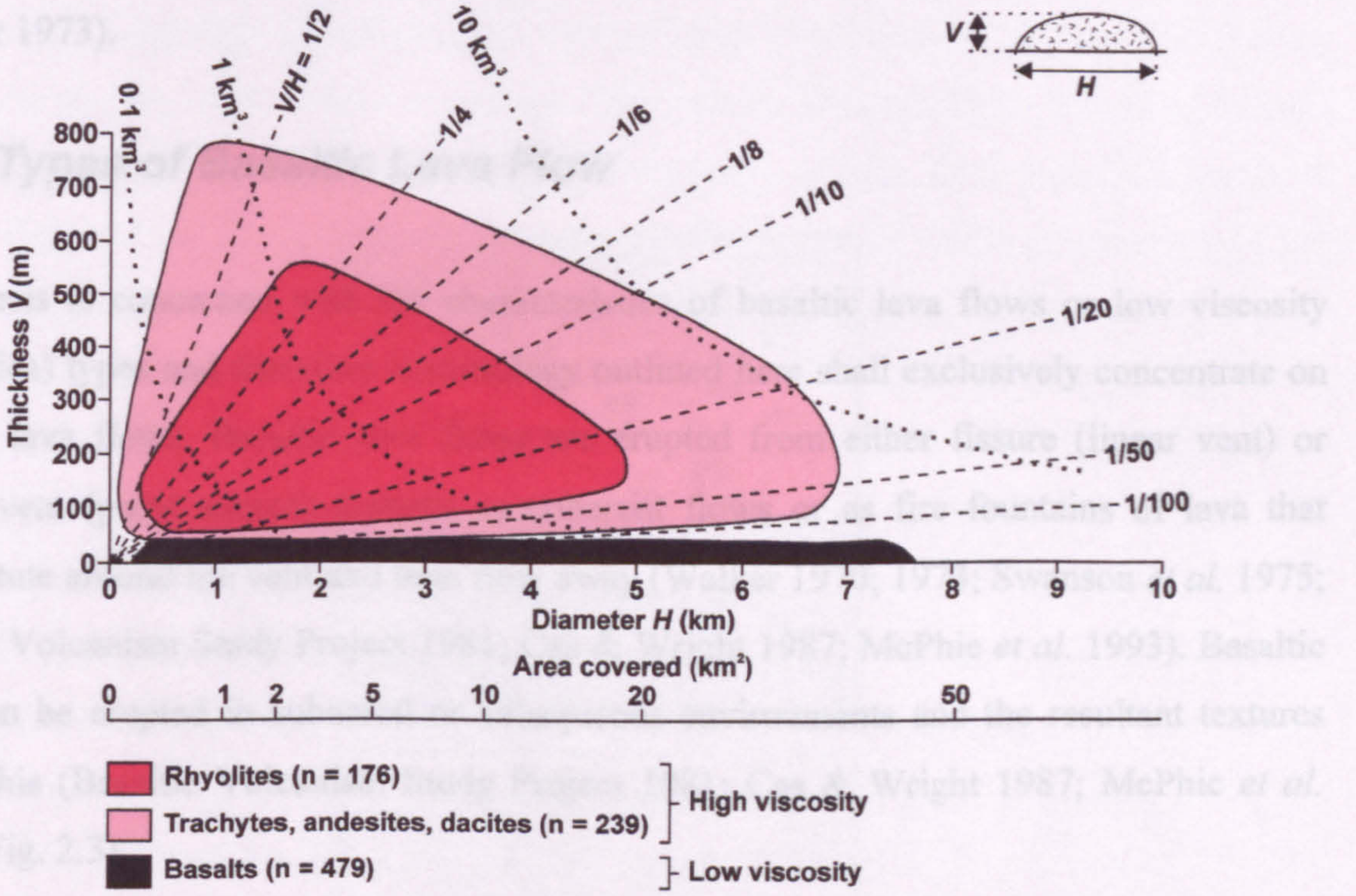

Fig. 2.1. Dimensions of lavas of different compositions. The two scales along the x-axis give the area covered by the extrusion and the diameter of a circle having this area. The broken lines give the aspect ratio V/H. The dotted lines give the volumes of circular disc-like bodies of the dimensions shown as a rough guide to the volumes of the lava extrusions. After Cas & Wright (1987) based on Walker (1973).

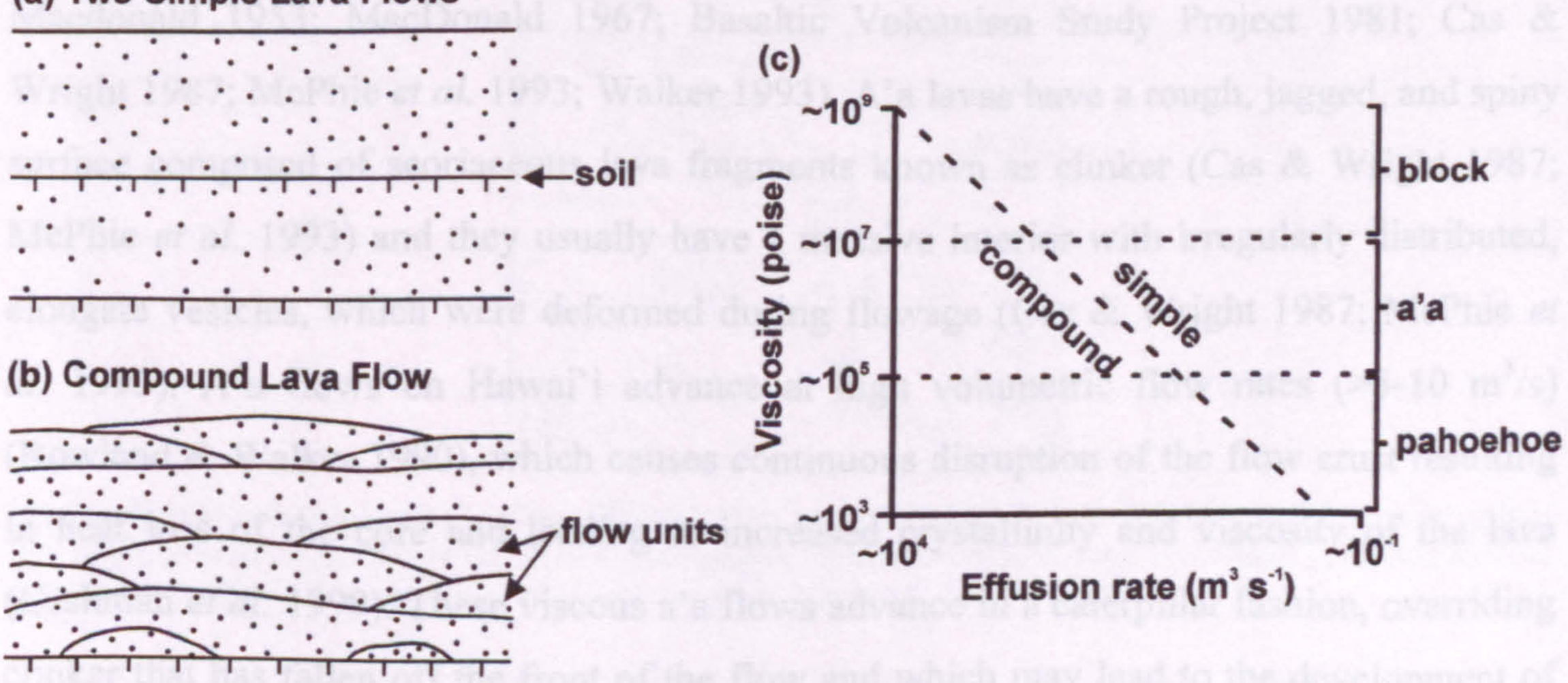

Fig. 2.2. Two main styles of lava flow architecture. (a) Two simple lava flows. (b) Compound lava flow made up of numerous flow units. (c) The postulated relationship between simple and compound lava flows as dependent on the effusion rate and the viscosity of the lava. (a) & (b) after Cas & Wright (1987) based on Walker (1970). (c) after Walker (1970).

rates, whereas compound lavas are considered to have formed from low effusion rate eruptions (Walker 1970; 1973). Topography can also influence the length and thickness of a flow, such as in a topographic depression, but is otherwise a relatively unimportant factor (Walker 1973).

2.1.1 Types of Basaltic Lava Flow

This thesis is concerned with the characteristics of basaltic lava flows or low viscosity (low-silica) types and therefore terminology outlined here shall exclusively concentrate on basaltic lava flows. Basaltic lava flows are erupted from either fissure (linear vent) or central vent (point source) systems as coherent flows or as fire fountains of lava that reconstitute around the vent and then flow away (Walker 1970; 1973; Swanson *et al.* 1975; Basaltic Volcanism Study Project 1981; Cas & Wright 1987; McPhie *et al.* 1993). Basaltic lavas can be erupted in subaerial or subaqueous environments and the resultant textures reflect this (Basaltic Volcanism Study Project 1981; Cas & Wright 1987; McPhie *et al.* 1993) (Fig. 2.3).

Most of the terminology used in describing subaerial basaltic lava flows originates from actively forming lava flows erupted from central vent systems on the island of Hawai`i (Wentworth & Macdonald 1953; MacDonald 1967; Basaltic Volcanism Study Project 1981; Cas & Wright 1987; McPhie *et al.* 1993; Walker 1993). Subaerial basaltic lava flows commonly exhibit either of two end-member flow types: a'a or pahoehoe (Wentworth & Macdonald 1953; MacDonald 1967; Basaltic Volcanism Study Project 1981; Cas & Wright 1987; McPhie *et al.* 1993; Walker 1993). A'a lavas have a rough, jagged, and spiny surface composed of scoriaceous lava fragments known as clinker (Cas & Wright 1987; McPhie *et al.* 1993) and they usually have a massive interior with irregularly distributed, elongate vesicles, which were deformed during flowage (Cas & Wright 1987; McPhie *et al.* 1993). A'a flows on Hawai`i advance at high volumetric flow rates (>5-10 m^3/s) (Rowland & Walker 1990), which causes continuous disruption of the flow crust resulting in heat loss of the core and leading to increased crystallinity and viscosity of the lava (Cashman *et al.* 1999). These viscous a'a flows advance in a caterpillar fashion, overriding clinker that has fallen off the front of the flow and which may lead to the development of channels in which lavas are constrained (Cas & Wright 1987; Rowland & Walker 1990; McPhie *et al.* 1993). A'a flows on Hawai`i range in thickness from 2-3 m, up to no more than 20 m, depending on the rate of effusion (Cas & Wright 1987; McPhie *et al.* 1993).

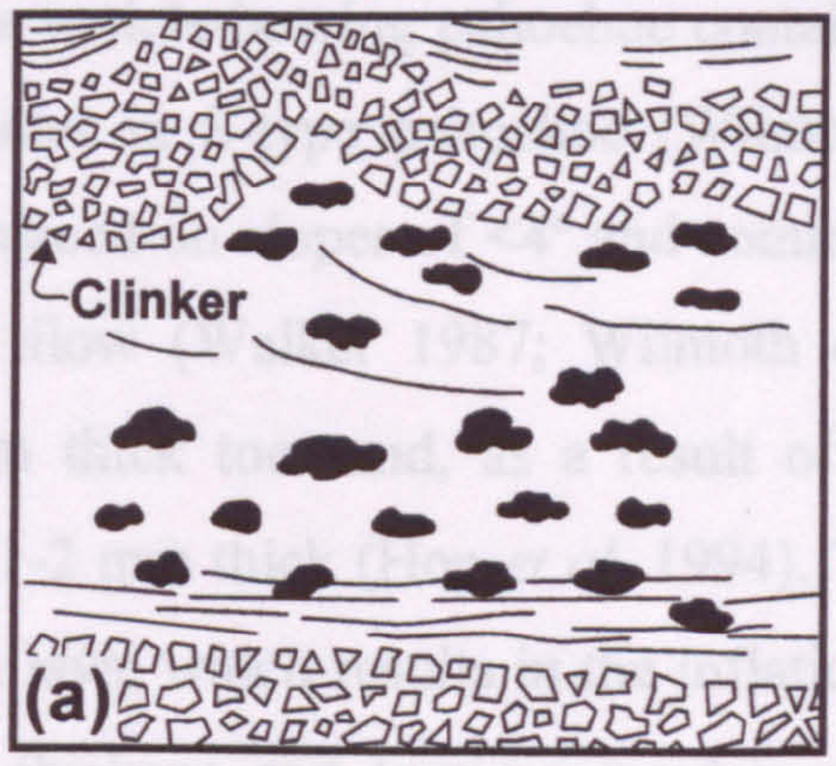

Fig. 2.3. Textures in ideal cross-sections through (a) a'a and (b) pahoehoe (mostly subaerial), and (c) pillow lava (subaqueous). Features that indicate younging are indicated with red arrows. Black areas are vesicles or former vesicles. After McPhie *et al.* (1993) based on Easton & Johns (1986).

Pahoehoe lavas form at low volumetric flow rates (<5-10 m^3/s) on Hawai`i (Rowland & Walker 1990) and are characterised by having a smooth, billowy or ropy surface (Wentworth & Macdonald 1953; MacDonald 1967; Basaltic Volcanism Study Project 1981; Cas & Wright 1987; McPhie *et al.* 1993; Walker 1993) and can be classified on their vesicle pattern as either S-type or P-type (Wilmoth & Walker 1993). S-type or spongy pahoehoe contains >30% vesicles that are commonly <4 mm in diameter (Wilmoth & Walker 1993). P-type or pipe vesicle-bearing pahoehoe contains <30% vesicles, which are usually larger than the vesicles in S-type pahoehoe (Wilmoth & Walker 1993). P-type pahoehoe flows that are emplaced on slopes of <4° and commonly exhibit pipe vesicles in the basal crust of the lava flow (Walker 1987; Wilmoth & Walker 1993). Pahoehoe advances as (thin) 10-50 cm thick toes and, as a result of rapid chilling, the toe will develop an insulating skin <1-2 mm thick (Hon *et al.* 1994). This thin insulating skin will contain the injection of fresh lava, which results in the inflation of the toe to as much as 4 m in thickness as the skin thickens and forms a rigid upper crust (Hon *et al.* 1994). Eventually the pressure (hydro 'magmastatic' head) exerted by the continued injection of fresh lava will rupture the insulating skin and the protrusion of a new toe will occur at the front of the flow (Hon *et al.* 1994). Locally increased supply rates of fresh lava can lead to the folding of the hot, flexible crust, producing a ropy surface that can be used as a palaeoflow indicator (MacDonald 1972; Fink & Fletcher 1978).

Tumuli and lava-rise pits are surface features on pahoehoe flow fields and are produced during the uplift of a lava crust during the inflation of a pahoehoe lava flow (Walker 1991). As the flow migrates away from the vent, upslope coalescence of toes leads to the formation of a lava tube network (Rowland & Walker 1990; Hon *et al.* 1994) (Fig. 2.4). Lava tube networks allow fresh lava to travel huge distances to the front of the flow without a major loss in temperature (Rowland & Walker 1990; Hon *et al.* 1994). Lava tubes can also form from roofing-over of lava channels and are commonly observed forming proximal to the vent (Peterson & Swanson 1974; Greeley 1987; Peterson *et al.* 1994; Dragoni *et al.* 1995). S-type pahoehoe is believed to spend less than an hour travelling within the tube network before it emerges at the front of the lava flow, whereas P-type pahoehoe is considered to have spent more than a day in the tube network (Wilmoth & Walker 1993) and consequently P-type pahoehoe is characteristic of the inflation mode of lava emplacement.

Lava flows on Hawai`i commonly begin as pahoehoe and change into a'a away from the vent (Cas & Wright 1987; McPhie *et al.* 1993). The transition from pahoehoe (near-Newtonian rheology) to a'a (Bingham rheology) lava is marked by surface crust

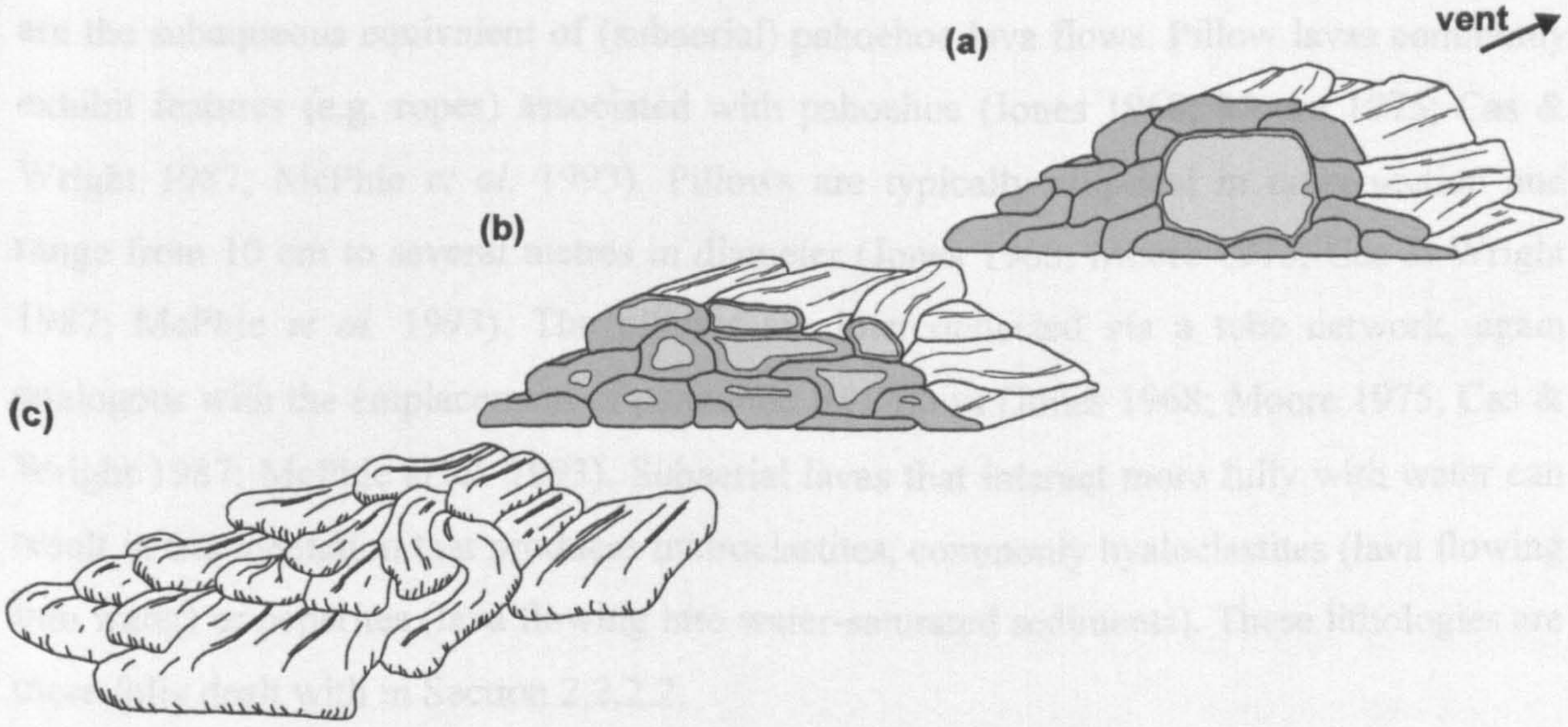

Fig. 2.4. Tube system in a pahoehoe lava flow. Master tubes (a) form by the coalescence of several adjacent smaller tubes or by roofing-over of open channels. Master tubes deliver lava to the distal parts of flows, where there is a system of small distributary tubes (b). At the flow front, the lava emerges in several small single flow unit tubes (c). Single flow unit tubes have cross-section areas of about 1 m^2. After McPhie *et al.* (1993) based on Rowland & Walker (1990).

differences, with lavas going from pahoehoe to slabby pahoehoe to scoriaceous-spinose a'a and finally, to clinker-dominated a'a at the distal parts of the lava flows, i.e. away from the vent (Lipman & Banks 1987). Across the transition vesicularity decreases, deformation of vesicles is greater, and plagioclase microlite crystallinity increases (Cashman *et al.* 1999; Polacci *et al.* 1999). The increase in crystallinity increases the viscosity and yield strength of the lava and at high strain rates leads to the formation of a'a with a distinctive clinker surface (Cashman *et al.* 1999). Recent studies have shown that a transition from a'a to pahoehoe lavas can occur but is restricted to where lavas flow from steep slopes to level ground and undergo a reduction in strain rate (Hon *et al.* 2003).

Pillow lavas are the characteristic basaltic lava flow type produced in subaqueous settings (Jones 1968; Moore *et al.* 1973; Moore 1975; Cas & Wright 1987; McPhie *et al.* 1993) and are the subaqueous equivalent of (subaerial) pahoehoe lava flows. Pillow lavas commonly exhibit features (e.g. ropes) associated with pahoehoe (Jones 1968; Moore 1975; Cas & Wright 1987; McPhie *et al.* 1993). Pillows are typically elliptical in cross-section and range from 10 cm to several metres in diameter (Jones 1968; Moore 1975; Cas & Wright 1987; McPhie *et al.* 1993). The pillows are interconnected via a tube network, again analogous with the emplacement of pahoehoe lava flows (Jones 1968; Moore 1975; Cas & Wright 1987; McPhie *et al.* 1993). Subaerial lavas that interact more fully with water can result in fragmentation that produces hydroclastites, commonly hyaloclastites (lava flowing into water) or peperites (lava flowing into water-saturated sediments). These lithologies are more fully dealt with in Section 2.2.2.2.

2.1.2 Continental Flood Basalts

Continental Flood Basalts (CFBs) are extremely voluminous, with lava fields ranging in volume from 10^5-10^7 km^3, compared to lava shield volcanoes (e.g. Hawai`i) that have volumes between 1,000–40,000 km^3 (Walker 1993). CFBs consist of vast 10-60 m thick sheets of lava with extremely low aspect ratios, which are commonly tholeiitic in composition (Cas & Wright 1987, and references therein). Simple lava flows, as described by Walker (1970), are characteristic of many CFB provinces, although compound lava flows do occur. Jerram (2002) referred to simple lava flows as tabular-classic facies and compound lava flows as compound-braided facies when describing lava flows from CFB provinces in terms of their facies architecture (Fig. 2.5).

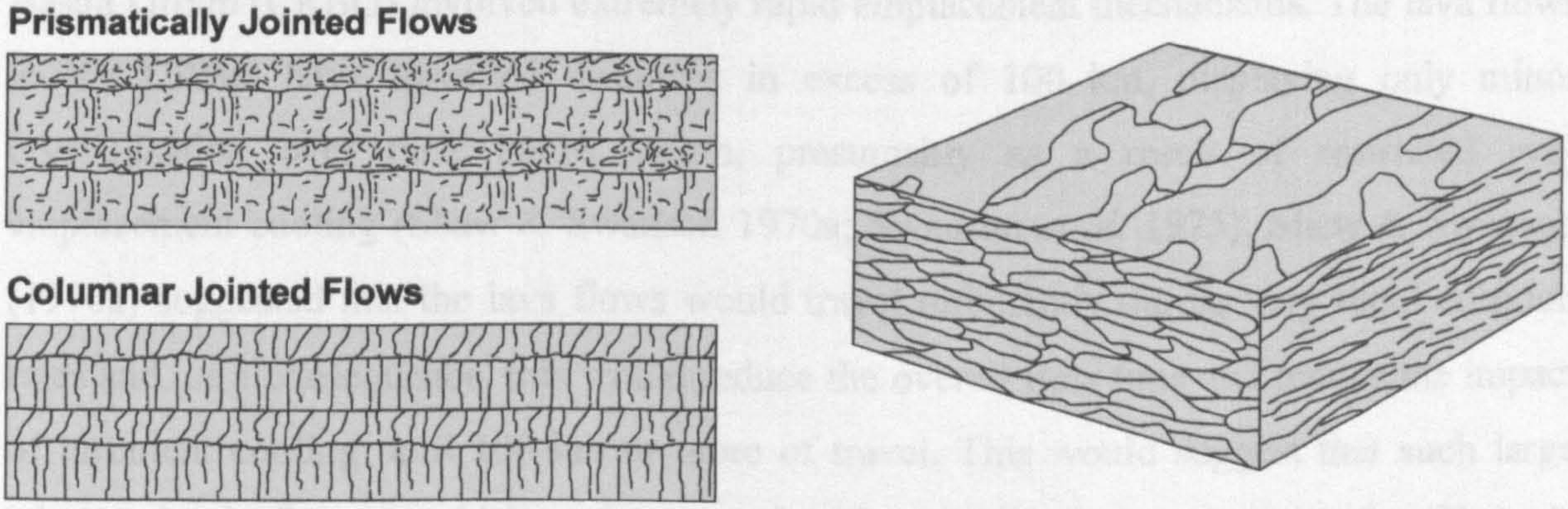

Fig. 2.5. Two main styles of facies architecture for lava flows in Continental Flood Basalt provinces. (a) Tabular-classic facies. Prismatic flows are erupted in arid environments whereas columnar jointed flows are erupted in wet environments. (b) Compound-braided facies. Lava flows are made up of numerous anastomosing pahoehoe flow sheets and lobes. After Jerram (2002).

2.1.2.1 Emplacement Mechanisms for CFBs

Initial investigations suggested that large flood basalts within CFB provinces were emplaced as high effusion rate turbulent flows (Shaw & Swanson 1970a; Swanson *et al.* 1975). However, more recent studies of the eruptions of pahoehoe lavas on Hawai`i have been extrapolated to suggest that long flood basalt flows of CFBs could have been emplaced by thermally efficient lava tube networks (Shaw & Swanson 1970a; Swanson *et al.* 1975; Greeley 1987; Keszthelyi 1995; Sakimoto & Zuber 1998) or as large inflated compound pahoehoe sheet flows, both of which are emplaced at lower effusion rates (Hon *et al.* 1994; Self *et al.* 1996; Self *et al.* 1997).

The hypothesis introduced by Shaw & Swanson (1970a) for the Yakima Basalt Subgroup (Grande Ronde, Wanapum, and Saddle Mountain basalt formations) of the Columbia River Basalt Group (CRBG) involved extremely rapid emplacement mechanisms. The lava flows in the CRBG have travelled distances in excess of 100 km, displaying only minor crystallisation over their entire length, presumably as a result of restricted syn-emplacement cooling (Shaw & Swanson 1970a; Swanson *et al.* 1975). Shaw & Swanson (1970a) suggested that the lava flows would travel turbulently during very rapid eruption rates and, as a consequence, this would reduce the overall flow time and reduce the impact of turbulent cooling until 100 km or more of travel. This would suggest that such large tabular-classic flows would have been emplaced over a week to a few months (Shaw & Swanson 1970a; Swanson *et al.* 1975; Reidel & Tolan 1992; Reidel 1998). According to Keszthelyi & Self (1998), rapidly emplaced lava flows should be dominated by a'a lava flow features, especially rubbly flow tops and bottoms. The transition from turbulent to laminar flow at the end of the eruption period may explain the preservation of pahoehoe flow features in localised areas (Reidel & Tolan 1992).

Self *et al.* (1996) & Self *et al.* (1997) have argued against a high effusion rate turbulent flow model for the emplacement of some of the CFB lava flows and suggested that some of the flows were emplaced as large inflated pahoehoe lava flow fields at low effusion rates over many years to decades. This hypothesis is based on field observations for the Roza Member of the Wanapum Basalt Formation within the CRBG and by comparing them to the features formed during the active emplacement of inflating pahoehoe flow fields on Hawai`i (Hon *et al.* 1994). The emplacement mechanism is analogous to that for thin pahoehoe sheets outlined in Section 2.1.1, but involves larger volumes and longer emplacement time periods. The inflation or 'swell' hypothesis for CFBs is summarised in Figure 2.6. As with pahoehoe sheets on Hawai`i, inflated CFBs display ropy surfaces,

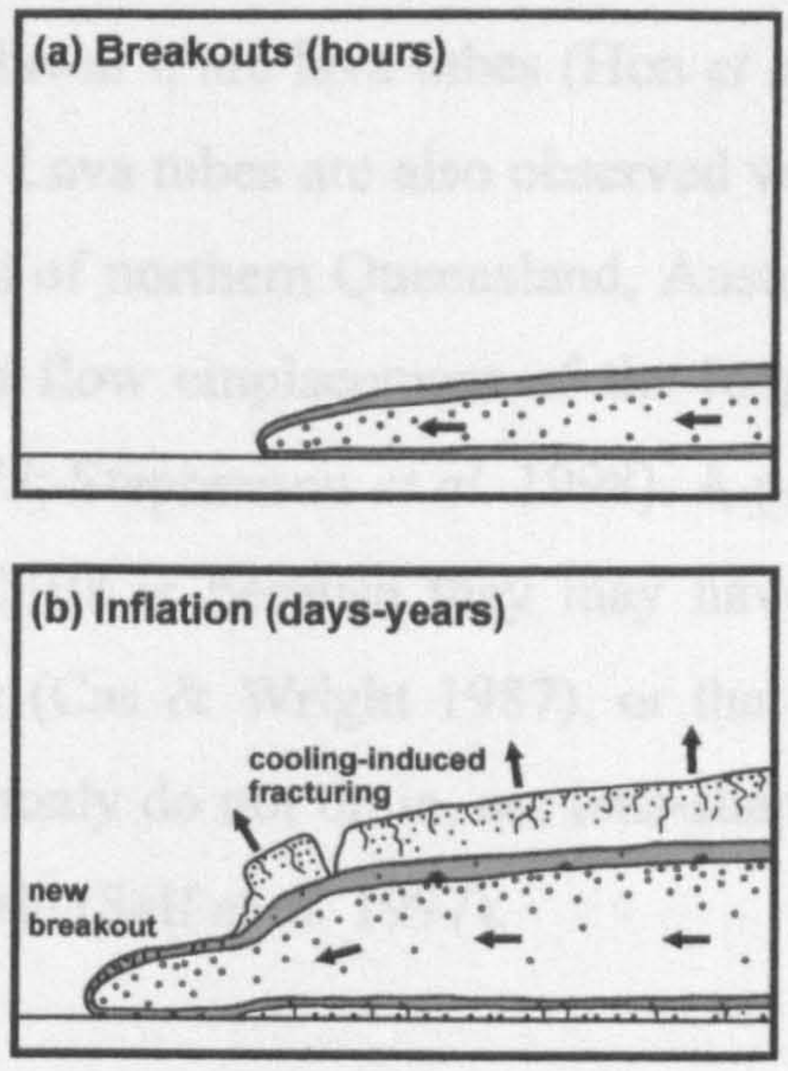

Fig. 2.6. Schematic cross-sections of emplacement of a generic inflating pahoehoe lava flow. Vertical scale varies from 1-5 m for Hawaiian flows to 5-50 m for Continental Flood Basalt flows. (a) Flow arrives as a small, slow-moving lobe of molten lava held inside a stretchable, chilled visco-elastic skin with a brittle crust on top. Bubbles are initially trapped in both the upper and basal crusts. (b) Continued injection of lava into the lobe results in inflation (lifting of the upper crust) and new breakouts. During inflation, bubbles rising from the fluid core become trapped in the visco-elastic mush at the base of the upper crust, forming horizontal vesicular zones (HVZ). The growth of the lower crust, in which pipe vesicles develop, is much slower. Relatively rapid cooling and motion during inflation results in irregular jointing in the upper crust. (c) After stagnation, diapirs of vesicular residuum form vertical cylinders and horizontal vesicle sheets within the crystallising lava core. Slow cooling of the stationary liquid core forms more regular joints. (d) Emplacement history of the lava flow is preserved in vesicle distribution and jointing patterns within the frozen lava. After Self *et al.* (1996).

lobes, tumuli, pipe vesicles (P-type pahoehoe), and so on. The large, inflated pahoehoe CFBs are also generally compound in nature, again analogous with the pahoehoe flow fields on Hawai`i.

One feature lacking from the CRBG, but which is observed to develop during the inflation of pahoehoe flow fields on Hawai`i, are lava tubes (Hon *et al.* 1994; Self *et al.* 1996; Self *et al.* 1997; Self *et al.* 1998). Lava tubes are also observed within the CFB province of the Cenozoic Volcanic Provinces of northern Queensland, Australia and are believed to have been of major importance in flow emplacement of the long lava flows observed in the province (Atkinson *et al.* 1975; Stephenson *et al.* 1998). A possible reason why lava tubes are not observed in some CFBs is because they may have been destroyed by internal flowage within ponded lavas (Cas & Wright 1987), or that lava tubes which formed on slopes of less than 0.5° commonly do not drain, are lens-shaped, and as a consequence are difficult to recognise in the field (Self *et al.* 1997).

2.1.2.2 Vesicle Patterns in CFBs

The lack of vesicles in the middle and bottom sections of thick lavas is a common feature associated with slowly solidifying flows that were emplaced rapidly (Aubele *et al.* 1988; Sahagian *et al.* 1989; Walker 1993). As the lava flow slowly solidifies there is time for the bubbles to migrate to the top of the flow and therefore produce the noticeable vesicular flow tops (Aubele *et al.* 1988; Sahagian *et al.* 1989; Walker 1993). However, large lava flows that have formed by endogenous (inflating) processes have been mistaken for rapidly emplaced lava flows and, therefore, detailed analysis of vesicle distribution, in terms of changing vesicularity and vesicle size through a lava flow, is needed to distinguish between them (Cashman & Kauahikaua 1997).

Cashman & Kauahikaua (1997) demonstrated that within inflated lava flows there is a rapid downward decrease in vesicularity and a downward increase in both average and maximum vesicle size, this layer is referred to as a horizontal vesicle zones (HVZ). This contrasts with the vesicle patterns observed for the rapidly emplaced ponded Alae lava lake, Hawai`i, which exhibits a downward increase in vesicularity and a downward decrease in maximum vesicle size (Peck 1978; Cashman & Kauahikaua 1997). Cashman & Kauahikaua (1997) also noted that inflated lava flows should have a normalised upper vesicular zone thickness (upper vesicular zone thickness/total flow thickness) in the range 0.4-0.6. This contrasts with rapidly emplaced lava flows, which have a normalised upper

vesicular zone thickness that decreases as flow thickness increases (Cashman & Kauahikaua 1997).

There are also a number of vesicle-related features that make inflated lava flows easily distinguishable from rapidly emplaced lava flows. For example, the lava flows from the CRBG, which have been identified as inflated lavas, particularly the Roza Member, exhibit horizontal vesicle zones, horizontal vesicle sheets, vertical cylinders and pipe vesicles (Self *et al.* 1997; Thordarson & Self 1998). Each injection of fresh lava into an inflating flow produces a horizontal vesicle zone (HVZ) as described above (Self *et al.* 1996; Self *et al.* 1998). Bubbles rise through the fluid core and become trapped at the base of the upper crust as it grows downwards due to cooling (Fig 2.6b) (Self *et al.* 1996; Self *et al.* 1998; Walker *et al.* 1999). Therefore, an inflated lava flow may exhibit a number of HVZs representing successive cycles of injection of fresh lava into the middle of the flow (Self *et al.* 1996; Self *et al.* 1998; Walker *et al.* 1999). After the stagnation of an inflating lava flow, due for example, to the cessation of injection of fresh lava, crystallisation of the dense core causes incompatible elements, including volatiles, to concentrate in the residuum (Self *et al.* 1996; Self *et al.* 1998). Secondary vesiculation can cause this residuum to rise as diapers (vertical cylinders), which can hit the base of the upper crust and spread to form horizontal vesicle sheets (HVSs) (Fig. 2.6c) (Self *et al.* 1996; Self *et al.* 1998). The depth between the lowermost horizontal vesicle zone and the uppermost horizontal vesicle sheet marks the base of the upper crust when inflation ended (Fig 2.6d) (Self *et al.* 1996; Self *et al.* 1998).

2.1.2.3 Development of Prismatic and Columnar Jointing in CFBs

Many large lava flows in CFB provinces exhibit prismatic or columnar jointing (Cas & Wright 1987). Prismatic jointing is formed as the result of volume reduction (contraction) during cooling (crystallisation) of lava flows from magmatic to atmospheric temperatures (Cas & Wright 1987; Walker 1993). The volume reduction can be as much as several percent and is accommodated in part by vertical to near-vertical joints that propagate perpendicular to the cooling surfaces, i.e. the top, bottom and sides of the lava flow (Cas & Wright 1987; Walker 1993). If the jointing consists of regular prisms that are uniform in size they are referred to as columnar jointing (Cas & Wright 1987; Walker 1993).

A columnar jointed lava flow is commonly segregated into two or three tiers, which are referred collectively as a multi-tiered flow (Tomkeieff 1940, and references therein; Spry 1962; Swanson 1967; Long & Wood 1986). Figure 2.7 shows a typical multi-tiered flow

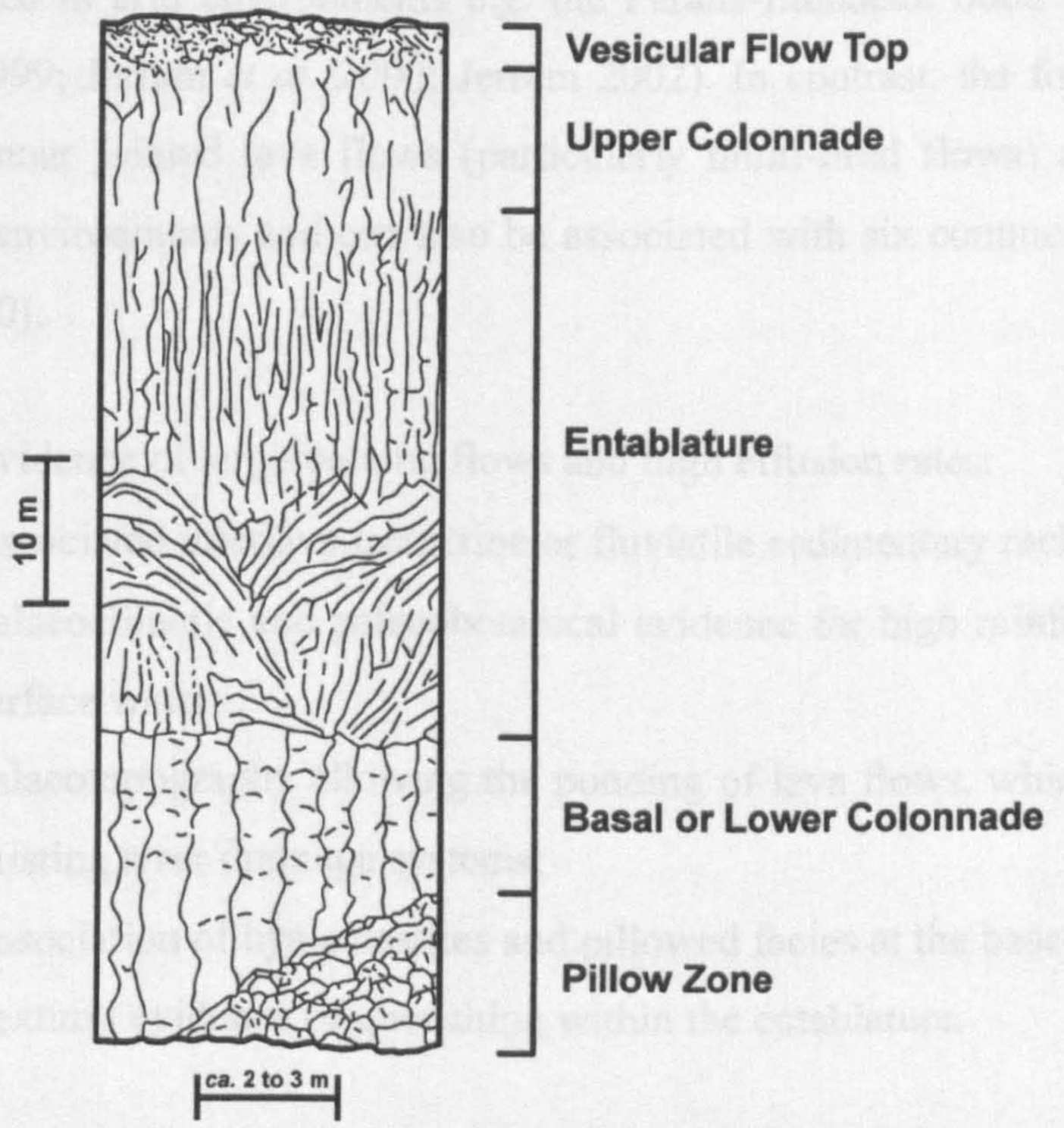

Fig. 2.7. Typical intraflow structures present in Grande Ronde Basalt flows, Columbia River Basalt Group, USA. Fractures in this figure are represented in a stylised manner, fracture widths are not to scale. After Long & Wood (1986).

from the Grande Ronde Basalt Formation of the CRBG. The nomenclature used for multi-tiered flows is that proposed by Long & Wood (1986). The basal tier is made up of regular, well-developed columns and is known as the (lower or basal) colonnade. The base of the colonnade may contain pillow lavas if the lava flow was erupted into a water-saturated environment. Overlying the colonnade is the entablature, which is characterised by irregular and hackly, curvi-columnar columns that frequently have a much smaller spacing than the columns in the colonnade. Sometimes overlying the entablature is an upper colonnade, which in turn is overlain by a vesicular flow top.

Prismatic, or poorly developed jointing appears to be a common feature of lava flows that have been erupted in arid environments e.g. the Paraná-Etendeka flood basalts, Namibia (Jerram *et al.* 1999; Jerram *et al.* 2000; Jerram 2002). In contrast, the formation of well-developed columnar jointed lava flows (particularly multi-tired flows) are indicative of eruption in wet environments and can also be associated with six common features, listed below (Lyle 2000):

(i) Evidence of large volume flows and high effusion rates;
(ii) Associated interlava lacustrine or fluviatile sedimentary rocks;
(iii) Palaeoclimatic and palaeobotanical evidence for high rainfall and abundant surface water;
(iv) Palaeotopography allowing the ponding of lava flows, which may dam pre-existing river drainage systems;
(v) Association of hyaloclastites and pillowed facies at the base of lava flows;
(vi) Textural evidence of quenching within the entablature.

2.1.3 Basaltic Plains Volcanism

Basaltic Plains Volcanism consists of large lava flows intermediate in style and volume between Hawaiian lavas and CFBs (Greeley 1982). The term Basaltic Plains Volcanism was introduced by Greeley (1976; 1977; 1982) to distinguish the Snake River Group Basalts, Snake River Plain, Idaho from the CRBG. Basaltic Plains basalts are similar to CFBs in being high volume flows, having fissure vent systems and planar geometries (Greeley 1982) and are similar to Hawaiian basalts, consisting of compound pahoehoe lava flow fields that are erupted from low lying shield volcanoes and emplaced via lava tube networks as well as lava channels (Greeley 1982). The compound flow fields erupted from the low-lying shield volcanoes are on average 35 m thick and are made up of flow units *ca.* 1-5 m thick (Greeley 1982). Lavas erupted from fissures are on average 10 m thick and

infill the low-lying areas inbetween shield volcanoes to give an overall planar geometry (Greeley 1982). Figure 2.8 is a block diagram depicting the main features of Basaltic Plains Volcanism.

2.2 Volcaniclastic Rocks

Due to the common misuse of terminology in the classification of volcaniclastic rocks in the literature, it is necessary to clarify the classification scheme used in this thesis. For example, the term agglomerate (a pyroclastic conglomerate) has in the past been applied to any volcaniclastic conglomerate/breccia, irrespective of being pyroclastic or epiclastic in origin, and has been associated with being a pyroclastic fall deposit in close proximity to a vent. However, in the majority of the classification schemes in use, an agglomerate is a pyroclastic rock (irrespective of its actual pyroclastic origin, i.e. fall, flow or surge) that contains more than 75% pyroclasts that have a mean diameter >64 mm and have an ellipsoidal, discoidal, or irregular shape, or have a cow-dung or bread crust texture (see Section 2.2.2). Cas & Wright (1987) have demonstrated that there are over 30 different ways to produce a volcaniclastic conglomerate/breccia, and agglomerate umbrellas less than half of them. The term *Volcaniclastic* was established by Fisher (1961; 1966) and redefined by Fisher & Smith (1991) to include:

> 'the entire spectrum of clastic materials composed in part or entirely of volcanic fragments, formed by any particle forming mechanism (e.g. pyroclastic, hydroclastic, epiclastic and autoclastic), transported by any mechanism, deposited in any physiogenetic environment or mixed with any other volcaniclastic type or with any non-volcanic fragment types in any proportion'.

Gillespie & Styles (1999) suggested that to be classified as a volcaniclastic rock, the rock must contain more than 10% by volume of volcanic debris. *Volcanic debris* is defined by Gillespie & Styles (1999) as:

> 'fragments originating by volcanic processes, either primary or after redeposition'.

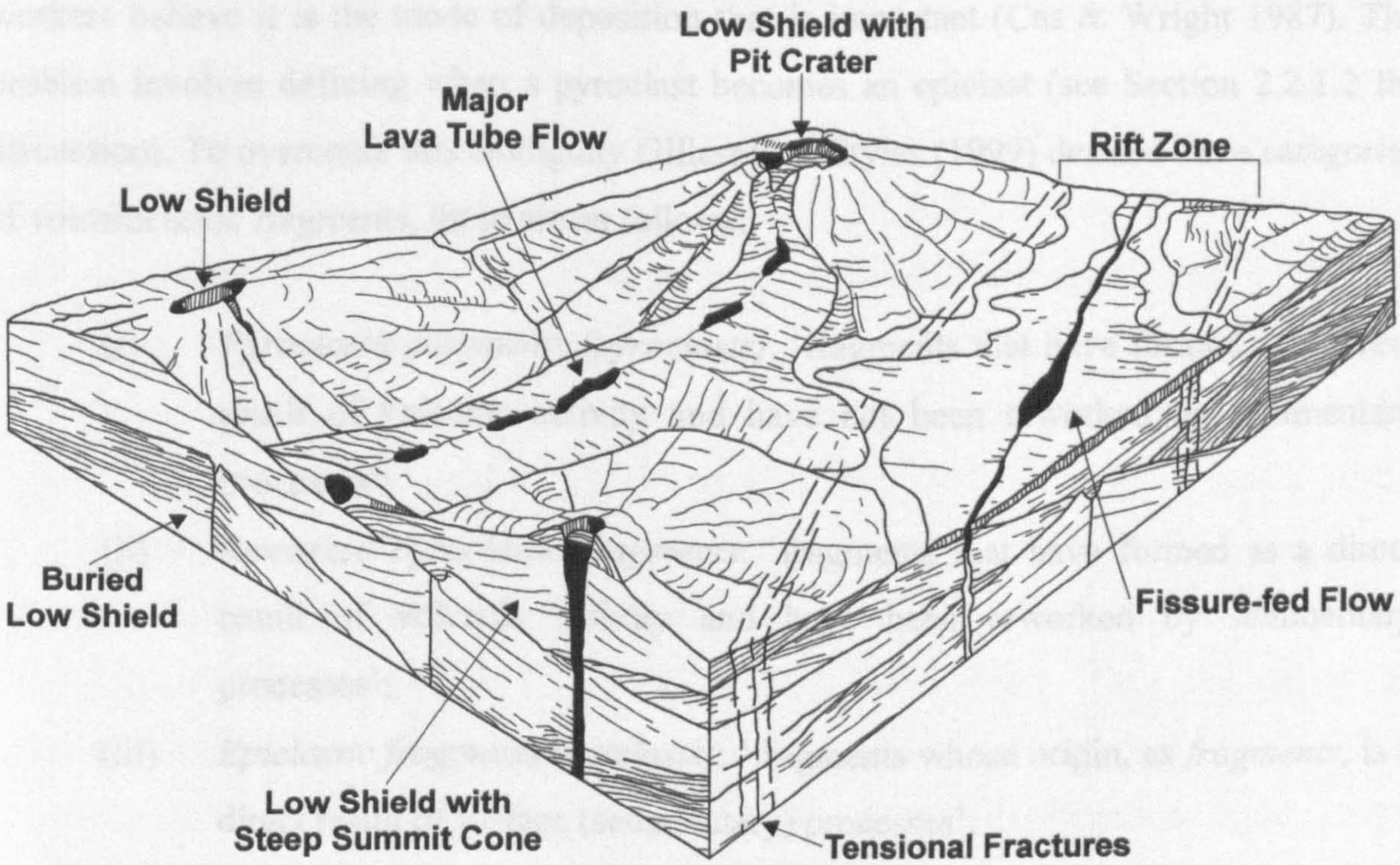

Fig. 2.8. Block diagram showing the relationship of low shields, major lava tube flows, and fissure flows within Basaltic Plains volcanic provinces. After Greeley (1977; 1982).

2.2.1 Volcaniclastic Fragments

Volcaniclastic rocks are classified on the recognition and distinction between various volcaniclastic fragments which make up the rocks (Fisher 1961; Schmid 1981; Fisher & Schmincke 1984; Cas & Wright 1987; Fisher & Smith 1991; Gillespie & Styles 1999). Volcaniclastic fragments have commonly been divided into two categories: (i) pyroclastic fragments (*pyroclasts*) and (ii) epiclastic fragments (*epiclasts*) (e.g. Fisher & Schmincke 1984; Cas & Wright 1987). However, problems have arisen in the classification of volcaniclastic rocks in differentiating between pyroclasts and epiclasts. This ambiguity has occurred because some workers believe the volcanic origin of the fragments (Fisher & Schmincke 1984) is the important aspect in the classification scheme, whereas other workers believe it is the mode of deposition that is important (Cas & Wright 1987). The problem involves defining when a pyroclast becomes an epiclast (see Section 2.2.1.2 for discussion). To overcome this ambiguity Gillespie & Styles (1999) defined three categories of volcaniclastic fragments, these are as follows:

(i) *Pyroclastic fragments (pyroclasts)*: 'fragments that have formed as a direct result of volcanic activity and have not been reworked by sedimentary processes';

(ii) *Reworked pyroclastic fragments*: 'fragments that have formed as a direct result of volcanic activity and have been reworked by sedimentary processes';

(iii) *Epiclastic fragments (epiclasts)*: 'fragments whose origin, as *fragments*, is a direct result of surface (sedimentary) processes'.

2.2.1.1 Pyroclastic Fragments (Pyroclasts)

Pyroclasts are generated by disruption as a direct result of explosive volcanic action and deposited by transport processes resulting directly from this activity (Cas & Wright 1987; McPhie *et al.* 1993; Gillespie & Styles 1999). Pyroclasts can be subdivided into six distinguishable categories: (i) *juvenile fragments*, (ii) *hydroclasts*, (iii) *autoclasts*, (iv) *cognate fragments*, (v) *accidental fragments*, and (vi) *alloclastic fragments*. The six categories of pyroclasts are defined by Fisher & Schmincke (1984) as follows:

(i) *Juvenile* (or *essential*) fragments are 'derived directly from the erupting magma and consist of dense or inflated particles of chilled melt, or crystals that were in the magma prior to eruption';

(ii) *Hydroclasts* are 'formed from steam explosions at magma-water interfaces, and also by rapid chilling and mechanical granulation of lava that comes in contact with water or water-saturated sediments';

(iii) *Autoclasts* are 'formed by mechanical friction or gaseous explosion during movement of lava';

(iv) *Cognate* (or *accessory*) fragments are 'fragmented co-magmatic volcanic rocks from previous eruptions of the same volcano';

(v) *Accidental* fragments are 'derived from the subvolcanic basement and therefore may be of any composition';

(vi) *Alloclastic* fragments are formed by the 'disruption of pre-existing volcanic rocks by igneous processes beneath the Earth's surface, with or without the intrusion of fresh magma'.

For the purposes of the classification scheme outlined in Section 2.2.2, pyroclasts are distinguished by their grain size (Fisher 1961) (Fig. 2.9). *Bombs* are pyroclasts that have a mean diameter >64 mm and have a shape (e.g. ellipsoidal, discoidal, irregular etc.) or texture (e.g. cow-dung, bread crust bombs etc.) which indicates that they were in a wholly or partly molten state during their formation and subsequent transport (MacDonald 1972; Schmid 1981; Fisher & Schmincke 1984; Cas & Wright 1987; Gillespie & Styles 1999). *Blocks* are pyroclasts that have a mean diameter >64 mm and which have an angular to sub-angular shape, indicating they were solid during transport (MacDonald 1972; Schmid 1981; Fisher & Schmincke 1984; Cas & Wright 1987; Gillespie & Styles 1999). *Lapilli* are pyroclasts of any shape with a mean diameter between 2 to 64 mm (MacDonald 1972; Schmid 1981; Fisher & Schmincke 1984; Cas & Wright 1987; Gillespie & Styles 1999). Ash grains are pyroclasts with a mean diameter <2 mm (MacDonald 1972; Schmid 1981; Fisher & Schmincke 1984; Cas & Wright 1987; Gillespie & Styles 1999). *Ash* grains are subdivided into coarse ash, which have a mean diameter between 0.063 to 2 mm and fine ash, which have a mean diameter <0.063 mm (MacDonald 1972; Schmid 1981; Fisher & Schmincke 1984; Cas & Wright 1987; Gillespie & Styles 1999). The boundaries between clast types correspond to divisions on the Wentworth Scale (Wentworth 1922).

A number of qualifier terms are added to the grain size names outlined above to further classify the pyroclasts. Pumice (or pumiceous) is a highly vesicular volcanic glass of silicic affinity with or without crystals, whereas scoria (or scoriaceous) is the basaltic or andesitic equivalent. These terms would be added to the front of the pyroclast name, for example, scoriaceous lapilli or pumiceous lapilli. Ash grains that are composed of volcanic glass are term glassy shards and these are subdivided into three forms: cuspate shards, platy shards,

Phi units	Clast or crystal size in mm Log Scale	Sedimentary clasts		Pyroclastic fragments	Crystalline Rocks
-8	256	Boulders		Blocks and Bombs	Very Coarsely Crystalline
-7	128	Cobbles			
-6	64	Pebbles	GRAVEL	Lapilli	Coarsely Crystalline
-5	32				
-4	16				
-3	8				
-2	4	Granules			
-1	2	Very Coarse Sand		Coarse Ash	Medium Crystalline
0	1	Coarse Sand			
1	0.5	Medium Sand	SAND		
2	0.25	Fine Sand			Finely Crystalline
3	0.125	Very Fine Sand			
4	0.063				
5	0.032				
6	0.016	Silt	MUD	Fine Ash	Very Finely Crystalline
7	0.008				
8	0.004				
		Clay			Cryptocrystalline

Fig. 2.9. Grain size chart for Sedimentary, Pyroclastic and Crystalline Rocks. Modified after Gillespie & Styles (1999).

and pumice/scoria shards. Accretionary lapilli are spheroidal, lapilli-sized aggregates of ash, which form two different textures (i) rim-type: a core of coarse ash surrounded by a rim of finer ash, this may alternate, and (ii) core-type: aggregate of coarse ash without the rim of finer ash. Fiamme are elongate, flattened, glassy lens with flame-like shapes. Alignment of the long dimensions of the fiammes produces a eutaxitic texture.

2.2.1.2 Epiclastic Fragments (Epiclasts)

Epiclasts are fragments that have formed by epiclastic (surface sedimentary) processes (i.e. weathering, erosion, transport and deposition) at the Earth's surface. Different workers disagree as to whether epiclasts have to come solely from the disruption of pre-existing consolidated rocks or whether unconsolidated deposits can be considered as a source. Schmid (1981) defined epiclasts as 'crystals, crystal fragments, glass and rock fragments that have been liberated from any type of pre-existing consolidated rock (volcanic or non-volcanic) by weathering or erosion and transported from the site of origin by gravity, air, water or ice'. This definition is accepted and used by Fisher & Schmincke (1984) and Fisher & Smith (1991). Cas & Wright (1987) however suggested that epiclasts are either 'produced by normal surface fragmentation processes or were finally deposited by normal surface processes, irrespective of their fragmentation mode, or both'. Therefore, the source for the epiclasts under the definition of Cas & Wright (1987) can be either pre-existing consolidated rocks or unconsolidated deposits. As a consequence, Gillespie & Styles (1999) introduced a third category referred to as reworked pyroclastic fragments (see Section 2.2.1).

However, classification schemes in current use for volcaniclastic rocks require the division of fragments into either pyroclasts or epiclasts. Schmid (1981) suggested that if the pyroclastic origin of the reworked pyroclasts is identifiable they should be treated as pyroclasts, but if there is any uncertainty in the origin of the fragments they should be treated as epiclasts as they have undergone epiclastic (surface) processes. McPhie *et al.* (1993) suggested that if the volcaniclastic rock is dominated by reworked pyroclasts the rock will have a narrow range in clast types and composition i.e. fairly homogeneous, whereas in lithologies dominated by epiclasts the rock will be heterogeneous in clast type and composition. However, exceptions to this rule do occur and care is required when trying to identify volcaniclastic fragments (Cas & Wright 1987; McPhie *et al.* 1993). Within this study reworked pyroclasts shall be considered as epiclasts, as they were deposited by epiclastic (surface) rather than pyroclastic processes.

2.2.2 Classification of Volcaniclastic Rocks

Cas & Wright (1987) stated that there are two schemes in naming volcaniclastic rocks (i) the non-genetic (lithological) and (ii) the genetic. The classification scheme in this thesis shall be primarily lithological, even though the resulting rock name shall imply a general origin for the rock, i.e. pyroclastic or epiclastic. The actual origin, or the genetic, classification of the volcaniclastic rocks (e.g. pyroclastic fall, pyroclastic flow, pyroclastic surge, lacustrine, fluvial, alluvial, etc.) shall be dealt with after all lithological and field facies characteristics have been evaluated. Care has to be taken in classifying ancient volcaniclastic rocks, as diagenesis rapidly alters glassy material to clays and destroys primary depositional textures (Fisher & Schmincke 1984; Cas & Wright 1987; Reading 1996; Tucker 1996a; Gillespie & Styles 1999).

2.2.2.1 Lithological Classification Scheme

The lithological classification scheme used in this study is based on the format proposed by Schmid (1981) (Fig. 2.10). This scheme involves dividing the volcaniclastic rock components into pyroclasts and epiclasts (volcanic (including reworked pyroclasts) and non-volcanic, and including minor amounts of biogenic, chemical sedimentary and authigenic constituents). This scheme will categorise the rock as one of three forms of volcaniclastic rock, which are (i) *pyroclastic rocks*, (ii) *tuffites*, and (iii) *epiclastic (or volcaniclastic sedimentary) rocks*. Pyroclastic rocks contain >75% pyroclastic fragments and <25% epiclasts. Tuffites, which are a mixture of pyroclastic and epiclastic fragments, contain 25-75% pyroclastic fragments and 25-75% epiclasts. Epiclastic rocks contain <25% pyroclastic fragments and >75% epiclasts. Once the rock has been categorised it can be further subdivided on its average fragment size to obtain its lithological rock name.

The classification scheme used here deals adequately with well sorted pyroclastic rocks. However, poorly sorted pyroclastic rocks should be additionally classified using the triangular plot proposed by Fisher & Schmincke (1984) (Fig. 2.11). Tuffs and lapillistones can be further subdivided depending on their fragmental composition and the qualifier terms *vitric*, *lithic*, and *crystal* can be added to the rock name, for example *lithic* lapillistone (Fig. 2.12). If the pyroclastic rock is made up of >50% reworked pyroclastic fragments then the qualifier term *reworked* should be added to the rock name, for example *reworked* lapillistone (Gillespie & Styles 1999). A rock composed of glass shards or formerly glassy shards have a vitriclastic texture in thin section (McPhie *et al.* 1993).

Average fragment size in mm	Pyroclastic rocks	Tuffites	Epiclastic rocks (or Volcaniclastic sedimentary rocks)
64	Agglomerate or Pyroclastic Breccia	Tuffaceous Conglomerate/Breccia	Volcaniclastic Conglomerate/Breccia
2	Lapillistone		
0.063	*Coarse* Tuff	Tuffaceous Sandstone	Volcaniclastic Sandstone
	Fine Tuff	Tuffaceous Mudstone	Volcaniclastic Mudstone
Amount of pyroclastic fragments by volume	100-75%	75-25%	25-0%
Amount of epiclastic fragments by volume	0-25%	25-75%	75-100%

Fig. 2.10. Classification of volcaniclastic rocks containing more than 10% volcanic debris. Adapted after Gillespie & Styles (1999) based on Schmid (1981).

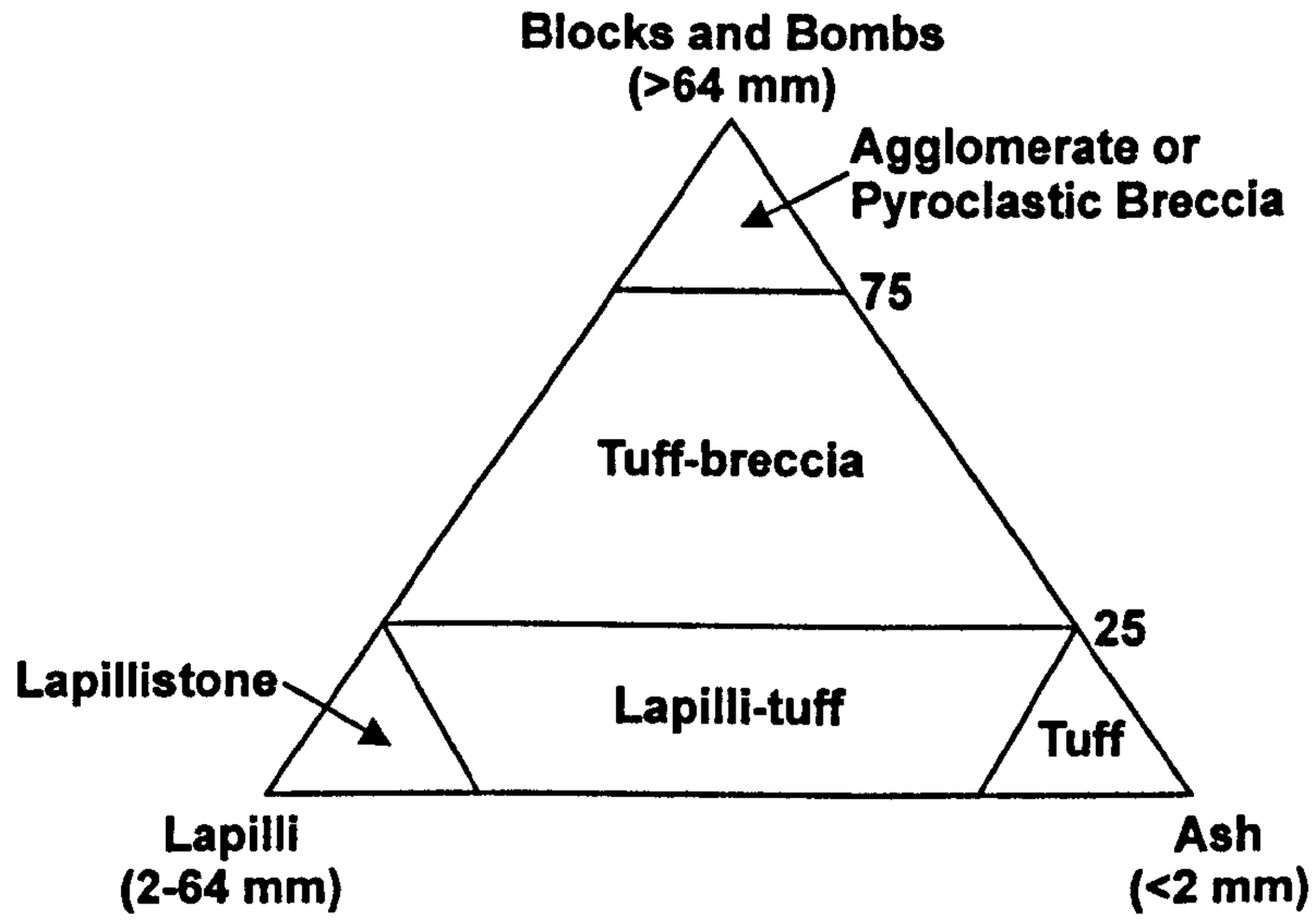

Fig. 2.11. Classification of poorly sorted pyroclastic rocks. After Fisher (1966).

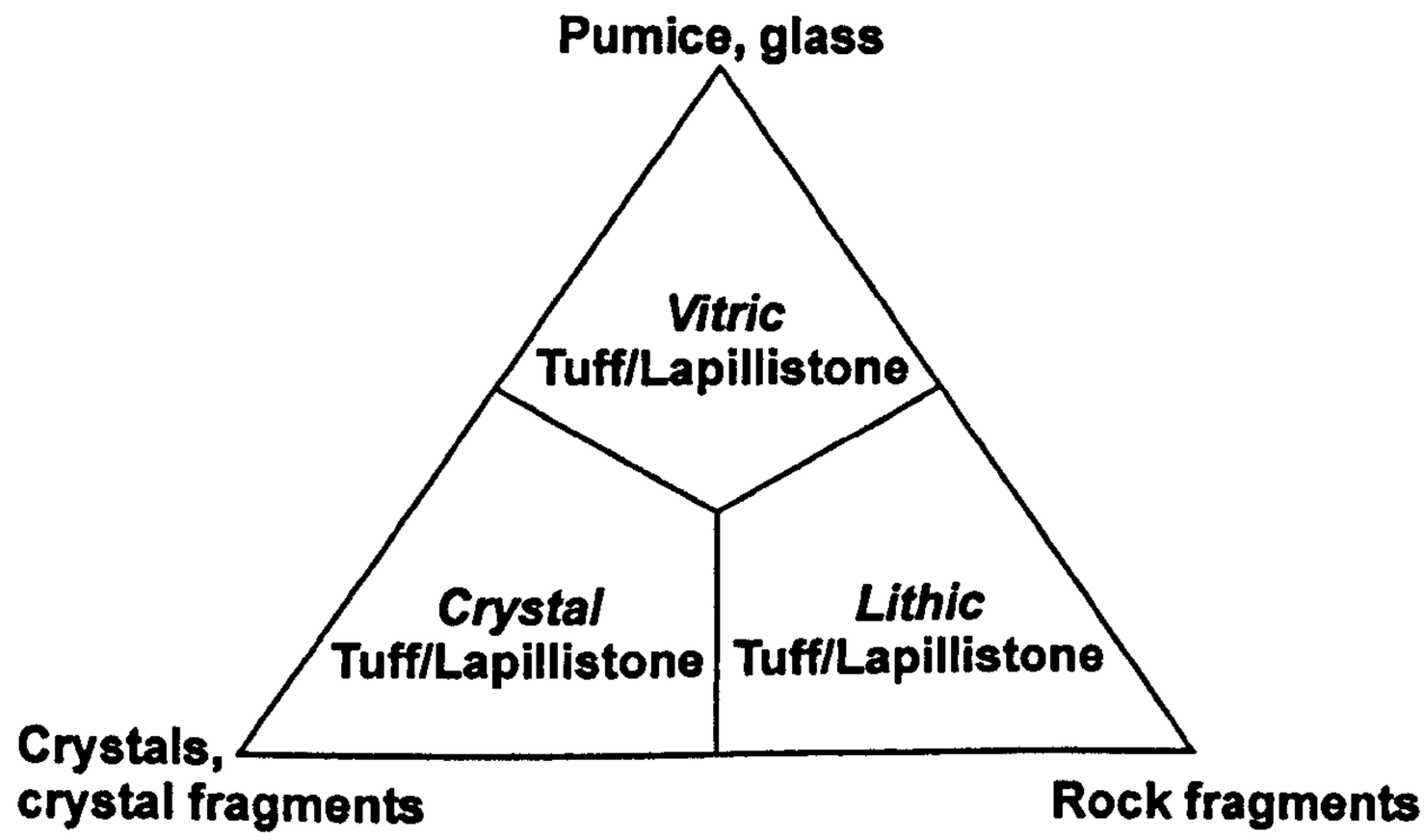

Fig. 2.12. Classification and nomenclature of tuffs and lapillistones based on their fragmental composition. Adapted after Schmid (1981).

Gillespie & Styles (1999) noted that in consolidated rocks, particularly ancient rocks, it is difficult or virtually impossible to accurately distinguish between the three main types of volcaniclastic rocks, i.e. the percentage of pyroclastic and epiclastic fragments, particularly if the fragments are all volcanic. If there is any ambiguity in naming the rock, but there is clearly a volcanic constituent, then the rock shall be classified under the tuffite category (Gillespie & Styles 1999).

2.2.2.2 Genetic Classification

The lithological classification scheme outlined in Section 2.2.2.1 constrains the clast-forming processes and begins to categorise the volcaniclastic rocks into two broad genetic groups: pyroclastic and epiclastic. Pyroclastic rocks can be further subdivided into five subgroups: autoclastites, hydroclastites, pyroclastic falls, pyroclastic flows, and pyroclastic surges. Autoclastic deposits and hydroclastites commonly involve the fragmentation of lava flows and are not the result of primary pyroclastic (not initiated by the original eruption) or epiclastic processes. As a consequence, autoclastic deposits and hydroclastites are considered separately and have their own genetic classification scheme in the literature. Autoclastitic deposits (autobreccias) are composed of abundant autoclasts, which were produced by the mechanical friction or the gaseous explosion during the movement of lava flows. Hydroclastites are the result of magma coming into contact with water and the rapid chilling and quenching that ensues causing fragmentation. Two main types of hydroclastites are recognised: hyaloclastites and peperites. Hyaloclastites are formed when lava flows into water or over water-saturated sediments, whereas peperites are formed when lava intrudes and mingles with unconsolidated or poorly consolidated, typically wet, sediments (White *et al.* 2000; Skilling *et al.* 2002).

Pyroclastic fall deposits are composed of pyroclasts that are produced and ejected by an explosive eruption of any composition. Pyroclastic flow deposits are the result of a hot, high-concentration, ground-hugging, highly mobile, gas-particle flow generated by a volcanic eruption. There are three different pyroclastic flow types that can be produced depending on the setting and mode of generation: (i) block and ash flows (or nuee ardentes or hot avalanches), (ii) scoria and ash flows, and (iii) pumice pyroclastic flows (deposits of which are know as ignimbrites). Pyroclastic surge deposits are the result of ground-hugging, dilute, particulate flows in which pyroclasts are carried laterally, entrained in turbulent gas. There are two types of pyroclastic surges (i) base surges, and (ii) ash cloud or ground surges (associated with pyroclastic flows).

Epiclastic processes that occur in a volcanic setting range from those that are observed in non-volcanic regions, e.g. fluvial or lacustrine, to those that are unique in volcanic provinces. The reader is referred to Reading (1996) for an overview of the 'normal' epiclastic processes that can occur within non- and volcanic regions. Lahars are unique to volcanic settings and is an umbrella term used to cover a wide range of processes and deposits which occur during a rapidly flowing mixture of debris and water that originated at a volcano edifice (Rodolfo 1989; Smith & Fritz 1989; Smith & Lowe 1991). The processes and deposits from a lahar range from volcaniclastic debris to hyperconcentrated flows and combinations of these inbetween (Janda *et al.* 1981; Pierson & Scott 1985; Lowe *et al.* 1986; Naranjo *et al.* 1986; Smith 1986; Rodolfo 1989; Smith & Lowe 1991; Coussot & Meunier 1996; Sohn *et al.* 1999; Kessler & Bédard 2000; Lavigne *et al.* 2000; Lirer *et al.* 2001). These debris and hyperconcentrated flow processes differ from their non-volcanic counterparts in that they are commonly lacking a clay component and usually travel far greater distances (Janda *et al.* 1981; Pierson & Scott 1985; Smith & Lowe 1991; Yarnold 1993; Coussot & Meunier 1996; Sohn *et al.* 1999; Kessler & Bédard 2000; Lirer *et al.* 2001). Another epiclastic lithology unique to volcanic settings is a volcaniclastic debris avalanche, which is a rapid and far reaching granular flow initiated from a large-volume landside (Smith & Lowe 1991; Calvari *et al.* 1998; Schneider & Fisher 1998; Kessler & Bédard 2000; Reubi & Hernandez 2000). Such volcaniclastic debris avalanches can transform into lahars distally from the volcanic edifice (Smith & Lowe 1991; Calvari *et al.* 1998; Schneider & Fisher 1998; Kessler & Bédard 2000; Reubi & Hernandez 2000).

The epiclastic processes, which are unique to volcanic settings, can be initiated by both volcanic and non-volcanic activity (Smith & Lowe 1991) and Figure 2.13 outlines the main generating events. However, due to the large volumes of volcanic debris preserved within the resulting deposits of these events, it has been postulated that they commonly occur during syn-eruption periods when there is a rapid and abrupt increase in debris from pyroclastic events (Smith 1987a; b; 1988; 1991; Haughton 1993; Bahk & Chough 1996; Orton 1996). This compares to inter-eruption periods, when the amount of volcanic debris available for transportation has been greatly removed by lahars during the syn-eruption periods (Smith 1987a; b; 1988; 1991; Haughton 1993; Bahk & Chough 1996; Orton 1996). The inter-eruption periods are characterised by the development of fluvial systems, which contrasts with syn-eruption periods dominated by rapidly aggrading braided channels and flooding episodes (Smith 1987a; b; 1988; 1991; Haughton 1993; Bahk & Chough 1996; Orton 1996).

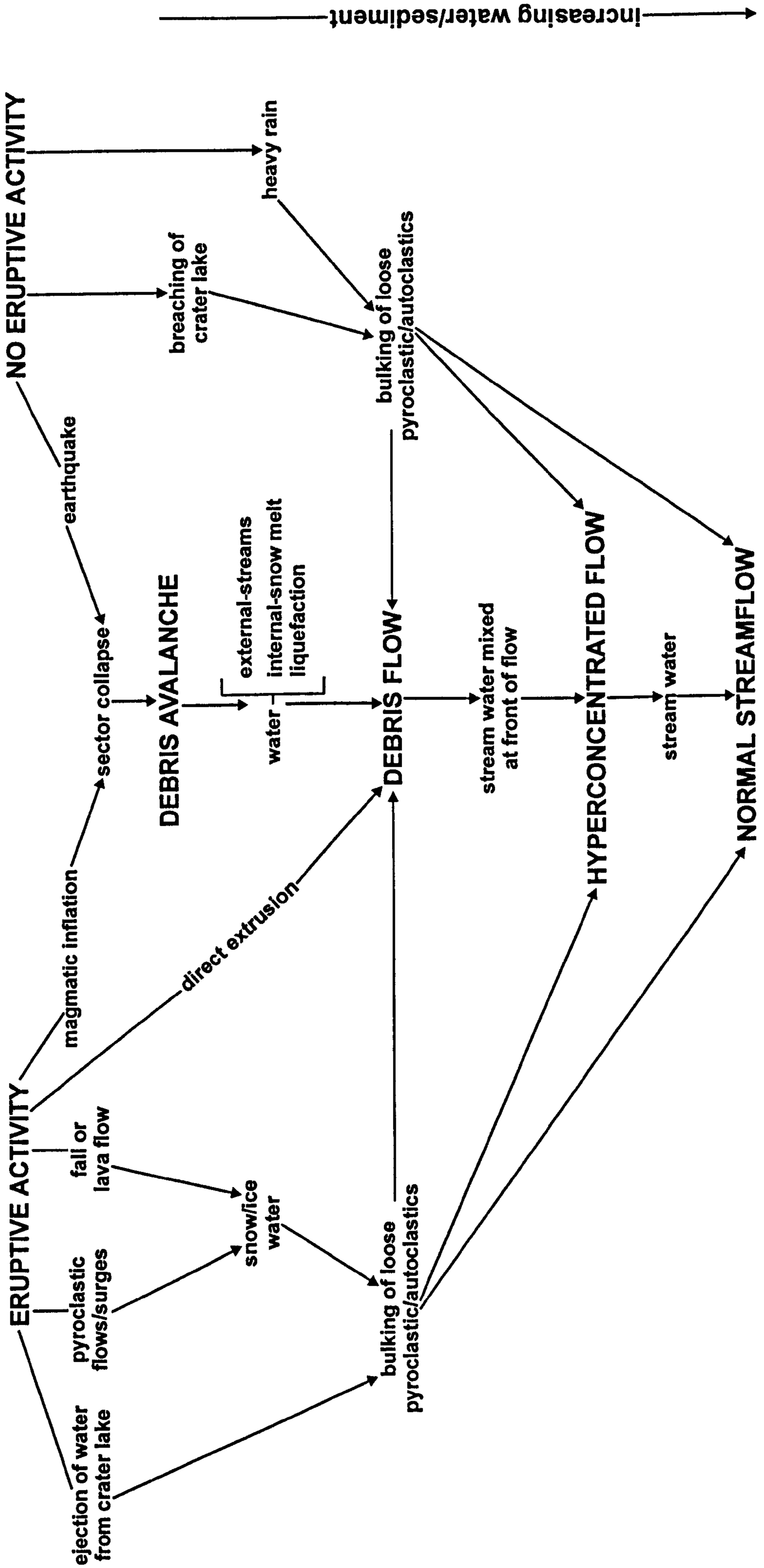

Fig. 2.13. Schematic diagram illustrating relationships of volcanic phenomena and the generation of debris avalanches, debris flows, and hyperconcentrated flows. Principal processes of sediment transport and deposition are vertically arranged in the centre according to the ratio of sediment to water in the moving flow; they can be related to one another by dilution or bulking processes. Processes that may release large volume of water, or sediment, or both, are listed near the top of the diagram. Paths drawn along the margins of the chart indicate the types of the flow phenomena that may be expected to result depending on the degree of dilution or bulking. After Smith & Lowe (1991).

By examining the lithofacies character and textural features of a volcaniclastic deposit it is possible to distinguish between pyroclastic falls, flows, surges and epiclastic deposits, as well as constraining the depositional setting (subaerial, subaqueous, etc.) and its proximity to the source region (McPhie *et al.* 1993). The lithofacies character of a volcaniclastic deposit is fundamental in recognising the mode of transport and depositional processes in the formation of the deposit (McPhie *et al.* 1993). This involves examining bedforms, geometry, structures, internal organisation and nature of contacts of the volcaniclastic deposit (McPhie *et al.* 1993). The presence of welding and other textural evidence of hot emplacement are significant in recognising primary pyroclastic deposits (McPhie *et al.* 1993).

Similar processes of transportation and deposition are involved in the formation of primary pyroclastic, reworked pyroclastic and epiclastic deposits. Regardless of the mode of fragmentation, the processes involved in transportation consist of clasts and interstitial fluid (gas or liquid). In primary pyroclastic deposits, transportation can be continuous, with the original mode of fragmentation with the interstitial fluid commonly involving volcanic gas, whereas reworked pyroclastic and epiclastic deposits involve surface sedimentary transporting agents (water, wind, etc.). Whether the deposit is pyroclastic, reworked pyroclastic or epiclastic three broad transport processes operate in the formation of the aforementioned deposits. The three broad transport processes are defined by McPhie *et al.* (1993) as follows:

(i) *Mass-flow* transport: 'groups of clasts, or clasts plus interstitial fluid (air, water, volcanic gas) move together and interact; mass flows vary widely in rheology and particle concentration';
(ii) *Traction* transport: 'clasts are entrained in moving interstitial fluid (air, water, volcanic gas) and are free to behave independently';
(iii) *Suspension* transport: 'clasts are fully suspended in interstitial fluid (air, water, volcanic gas)'.

Although it may be possible to distinguish between deposits formed by different transport methods, difficultly arises in distinguishing between deposits that have formed from the same transport method. For example, it may be possible to distinguish between a pyroclastic flow and a pyroclastic surge deposit, but it can be near impossible to distinguish between a non-welded pyroclastic flow from a water supported epiclastic mass flow deposit (McPhie *et al.* 1993). The only way to discriminate between these two types

of deposit is to identify welding and other textural features of hot emplacement, which are indicative of a primary pyroclastic mode of origin.

For the purpose of this study, which is examining ancient volcaniclastic rocks, it is essential to compare and contrast the deposits observed with deposits formed by the various transport methods outlined in Table 2.1. To summarise all the known volcaniclastic rock types here would be both time consuming and repetitive, for example Cas & Wright (1987) list over 40 different volcaniclastic rocks based on their grain size and texture alone. Therefore, the volcaniclastic rocks described in this thesis shall be compared and contrasted with the various volcaniclastic rocks reported in Fisher & Schmincke (1984), Cas & Wright (1987), McPhie *et al.* (1993) and other relevant sources in the appropriate sections.

GENETIC CATEGORY	DOMINANT TRANSPORT		
	Mass-flow	Traction	Suspension
Primary Pyroclastic Deposits	• Pyroclastic flows	• Pyroclastic surges	• Fallout • Water-settled fallout
Reworked Pyroclastic Deposits & Epiclastic Deposits	• Turbidity currents • Debris flows, mud flows • Grain flows • Density-modified grain flows • Slides, debris avalanches	• Fluvial and shallow subaqueous currents • Waves	• Suspension associated with mass flows • Hemipelagic suspension

Table 2.1 Mass-flow, traction and suspension transport processes that operate in the formation of pyroclastic, reworked pyroclastic and epiclastic deposits. Modified after McPhie *et al.* (1993).

2.3 Colour Appellations

All colour appellations used in this study are based upon dry samples viewed in natural light. The colour names and their numerical designations presented are based upon the Munsell system of colour identification used in the Rock-Color Chart (Rock-Color Chart Committee 1995). A complete description of how colour names are determined as well as their numerical designations can be seen in Figure 2.14.

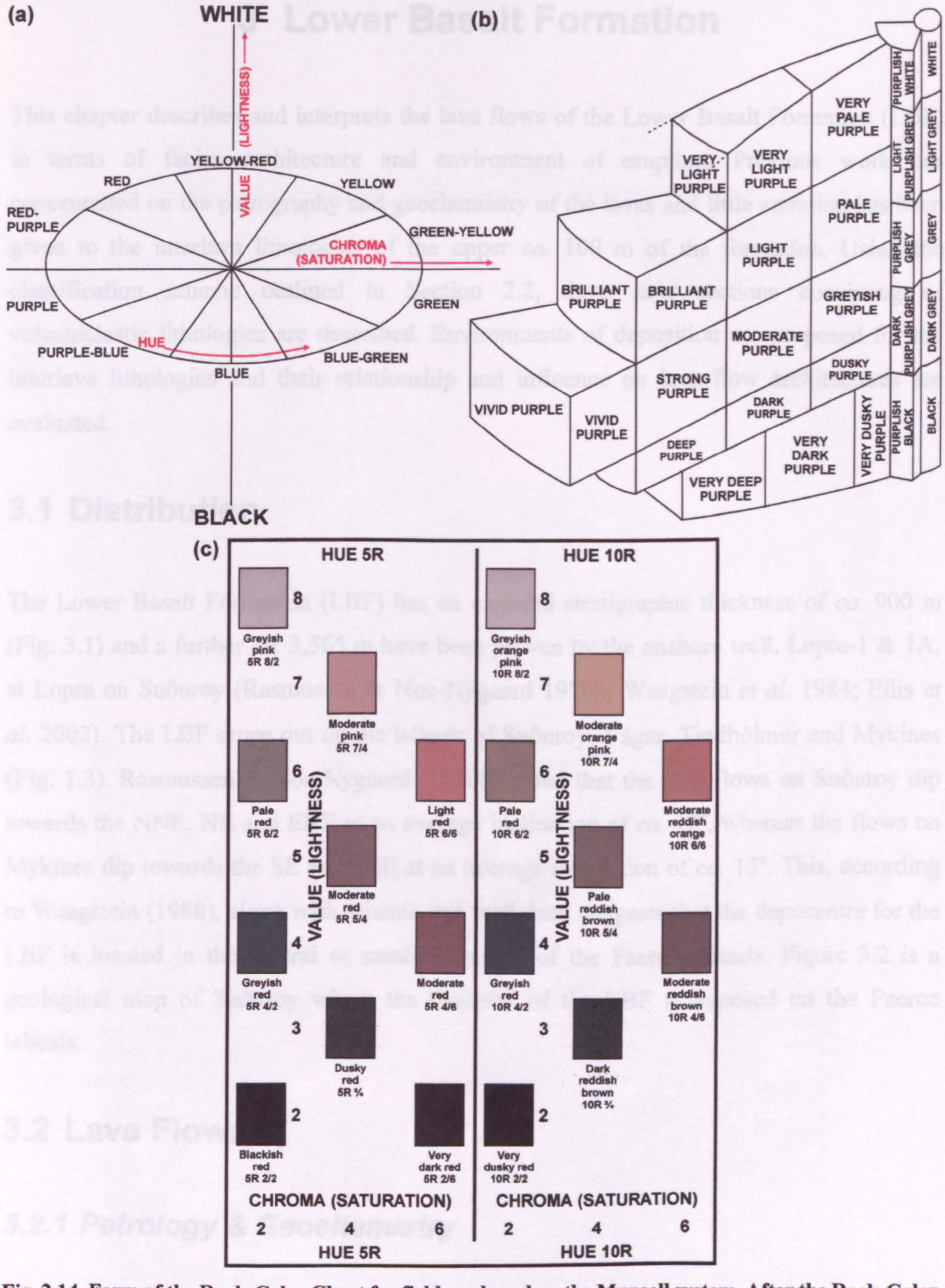

Fig. 2.14. Form of the Rock-Color Chart for field use based on the Munsell system. After the Rock-Color Chart Committee (1995) (a) The dimensions of the colour solid, approximately a sphere, which has a natural grey axis grading from white at the top to black at the bottom. This property of lightness is called *value*. Around the circumference or equator of the solid are the 10 major *hues*, each of which is separated into 10 numbered divisions, so that 5 marks the middle of the *hue* and 10 marks the boundary between one *hue* and the next. Thus any particular *hue* can be designated by a number and a letter such as 5R or 10YR. Any single vertical section through the neutral grey axis and a particular *hue* constitutes a colour chart on which the colours grade in *value* from light at the top to dark at the bottom, and in *chroma* (degree of saturation) from grey at the left to the most vivid colours at the right. Both *value* and *chroma* are numbered so any particular colour can be given a numerical designation representing *hue*, *value*, and *chroma* such as 5R 6/4 and 10YR 8/2. (b) The purple section of the colour solid. (c) A sample page from the Rock-Color Chart. The Munsell colour chips cannot be reproduced with any degree of accuracy and the colours presented here should be regarded as a representation only.

3 Lower Basalt Formation

This chapter describes and interprets the lava flows of the Lower Basalt Formation (LBF) in terms of facies architecture and environment of eruption. Previous work has concentrated on the petrography and geochemistry of the lavas and little attention has been given to the interlava lithologies of the upper *ca.* 100 m of the formation. Using the classification scheme outlined in Section 2.2, three new sections consisting of volcaniclastic lithologies are described. Environments of deposition are proposed for the interlava lithologies and their relationship and influence on lava flow architectures are evaluated.

3.1 Distribution

The Lower Basalt Formation (LBF) has an exposed stratigraphic thickness of *ca.* 900 m (Fig. 3.1) and a further *ca.* 3,565 m have been proven by the onshore well, Lopra-1 & 1A, at Lopra on Suðuroy (Rasmussen & Noe-Nygaard 1970b; Waagstein *et al.* 1984; Ellis *et al.* 2002). The LBF crops out on the islands of Suðuroy, Vágar, Tindhólmur and Mykines (Fig. 1.3). Rasmussen & Noe-Nygaard (1970b) noted that the lava flows on Suðuroy dip towards the NNE, NE and ENE at an average inclination of *ca.* 12°, whereas the flows on Mykines dip towards the SE and ESE at an average inclination of *ca.* 15°. This, according to Waagstein (1988), along with seismic and well data, suggests that the depocentre for the LBF is located in the central or southern region of the Faeroe Islands. Figure 3.2 is a geological map of Suðuroy where the majority of the LBF is exposed on the Faeroe Islands.

3.2 Lava Flows

3.2.1 Petrology & Geochemistry

The LBF flows are Fe-rich tholeiites, which are primarily aphyric, finely to medium crystalline basalts displaying an intergranular texture (Rasmussen & Noe-Nygaard 1970b; Hald & Waagstein 1984; Waagstein & Hald 1984; Waagstein 1988; Larsen *et al.* 1999) (Fig. 3.3). However, infrequent plagioclase-phyric basalts also occur (Rasmussen & Noe-Nygaard 1970b; Hald & Waagstein 1984; Waagstein & Hald 1984; Waagstein 1988; Larsen *et al.* 1999). The average modal mineralogy of the LBF lava flows is presented in Table 3.1. The lava flows of the LBF are fairly homogenous and show very little variation,

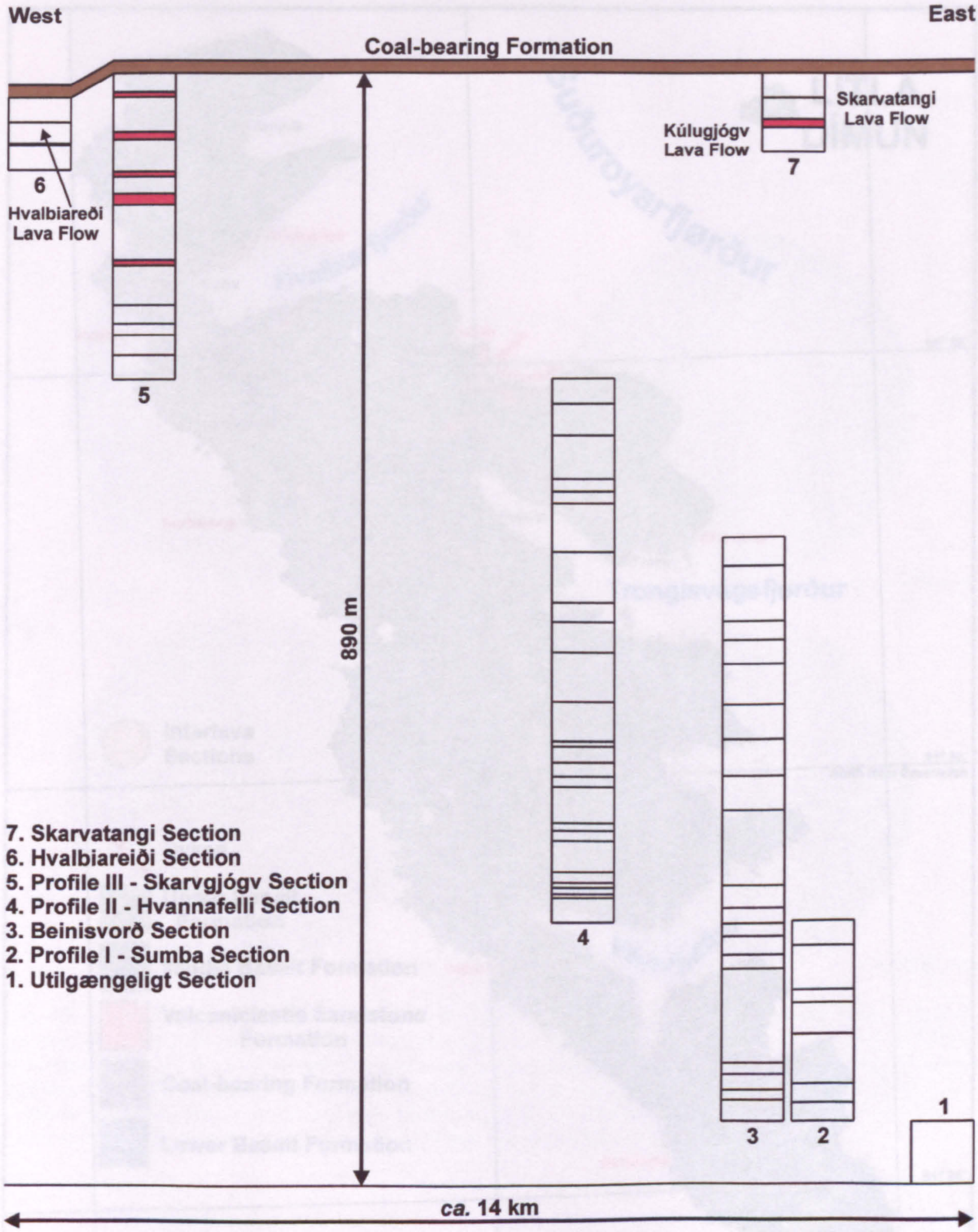

Fig. 3.1. Stratigraphic logs for the exposed 890 m of the Lower Basalt Formation (LBF), Suðuroy, Faeroe Islands. Sections 1, 2, 4 and 5 form the ideal section of Rasmussen & Noe-Nygaard (1969; 1970b). Volcaniclastic rocks that have been identified are highlighted in red. Three lava flows that are discussed in the text are indicated. The average lava flow thickness for the exposed LBF sequence is *ca.* 25 m, although flow thicknesses range from *ca.* 10 to *ca.* 70 m.

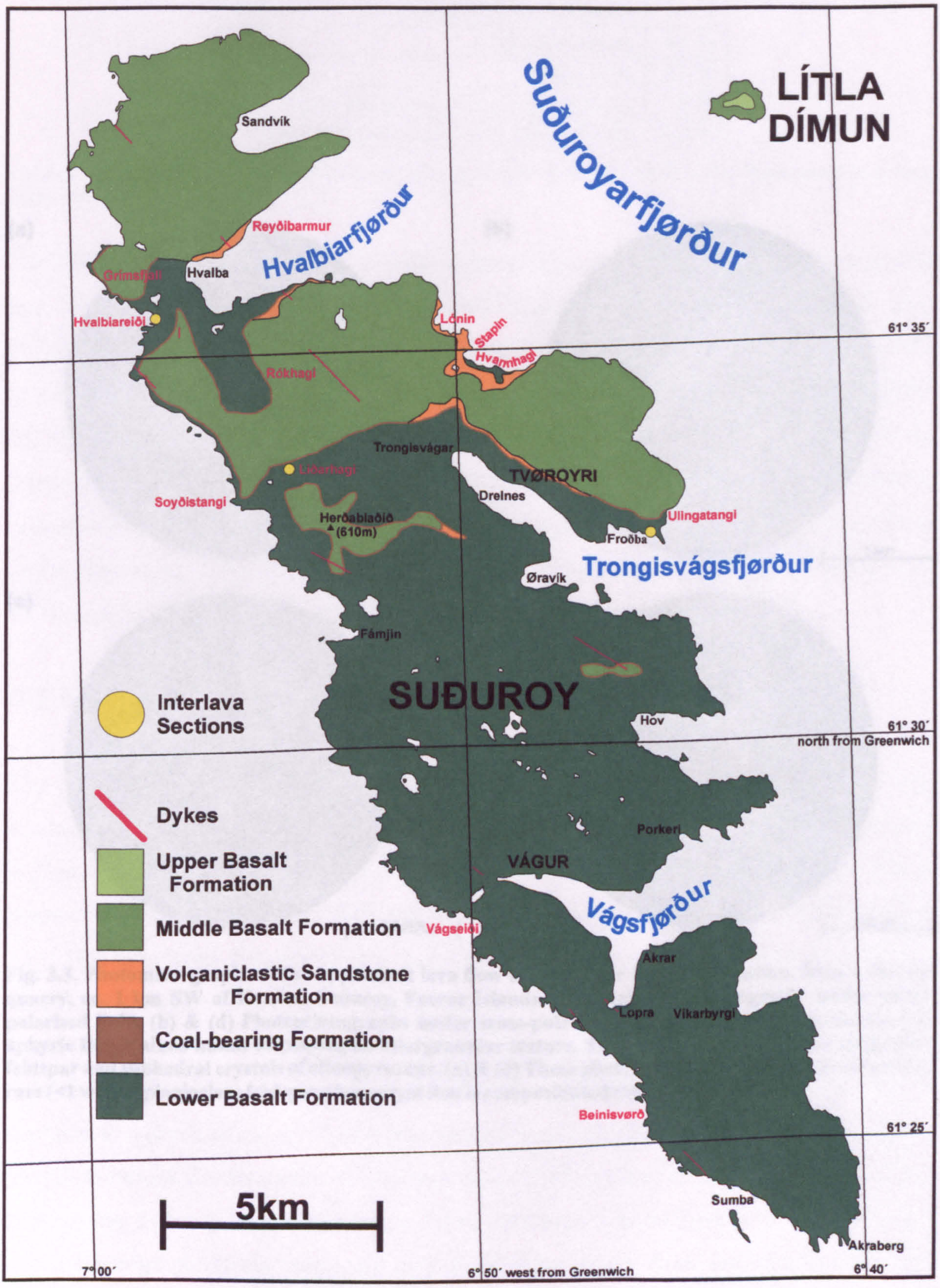

Fig. 3.2. Geological map of Suðuroy, Faeroe Islands. After Rasmussen & Noe-Nygaard (1969; 1970a; b).

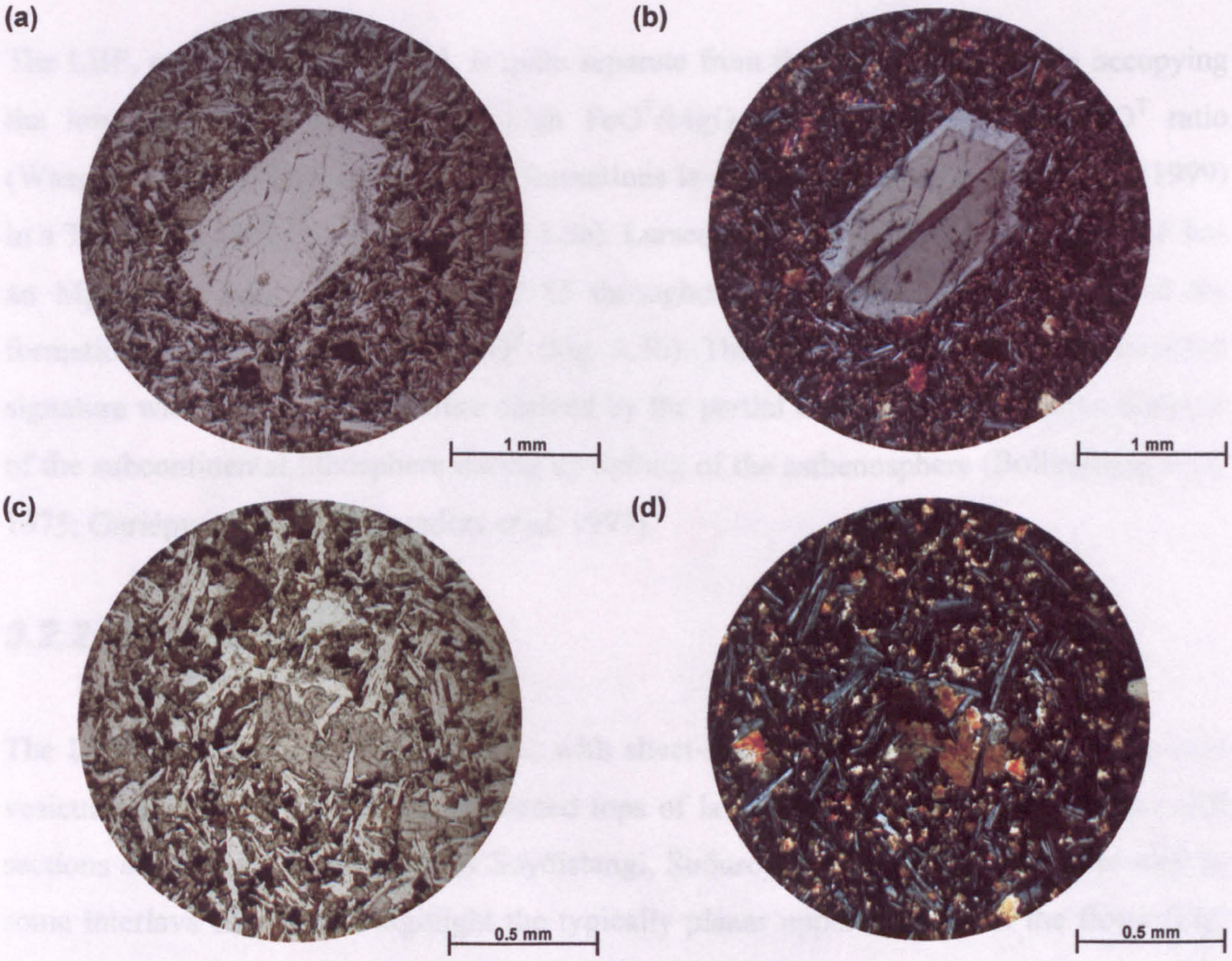

Fig. 3.3. Photomicrographs of the uppermost lava flow of the Lower Basalt Formation, from a disused quarry, *ca.* 1 km SW of Hvalba, Suðuroy, Faeroe Islands. (a) & (c) Photomicrographs under plane-polarised light. (b) & (d) Photomicrographs under cross-polarised light. The lava is a predominantly aphyric fine grained basalt displaying an intergranular texture. The lava consists of laths of plagioclase feldspar and subhedral crystals of clinopyroxene. (a) & (b) These photomicrographs contain an extremely rare (<1 vol.%) plagioclase feldspar phenocryst that is compositional zoned.

chemically or texturally, within individual lava flows as well as over the 4.5 km thickness of the LBF.

Plagioclase Feldspars	36 %
Clinopyroxenes	44 %
Black ores	11 %
Glass and green alteration products	9 %
Olivine and pseudomorphs after olivine	0.2 %

Table 3.1. The average modal mineralogy of a lava flow from the LBF. After Rasmussen and Noe-Nygaard (1970b).

The LBF, as depicted in Fig. 3.4, is quite separate from the other formations in occupying the low-Ti tholeiite field, with a high FeO^T/MgO ratio and a low TiO_2/FeO^T ratio (Waagstein 1988). This separation of formations is also replicated by Larsen *et al.* (1999) in a TiO_2/FeO^T vs. Mg # diagram (Fig. 3.5a). Larsen *et al.* (1999) showed that the LBF has an Mg # that falls between 40 and 55 throughout the upper 3 km thickness of the formation, and with 12-16 wt.% FeO^T (Fig. 3.5b). The LBF flows have a LREE-enriched signature which suggests they were derived by the partial melting of deep mantle blobs or of the subcontinental lithosphere during upwelling of the asthenosphere (Bollingberg *et al.* 1975; Gariépy *et al.* 1983; Saunders *et al.* 1997).

3.2.2 Morphology

The LBF flows are laterally extensive, with sheet-like geometries, and are massive with vesicular and rubbly top zones. Reddened tops of lava flows typically inweather the cliff sections at Beinisvørð and north of Soyðistangi, Suðuroy. These reddened tops, as well as some interlava lithologies, highlight the typically planar upper surfaces to the flows (Fig. 3.6). This layer cake appearance and associated terraced terrain is characteristic of simple lava flows (Walker 1970), also known as tabular-classic flow facies (Jerram 2002) (Figs. 2.2 & 2.5), which are common within subaerial Continental Flood Basalt (CFB) provinces (Cas & Wright 1987, and references therein). The subaerial lava flows are believed to continue to a depth of *ca.* 2,550 m within wells Lopra-1 & 1A (Ellis *et al.* 2002), giving an overall thickness for the subaerial sequence of *ca.* 3,450 m. Individual flows can be traced E-W across Suðuroy, a distance of *ca.* 9 km. Although it is difficult to determine aspect ratios (average thickness/horizontal extent) of these flows from two-dimensional cliff exposures, it is clear that low values (<0.005) are common, which suggests high effusion rates during eruption (Walker 1973).

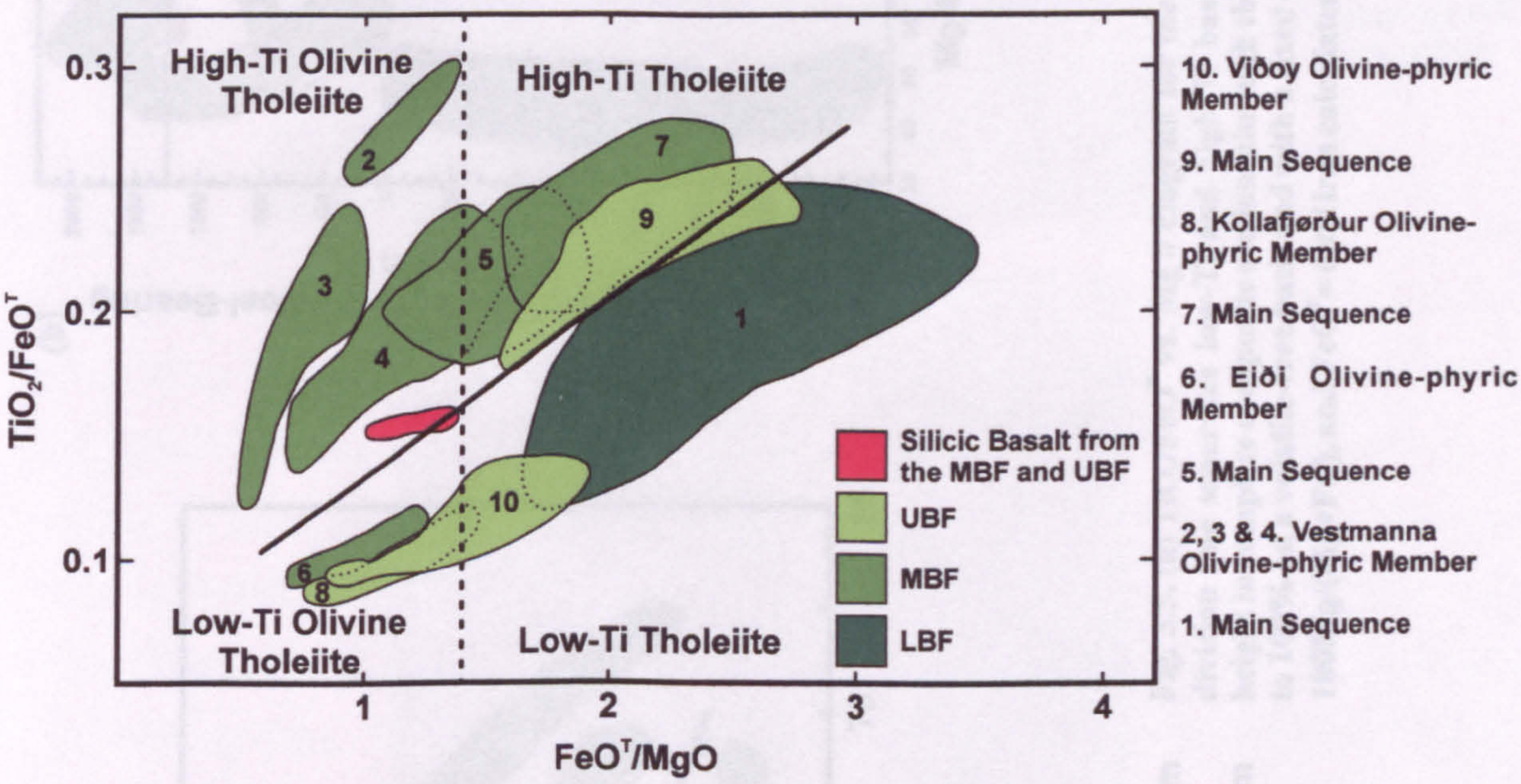

Fig. 3.4. TiO_2/FeO^T vs. FeO^T/MgO diagram for basalt lavas from the Faeroe Plateau Lava Group, Faeroe Islands (FeO^T = total iron recalculated as FeO). The oblique full line and the vertical stippled line mark the proposed boundaries between high-Ti olivine tholeiites, high-Ti tholeiites, low-Ti olivine tholeiites, and low-Ti tholeiites. LBF = Lower Basalt Formation, MBF = Middle Basalt Formation, UBF = Upper Basalt Formation. After Waagstein (1988).

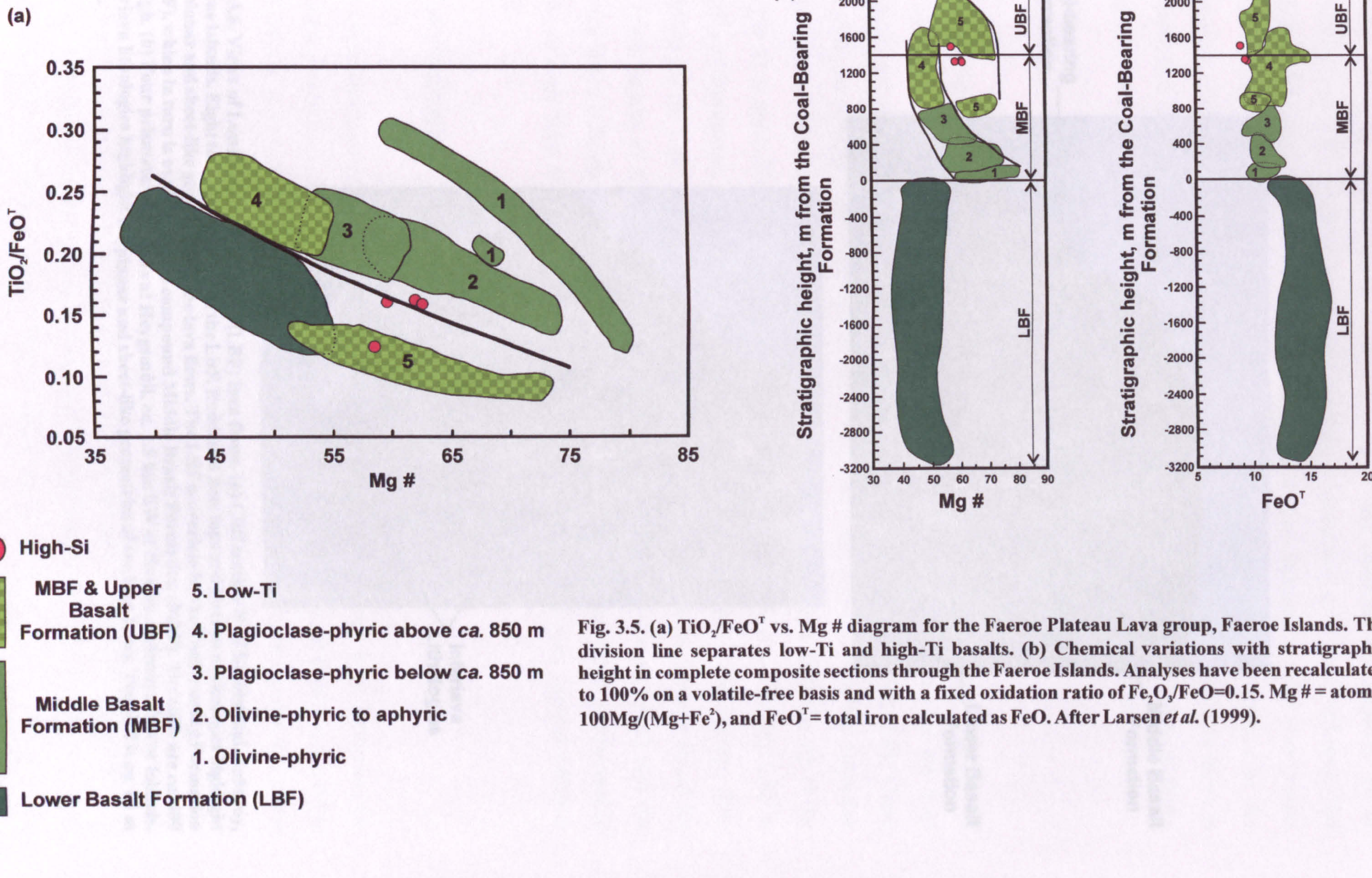

Fig. 3.5. (a) TiO_2/FeO^T vs. Mg # diagram for the Faeroe Plateau Lava group, Faeroe Islands. The division line separates low-Ti and high-Ti basalts. (b) Chemical variations with stratigraphic height in complete composite sections through the Faeroe Islands. Analyses have been recalculated to 100% on a volatile-free basis and with a fixed oxidation ratio of $Fe_2O_3/FeO=0.15$. Mg # = atomic $100Mg/(Mg+Fe^2)$, and FeO^T = total iron calculated as FeO. After Larsen *et al.* (1999).

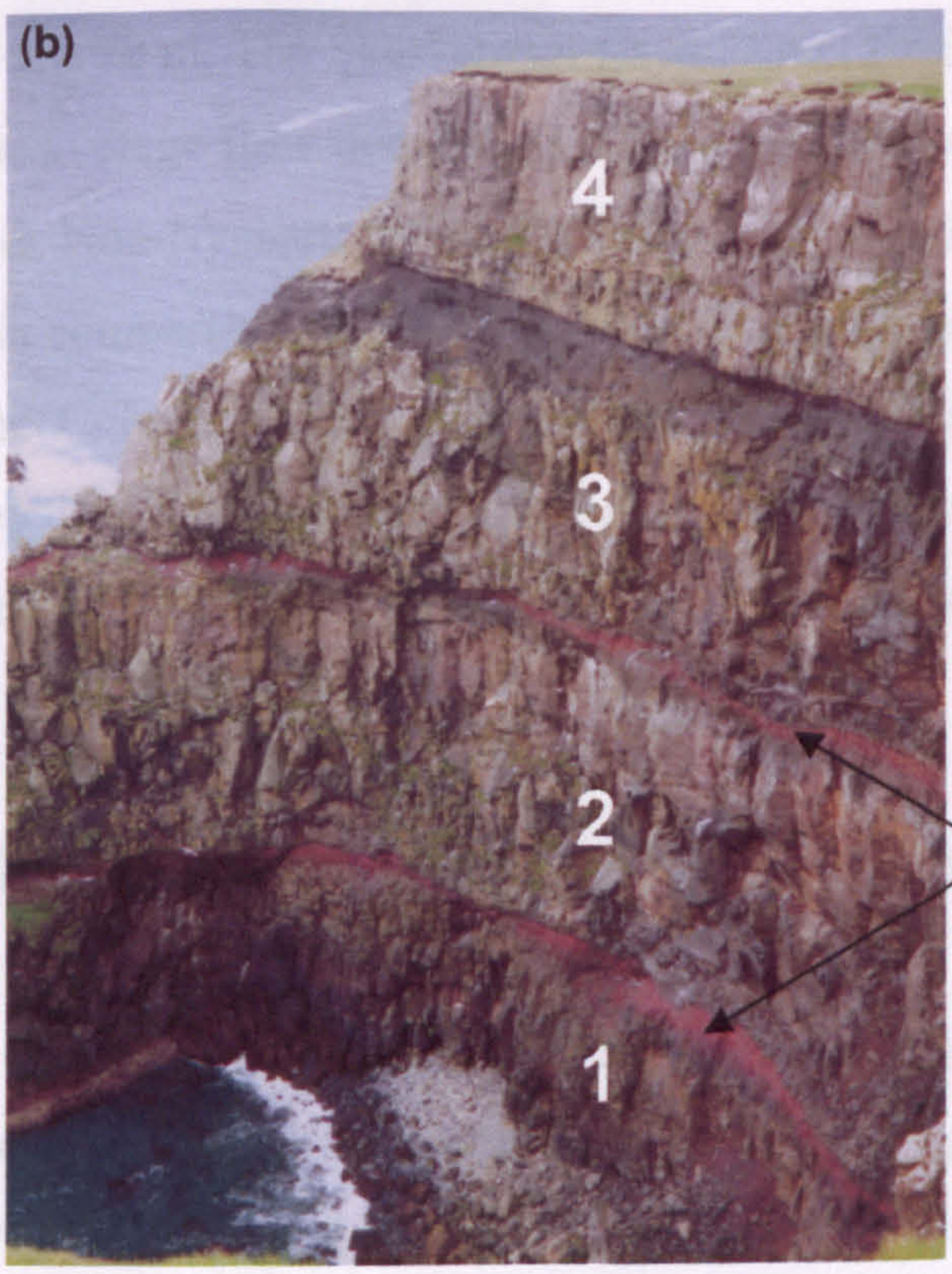

Fig. 3.6. Views of Lower Basalt Formation (LBF) lava flows. (a) Cliff section N of Soyðistangi, Suðuroy, Faeroe Islands. Eight tabular lava flows of the LBF. Reddened flow tops and interlava lithologies highlight the planar and sheet-like geometries of the lava flows. The LBF is overlain by the Coal-bearing Formation (CBF), which in turn is overlain by the compound Middle Basalt Formation (MBF). The cliffs are *ca.* 400 m high. (b) Four prismatic lava flows at Heygsmúli, *ca.* 1.5 km SW of Hvalba, Suðuroy, Faeroe Islands. Interlava lithologies highlight the planar and sheet-like geometries of the lava flows. The cliff is *ca.* 80 m high.

Flow edges are rare within the LBF, but Rasmussen & Noe-Nygaard (1970b) have observed wedging out of flows in the following cliff sections on Suðuroy: N of Bølluhálsur, *ca.* 2.5 km NW of Sumba and N of Lomvigastakkur, *ca.* 1 km S of Lopra. The erosion of flow tops is observed within the LBF and a good example is quite clearly seen in the cliffs S of Vágseiði, Suðuroy (Fig. 3.7), suggesting substantial hiatuses in the outpouring of the LBF. Waagstein (1988) has suggested that interfingering of lava flows is commonplace within the LBF, based on the variation in thickness and number of flows along cliff sections as well as misfits between overlapping geochemical profiles.

3.2.3 Flow Thicknesses

The stratigraphically lowest (and therefore oldest) lava flows from the exposed sequence of the LBF crop out at the Beinisvørð cliff section, *ca.* 3 km NW of Sumba, in the S of Suðuroy, comprising *ca.* 19 tabular flows within a thickness of 469 m (Fig. 3.8). These data yield an average flow thickness of *ca.* 25 m. However, flows within this sequence range from *ca.* 10 m to *ca.* 70 m. The Skarvatangi Lava Flow (2nd flow from the top of the LBF) is 17 m thick. The average flow thickness for the entire (exposed and drilled) LBF is *ca.* 20 m (Rasmussen & Noe-Nygaard 1970b; Waagstein *et al.* 1984). The average flow thickness for the LBF is comparable to the 15 to 35 m average flow thicknesses found for the flood basalts of the Columbia River Basalt Group (CRBG) (Waters 1961) and the Deccan Traps (Choubey 1973; Subbarao & Sukheswala 1981). They are also comparable to the average flow thickness of 17 m for the flood basalts of eastern Iceland (Walker 1963).

3.2.4 Reddened Tops and Environment of Eruption

The contemporaneous subaerial chemical weathering of lava flow tops produces the distinctive reddened tops observed throughout CFB provinces (e.g. Wilkins *et al.* 1994; Widdowson *et al.* 1997). These reddened flow tops are dominant throughout the lower sections of the LBF (e.g. at Beinisvørð) (Fig 3.8). If these reddened tops show a weathering profile down through fine-grained altered material into fresh basalt, and retain relic features of the unaltered lava flow they are termed saprolitic boles (Widdowson *et al.* 1997). These saprolitic boles are prevalent throughout the upper sections of the upper LBF. To form saprolitic boles the lava flow tops need to have been exposed for hundreds or even thousands of years (Wilkins *et al.* 1994; Widdowson *et al.* 1997) and according to the calculations of Nahon (1991) 1 mm of basalt will remain fresh, depending on the climate, for 40 to 68 years.

Fig. 3.7. Cliff section S of Vágseiði, *ca.* 1 km S of Vágur, Suðuroy, Faeroe Islands. The flow top of the basal lava is an erosional surface, which has produced the relatively steep-sided hummock. The hummock may have been formed by two adjacent channels. The presence of this erosional surface suggests substantial hiatuses in the outpouring of the Lower Basalt Formation.

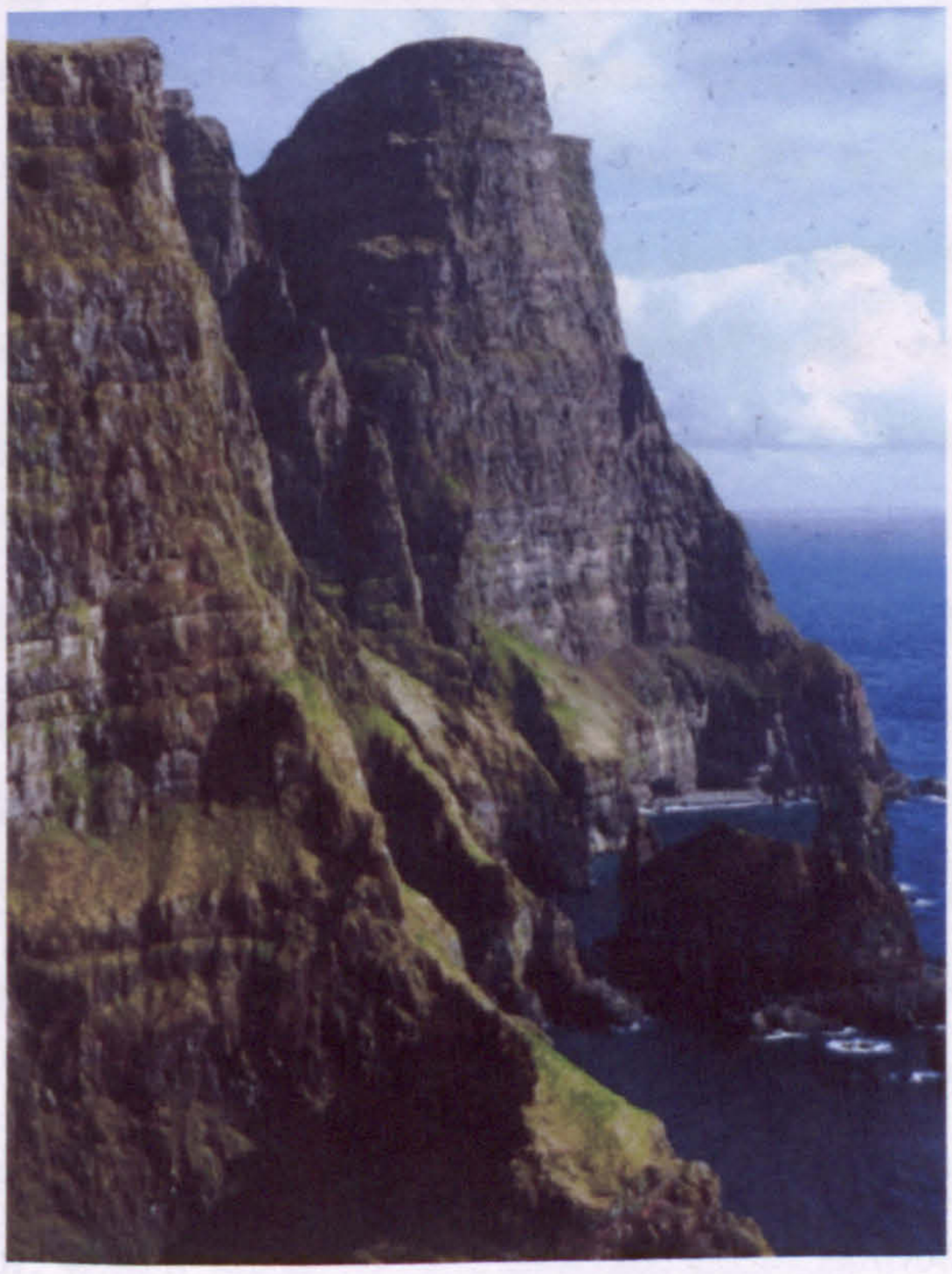

Fig. 3.8. Beinisvørð cliff section, *ca.* 3 km NW of Sumba, Suðuroy, Faeroe Islands. The cliff section consists of the stratigraphically lowest (and therefore oldest) lavas from the exposed sequence of the Lower Basalt Formation. The cliff section is *ca.* 469 m high and comprises *ca.* 19 tabular lava flows identified from their reddened flow tops. These data yield an average flow thickness of *ca.* 25 m. However, flows within this sequence range from *ca.* 10 m to *ca.* 70 m.

The formation of bole horizons can lead to the development of a soil profile upon lava flow tops. Reddened soil profiles have been recognized from the upper parts of the LBF (Parra *et al.* 1987). Argillisation, the replacement or alteration of feldspars to form clay minerals, of basalt lavas by meteoric fluids has given rise to the formation of either eutrophic (containing high levels of plant nutrients) or vertic (containing abundant swelling-clay) soil profiles, implying a warm temperate climate with alternating moist and dry seasons (Parra *et al.* 1987). The argillites analysed by Parra *et al.* (1987) still retain a high SiO_2 content, placing them in the kaolinitised basalt field and therefore still within the bole field rather than the extreme alteration laterite field (Schellmann 1986; Widdowson *et al.* 1997). To form a 1 to 2 m thick kaolinitic basalt i.e. a reddened bole, under humid temperate conditions would take 68,000-136,000 years (Nahon 1991).

3.2.5 Development of Prismatic and Columnar Jointing

Prismatic or poorly developed jointed lava flows are common throughout the 900 m of the exposed LBF (Fig. 3.9). Prismatic jointed lava flows are more prevalent in the lower sections of the LBF and particularly good examples are observed in the cliff section at Beinisvørð, Suðuroy (Fig. 3.8). At the base of prismatic lava flows, in the upper sections of the LBF, brecciation and pillow-like lobes are evident. This is quite clearly observed in the Hvalbiareiði Lava Flow (2nd flow from the top of the LBF), in Hvalbiareiði Bay, 1.5 km SW of Hvalba, Suðuroy (Fig. 3.10). Here, a *ca.* 15 m thick prismatic lava flow has breccia pockets and pillow-like lobes (pinch-and-swell structures) within *ca.* 1.0-1.5 m of the base. These structures are interpreted to be part of the lava flow because they have a sharp contact with the underlying unit and the breccia has a gradational contact with the lava flow. The pillow-like lobes are defined by having elliptical shapes, which form a pinch-and-swell structures along the base of the lava flow. The pinch-and-swell structures make the upper surface of the underlying sedimentary rock appear hummocky. The pillow-like lobes are suggestive of a wet substrate (cf. Campbell *et al.* 2001). The breccia pockets are commonly found located within the pinch/nip sections of the pinch-and-swell structures. The breccias consist of blocky, almost jigsaw fit, clasts of basalt, which are compositionally and texturally the same as the basalt from the overlying lava flow. The breccias are matrix poor, which suggests that they are either autobreccias or hyaloclastites rather than peperites (cf. McPhie *et al.* 1993). As the breccias are found in conjunction with the pillow-like lobes it implies that the breccias formed from quenching in surface water rather than from autobrecciation (cf. McPhie *et al.* 1993); consequently they are recognised as hyaloclastites. The lava flow overlies and has a sharp contact with a *ca.* 1.5

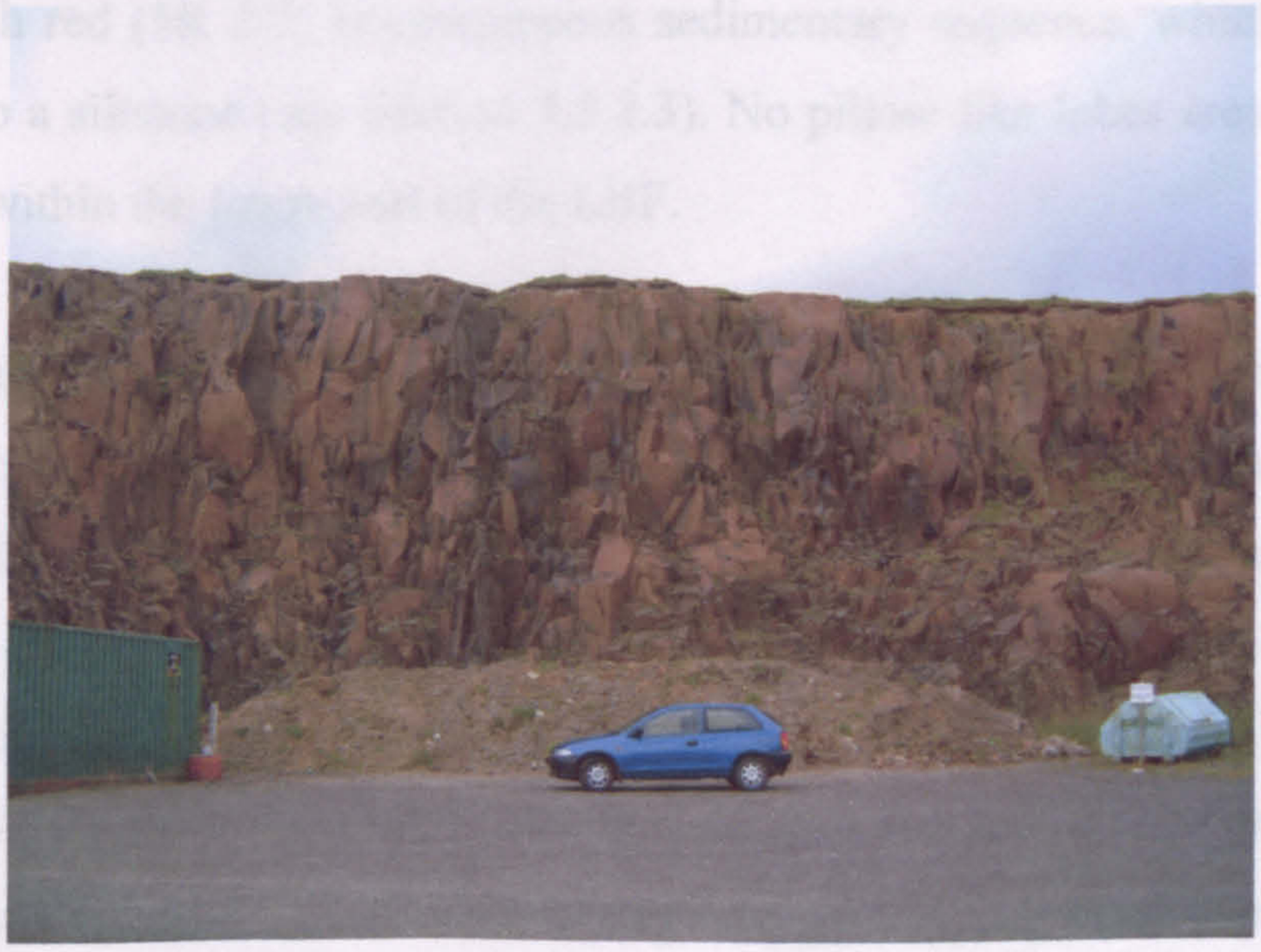

Fig. 3.9. Prismatically jointed lava flow in a disused quarry *ca.* 1 km SE of Tvøroyri, Suðuroy, Faeroe Islands. Prismatically jointed lavas are indicative of lava flows erupted into a dry environment. The lava flow is *ca.* 9 m thick.

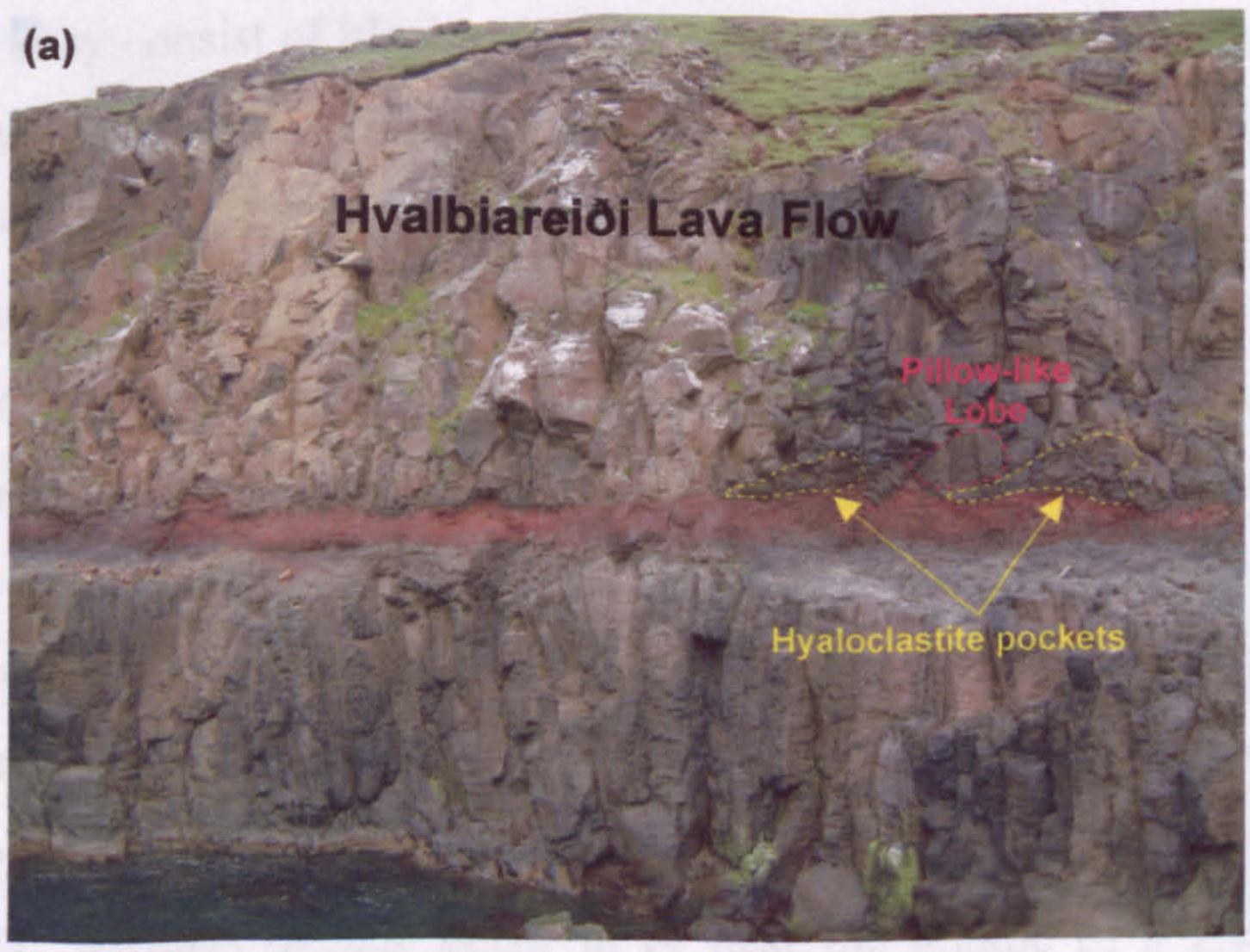

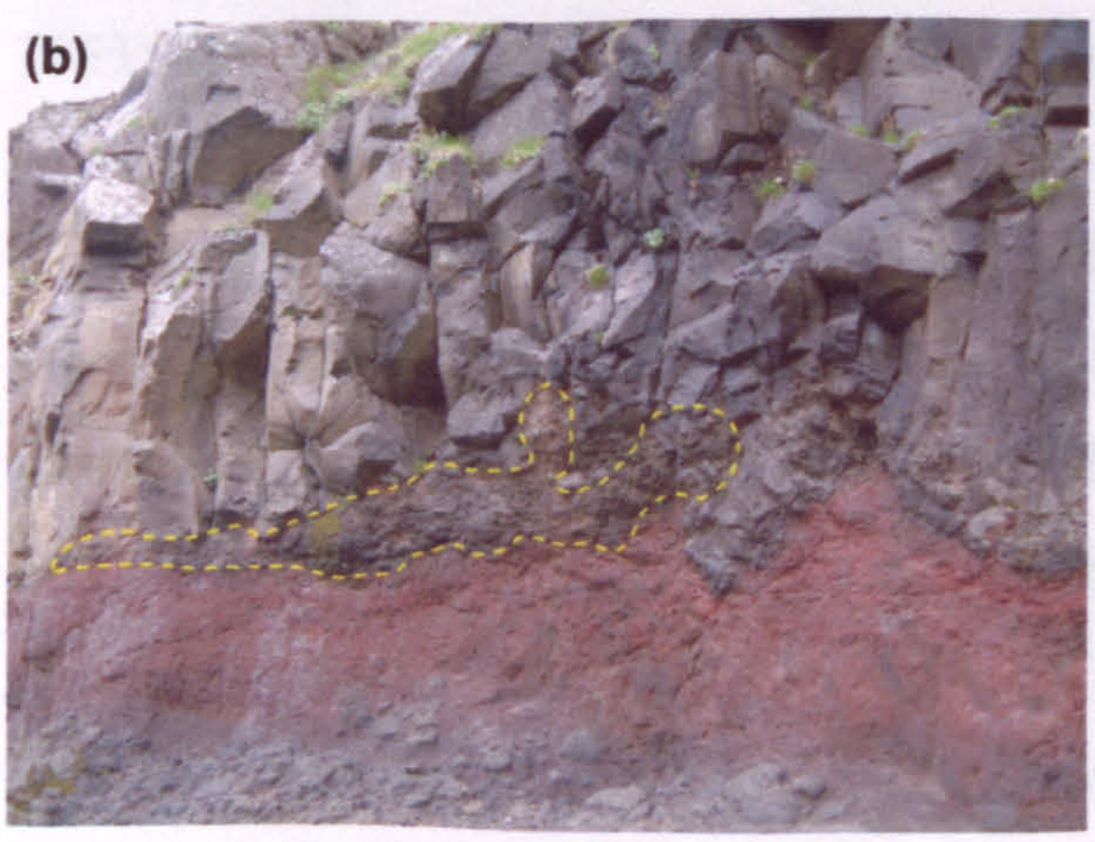

Fig. 3.10. Prismatically jointed Hvalbiareiði Lava Flow (2nd flow from the top of the LBF), in Hvalbiareiði Bay, 1.5 km SW of Hvalba, Suðuroy, Faeroe Islands. (a) The base of the lava flow exhibits pillow-like lobes and contains hyaloclastite pockets, both indicative of the lava flow advancing into standing water. Notice the hummocky boundary between the lava flow and the underlying sedimentary rock. The Hvalbiareiði Lava Flow is *ca.* 17 m thick. (b) The yellow dotted line delineates the left-handside hyaloclastite pocket in (a). (c) A yellow dotted line delineates the right-handside hyaloclastite pocket in (a). The pillow-like lobe is identified by its elliptical shape. Notice how both hyaloclastites are contained within the base of the lava flow. The compass is *ca.* 10 x 6 cm.

m thick blackish red (5R 2/2) heterogeneous sedimentary sequence, which ranges from a conglomerate to a siltstone (see Section 3.3.2.3). No pillow-like lobes are observed within the flow bases within the lower part of the LBF.

The Skarvatangi Lava Flow, *ca.* 1 km E of Froðba, Suðuroy, is prismatically jointed and has basal breccia pockets but no pillow-like lobes (Fig. 3.11). The flow extends from Skarvatangi point and is exposed for at least *ca.* 1 km along its length, inland. It is the 2nd lava flow from the top of the LBF and is the next lava flow above the columnar jointed Kúlugjógv Lava Flow (see below). The Skarvatangi Lava Flow is *ca.* 17 m thick and overlies a *ca.* 6-7 m thick volcanic fluviatile sedimentary sequence. The contact between the Skarvatangi Lava Flow and the underlying sedimentary sequence is planar and sharp rather than the hummocky contact observed beneath the Hvalbiareiði Lava Flow, which is at a similar stratigraphic position (Fig. 3.1). The breccia pockets range in size from 6 x 0.6 m to 14 x 6 m. They consist of blocky clasts of basalt from the overlying lava flow set in a matrix of volcaniclastic siltstone, presumably of the same composition as the underlying siltstone (see Section 3.3.2.2). Some of the blocky clasts have a jigsaw fit texture. The breccia appears to be a blocky peperite comparable to those described by Busby-Spera & White (1987) and Skilling *et al.* (2002), which suggests that the siltstone was locally 'wet' at the time of eruption of the lava flow. The width of the prisms within the lower 2-3 m of the Skarvatangi Lava Flow is on the order of *ca.* 60 cm, whereas in the remaining 14-15 m the width increases to *ca.* 2 m. The transition in size between the two sets of prisms is sharp and planar and therefore may represent a median parting, which is where the cooling surfaces that propagated from the top and bottom of the flow meet (Walker 1993). However, median partings usually occur in or near the middle of a lava flow (Walker 1993) but in the Skarvatangi Lava Flow the offset may represent uneven cooling rates.

The occurrence of multi-tiered flows is extremely rare within the LBF, but many of the common features associated with such flows are observed (see Section 2.1.2.3). There is, however, one lava flow that can quite clearly be divided into a colonnade and entablature. The multi-tiered lava flow is observed dipping to the ENE in a roadside section N of Hov, Suðuroy (Fig. 3.12). The base of the lava flow is not observed but the colonnade has a minimum thickness of *ca.* 8-10 m. The colonnade is composed of regular columns that have a uniform width of *ca.* 1.8 m. There is a sharp and planar contact between the colonnade and the overlying entablature. The maximum observed thickness of the entablature is *ca.* 8-10 m, but the top of the flow is not observed. The entablature consists of 20-30 cm wide curvi-columnar columns.

Fig. 3.11. Views of the Skarvatangi Lava Flow, *ca.* 1 km E of Froðba, Suðuroy, Faeroe Islands. (a) The Skarvatangi Lava Flow overlies and has a sharp planar contact with, a fluviatile sedimentary sequence. The fluviatile sedimentary sequence consists of a volcaniclastic conglomerate overlain by a volcaniclastic siltstone (VS). A blocky peperite is observed at the base of the lava flow. This has formed from the interaction between the hot lava and the water-saturated sediment. (b) The Skarvatangi Lava Flow exhibits what appears to be a median parting where there is a change in the width of individual columns. Below the median parting the columns have an average width of *ca.* 60 cm and above the median parting the columns have an average width of *ca.* 2 m. (c) A blocky peperite contained within the base of the lava flow. Notice the sharp contact between the underlying sedimentary rock and the blocky peperite, which suggests that the peperite is part of the lava flow. (d) A close up of the blocky peperite in (c). The peperite consists of angular clasts of basalt from the overlying lava flow set in a matrix of volcaniclastic siltstone, presumably of the same composition as the underlying siltstone. Some of the blocky clasts have a jigsaw fit texture. The red dotted line delineates the extent of the blocky peperite. The lack of peperite along the entire length of the lava flow suggests that the water was restricted to certain areas within the sediment. The hammer is *ca.* 40 cm long and the compass is *ca.* 10 x 6 cm.

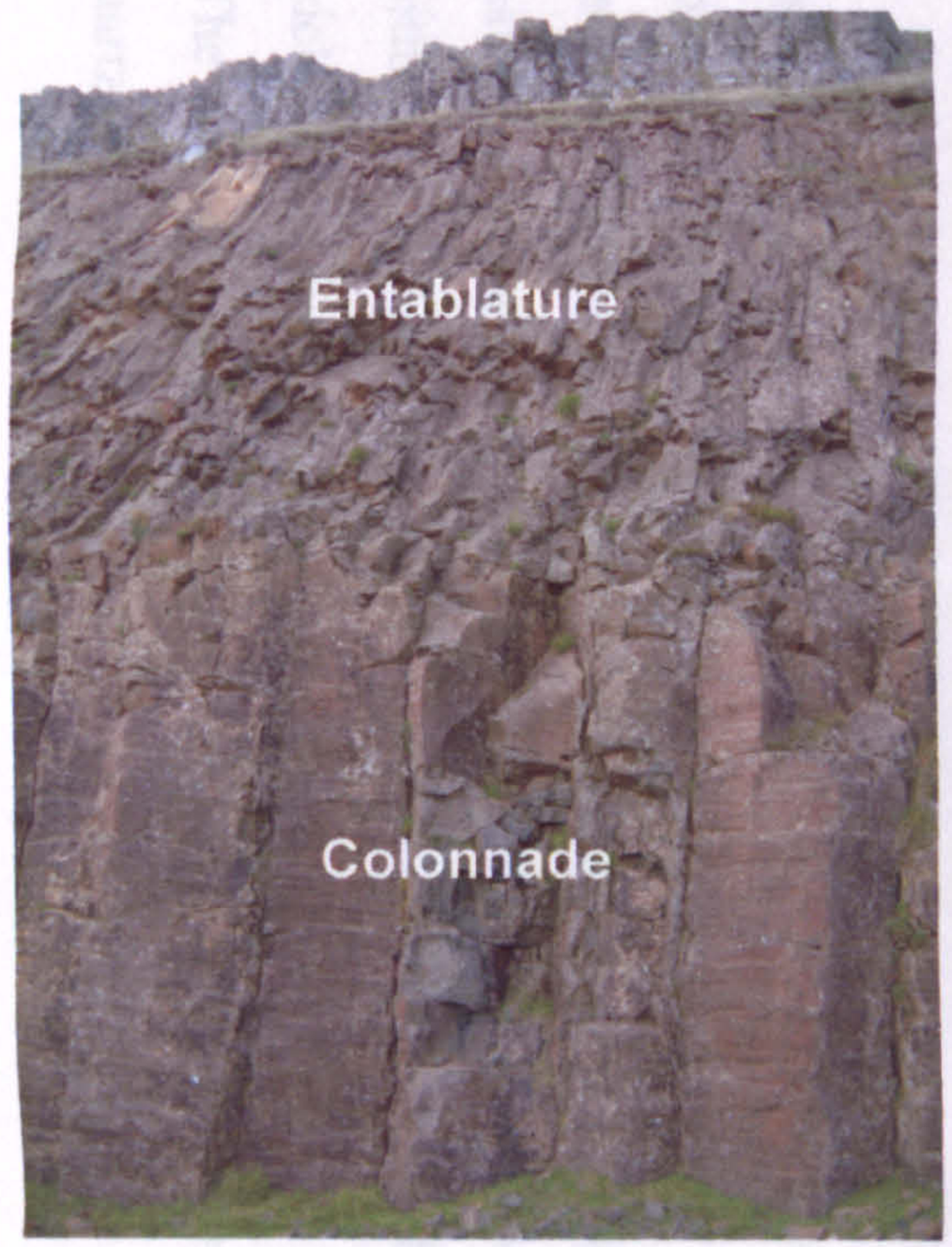

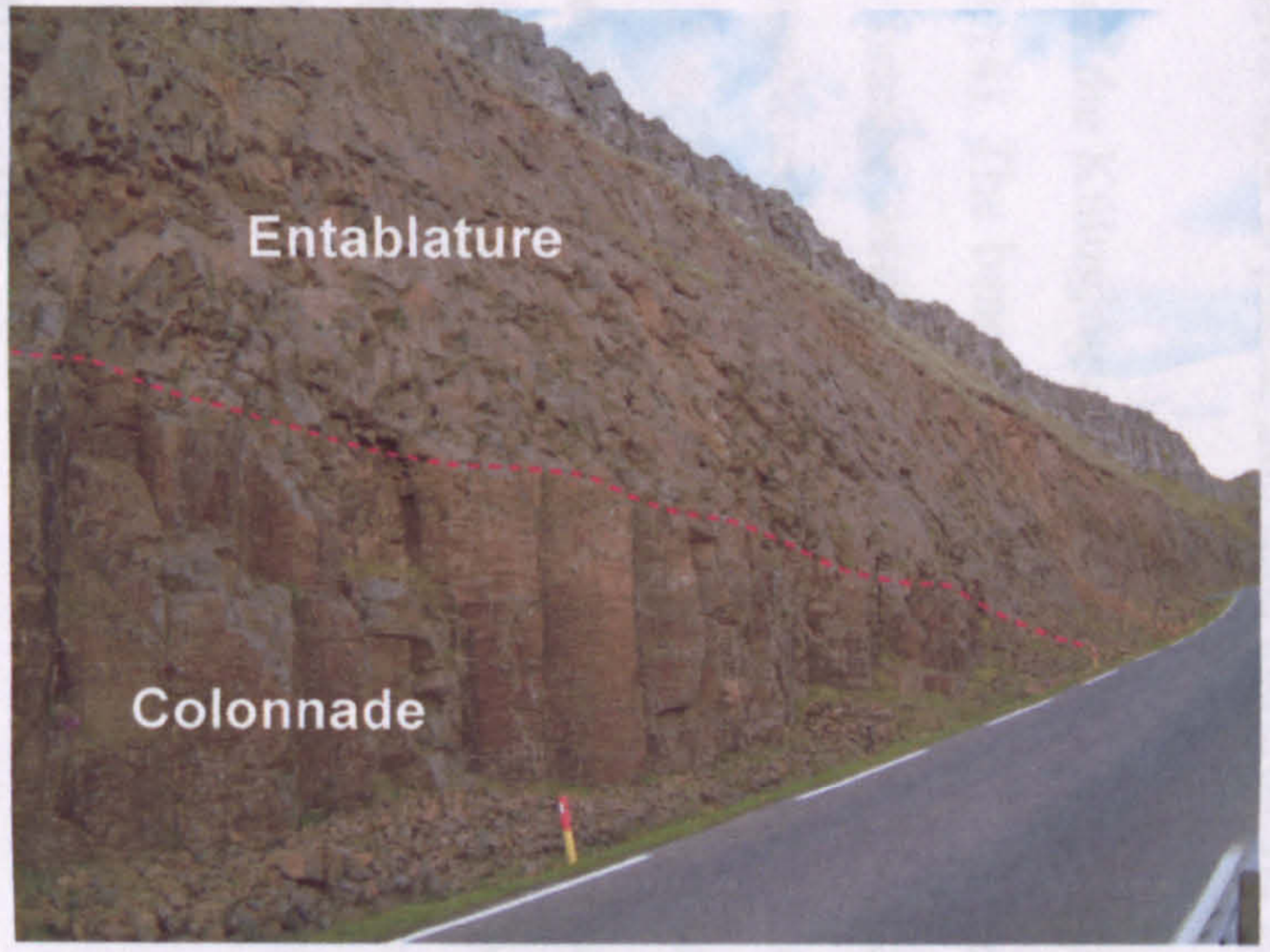

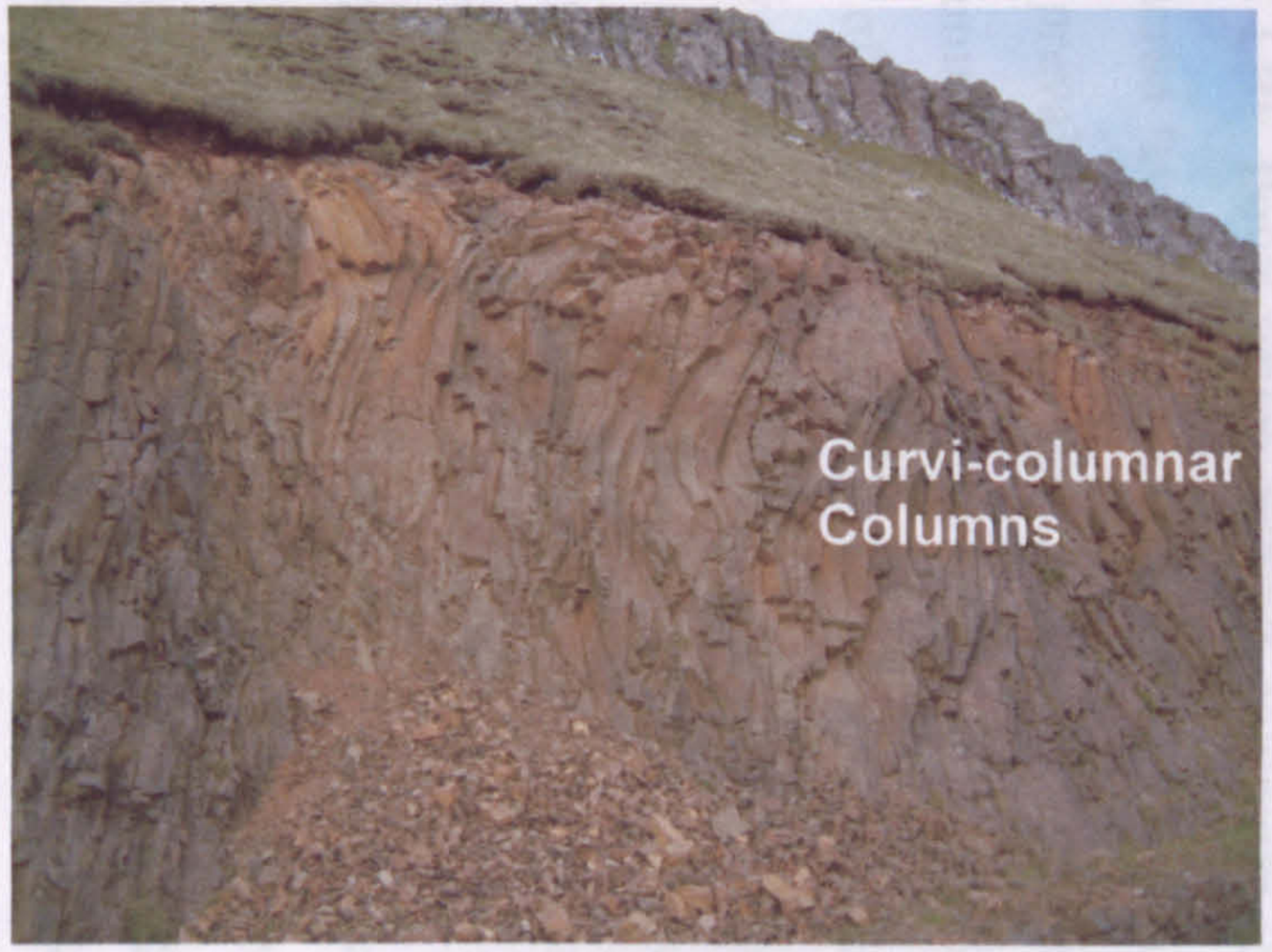

Fig. 3.12. Views of a multi-tiered lava flow dipping to the ENE in a roadside section N of Hov, Suðuroy, Faeroe Islands. The base of the lava flow is not observed but the colonnade has a minimum thickness of *ca.* 8-10 m. The colonnade is composed of regular columns that have a uniform width of *ca.* 1.8 m. There is a sharp and planar contact between the colonnade and the overlying entablature. The maximum observed thickness of the entablature is *ca.* 8-10 m, but the top of the flow is not observed. The entablature consists of 20-30 cm wide curvi-columnar columns.

The majority of the LBF flows which exhibit columnar jointing would belong to the colonnade of multi-tiered lava flows of Long & Wood (1986). The columnar jointed lava flows become more prevalent in the upper sections of the exposed 900 m thick LBF. A good example of columnar jointing is observed in the Kúlugjógv Lava Flow, which is the 3rd flow from the top of the LBF. The Kúlugjógv Lava Flow is exposed in a coastal section E of Froðba, Suðuroy and is exposed for *ca.* 700 m inland. The thickness of the flow varies along its length, but is on average *ca.* 20 m. In the coastal exposure, the Kúlugjógv Lava Flow displays superb fan-shaped columns (Fig. 3.13). The orientation of the fan-shaped columnar jointing can be used to recognise relief of *ca.* 20-30 m on the underlying land surface. The Kúlugjógv Lava Flow overlies a volcaniclastic breccia, composed of apparently unbedded clasts of vesiculated and non-vesiculated basalt, which has been differentially eroded and subsequently inundated by the Kúlugjógv Lava Flow. The base of the lava flow exhibits vesicles with *ca.* 1 cm diameters, as well as pillow-like lobes. The upper surface of the lava flow is planar and dips towards the ENE.

The inland exposure of the Kúlugjógv Lava Flow crops out alongside the main road 200 m SW of Hámar (Fig. 3.14). The base of the flow is not exposed at this locality. The tops of the pronounced rusty orange weathering columns have what appears to be a sharp contact with differentially weathered grey columns. The columns are very regular and have a uniform width of *ca.* 2 m. Individual columns exhibit horizontal markings, also referred to as chisel marks (James 1920), that alternate from smooth to rough portions over a distance of *ca.* 8-10 cm (Fig. 3.15). This alternation is considered to indicate the direction in which the column joint surface propagated (DeGraff & Aydin 1987). These chisel structures represent a cycle of stress build-up and stress-release, which also produce the fractures that define the columns (Ryan & Sammis 1978).

3.2.6 Internal Structure

The lava flows are massive, with a very uniform and disperse vesicular pattern except for the densely populated vesicular and rubbly flow top. The vesicular and rubbly flow tops are generally several metres in thickness (Rasmussen & Noe-Nygaard 1970b; Waagstein 1988). Pipe vesicles are rare or absent from the base of the lava flows. There is also a lack of vesicles within the lower and middle sections of the lava flows from the LBF. Horizontal vesicle sheets and vertical vesicle cylinders are similarly lacking from the LBF lava flows. The vesicles are commonly infilled with secondary minerals, such as chalcedony, quartz and calcite.

West

East

Fig. 3.13. Views of the fan-shaped columns within the Kúlugjógv Lava Flow, *ca.* 700 m east of Froðba, Suðuroy, Faeroe Islands. The orientation of the fan-shaped columnar jointing can be used to recognise relief of *ca.* 20-30 m on the underlying land surface. The Kúlugjógv Lava Flow overlies a volcaniclastic breccia (VB), composed of apparently unbedded clasts of vesiculated and non-vesiculated basalt, which has been differentially eroded and subsequently inundated by the Kúlugjógv Lava Flow. The base of the lava flow exhibits vesicles with an *ca.* 1 cm diameter, as well as pillow-like lobes. The upper surface of the lava flow is planar and dips towards the ENE.

Fig. 3.14. View of the colonnade tier of the Kúlugjógv Lava Flow, *ca.* 200 m SW of Hámar, Suðuroy, Faeroe Islands. The base of the flow is not exposed at this locality. The tops of the pronounced rusty orange weathering columns have what appears to be a sharp contact with differentially weathered grey columns. The columns are very regular and have a uniform width of *ca.* 2 m.

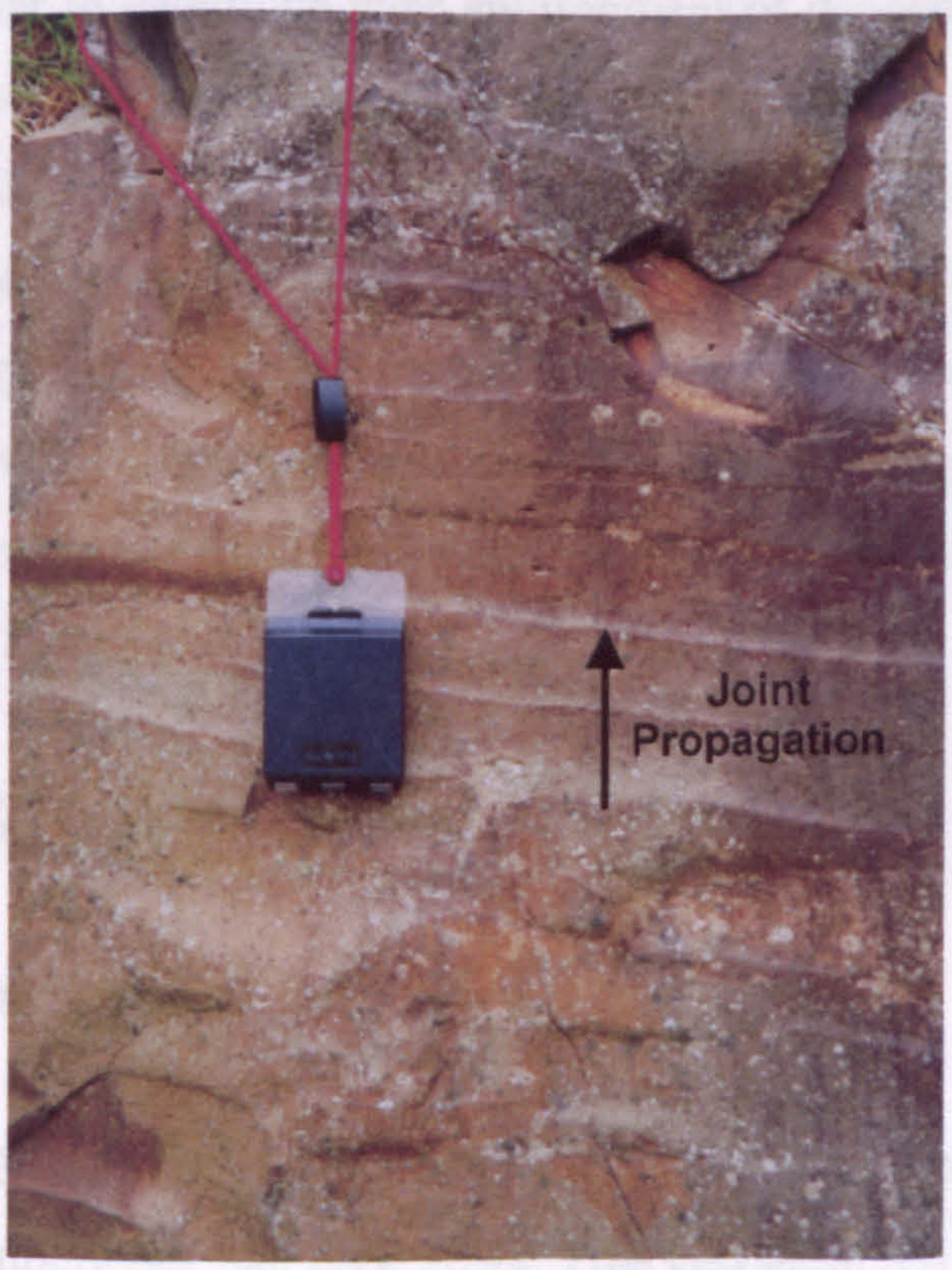

Fig. 3.15. View of the chisel structures on a column from the Kúlugjógv Lava Flow, *ca.* 200 m SW of Hámar, Suðuroy, Faeroe Islands. The chisel markings alternate from smooth to rough portions over a distance of *ca.* 8-10 cm. This alternation is considered to indicate the direction in which the column joint surface propagated. These chisel structures represent a cycle of stress build-up and stress-release, which also produce the fractures that define the columns. The compass is *ca.* 10 x 6 cm.

3.3 Interlava Lithologies

3.3.1 Occurrence

Individual lava flows within the LBF are most easily distinguished by the presence of tuffaceous (sometimes) reddened sedimentary rocks and palaeosols with which they are interbedded. These deposits are often laterally continuous (>5 km) and are typically 2-4 m thick, although sequences up to 10 m do occur. Parra *et al.* (1987) noted that the palaeosols in the Hov, Øravik and Nes profiles have a limited lateral extent of only a few metres. Interlava lithologies become more prevalent and represent 15% of the rocks in the upper sections of the LBF (Hald & Waagstein 1984). Interlava sedimentary units within the LBF cover a range of lithologies, from lutites (claystones, argillites (weakly metamorphosed claystones)), through arenites, rudites (volcaniclastic breccias and conglomerates), and coals (Rasmussen & Noe-Nygaard 1970b). Rasmussen & Noe-Nygaard (1970b) recorded thirteen localities with small amounts of coal.

New interlava units from the upper part of the LBF were studied in the field and petrographically in order to determine their environment of deposition and provenance. A tuffaceous claystone was studied from inbetween two lava flows that crops out along a roadside cutting, *ca.* 500 m E of the southern entrance to the tunnel at Liðarhagi, Suðuroy. A sedimentary sequence was investigated E of Froðba, Suðuroy which consists of two intercalated sedimentary units separated by the Kúlugjógv Lava Flow and overlain by the Skarvatangi Lava Flow. A sedimentary unit of a similar stratigraphic position to the previous locality was examined from underneath the Hvalbiareiði Lava Flow, Hvalbiareiði, 1.5 km SW of Hvalba, Suðuroy.

3.3.2 Lithology & Petrography

3.3.2.1 Liðarhagi Section

At Liðarhagi, a *ca.* 1.2 m thick greyish red (5R 4/2) to blackish red (5R 2/2) tuffaceous claystone is observed inbetween two lava flows. This claystone has sharp upper and lower contacts with the overlying and underlying lava flows. It has been brecciated into angular pebbles averaging *ca.* 1 cm across that form a jigsaw fit texture, cemented together by calcite. The brecciation has most likely formed as a result of compaction from the load of the overlying lava flow(s) and not from an interaction between the claystone and the overlying flow. This is supported by the sharp contact observed between the claystone and

the overlying lava flow. The claystone has a faint, thickly laminated appearance and in thin section, it is generally too fine-grained and too opaque to recognise any identifiable components. The only identifiable grains are rare (<1 vol.%), extremely small (<0.2 mm), rounded, orange grains, which are near isotropic; these are palagonitised basaltic glass (Fig. 3.16). This tuffaceous claystone is most likely an argillite analogous to those described by Parra *et al.* (1987).

3.3.2.2 Kúlugjógv Section

An idealised stratigraphic log through the Kúlugjógv sedimentary sequence can be seen in Figure 3.17. A poorly sorted volcaniclastic breccia is in a steep angular contact relationship with the underlying fan-shaped section of the Kúlugjógv Lava Flow and juxtaposed against a basaltic sill, which makes it impossible to determine the breccia's true geometry. The volcaniclastic breccia is *ca.* 10 m thick and consists of sub-angular clasts of vesicular and non-vesicular basalt, which have a maximum size of *ca.* 10 cm (Fig. 3.18). The breccia is predominantly grey, poorly sorted, and matrix supported. However, the upper *ca.* 30 cm of the breccia is red and shaly in texture and contains rare clasts of basalt. The unit has sub-parallel hydrothermal veins running down through it from the overlying lava flow. Overlying the breccia is the *ca.* 20 m thick Kúlugjógv Lava Flow, which is in turn overlain by a sedimentary sequence *ca.* 6-7 m thick.

This sedimentary sequence infills the rubbly flow top of the Kúlugjógv Lava Flow. Two distinct units are evident within the sedimentary sequence (Fig. 3.11a & c). The basal unit is a poorly sorted volcaniclastic conglomerate *ca.* 4-5 m thick (Figs. 3.19 & 3.20), which contains various basalt clasts that show a range in the degree of weathering they have undergone. Approximately 5 vol.% of the large basalt clasts are amygdaloidal in nature. The clasts are predominantly well rounded and have low to high sphericities and long axes of the low sphericity clasts are aligned parallel to bedding (Fig. 3.19f). This tentative palaeoflow indicator suggests that transport was either to the ESE or the WNW. The largest low sphericity clast observed is *ca.* 12 x 4.5 cm. The unit contains small angular light olive (10Y 5/4) clasts, which in thin section contain deformed amygdales; these clasts are interpreted here as chloritised basalts (Figs. 3.19e & 3.20e,f). There are *ca.* 1-2 vol.% reddened bole clasts (Figs. 3.19b); the largest observed is *ca.* 60 x 20 cm, which contains pre-existing fragments of basalt. There are also 1-2 vol.% of clasts of brownish mudstone (Fig. 3.19c). The remainder of the unit consists of a very dusty red (10R 2/2) matrix, which in thin section contains *ca.* 1 vol.% palagonitised orange basaltic glassy material <1 mm in size. The upper surface has a sharp contact and is overlain by a very dusky red (10R 2/2) to

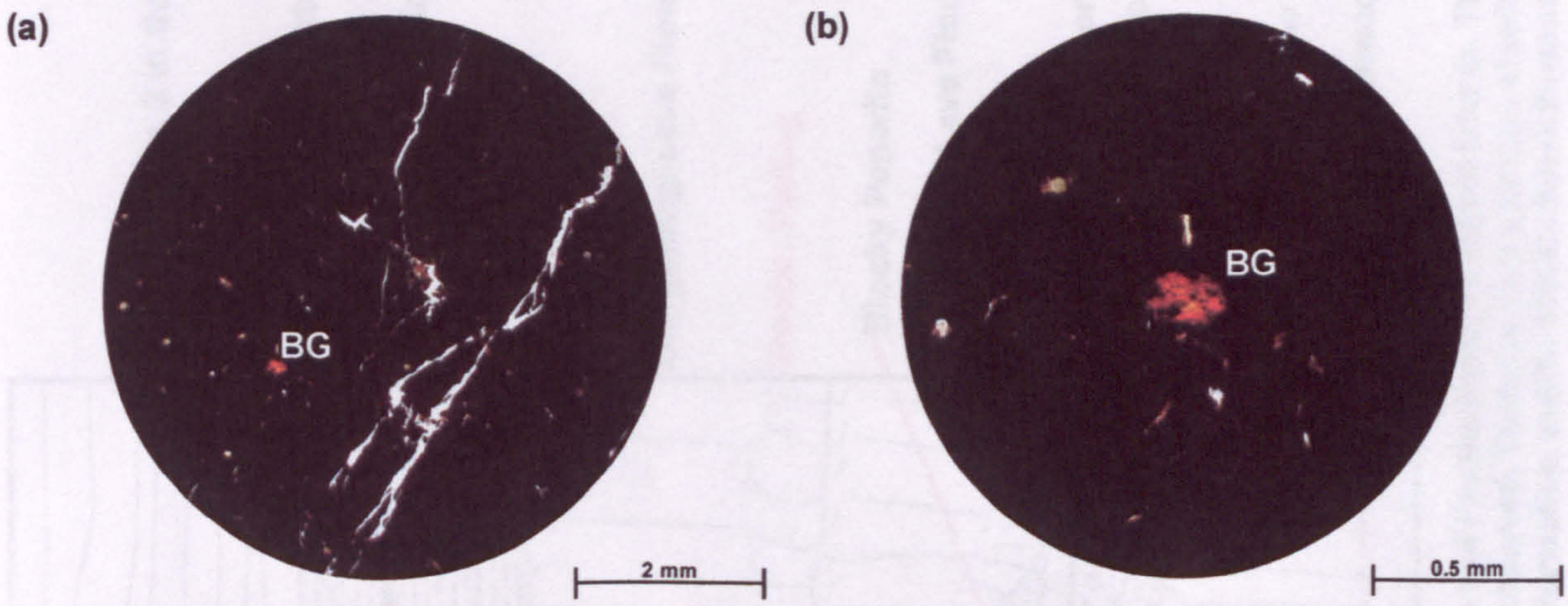

Fig. 3.16. Photomicrographs of a volcaniclastic claystone that crops out inbetween two lava flows, *ca.* 500 m E of the southern entrance to the tunnel at Liðarhagi, Suðuroy, Faeroe Islands. Both photomicrographs are under plane-polarised light. (a) & (b) The claystone is generally too fine-grained and too opaque to recognise any identifiable components. The only identifiable grains are rare (<1 vol.%), extremely small (<0.2 mm), rounded, orange grains, which are near isotropic; these are palagonitised basaltic glass (BG).

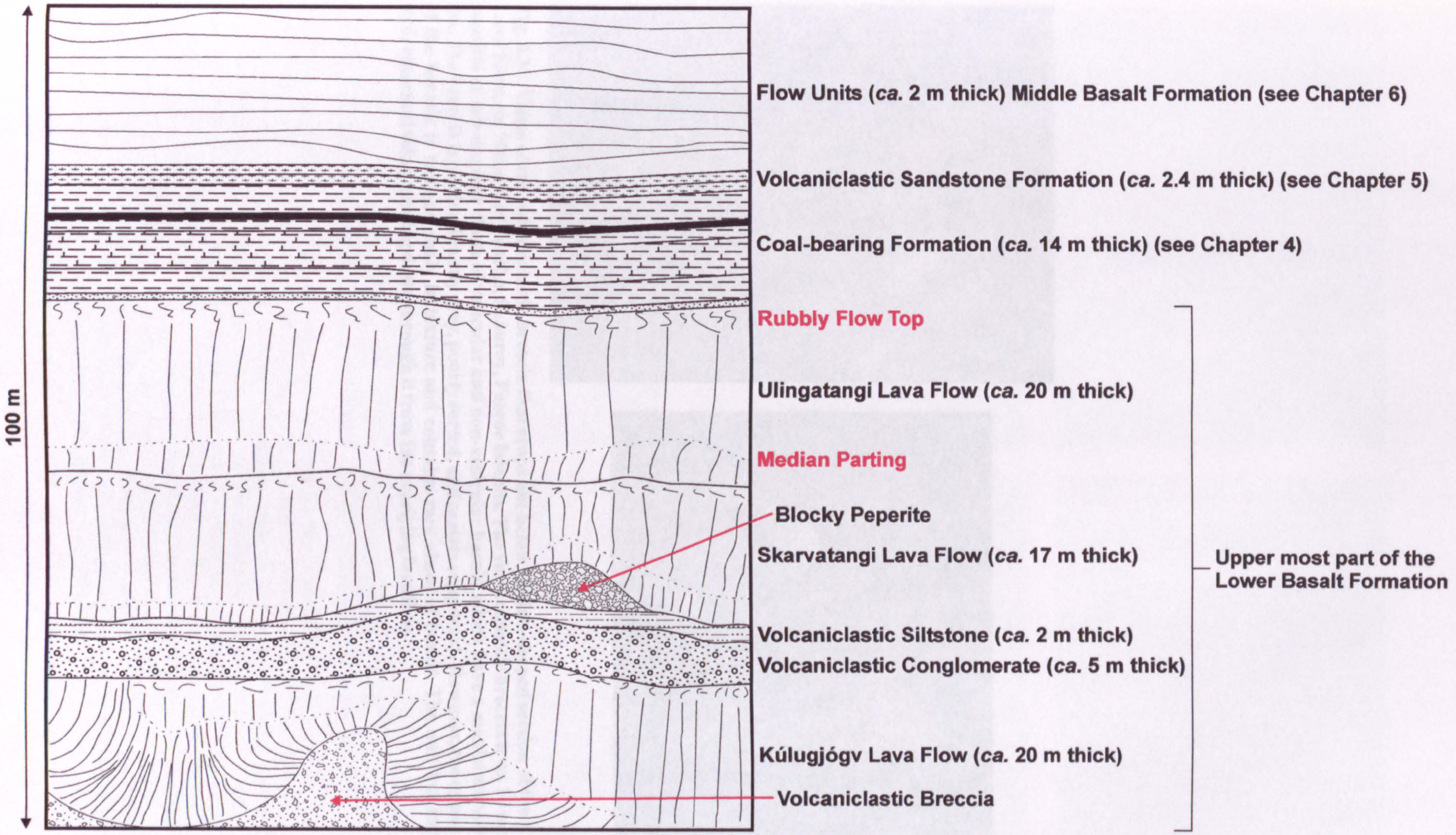

Fig. 3.17. Idealised stratigraphic log in the region of Kúlugjógv, *ca.* 1 km E of Froðba, Suðuroy, Faeroe Islands. The section comprises 3 tabular lava flows from the upper most part of the Lower Basalt Formation. The base of the section is not observed. The lavas have a number of sedimentary sequences interbedded within them. The lavas are overlain by the Coal-bearing Formation, Volcaniclastic Sandstone Formation, and the Middle Basalt Formation.

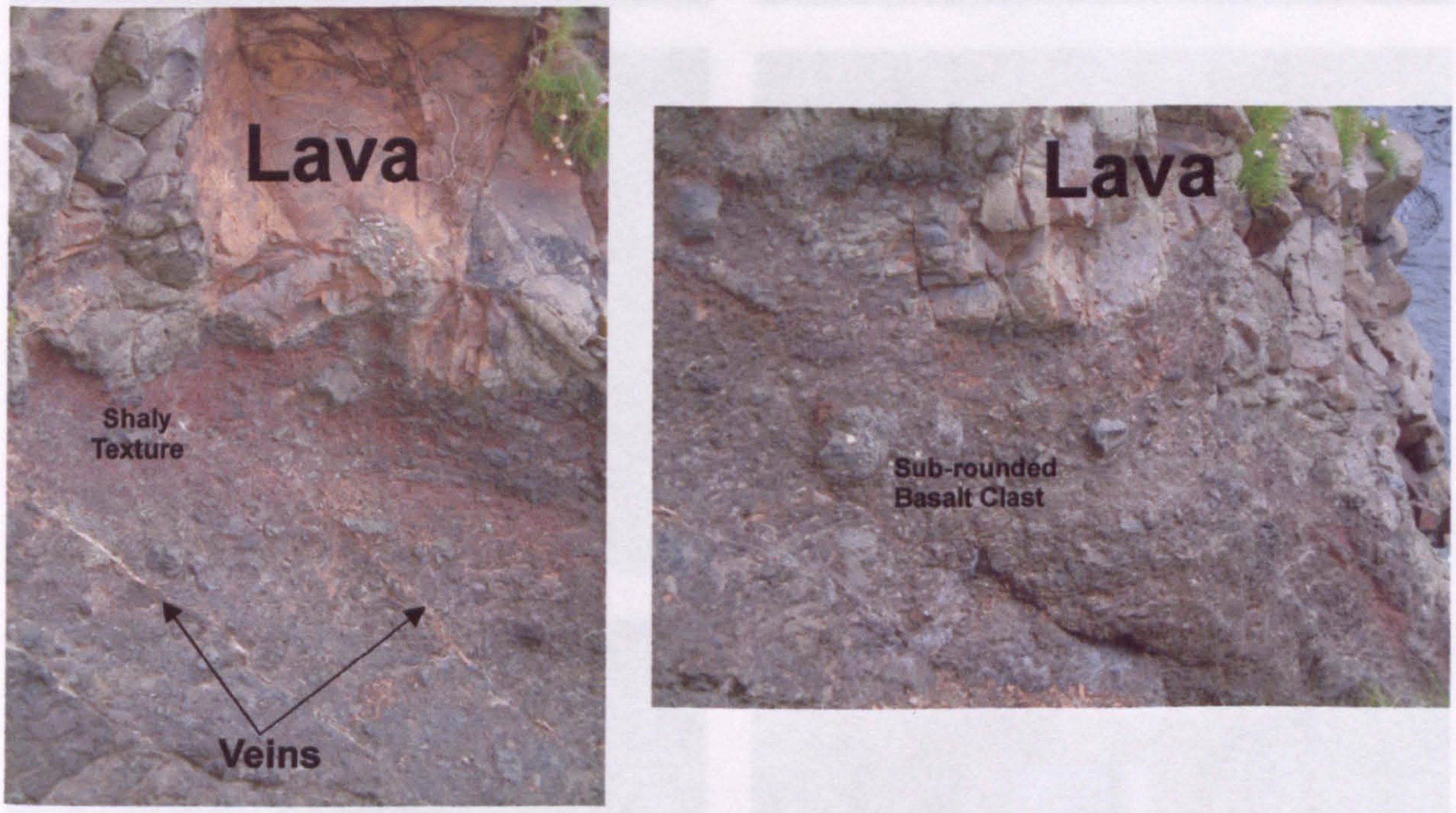

Fig. 3.18. Views of the volcaniclastic breccia that crops out below the fan-shaped section of the Kúlugjógv Lava Flow, *ca.* 700 m E of Froðba, Suðuroy, Faeroe Islands. The volcaniclastic breccia is *ca.* 10 m thick and consists of sub-angular clasts of vesicular and non-vesicular basalt, which have a maximum size of *ca.* 10 cm. The breccia is predominantly grey, poorly sorted, and matrix supported. However, the upper *ca.* 30 cm of the breccia is red and shaly in texture and contains rare clasts of basalt. The unit has sub-parallel hydrothermal veins running down through it from the overlying lava flow.

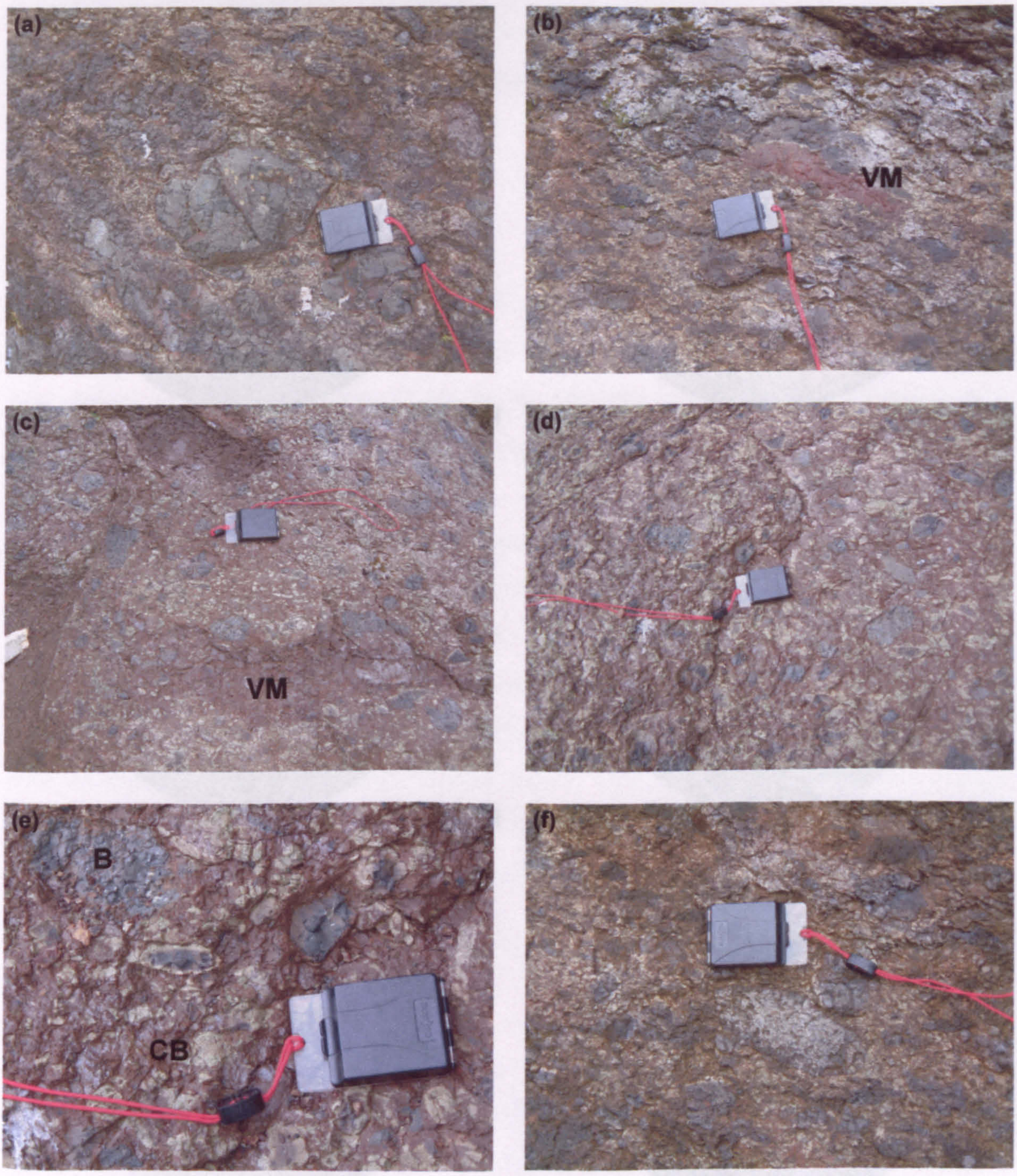

Fig. 3.19. Views of the volcaniclastic conglomerate from the fluviatile sedimentary sequence overlying the Kúlugjógv Lava Flow, *ca.* 1 km E of Froðba, Suðuroy, Faeroe Islands. (a) The conglomerate is poorly sorted and contains various clasts of basalt (B) which range in size and sphericity, here a large sub-rounded, high sphericity basalt clast is observed. (b) The conglomerate also contains rare (1-2 vol.%) mudstone/bole clasts (VM). (c) The basalt clasts show a range in the degree of weathering they have undergone. The yellowish clasts are chloritised basalts (CB). The photograph also illustrates a volcaniclastic mudstone clast. (d) A typical view of the conglomerate showing the range in the degree of weathering of the basalt clasts. (e) A close up of some of the basalt clasts. Some of the less altered basalt clasts exhibit rims of altered chloritised basalt. The clasts are set in a volcaniclastic mud to sand grade matrix. (f) A low sphericity basalt clast that is well rounded and aligned to the planar upper surface, suggesting flow in a water-borne environment. The compass is *ca.* 10 x 6 cm.

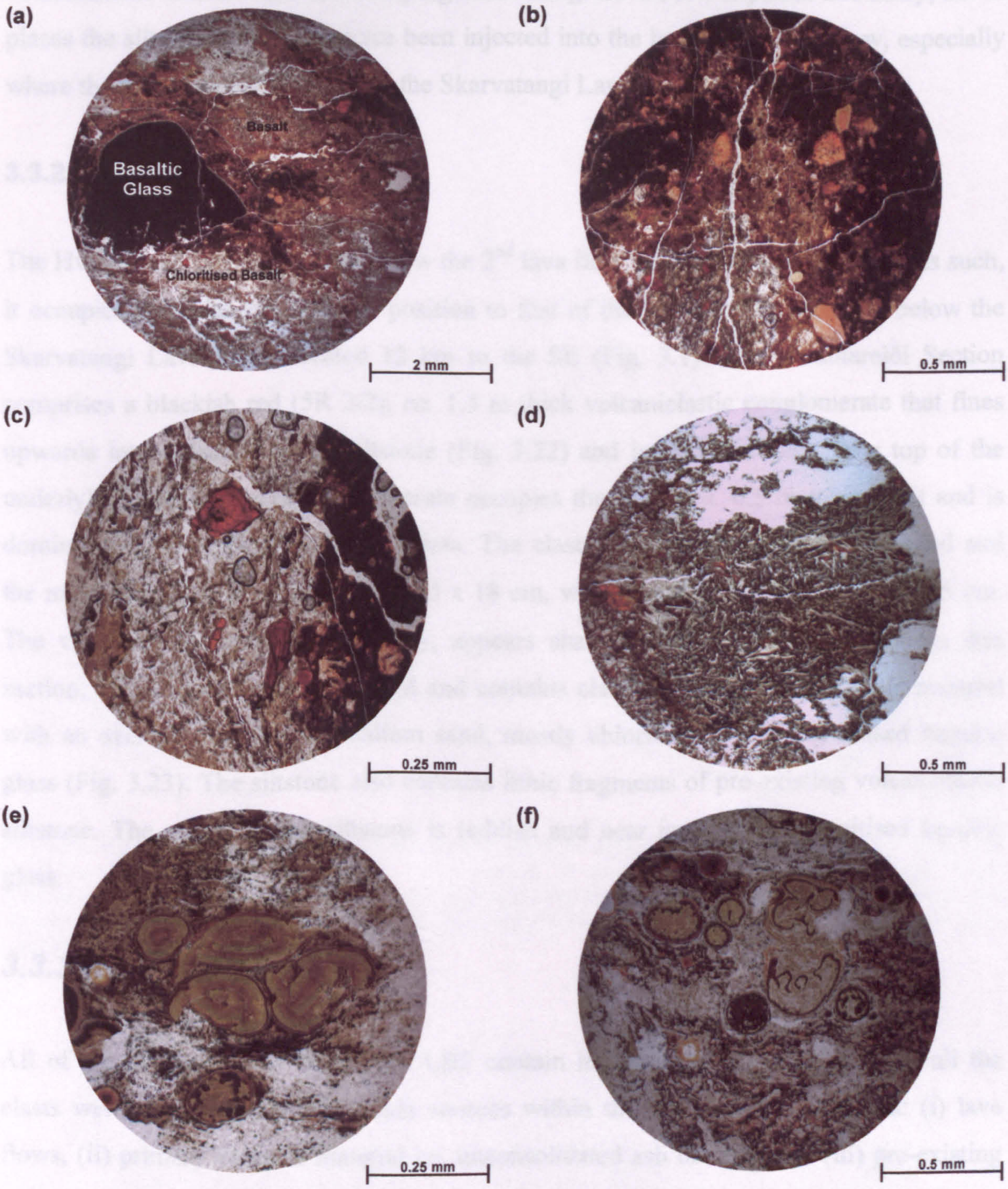

Fig. 3.20. Photomicrographs of the volcaniclastic conglomerate from the fluviatile sedimentary sequence overlying the Kúlugjógv Lava Flow, *ca.* 1 km E of Froðba, Suðuroy, Faeroe Islands. All of the photomicrographs are under plane-polarised light. (a) Clasts of basaltic glass, basalt and chloritised basalt within a matrix of volcaniclastic mudstone containing grains of orange palagonitised basaltic glass. (b) Volcaniclastic mudstone matrix containing grains of orange, transparent palagonitised basaltic glass. (c) Palagonitised basaltic glass within altered volcaniclastic mudstone matrix. (d) Angular equigranular basalt clast. (e) & (f) Fractured amygdales within altered chloritised basalt.

a greyish brown (5YR 3/2) volcaniclastic siltstone devoid of any significant clasts apart from some fine sand grade basaltic material (Fig. 3.21). The volcaniclastic siltstone is thickly laminated to very thinly bedded over its 2 m thickness. The contact between the volcaniclastic siltstone and the overlying Skarvatangi Lava Flow is planar and sharp, but in places the siltstone appears to have been injected into the base of the lava flow, especially where the blocky peperites occur in the Skarvatangi Lava Flow (see Section 3.2.5).

3.3.2.3 Hvalbiareiði Section

The Hvalbiareiði Section occurs below the 2nd lava flow from the top of the LBF. As such, it occupies a similar stratigraphic position to that of the sedimentary sequence below the Skarvatangi Lava Flow, located 12 km to the SE (Fig. 3.1). The Hvalbiareiði Section comprises a blackish red (5R 2/2), *ca.* 1.5 m thick volcaniclastic conglomerate that fines upwards into a volcaniclastic siltstone (Fig. 3.22) and infills the rubbly flow top of the underlying lava flow. The conglomerate occupies the lower *ca.* 0.5 m of the unit and is dominated by amygdaloidal basalt clasts. The clasts are predominantly sub-rounded and the maximum clast size observed is 30 x 18 cm, with an average size is *ca.* 20 x 15 cm. The volcaniclastic siltstone is blocky, appears shaly, and is thickly laminated. In thin section, the siltstone is poorly sorted and contains clasts of sub-rounded opaque material with an average size fine to medium sand, mostly chloritised and palagonitised basaltic glass (Fig. 3.23). The siltstone also contains lithic fragments of pre-existing volcaniclastic siltstone. The matrix to the siltstone is reddish and near isotropic palagonitised basaltic glass.

3.3.3 Provenance

All of the interlava units within the LBF contain intraformational clasts, that is, all the clasts were derived from three main sources within the LBF depositional area: (i) lava flows, (ii) primary volcanic material i.e. unconsolidated ash or tuffs, and (iii) pre-existing sedimentary units and palaeosols. The phenoclasts in many of the sedimentary rocks are dominated by fragments eroded from lava flows, although the range in composition and varying degrees of weathering of the phenoclasts suggests that the fragments were eroded from different lava flows at different stages in their weathering history. The fine-grained matrices to the majority of the sedimentary rocks consist of material eroded from primary pyroclastic and epiclastic sedimentary rocks made up of tuffaceous material.

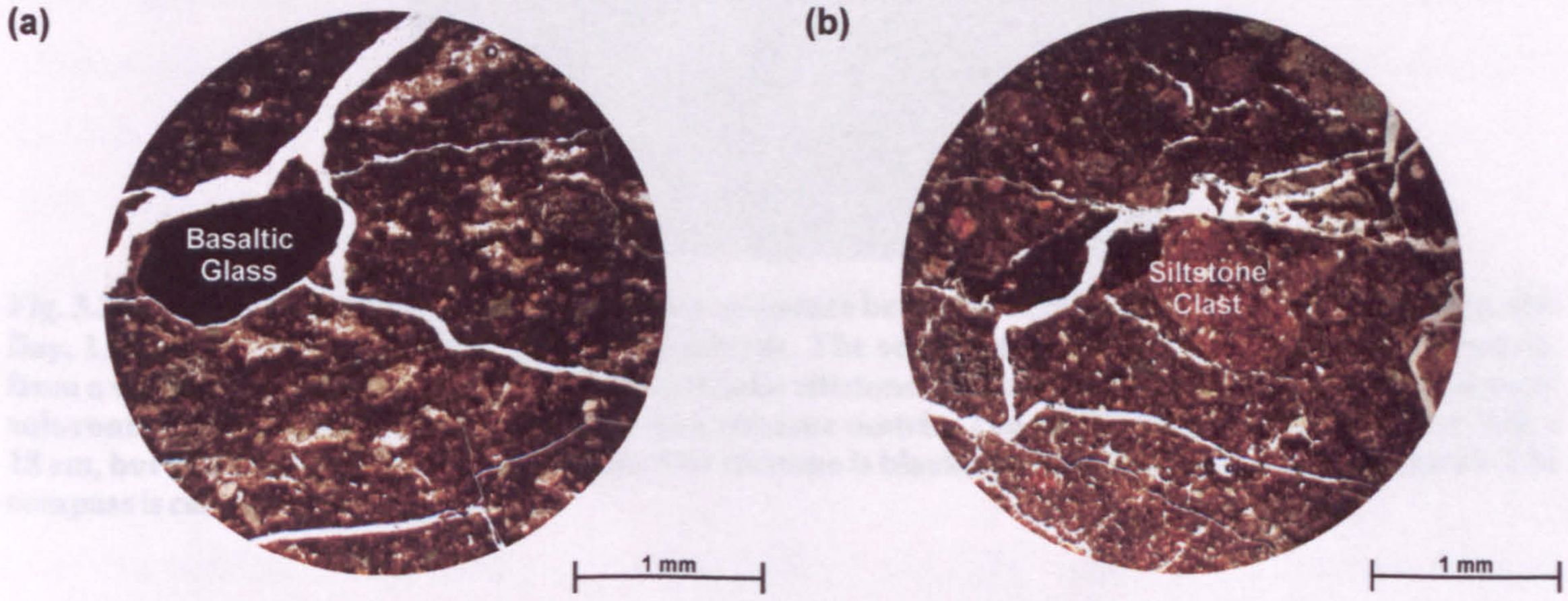

Fig. 3.21. Photomicrographs of the volcaniclastic siltstone from the fluviatile sedimentary sequence overlying the Kúlugjógv Lava Flow, *ca.* 1 km E of Froðba, Suðuroy, Faeroe Islands. Both photomicrographs are under plane-polarised light and contain rare, rounded sand grade clasts set in the siltstone matrix. (a) A well rounded clast of palagonitised basaltic glass. (b) Palagonitised basaltic glass and siltstone clasts.

Fig. 3.22. View of the volcaniclastic sedimentary sequence below the Hvalbiareiði Lava Flow, Hvalbiareiði Bay, 1.5 km SW of Hvalba, Suðuroy, Faeroe Islands. The sequence is *ca.* 1.5 m thick and fines upwards from a volcaniclastic conglomerate to a volcaniclastic siltstone. The conglomerate predominantly contains sub-rounded amygdaloidal basalt clasts set in a siltstone matrix. The maximum clast size observed is 30 x 18 cm, but the average size is *ca.* 20 x 15 cm. The siltstone is blackish red, shaly and thickly laminated. The compass is *ca.* 10 x 6 cm.

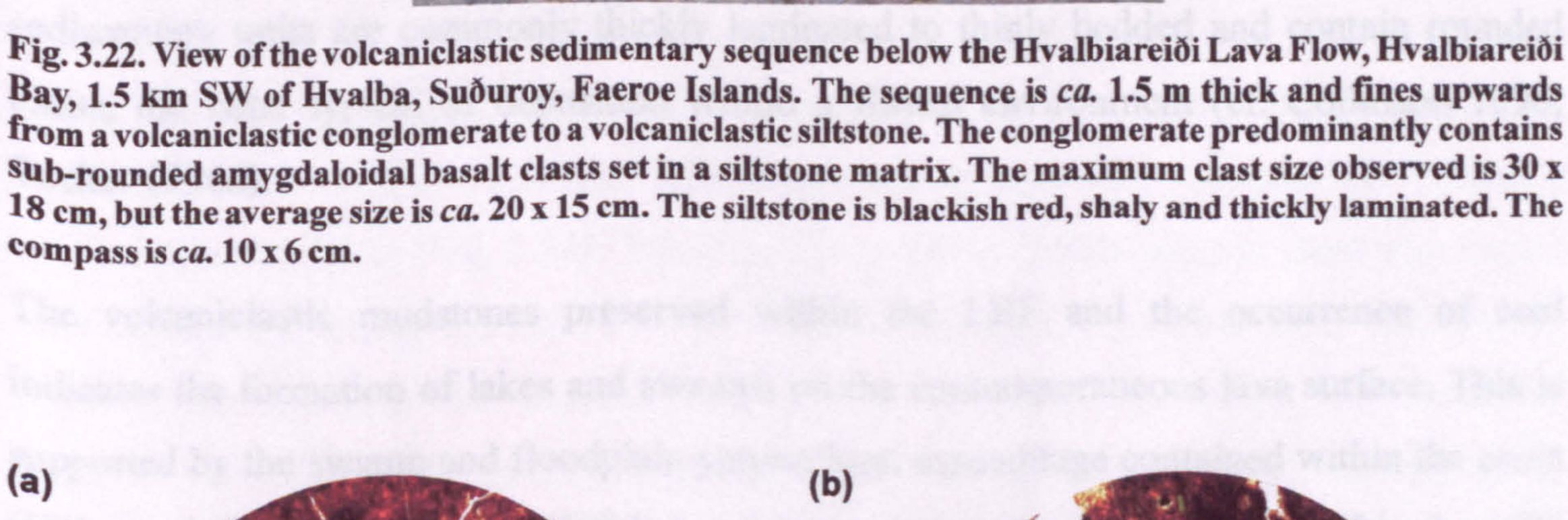

Fig. 3.23. Photomicrographs, under plane-polarised light, of the volcaniclastic siltstone from the volcaniclastic sedimentary sequence below the Hvalbiareiði Lava Flow, Hvalbiareiði Bay, 1.5 km SW of Hvalba, Suðuroy, Faeroe Islands. Both photomicrographs are under plane-polarised light. (a) & (b) The siltstone is dominated by reddish and near isotropic material, most probably palagonitised basaltic glass. The siltstone contains rounded sand grade clasts of least altered basaltic glass (BG) and chloritic glass (CG).

3.3.4 Environment of Deposition

The interlava lithologies preserved within the LBF were deposited in a terrestrial environment under warm and humid conditions and do not show any evidence for a marine influence. The occurrence of palaeosols within the LBF supports an alluvial setting (cf. Retallack 1981; 1988; 1997; 2001). The lack of pyroclastic textures (glass shards, welding, angular grains, etc.) within the interlava lithologies suggests that they formed by epiclastic processes (cf. Fisher & Schmincke 1984; Cas & Wright 1987; McPhie *et al.* 1993). Channel structures with reliefs of up to 20 m, e.g. E of Froðba, Suðuroy, suggests relatively high energy systems were achieved where there was an abundance of surface water sourced primarily from rainfall draining off elevated parts of the volcanic land surface (cf. Collinson 1996; Tucker 1996a). Units from the LBF display a range in clast types indicating a heterogeneous source, which is a common feature of epiclastic sandstones within a volcanic setting (Fisher & Schmincke 1984; Cas & Wright 1987; McPhie *et al.* 1993). The alignment of clasts in the Skarvatangi deposits suggests that the flow direction within the fluvial channel was either to the ESE or the WNW. The sedimentary units are commonly thickly laminated to thinly bedded and contain rounded clasts, the latter typical of deposition within a fluvial environment (cf. Collinson 1996; Tucker 1996a).

The volcaniclastic mudstones preserved within the LBF and the occurrence of coal indicates the formation of lakes and swamps on the contemporaneous lava surface. This is supported by the swamp and floodplain palynofloral assemblage contained within the coals (Ellis *et al.* 2002). Parra *et al.* (1987) have shown that many of the lutites within the LBF have formed from the argillisation of tuffaceous material in lacustrine environments and as a result of hydrothermal processes. The preservation of coal suggests that the surrounding land surface was heavily vegetated.

3.4 Location of Vents

The eruption sites for the LBF lavas are not observed on the Faeroe Islands, but are assumed to have taken the form of NW-SE trending fissures (Rasmussen & Noe-Nygaard 1970b). However, a possible vent from the LBF is identified at Stapin, Suðuroy and is more appropriately described in Section 5.3.1. The strong parallel trend of the inter-island fjords and the similar trending outcrop of the Volcaniclastic Sandstone Formation reinforce a NW-SE trending fissure model. Rasmussen & Noe-Nygaard (1970b) suggested that the

fissures were situated to the west of the Faeroe Islands. However, Waagstein (1988) suggested that the LBF was erupted locally because of the overlapping geochemical profiles (e.g. Y/Zr ratios) observed within the lavas (Hald & Waagstein 1984). As a result of these findings, Hald & Waagstein (1984) and Waagstein (1988) concluded that the LBF consisted of small flow groups that originated from a number of independent volcanic systems. Larsen *et al.* (1999) geochemically and stratigraphically correlated the LBF to the Nansen Fjord Formation, East Greenland. These data suggest that the two formations formed a pre-break-up succession above a thinning lithosphere in the NE Atlantic, with the subsequent line of opening to the west of the Faeroe Islands (Larsen *et al.* 1999). The drilling of a road tunnel between the islands of Vágar and Suðuroy in 2002 only encountered a small number of dykes rather than a eruption dyke swarm (B.R. Bell *pers. comm.*), suggesting that the Fjords do not contain the eruption sites for the LBF (cf. Swanson *et al.* 1975). Therefore, it seems most likely that the lava flows were erupted to the west of the Faeroe Islands as Larsen *et al.* (1999) postulated.

3.5 Synthesis

The lavas and intercalated sedimentary accumulations of the Lower Basalt Formation (LBF) preserve evidence consistent with eruption and deposition, respectively, within a terrestrial environment (Fig. 3.24). The lavas are typically rubbly-topped, sheet-like bodies with significant lateral extents (>9 km) and no features associated with subaqueous eruption, for example the development of pillows or the formation of substantial hyaloclastite breccias (Fisher & Schmincke 1984; Cas & Wright 1987; McPhie *et al.* 1993), have been observed. However, volcaniclastic rocks have been recovered from a depth of 2,550 to 3,565 m from the Lopra-1 & 1A wells (Ellis *et al.* 2002), possibly representing a hyaloclastite sequence. The laterally extensive tabular-classic facies architecture observed throughout the LBF is typical of large volume eruptions common within Continental Flood Basalt (CFB) provinces (Cas & Wright 1987; Walker 1993; Jerram 2002).

The LBF lava flows have characteristics consistent with having been emplaced rapidly as a'a flows rather than inflated pahoehoe flows (cf. Shaw & Swanson 1970a; b; Rowland & Walker 1990; Reidel & Tolan 1992; Hon *et al.* 1994; Self *et al.* 1996; Cashman & Kauahikaua 1997; Self *et al.* 1997; Keszthelyi & Self 1998; Reidel 1998; Self *et al.* 1998; Thordarson & Self 1998). The vesicle distribution patterns within the LBF lava flows are characterised by vesicle-rich upper crusts and vesicle-poor cores and basal crusts,

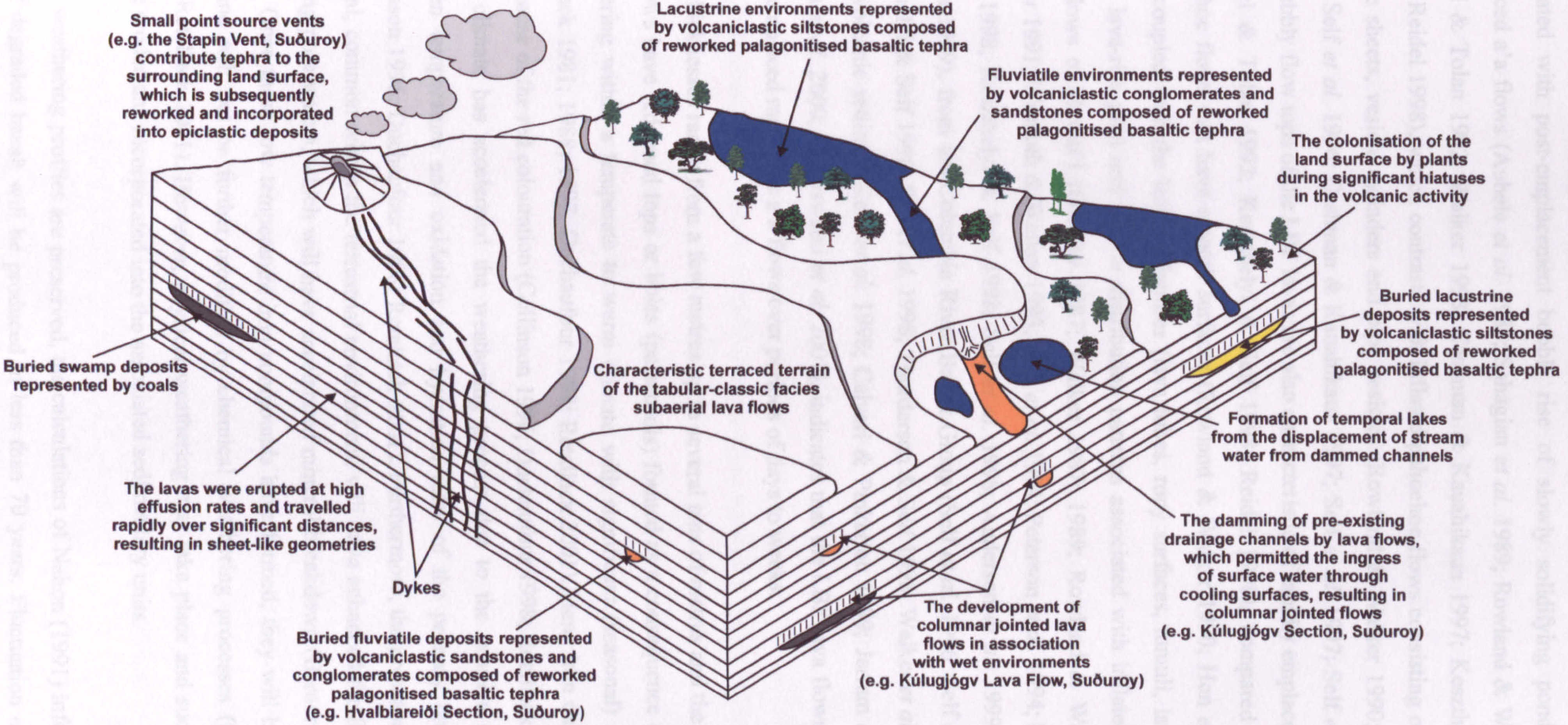

Fig. 3.24. Schematic palaeogeographical block diagram for the Lower Basalt Formation with the main elements highlighted. Length of each horizontal dimension of the figure is very approximately 1-2 km.

associated with post-emplacement bubble rise of slowly solidifying ponded, rapidly emplaced a'a flows (Aubele *et al.* 1988; Sahagian *et al.* 1989; Rowland & Walker 1990; Reidel & Tolan 1992; Walker 1993; Cashman & Kauahikaua 1997; Keszthelyi & Self 1998; Reidel 1998), which contrasts with inflated pahoehoe flows consisting of horizontal vesicle sheets, vesicle cylinders and pipe vesicles (Rowland & Walker 1990; Hon *et al.* 1994; Self *et al.* 1996; Cashman & Kauahikaua 1997; Self *et al.* 1997; Self *et al.* 1998). The rubbly flow tops of the LBF lavas are also characteristic of rapidly emplaced a'a flows (Reidel & Tolan 1992; Keszthelyi & Self 1998; Reidel 1998), compared to inflated pahoehoe flows that have smooth surfaces (Rowland & Walker 1990; Hon *et al.* 1994). This, coupled with the lack of features (lava tubes, ropy surfaces, tumuli, lava inflation clefts, lava-rise pits) and vesicle distribution patterns associated with inflated pahoehoe lava flows of Hawai`i (Greeley 1987; Walker 1987; 1989; Rowland & Walker 1990; Walker 1991; Wilmoth & Walker 1993; Hon *et al.* 1994; Peterson *et al.* 1994; Kauahikaua *et al.* 1998; Keszthelyi & Self 1998; Self *et al.* 1998; Anderson *et al.* 1999; Crown & Baloga 1999), from the Columbia River Basalt Group (Self *et al.* 1996; Self *et al.* 1997; Keszthelyi & Self 1998; Self *et al.* 1998; Thordarson & Self 1998; Walker *et al.* 1999) and other volcanic settings (Kent *et al.* 1998; Calvari & Pinkerton 1999; Jerram *et al.* 1999; Jerram *et al.* 2000; Duraiswami *et al.* 2001), indicates that the LBF lava flows were most likely emplaced rapidly as a'a flows over periods of days to weeks.

Flow thicknesses range from a few metres up to several tens of metres and the majority of the flows have reddened tops or boles (palaeosols) formed as a consequence of subaerial weathering within a temperate to warm climate with significant (seasonal) rainfall (cf. Retallack 1981; 1988; 1997; Duchaufour 1998; Retallack 2001). Here, iron oxides are the main cause of the red colouration (Collinson 1996; Duchaufour 1998; Retallack 2001). The warm climate has accelerated the weathering process due to the positive correlations between temperature and oxidation and hydration rates of the primary lava minerals (Collinson 1996; Duchaufour 1998; Retallack 2001). Furthermore, the presence of organic material, common within the terrestrial environment, will have enhanced the formation of reducing pore waters, which will have accelerated mineral breakdown (Berner & Cochran 1998). Once these low temperature iron compounds have formed, they will be relatively inert and will not be further modified by chemical weathering processes (Duchaufour 1998; Retallack 2001). However, physical weathering may take place and such materials may be eroded and incorporated into the associated sedimentary units.

Where weathering profiles are preserved, the calculations of Nahon (1991) infer that *ca.* 1 mm of degraded basalt will be produced in less than 70 years. Fluctuation of the water

table and increasing rainfall will further accelerate the weathering process (Nahon 1991; Duchaufour 1998; Retallack 2001). The thickest bole is some 2 m thick, suggesting a hiatus in the volcanic activity of up to 140 kyrs. Flows lacking oxidised tops point towards relatively rapid sequential eruptions, although not necessarily from the same vent or fissure. According to Ellis *et al.* (2002) the LBF was erupted within *ca.* 3 myrs and assuming an average flow thickness of *ca.* 20 m throughout the *ca.* 3.5 km thick subaerial sequence of lava flows (exposed and drilled), suggests that the *ca.* 175 flows were erupted sequentially no more than every *ca.* 17 kyrs. If hiatuses in the volcanic activity did last for as long as 140 kyrs it suggests that the lava flows were erupted at considerably shorter intervals. For example, if there were just 20 m of bole in the sequence, hiatuses would have lasted in the order of *ca.* 1.4 myrs, suggesting that the 174 (one flow deducted due to the presence of bole) lava flows were erupted no more than every *ca.* 9 kyrs. However, to give a full assessment of the rates would involve logging the LBF to give each flow thickness, (to confirm the amount of flows), as well as the thickness of the boles present. Secondly, these data would need to be bracketed by high resolution (thousands of years) geochronological data, which is presently unattainable. Therefore, the use of the above calculations, involving the development of boles, help to further constrain relative timescales in the CFBs.

Joint development is commonly of the prismatic type, especially within the lower part of the exposed sequence, although most of the flows at the top of the LBF preserve classic columnar jointing, typical of the regular cooling of ponded flows (Spry 1962; Walker 1970; Long & Wood 1986; Jerram 2002). The formation of prismatic joints has been interpreted by Jerram (2002) as evidence for a relatively dry environment during volcanism. Conversely, the development of columnar joints and multi-tiered flows in the upper part of the LBF is evidence for the eruption of lavas into a wet subaerial environment (cf. Saemundsson 1970; Lyle 2000; Jerram 2002). This is supported, in part, by the presence of fluviatile, lacustrine and swamp facies strata found below the columnar jointed flows. Parra *et al.* (1987) have demonstrated that many of the clay-rich beds observed throughout the LBF have formed by the argillisation of tuffaceous sandstones in lacustrine environments or by argillisation of basalt lavas by meteoric waters. These data imply that there was sufficient rainfall and abundant surface water on the contemporaneous volcanic land surface. The climate during the eruption of the uppermost interval of the LBF was humid and warm temperate, which also implies high rainfall and seasonal lakes (Parra *et al.* 1987; Lund 1989).

The presence of pillow-like lobes and brecciated (hyaloclastite and blocky peperite) pockets at the base of some of the lava flows are indicative of the flows advancing into standing water (cf. Lyle 2000; Carr & Jones 2001). The hyaloclastite pockets at the base of the Hvalbiareiði Lava Flow contain little or no sediment, suggesting that the lava flowed into water alone rather than a water-rich sediment (cf. Kokelaar 1982; Busby-Spera & White 1987; McPhie *et al.* 1993; Skilling *et al.* 2002). Conversely, the blocky peperite pockets at the base of the Skarvatangi Lava Flow contain abundant sediment, indicating that the lava flowed into a water-rich sediment (cf. Kokelaar 1982; Busby-Spera & White 1987; Skilling *et al.* 2002). The brecciation of the lava flow only occurs in small pockets rather than along the entire length of the flow, suggesting that either the pools and water-rich sediments occurred as small localised features, or, that the lava flow had cooled sufficiently in places to produce a glassy boundary layer to insulate the inner part of the lava (cf. Pichler 1965), or a superheated layer of water vapour insulated the lava (cf. Williams & McBirney 1979; Kokelaar 1982).

The damming of pre-existing river channels by lava flows, displacing river systems, is preserved east of Froðba, Suðuroy, where the fan-shaped section of Kúlugjógv Lava Flow has infilled a small channel. The displaced water from such lava dams, together with high levels of rainfall can lead to the textural quenching of the upper sections of lava flows (cf. Lyle & Preston 1998; Lyle 2000). Textural quenching, in the form of curvi-columnar columns is preserved in the entablature tier of the lava flow at Hov. Such textural quenching is interpreted as the result of water ingress through cooling surfaces along master joints (cf. Saemundsson 1970; Long & Wood 1986), which modifies the internal isotherms of the cooling lava flow (cf. Lyle & Preston 1998).

The interbedded volcaniclastic sandstones and siltstones, claystones and coals, are characteristic of fluvial, deltaic and lacustrine environments and there is no evidence of a marine influence (e.g. Collinson 1996; Tucker 1996a). The sedimentary units comprise both fine-grained, often laterally extensive (>5 km), deposits and coarser, channel-like units, all of which were deposited in an alluvial environment. The lithologies range from tuffaceous mudstones to volcaniclastic conglomerates/breccias and coals. The tuffaceous mudstones are extremely clay-rich, containing palagonitised basaltic glass grains less than 200 μm in size. The sandstones and conglomerates/breccias are poorly sorted and clast supported. The clasts are all intraformational, with no evidence of any external sources. The clasts display a high degree of rounding and are commonly aligned parallel to bedding. The clasts are dominated by basalt, derived from lavas at various stages of surface oxidation, indicating numerous exposed flows within the contemporaneous lava surface.

The units also contain clasts of pre-existing volcaniclastic mudstones, typical of an evolving sedimentary sequence in a volcanic setting, where epiclastic volcanic units progress from mudstones to sandstones with time (cf. Nakayama & Yoshikawa 1997). The sandstones, conglomerates and breccias also contain a significant proportion of reworked palagonitised glassy material. The preservation of thin coals from 13 localities (Rasmussen & Noe-Nygaard 1970b) indicates that the surrounding volcanic land surface was vegetated, thus aiding the surface weathering of the volcanic lithologies (cf. Berner & Cochran 1998).

The increase in abundance of interlava lithologies and the development of coal-forming swamps in the upper section of the LBF is a consequence of a gradual waning of the volcanic activity, thus allowing time for erosion and associated sediment transportation and deposition to take place (cf. Cas & Wright 1987; Smith 1991; McPhie *et al.* 1993; Collinson 1996). Rates of basin subsidence must been high enough to allow the accumulation of the deposits, otherwise there would not have been enough accommodation space available to allow the build up of the deposits (cf. Smith 1991). It seems apparent from the range of lava clast lithologies in the volcaniclastic sandstones, that as soon as a lava flow had solidified it was being actively eroded. The scale of erosion is evident along the Vágseiði cliff profile and from the channel infilled by the Kúlugjógv Lava Flow, which indicates relief of up to 30 m. The rate of erosion is determined by the climate (Collinson 1996) and, as discussed above, there are clear indications that there was abundant surface water and high levels of rainfall to sustain a high rate of erosion. Conversely, the lower section of the LBF is generally lacking in interlava lithologies, which is typical of a drier climate (Collinson 1996) and this is supported by the abundance of prismatically jointed flows (cf. Jerram 2002, see above).

4 Coal-bearing Formation

Sections from the Coal-bearing Formation (CBF) have been described in detail by Rasmussen & Noe-Nygaard (1969; 1970b) and have been thoroughly examined for palynofloral assemblages (Lund 1983; 1989). Whilst the distribution and lithologies of the CBF and the relationship of this formation to the LBF are discussed, this chapter concentrates on the ironstone deposits found within the CBF. These units have not been previously reported in the literature and two principal localities are considered in detail. The ironstones are described in terms of petrography, crystallography and geochemistry in order to aid in the understanding of the environments of deposition of the formation. The second half of the chapter focuses on the sandstone and conglomerate beds overlying the coal seams, also rocks which have not been previously described in the literature. Again, these beds are examined to interpret the environments of deposition of the CBF.

4.1 Distribution

After the Lower Basalt Formation (LBF) was emplaced a period followed in which erosion cut down to at least the top of the second highest flow, and the continuing quiescence allowed the Coal-bearing Formation (CBF) to be deposited. The CBF crops out on the islands of Tindhólmur, Vágar and Suðuroy, where the coals have been mined. It forms a sub-horizontal sequence, which is always found overlying the LBF. On Vágar the CBF crops out in the north-western part of the island (Fig. 4.1). At Álkuklettur, just north of Bøur, it rises from sea level and follows the topography northwest to Barðið to reach a height of 300 m where it then drops to sea level at Víkar, to the east.

The CBF covers an area of 23 km^2 on Suðuroy and it is only on this island that the formation contains any substantial amount of coal (Fig. 4.2). The formation is usually only accessible and exposed in completeness in mine workings, which except for one on the east side of Rokhagi valley are now all closed. On Suðuroy the CBF has been subdivided into four separate coalfields: (i) Grímsfjall, (ii) Northern, (iii) Southern, and (iv) Kolheyggjur-Hovstúgva (Rasmussen & Noe-Nygaard 1970b). The Grímsfjall coalfield (*ca.* 1.5 km^2) follows the topography from Kolaratangi to the south around Grímsfjall and then northeastwards to Hvalba at a height between 0 and 50 m above sea level. The northern coalfield (*ca.* 19 km^2) starts from Ulingatangi, east of Froðba, at sea level and follows the topography along the mountainside to the west, north of Trongisvágur, where it reaches a height of 250 m eventually reaching sea level again at Tjørnunes, east of Nes in the north

Fig. 4.1. Geological map of western Vágar, Tindhólmur, and Gáshólmur, Faeroe Islands. After Rasmussen & Noe-Nygaard (1969; 1970a; b).

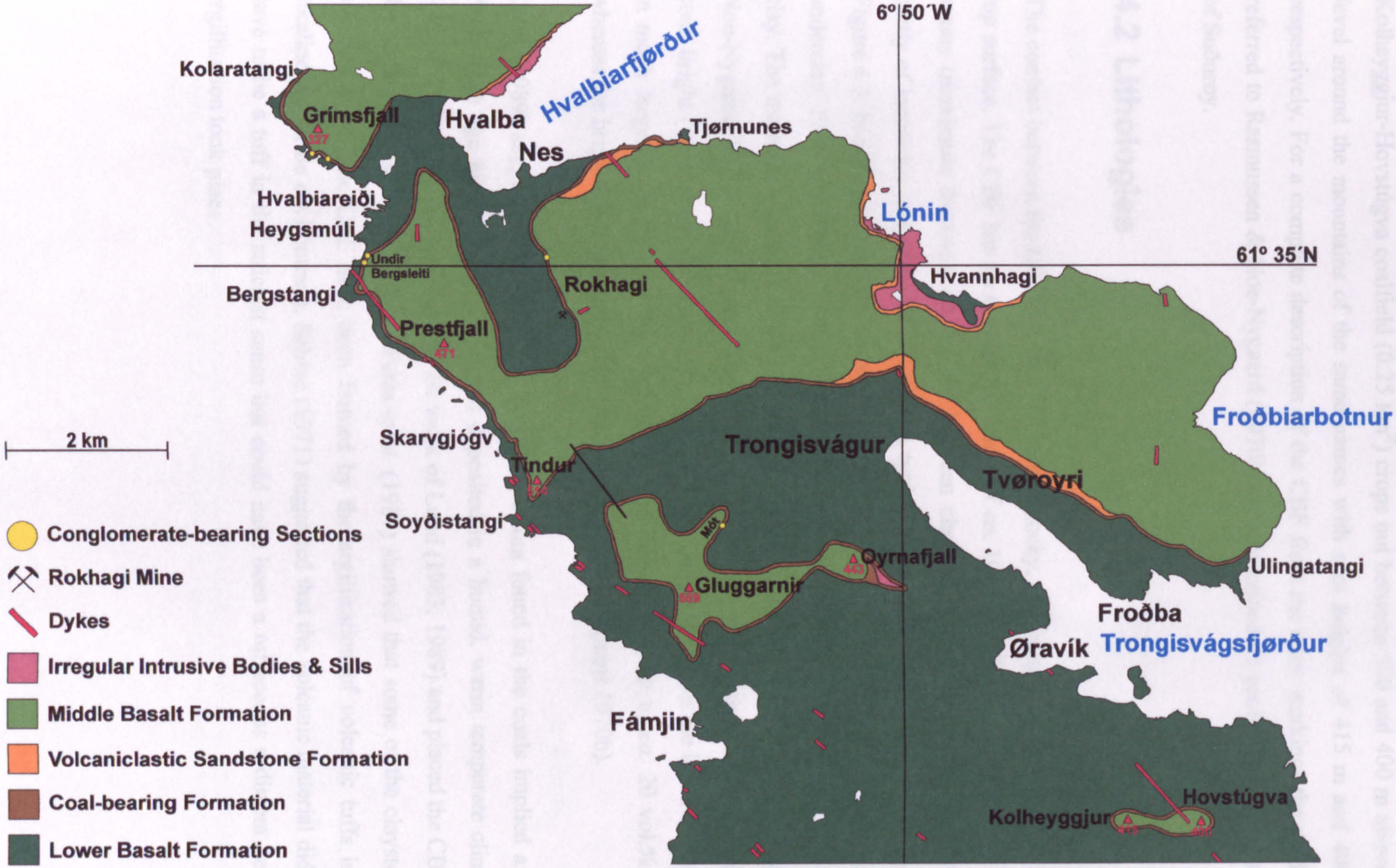

Fig. 4.2. Geological map displaying the four coal fields on Suðuroy, Faeroe Islands. Spot heights are in metres. After Rasmussen & Noe-Nygaard (1969; 1970a; b).

of the island. The southern coalfield (*ca.* 2.6 km^2) crops out at a height between 300 and 350 m around the mountainsides of Gluggarnir (569 m) and Oyrnafjall (443 m). The Kolheyggjur-Hovstúgva coalfield (0.25 km^2) crops out between 300 and 400 m above sea level around the mountains of the same names with spot heights of 415 m and 400 m, respectively. For a complete description of the CBF from the mine workings the reader is referred to Rasmussen & Noe-Nygaard (1970b) who described 41 profiles from the island of Suðuroy.

4.2 Lithologies

The contact between the LBF and the CBF is hummocky, reflecting the erosion of the LBF top surface. The CBF has an average thickness of *ca.* 10 m and there are usually two coal seams (maximum thickness *ca.* 1.8 m) between claystones and shales interpreted to be partly of lacustrine in origin (Lund 1989). A typical sequence through the CBF is given in Figure 4.3. In at least two localities previously unreported ironstone beds have replaced the underclay. Elsewhere basaltic sandstones and conglomerates replace, or overlie, the roof clay. The macerals within the coals are believed to be partly allochthonous (Rasmussen & Noe-Nygaard 1970b). Rasmussen & Noe-Nygaard (1970b) state that there are two types of coal: bright (vitrain) and dull (durain). The dull coals usually occur in the lower seam and in much larger amounts than the bright coals and they contain up to *ca.* 20 vol.% ash whereas the bright coals have <5 vol.% (Rasmussen & Noe-Nygaard 1970b).

Lund (1989) suggested that the non-marine microflora found in the coals implied a late Palaeocene age for the CBF, which was deposited in a humid, warm temperate climate. Jolley (1997), however, re-examined the work of Lund (1983; 1989) and placed the CBF in the earliest Ypresian (*ca.* 57 Ma). Parra *et al.* (1987) showed that some of the claystones associated with the CBF have been formed by the argillisation of volcanic tuffs in an alkaline lacustrine environment. Sabine (1971) suggested that the volcanic material did not have to be a tuff in the strictest sense but could have been a tuffaceous sediment before argillisation took place.

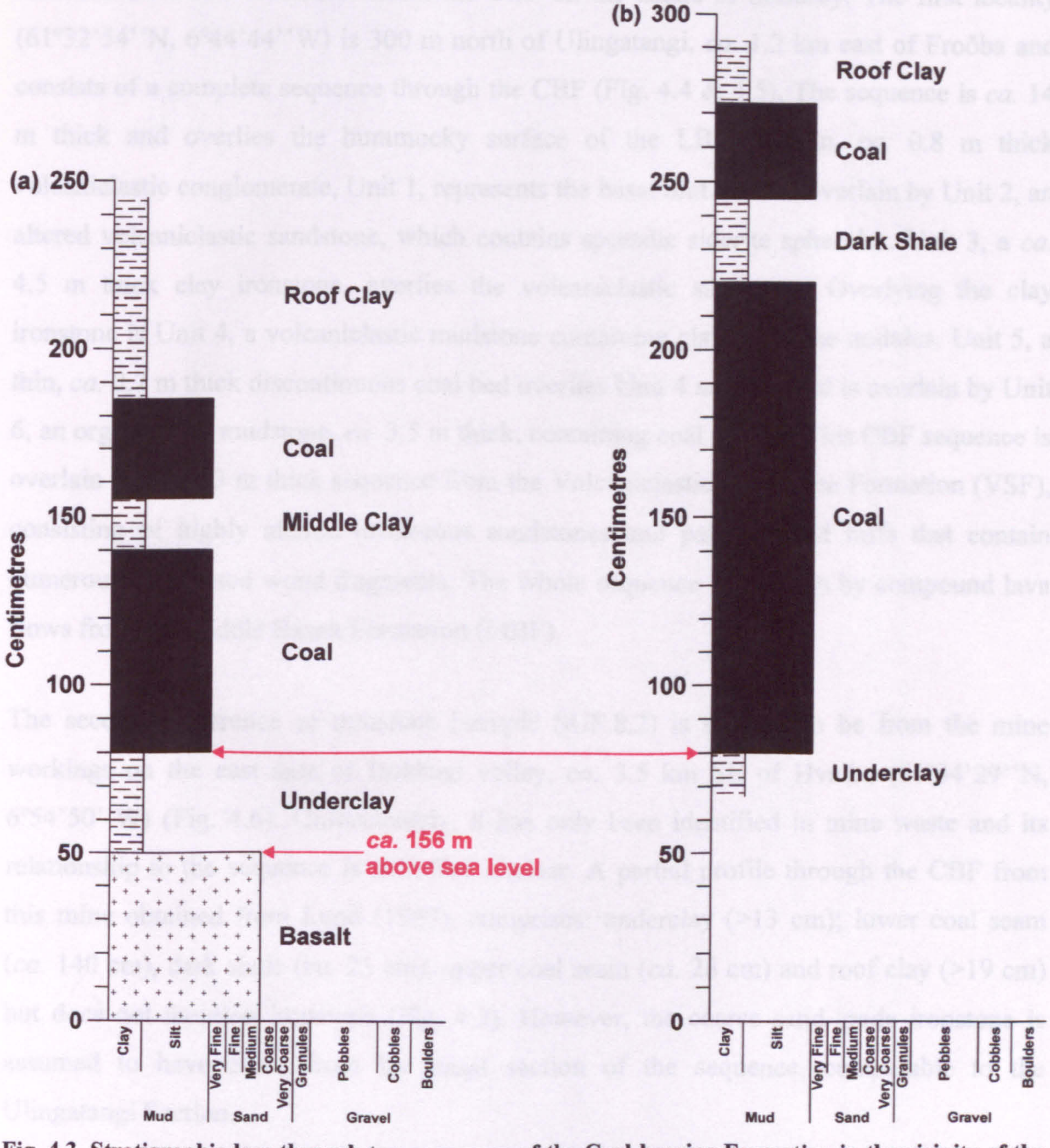

Fig. 4.3. Stratigraphic logs through two sequences of the Coal-bearing Formation in the vicinity of the Rokhagi Mine, Suðuroy, Faeroe Islands. (a) After Rasmussen & Noe-Nygaard (1969; 1970b). (b) After Lund (1989).

4.3 Ironstone Beds

4.3.1 Occurrence

Previously unreported ironstone beds, containing siderite ($FeCO_3$) spherules have been recorded from two localities within the CBF on the island of Suðuroy. The first locality (61°32'54''N, 6°44'44''W) is 300 m north of Ulingatangi, *ca.* 1.2 km east of Froðba and consists of a complete sequence through the CBF (Fig. 4.4 & 4.5). The sequence is *ca.* 14 m thick and overlies the hummocky surface of the LBF. A thin, *ca.* 0.8 m thick volcaniclastic conglomerate, Unit 1, represents the basal unit. This is overlain by Unit 2, an altered volcaniclastic sandstone, which contains sporadic siderite spherules. Unit 3, a *ca.* 4.5 m thick clay ironstone, overlies the volcaniclastic sandstone. Overlying the clay ironstone is Unit 4, a volcaniclastic mudstone containing clay ironstone nodules. Unit 5, a thin, *ca.* 0.7 m thick discontinuous coal bed overlies Unit 4 and the coal is overlain by Unit 6, an organic-rich mudstone, *ca.* 3.5 m thick, containing coal streaks. This CBF sequence is overlain by a *ca.* 3 m thick sequence from the Volcaniclastic Sandstone Formation (VSF), consisting of highly altered tuffaceous sandstones and palagonitised tuffs that contain numerous carbonised wood fragments. The whole sequence is overlain by compound lava flows from the Middle Basalt Formation (MBF).

The second occurrence of ironstone (sample SUF.8.2) is thought to be from the mine workings on the east side of Rokhagi valley, *ca.* 3.5 km SE of Hvalba (61°34'29''N, 6°54'50''W) (Fig. 4.6). Unfortunately, it has only been identified in mine waste and its relationship to the sequence is therefore unclear. A partial profile through the CBF from this mine obtained from Lund (1989), comprises: underclay (>13 cm); lower coal seam (*ca.* 140 cm), dark shale (*ca.* 25 cm), upper coal seam (*ca.* 28 cm) and roof clay (>19 cm) but does not mention ironstone (Fig. 4.3). However, the coarse sand-grade ironstone is assumed to have come from the basal section of the sequence, comparable to the Ulingatangi Section.

4.3.2 Petrography

4.3.2.1 Ulingatangi Section

Unit 1 is a medium bluish grey (5B 5/1) poorly sorted granule-grade volcaniclastic conglomerate, which is *ca.* 0.8 m thick (Fig. 4.7). The conglomerate is matrix supported and consists of sub-rounded basalt clasts. The average clast size of the conglomerate is *ca.*

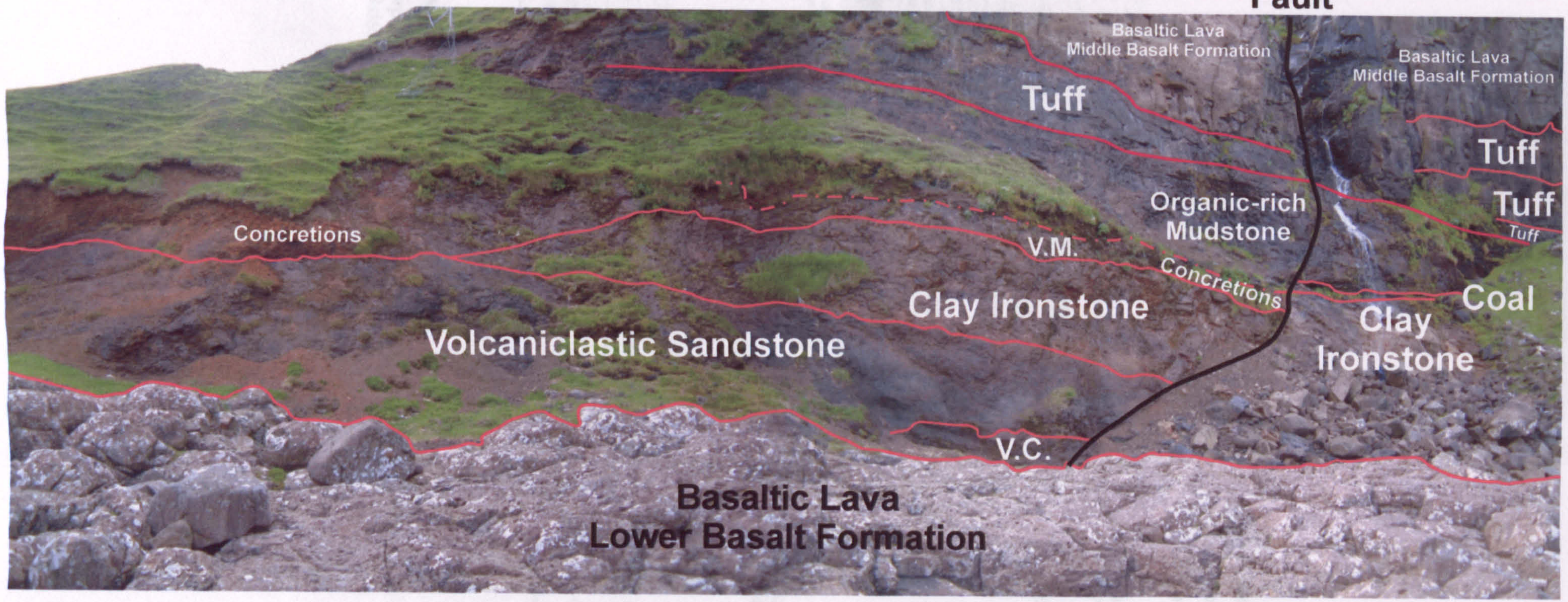

Fig. 4.4. View of the Ulingatangi Section, *ca.* 300 m N of Ulingatangi, *ca.* 1.2 km E of Froðba, Suðuroy, Faeroe Islands. The Coal-bearing Formation (CBF) overlies the Lower Basalt Formation and is *ca.* 14 m thick at this locality. The CBF is overlain by a 3 m thick sequence of tuffs from the Volcaniclastic Sandstone Formation, which in turn is overlain by lava flow units from the Middle Basalt Formation. V.C. = Volcaniclastic Conglomerate. V.M. = Volcaniclastic Mudstone. See Figure 4.5 for a stratigraphic log of the section.

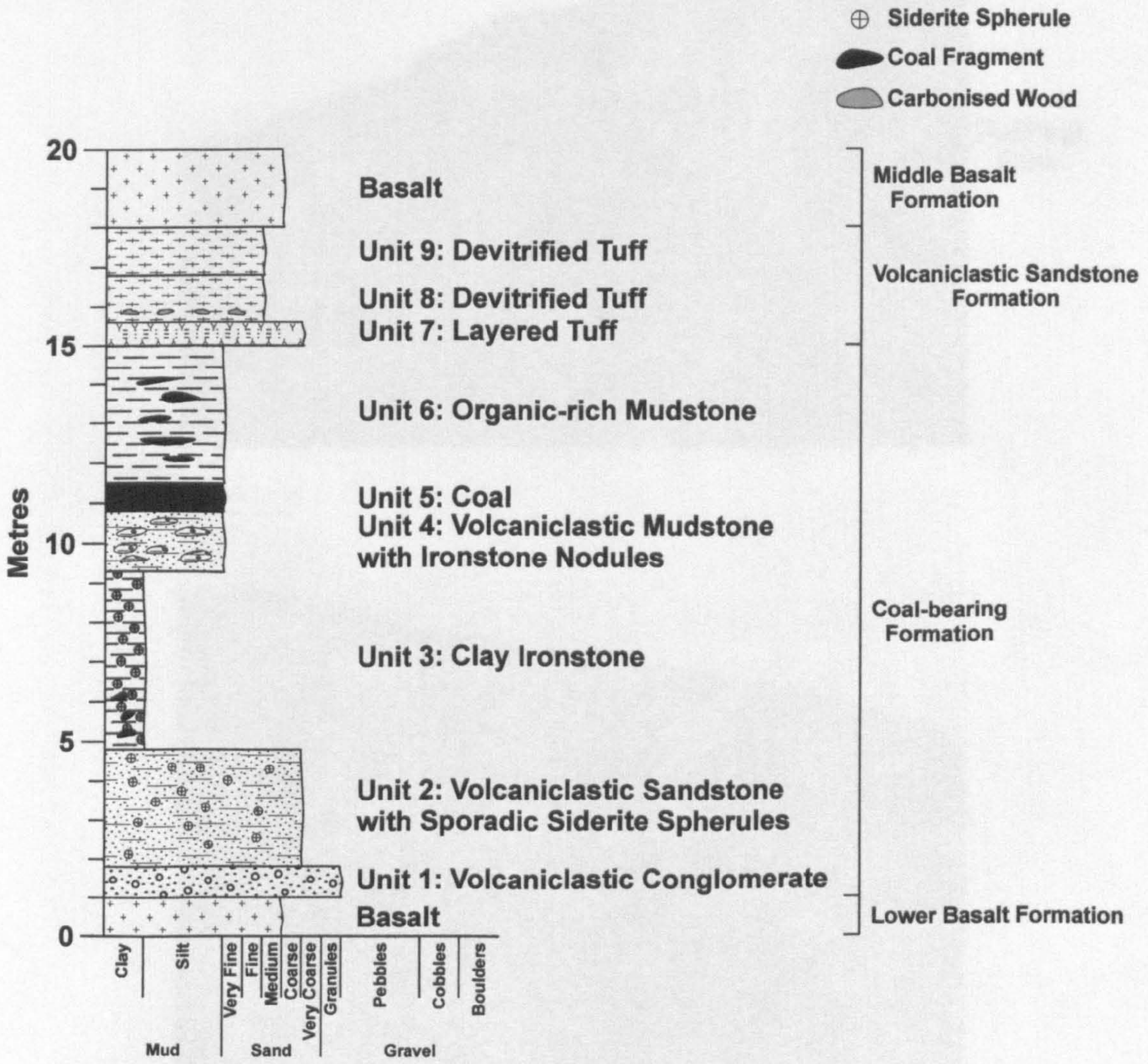

Fig. 4.5. Stratigraphic log of the Ulingatangi Section, *ca.* 300 m N of Ulingatangi, *ca.* 1.2 km E of Froðba, Suðuroy, Faeroe Islands.

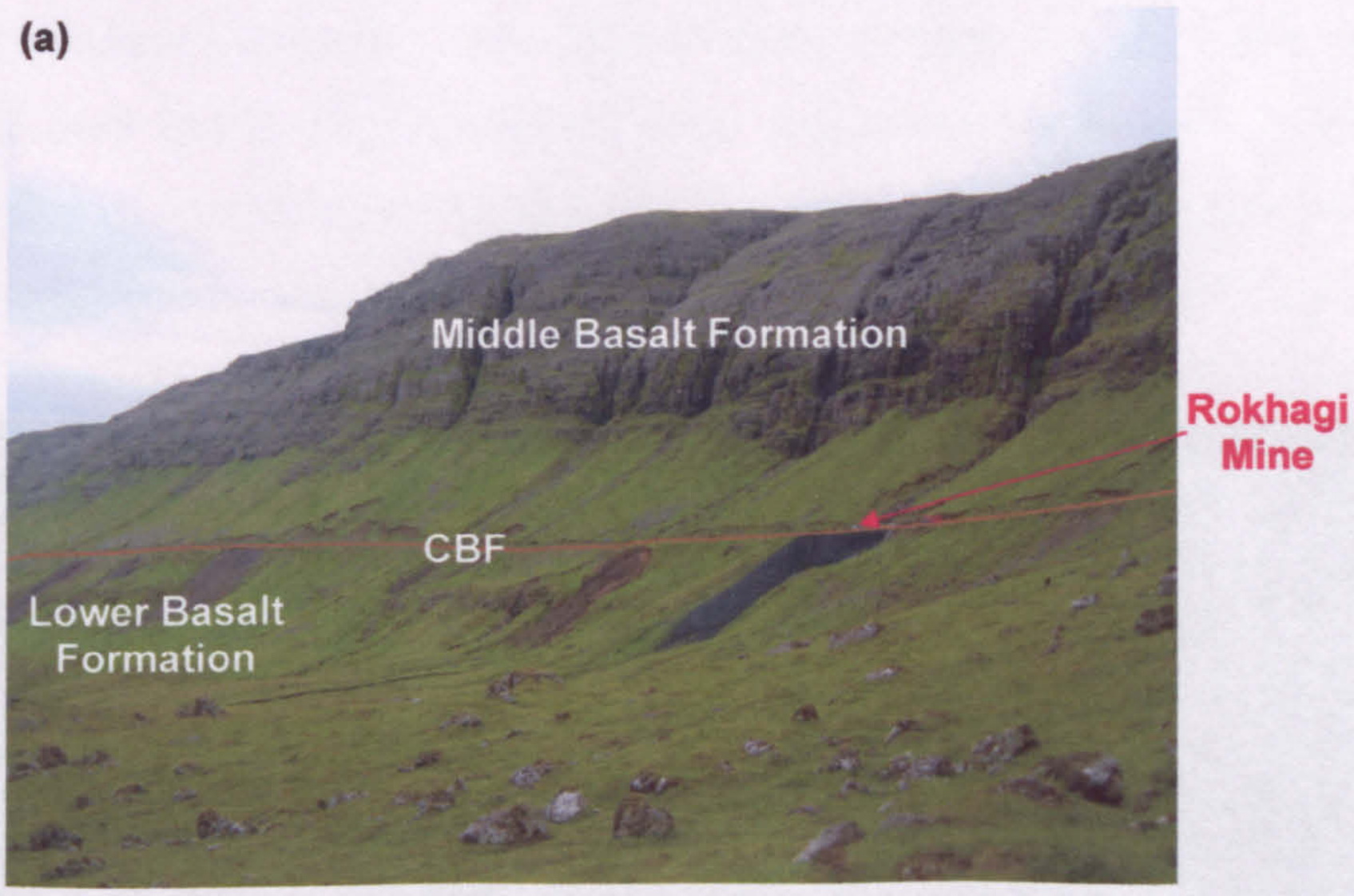

Fig. 4.6. (a) View of the Rokhagi mine, Suðuroy, Faeroe Islands. The mine is identified by its distinctive black mine waste, from where sample SUF.8.2 was collected. (b) View of the top of the mine waste at Rokhagi mine. Other disused mines can be identified by their brown mine waste. The track way marks the level of the Coal-bearing Formation (CBF). Underneath the mines are lava flows of the Lower Basalt Formation (LBF). The mountainside above the mines are made up of compound lava flows of the Middle Basalt Formation (MBF).

Fig. 4.7. View of Unit 1, Granule-grade conglomerate, from the base of the Ulingatangi Section, *ca.* 300 m N of Ulingatangi, *ca.* 1.2 km E of Froðba, Suðuroy, Faeroe Islands. The hammer head is *ca.* 16 cm wide.

0.3 x 0.3 cm with maximum sizes of 5 x 2 cm. The long axes of the clasts are commonly aligned parallel to the upper bedding plane.

Unit 2 is a brownish black (5YR 2/1) mottled coarse sand-grade volcaniclastic sandstone, which is *ca.* 3 m thick. The sandstone is blocky and thinly to thickly laminated. It reacts sluggishly with 10% hydrochloric (HCl) acid, although a series of fractures develop. In thin section, the sandstone comprises near opaque clasts, average size *ca.* 1 mm, with the slightest hint of dark red in plane-polarised light, suggesting enrichment in iron, and probably consisting of iron oxide or oxyhydrate (Fig. 4.8). Some of the clasts consist of highly altered glassy basalt, with a maximum size of *ca.* 4 mm and some of these contain lath-shaped crystals <100 μm in size that have been pseudomorphed by a yellowish brown mineral, these are most likely remnants of plagioclase feldspar crystals. The presence of pseudomorphed plagioclase feldspar laths and the highly altered nature of the groundmass suggests that the sandstone formed from the intense alteration of basaltic material. The lamination may indicate a basaltic volcaniclastic deposit.

Fractures between clasts have been filled by yellowish brown siderite (Fig. 4.8) and it is this cement that reacts with the HCl acid. Also within the fractures are rare colourless siderite spherules with an average grain size of *ca.* 200 μm (rarely *ca.* 2.0 mm) (Figs. 4.8 & 4.9). These are commonly enclosed within the siderite cement, suggesting that growth took place *in situ* before the cementation event. The siderite cement enclosing the spherules is commonly in optical continuity with them. The spherules usually contain occluded fragments of broken basaltic material, indicating *in situ* mode of formation. Some of the larger spherules exhibit concentric zones with distinct and separate phases of siderite growth. This zonation is discussed in detail in Section 4.3.3.2.

Unit 3 is a massive, dense, light olive grey (5Y 6/1) clay ironstone (sample SUF.1.2) containing 30-40 vol.% siderite spherules. The ironstone is *ca.* 4.5 m thick and the basal 1.5 m contains discoidal coal fragments with a maximum size of *ca.* 15 x 2 cm (Fig. 4.10). In thin section, the ironstone consists of a clay-rich matrix that has been significantly compacted around larger grains (Figs. 4.11a-b). Irregular, sometimes cuspate to platy, lithic fragments occur throughout the unit. These fragments are <1 mm in size and consist of palagonitised and chloritised basaltic glass. The siderite spherules have a maximum grain size of *ca.* 1 mm and exhibit the following morphologies: perfect spherules (10 vol.%) (Figs. 4.11c-d), bow-ties (50 vol.%) (Figs. 4.11e-h), fan-shapes (40 vol.%), and numerous irregular sub-rectangular grains. Under the scanning electron microscope (SEM) trigonal siderite crystals are observed (Fig. 4.12a). The crystallography of the spherules is

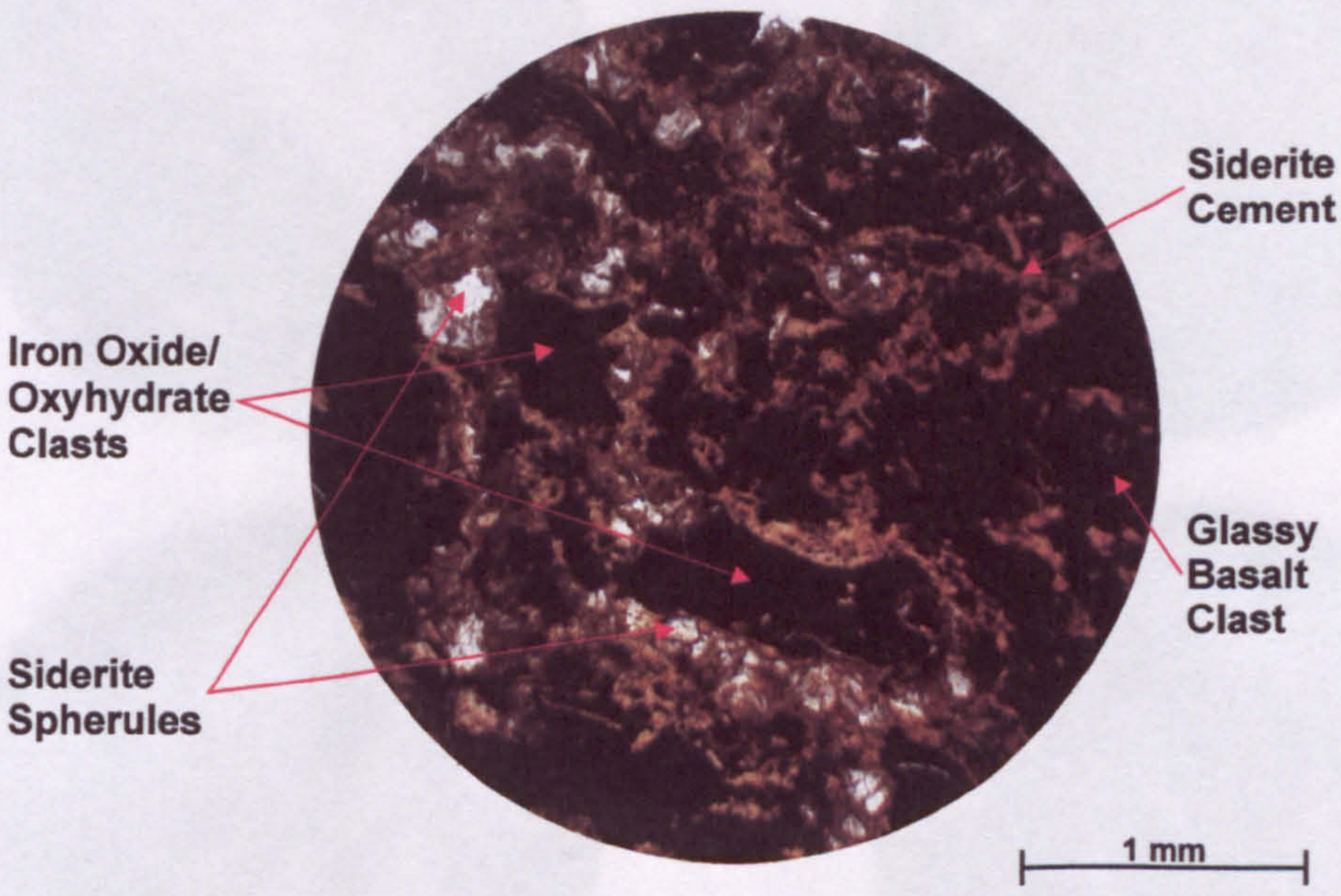

Fig. 4.8. Photomicrograph, under plane-polarised light, of Unit 2, volcaniclastic sandstone, Ulingatangi Section, Suðuroy, Faeroe Islands. Showing opaque iron oxide/oxyhydrate clasts and clasts of glassy basalt. The fractures have been filled by brownish-yellow siderite cement and siderite spherules.

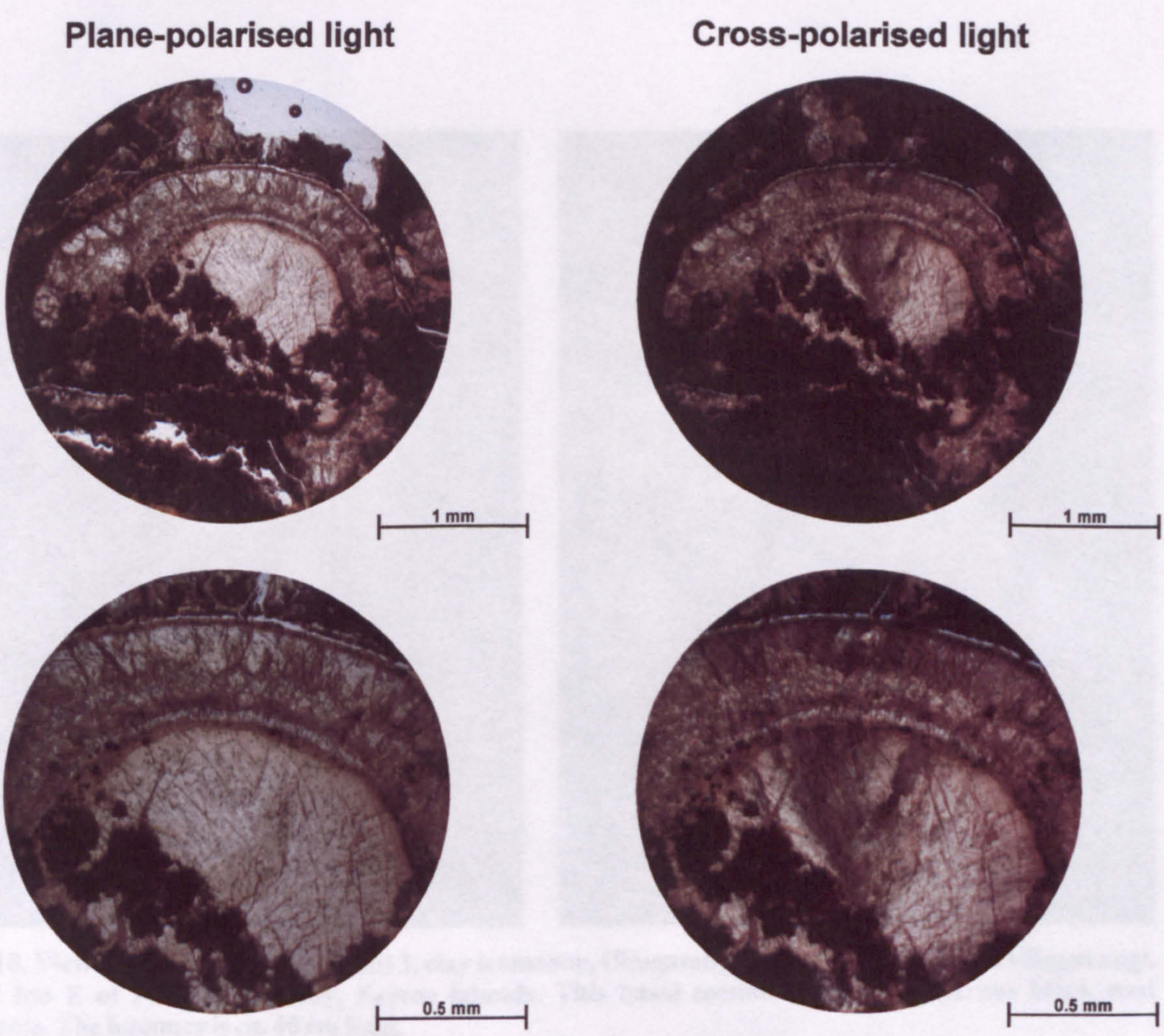

Fig. 4.9. Photomicrographs of a large siderite spherule from Unit 2, volcaniclastic sandstone, Ulingatangi Section, *ca.* 300 m north of Ulingatangi, *ca.* 1.2 km east of Froðba, Suðuroy, Faeroe Islands. The siderite spherule exhibits concentric zones of growth. See Section 4.3.3 for a detailed description.

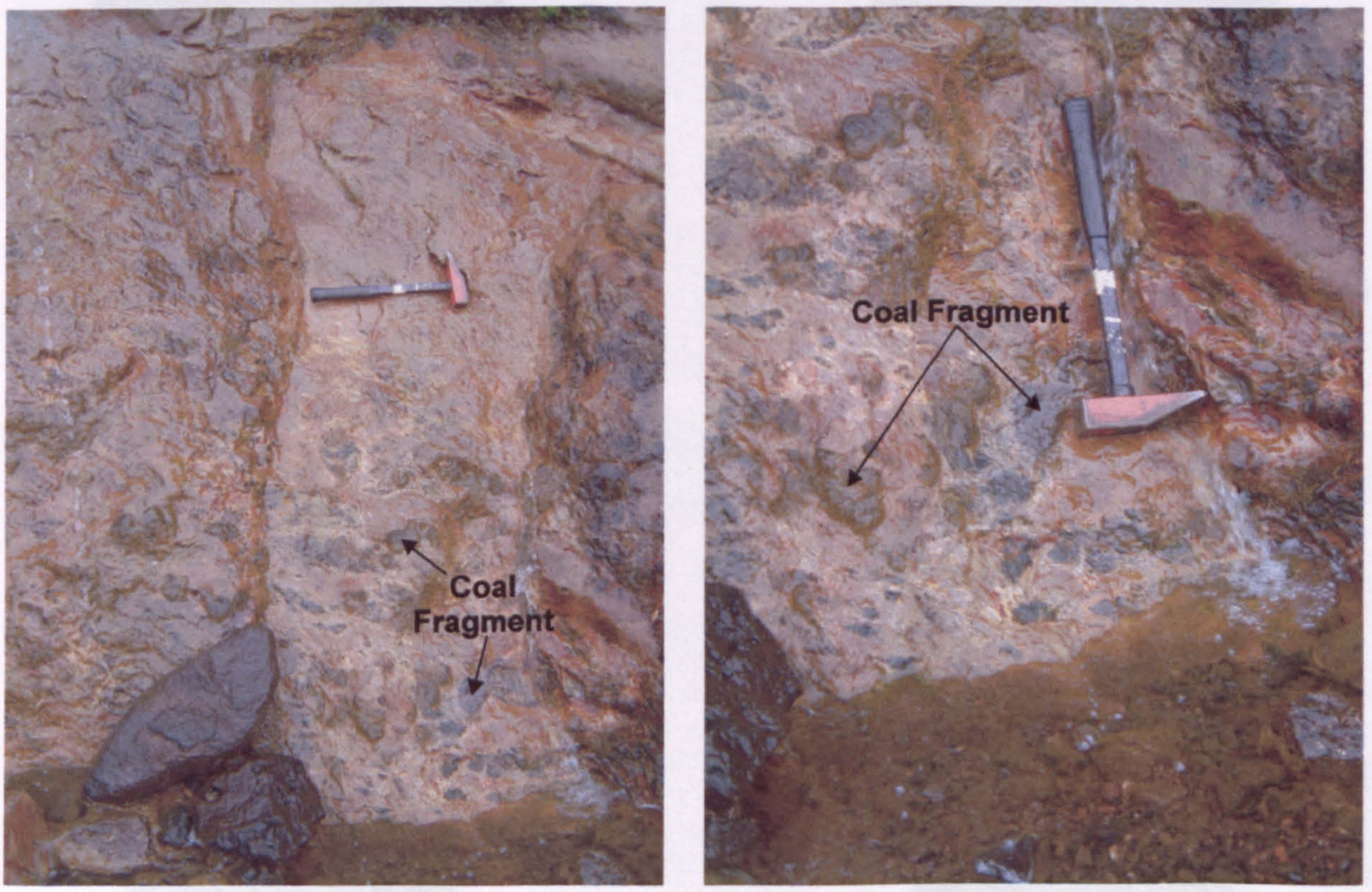

Fig. 4.10. Views of the basal 1.5 m of Unit 3, clay ironstone, Ulingatangi Section, *ca.* 300 m N of Ulingatangi, *ca.* 1.2 km E of Froðba, Suðuroy, Faeroe Islands. This basal section contains numerous black coal fragments. The hammer is *ca.* 40 cm long.

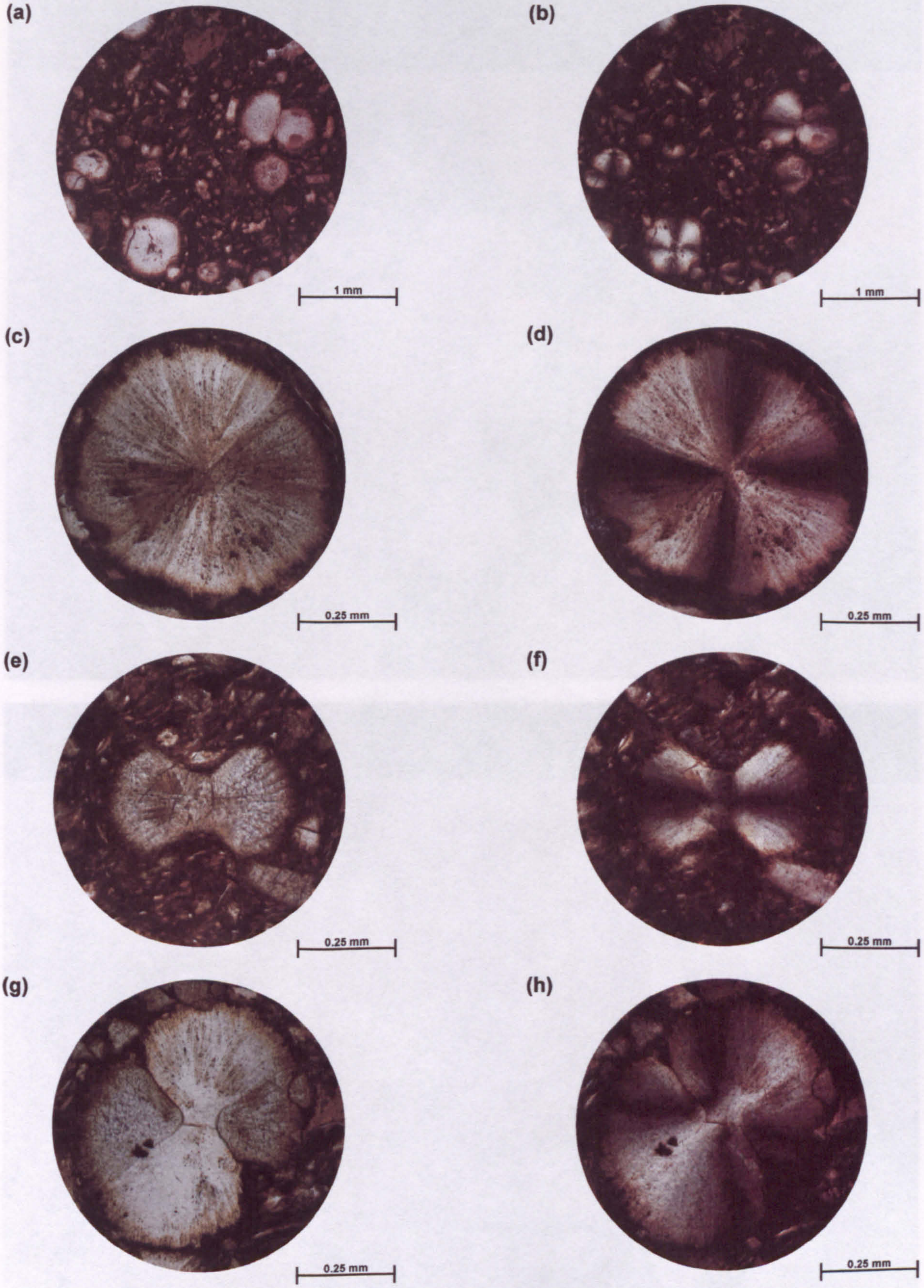

Fig. 4.11. Photomicrographs of sample SUF.1.2, Unit 3, clay ironstone, Ulingatangi Section, *ca.* 300 m north of Ulingatangi, *ca.* 1.2 km east of Froðba, Suðuroy, Faeroe Islands. (a) Siderite spherules in a clayey matrix, bow-tie right of centre, perfect spherule bottom left, and a palagonite clast top centre of view. (b) Same view as in (a) under cross-polarised light. Notice the Maltese Cross extinction patterns. (c) A perfect spherule consisting of a cryptocrystalline centre surrounded by individual siderite crystals. (d) Same view as in (c) under cross-polarised light, which shows that the crystals are orientated parallel to the c-axis. (e) A bow-tie shaped siderite spherule which has formed from split crystal growth. (f) Same view as in (e) in cross-polarised light. (g) A bow-tie shaped siderite spherule that has continued to grow to a stage of almost forming a sphere. (h) Same view as in (g) under cross-polarised light. For further details on crystal formation see Section 4.3.3.

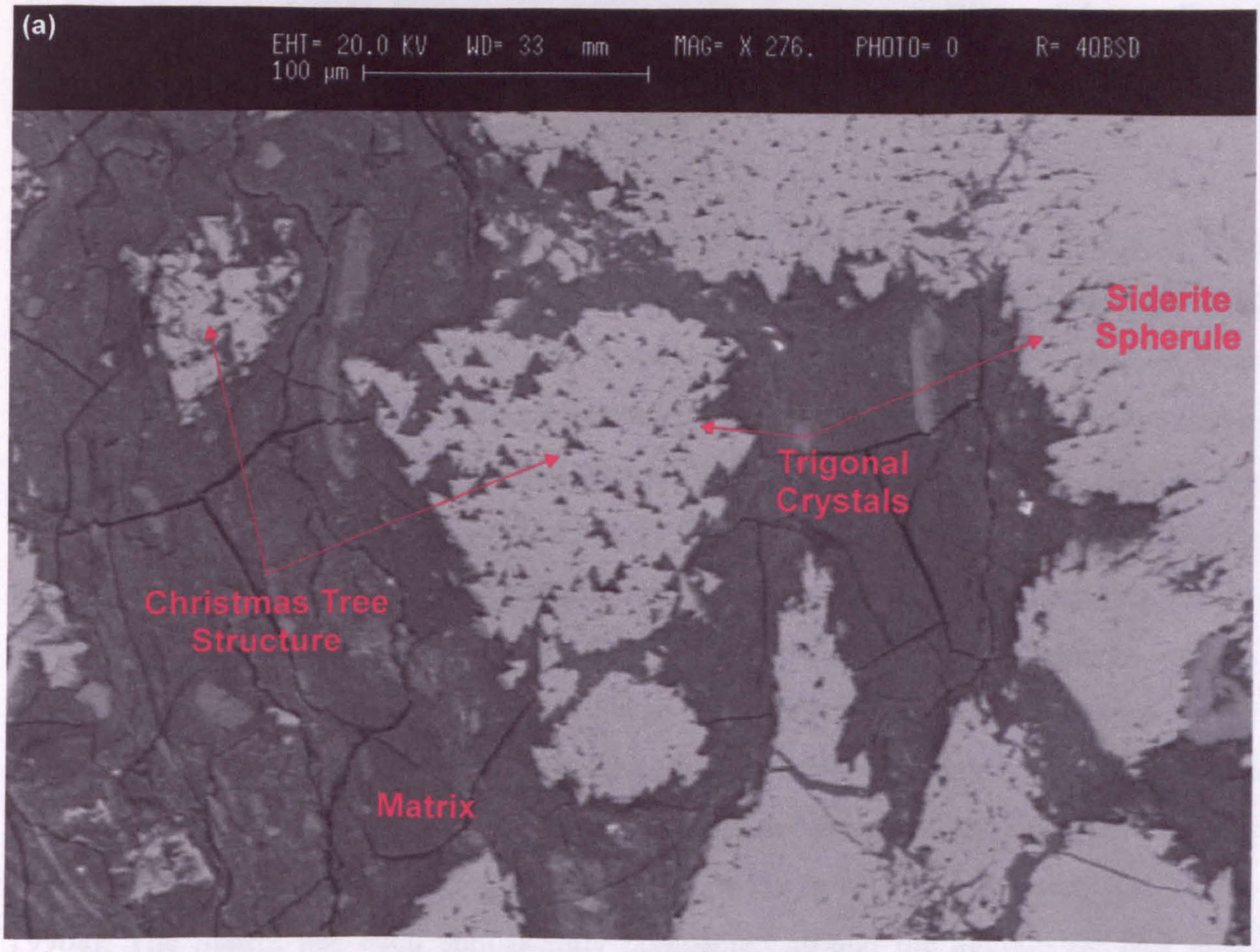

Fig. 4.12. SEM photomicrographs of sample SUF.1.2, Unit 3, clay ironstone, Ulingatangi Section, *ca.* 300 m north of Ulingatangi, *ca.* 1.2 km east of Froðba, Suðuroy, Faeroe Islands. (a) Small trigonal siderite crystals cumulating to form a Christmas tree pattern structure. Notice the trigonal siderite crystals growing on the periphery of siderite spherules in the top left of the picture. This suggests the trigonal crystals grew at a very late stage. (b) The central siderite spherule has shattered as a result of compaction, suggesting that the spherules grew before compaction and therefore did not grow during burial.

discussed in Section 4.3.3. Where a spherule-to-spherule contact is observed the smaller of the two spherules is commonly shattered into small irregular pieces, suggesting that the spherules formed before compaction (Fig. 4.12b).

Unit 4 is a thin, *ca.* 1.5 m thick brownish black (5YR 2/1) volcaniclastic mudstone. The mudstone contains light olive grey (5Y 6/1) nodules with well-developed spheroidal weathering (Fig. 4.13). The nodules are elliptical in shape and have a higher density than the mudstone host. The nodules are all aligned parallel to the bedding plane and range in size from 8 x 2 cm up to 25 x 9 cm and they are commonly thinly laminated. The nodules contain iron stained spherical aggregates up to 7 mm in diameter within a clayey-matrix (Fig. 4.14). In thin section, these aggregates consist of irregular, sub-rectangular crystals of siderite <200 μm in size, with rare, *ca.* 5-10 vol.%, bow-tie bundles of siderite crystals with an average grain size of *ca.* 2 mm. These commonly have a brown oxidised rim of either goethite or haematite. Sharp boundaries between the aggregates and the clay-rich matrix define the spherical shape. The nodularity and difference in grain size between the spherical aggregates and the clay-rich matrix may be the result of bioturbation (cf. Tucker 1996a). The matrix has been significantly compacted around the aggregates; that must have formed early for them to have kept their spherical shape.

Unit 5 is a thin, *ca.* 0.7 m thick discontinuous coal seam, which is overlain by Unit 6, a *ca.* 3.5 m thick dark grey (N3) organic-rich mudstone containing numerous coal streaks aligned parallel to bedding.

4.3.2.2 Rokhagi Section

The coarse sand-grade ironstone bed from the Rokhagi Section is found as small broken up samples in the mine waste. It is not observed *in situ* and its stratigraphic position is unknown. No occurrence of ironstone is mentioned in the descriptions of the CBF sequence from within the Rokhagi mine (Rasmussen & Noe-Nygaard 1970b; Lund 1989).

The sample SUF.8.2 is olive grey (5Y 4/1) with slight orange (iron) staining in hand specimen. The sample contains small coal bands, *ca.* 1-2 mm thick and is friable, liberating spherical grains <1 mm in size. In thin section, the sample is dominated (*ca.* 90 vol.%) by siderite spherules (Figs. 4.15a-b) that are closely packed together and have a yellowish brown oxidised rim, most likely goethite or haematite. The spherules have an average grain size of *ca.* 0.5 mm but can reach a maximum of *ca.* 1.0 mm. The sample contains a range of morphologies: perfect spherules (Figs. 4.16a-b), bow-ties (Figs. 4.16c-d), fan-shapes, and irregular sub-rectangular grains. The crystals in the sample are generally broken,

Fig. 4.13. View of Unit 4, clay ironstone nodules contained within the volcaniclastic mudstone overlying Unit 3, the clay ironstone. Ulingatangi Section, *ca.* 300 m N of Ulingatangi, *ca.* 1.2 km E of Froðba, Suðuroy, Faeroe Islands. Notice the apparent conchoidal fracture around some of the nodules. The white card is *ca.* 16 x 6 cm.

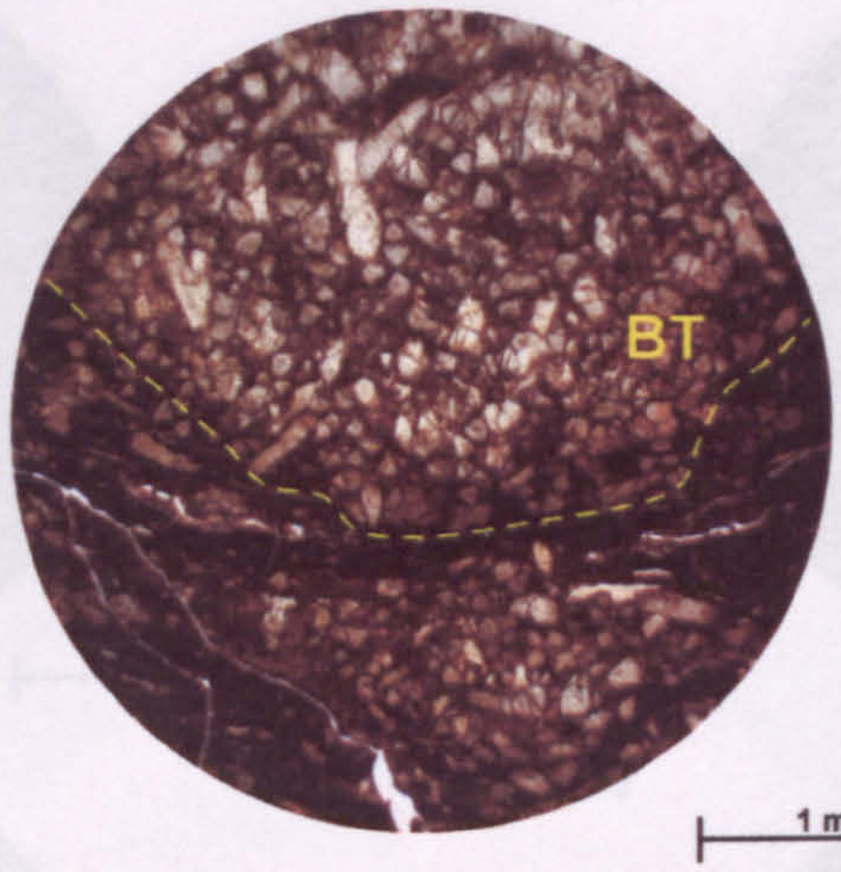

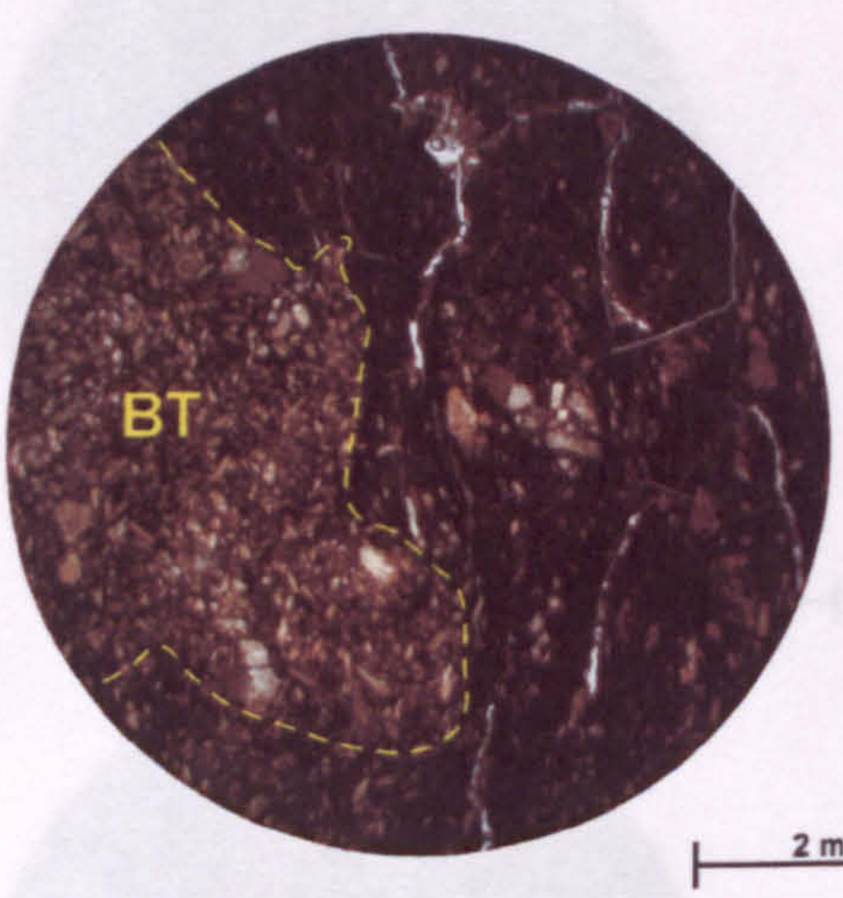

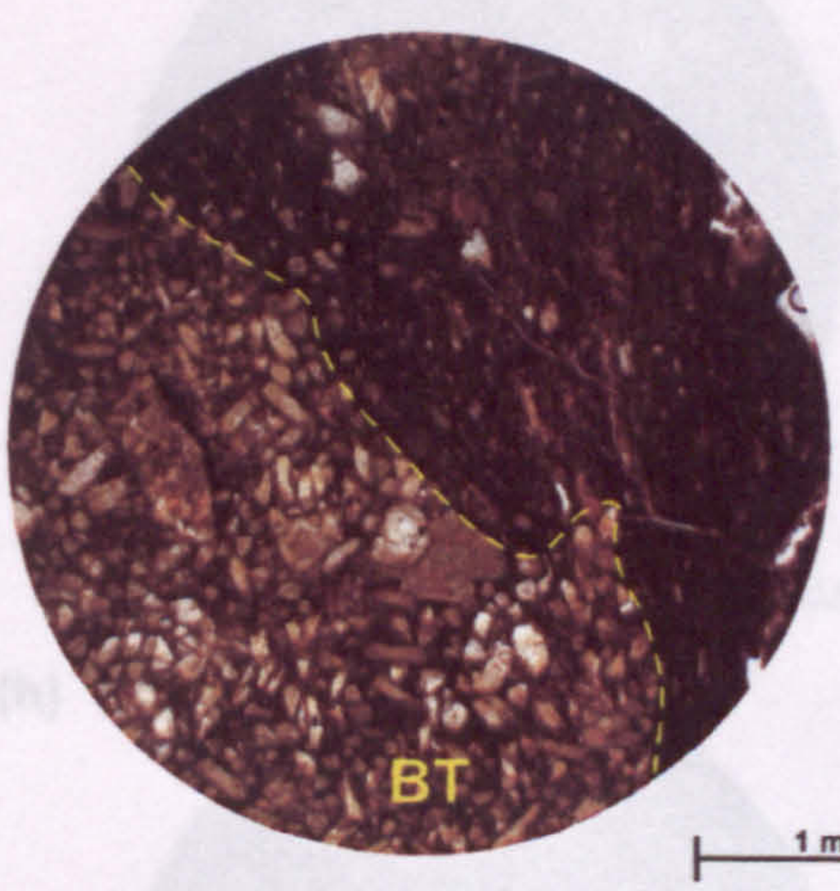

Fig. 4.14. Photomicrographs of bioturbation tubes (BT) from within ironstone nodules from Unit 4, volcaniclastic mudstone, Ulingatangi Section, *ca.* 300 m north of Ulingatangi, *ca.* 1.2 km east of Froðba, Suðuroy, Faeroe Islands. All of the photomicrographs are under plane-polarised light. The sharp contact between the tubes, filled with broken pieces of siderite spherules, and compaction of the clayey matrix around the tubes suggests that they formed prior to compaction.

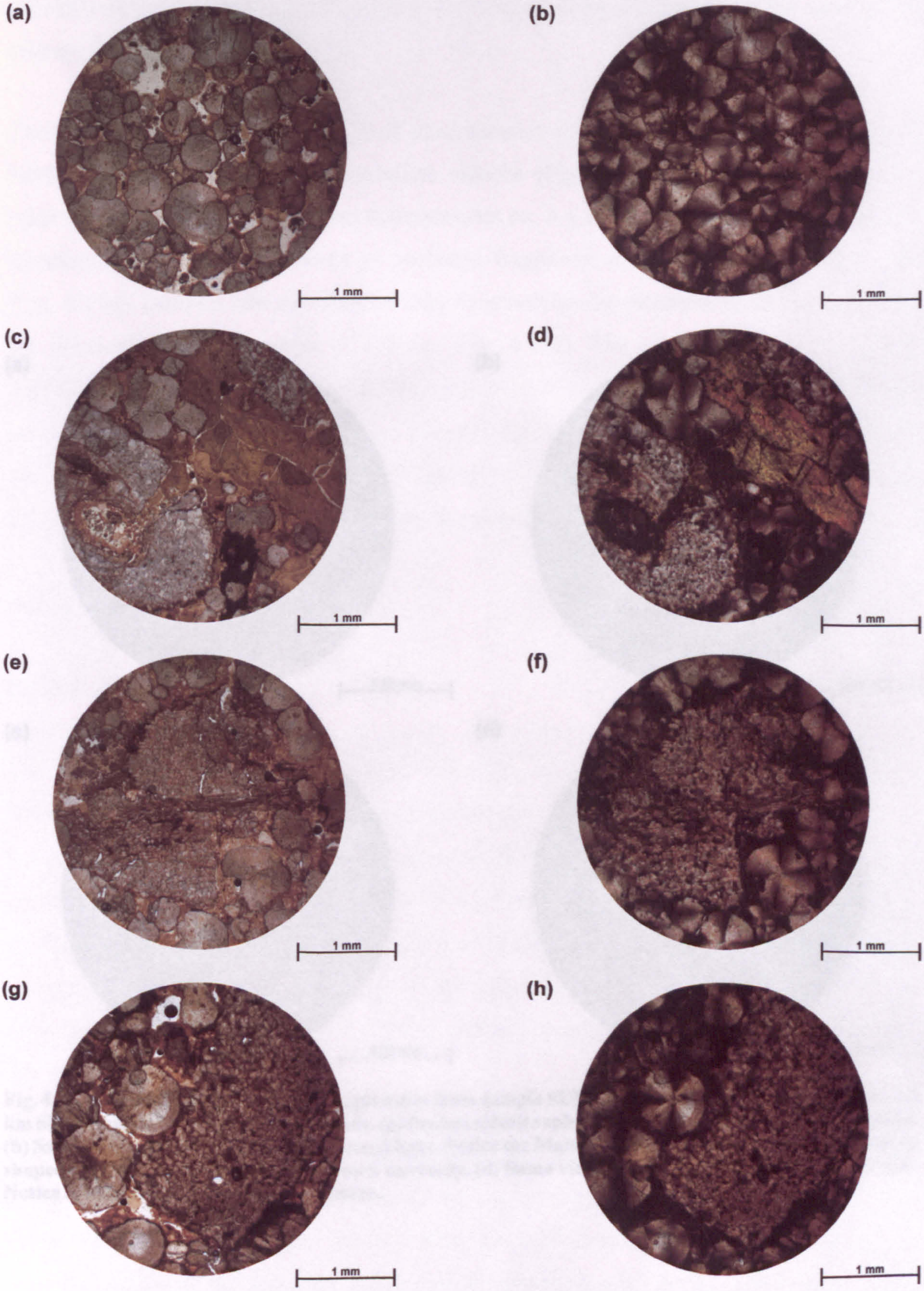

Fig. 4.15. Photomicrographs of sample SUF.8.2, ironstone, Rokhagi Section, *ca.* 3.5 km SE of Hvalba, Suðuroy, Faeroe Islands. (a) Siderite spherules that are clast supported; as a result of compaction some of the spherules have shattered. Notice the weakly developed yellowish siderite cement. (b) Same view as (a) under cross-polarised light. Notice the Maltese Cross extinction patterns. (c) The left hand side of the photomicrograph contains a clast of organic material that has been replaced by microcrystalline siderite. The right hand side of the photomicrograph contains a brownish clayey clast. (d) Same view as in (c) but in cross-polarised light. Notice the high birefringence and serpentine structure of the clayey clast, possibly berthierine or chamosite. (e) Cellular structure can be observed within a woody fragment, which has been replaced by siderite. (f) Same view as in (e) under cross-polarised light. (g) Pseudomorphed clast of organic material by microcrystalline siderite in the bottom right of the photomicrograph. Notice the zoning to the siderite spherule in the centre of the view. (h) Same view as in (g) under cross-polarised light.

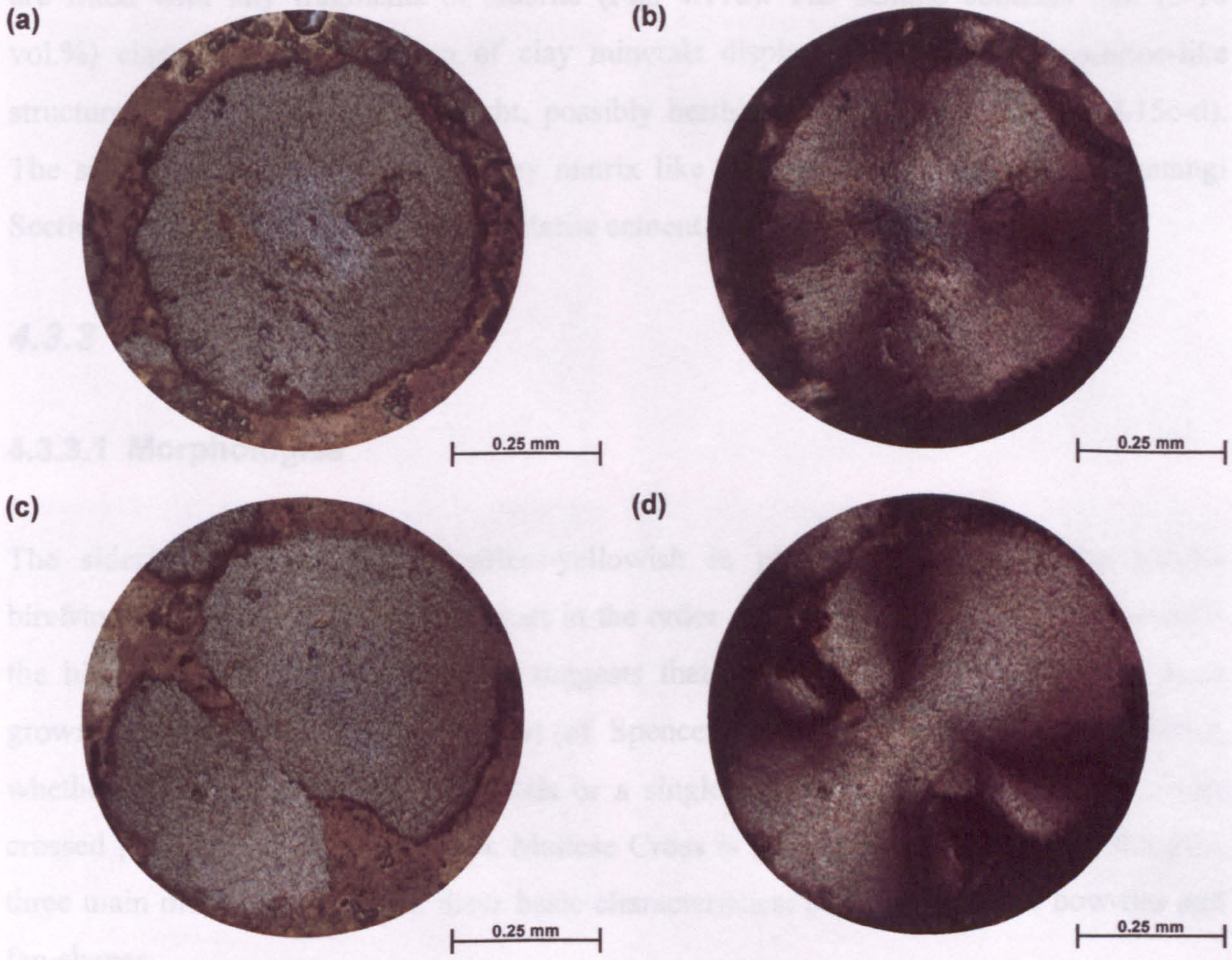

Fig. 4.16. Photomicrographs of siderite spherules from sample SUF.8.2, ironstone, Rokhagi Section, *ca.* 3.5 km SE of Hvalba, Suðuroy, Faeroe Islands. (a) Perfect siderite spherule showing no internal segmentation. (b) Same view as in (a) under cross-polarised light. Notice the Maltese Cross extinction pattern. (c) Bow-tie shaped siderite spherule, which has grown unevenly. (d) Same view as in (c) under cross-polarised light. Notice the Maltese Cross extinction pattern.

probably as a result of compaction (Figs. 4.17a-b). The crystallography of the spherules is discussed in detail in Section 4.3.3.

The sample contains *ca.* 5-10 vol.% of plant remains with the cellular structure preserved, having been replaced by microcrystalline siderite (Figs. 4.15c-h). The largest observed plant material is a tabular fragment that measures *ca.* 6 x 1 mm. Charcoal (burnt wood) (cf. Retallack 2001) is also observed as occluded fragments within siderite under the SEM (Fig. 4.17c). Borings into the sides of siderite spherules are observed under the SEM and are filled with tiny fragments of siderite (Fig. 4.17d). The sample contains rare (5-10 vol.%) clasts that are made up of clay minerals displaying distinctive serpentine-like structures under cross-polarised light, possibly berthierine or chamosite (Figs. 4.15c-d). The sample does not contain a clayey matrix like sample SUF.1.2, Unit 3, Ulingatangi Section, but has a weakly developed siderite cement.

4.3.3 Crystallography

4.3.3.1 Morphologies

The siderite spherules are colourless-yellowish in plane-polarised light and exhibit birefringences on the Michel Levy chart in the order of 0.240. As all the spherules exhibit the highest birefringence possible it suggests that crystals forming the spherules have grown parallel to the c-axis (optic axis) (cf. Spencer 1925; Deans 1934; Hounslow 2001), whether it be numerous fibrous crystals or a single crystal (see Section 4.3.3.3). Under crossed polars a characteristic black Maltese Cross is observed. For grains over 0.5 mm, three main morphologies share these basic characteristics: perfect spherules, bow-ties and fan-shapes.

The perfect spherules show no segmentation and appear to be uniform in structure, compared to the spherules made up of distinctive fan-shaped segments. The black Maltese Cross observed under crossed polars within the perfect spherules commonly originates from the centre of the spherule, but off-centre exceptions do occur. The centres of the perfect spherules appear to be cryptocrystalline in structure, and have fibrous crystals radiating around the centre; spherules with this type of structure are known as sphaerosiderite or spherulitic siderite (Figs 4.18a-b).

The simplest bow-tie morphology observed is made up of two fans, commonly truncated at their bases, growing away from each other. However, a variation to this is observed; at

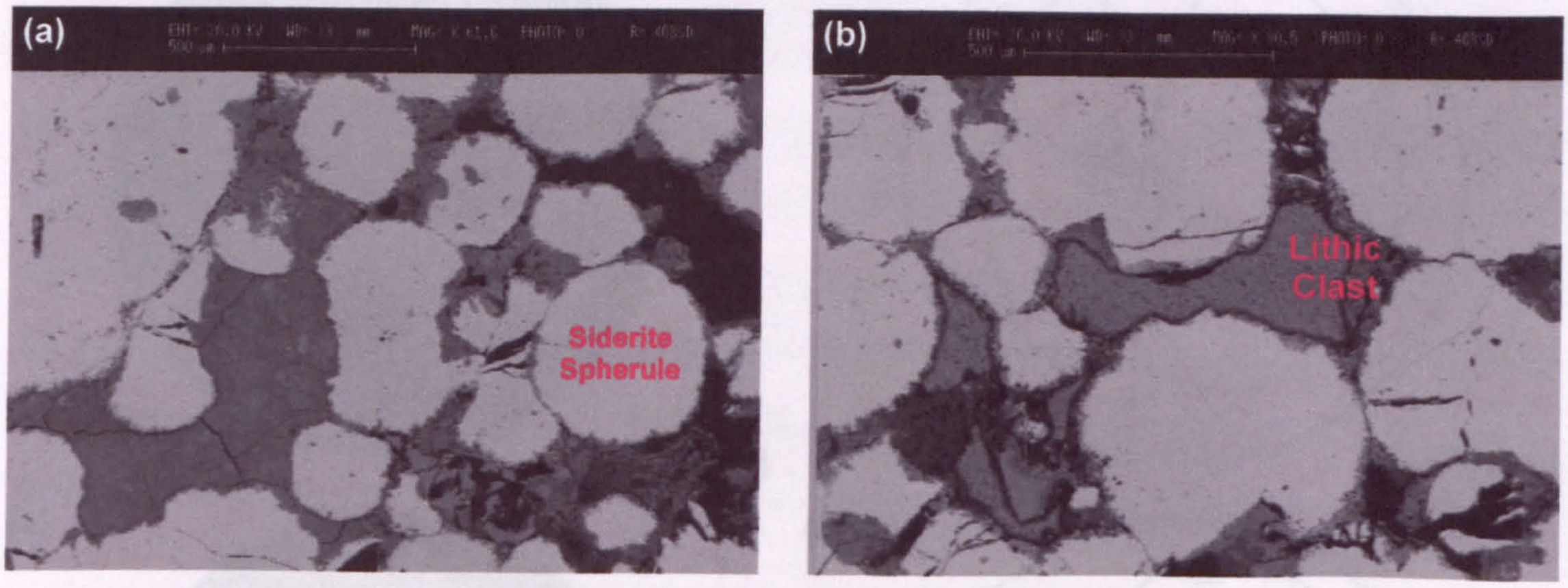

Fig. 4.17. SEM photomicrographs of sample SUF.8.2, ironstone, Rokhagi Section, *ca.* 3.5 km SE of Hvalba, Suðuroy, Faeroe Islands. (a) As a result of compaction a smaller siderite spherule has shattered, suggesting growth before burial. (b) A lithic clast that has been compacted around siderite spherules. (c) The red circle is highlighting an occluded charcoal fragment in siderite. (d) A boring into the side of a siderite spherule.

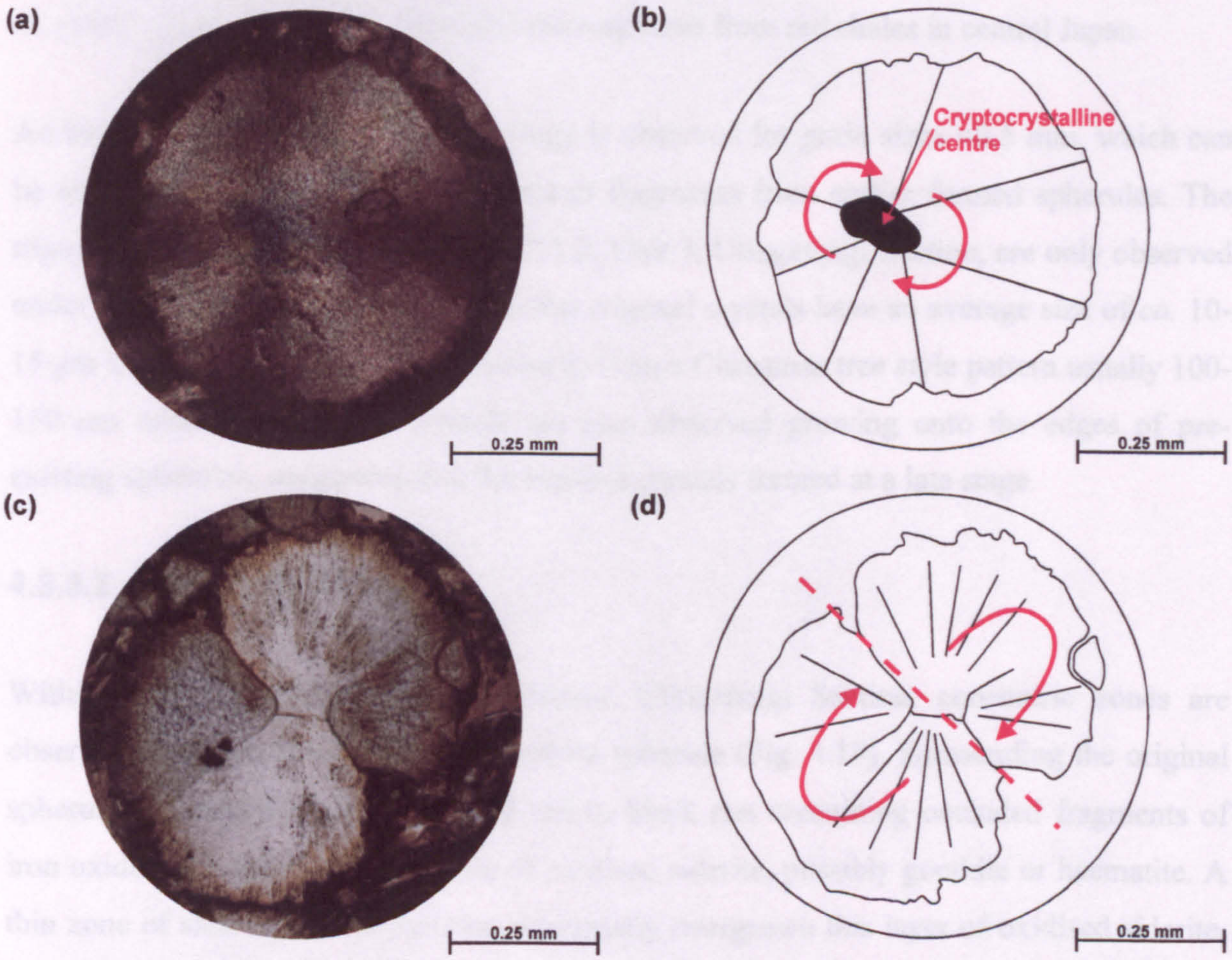

Fig. 4.18. Siderite spherule morphologies from the ironstone deposits of the Coal-bearing Formation. (a) A perfect siderite spherule from sample SUF.8.2, ironstone, Rokhagi Section, *ca.* 3.5 km SE of Hvalba, Suðuroy, Faeroe Islands. The photomicrograph is under cross-polarised light. (b) A line drawing of a perfect spherule in (a). The spherule has a cryptocrystalline centre surrounded by radiating, fibrous siderite crystals indicated by the arrows. This perfect spherule is a sphaerosiderite. (c) Bow-tie siderite spherule from sample SUF.1.2, Unit 3, clay ironstone, Ulingatangi Section, *ca.* 300 m north of Ulingatangi, *ca.* 1.2 km east of Froðba, Suðuroy, Faeroe Islands. The photomicrograph is under plane-polarised light. (d) A line drawing of the bow-tie siderite spherule in (c). The spherule shows spiralling growth to the right, which is symmetrical about an inverted mirror plane. This siderite spherule is a single crystal that has grown by the split crystal method. See Section 4.3.3.3 for further details.

some stage as the fan grows away from the centre of the bow-tie it begins to spiral to one side. The striking observation about this process is that it appears to be symmetrical about an inverted mirror plane running between the two fans (Figs. 4.18c-d). The spiralling can occur on either the left or right hand sides of the fans. Sometimes the spiralling results in the formation of what appears to be a perfect spherule, but individual fan-shaped segments can be identified within them, suggesting they grew from bow-tie morphologies. These bow-tie shaped spherules are very similar to the crystal structures observed by Minoura *et al.* (1991) for rhodochrosite ($MnCO_3$) microspheres from red shales in central Japan.

An irregular, sub-rectangular morphology is observed for grain sizes <0.5 mm, which can be either early fan development or broken fragments from earlier formed spherules. The trigonal siderite crystals in sample SUF.1.2, Unit 3, Ulingatangi Section, are only observed under the SEM (Fig. 4.12a). These perfect trigonal crystals have an average size of *ca.* 10-15 μm and occur in overlapping clusters to form a Christmas tree style pattern usually 100-150 μm wide. The trigonal crystals are also observed growing onto the edges of pre-existing spherules, suggesting that the trigonal crystals formed at a late stage.

4.3.3.2 Concentric Zonation

Within Unit 2, a volcaniclastic sandstone, Ulingatangi Section, concentric zones are observed surrounding a large 2 mm siderite spherule (Fig. 4.19). Surrounding the original spherule is a relatively thin and dark red to black rim containing occluded fragments of iron oxide. This rim is characteristic of oxidised siderite, possibly goethite or haematite. A thin zone of siderite (<0.05 mm) has syntaxially overgrown this layer of oxidised siderite. This very thin zone of siderite has an even thinner and poorly developed rim of oxidised siderite. A second concentric zone *ca.* 0.10-0.15 mm wide has syntaxially overgrown the previous thin zone of siderite. The rim to this second zone has not been oxidised but has a distinctive saw-tooth contact with a third and final concentric zone, *ca.* 0.10-0.15 mm wide. Each saw-tooth defines a segment within the outer concentric zone. This third, and outer, zone of siderite has an oxidised rim. Again, this third concentric zone is in optical continuity with the previous zones and the original spherule.

4.3.3.3 Crystal Formation

There are three ways to produce spherules: (i) overgrowth of crystals on an extraneous body (i.e. ooid) (Fig. 4.20a), (ii) growth of crystals from a cryptocrystalline centre (Fig. 4.20b), and (iii) split crystal growth (Fig. 4.20c) (Grigor'ev 1965). The spherules produced

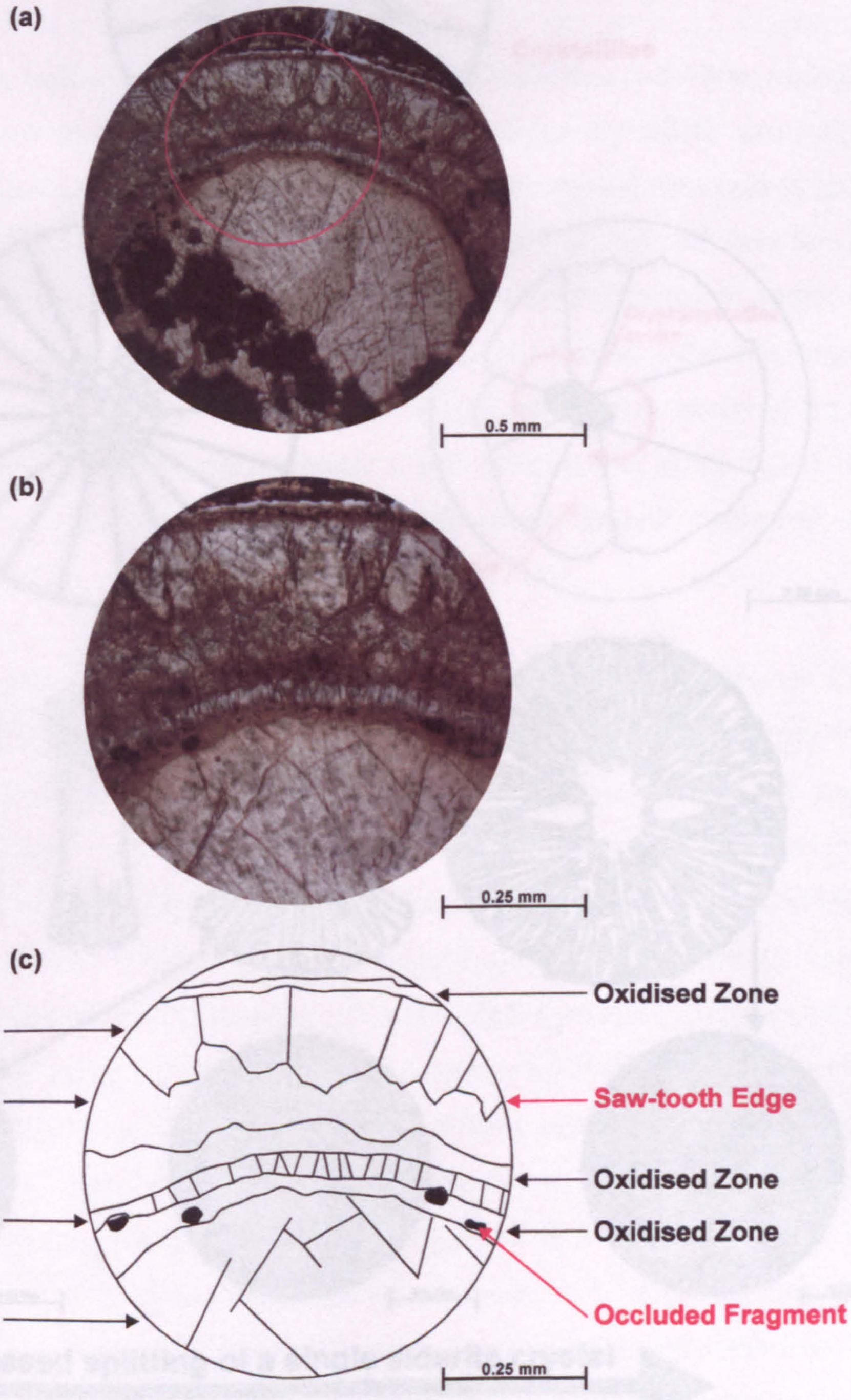

Fig. 4.19. Concentric zoning to a siderite spherule from Unit 2, volcaniclastic sandstone, Ulingatangi Section, *ca.* 300 m N of Ulingatangi, *ca.* 1.2 km E of Froðba, Suðuroy, Faeroe Islands. (a) Photomicrograph under plane polarised light that shows the location of (b) & (c). (b) Plane-polarised light photomicrograph of three siderite growth zones. (c) Line drawing of (b). The drawing picks out 6 different zones. Three zones represent periods of oxidation. The diagram also identifies three zones of different siderite growth mechanisms. See Section 4.3.3.3 for further details.

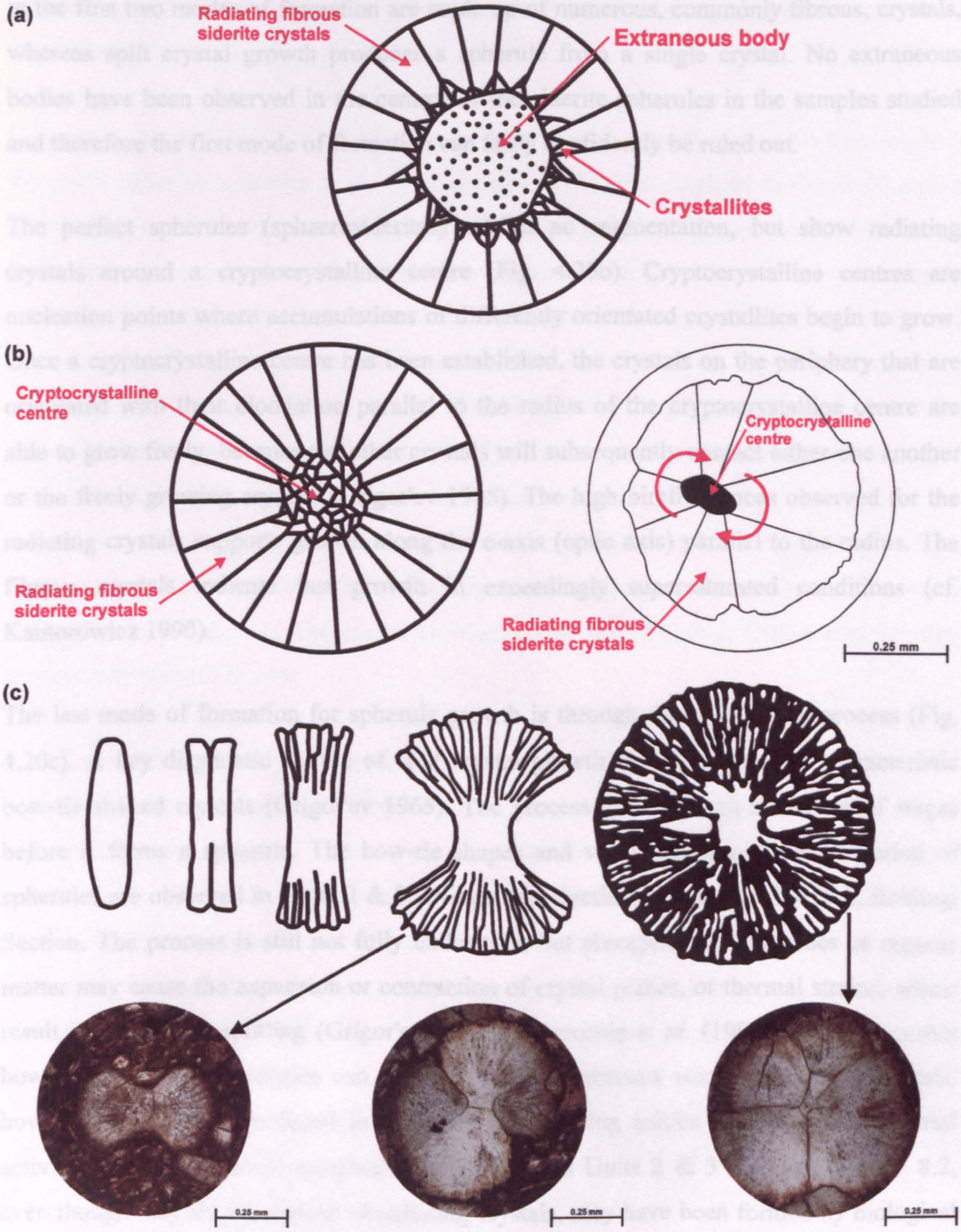

Fig. 4.20. Modes of spherule formation after Grigor'ev (1965). (a) Growth of numerous crystallites on an extraneous body. The crystals eventually become orientated parallel to the c-axis and grow in this direction forming a radiating extinction pattern. (b) Growth from the accumulation of crystallites. Crystals on the periphery of the cryptocrystalline centre become orientated parallel to the c-axis and grow in this direction forming a radiating extinction pattern. This mode of formation is compared to a spherule from sample SUF.8.2, ironstone, Rokhagi Section, *ca.* 3.5 km SE of Hvalba, Suðuroy, Faeroe Islands. (c) Growth by the split crystal mechanism. The schematic drawings of Grigor'ev (1965) show various stages in the formation of a spherule through splitting of a single crystal. This is compared to three split crystals from sample SUF 1.2, Unit 3, clay ironstone, Ulingatangi Section, *ca.* 300 m N of Ulingatangi, *ca.* 1.2 km E of Froðba, Suðuroy, Faeroe Islands. The degree of splitting increases from left to right. The first photomicrograph shows a typical bow-tie morphology, which progresses through a spiralling bow-tie to a spherule made up of segments of a split crystal.

in the first two modes of formation are made up of numerous, commonly fibrous, crystals, whereas split crystal growth produces a spherule from a single crystal. No extraneous bodies have been observed in the centres of the siderite spherules in the samples studied and therefore the first mode of formation can fairly confidently be ruled out.

The perfect spherules (sphaerosiderites) exhibit no segmentation, but show radiating crystals around a cryptocrystalline centre (Fig. 4.20b). Cryptocrystalline centres are nucleation points where accumulations of differently orientated crystallites begin to grow. Once a cryptocrystalline centre has been established, the crystals on the periphery that are orientated with their elongation parallel to the radius of the cryptocrystalline centre are able to grow freely, because the other crystals will subsequently contact either one another or the freely growing crystals (Grigor'ev 1965). The high birefringences observed for the radiating crystals supports growth along the c-axis (optic axis) parallel to the radius. The fibrous crystals indicate fast growth in exceedingly supersaturated conditions (cf. Kantorowicz 1990).

The last mode of formation for spherule growth is through the split crystal process (Fig. 4.20c). A key diagnostic feature of split crystal growth is the presence of characteristic bow-tie shaped crystals (Grigor'ev 1965). The process goes through a number of stages before it forms a spherule. The bow-tie shapes and various stages to the formation of spherules are observed in Units 2 & 3, Ulingatangi Section and sample SUF.8.2, Rokhagi Section. The process is still not fully understood but absorption of impurities or organic matter may cause the expansion or contraction of crystal planes, or thermal strains, which result in the crystal splitting (Grigor'ev 1965). Verrecchia *et al.* (1995) have shown that bow-tie shaped morphologies can be made up of numerous acicular radiating crystals, however, these were produced in a system precipitating calcite through cyanobacterial activity. Thus, the bow-tie morphologies observed in Units 2 & 3 and sample SUF 8.2, even though they do not consist of radiating crystals, may have been formed by biological factors, this has tentatively been suggested for the formation of siderite spherules from the Upper Carboniferous, England, by Hounslow (2001). Petrun (1958) suggested that split crystal formation in calcite crystals was caused by isomorphic impurities of manganese, with crystals containing 4-12 wt.% $MnCO_3$. This could be a possible reason for the split crystal growth observed in the present siderite spherules, as they contain 1-13 wt.% $MnCO_3$ (see Section 4.3.4). Fernández-Díaz *et al.* (1996) have shown that under high values of supersaturation calcite crystals will form spheres and at lower values dumbbell-like forms are observed. Therefore, the bow-tie shaped and associated siderite spherule

morphologies may have formed under supersaturated conditions analogous with those described by Fernández-Díaz *et al.* (1996).

Concentric zonation is a common feature associated with the formation of spherules. It is the result either of a change in the concentration of the pore fluid, or in the precipitating conditions, or is due to a mechanical agent (Grigor'ev 1965). Once conditions become favourable again, growth continues on the periphery of the spherule and this can occur in two ways (Fig. 4.21). The first involves the formation of new crystallites on the surface of the spherule. These crystallites will grow in the same way as crystallites around a cryptocrystalline centre, that is to say that the preferred growth orientation will be perpendicular to the surface of the spherule. The second method involves the formation of new embryonic split crystals on the surface of the spherule. If this occurs then the boundary between the original spherule and the new concentric zone will exhibit a saw-tooth appearance (Grigor'ev 1965). Therefore, each segment defined by the saw-tooth texture is a new spherule. The concentric zones observed in Unit 2, Ulingatangi Section, exhibit both types of growth.

It has been demonstrated that two modes of formation exist for the formation of siderite spherules. The primary mode of formation is by the process of split crystal growth. This is supported by the range of bow-tie morphologies observed as well as the saw-tooth concentric growth zones. The majority of siderite spherules are, therefore, not made up of groups of fibrous crystals but of subunits of a single crystal. However, the perfect spherules (sphaerosiderites) are made up of fibrous crystals radiating round a cryptocrystalline centre. Both modes of formation occur under supersaturated conditions.

4.3.4 Mineral Chemistry

Electron probe micro-analysis techniques have been used to confirm the compositions of the siderite spherules. All mineral analyses were determined on a Cameca SX50 electron probe micro-analyser in the Division of Earth Sciences, University of Glasgow, utilizing wavelength-dispersal techniques. Standard operating conditions were a 20 kV accelerating voltage, a 10 nA beam current, and an integrated counting time of 20 seconds per element. The beam diameter was in the region of 10 μm. Standards comprised well-characterised natural silicates and pure metals. ZAF and dead-time corrections were applied.

Two perfect spherules (sphaerosiderites) were picked from each sample, SUF.1.2 (Unit 3, Ulingatangi Section) and SUF.8.2 (Rokhagi Section), which did not contain any or very

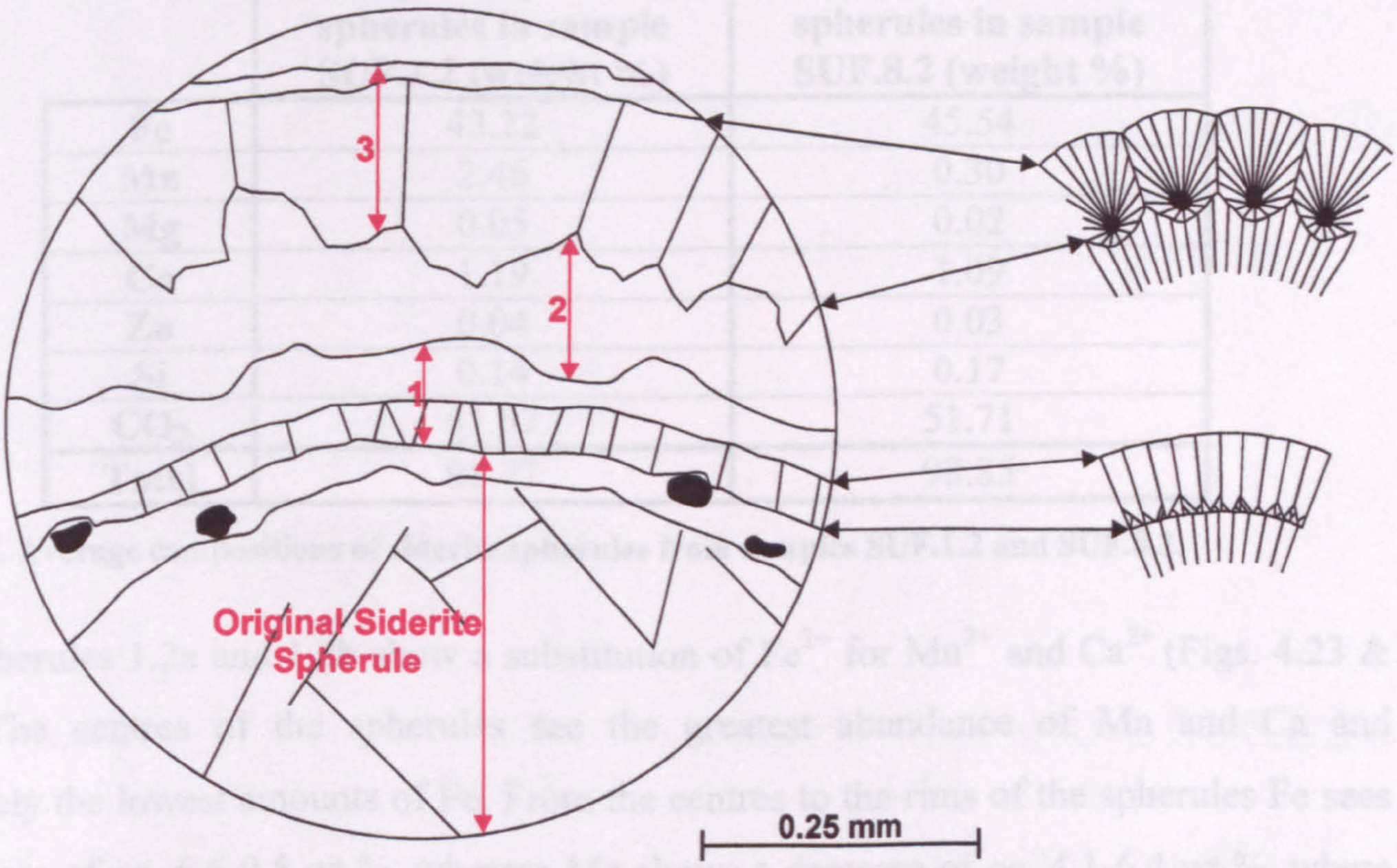

Fig. 4.21. Formation of concentric zoning in a siderite spherule from Unit 2, volcaniclastic sandstone, Ulingatangi Section, *ca.* 300 m N of Ulingatangi, *ca.* 1.2 km E of Froðba, Suðuroy, Faeroe Islands. The line drawing is of three concentric growth zones onto the periphery of an already formed spherule. See Figure 4.19 for the photomicrograph of the siderite spherule. The two-headed red arrows identify the growth zones. The zones usually consist of a siderite overgrowth and an oxidised rim, apart from zone 2 which has no oxidised rim. Zones 1 and 3 are compared to the diagrams of Grigor'ev (1965) for the formation of concentric zoning in spherulites. Zone 1 represents the formation of new crystallites of normal crystals on the surface of the original spherule. Zone 3 represents the formation of new embryonic spherules on the surface of the previous growth zone, which grow through the split crystal growth mechanism.

few occluded matrix fragments. Analyses were obtained along traverses across the spherules. Sample SUF.1.2 contains the spherules 1.2a and 1.2b, which were 519 μm and 459 μm wide and had 50 and 40 analyses taken across the diameters of the spherules, respectively (Fig 4.22a-b). Sample SUF.8.2 contains spherules 8.2a and 8.2b, which were 651 μm and 598 μm wide, respectively; each had 50 analyses taken across the diameters of the spherules (Fig. 4.22c-d). Average compositions for the spherules from samples SUF.1.2 and SUF.8.2 can be seen in Table 4.1 (see Appendix A for the all the siderite spherule analyses). Both samples are generally quite pure, containing 90-94 wt.% $FeCO_3$.

	Average composition of spherules in sample SUF.1.2 (weight %)	Average composition of spherules in sample SUF.8.2 (weight %)
Fe	43.22	45.54
Mn	2.46	0.30
Mg	0.05	0.02
Ca	1.19	1.09
Zn	0.04	0.03
Si	0.14	0.17
CO_3	51.67	51.71
Total	98.77	98.85

Table 4.1. Average compositions of siderite spherules from samples SUF.1.2 and SUF.8.2.

Both spherules 1.2a and 1.2b show a substitution of Fe^{2+} for Mn^{2+} and Ca^{2+} (Figs. 4.23 & 4.24). The centres of the spherules see the greatest abundance of Mn and Ca and conversely the lowest amounts of Fe. From the centres to the rims of the spherules Fe sees an increase of *ca.* 6.6-9.5 wt.%, whereas Mn shows a decrease of *ca.* 4.1-6.4 wt.%, where the amount of Mn in the rims of the spherules is negligible. Ca also shows a decrease from the centres to the rims from *ca.* 1.8-2.0 wt.% to amounts that are negligible. Mg concentrations are very constant across the spherules with amounts varying on average by only 0.07 wt.%. This chemical zonation observed within the perfect spherules of sample SUF.1.2 can be quite clearly seen in the elemental maps of spherule 1.2c (Fig. 4.25).

Spherules 8.2a and 8.2b both show a substitution of Fe^{2+} for Mn^{2+} and Ca^{2+} (Figs. 4.26 & 4.27), but it is not as marked as that observed in the spherules from sample SUF.1.2. The centres of the spherules have the greatest abundance of Ca and conversely the lowest amounts of Fe. From the centres to the rims of the spherules there is an increase of *ca.* 2.7-3.0 wt.% Fe, whereas Ca shows a decrease of *ca.* 1.7-1.9 wt.%. Mn concentrations are high towards the centre of the spherules with *ca.* 0.5 wt.%; this then decreases towards the rim to negligible amounts before it increases at the rims to *ca.* 0.75 wt.%. Mg is constant across the spherules with amounts varying on average by only 0.07 wt.%.

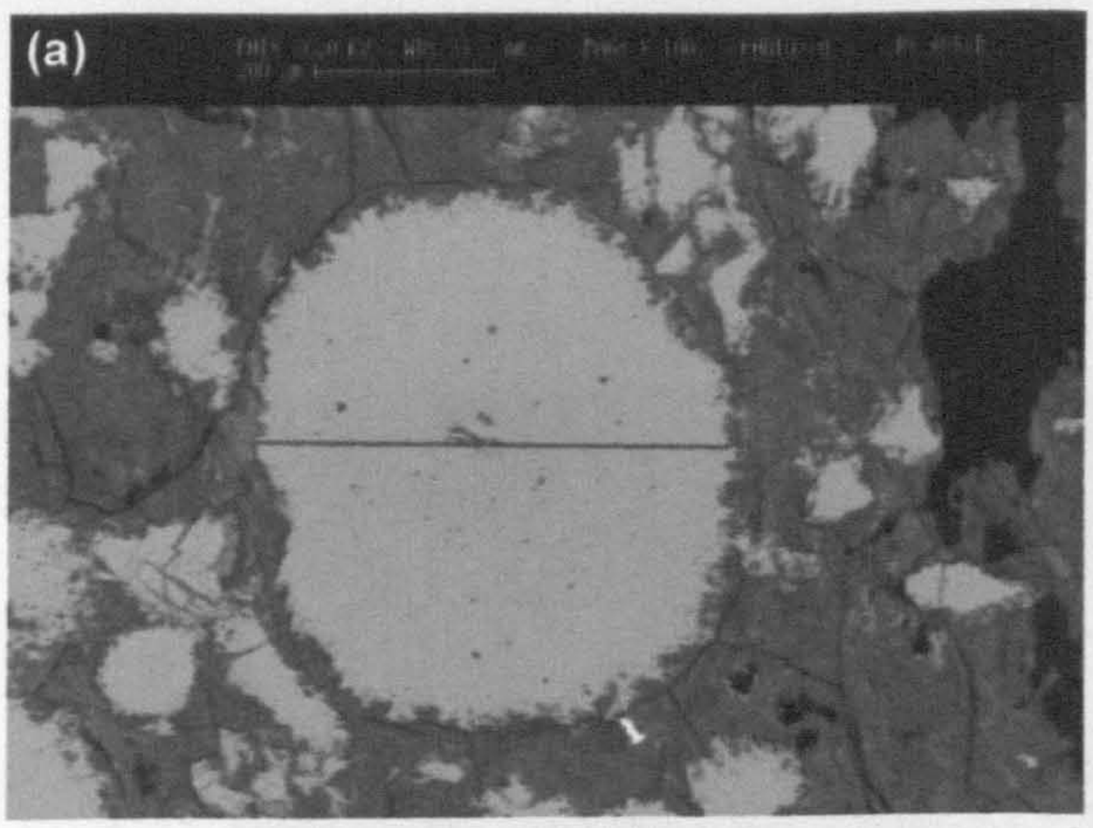

Siderite Spherule SUF.1.2a
519 µm wide
50 analysis points
4 erroneous results

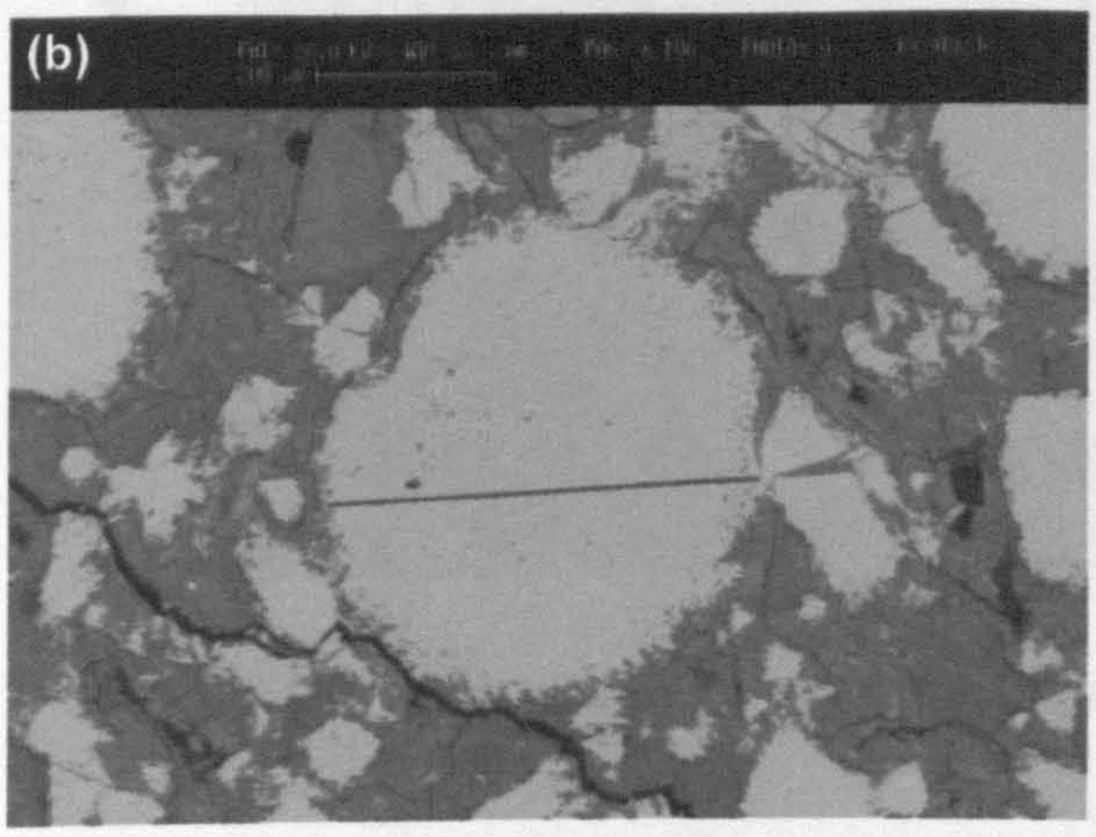

Siderite Spherule SUF.1.2b
459 µm wide
40 analysis points

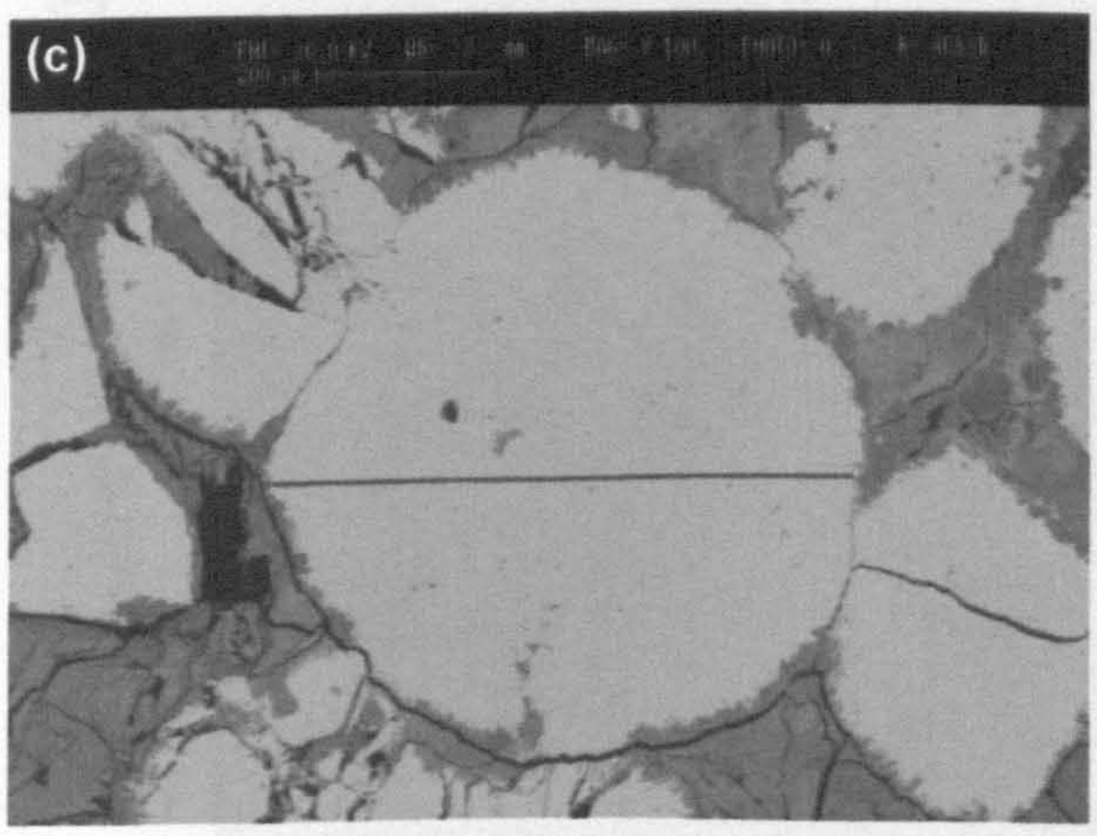

Siderite Spherule SUF.8.2a
651 µm wide
50 analysis points

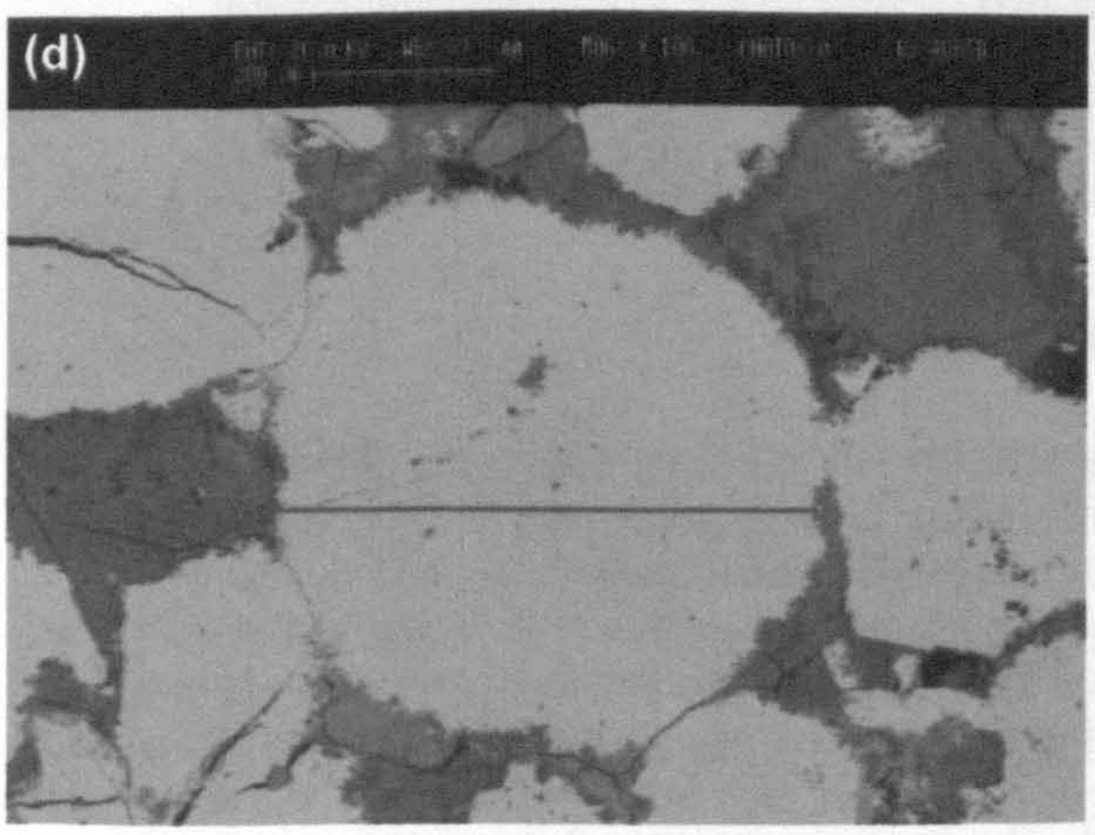

Siderite Spherule SUF.8.2b
598 µm wide
50 analysis points

Fig. 4.22. SEM photomicrographs of four siderite spherules that were geochemically analysed along traverses, highlighted by the red lines. (a) & (b) Siderite spherules from sample SUF.1.2, Unit 3, clay ironstone, Ulingatangi Section, *ca.* 300 m N of Ulingatangi, *ca.* 1.2 km E of Froðba, Suðuroy, Faeroe Islands. (c) & (d) Siderite spherules from sample SUF.8.2, ironstone, Rokhagi Section, *ca.* 3.5 km SE of Hvalba, Suðuroy, Faeroe Islands. The results from the analyses can be seen in Figures 4.23, 4.24, 4.26. and 4.27.

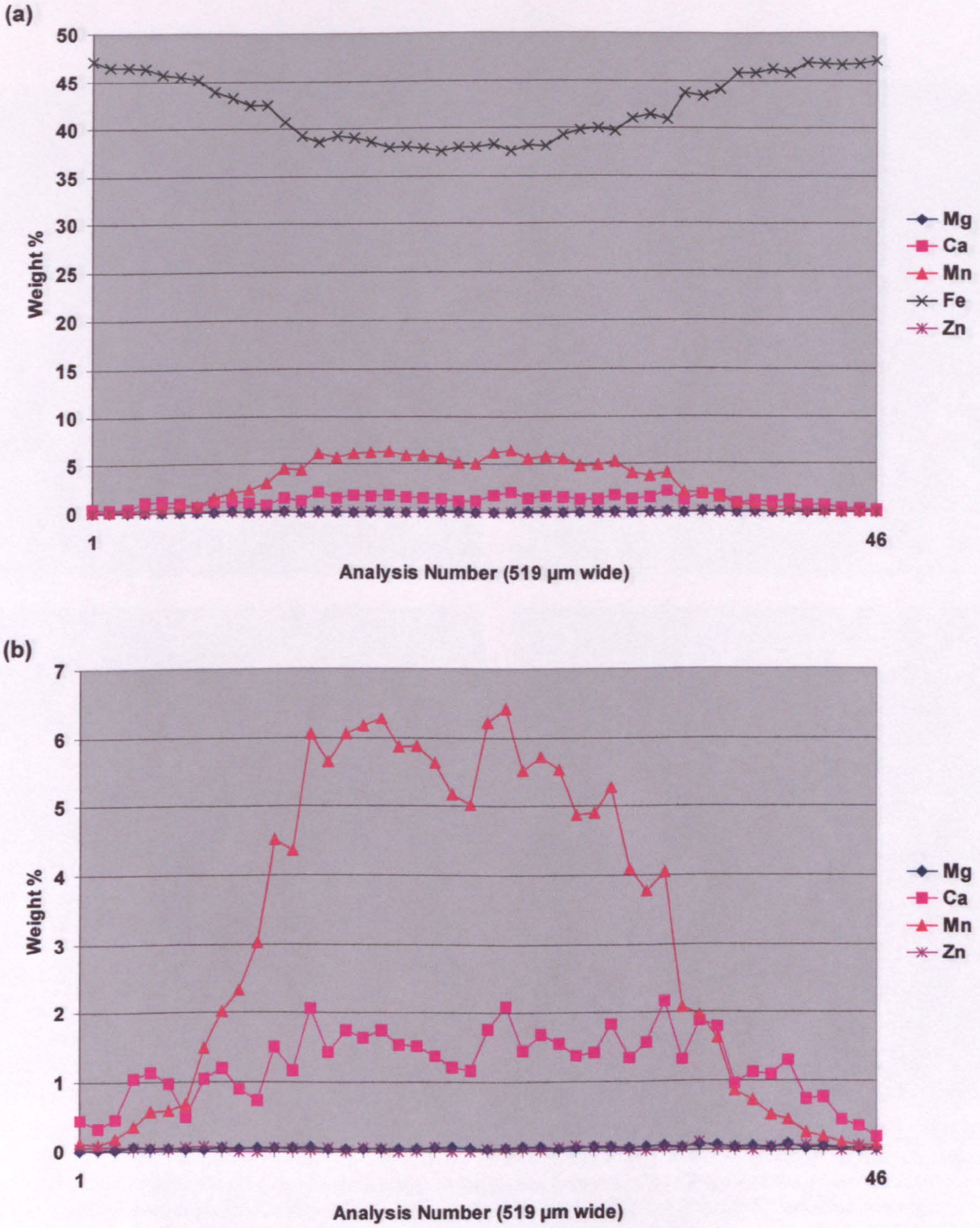

Fig. 4.23. Mineral chemistry data for the siderite spherule SUF.1.2a, Unit 3, clay ironstone, Ulingatangi Section, *ca.* 300 m N of Ulingatangi, *ca.* 1.2 km E of Froðba, Suðuroy, Faeroe Islands. 50 spot analyses were taken across the 519 µm wide spherule; there were four erroneous results. (a) & (b) The graphs show that the centre of the spherule sees the greatest abundance of Mn and Ca and conversely the lowest amounts of Fe. From the centre to the rim of the spherule Fe sees an increase of *ca.* 9.5 wt.%, whereas Mn shows a decrease of *ca.* 6.4 wt.%, where the amount of Mn in the rim of the spherule is negligible. Ca also shows a decrease from the centre to the rim in the order of *ca.* 2.0 wt.%. Mg and Zn concentrations are very constant across the spherule with amounts varying by only 0.08 and 0.12 wt.%, respectively.

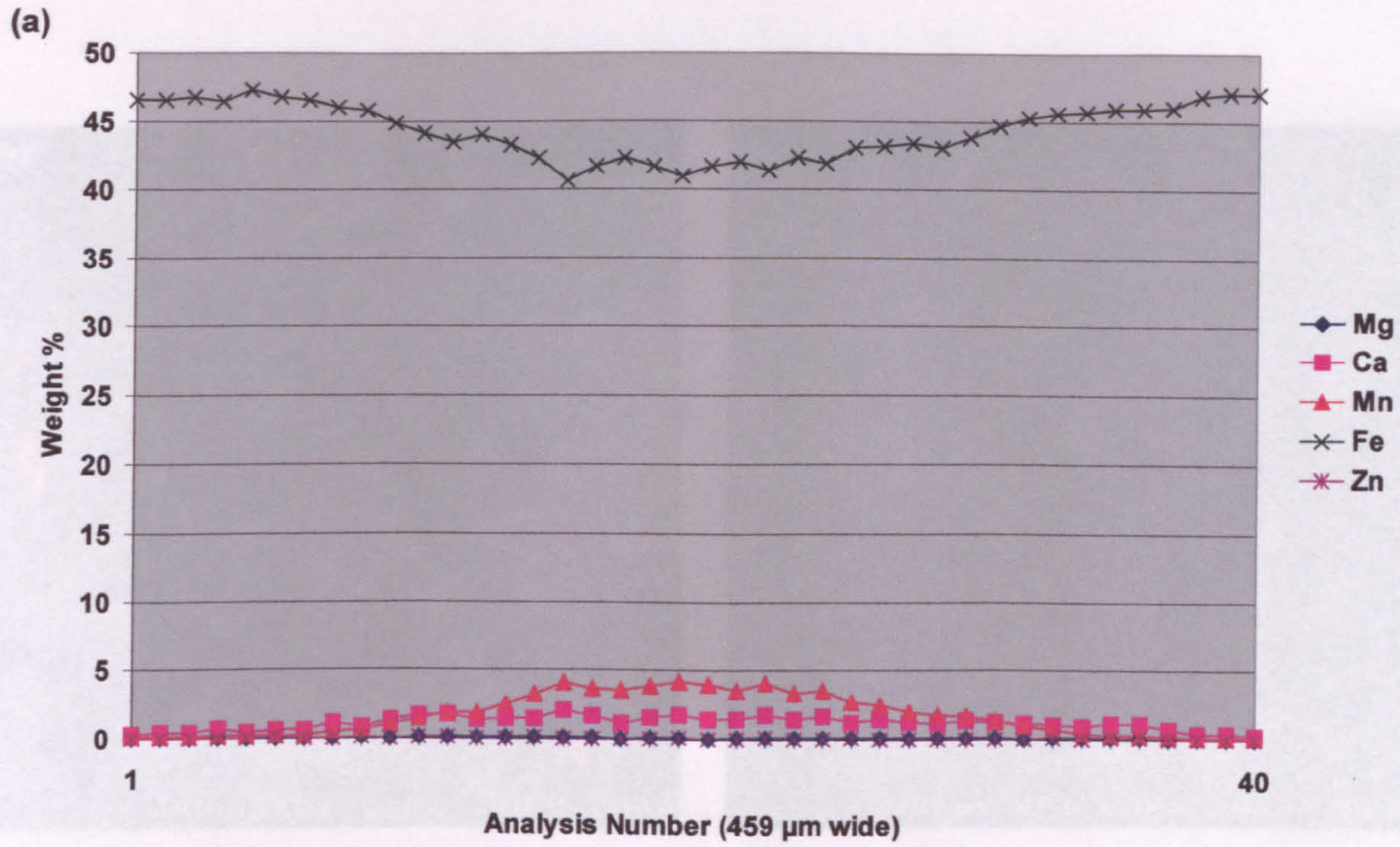

Fig. 4.24. Mineral chemistry data for the siderite spherule SUF.1.2b, Unit 3, clay ironstone, Ulingatangi Section, *ca.* 300 m N of Ulingatangi, *ca.* 1.2 km E of Froðba, Suðuroy, Faeroe Islands. 40 spot analyses were taken across 459 µm wide spherule. (a) & (b) The graphs show that the centre of the spherule sees the greatest abundance of Mn and Ca and conversely the lowest amounts of Fe. From the centre to the rim of the spherule Fe sees an increase of *ca.* 6.6 wt.%, whereas Mn shows a decrease of *ca.* 4.1 wt.%, where the amount of Mn in the rim of the spherule is negligible. Ca also shows a decrease from the centre to the rim in the order of *ca.* 1.8 wt.%. Mg and Zn concentrations are very constant across the spherule with amounts varying by only 0.07 and 0.09 wt.%, respectively.

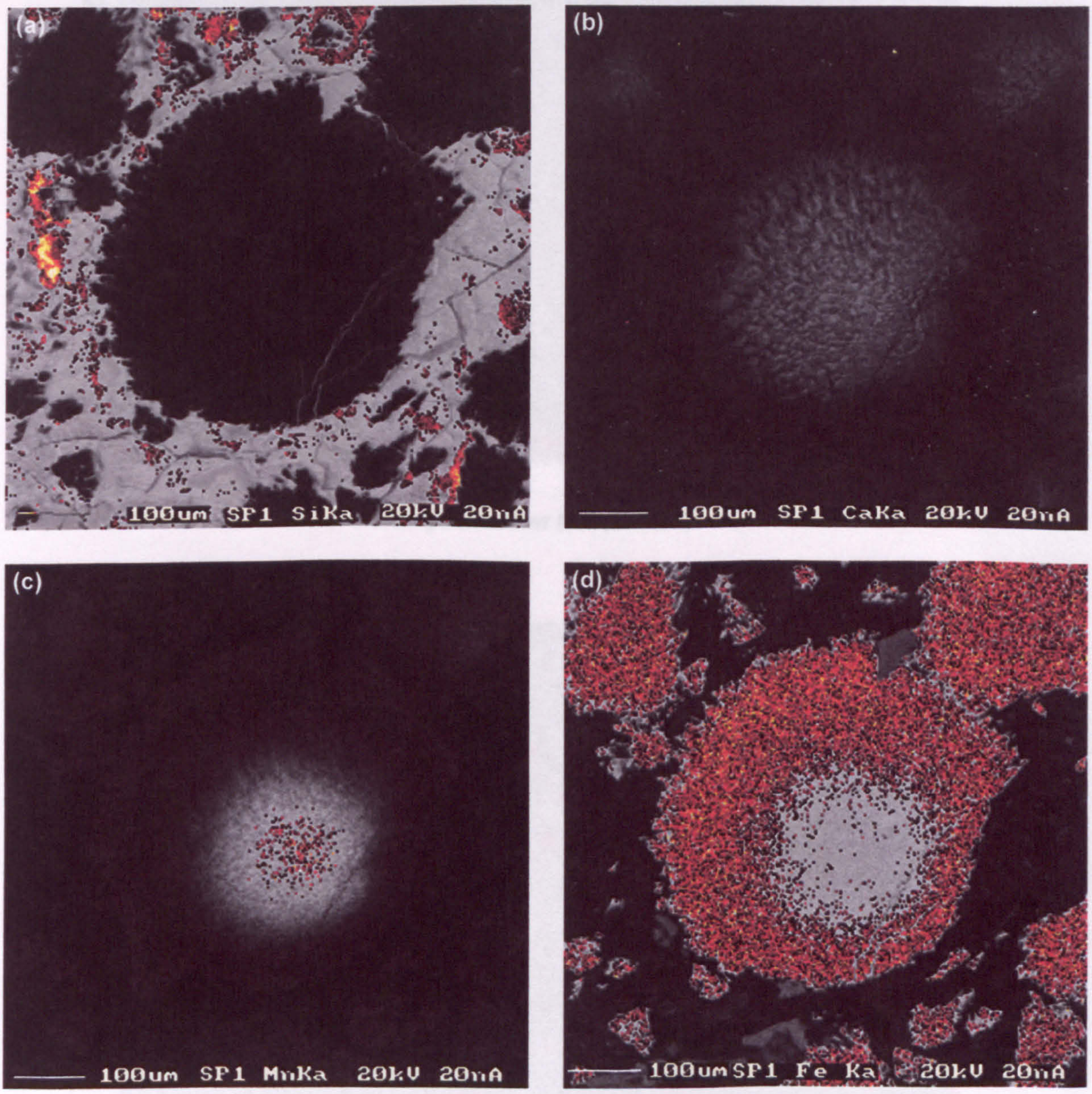

Fig. 4.25. Elemental maps of a siderite spherule SUF.1.2c from Unit 3, clay ironstone, Ulingatangi Section, *ca.* 300 m N of Ulingatangi, *ca.* 1.2 km E of Froðba, Suðuroy, Faeroe Islands. Areas of highest concentration of a particular element display the brightest colours. The elemental maps compare very well to the mineral compositions of the siderite spherules (see Figs. 4.23 & 4.24). (a) Elemental map for silicon (Si). Silicon is used to define the shape of the spherule, which appears black, due to the lack of silicon in the spherule. Silicon is concentrated within the clayey matrix of the rock. (b) Elemental map for calcium (Ca). Calcium appears to be diffuse throughout the spherule apart from the rim regions, which show a marked depletion. (c) Elemental map for manganese (Mn). The core of the spherule shows enrichment in manganese and depletion at the rim. (d) Elemental map for iron (Fe). The core of the spherule shows depletion in iron compared to the rim.

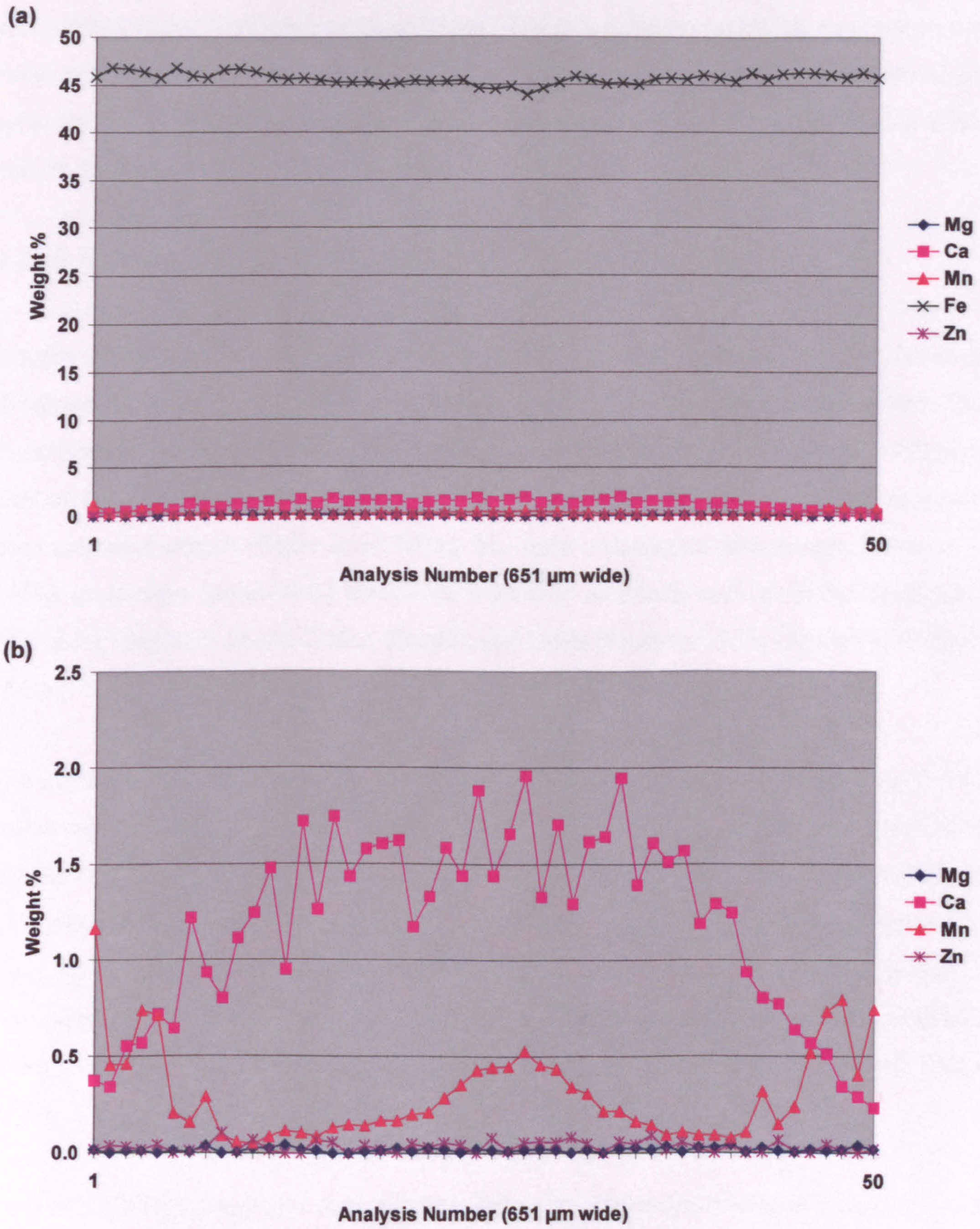

Fig. 4.26. Mineral chemistry data for the siderite spherule SUF.8.2a, ironstone, Rokhagi Section, *ca.* 3.5 km SE of Hvalba, Suðuroy, Faeroe Islands. 50 spot analyses were taken across the 651 µm wide spherule. (a) & (b) The graphs show that the centre of the spherule has the greatest abundance of Ca and conversely the lowest amounts of Fe. From the centre to the rim of the spherule there is an increase of *ca.* 3.0 wt.% Fe, whereas Ca shows a decrease of *ca.* 1.7 wt.%. Mn concentrations are high towards the centre of the spherule with *ca.* 0.5 wt.%; this then decreases towards the rim to negligible amounts before it increases at the rims to *ca.* 0.75 wt.%. Mg and Zn concentrations are fairly constant across the spherule with amounts varying by only 0.04 and 0.11 wt.%, respectively.

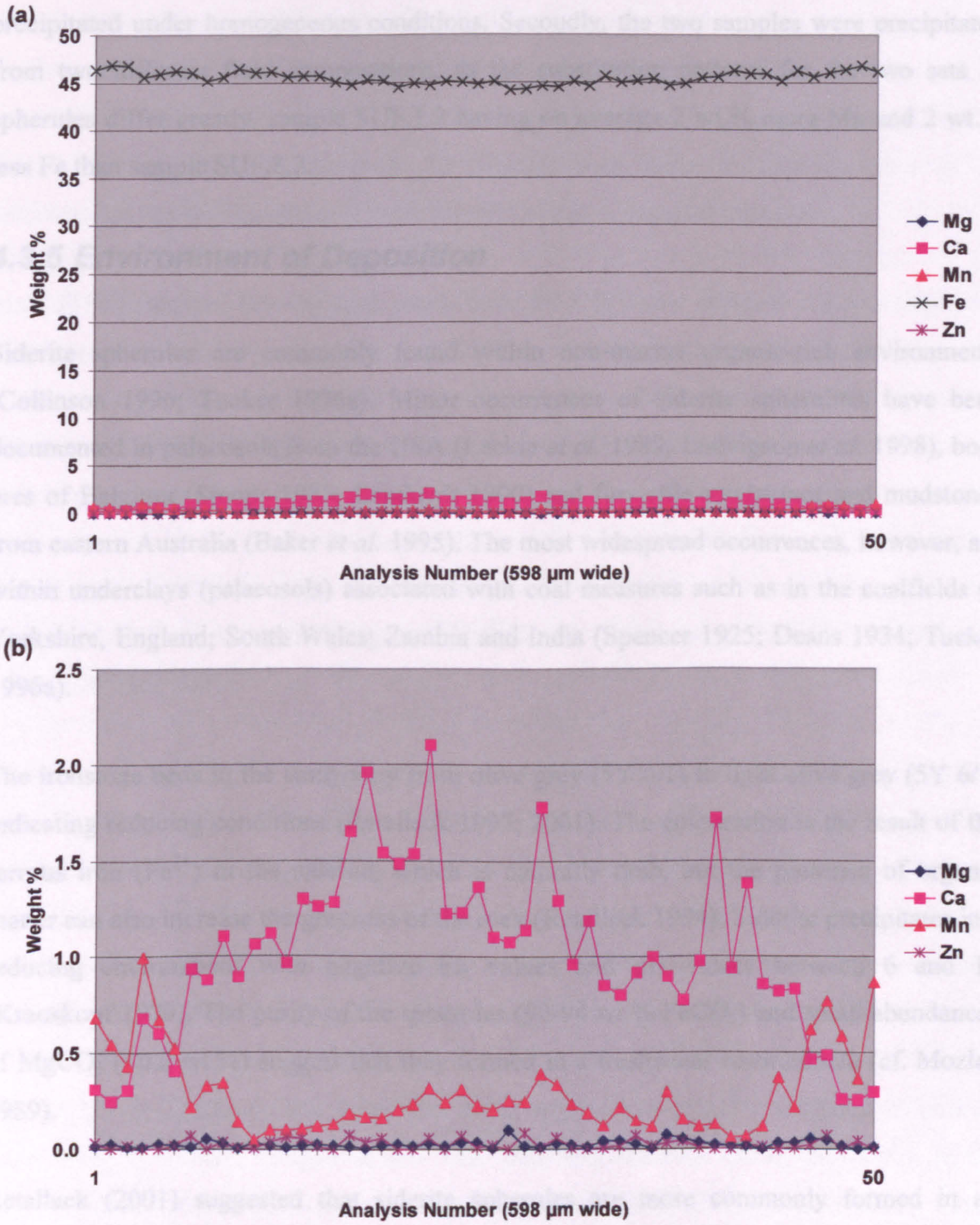

Fig. 4.27. Mineral chemistry data for the siderite spherule SUF.8.2b, ironstone, Rokhagi Section, *ca.* 3.5 km SE of Hvalba, Suðuroy, Faeroe Islands. 50 spot analyses were taken across the 598 µm wide spherule. (a) & (b) The graphs show that the centre of the spherule has the greatest abundance of Ca and conversely the lowest amounts of Fe. From the centre to the rim of the spherule there is an increase of *ca.* 2.7 wt.% Fe, whereas Ca shows a decrease of *ca.* 1.9 wt.%. Mn concentrations are high towards the centre of the spherule with *ca.* 0.4 wt.%; this then decreases towards the rim to negligible amounts before it increases at the rims to *ca.* 0.75 wt.%. Mg and Zn concentrations are fairly constant across the spherule with amounts varying by only 0.1 and 0.08 wt.%, respectively.

From the chemical analyses obtained from the samples SUF.1.2 and SUF.8.2 two trends are observed. Firstly, the mineral chemistries obtained from the two samples are replicated from spherule to spherule within each sample, suggesting that the spherules were precipitated under homogeneous conditions. Secondly, the two samples were precipitated from two different fluid compositions, as the substitution patterns for the two sets of spherules differ greatly, sample SUF.1.2 having on average 2 wt.% more Mn and 2 wt.% less Fe than sample SUF.8.2.

4.3.5 Environment of Deposition

Siderite spherules are commonly found within non-marine organic-rich environments (Collinson 1996; Tucker 1996a). Minor occurrences of siderite spherulites have been documented in palaeosols from the USA (Leckie *et al.* 1989; Ludvigson *et al.* 1998), bog-ores of Belgium (Stoops 1983; Landuydt 1990) and fluviatile sandstones and mudstones from eastern Australia (Baker *et al.* 1995). The most widespread occurrences, however, are within underclays (palaeosols) associated with coal measures such as in the coalfields of Yorkshire, England; South Wales; Zambia and India (Spencer 1925; Deans 1934; Tucker 1996a).

The ironstone beds in the study vary from olive grey (5Y 4/1) to light olive grey (5Y 6/1) indicating reducing conditions (Retallack 1997; 2001). The colouration is the result of the ferrous iron (Fe^{2+}) in the siderite, which is naturally drab, but the presence of organic matter can also increase the greyness of the rock (Retallack 1994). Siderite precipitates in a reducing environment with negative Eh values and pH values between 6 and 10 (Krauskopf 1979). The purity of the spherules (90-94 wt.% $FeCO_3$) and small abundances of $MgCO_3$ (<0.2 wt.%) suggest that they formed in a freshwater environment (cf. Mozley 1989).

Retallack (2001) suggested that siderite spherules are more commonly formed in an intermediate redox (near-neutral Eh) environment. Intermediate redox environments can be partly or periodically waterlogged compared to reducing environments that are continually waterlogged (Baas-Becking *et al.* 1960). Berner (1981) suggested that a sediment goes through four phases during diagenesis, with increasing reduction: i) oxic, ii) post-oxic iii) sulphidic and iv) methanic. The post-oxic to methanic phases are all under anoxic conditions. Siderite is known to precipitate in the post-oxic and methanic phases, whereas sulphides are precipitated in the sulphidic phase (Berner 1981). The lack of any sulphide minerals, particularly pyrite (FeS_2), suggests that the environments never reached

extreme reduction, i.e. continually waterlogged. However, as dissolved sulphate (SO_4) is extremely low in freshwater pore fluids sulphides are less common in non-marine environments (Berner 1981). Moore (1992) suggested that in a non-marine environment the sulphidic phase is of little importance and a sediment in a non-marine environment may reach extreme reduction without precipitating pyrite in the process. Therefore, the lack of any sulphide minerals cannot be used as an indicator of the degree of reduction in non-marine settings, and consequently the siderite may have been precipitated in an environment that was continually waterlogged i.e. one of extreme reduction.

Lund (1989) showed that the coal seams from the CBF were deposited in a eutrophic to mesotrophic lacustrine environment, which was surrounded by swamps. Over time the lacustrine environment changed to more oligotrophic conditions (Lund 1989). Eutrophic lakes are characterised by an abundance of dissolved plant nutrients and by a seasonal deficiency of oxygen in the hypolimnion (lowermost layer of the water column in a lake). The greyness of the beds, the association with overlying coal seams, the reducing waterlogged environment, and the close proximity of swamp environments suggests that the ironstone beds most likely represent palaeosols known as gleysols (cf. Mack *et al.* 1993; Retallack 2001).

Gleization (or gleying) is the soil forming process that produces distinctive grey gley soil beds (Retallack 2001). Gleization can also account for the presence of siderite spherules and spherulites, which suggest growth under supersaturated conditions at very fast rates (see Section 4.3.3.3). Gleization occurs in a post-oxic non-sulphidic waterlogged environment (Retallack 2001). Organic decomposition by aerobic micro-organisms consumes all the dissolved oxygen, but not enough to bring about sulphate (SO_4) reduction to produce hydrogen sulphide (H_2S), consequently, no sulphide minerals are precipitated (Berner 1981). Continued decomposition of the organic matter under anaerobic conditions takes place by nitrate, manganese and iron reduction, whereby ferric iron (Fe^{3+}), in the form of ferric hydroxides, is reduced to produce ferrous iron (Fe^{2+}) (Berner 1981). Ferric iron reduction and the lack of O_2 and H_2S may lead to supersaturated levels of bicarbonate (HCO_3), Fe^{2+} and Mn^{2+} in the pore fluids (Berner 1981; Kantorowicz 1990). These are favourable conditions to precipitate siderite ($FeCO_3$) and rhodochrosite ($MnCO_3$) (Berner 1981). These two minerals produce a complete series from Fe-rich to Mn-rich end-members (Chang 1996). The mineral chemistries obtained for the siderite spherules in samples SUF.1.2 and SUF.8.2 (see Section 4.3.4) show a marked substitution of Fe^{2+} for Mn^{2+}, supporting the model of supersaturated levels of Fe^{2+} and Mn^{2+} in the pore fluids. The concentration of Fe^{2+} in the pore fluids must have substantially exceeded the

concentration of Mn^{2+} because siderite spherules were precipitated rather than rhodochrosite. Ferric iron reduction is a much slower process than manganese reduction and as a consequence Mn^{2+} concentrations are higher in the cores of the siderite spherules before ferric iron reduction became dominant.

An accumulation of organic matter built up on the lake bottom rapidly became anoxic. Under anaerobic decomposition the organic matter was transformed into peat, which ultimately formed the coal overlying the ironstone beds. The lack of oxygen in the environment also prohibited the activity of animals and plants, and consequently the ironstone beds show little evidence of bioturbation or rootlets. There absence is a common feature associated with gleysols (Retallack 2001).

4.3.5.1 Ulingatangi Section

The basal volcaniclastic conglomerate (Unit 1) at Ulingatangi consists of aligned elliptical clasts, which suggest transport in a fluvial system (cf. Collinson 1996; Tucker 1996a). The conglomerate is overlain by Unit 2, a brownish black (5YR 2/1) volcaniclastic sandstone. The brownish black colour is due to the presence of ferric iron oxyhydrates (ferrihydrite and goethite) and ferric iron oxides (haematite) that indicates oxidising conditions (Retallack 2001). Rocks containing iron oxyhydrates and oxides are commonly termed ferruginous. The presence of the clay ironstone above and siderite spherules in the volcaniclastic sandstone tentatively suggests that the sandstone underwent soil-forming processes (cf. Retallack 2001). Ferruginous soils are typical of well-drained environments (Baas-Becking *et al.* 1960). However, the ferruginous sandstone contains sporadic siderite spherules and abundant siderite cement, which indicate a reducing environment. This suggests that the environment underwent alternating waterlogged (reducing) and well-drained (oxidising) periods. Periodically waterlogged palaeosols have been termed semi-gleysols by Besly & Fielding (1989).

The sporadic siderite spherules are only observed within fractures in the semi-gleysol, which has subsequently been cemented together by disseminated siderite, suggesting that the porosity was restricted to the fractures. One of the siderite spherules in the semi-gleysol exhibits concentric zonation implying four episodes of growth. The initial formation of the spherule was under reducing conditions, and was followed by a period in an oxidising environment whereby an oxidised rim was formed. This pattern of alternating reducing and oxidising conditions is repeated for a further three cycles; there are four cycles in total.

This pattern of zoning supports an environment that was periodically waterlogged and records a water table that fluctuated at least four times.

The volcaniclastic sandstone is overlain by Unit 3, the clay ironstone (gleysol), which was clearly formed under waterlogged, reducing conditions as described in Section 4.3.5. The clay ironstone is overlain by Unit 4, a brownish black (5YR 2/1) mudstone. The mudstone appears to have undergone alternating waterlogged (reducing) and well-drained (oxidising) periods akin to Unit 2, the volcaniclastic sandstone (semi-gleysol) underneath the clay ironstone. This is supported by the presence of ironstone nodules contained within the iron oxyhydrate and oxide rich mudstone. The clayey matrix in the ironstone nodules was most likely more organic-rich than the host mudstone, and thus an ideal site for the precipitation of siderite spherules. The abundant borings observed in the ironstone nodules suggests that the environment was oxygenated after the siderite spherules were precipitated, supporting a model for a periodically waterlogged environment. The mudstone (semi-gleysol) is overlain by a coal seam and an organic-rich mudstone that formed in a lacustrine environment (Lund 1983; 1989).

The Ulingatangi Section begins with the deposition of a fluvial conglomerate; this was followed by the deposition of a volcaniclastic sandstone. The sandstone was periodically waterlogged and in it siderite was precipitated as spherules or cement. From the zonation in one of the siderite spherules it can be demonstrated that it experienced at least four water table fluctuations. The sandstone became permanently waterlogged and a lake developed on the surface into which a clay unit was deposited. This clay unit was permanently waterlogged and consequently a reducing environment ensued into which siderite spherules were precipitated. The top of the clay unit underwent water table fluctuations and consequently saw the development of ironstone nodules during waterlogged periods. Eventually a subsequent lake developed on the surface of the claystone and plant materials accumulated leading to the formation of the coal seam and the organic-rich mudstone. The alternation between well-drained and waterlogged conditions most probably represents dry and wet seasons. The section may represent an alluvial floodplain environment (cf. Collinson 1996) or marginal areas of a lacustrine system (cf. Talbot & Allen 1996). The environment saw the formation of small seasonal lakes above actively forming gley soils.

4.3.5.2 Rokhagi Section

The coarse sand-grade ironstone from the Rokhagi Section was produced under a post-oxic reducing waterlogged environment, although it formed slightly differently from the clay

ironstone in the Ulingatangi Section. The Rokhagi ironstone has evidence of bioturbation and has little or no clay matrix. Bioturbation suggests that after the siderite spherules were precipitated the environment became oxygenated. This is supported by the oxidised rims, most likely goethite, of the spherules. The lack of a clay-matrix in the sample suggests that the siderite spherules either coalesced to form distinct, more resistant nodules within ironstone beds (cf. Kantorowicz 1990) or were precipitated directly from the hypolimnion. These scenarios are difficult to distinguish because the sample is from mine waste and not observed *in situ*.

Kantorowicz (1990) has demonstrated that the bicarbonate in siderite spherules from clay ironstones have $\delta^{13}C$ compositions that indicate mixing of freshwater bicarbonate and bicarbonate formed in a post-oxic ferric iron reduction environment, whereas the bicarbonate in siderite spherules from nodules have $\delta^{13}C$ compositions that indicate freshwater bicarbonate alone. If sample SUF.8.2 represent nodules then the siderite spherules might, therefore, contain carbonate from only a freshwater source.

The presence of alternating small coal bands within the ironstone suggests periods of organic accumulation and periods of no accumulation. This may represent dry and wet seasons, a view supported by the presence of charcoal - burnt wood remains of forest fires - occluded within siderite spherules. Forest fires occur during dry seasons and the charcoal produced can then be transported and deposited within lacustrine or swamp environments. Alternations of wet and dry seasons are common features of many swamp environments (Retallack 2001).

The Rokhagi sample represents an ironstone that formed in an environment that had very low sedimentation rates but accumulated organic matter. This type of setting could be the basin plain of a lacustrine system (cf. Talbot & Allen 1996). In this setting the siderite spherules were precipitated directly from the anoxic hypolimnion, through the anaerobic decomposition of the organic matter.

4.4 Conglomerate and Sandstone Beds

4.4.1 Occurrence

Rasmussen & Noe-Nygaard (1970b) recorded seven sequences from the CBF that contain conglomeratic deposits. Six of these are on the island of Suðuroy (Figs. 4.2 & 4.28) and the remaining sequence is found on the island of Vágar (Fig. 4.1). The sequence on Vágar lies

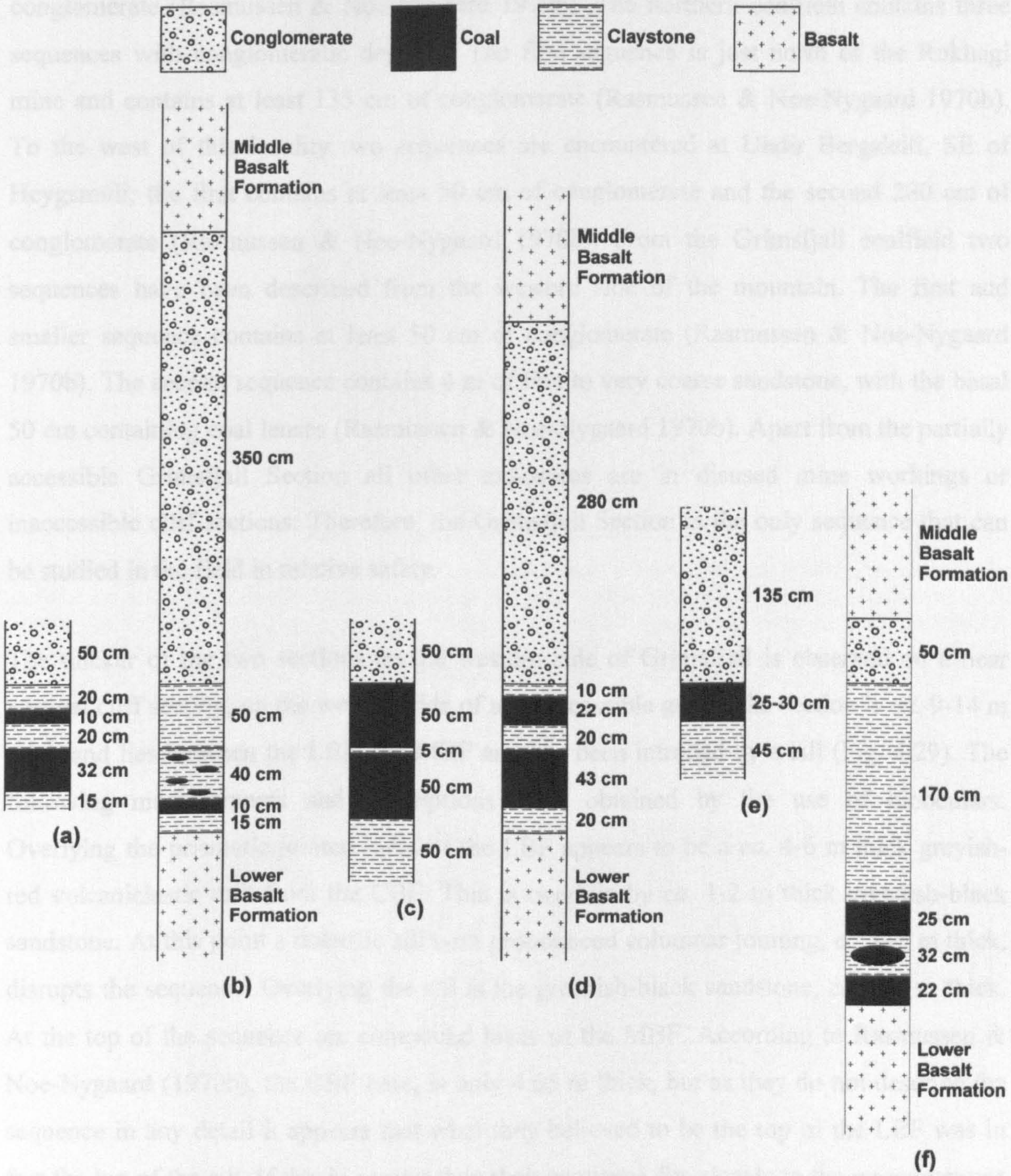

Fig. 4.28. Stratigraphic logs for the six conglomerate-bearing sections from the Coal-bearing Formation on Suðuroy, Faeroe Islands. (a) & (b) are two sections from the west side of Grímsfjall. (c) & (d) are two sections from Undir Bergsleiti, SE of Heygsmúli. (e) A section from a disused mine N of the Rokhagi mine. (f) A section from the NE side of Mót, NE of Gluggarnir. See Figure 4.2 for the locations of these sections. Adapted after Rasmussen & Noe-Nygaard (1969; 1970b).

to the west of Hjallabólsflesjar and contains a fluviatile conglomerate 2-3 m in thickness (Rasmussen & Noe-Nygaard 1970b). The conglomerates on Suðuroy are found in the southern, northern and Grímsfjall coalfields. The sequence through the CBF on the north east side of Mót, NE of Gluggarnir, in the southern coalfield, contains 50 cm of conglomerate (Rasmussen & Noe-Nygaard 1970b). The northern coalfield contains three sequences with conglomeratic deposits. The first sequence is just north of the Rokhagi mine and contains at least 135 cm of conglomerate (Rasmussen & Noe-Nygaard 1970b). To the west of this locality two sequences are encountered at Undir Bergsleiti, SE of Heygsmúli; the first contains at least 50 cm of conglomerate and the second 280 cm of conglomerate (Rasmussen & Noe-Nygaard 1970b). From the Grímsfjall coalfield two sequences have been described from the western side of the mountain. The first and smaller sequence contains at least 50 cm of conglomerate (Rasmussen & Noe-Nygaard 1970b). The second sequence contains 4 m of fine to very coarse sandstone, with the basal 50 cm containing coal lenses (Rasmussen & Noe-Nygaard 1970b). Apart from the partially accessible Grímsfjall Section all other exposures are in disused mine workings or inaccessible cliff sections. Therefore, the Grímsfjall Section is the only sequence that can be studied in the field in relative safety.

The thicker of the two sections on the western side of Grímsfjall is observed on a near vertical cliff section, on the western side of an inaccessible gully. The section is *ca.* 9-14 m thick and lies between the LBF and MBF and has been intruded by a sill (Fig. 4.29). The following measurements and descriptions were obtained by the use of binoculars. Overlying the prismatic jointed lavas of the LBF appears to be a *ca.* 4-6 m thick greyish-red volcaniclastic unit from the CBF. This is overlain by *ca.* 1-2 m thick greenish-black sandstone. At this point a doleritic sill with pronounced columnar jointing, *ca.* 6-8 m thick, disrupts the sequence. Overlying the sill is the greenish-black sandstone, *ca.* 4-6 m thick. At the top of the sequence are compound lavas of the MBF. According to Rasmussen & Noe-Nygaard (1970b), the CBF here, is only 4.65 m thick, but as they do not describe the sequence in any detail it appears that what they believed to be the top of the LBF was in fact the top of the sill. If this is correct then their sequence fits closely to the measurements of the sequence given above.

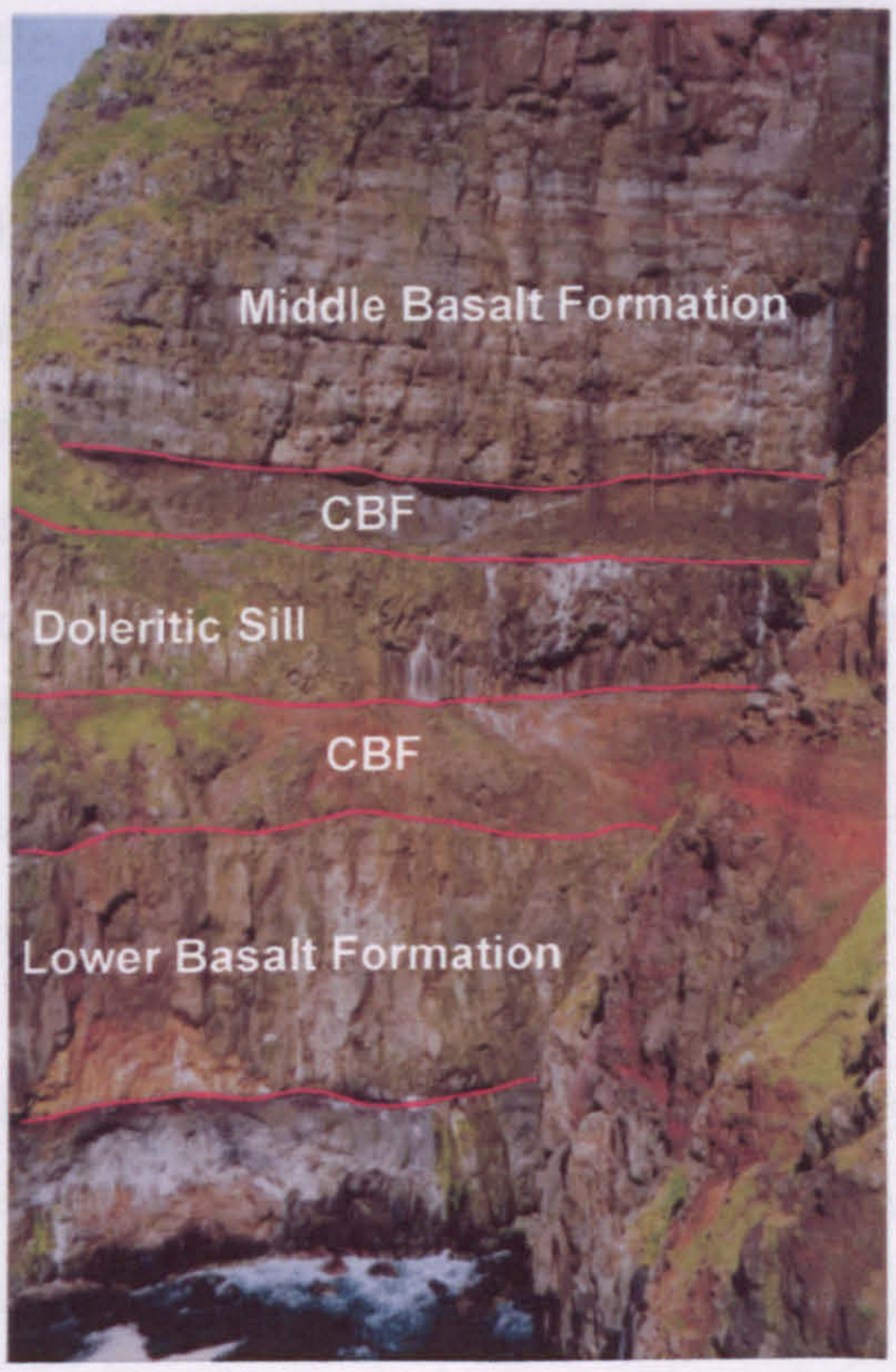

Fig. 4.29. View of the inaccessible cliff face at Grímsfjall, Suðuroy, Faeroe Islands. The section comprises a *ca.* 9-14 m thick sedimentary sequence from the Coal-bearing Formation (CBF) inbetween the Lower & Middle basalt formations. The sequence is disrupted by a *ca.* 6-8 m thick columnar jointed doleritic sill. The bottom half of the CBF is represented by a *ca.* 4-6 m thick volcaniclastic breccia overlain by a *ca.* 1-2 m thick olive grey volcaniclastic sandstone. The sequence above the doleritic sill is represented by a *ca.* 6-8 m thick olive grey volcaniclastic sandstone.

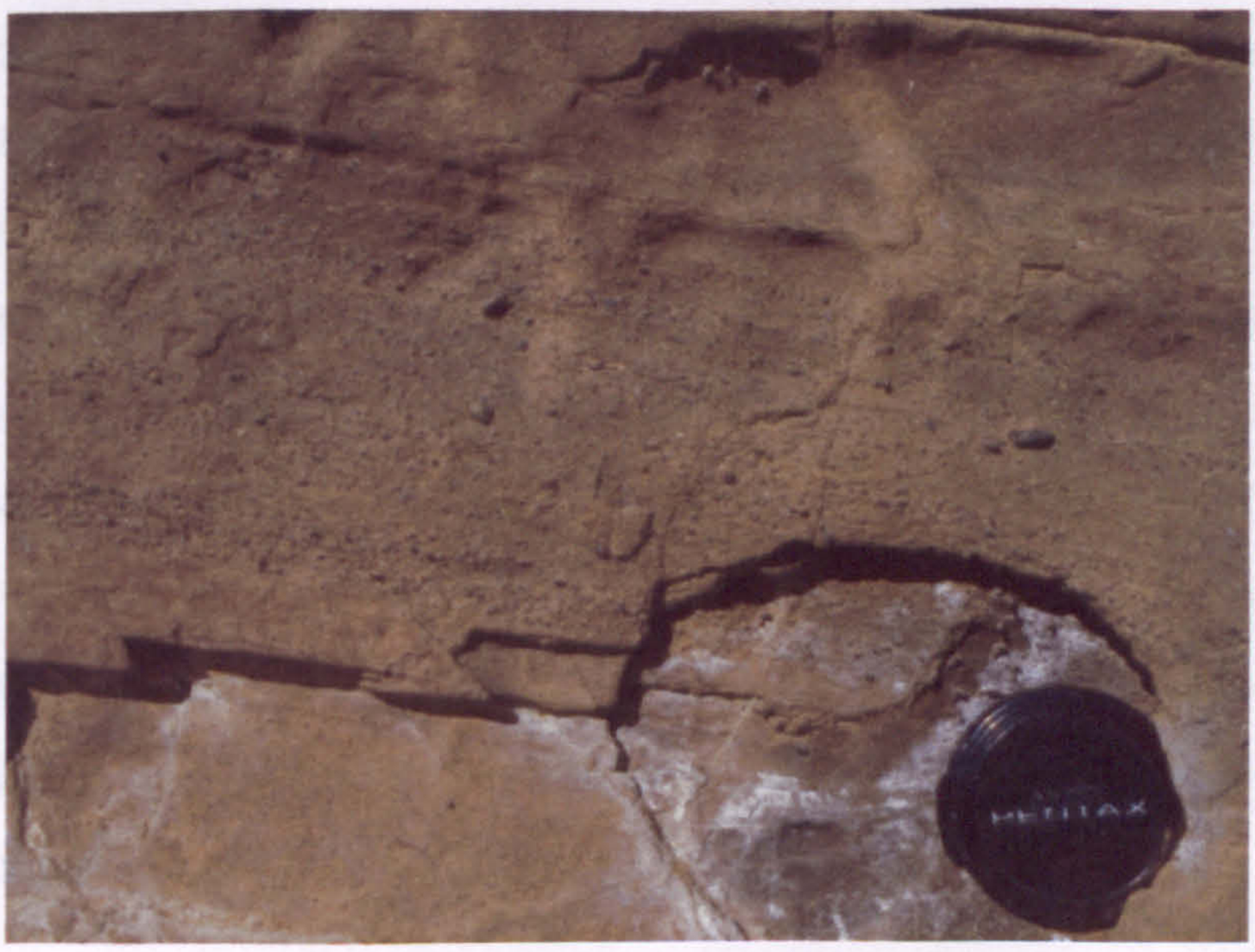

Fig. 4.30. View of a thinly to medium bedded (6-15 cm) olive grey basaltic sandstone from the accessible eastern side of the Grímsfjall Section, Suðuroy, Faeroe Islands. The contacts between beds are commonly sharp and planar and the sandstone is mainly fine to medium grained, although some of the beds contain coarse sand to granule grade clasts (0.5-5.0 mm). The lens cap is *ca.* 6 cm in diameter.

4.4.2 Petrography

4.4.2.1 Grímsfjall Section

Approximately 3-4 m of the sandstone unit that crops out above the sill on the western side of the gully also crops out on the accessible eastern side. The sandstone is olive grey (5Y 3/2) and is thinly to medium bedded (6-15 cm) (Fig. 4.30). The contacts between beds are commonly sharp and planar (Figs. 4.30 & 4.32f). The unit is mainly a fine to medium grained basaltic sandstone (Figs. 4.31 & 4.32). Some of the beds contain coarse sand to granule grade clasts (0.5-5.0 mm) (Figs. 4.33 & 4.34). The fine to medium grained sandstone is poorly to moderately well sorted and elongate clasts are aligned parallel to bedding. The sandstone is clast supported and there is virtually no matrix or cement.

The sandstone is dominated by *ca.* 0.5 mm clasts of palagonitised basaltic glass (*ca.* 60-65 vol.%) (Fig. 4.31). Palagonite is formed from the hydration (palagonitisation) of basaltic glass, commonly sideromelane but also tachylite. Secondary minerals can be produced as the result of palagonitisation; these may include: various clays, zeolites, opal, carbonate, and Fe-Mn oxides or carbonates (Hay & Iijima 1968; Fisher & Schmincke 1984). However, on the whole no secondary minerals, apart from clays, have been observed within the sandstone. The palagonitised clasts are commonly a dirty green-yellow in plane polarised light and isotropic to weakly birefringent in crossed polars. Rare phenocrysts of plagioclase feldspar and rarer phenocrysts of pyroxene are observed within the usually highly vesiculated palagonitised glass (Fig. 4.31f). The degree of palagonitisation of the sandstone is extremely varied, from orange translucent palagonite platy shards to various clays, comprising smectite and chlorite. Primary textures and clast margins have become obscured due to the hydration process, which is a common feature associated with palagonitisation (Hay & Iijima 1968; Fisher & Schmincke 1984; Cas & Wright 1987). However, the orange translucent palagonitised platy shards are more easily identified by their higher refractive index (1.600-1.700 on the Michel Levy chart), as they have undergone a smaller degree of palagonitisation and closer to their original composition of fresh basaltic glass (Fig. 4.31d). The usually sharp edges to these platy shards have been to some extent rounded.

Prominent speckled murky grey clasts (*ca.* 20 vol.%) that contain opaque iron oxides and are weakly birefringent in crossed polars are also present within the sandstones. The clasts are sub-rounded and have an average clast size of *ca.* 0.25 mm and rarely contain laths of plagioclase feldspar. The clasts are most probably the eroded remnant of weathered basalt

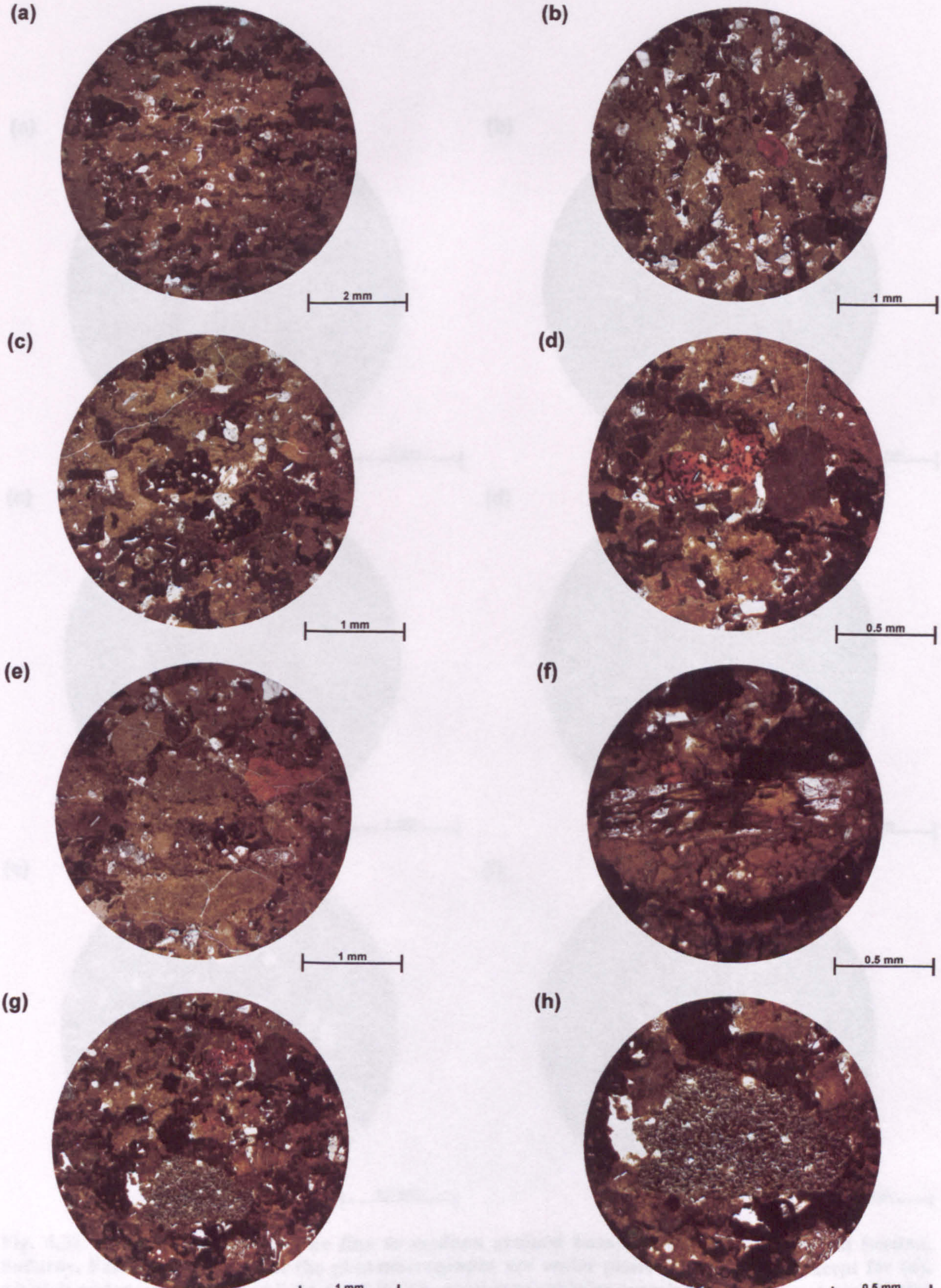

Fig. 4.31. Photomicrographs of a fine to medium grained basaltic sandstone, Grímsfjall Section, Suðuroy, Faeroe Islands. All photomicrographs are under plane-polarised light. (a) to (e) General views showing that the sandstone is dominated by dirty green-yellow palagonitised basaltic glass clasts. The scale of palagonitisation throughout the sandstone is extremely varied, from orange translucent glass to various clays. (d) An orange translucent palagonitised glass clast, which is easily identified by its higher refractive index because it has undergone a smaller degree of palagonitisation and closer to its original composition. (f) Some of the palagonitised glass clasts contain phenocrysts of plagioclase feldspar. (g) & (h) The sandstone also contains basalt clasts, derived from lava flows, these views show a typical trachytic clast.

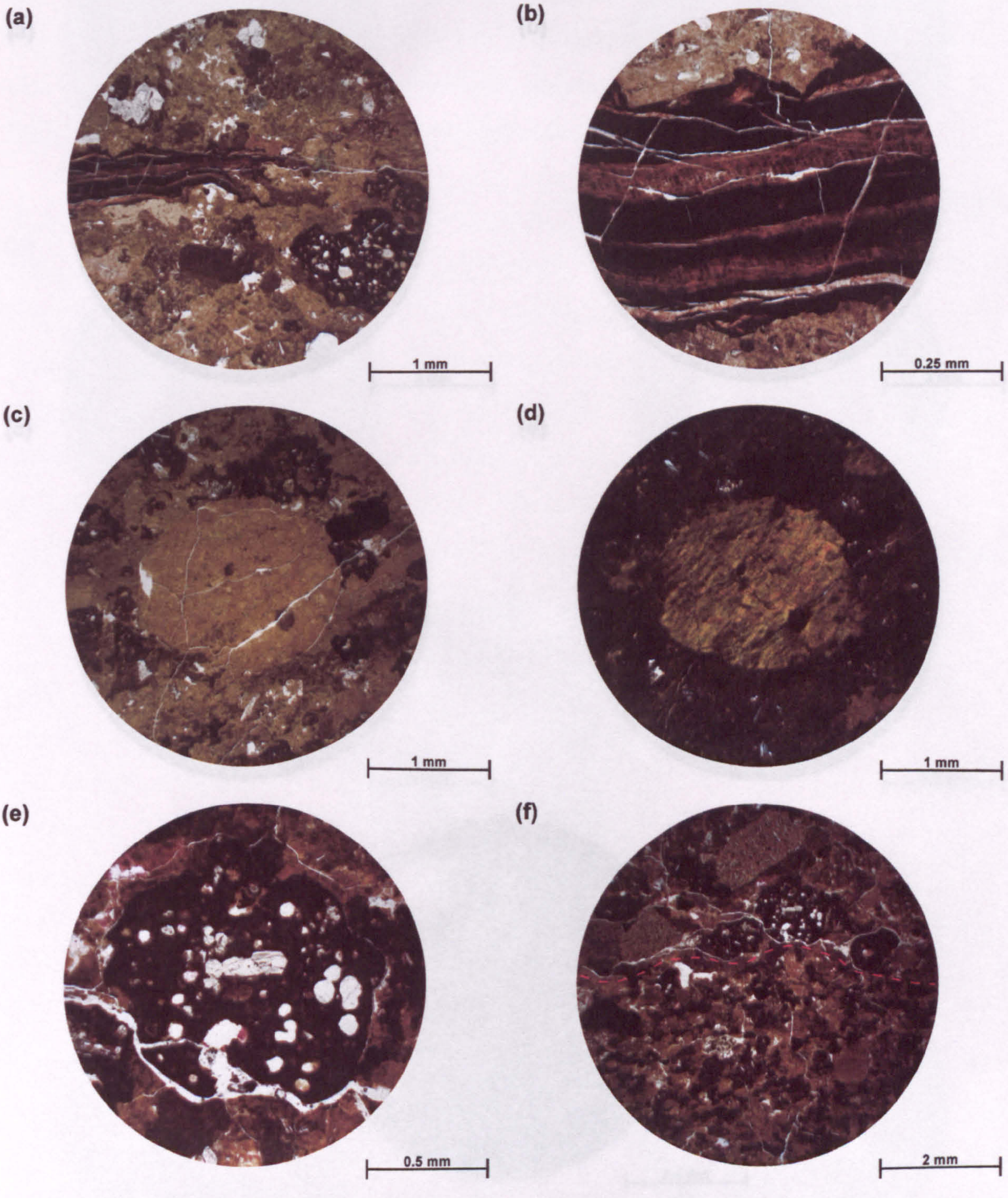

Fig. 4.32. Photomicrographs of the fine to medium grained basaltic sandstone, Grímsfjall Section, Suðuroy, Faeroe Islands. All of the photomicrographs are under plane-polarised light except for (d), which is under cross-polarised light. (a) & (b) The sandstone contains prominent organic material. Notice the well preserved cellular structure of the organic material in (b). (c) & (d) A clayey clast that has a distinctive serpentine-like structure, this is most likely berthierine or chamosite. (e) Vesiculated, opaque basaltic glass, most likely scoria. (f) A planar boundary between the fine to medium grained basaltic sandstone (bottom half of view) and the coarse sand to granule grade layer (top half of view).

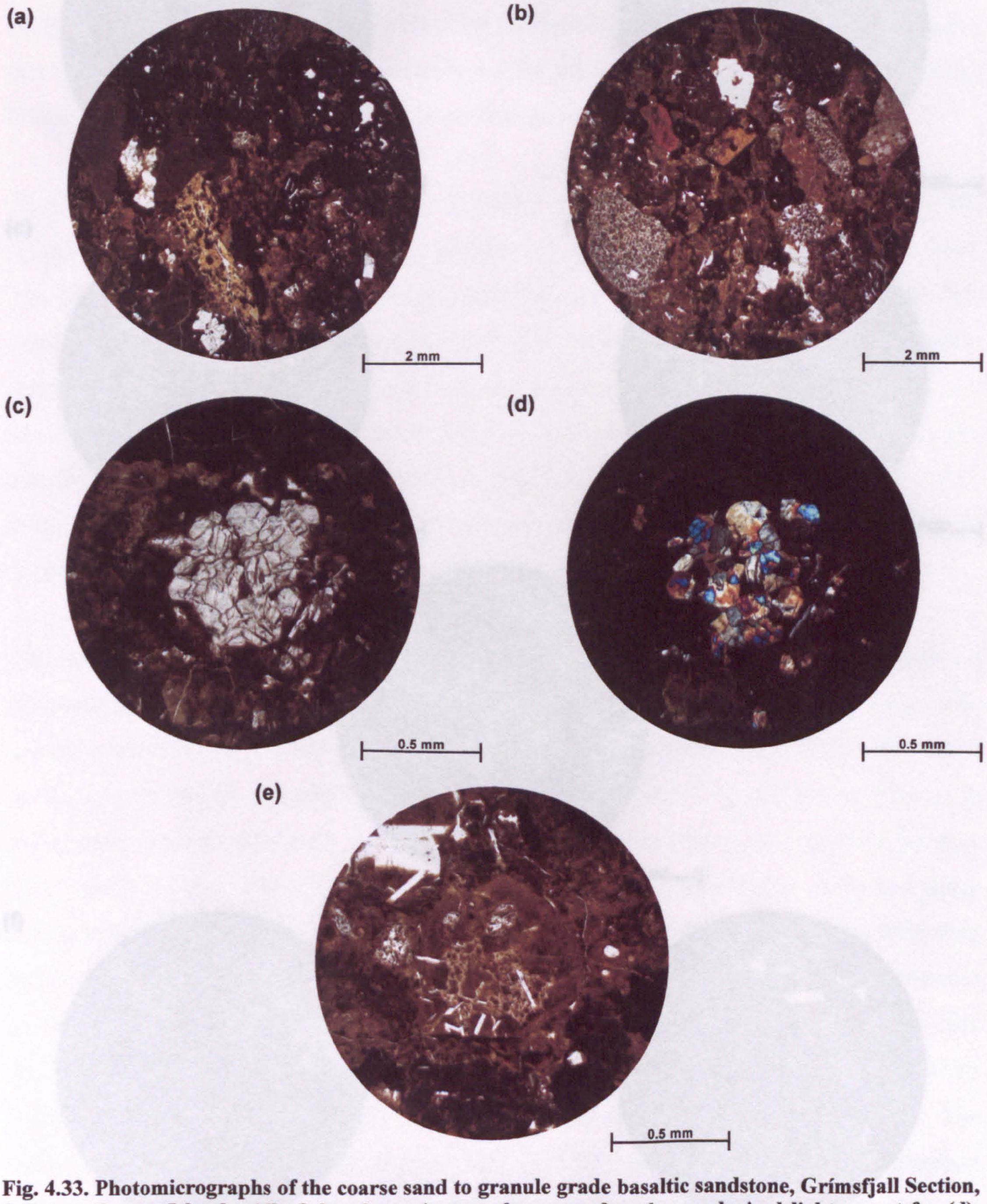

Fig. 4.33. Photomicrographs of the coarse sand to granule grade basaltic sandstone, Grímsfjall Section, Suðuroy, Faeroe Islands. All of the photomicrographs are under plane-polarised light except for (d), which is under cross-polarised light. (a) & (b) General views of the basaltic sandstone, which is similar to the fine to medium grained basaltic sandstone seen in Figs. 4.31 & 4.32, but contains more basalt clasts. (c) & (d) Some of the palagonitised basaltic glass clasts contain cumulates of clinopyroxene. (e) Some of the palagonitised glass clasts contain phenocrysts of plagioclase feldspar.

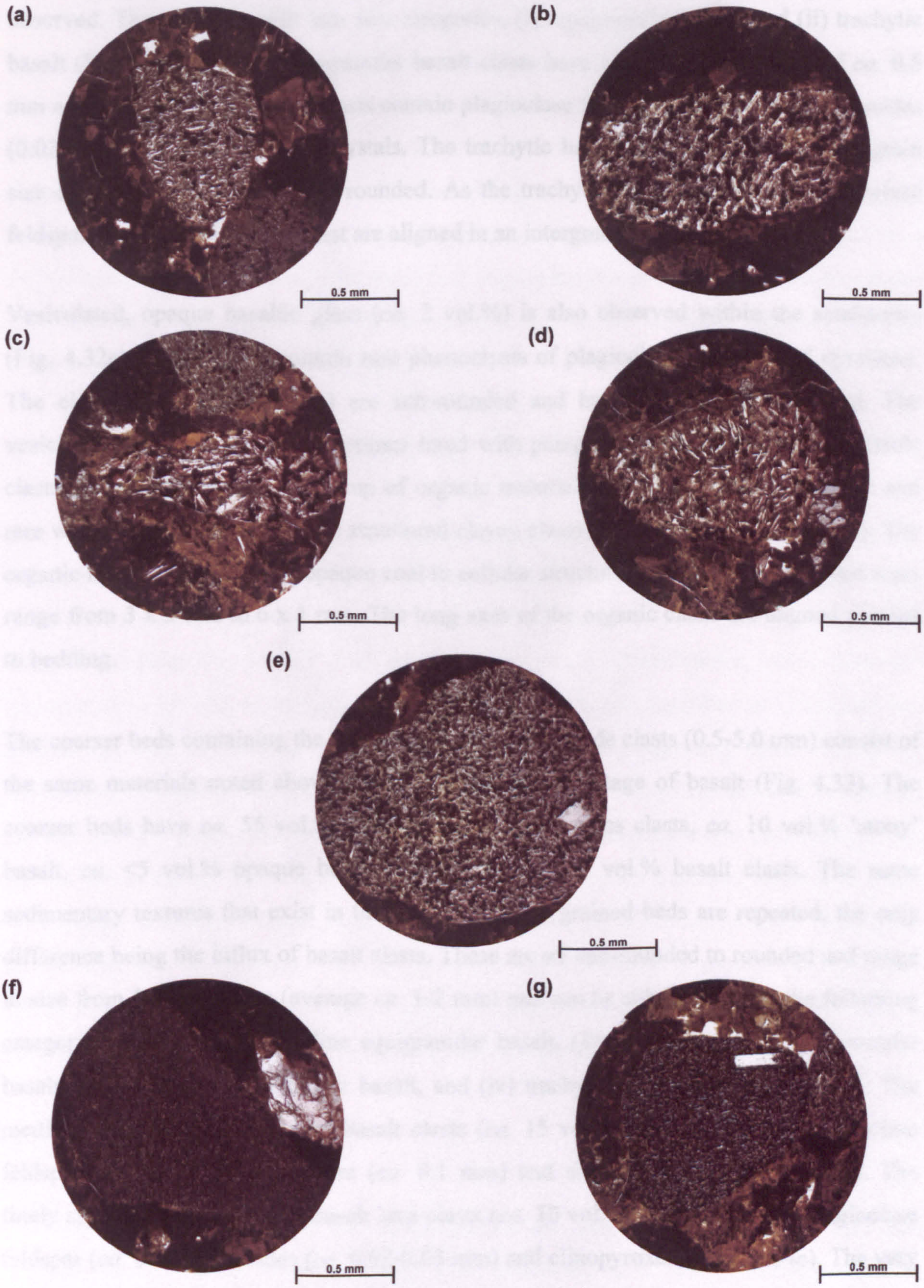

Fig. 4.34. Photomicrographs of the coarse sand to granule grade basaltic sandstone, Grímsfjall Section, Suðuroy, Faeroe Islands. All of the photomicrographs are under plane-polarised light. (a) to (d) Medium crystalline equigranular basalt clasts that contain laths of plagioclase feldspar (*ca.* 0.1-0.2 mm), oxides (*ca.* 0.1 mm) and clinopyroxene. (e) Finely crystalline equigranular basalt clast that contains laths of plagioclase feldspar (*ca.* 0.1 mm), oxides (*ca.* 0.02-0.03 mm) and clinopyroxene. (f) Very finely crystalline basalt clast that contains laths of plagioclase feldspar (*ca.* 0.05 mm) set in an intergranular texture of clinopyroxene and oxides. (g) Trachytic basalt clast that contains laths of plagioclase feldspar (*ca.* 0.1 mm) that are aligned in an intergranular texture consisting of clinopyroxene and oxides.

lava, referred to here as 'stony' basalt. Other basalt clasts totalling *ca.* 10 vol.% are also observed. These can be split into two categories, (i) equigranular basalt, and (ii) trachytic basalt (Fig. 4.31g-h). The equigranular basalt clasts have an average grain size of *ca.* 0.5 mm and are sub-rounded. The clasts contain plagioclase feldspar (*ca.* 0.1 mm), iron oxides (0.02-0.03 mm) and pyroxene crystals. The trachytic basalt clasts have an average grain size of *ca.* 0.5 mm and are sub-rounded. As the trachytic name implies, the plagioclase feldspars (*ca.* 0.1 mm) in the clast are aligned in an intergranular groundmass.

Vesiculated, opaque basaltic glass (*ca.* 2 vol.%) is also observed within the sandstones (Fig. 4.32e). These clasts contain rare phenocrysts of plagioclase feldspar and pyroxene. The clasts (*ca.* 0.25-0.75 mm) are sub-rounded and have been partially altered. The vesicles are unfilled but are sometimes lined with palagonite. The remaining identifiable clasts in the sandstone are made up of organic material (*ca.* 3 vol.%) (Fig. 4.32a-b) and rare well-rounded serpentine-like structured clayey clasts (*ca.* 2 vol.%) (Fig. 4.32c-d). The organic material ranges from opaque coal to cellular structured woody material. Clast sizes range from 3 x 2 mm to 6 x 1 mm. The long axes of the organic clasts are aligned parallel to bedding.

The coarser beds containing the coarse sand to granule grade clasts (0.5-5.0 mm) consist of the same materials noted above but have a higher percentage of basalt (Fig. 4.33). The coarser beds have *ca.* 55 vol.% palagonitised basaltic glass clasts, *ca.* 10 vol.% 'stony' basalt, *ca.* <5 vol.% opaque basaltic glass, and *ca.* 35 vol.% basalt clasts. The same sedimentary textures that exist in the fine to medium grained beds are repeated, the only difference being the influx of basalt clasts. These are all sub-rounded to rounded and range in size from 0.5 to 5.0 mm (average *ca.* 1-2 mm) and can be subdivided into the following categories: (i) medium crystalline equigranular basalt, (ii) finely crystalline equigranular basalt, (iii) very finely crystalline basalt, and (iv) trachytic basalt clasts (Fig. 4.34). The medium crystalline equigranular basalt clasts (*ca.* 15 vol.%) contain laths of plagioclase feldspar (*ca.* 0.1-0.2 mm), oxides (*ca.* 0.1 mm) and clinopyroxene (Fig. 4.34a-d). The finely crystalline equigranular basalt lava clasts (*ca.* 10 vol.%) contain laths of plagioclase feldspar (*ca.* 0.1 mm), oxides (*ca.* 0.02-0.03 mm) and clinopyroxene (Fig. 4.34e). The very finely crystalline basalt clasts, which are light grey to colourless contain laths of plagioclase feldspar that are *ca.* 0.05 mm in size and are set in an intergranular groundmass consisting of clinopyroxene and oxides (Fig. 4.34f). The trachytic basalt clasts contain laths of plagioclase feldspar (*ca.* 0.1 mm) that are aligned in an intergranular groundmass consisting of clinopyroxene and oxides (Fig. 4.34g).

4.4.3 Provenance

The conglomerates and sandstones all contain intraformational clasts derived from within the depositional area. The sandstone described from Grímsfjall is mainly composed of volcanic materials, the majority of which are reworked palagonitised basaltic glass derived from unconsolidated ash deposits. The remaining volcanic materials display a range of basalt textures most likely derived from the erosion of exposed lava flows of the LBF. Five different clast categories have been identified, suggesting that at least 5 different lava flows were eroded. The presence of organic material within the deposits indicates that the surrounding land surface was vegetated.

4.4.4 Environment of Deposition

The sandstones and conglomerates appear to be fluvial in origin as they are heterogeneous, intraformational, clast-supported, immature lithic arenites that consist of sub-rounded clasts (cf. Collinson 1996; Tucker 1996b). The presence of plant material within the deposits supports the premise that the coals are partly allochthonous (plant materials transported to the site of formation) in origin. The sandstone described at Grímsfjall has alternating beds that are basalt lava clast-poor and –rich suggesting either fluctuating erosion rates or water flow energy levels. This alternation may reflect seasonal variations, i.e. wet and dry, during drier climates water flow energy levels are lower only transporting ash and minor basalt clasts compared to wetter climates that see a marked increase in water flow energy levels as a result of higher surface runoff (cf. Collinson 1996). The higher levels of surface runoff maybe directly related to higher amounts of rainfall (cf. Collinson 1996), as a consequence, channels may flood, increasing water flow energy levels which is able to transport a larger amount of basalt clasts than during drier periods.

4.5 Synthesis

The Coal-bearing Formation (CBF) is exposed on the islands of Tindhólmur, Vágar and Suðuroy and preserves lithologies that were deposited in a humid, warm temperate terrestrial environment (Lund 1983; 1989; Jolley 1997) (Fig. 4.35). The CBF has an average thickness of *ca.* 10 m and commonly contains two coal seams interbedded with claystones and shales. In at least two localities the basal claystone (under clay) has been replaced by previously unreported ironstone deposits and in seven localities the upper

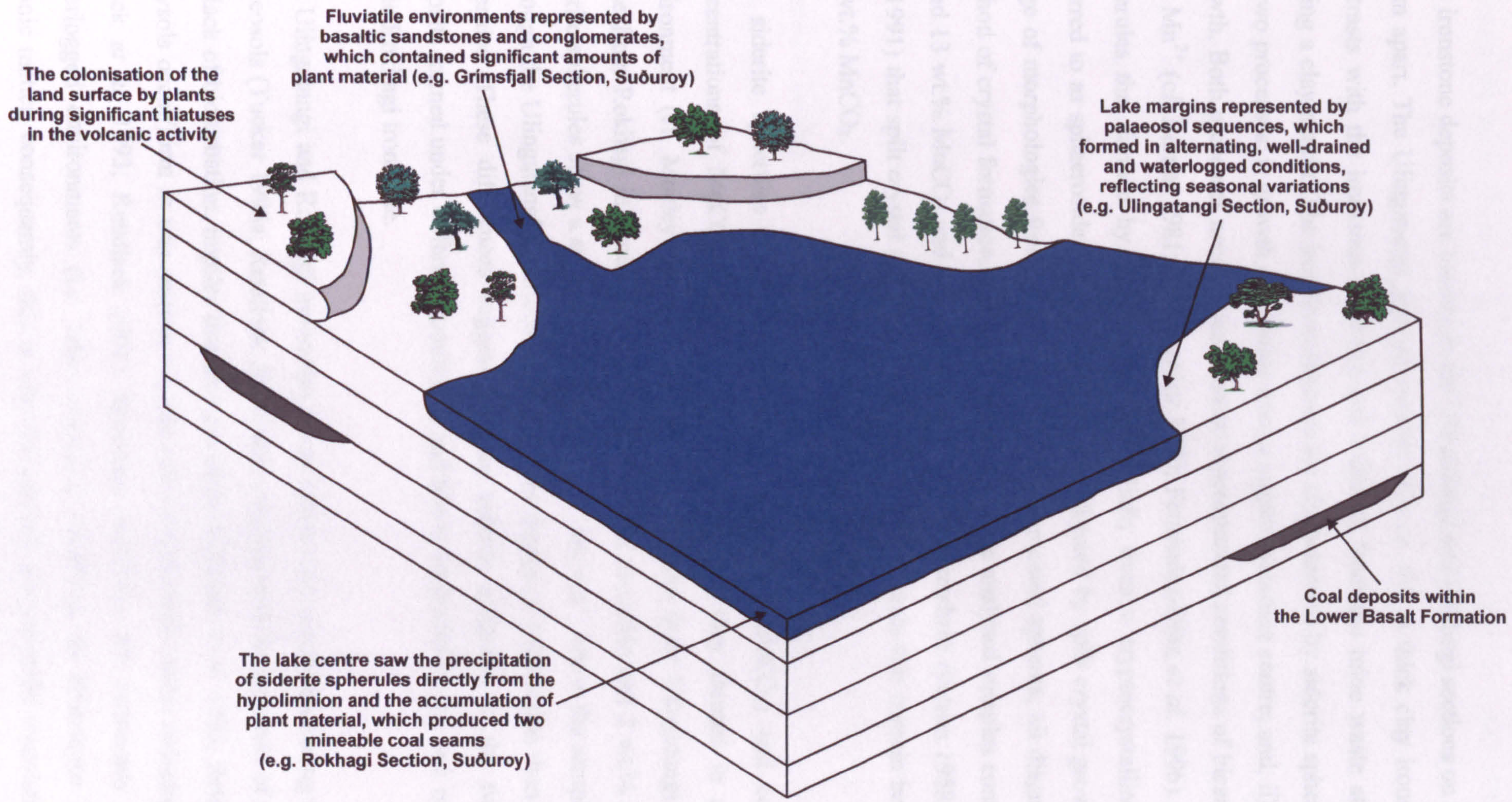

Fig. 4.35. Schematic palaeogeographical block diagram for the Coal-bearing Formation with the main elements highlighted. Subsidence at the end of the Lower Basalt Formation times allowed erosion to cut down to at least the second highest lava flow. Within the resulting topographic low a lake developed on Suðuroy, at least 10 km across. Length of each horizontal dimension of the figure is very approximately 4-5 km.

claystone (roof clay) has been replaced or is overlain by fluvial sandstones and conglomerates.

The ironstone deposits are located in the Ulingatangi and Rokhagi sections on Suðuroy, *ca.* 4 km apart. The Ulingatangi Section consists of a *ca.* 4.5 m thick clay ironstone, which contrasts with the ironstone collected and analysed from the mine waste at Rokhagi in having a clay matrix. The ironstone deposits are characterised by siderite spherules formed by two processes: i) growth of crystals from a cryptocrystalline centre; and, ii) split crystal growth. Both processes need to occur under supersaturated conditions of bicarbonate, Fe^{2+} and Mn^{2+} (cf. Berner 1981; Kantorowicz 1990; Fernández-Díaz *et al.* 1996). The siderite spherules that formed by crystals growing radially from a cryptocrystalline centre are referred to as sphaerosiderites. Siderite spherules formed by split crystal growth display a range of morphologies from fans to bow-ties to segmented spheres, all diagnostic of this method of crystal formation. The siderite crystals in the analysed samples contain between 1 and 13 wt.% $MnCO_3$ and it has been demonstrated elsewhere (Petrun 1958; Minoura *et al.* 1991) that spilt crystal growth occurs in carbonate crystals that contain between 4 and 12 wt.% $MnCO_3$.

The siderite spherules are extremely pure (90-94 wt.% $FeCO_3$) and contain small concentrations of $MgCO_3$ (<0.2 wt.%), suggesting that they formed in a freshwater environment (cf. Mozley 1989). However, the spherules from Ulingatangi differ from those from Rokhagi in containing on average 2 wt.% more Mn and 2 wt.% less Fe. The siderite spherules show a substitution of Fe^{2+}, Mn^{2+} and Ca^{2+} across the samples analysed, although the Ulingatangi spherules show a greater degree of substitution than the Rokhagi spherules. These differences suggest that the siderite spherules in the two ironstone deposits formed under different conditions, and this is supported by the lack of clay matrix in the Rokhagi ironstone.

The Ulingatangi and Rokhagi ironstones occur below coal seams, indicating that they are palaeosols (Tucker 1996a; Retallack 2001) and, coupled with the greyness of the beds and the lack of bioturbation, implies that they are gleysols (Mack *et al.* 1993; Retallack 2001). Gleysols occur/form in non-marine, organic-rich environments under reducing conditions (Mack *et al.* 1993; Retallack 2001). Reducing conditions are commonly achieved in waterlogged environments (i.e. lakes, swamps) involving an abundance of decaying organic matter; consequently, this is why the gleysols are generally associated with coal seams (Mack *et al.* 1993; Retallack 2001). Lund (1983; 1989) and Parra *et al.* (1987) have shown that the claystones in the CBF were deposited within a lacustrine environment, thus

it follows that the gleysols formed within a lacustrine system. The lack of clay matrix in the Rokhagi ironstone implies that sedimentation rates were extremely low and may represent the basin plain of the lacustrine system (cf. Talbot & Allen 1996). If this is correct, it suggests that the spherules were precipitated directly from an anoxic hypolimnion. This compares to the Ulingatangi Section, which preserves reddened lithologies containing ferric oxyhydrates and iron oxides formed during periods of oxidisation, thus indicating a well-drained environment. Concentric zonation of siderite spherules at Ulingatangi record a cycle of at least four reducing and oxidising periods, i.e. waterlogged and well-drained environments. This suggests that the Ulingatangi Section formed at the margin of a lacustrine system that underwent seasonal variations i.e. fluctuating water levels within the lake.

The abundance of organic material within the ironstones and the occurrence of coal indicate that the surrounding land surface was heavily vegetated. The occurrence of plant remains in the fluvial conglomerates and sandstones in the upper section of the CBF, West Suðuroy, support the premise that the coal macerals are partly allochthonous and that the lake environment was at least 10 km across. The sandstone at Grímsfjall (Fig. 4.2) is thinly to medium bedded, alternating from fine- to medium-grained sandstones to coarse sand- to granule-grade sandstones. This alternation between dominant grain-sizes implies fluctuating water flow (energy) levels, most likely reflecting an increase in surface water run-off (cf. Collinson 1996). The sandstones are clast supported, poorly sorted and are composed primarily of palagonitised basaltic glass derived from the reworking of unconsolidated ash deposits, suggesting that volcanism was occurring distally to the Faeroe Islands. They also consist of varying amounts of basalt clasts, derived from the erosion of numerous Lower Basalt Formation (LBF) lava flows. The range in basalt textures implies that numerous lava flows were being eroded at the same time.

5 Volcaniclastic Sandstone Formation

The Volcaniclastic Sandstone Formation (VSF) was referred to as the Tuff-Agglomerate Zone by Rasmussen & Noe-Nygaard (1970b) and has been renamed here because of subsequent refinements in terminology (see Section 2.2 for further explanation) and advances in our understanding of processes that occur in volcanic settings. Previously, the formation has not been described in great detail in the literature and this chapter examines the volcaniclastic lithologies from three significant traverses on Suðuroy. The rocks are initially described using the lithological classification scheme outlined in Section 2.2, before genetic interpretations and environments of deposition are presented.

5.1 Distribution

The VSF crops out on the islands of Vágar, Tindhólmur and Suðuroy in a NW-SE trending corridor approximately parallel to the dominant fjord elongation (Figs. 1.3 & 5.1-insert). The VSF overlies the Coal-bearing Formation (CBF) as seen at Ulingatangi, *ca.* 1.2 km east of Froðba, Suðuroy (Fig. 4.4). The maximum thickness of the VSF is difficult to estimate as numerous doleritic sills have intruded the formation and the top of the formation is sometimes transitional with lavas of the Middle Basalt Formation (MBF). The VSF on Vágar extends from Bøur, northwestwards to Barðið, and then eastwards towards Víkar (Fig. 4.1). Along this section the VSF has an exposed thickness of *ca.* 6 m (Rasmussen & Noe-Nygaard 1970b). The best exposures of the VSF occur on the island of Suðuroy (Fig. 5.1) in three main traverses. From east to west, they are as follows: the Húsagarðsá-Hvannagjógv Traverse, the Hvannhagi-Lónin Traverse, and the Reyðibarmur-Hvalba Traverse. Minor occurrences occur along the coastline from Myrkagjógv westwards towards Flekksá and at Ulingatangi, *ca.* 1.2 km E of Froðba.

5.2 Húsagarðsá–Hvannagjógv Traverse

The Húsagarðsá–Hvannagjógv Traverse, Suðuroy, is *ca.* 5.5 km long (Fig. 5.1) and the VSF has a maximum exposed thickness of *ca.* 30 m. The VSF is poorly exposed along the majority of the traverse, but good exposures are observed between the streams of Svalbarðaá and Myllá (sometimes known by its waterfall's name, Bláfossur) (Fig. 5.2). Another partial exposure is observed in the stream section of Hvannagjógv.

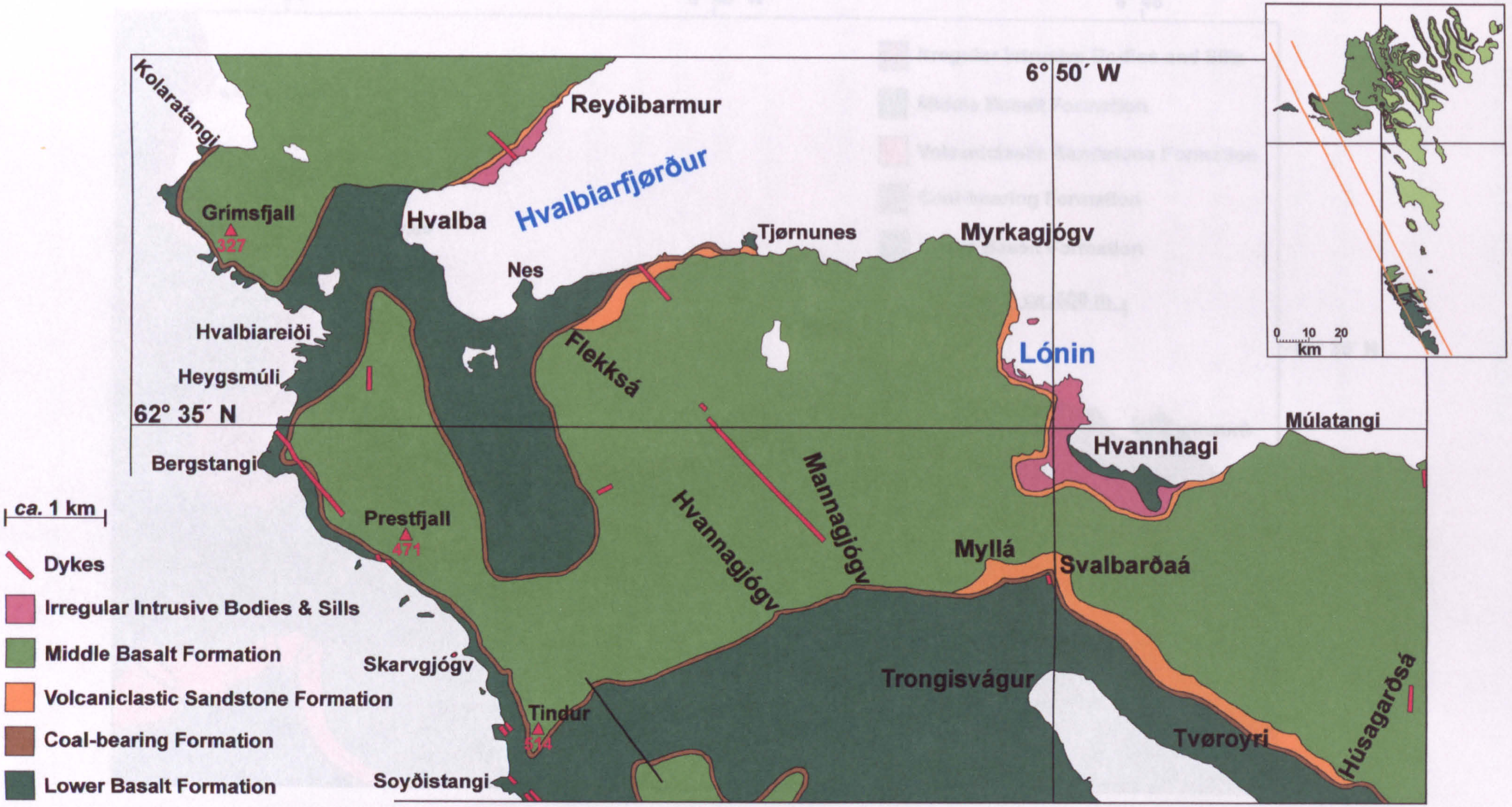

Fig. 5.1. Geological map showing the location of the Volcaniclastic Sandstone Formation (VSF) on Suðuroy, Faeroe Islands. Spot heights are in metres. The insert shows a map of the Faeroe Islands and the zone (parallel orange lines) in which the VSF is found. After Rasmussen & Noe-Nygaard (1969; 1970a; b).

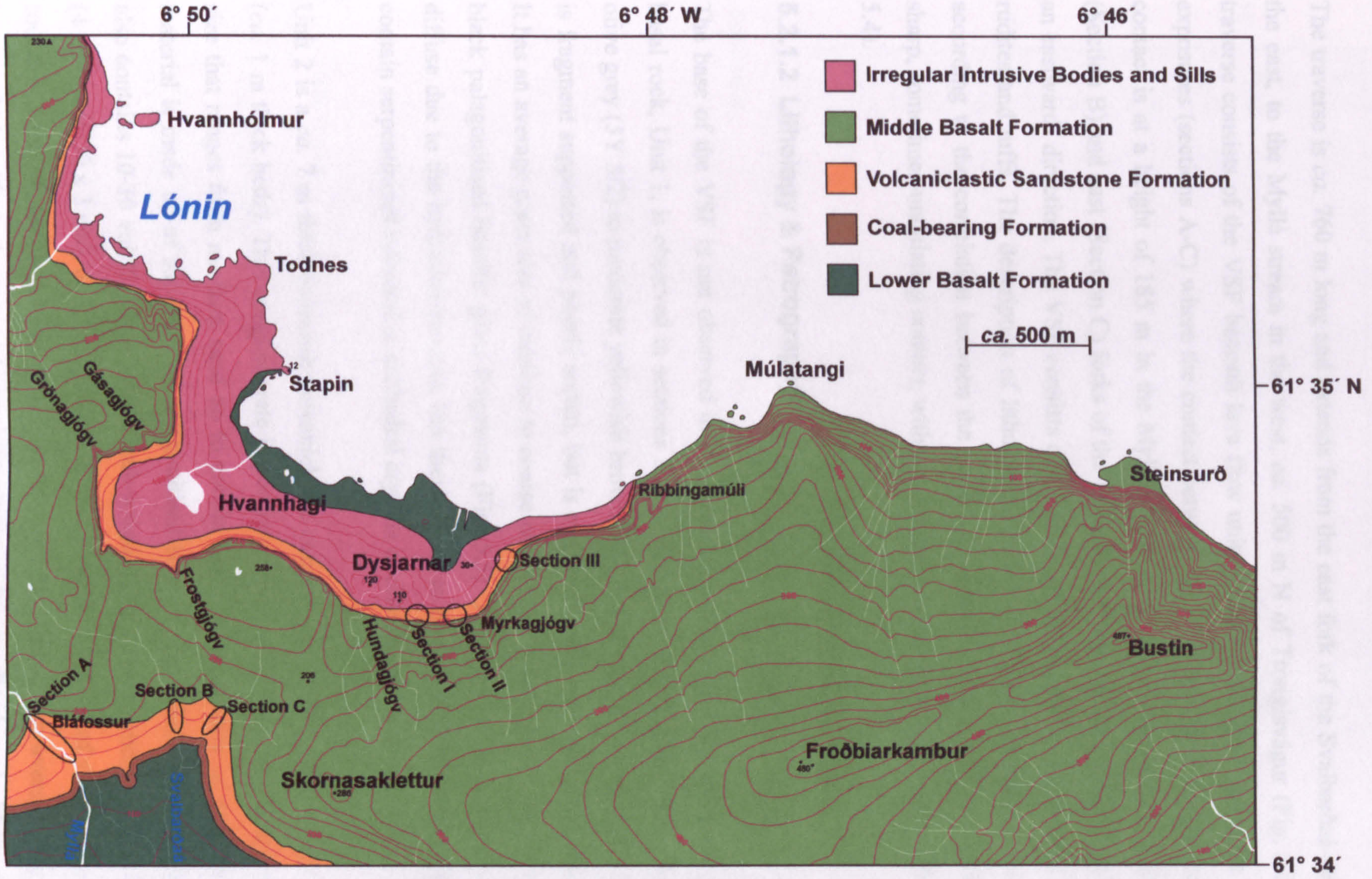

Fig. 5.2. Geological map of the area north of Trongisvágur, Suðuroy, Faeroe Islands. The map shows the location of sections A-C of the Svalbarðaá-Myllá Volcaniclastic Sandstone Formation (VSF) traverse. The map also shows the location of sections I-III of the Dysjarnar Traverse, part of the larger Hvannhagi-Lónin Traverse. Spot heights are in metres.

5.2.1 Svalbarðaá–Myllá Traverse

5.2.1.1 Overview of Traverse

The traverse is *ca.* 760 m long and extends from the east fork of the Svalbarðaá stream in the east, to the Myllá stream in the west, *ca.* 500 m N of Trongisvágur (Fig. 5.2). The traverse consists of the VSF beneath lava flow units of the MBF. There are three stream exposures (sections A-C) where the contact between the VSF and MBF is observed. The contact is at a height of 185 m in the Myllá stream (Section A) and 160 m in the west (Section B) and east (Section C) forks of the Svalbarðaá stream, giving a dip of *ca.* 1.5° in an eastwards direction. The VSF consists of a mixture of volcaniclastic (epiclastic) lutites-rudites and tuffs. The description of lithologies (units 1-9) shall be in stratigraphic order according to the correlation between the three exposures in Figure 5.3. The VSF has a sharp, sometimes-undulating contact, with *ca.* 2 m thick basalt flow units of the MBF (Fig. 5.4).

5.2.1.2 Lithology & Petrography

The base of the VSF is not observed in the three sections due to poor exposure, but the basal rock, Unit 1, is observed in sections B & C and is *ca.* 7-8 m thick. Unit 1 is a light olive grey (5Y 5/2) to moderate yellowish brown (10YR 5/4) massive coarse tuff. This tuff is fragment supported and poorly sorted, but is extremely homogeneous in fragment type. It has an average grain size of medium to coarse sand and is made up of reddish to greyish black palagonitised basaltic glass fragments (Fig. 5.5). The margins of the fragments are diffuse due to the hydration process, but they appear to be angular. The larger fragments contain serpentinised euhedral to subhedral crystals of olivine up to 2 mm in size.

Unit 2 is a *ca.* 7 m thick brownish volcaniclastic conglomerate that is very thickly bedded (*ca.* 1 m thick beds). This conglomerate is poorly sorted, matrix supported and has a clast size that ranges from medium sand up to cobble grade. The majority of this sand grade material is made up of sub-rounded palagonitised basaltic glass clasts. The conglomerate also contains 10-30 vol.% sub-angular to sub-rounded, very large pebbles to cobble grade (4 x 2 cm to 30 x 3 cm), dark basalt clasts. It also contains 10 vol.% of sub-angular to sub-rounded clasts of the underlying greyish coarse tuff, which have an average size of very large pebbles (6 x 4 cm) and are characterised by needle-shaped, blackish-green, serpentinised olivine crystals 2-4 mm long. The lava and tuff clasts decrease in size to

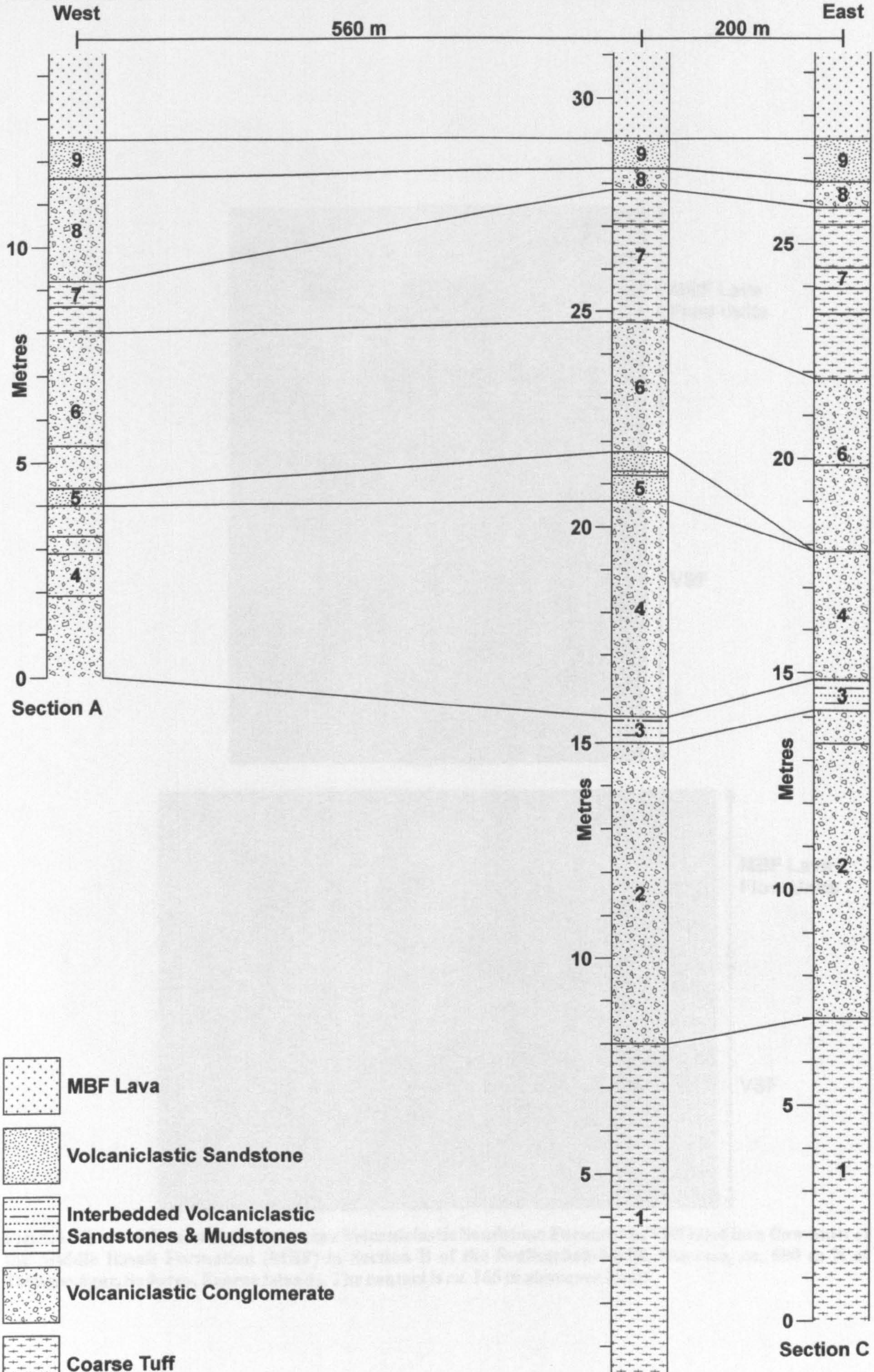

Fig. 5.3. Graphic logs of the Volcaniclastic Sandstone Formation (VSF) below the Middle Basalt Formation (MBF) lavas, Svalbarðaá-Myllá Traverse, *ca.* 500 m N of Trongisvágur, Suðuroy, Faeroe Islands.

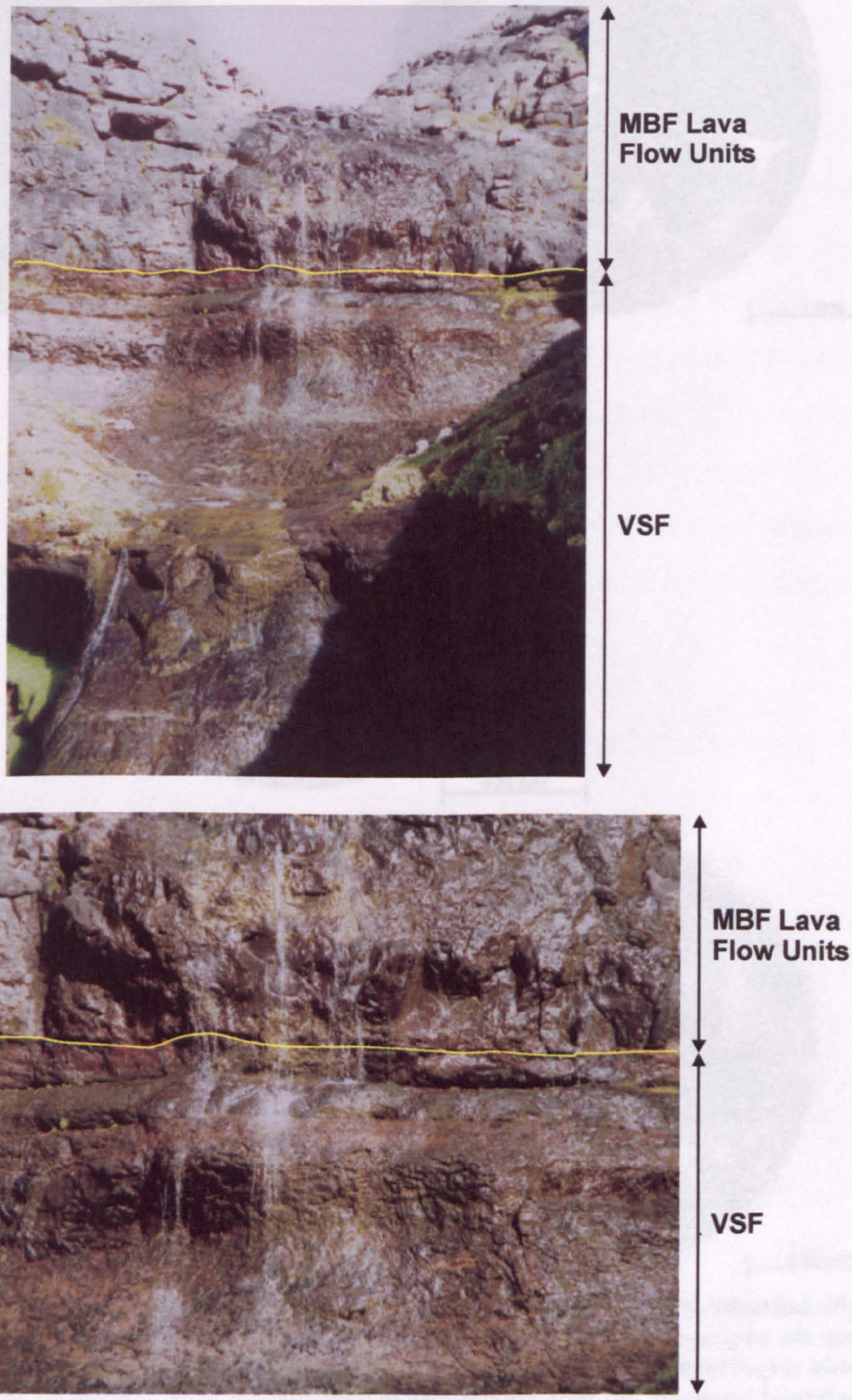

Fig. 5.4. Views of the contact between the Volcaniclastic Sandstone Formation (VSF) and lava flow units of the Middle Basalt Formation (MBF) in Section B of the Svalbarðaá-Myllá Traverse, *ca.* 500 m N of Trongisvágur, Suðuroy, Faeroe Islands. The contact is *ca.* 165 m above sea level.

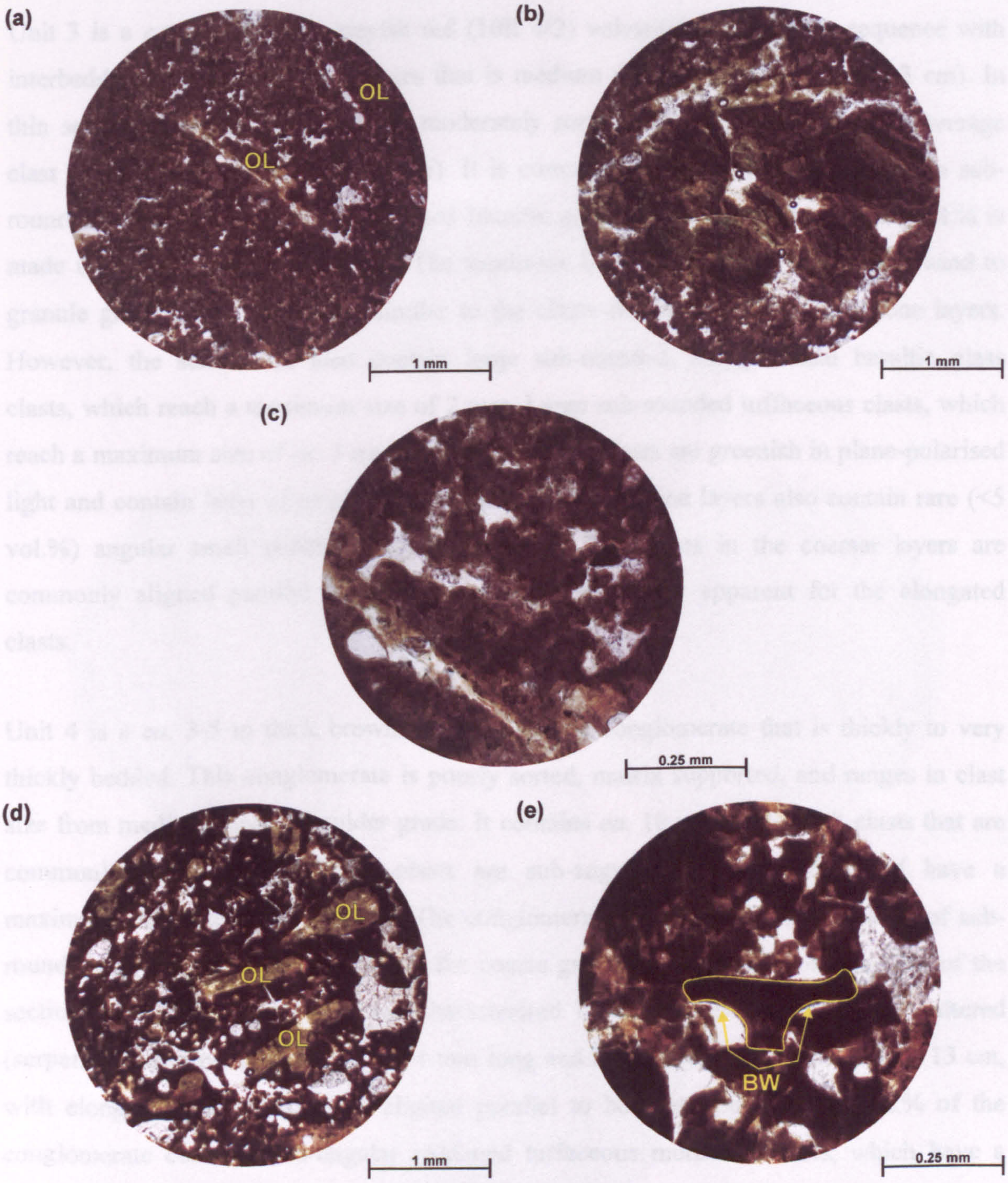

Fig. 5.5. Photomicrographs of Unit 1, coarse tuff, from the base of sections B & C, Svalbarðaá-Myllá Traverse, *ca.* 500 m N of Trongisvágur, Suðuroy, Faeroe Islands. All of the photomicrographs are under plane-polarised light. (a) The tuff is fairly homogeneous in fragment type, which consists of highly altered (palagonitised) basaltic glass fragments. As a consequence of palagonitisation the fragment boundaries have been obscured. Serpentinised euhedral and subhedral needle shaped crystals of olivine occur in larger glass fragments (OL). (b) Fragment boundaries although obscured by palagonitisation sometimes display angular edges. The photomicrograph also shows that there is little or no matrix to the unit. (c) Glass fragments displaying diffused boundaries due to palagonitisation. (d) Some of the larger basaltic glassy fragments contain serpentinised greenish needle-shaped olivine crystals (OL). (e) The centre of the photomicrograph contains a basaltic glass fragment that has cuspate margins, which are the remnants of former bubble walls (BW).

small pebbles (2-8 mm) towards the top of the unit, suggesting that the conglomerate fines upwards.

Unit 3 is a *ca.* 70 cm thick greyish red (10R 4/2) volcaniclastic siltstone sequence with interbedded volcaniclastic sandstones that is medium to thickly laminated (0.5-3 cm). In thin section, the siltstone layers are moderately sorted, clast supported, with an average clast size of very coarse silt (Fig. 5.6). It is composed of 90 vol.% sub-angular to sub-rounded opaque to orange palagonitised basaltic glass clasts. The remaining 10 vol.% is made up of tuffaceous lithic clasts. The sandstone layers range from very coarse sand to granule grade clasts, which are similar to the clasts described from the siltstone layers. However, the sandstones also contain large sub-rounded, amygdaloidal basaltic glass clasts, which reach a maximum size of 2 mm. Large sub-rounded tuffaceous clasts, which reach a maximum size of *ca.* 3 mm also occur. These clasts are greenish in plane-polarised light and contain laths of plagioclase feldspar. The sandstone layers also contain rare (<5 vol.%) angular small pebble grade basalt clasts. The clasts in the coarser layers are commonly aligned parallel to bedding, which is especially apparent for the elongated clasts.

Unit 4 is a *ca.* 3-5 m thick brownish volcaniclastic conglomerate that is thickly to very thickly bedded. This conglomerate is poorly sorted, matrix supported, and ranges in clast size from medium sand to boulder grade. It contains *ca.* 10 vol.% of basalt clasts that are commonly amygdaloidal. These clasts are sub-angular to sub-rounded and have a maximum clast size of 45 x 20 cm. The conglomerate also contains *ca.* 10 vol.% of sub-rounded greyish tuff clasts, similar to the coarse grey tuff described from the base of the section (Unit 1). These clasts are characterised by needle shaped dark green altered (serpentinised) olivine crystals *ca.* 2-4 mm long and have a maximum size of 45 x 13 cm, with elongated clasts frequently aligned parallel to bedding. Less than 5 vol.% of the conglomerate contains sub-angular reddened tuffaceous mudstone clasts, which have a maximum size of 10 x 6 cm, but usually have sizes of 4 x 2 cm. Some of the beds are densely populated with large clasts while others are sparsely populated. The majority of the sand grain material is made up of palagonitised basaltic glass material.

Unit 5 is an olive grey (5Y 3/2) to blackish red (5R 2/2) thickly to very thickly laminated volcaniclastic sandstone (Fig. 5.7). This sandstone is 0.4-1.2 m thick and, in the upper 45 cm, thin (<1 cm) mudstone lamina occur. It is poorly to moderately sorted, matrix supported and an average clast size of very fine to fine sand (Fig. 5.8). The sandstone contains rare (<5 vol.%) sub-angular to sub-rounded clasts of basalt, which have a

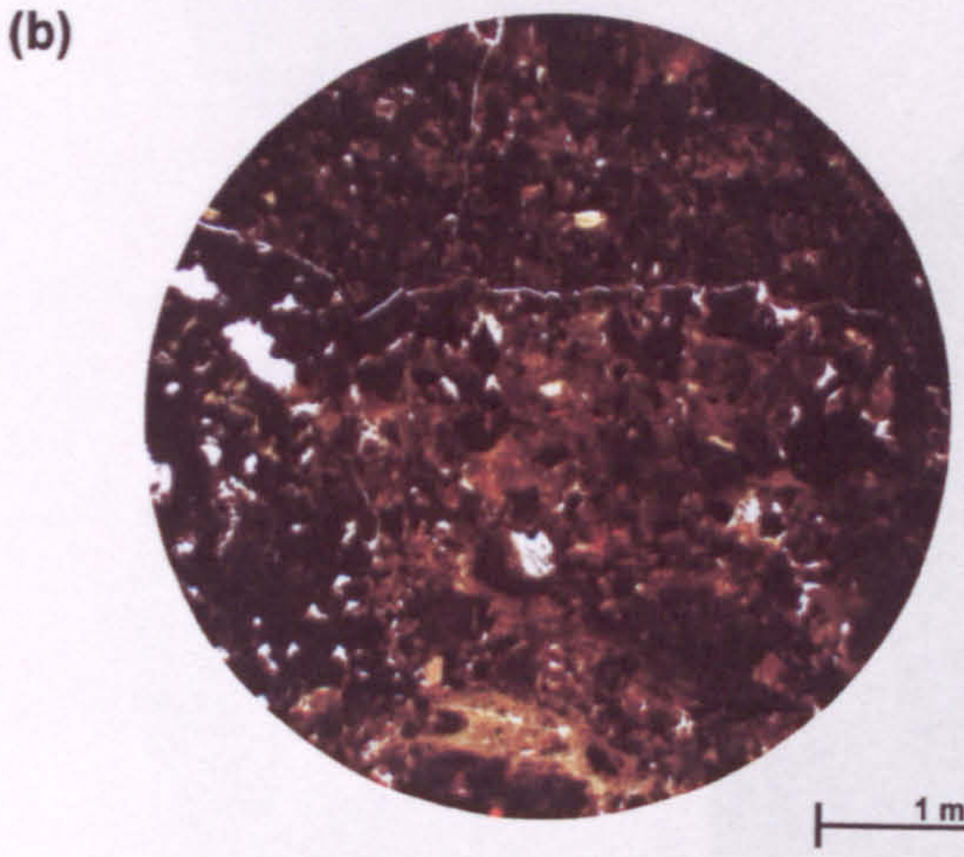

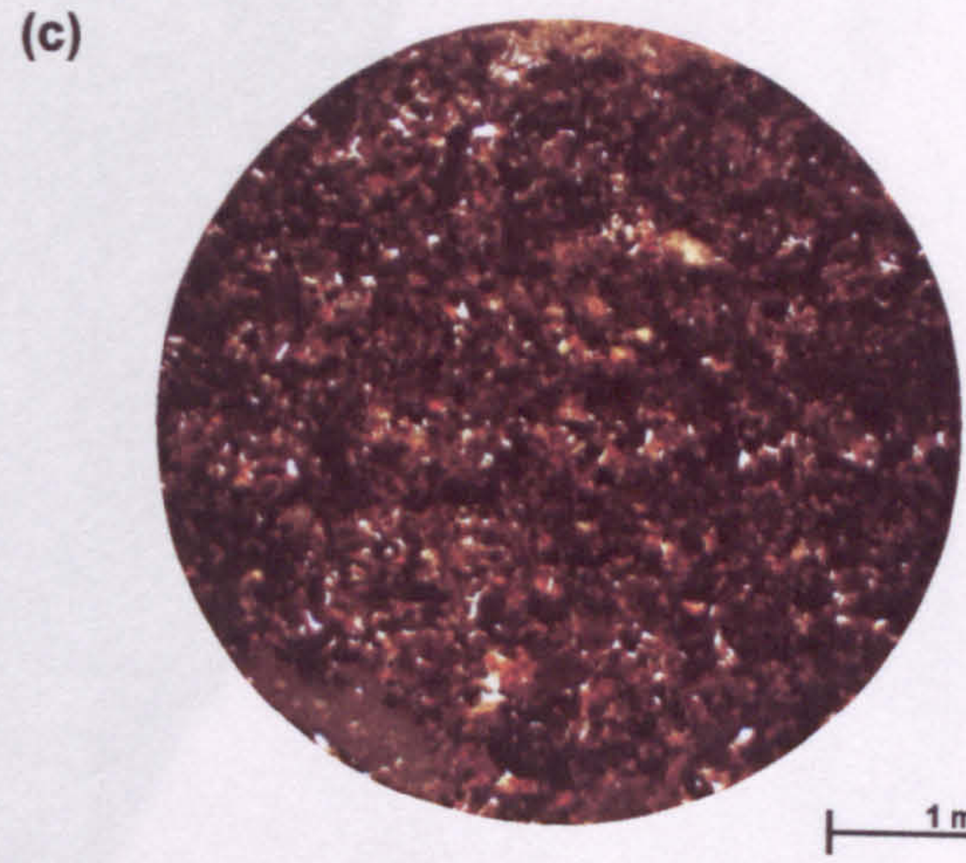

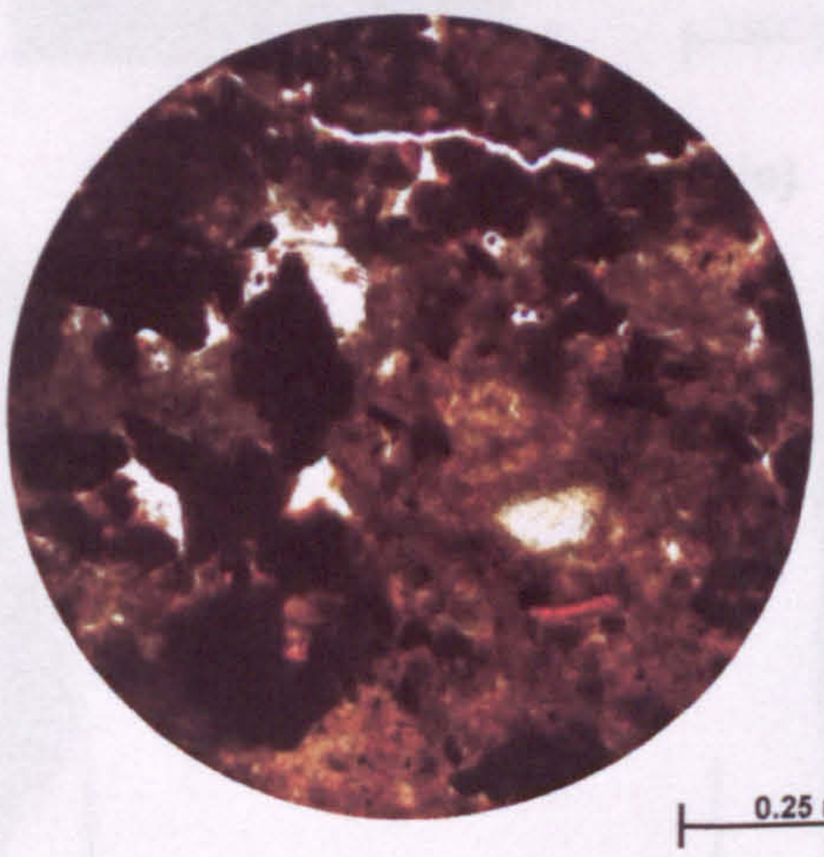

Fig. 5.6. Thin section photograph and photomicrographs from the interbedded volcaniclastic siltstones and sandstones (Unit 3), from sections B & C, Svalbarðaá-Myllá Traverse, *ca.* 500 m N of Trongisvágur, Suðuroy, Faeroe Islands. (a) Thin section photograph showing the medium to thick lamina (0.5-3 cm) of the unit. (b) to (d) Photomicrographs of siltstone lamina under plane-polarised light. The siltstone lamina are poorly sorted and are dominated by palagonitised basaltic glass fragments.

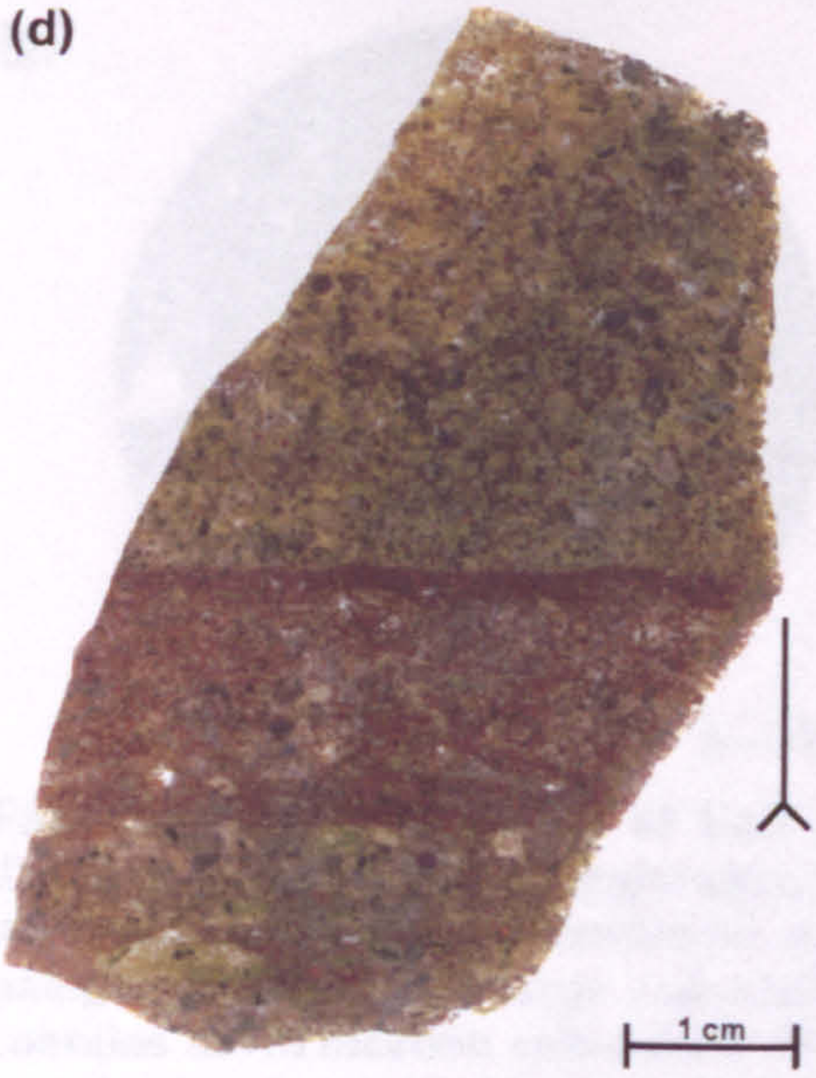

Fig. 5.7. Photographs of Unit 5, volcaniclastic sandstone, from Section B, Svalbarðaá-Myllá Traverse, *ca.* 500 m N of Trongisvágur, Suðuroy, Faeroe Islands. The sandstone is thickly to very thickly laminated. (a) & (b) Field photographs of the volcaniclastic sandstone, which is *ca.* 1.2 m thick. The compass is *ca.* 10 x 6 cm. (c) & (d) Hand specimen and thin section photographs of the layering within the sandstone. (e) Diffusely layered thin section from the sandstone, which is coarser grained than the layers in (c) & (d).

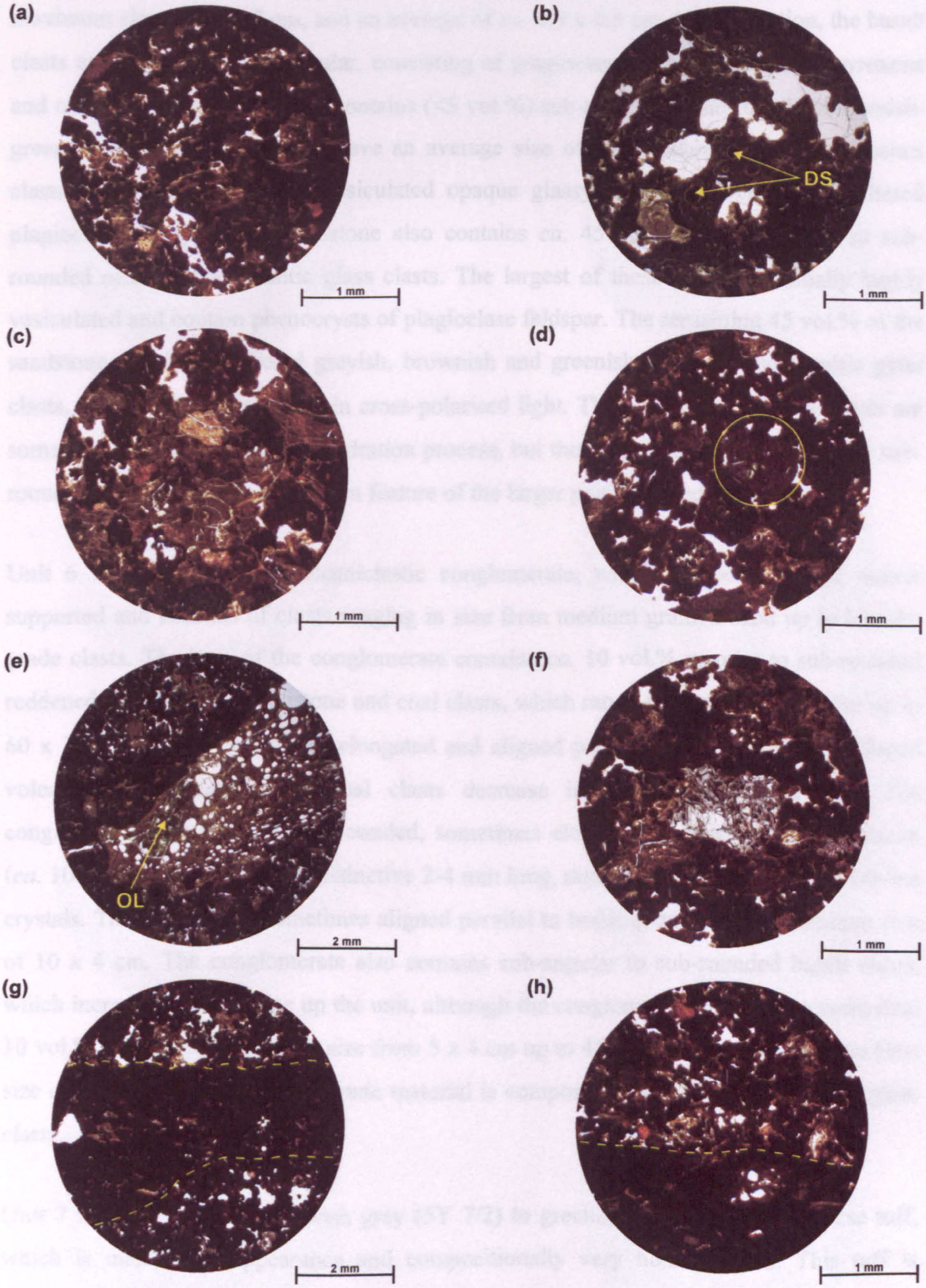

Fig. 5.8. Photomicrographs of Unit 5, volcaniclastic sandstone from Section B, Svalbarðaá-Myllá Traverse, *ca.* 500 m N of Trongisvágur, Suðuroy, Faeroe Islands. All of the photomicrographs are in plane-polarised light. (a) The sandstone contains *ca.* 90 vol.% basaltic glass clasts at various stages of palagonitisation. (b) A large vesiculated near opaque basaltic glass clast, most likely scoria. The clast contains devitrification spherulites (DS) and the occasional plagioclase feldspar lath. (c) Various sub-angular to sub-rounded basaltic glass clasts at various stages of palagonitisation. (d) A 'stony' basalt lava clast is enclosed in the yellow circle. The lava clast is equigranular and consists of plagioclase feldspar laths, clinopyroxenes and oxides. (e) The top left of the photomicrograph consists of a tuffaceous clast made up basaltic glassy clasts. The centre of the photomicrograph consists of a flattened orange vesiculated basaltic glass clast. The clast also contains an altered subhedral olivine crystal (OL). (f) The colourless clast is equigranular basalt lava consisting of plagioclase feldspar laths, clinopyroxene and oxides. (g) & (h) Views of thin mudstone layers interbedded within the sandstone.

maximum size of 4 x 1.5 cm, and an average of *ca.* 0.5 x 0.5 cm. In thin section, the basalt clasts are commonly equigranular, consisting of plagioclase feldspar laths, clinopyroxene and oxides. The sandstone also contains (<5 vol.%) sub-angular to sub-rounded brownish-green tuffaceous clasts, which have an average size of small pebbles. These tuffaceous clasts usually contain highly vesiculated opaque glassy clasts, with crystals of altered plagioclase feldspar. The sandstone also contains *ca.* 45 vol.% of sub-angular to sub-rounded near opaque basaltic glass clasts. The largest of these clasts are usually highly vesiculated and contain phenocrysts of plagioclase feldspar. The remaining 45 vol.% of the sandstone consists of altered greyish, brownish and greenish palagonitised basaltic glass clasts, which are near isotropic in cross-polarised light. The clast edges of these clasts are somewhat obscured due to the hydration process, but they appear to be sub-angular to sub-rounded. Vesiculation is a common feature of the larger palagonitised glass clasts.

Unit 6 is a 3-4 m thick volcaniclastic conglomerate, which is poorly sorted, matrix supported and consists of clasts ranging in size from medium grained sand up to boulder grade clasts. The base of the conglomerate contains *ca.* 10 vol.% angular to sub-rounded reddened volcaniclastic mudstone and coal clasts, which range in size from 3 x 1 cm up to 60 x 30 cm and are sometimes elongated and aligned parallel to bedding. The reddened volcaniclastic mudstone and coal clasts decrease in abundance up the unit. The conglomerate also contains sub-rounded, sometimes elongated, greyish coarse tuff clasts (*ca.* 10 vol.%), which contain distinctive 2-4 mm long, needle-shaped serpentinised olivine crystals. These clasts are sometimes aligned parallel to bedding and have a maximum size of 10 x 4 cm. The conglomerate also contains sub-angular to sub-rounded basalt clasts, which increase in abundance up the unit, although the conglomerate contains no more than 10 vol.%. These clasts range in size from 5 x 4 cm up to 45 x 30 cm, with an average clast size of *ca.* 7 x 5 cm. The sand grade material is composed of palagonitised basaltic glass clasts.

Unit 7 is a 1-4 m thick yellowish grey (5Y 7/2) to greenish grey (5GY 6/1) coarse tuff, which is massive in appearance and compositionally very homogeneous. This tuff is moderately sorted and is dominated by sub-angular to sub-rounded clasts of near opaque palagonitised basaltic glass fragments, with an average fragment size of very fine to fine sand, although fragments up to 3 mm do occur (Fig. 5.9). The fragments show a range in colouration in plane-polarised light, which is the result of palagonitisation; and as a consequence fragment margins are obscured. Some of the fragments contain phenocrysts of plagioclase feldspar and the largest fragments contain euhedral to subhedral serpentinised greenish crystals of olivine, which are a very distinctive feature in hand

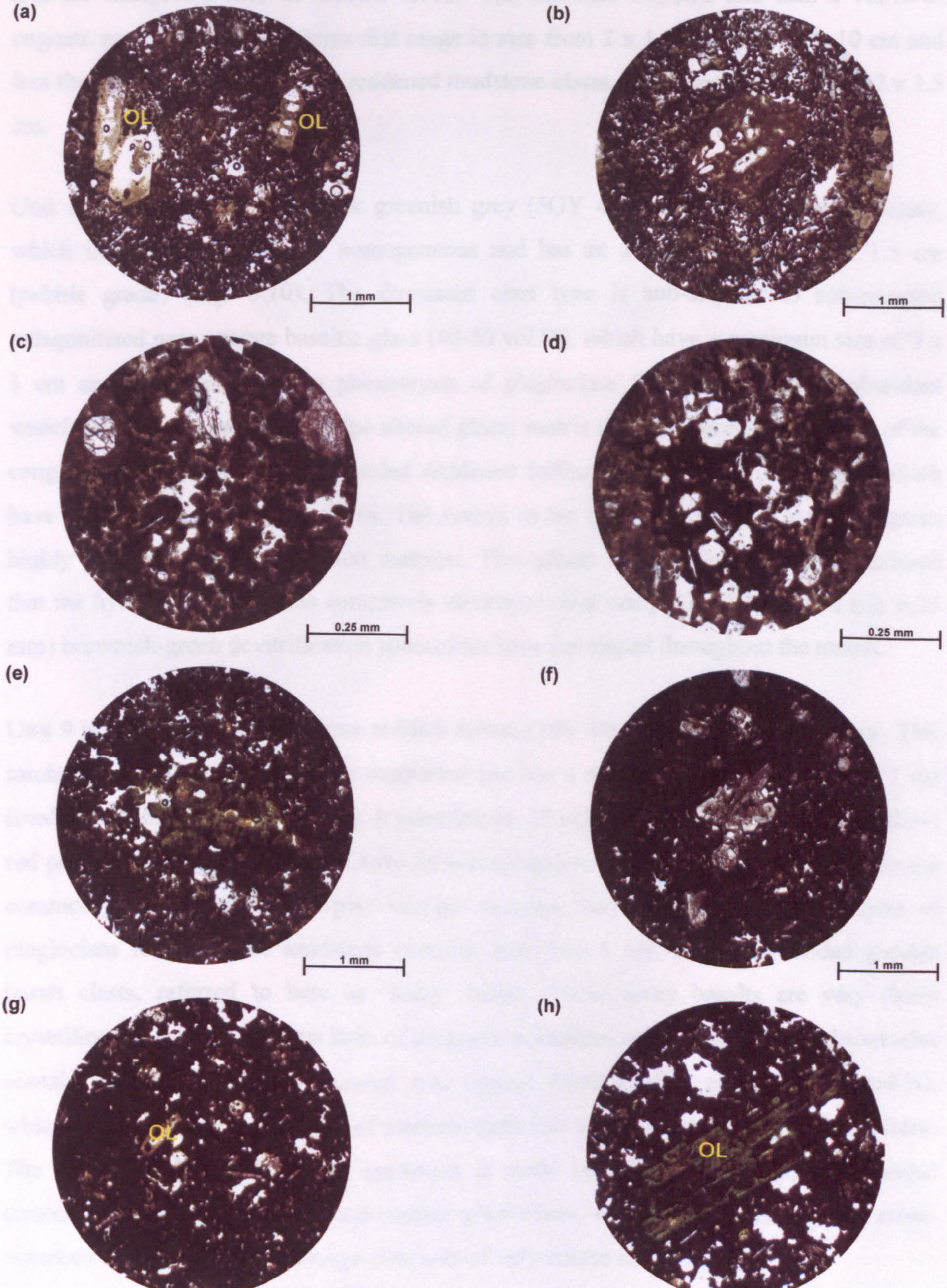

Fig. 5.9. Photomicrographs of Unit 7, coarse tuff, from sections B & C, Svalbarðaá-Myllá Traverse, *ca.* 500 m N of Trongisvágur, Suðuroy, Faeroe Islands. All of the photomicrographs are under plane-polarised light. (a) to (h) The tuff is dominated by palagonitised basaltic glass fragments with an average grain size of very fine to fine sand. The largest glass fragments contain euhedral to subhedral serpentinised greenish crystals of olivine (OL). Rare sub-angular highly vesiculated opaque glassy fragments (scoria) also occur, as seen in (d).

specimen. Rare, sub-angular, highly vesiculated opaque basaltic glass fragments also occur and are interpreted here as basaltic scoria. The tuff also contains less than 2 vol.% of cognate angular basalt fragments that range in size from 2 x 1.5 cm up to 15 x 10 cm and less than 2 vol.% of (accidental) reddened mudstone clasts, with a maximum size of 2 x 1.5 cm.

Unit 8 is a 0.5-2.4 m thick dark greenish grey (5GY 4/1) volcaniclastic conglomerate, which is poorly sorted, fairly homogeneous and has an average clast size 2 x 1.5 cm (pebble grade) (Fig. 5.10). The dominant clast type is sub-angular to sub-rounded palagonitised near opaque basaltic glass (40-50 vol.%), which have a maximum size of 9 x 3 cm and commonly contain phenocrysts of plagioclase feldspar as well as abundant vesicles, which are infilled with the altered glassy matrix material. Less than 5 vol.% of the conglomerate consists of sub-rounded reddened tuffaceous mudstone lithologies, which have a maximum size of 7 x 4 cm. The matrix to the conglomerate is a brownish-green highly palagonitised basaltic glass material. This glassy material is so extremely altered that the hydration process has completely destroyed clast margins and that small (*ca.* 0.25 mm) brownish-green devitrification spherulites have developed throughout the matrix.

Unit 9 is a 0.7-1 m thick moderate reddish brown (10R 4/6) volcaniclastic sandstone. This sandstone is poorly sorted, matrix supported and has a maximum clast size of 1.5 x 1 cm (medium pebble grade) (Fig. 5.11). It contains *ca.* 15 vol.% angular to sub-angular yellow-red palagonitised glass clasts that have an average grain size of fine sand. These clasts are commonly vesiculated and display cuspate margins, and larger clasts contain laths of plagioclase feldspar. The sandstone contains less than 5 vol.% of sub-rounded greyish basalt clasts, referred to here as 'stony' basalt. These stony basalts are very finely crystalline and contain obvious laths of plagioclase feldspar and oxides. The sandstone also contains sub-angular to sub-rounded near opaque basaltic glass clasts (*ca.* 35 vol.%), which have an average clast size of medium sand and larger clasts are highly vesiculated. The remaining 35 vol.% of the sandstone is made up of sub-angular to sub-rounded creamish to brownish palagonitised basaltic glass clasts, which are near isotropic in cross-polarised light and have an average clast size of very coarse silt.

5.2.1.3 Provenance

All of the volcaniclastic units observed within the Svalbarðaá-Myllá Traverse contain clasts derived from within the depositional catchment area. The sedimentary units contain clasts that are dominantly from the reworking of basaltic ash and lapilli grade deposits,

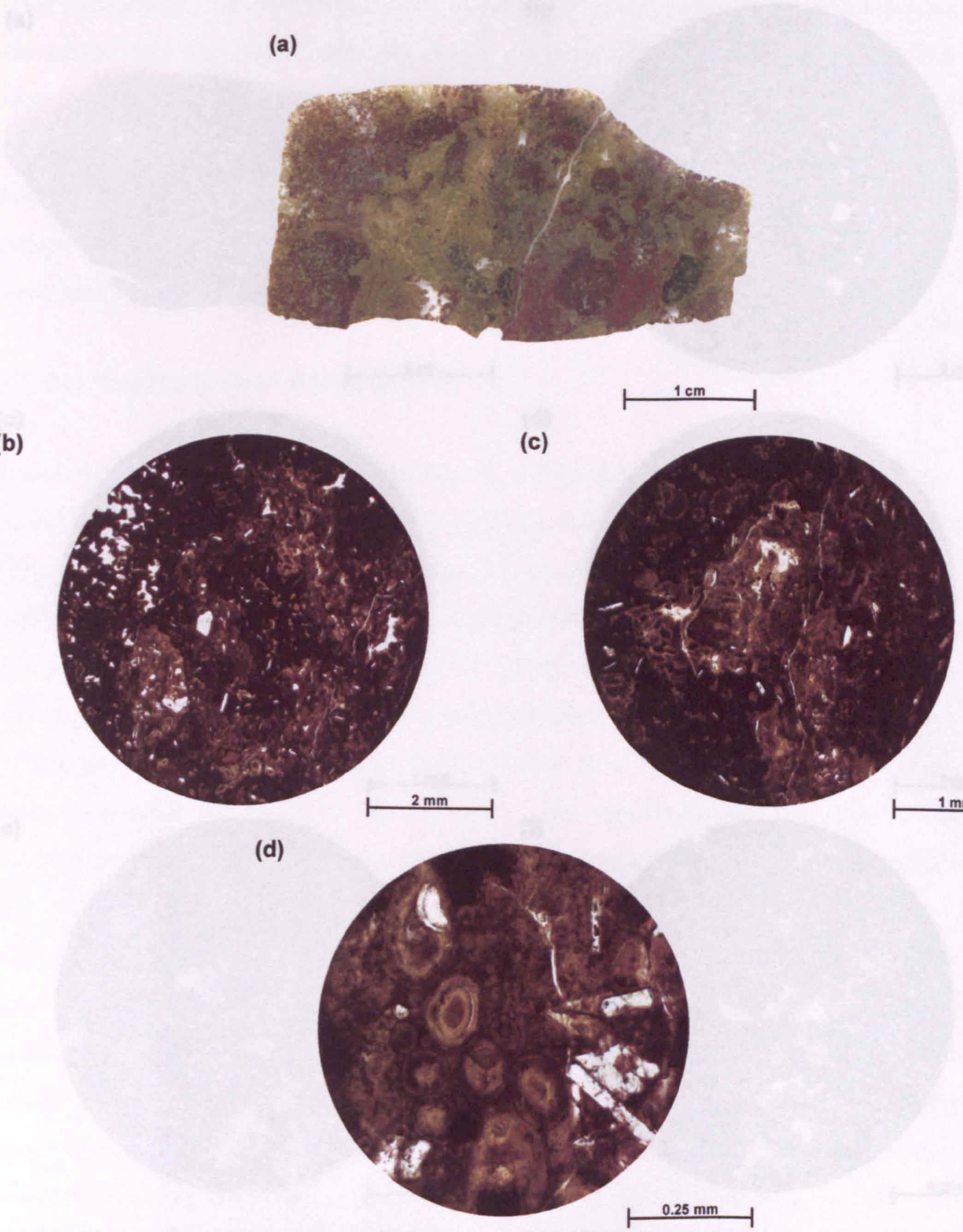

Fig. 5.10. Thin section photograph and photomicrographs of the Unit 8, volcaniclastic conglomerate, from Section B, Svalbarðaá-Myllá Traverse, *ca.* 500 m N of Trongisvágur, Suðuroy, Faeroe Islands. (a) Thin section showing the colour variation of the conglomerate, reflecting different stages of clast alteration. Basaltic glassy clasts are more evident looking at the thin section with the naked eye than under the microscope. All the photomicrographs are under plane-polarised light. (b) & (c) Opaque basaltic glassy clasts are evident, these clasts commonly contain tiny laths of plagioclase feldspar. The clasts are set in a brownish-green highly palagonitised basaltic glass matrix. (c) The top left of the photomicrograph contains highly vesiculated basaltic scoria. The vesicles have been infilled by the altered matrix. (d) The highly altered brownish-green glassy matrix has begun to devitrify and contains abundant devitrification spherulites, which take the form of small (*ca.* 0.25 mm) brownish-green ovals.

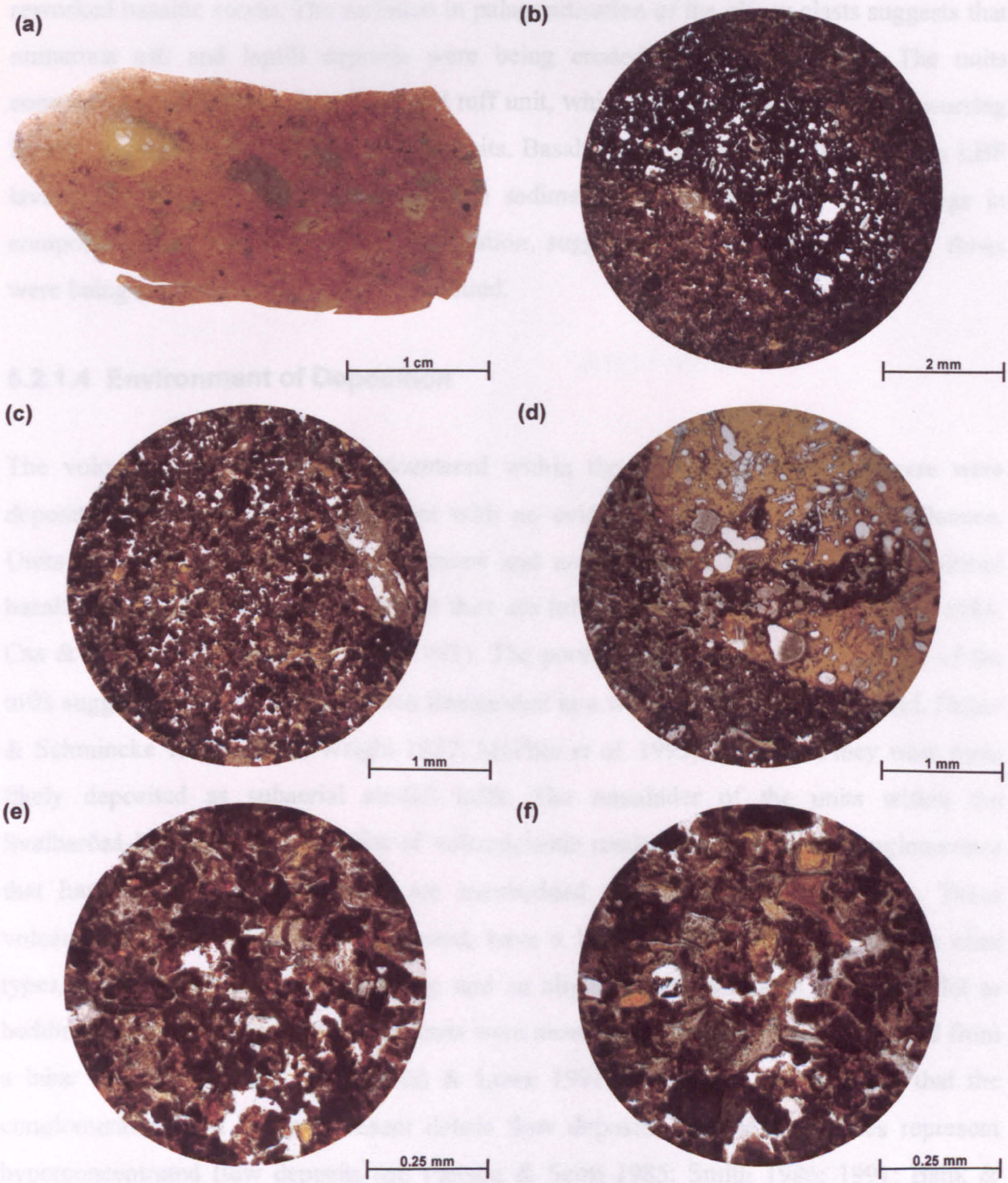

Fig. 5.11. Thin section photograph and photomicrographs of Unit 9, volcaniclastic sandstone, from Section B, Svalbarðaá-Myllá Traverse, *ca.* 500 m N of Trongisvágur, Suðuroy, Faeroe Islands. All of the photomicrographs are under plane-polarised light. (a) The moderate reddish brown sandstone is poorly sorted and is heterogeneous in clast type. (b) A large highly vesiculated opaque basaltic glass clast, most likely scoria, which contains tiny laths of plagioclase feldspar. (c) The sandstone is dominated by various basaltic glass clasts displaying a range of colours from orange to opaque, a consequence of palagonitisation. There is little or no matrix in the pore spaces. (d) The edge of a relatively fresh orange basaltic glass clast, which is highly vesiculated and contains abundant laths of plagioclase feldspar. A fracture in the glass clast has been infilled by finer basaltic glassy material. (e) & (f) The clast boundaries although obscured by the process of palagonitisation appear fairly angular. The pore spaces contain very little or no matrix material. The basaltic glassy clasts display a range in colouration, suggesting various stages of palagonitisation.

most likely derived from pyroclastic air-fall events. This is supported by the abundance of palagonitised basaltic glass clasts and the occurrence of highly vesiculated near opaque reworked basaltic scoria. The variation in palagonitisation of the glassy clasts suggests that numerous ash and lapilli deposits were being eroded contemporaneously. The units commonly contain clasts from the basal tuff unit, which shows that erosion was occurring locally, soon after the deposition of the units. Basalt clasts, most likely derived from LBF lava flows, are also contained within the sedimentary units. The lava clasts range in composition and stages of surface oxidisation, suggesting that numerous exposed flows were being eroded, transported and deposited.

5.2.1.4 Environment of Deposition

The volcaniclastic lithologies encountered within the Svalbarðaá-Myllá Traverse were deposited in a terrestrial environment with no evidence indicating a marine influence. Units 1 and 7 are extremely homogenous and are dominated by angular palagonitised basaltic glass fragments indicating that they are tuff beds (cf. Fisher & Schmincke 1984; Cas & Wright 1987; McPhie *et al.* 1993). The poorly to moderately sorted nature of the tuffs suggests that they have not been transported in a water-borne environment (cf. Fisher & Schmincke 1984; Cas & Wright 1987; McPhie *et al.* 1993); therefore, they were most likely deposited as subaerial air-fall tuffs. The remainder of the units within the Svalbarðaá-Myllá Traverse consist of volcaniclastic mudstones through to conglomerates that have tabular geometries and are interbedded with pyroclastic lithologies. These volcaniclastic units are matrix supported, have a high degree of heterogeneity in clast types, a high degree of clast rounding and an alignment of elongated clasts parallel to bedding. These data suggest that the clasts were most likely transported and deposited from a lahar event (cf. Smith 1991; Smith & Lowe 1991). If correct, this suggests that the conglomerates most likely represent debris flow deposits and the sandstones represent hyperconcentrated flow deposits (cf. Pierson & Scott 1985; Smith 1986; 1991; Bahk & Chough 1996; Coussot & Meunier 1996; Sohn *et al.* 1999; Lirer *et al.* 2001).

5.2.2 Hvannagjógv Section

5.2.2.1 Overview of Section

The Hvannagjógv Section crops out *ca.* 2.2 km west of the Myllá stream section (Fig. 5.1). The section is *ca.* 7.5 m thick, consisting of interbedded brecciated MBF lavas and volcaniclastic rock units (Fig. 5.12). At approximately 200 m above sea level the lavas are

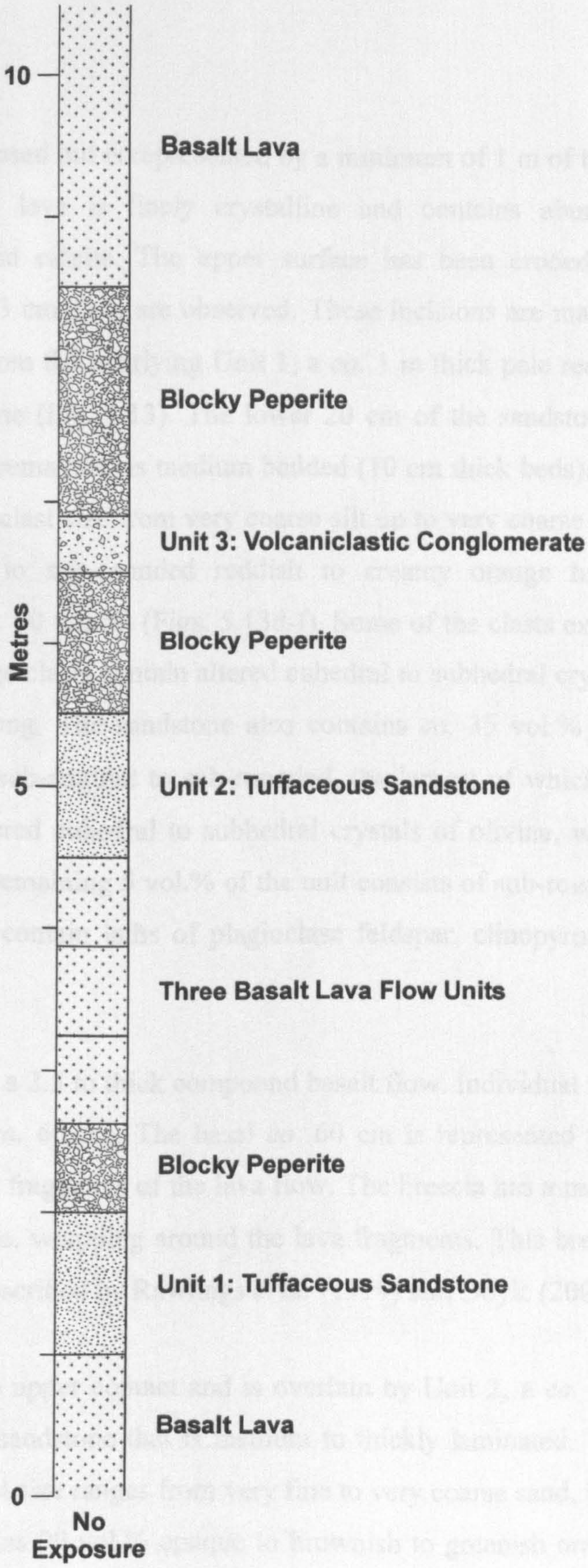

Fig. 5.12. Graphic log of the transitional zone between the Volcaniclastic Sandstone Formation (VSF) and the Middle Basalt Formation (MBF) lavas, Hvannagjógv Section, *ca.* 2.5 km WNW of Trongisvágur, Suðuroy, Faeroe Islands.

not brecciated and exhibit compound structures consistent with belonging to the MBF (see Chapter 6).

5.2.2.2 Lithology & Petrology

The base of the section is poorly exposed but is represented by a minimum of 1 m of basalt from the MBF. The greyish blue lava is finely crystalline and contains abundant amygdales, infilled with zeolites and calcite. The upper surface has been eroded and prominent v-shaped incisions, *ca.* 2-3 cm deep are observed. These incisions are mantled by a *ca.* 1 cm thick greenish layer from the overlying Unit 1, a *ca.* 1 m thick pale reddish brown (10R 5/4) tuffaceous sandstone (Fig. 5.13). The lower 20 cm of the sandstone is medium to thickly laminated but the remainder is medium bedded (10 cm thick beds). The sandstone is poorly sorted, ranges in clast size from very coarse silt up to very coarse sand and is dominated by sub-angular to sub-rounded reddish to creamy orange highly palagonitised basaltic glass clasts (*ca.* 60 vol.%) (Figs. 5.13d-f). Some of the clasts exhibit cuspate margins and the largest orange clasts contain altered euhedral to subhedral crystals of olivine, which are *ca.* 1-2 mm long. The sandstone also contains *ca.* 35 vol.% near opaque basaltic glass clasts that are sub-angular to sub-rounded, the largest of which are typically vesiculated and contain altered euhedral to subhedral crystals of olivine, which have a maximum size of 2 mm. The remaining 5 vol.% of the unit consists of sub-rounded clasts of equigranular basalt, which contain laths of plagioclase feldspar, clinopyroxene and oxides.

Overlying the tuffaceous sandstone is a 2.5 m thick compound basalt flow. Individual flow units have an average thickness of *ca.* 60 cm. The basal *ca.* 60 cm is represented by a jigsaw fit breccia, comprising angular fragments of the lava flow. The breccia has a matrix derived from the underlying sandstone, wrapping around the lava fragments. This breccia is a blocky peperite similar to those described by Rawlings *et al.* (1999) and Doyle (2000).

The compound lava flow has a sharp upper contact and is overlain by Unit 2, a *ca.* 1 m thick olive grey (5Y 3/2) tuffaceous sandstone that is medium to thickly laminated. This sandstone is poorly sorted and the clast size ranges from very fine to very coarse sand, with an average size of fine sand. It contains 90 vol.% opaque to brownish to greenish orange sub-angular to sub-rounded palagonitised basaltic clasts (Fig. 5.14). The largest clasts are highly vesiculated and commonly contain euhedral to subhedral crystals of serpentinised olivine. Some of the clasts exhibit cuspate margins and the margins of the finer clasts are obscured due to the hydration process. The remaining 10 vol.% of the unit is made up of

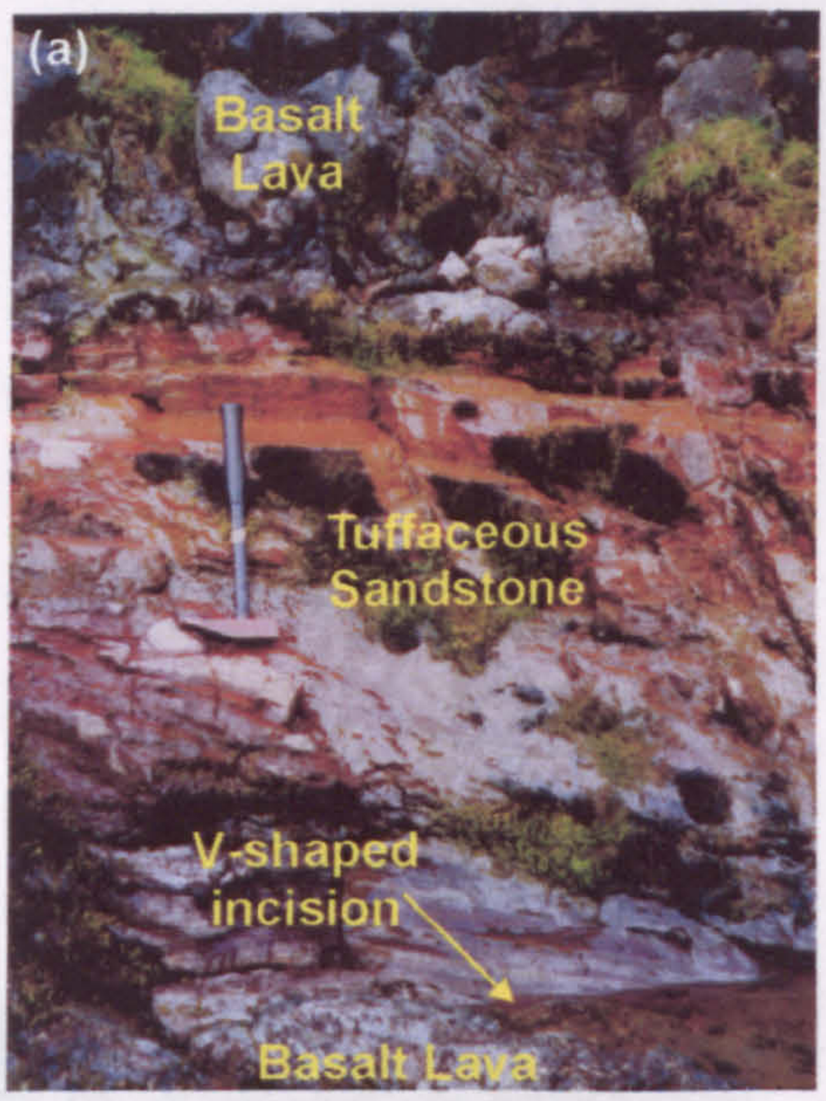

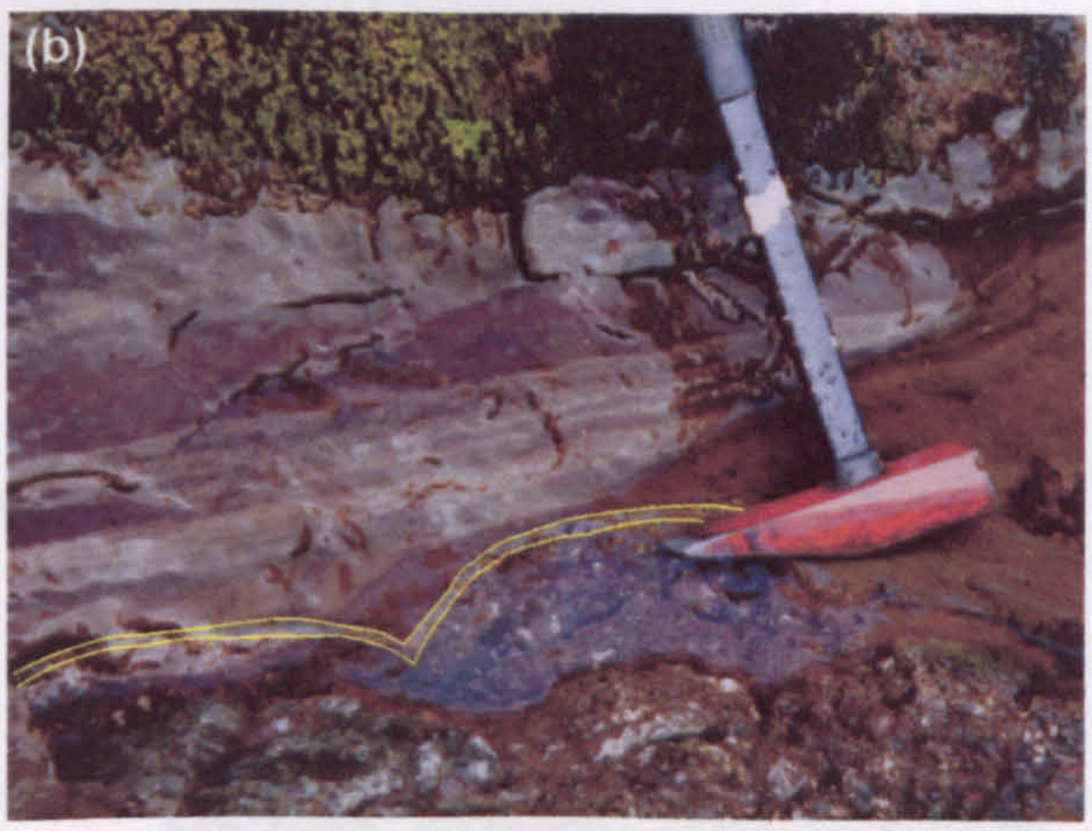

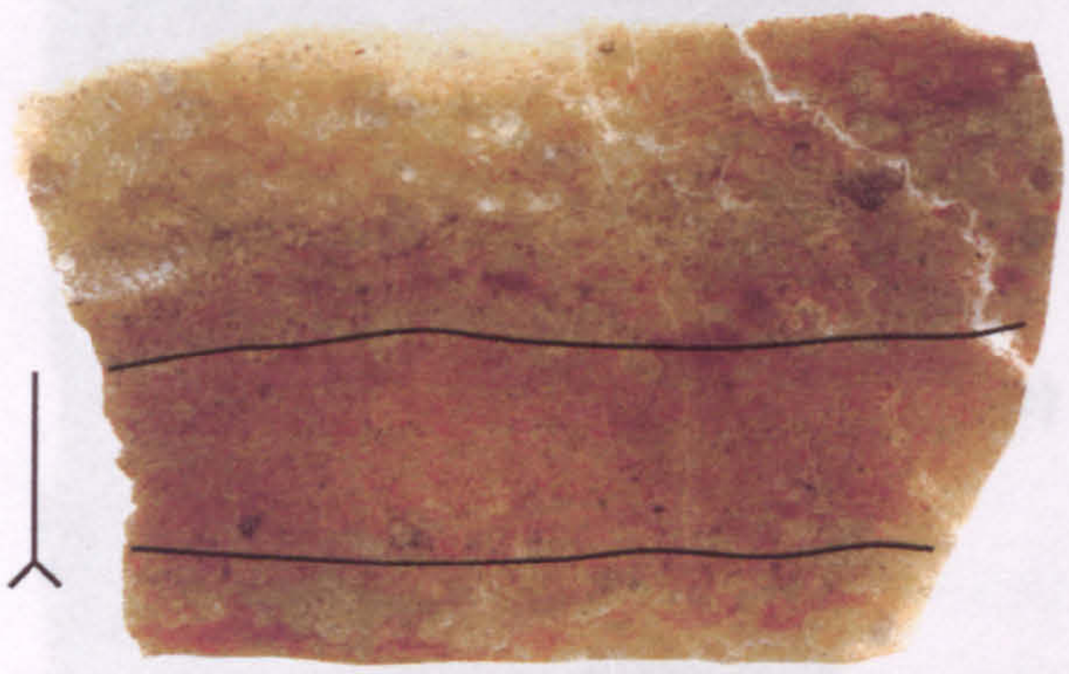

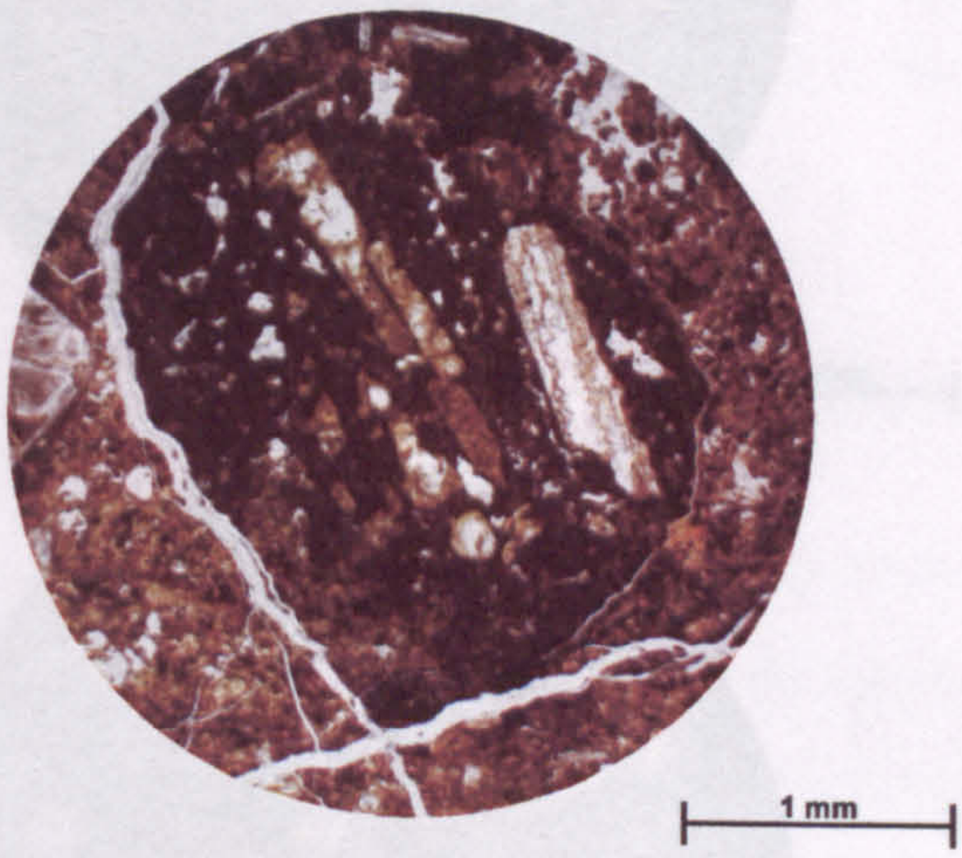

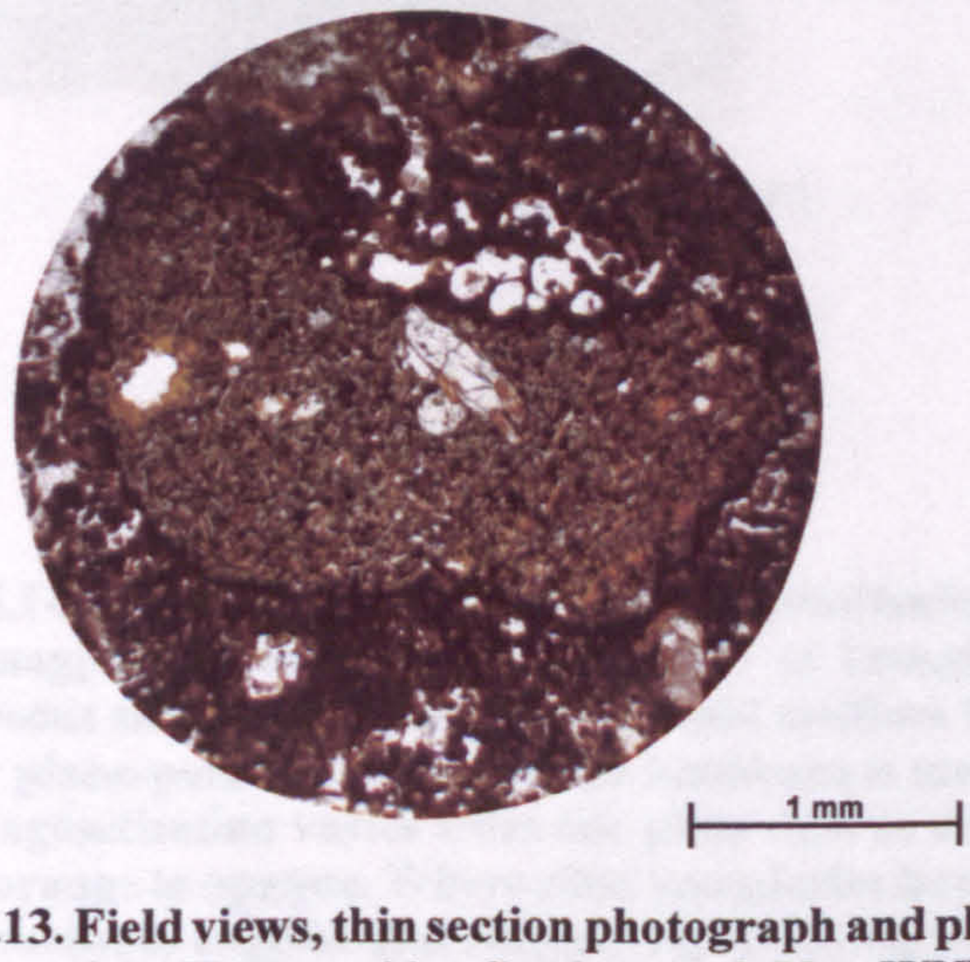

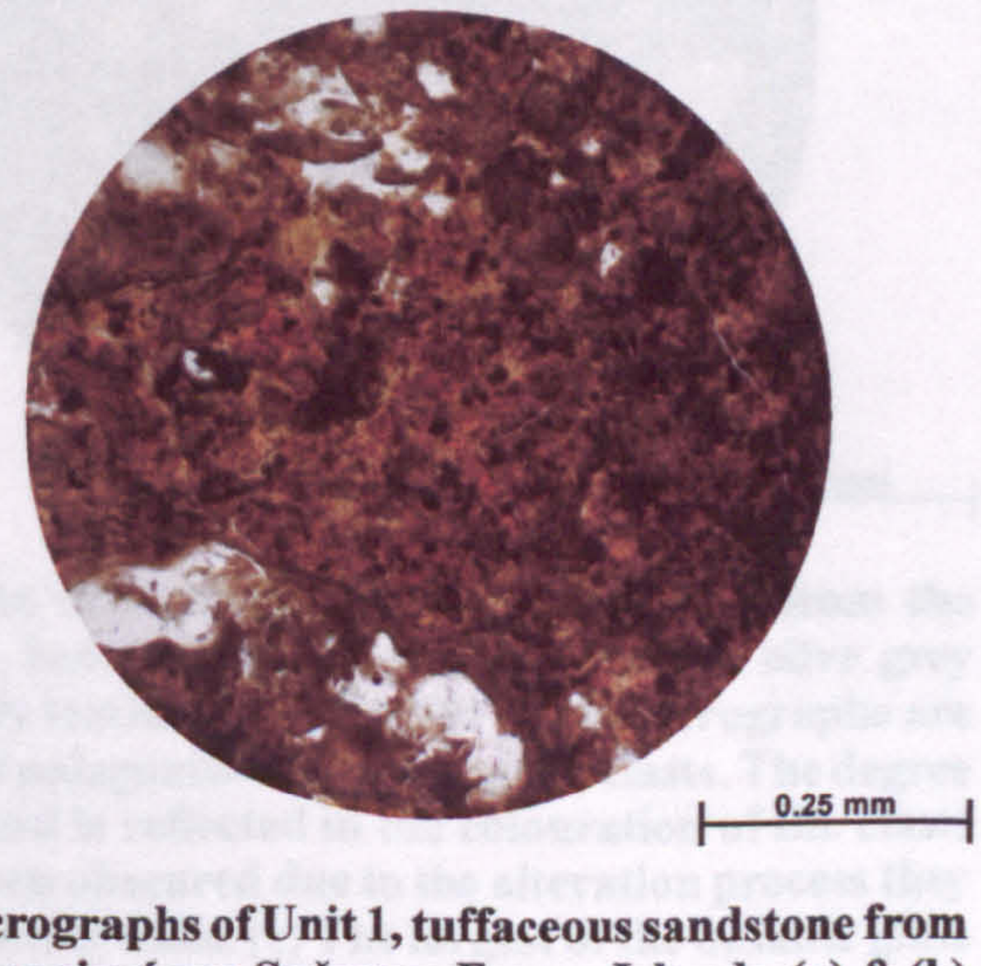

Fig. 5.13. Field views, thin section photograph and photomicrographs of Unit 1, tuffaceous sandstone from the base of the Hvannagjógv Section, *ca.* 2.5 km WNW of Trongisvágur, Suðuroy, Faeroe Islands. (a) & (b) The upper surface of the basalt lava flow has been eroded producing prominent v-shaped incisions. The incisions are mantled by a *ca.* 1 cm thick greenish layer from the overlying 1 m thick pale reddish brown tuffaceous sandstone. (c) The lower 20 cm of the tuffaceous sandstone is medium to thickly laminated and is dominated (60 vol.%) by reddish to creamy orange highly palagonitised basaltic glass clasts. All of the photomicrographs are under plane-polarised light. (d) The sandstone also contains *ca.* 35 vol.% near opaque basaltic glass clasts interpreted here as basaltic scoria. The largest of these clasts are commonly highly vesiculated and contain phenocrysts of highly altered olivine crystals. (e) The sandstone is made up of *ca.* 5 vol.% sub-rounded clasts of equigranular basalt lava. The lava is made up of laths of plagioclase feldspar, clinopyroxene and oxides, rare phenocrysts of plagioclase feldspar also occur. (f) The basaltic glass clasts are highly palagonitised, obscuring clast boundaries but occasionally angular edges are observed.

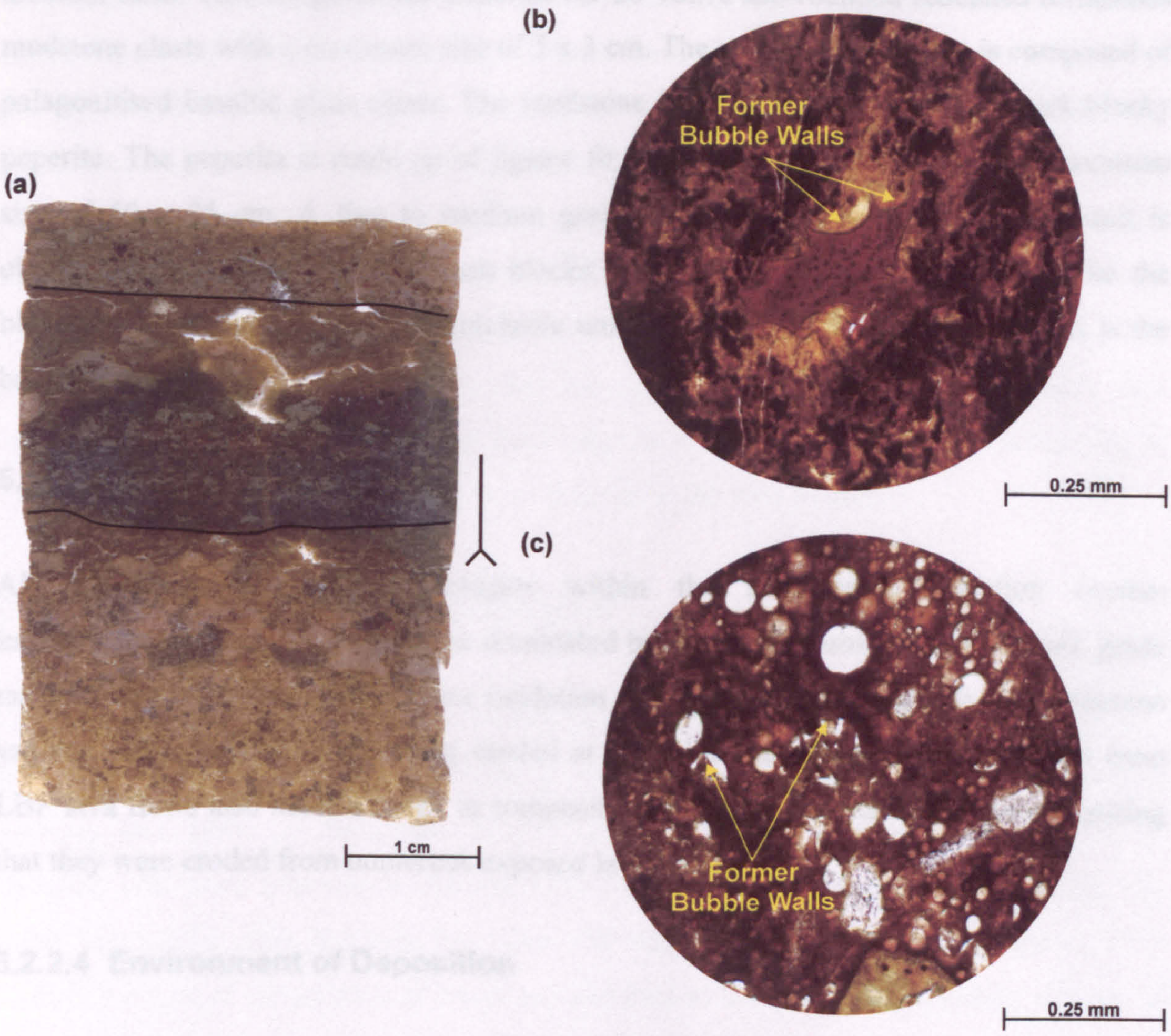

Fig. 5.14. Thin section photograph and photomicrographs of Unit 2, tuffaceous sandstone, from the Hvannagjógv Section, *ca.* 2.5 km WNW of Trongisvágur, Suðuroy, Faeroe Islands. (a) The olive grey tuffaceous sandstone is poorly sorted and medium to thickly laminated. All of the photomicrographs are under plane-polarised light. (b) The sandstone is made up of palagonitised basaltic glass clasts. The degree of palagonitisation varies from one glass clast to another and is reflected in the colouration of the clasts from orange to opaque. Where clast boundaries have not been obscured due to the alteration process they are sometimes angular and cuspate, representing former bubble walls. (c) The largest of the basaltic glass clasts are commonly highly vesiculated and have cuspate margins, the remains of former bubble walls.

sub-rounded clasts of equigranular basalt, which contain laths of plagioclase feldspar, clinopyroxene and oxides.

Overlying the tuffaceous sandstone is a *ca.* 1 m thick blocky peperite similar to the one described above. Unit 3 is a *ca.* 40 cm thick volcaniclastic sandstone that is medium to thickly bedded, poorly sorted, clast supported and has an average clast size of fine to medium sand. This conglomerate contains *ca.* 20 vol.% sub-rounded reddened tuffaceous mudstone clasts with a maximum size of 5 x 3 cm. The remaining 80 vol.% is composed of palagonitised basaltic glass clasts. The sandstone is overlain by a *ca.* 1.6 m thick blocky peperite. The peperite is made up of jigsaw fit basalt fragments, which have a maximum size of 50 x 25 cm. A fine to medium grained matrix akin to the underlying unit is observed wrapping around the basalt blocks. Basalt flow units of the MBF overlie the blocky peperite and no other volcaniclastic units are observed, suggesting that this is the base of the MBF.

5.2.2.3 Provenance

All of the volcaniclastic lithologies within the Hvannagjógv Section contain intraformational clasts. The units are dominated by reworked basaltic ash and lapilli grade material, and the variation in surface oxidation states of the clasts suggests that numerous ash and lapilli deposits were being eroded at the same time. Basalt clasts, derived from LBF lava flows also show a range in composition and surface oxidation states suggesting that they were eroded from numerous exposed lava flows.

5.2.2.4 Environment of Deposition

The volcaniclastic rocks within the Hvannagjógv Section have a high degree of heterogeneity, which suggests that they were formed by epiclastic processes (cf. Fisher & Schmincke 1984; Cas & Wright 1987; McPhie *et al.* 1993). As the lava flow units are extremely brecciated (blocky peperites) it suggests that the sedimentary units were water-rich at the time of eruption (cf. Skilling *et al.* 2002, and references therein). The general lack of rounding suggests that the clasts have only been transported to a limited extent. It is unclear whether the units were deposited within a fluvial or lacustrine environment. The mantling of the basal lava flow is a common feature associated with the deposition of tuff units (cf. Fisher & Schmincke 1984; Cas & Wright 1987; McPhie *et al.* 1993). Therefore, the basal tuffaceous sandstone may have been deposited originally as a tuff bed, which has subsequently been reworked, but preserving the basal tuff-like characteristics.

5.2.3 Summary

The Húsagarðsá to Hvannagjógv Traverse records episodes of pyroclastic and epiclastic deposition. Two units of olivine-phyric vitric basaltic tuffs were deposited within the VSF. These tuffs are extremely homogeneous, massive in appearance, poorly sorted, have glass shards and they mantle the topography, tentatively suggesting that they may even have been deposited by aeolian processes as subaerial air-fall tuffs rather than in a subaqueous environment. The volcaniclastic conglomerates through to mudstones within the traverse are interbedded with pyroclastic lithologies, which implies that they were formed contemporaneously with volcanism. The tabular geometries, matrix supported fabric and heterogeneous clast compositions, of the units suggests that they represent volcaniclastic debris and hyperconcentrated flow deposits formed during a lahar event (cf. Smith & Lowe 1991, and others). The top of the VSF in the west at Hvannagjógv is transitional with MBF lava flow units, which have generally been brecciated as a consequence of water-saturated volcaniclastic units. The absence of flow units in the VSF along the Svalbarðaá-Myllá Traverse implies that the MBF flows were erupted to the west of Myllá.

5.3 Hvannhagi–Lónin Traverse

The Hvannhagi to Lónin Traverse is located in the bays *ca.* 2.5 km N of Tvøroyri, Suðuroy (Fig. 5.2). The traverse is *ca.* 2.5 km long by *ca.* 150 m high and consists of a sequence between lava flows of the Lower Basalt Formation (LBF) and the MBF (Fig. 5.15). Doleritic sills have extensively disrupted the VSF in this traverse. The sills occupy the entire base of the cliffs in Lónin Bay. The VSF has a maximum exposed thickness of *ca.* 30 m in the east of the traverse at Dysjarnar and dips to the ENE. An extensive outcrop of agglomerate occupies the wave cut platform S of Stapin.

5.3.1 Vents

A mass of agglomerate crops out on the wave cut platform S of Stapin, which has a domed and annular shape (Fig. 5.16). The outcrop has an exposed thickness of *ca.* 10 m and extends for *ca.* 150 m S of Stapin, but is only *ca.* 2 m thick on its southern margin. A thin sedimentary sequence, comprising a *ca.* 0.5 m thick shale and a *ca.* 0.2 m thick coal overlie the southern margin of the agglomerate (Fig. 5.17a-b) and *ca.* 1.8 m thick shaly unit overlies the northern margin (Fig. 5.17c-d). Doleritic dykes and sills have intruded the northern and southern margins of the agglomerate (see Section 5.3.2) (Fig. 5.17). The

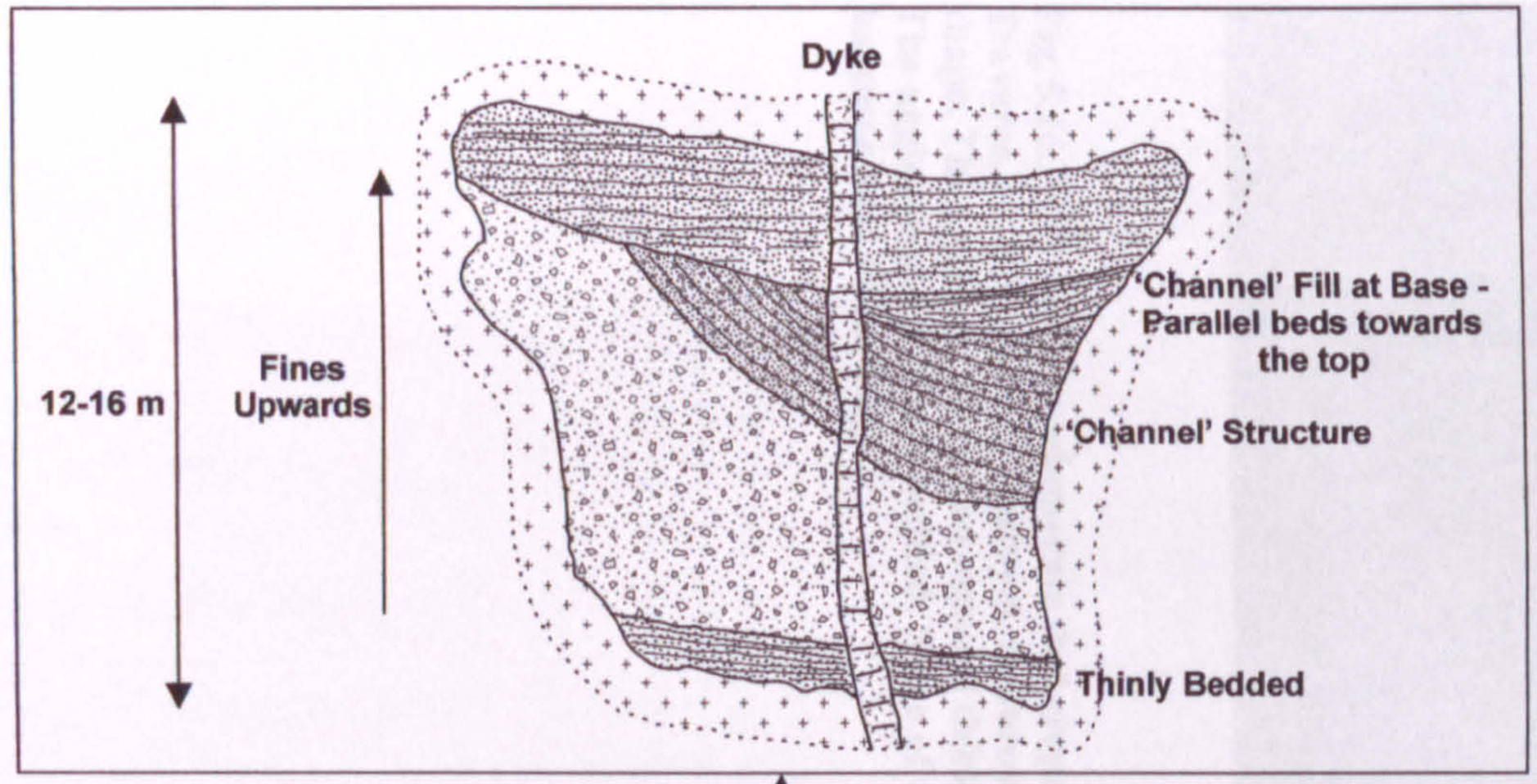

Fig. 5.15. Cross-section of the Hvannhagi-Lónin Traverse, *ca.* 2.5 km N of Tvøroyri, Suðuroy, Faeroe Islands. The insert is a representation of the Lónin raft, which is contained within doleritic sills. LBF = Lower Basalt Formation, VSF = Volcaniclastic Sandstone Formation, and MBF = Middle Basalt Formation

Fig. 5.16. Views of the agglomerate that crops out on the wave cut platform S of Stapin, Hvannhagi-Lónin Traverse, *ca.* 2.5 km N of Tvøroyri, Suðuroy, Faeroe Islands. (a) The exposure is domed and annular in shape. The agglomerate has an exposed thickness of *ca.* 10 m and has a horizontal extent of *ca.* 150 m. (b) The agglomerate is thinly bedded. Some of the bedding planes have been highlighted by red lines. The hammer is *ca.* 40 cm long.

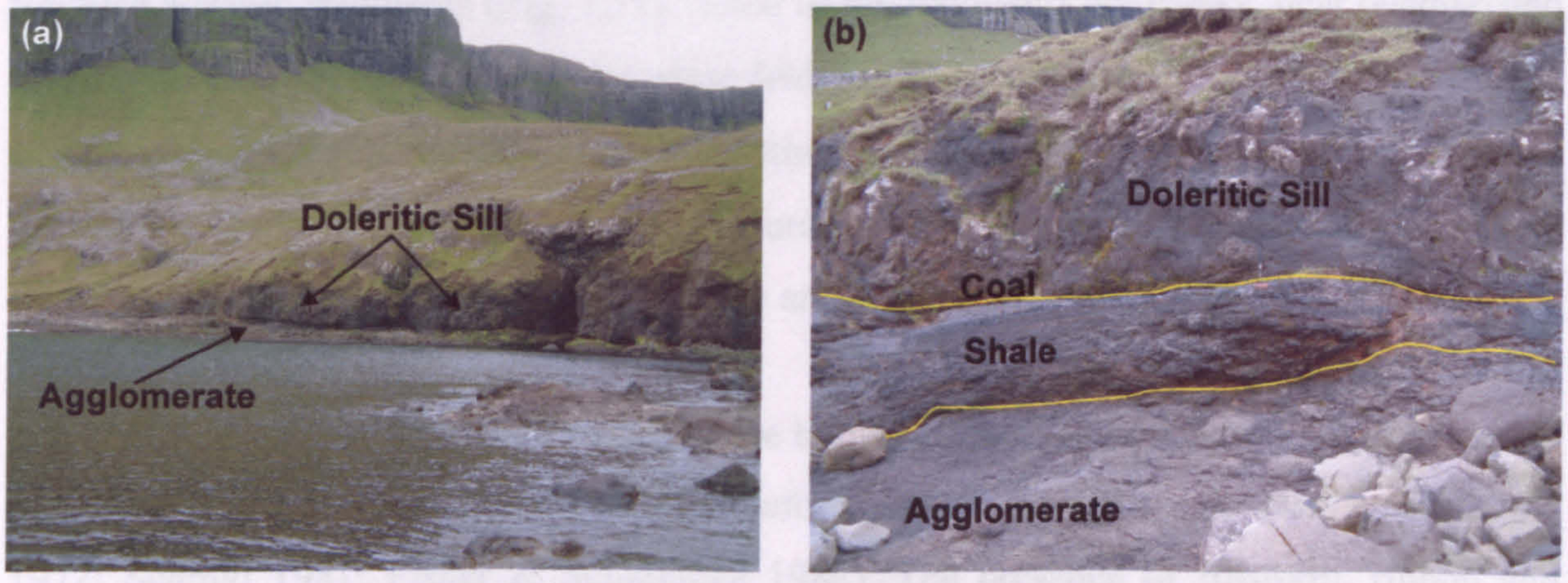

Fig. 5.17. Views of the agglomerate S of Stapin, Hvannhagi-Lónin Traverse, *ca.* 2.5 km N of Tvøroyri, Suðuroy, Faeroe Islands. (a) & (b) The southern extent of the agglomerate is *ca.* 2 m thick and is overlain by a *ca.* 0.5 m thick shale and a *ca.* 0.2 m thick coal from the Coal-bearing Formation (CBF). Overlying the coal is a doleritic sill, which contains large rafts of the underlying coal and shale. (c) & (d) The northern margin of the agglomerate is overlain by shale from the CBF, which has been intruded by a doleritic sill that displays lobate margins. The hammer is *ca.* 40 cm long.

agglomerate is thinly bedded and poorly sorted (Fig. 5.16b), and is made up of nearly 100 vol.% basaltic fragments with lobate margins, ranging in size from coarse ash grade to blocks and bombs with a maximum size of *ca.* 70 cm (Fig. 5.18). The average dimensions of the fragments are of the order of *ca.* 10 cm. Rare occurrences of fusiform, ribbon and cow-dung bombs are observed within the exposure (Fig. 5.18e). Some of the cow-dung bombs exhibit vesicle-poor cores but highly vesicular rims (Fig. 5.18f). The agglomerate has no matrix and what little cement is present is zeolitic in composition. In thin section, the agglomerate is extremely poorly sorted, clast supported and consists of various sub-rounded basaltic fragments (Fig. 5.19). Some of the fragments are glassy, near opaque, and contain tiny infrequent laths of plagioclase feldspar. These fragments have irregular shaped amygdales of zeolite group minerals. Other basaltic fragments are aphyric, finely crystalline, displaying an intergranular texture and are composed of laths of plagioclase feldspar, subhedral crystals of clinopyroxene and oxides.

The lobate margins and sinuous shapes of the bombs are indicative that the fragments acted plastically at the time of deposition and therefore are true pyroclasts (cf. MacDonald 1967; 1972; Schmid 1981; Fisher & Schmincke 1984). The presence of fusiform, ribbon and cow-dung bombs supports this interpretation and these bombs are characteristic of primary pyroclastic deposits (MacDonald 1967; 1972; Fisher & Schmincke 1984). Cow-dung bombs are formed from masses of very fluid lava that have not been projected to any great height to allow solidification and therefore have remained fluidal on impact suggesting that they have landed in close proximity to the vent (cf. MacDonald 1972). These data suggest that the unit can be qualified as an agglomerate in the true lithological definition of the term (Schmid 1981). The presence of the agglomerate, the annular shape of the outcrop and presence of bedding suggests that the unit was deposited near a vent, named here as the Stapin Vent.

According to D.W. Jolley (*pers. comm.*) the shale and coal overlying the agglomerate is biostratigraphically similar to those deposited in the CBF and unrelated to coals deposited in the LBF. This suggests that the vent was active prior to the deposition of the CBF and is either associated with the LBF volcanism or small localised vents of early CBF age and not with the VSF. If the vent was associated with the VSF, the shale and coal deposits would most likely have been destroyed by the development of the vent and consequently would not be mantling the agglomerate.

Fig. 5.18. Views of the agglomerate S of Stapin, Hvannhagi-Lónin Traverse, *ca.* 2.5 km N of Tvøroyri, Suðuroy, Faeroe Islands. (a) to (d) The agglomerate is composed entirely of basaltic fragments of a pyroclastic origin. The agglomerate is poorly sorted and ranges in size from coarse ash up to blocks and bombs with a maximum size of *ca.* 70 cm. The pyroclasts commonly have lobate margins and fusiform, ribbon and cow-dung bombs occur. (e) A large cow-dung bomb, which has formed when ejected lava has remained fluidal on impact, suggesting that the material was not projected to any great height to allow solidification. (f) A pyroclastic bomb that displays a vesicle poor core and a highly vesicular rim, typical of pyroclastic bombs. The compass is *ca.* 10 x 6 cm, the lens cap is *ca.* 6 cm across and the hammer is *ca.* 40 cm long.

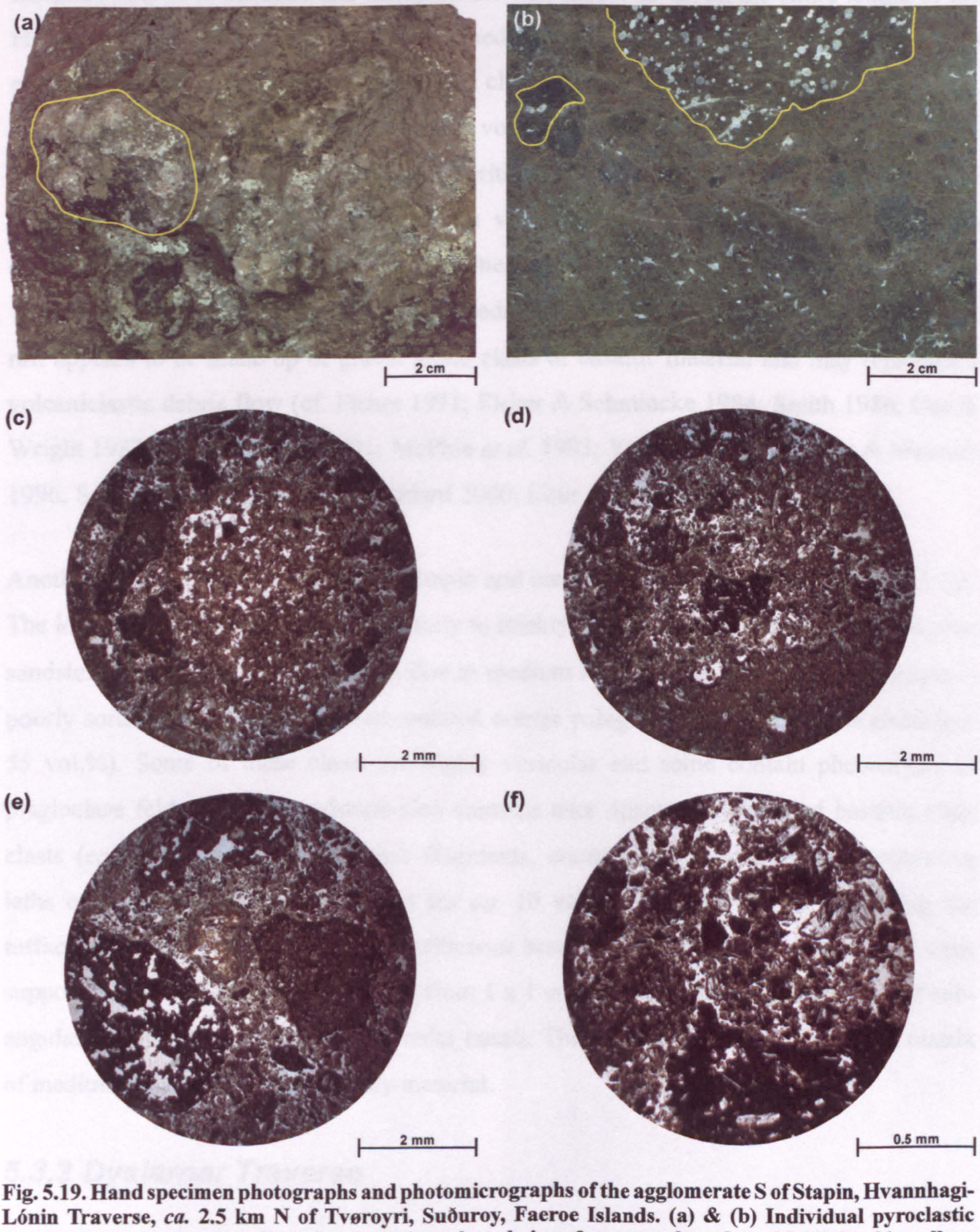

Fig. 5.19. Hand specimen photographs and photomicrographs of the agglomerate S of Stapin, Hvannhagi-Lónin Traverse, *ca.* 2.5 km N of Tvøroyri, Suðuroy, Faeroe Islands. (a) & (b) Individual pyroclastic fragments are hard to identify in hand specimen but obvious fragments have been highlighted in yellow. All of the photomicrographs are under plane-polarised light. (c) to (f) The agglomerate is extremely poorly sorted, clast supported and consists of various sub-rounded basaltic fragments. Some of the basaltic fragments display a range of glassy textures and variations in colour from orange to near opaque. The glassy fragments contain tiny laths of plagioclase feldspar and some contain irregular shaped amygdales of zeolitic group minerals. Other basaltic fragments are aphyric and finely crystalline displaying an intergranular texture. These fragments are composed of laths of plagioclase feldspar, subhedral crystals of clinopyroxene and oxides. The agglomerate has a small proportion of zeolitic cement.

5.3.2 Sills

Doleritic sills have intruded and disrupted the CBF and VSF along the entire length of the Hvannhagi–Lónin Traverse. The sills are medium to finely crystalline and consist of laths of plagioclase feldspar *ca.* 0.1 mm long and clinopyroxene *ca.* 0.25 mm in size (Fig. 5.20). The sills are equigranular and contain *ca.* 5 vol.% vesicles/amygdales, suggesting that they were intruded at a shallow depth. The doleritic sills are extremely well exposed in Lónin Bay and consist of columns orientated in various directions. Large rafts/xenoliths are observed within the sills west of Todnes. One such raft, observed in Lónin Bay, is *ca.* 12-16 m high by 14-18 m wide and exhibits bedding and channel structures (Fig. 5.21). The raft appears to be made up of gravel grade clasts of basaltic material and may represent a volcaniclastic debris flow (cf. Fisher 1971; Fisher & Schmincke 1984; Smith 1986; Cas & Wright 1987; Smith & Lowe 1991; McPhie *et al.* 1993; Yarnold 1993; Coussot & Meunier 1996; Sohn *et al.* 1999; Kessler & Bédard 2000; Lirer *et al.* 2001).

Another large raft is located north of Stapin and measures *ca.* 20 m by *ca.* 8 m (Fig. 5.22). The lower 5 m of the raft consists of thinly to thickly bedded greenish to greyish tuffaceous sandstones ranging in clast size from fine to medium sand. In thin section, the sandstone is poorly sorted and comprises of sub-rounded orange palagonitised basaltic glass clasts (*ca.* 55 vol.%). Some of these clasts are highly vesicular and some contain phenocrysts of plagioclase feldspar. The sandstone also contains near opaque sub-rounded basaltic glass clasts (*ca.* 35 vol.%). Greyish basalt fragments, commonly sub-rounded and containing laths of plagioclase feldspar, account for *ca.* 10 vol.% of the sandstone. Overlying the tuffaceous sandstone is a 2.9 m thick tuffaceous breccia. This breccia is poorly sorted, clast supported, with a clast size that ranges from 1 x 1 cm to 10 x 6 cm, and is made up of sub-angular to sub-rounded clasts of vesicular basalt. The clasts are contained within a matrix of medium sand palagonitised glassy material.

5.3.3 Dysjarnar Traverse

5.3.3.1 Overview of Traverse

This traverse is *ca.* 1 km long and extends from the inaccessible Ribbingamúli point westwards to the landslip at Dysjarnar, *ca.* 2 km N of Tvøroyri, Suðuroy (Fig. 5.2). The traverse consists of three stream exposures (sections I-III), which are located within a 400 m stretch of the traverse (Figs. 5.23 & 5.24). In this traverse the contact between the VSF and MBF goes from a height of 110 m in Section I to 85 m in Section III, a dip of *ca.* 4° to

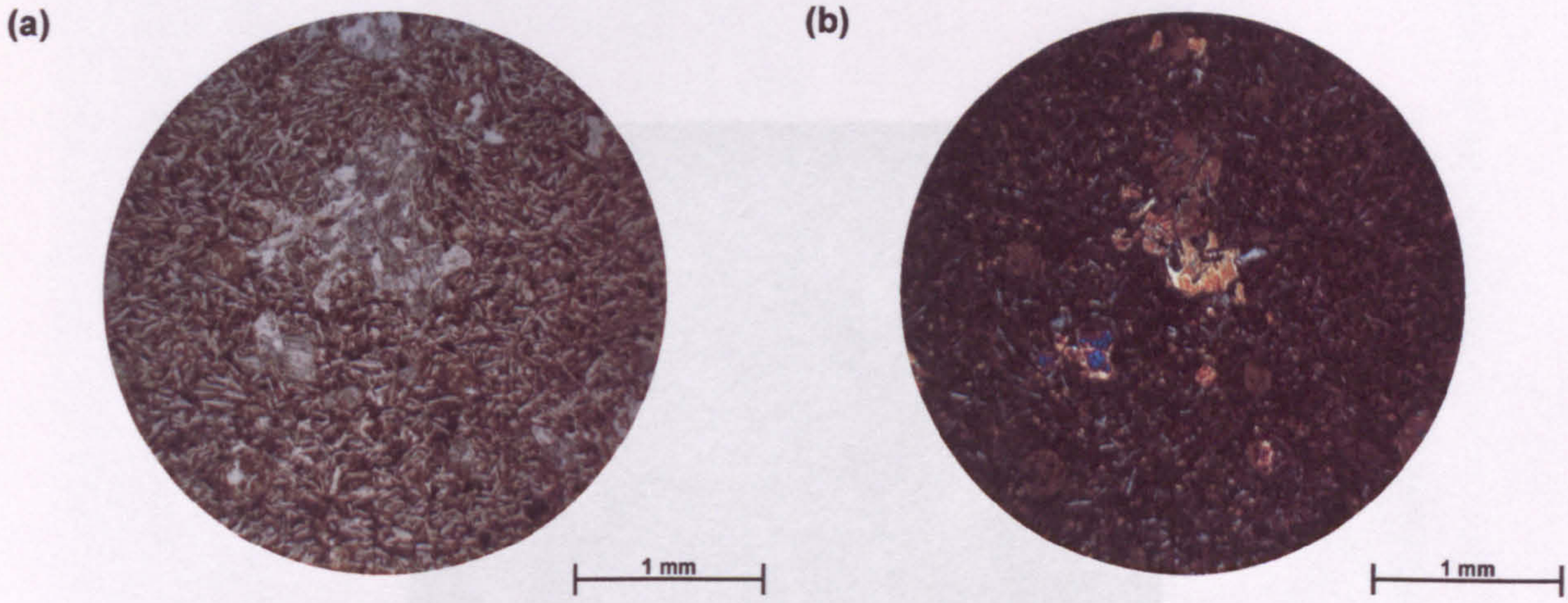

Fig. 5.20. Photomicrographs of the doleritic sills intruding the northern margin of the agglomerate S of Stapin, Hvannhagi-Lónin Traverse, *ca.* 2.5 km N of Tvøroyri, Suðuroy, Faeroe Islands. The sills are finely crystalline, equigranular and contain *ca.* 5 vol.% vesicles/amygdales, suggesting that they were intruded at a shallow level. The sills contain laths of plagioclase feldspar (*ca.* 0.1 mm long), clinopyroxenes (*ca.* 0.25 mm) and oxides. (a) Photomicrograph under plane-polarised light. (b) Same view as in (a) but under cross-polarised light.

Fig. 5.21. Views of the large raft contained within doleritic sills at Lónin Bay, *ca.* 2.5 km N of Trongisvágur, Suðuroy, Faeroe Islands. The raft is *ca.* 12-16 m high by 14-18 m wide. The raft is composed of poorly sorted sandstones and conglomerates which exhibit possible bedding and channel structures, suggesting that the raft was once a deposit from a lahar.

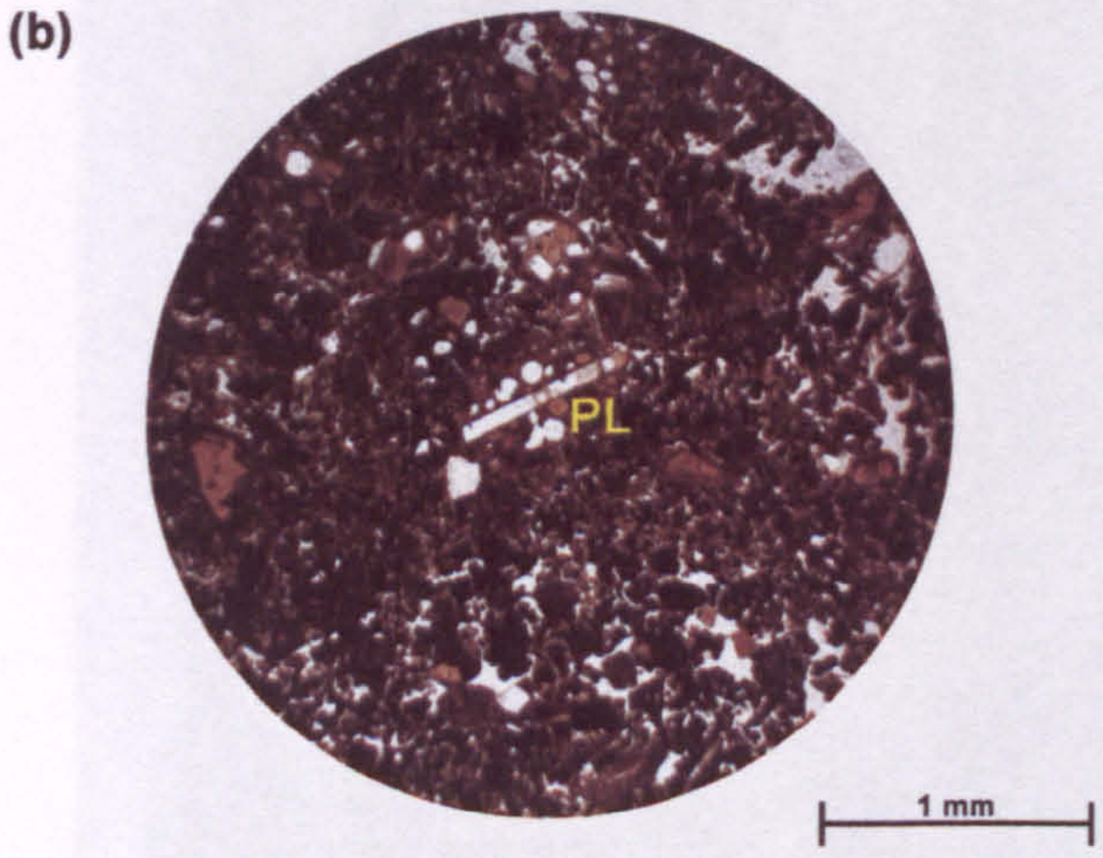

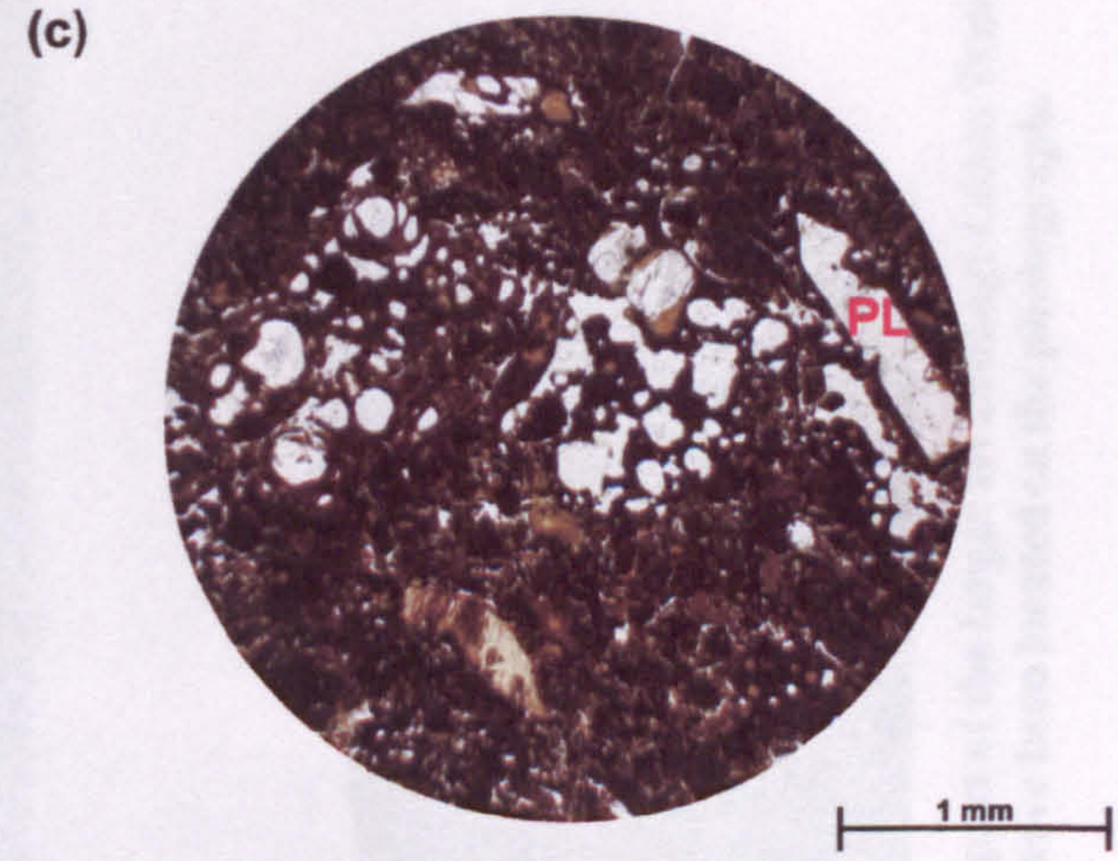

Fig. 5.22. View and photomicrographs of a large raft contained within doleritic sills N of Stapin, Hvannhagi-Lónin Traverse, *ca.* 2.5 km N of Tvøroyri, Suðuroy, Faeroe Islands. (a) The raft is *ca.* 20 m long by 8 m wide and the lower 5 m consists of thinly to thickly bedded greenish to greyish tuffaceous sandstones. Overlying the sandstones is a *ca.* 3 m thick tuffaceous breccia. All of the photomicrographs are under plane-polarised light. (b) The sandstones are poorly sorted and consist of orange to opaque palagonitised basaltic glass fragments. Some of the orange palagonitised fragments are highly amygdaloidal and contain phenocrysts of plagioclase feldspar (PL). (c) Near opaque basaltic glass fragments are highly amygdaloidal and most likely represent basaltic scoria. Some of the glass fragments contain phenocrysts of plagioclase feldspar and serpentinised olivine crystals.

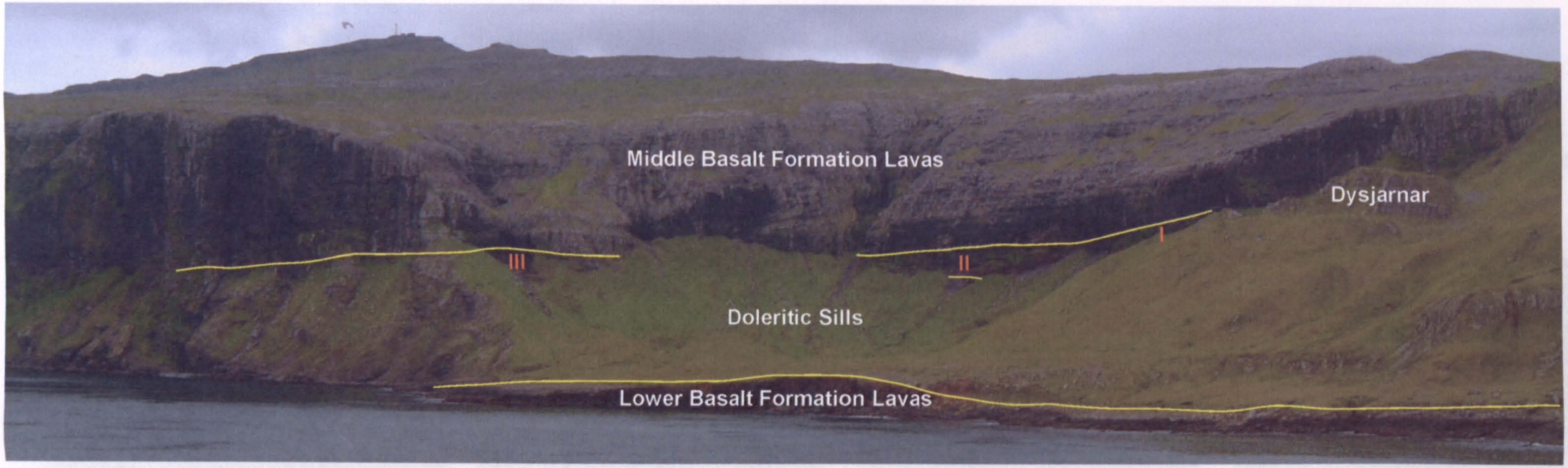

Fig. 5.23. Views of the Dysjarnar Traverse, part of the larger Hvannhagi-Lónin Traverse, *ca.* 2 km N of Tvøroyri, Suðuroy, Faeroe Islands. The three sections (I-III) from the Volcaniclastic Sandstone Formation (VSF) have been located on the photograph.

East

West

Ribbingamúli Point
East of Section III

Section III

Section II

Section I

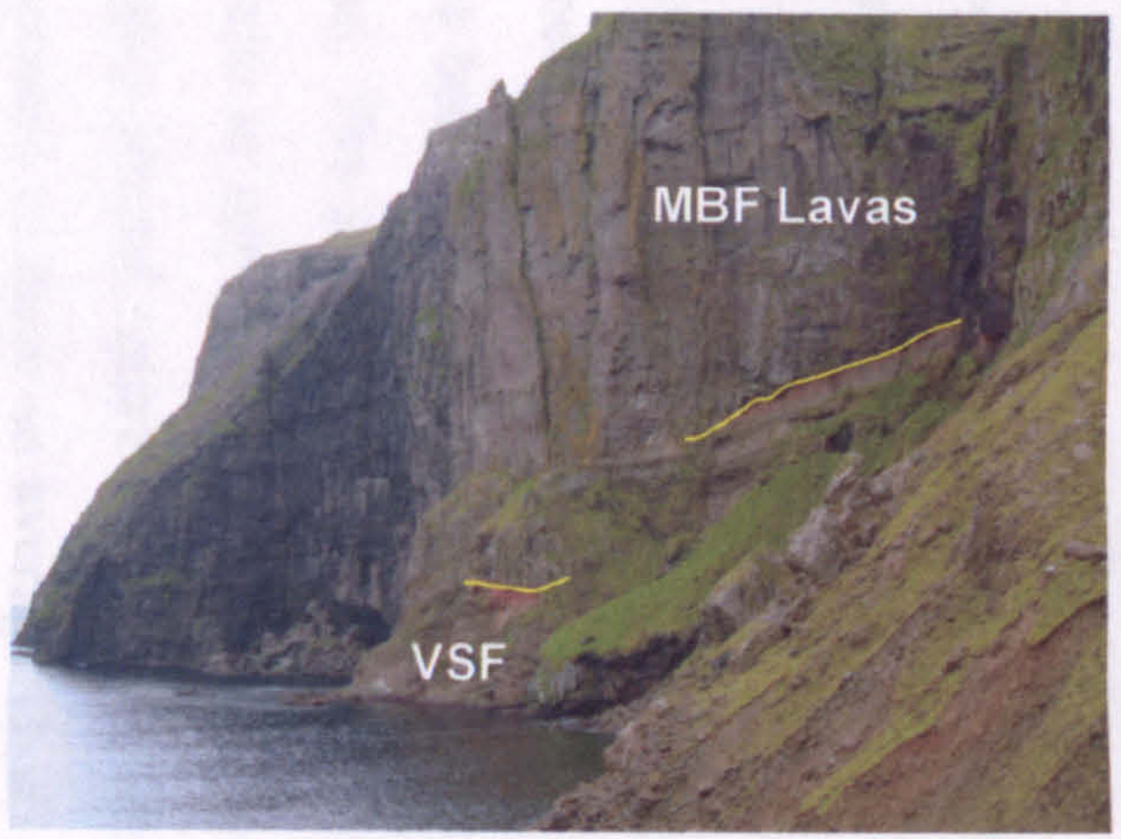

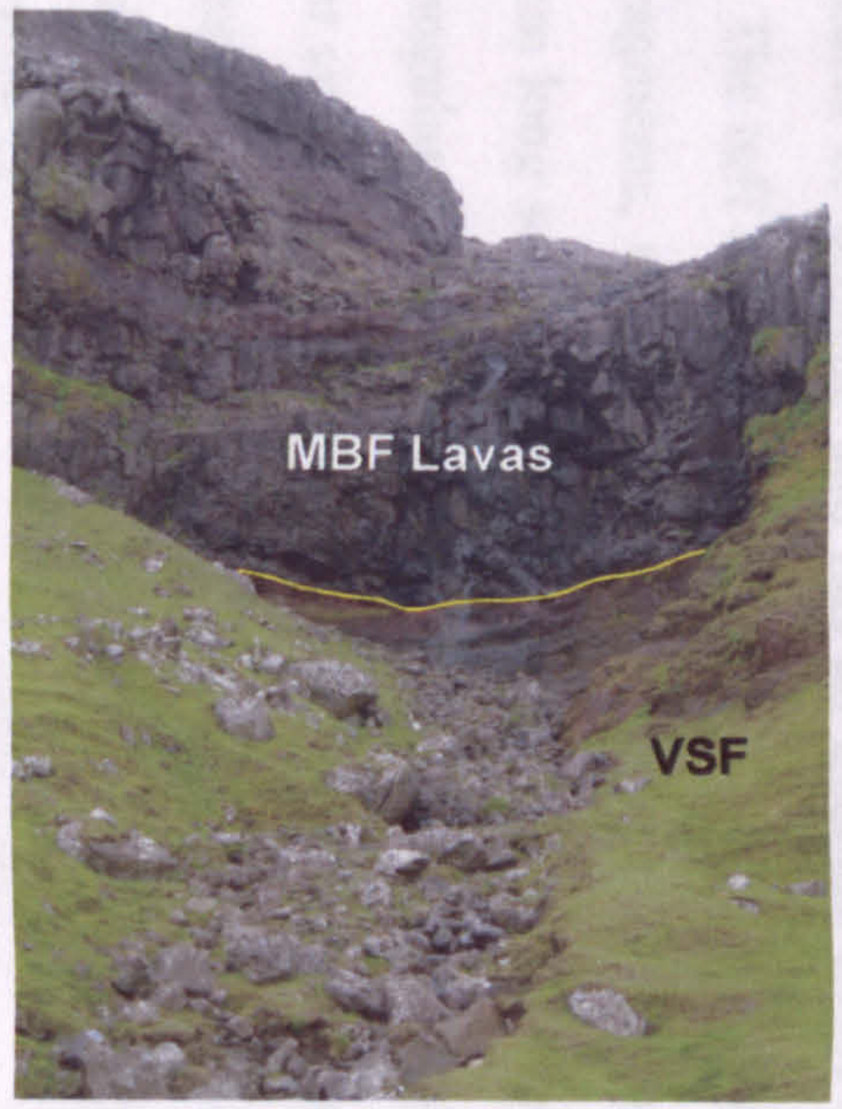

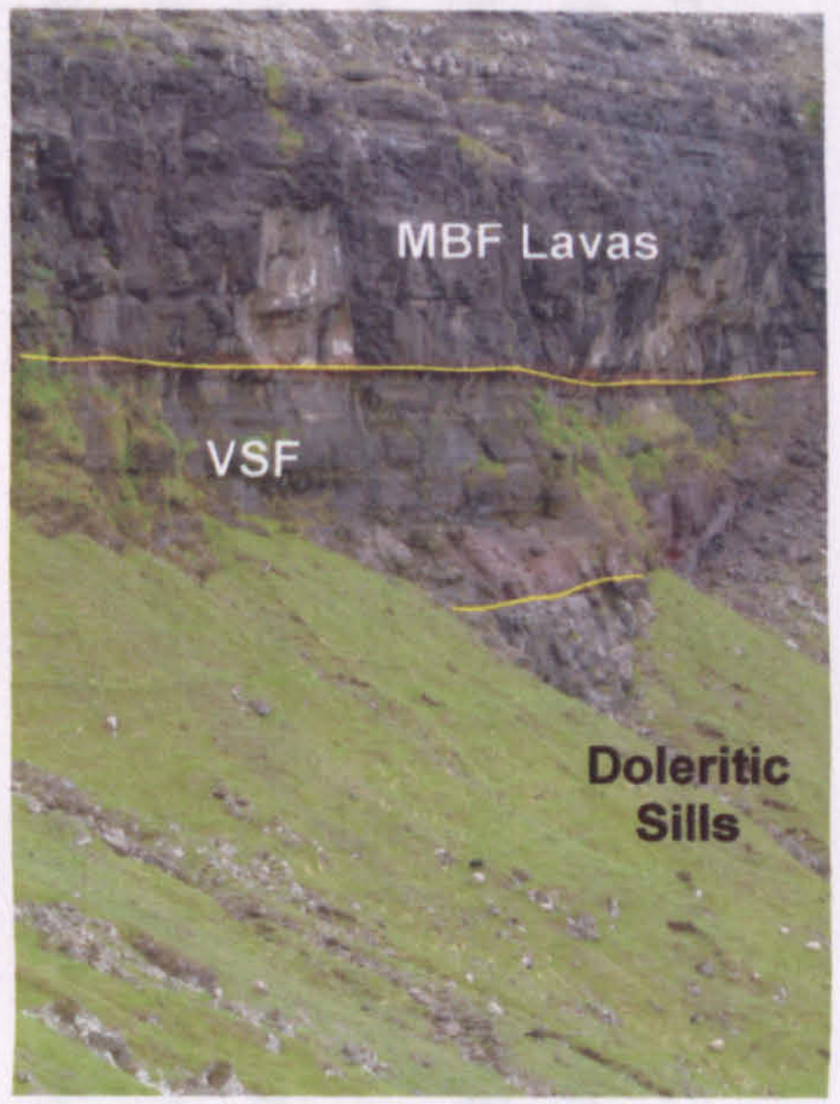

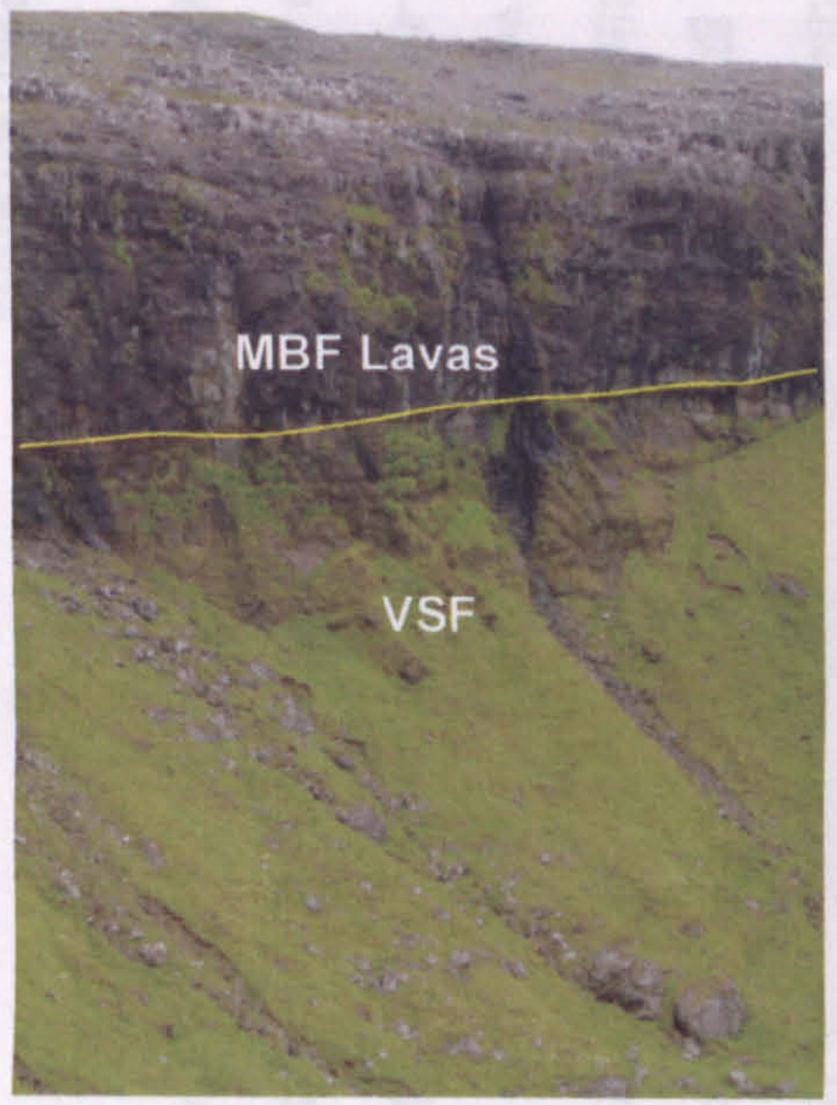

Fig. 5.24. Views of the Volcaniclastic Sandstone Formation (VSF) and Middle Basalt Formation (MBF) contact along the Dysjarnar Traverse, part of the larger Hvannhagi-Lónin Traverse, *ca.* 2 km N of Tvøroyri, Suðuroy, Faeroe Islands.

the ENE. The base of the traverse is composed of doleritic sills that have invaded and disrupted the VSF. The greatest observed thickness of the VSF is *ca.* 26 m in Section II; this is a minimum thickness due to the intrusion of the sills. In this traverse, the VSF consists of a mixture of volcaniclastic (epiclastic) lutites-arenites and tuffs. The description of lithologies (units 1-6) will be presented in stratigraphic order according to the correlation between the three exposures given in Figure 5.25. The VSF has a sharp, sometimes-undulating, upper contact with 2 m thick basalt flow units of the MBF.

5.3.3.2 Lithology & Petrography

Doleritic sills are observed at the base of sections I and II. The sills are greyish and sometimes contain xenoliths of tuffaceous material several tens of centimetres across. The contact between the sills and the overlying VSF is sharp and undulating. Overlying the sill in Section II, and also occurring at the base of Section III, is Unit 2, a *ca.* 12 m thick tuff bed. This tuff bed is thickly to very thickly bedded except for the lower 30 cm, which is thinly bedded. The lower 4 m is light olive grey (5Y 6/1) whereas the upper 8 m is reddened as a result of surface oxidisation. This tuff is poorly sorted, fragment supported, does not contain any matrix or cement, and has an average grain size of medium sand (coarse ash) (Fig. 5.26). The tuff is dominated (>85 vol.%) by angular to sub-rounded near opaque basaltic glass fragments, which contain abundant amygdales. Some of the larger fragments contain 1-2 mm long serpentinised euhedral and skeletal crystals of olivine. The tuff contains 10 vol.% angular basalt fragments with an average size of *ca.* 6 cm (lapilli) but a maximum fragment size of *ca.* 25 cm is noted. The tuff also contains sub-rounded to rounded lithic fragments of basalt (5 vol.%), which commonly contain serpentinised euhedral olivine phenocrysts set in a groundmass of very finely crystalline plagioclase feldspar laths and clinopyroxene.

Unit 3 only crops out in Section II and is a *ca.* 5.5 m thick sequence of interbedded tuffaceous sandstones and volcaniclastic mudstones. Unit 3 is not observed in sections I and III, suggesting that it is a localised unit. However, due to the disruption of sills in Section I it is impossible to be certain whether the Unit 3 continues to the west. The sandstone beds range in thickness from 8 cm up to 2 m, with an average thickness of *ca.* 50 cm (Fig. 5.27). The mudstone beds range in thickness from 1 cm up to 13 cm, with an average thickness of *ca.* 6 cm. The greenish black (5G 2/1) sandstone beds are poorly sorted and consist of sub-angular to sub-rounded highly palagonitised basaltic glass clasts (Figs. 5.28a-b). Due to the highly altered nature of the sandstone, clast margins have been obscured, although the unit appears to have an average clast size of medium sand, with

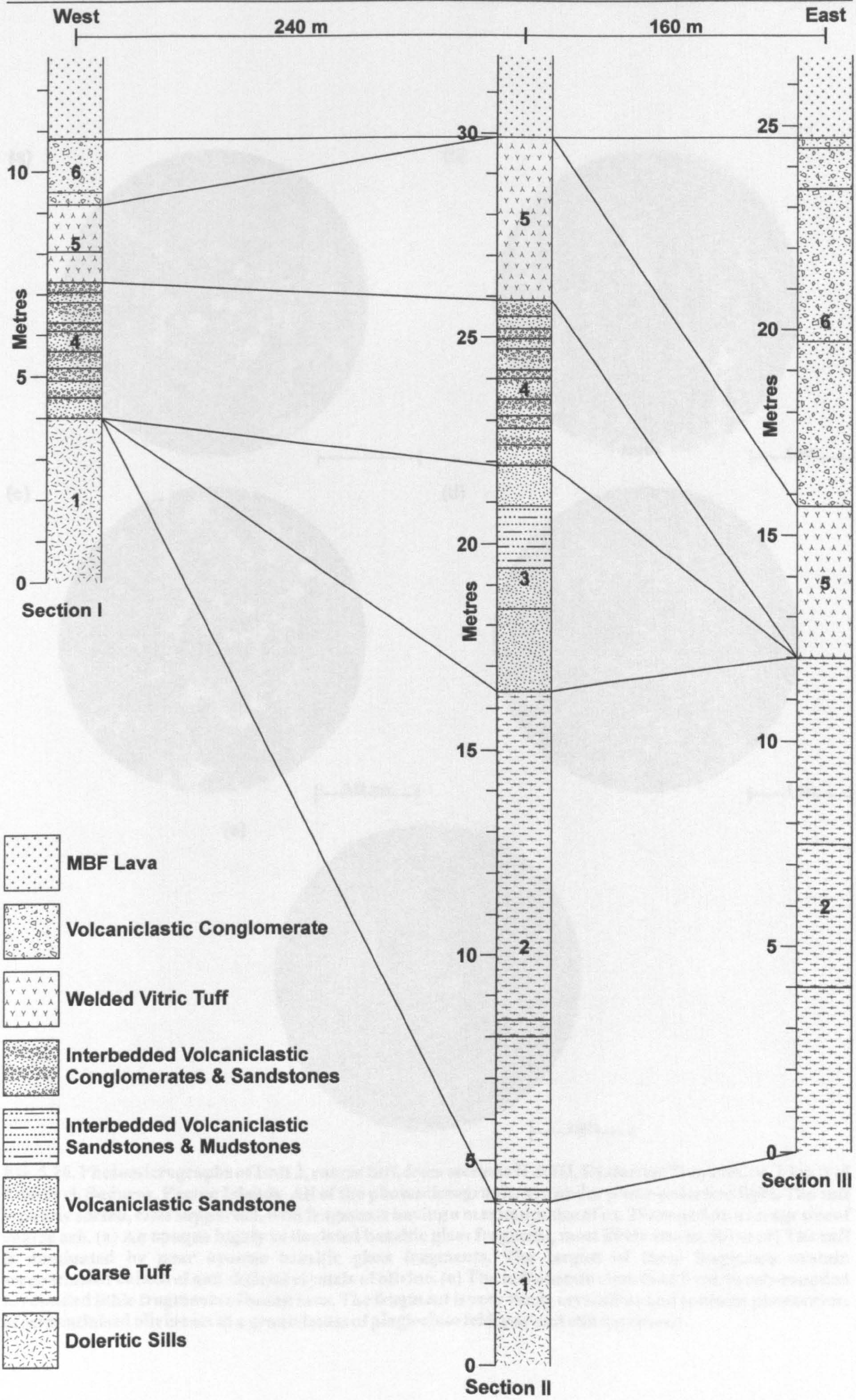

Fig. 5.25. Graphic logs of the Volcaniclastic Sandstone Formation (VSF) inbetween doleritic sills and Middle Basalt Formation (MBF) lavas, Dysjarnar Traverse, part of the larger Hvannhagi-Lónin Traverse, *ca.* 2 km N of Tvøroyri, Suðuroy, Faeroe Islands.

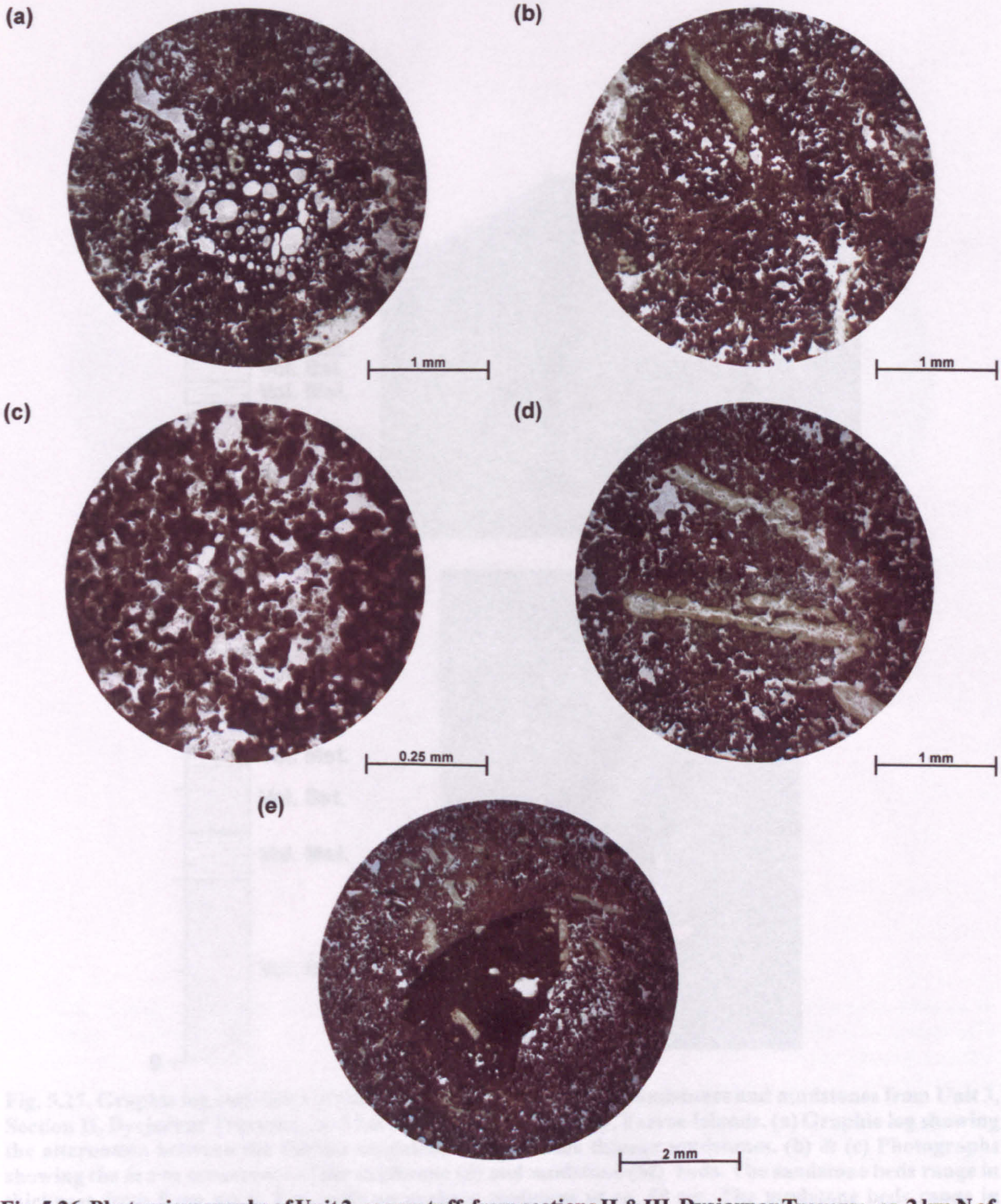

Fig. 5.26. Photomicrographs of Unit 2, coarse tuff, from sections II & III, Dysjarnar Traverse, *ca.* 2 km N of Tvøroyri, Suðuroy, Faeroe Islands. All of the photomicrographs are under plane-polarised light. The tuff is poorly sorted, clast supported, with fragments having a maximum size of *ca.* 25 cm and an average size of coarse ash. (a) An opaque highly vesiculated basaltic glass fragment, most likely scoria. (b) to (d) The tuff is dominated by near opaque basaltic glass fragments. The largest of these fragments contain serpentinised euhedral and skeletal crystals of olivine. (e) The tuff contains less than 5 vol.% sub-rounded to rounded lithic fragments of basalt lava. The fragment is very finely crystalline and contains phenocrysts of serpentinised olivine set in a groundmass of plagioclase feldspar and clinopyroxene.

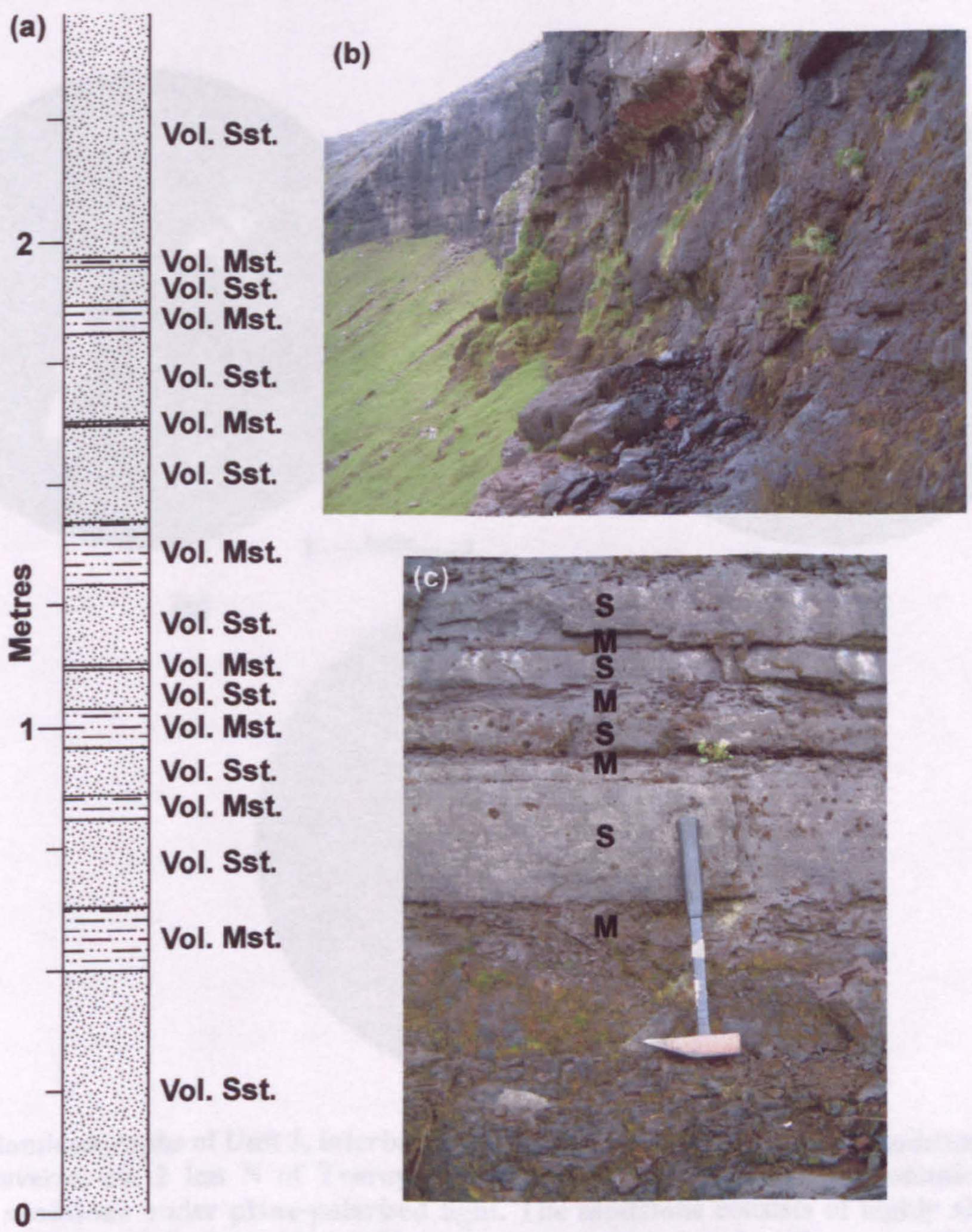

Fig. 5.27. Graphic log and views of the interbedded volcaniclastic sandstones and mudstones from Unit 3, Section II, Dysjarnar Traverse, *ca.* 2 km N of Tvøroyri, Suðuroy, Faeroe Islands. (a) Graphic log showing the alternation between the thicker sandstone beds and the thinner mudstones. (b) & (c) Photographs showing the *in situ* occurrence of the sandstone (S) and mudstone (M) beds. The sandstone beds range in thickness from 8 cm up to 2 m, with an average thickness of *ca.* 50 cm. The mudstone beds range in thickness from 1 cm up to 13 cm, with an average thickness of *ca.* 6 cm. The hammer is *ca.* 40 cm long.

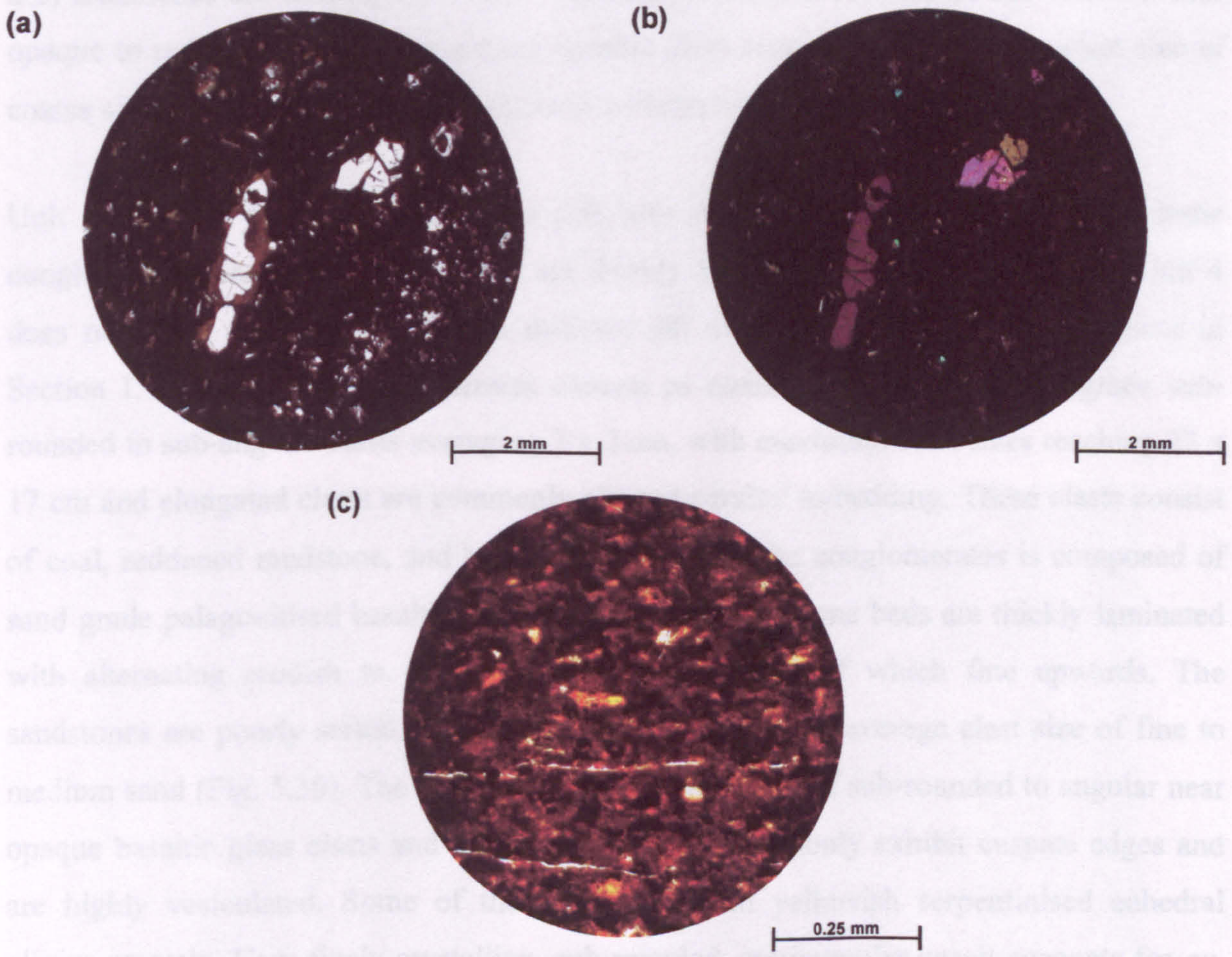

Fig. 5.28. Photomicrographs of Unit 3, interbedded volcaniclastic sandstones and mudstones, Section II, Dysjarnar Traverse, *ca.* 2 km N of Tvøroyri, Suðuroy, Faeroe Islands. (a) Photomicrograph of a volcaniclastic sandstone under plane-polarised light. The sandstone consists of highly altered basaltic glass clasts that have partially devitrified and have an average clast size of medium sand. The largest clasts commonly contain relatively fresh euhedral or skeletal crystals of olivine. (b) Same view as in (a) but under cross-polarised light. (c) Photomicrograph of a volcaniclastic mudstone under plane-polarised light. The mudstone has an average grain size of coarse silt. The mudstone appears to be made up of near opaque and orange-reddish basaltic palagonitised glass clasts.

clasts up to 2 mm in size. The basaltic glass clasts are either near opaque or murky brown and have partially devitrified. Some of the clasts contain laths of plagioclase feldspar *ca.* 0.25 mm long and the largest clasts contain relatively fresh euhedral or skeletal crystals of olivine. The sandstones also contain sub-rounded reddish clasts of volcaniclastic mudstone. The unit is classified here as a tuffaceous sandstone because of the highly altered nature of the unit, which makes it difficult to tell whether the clasts have a pyroclastic or epiclastic mode of origin, although they are most likely epiclastic in origin. The very dusky red (10R 2/2) mudstones are moderately sorted, clast supported, and consists of sub-rounded near opaque to reddish-orange palagonitised basaltic glass clasts, with an average clast size of coarse silt (Fig. 5.28c). The mudstones have a distinctive conchoidal fracture.

Unit 4 is a *ca.* 4 m thick dusky red (5R 3/4) sequence of interbedded volcaniclastic conglomerates and sandstones, which are thickly bedded (20-50 cm) (Fig. 5.29). Unit 4 does not occur in Section III and a doleritic sill truncates the base of the sequence in Section I. Some of the conglomerates contain as much as 25 vol.% cobble grade sub-rounded to sub-angular clasts averaging 7 x 2 cm, with maximum clast sizes reaching 22 x 17 cm and elongated clasts are commonly aligned parallel to bedding. These clasts consist of coal, reddened mudstone, and basalt. The matrix of the conglomerates is composed of sand grade palagonitised basaltic glass material. The sandstone beds are thickly laminated with alternating reddish to creamy lamina, the majority of which fine upwards. The sandstones are poorly sorted, matrix supported, and have an average clast size of fine to medium sand (Fig. 5.30). The sandstones contain 40 vol.% of sub-rounded to angular near opaque basaltic glass clasts and the largest of these commonly exhibit cuspate edges and are highly vesiculated. Some of these clasts contain yellowish serpentinised euhedral olivine crystals. Very finely crystalline, sub-rounded, equigranular basalt accounts for *ca.* 10 vol.% of the clasts in the sandstones. The sandstones also contain rounded lithic clasts, which are predominantly reddish volcaniclastic mudstones and sandstones (*ca.* 10 vol.%). The remaining 40 vol.% of the sandstones are made up of dirty brownish to orange sub-rounded palagonitised basaltic glass clasts which forms the matrix of the unit.

Unit 5 is a very pale orange (10YR 8/2) welded tuff, which ranges in thickness from *ca.* 2 m in Section I to *ca.* 4 m in Section III. This tuff is poorly sorted and is characterised by its elongated dark brown flattened basaltic fiamme-like fragments (Fig. 5.31). These fiamme define a planar foliation or eutaxitic texture. Typical sizes of the fiamme are 15 x 5 cm, 10 x 2 cm, and 25 x 8 cm. The welded tuff also contains <10 vol.% angular fragments of coal, reddened mudstone, and basalt ranging in size from 0.5 cm to 10 cm. In thin section, the tuff is composed of >90 vol.% orange cuspate glass shards sintered together, with an

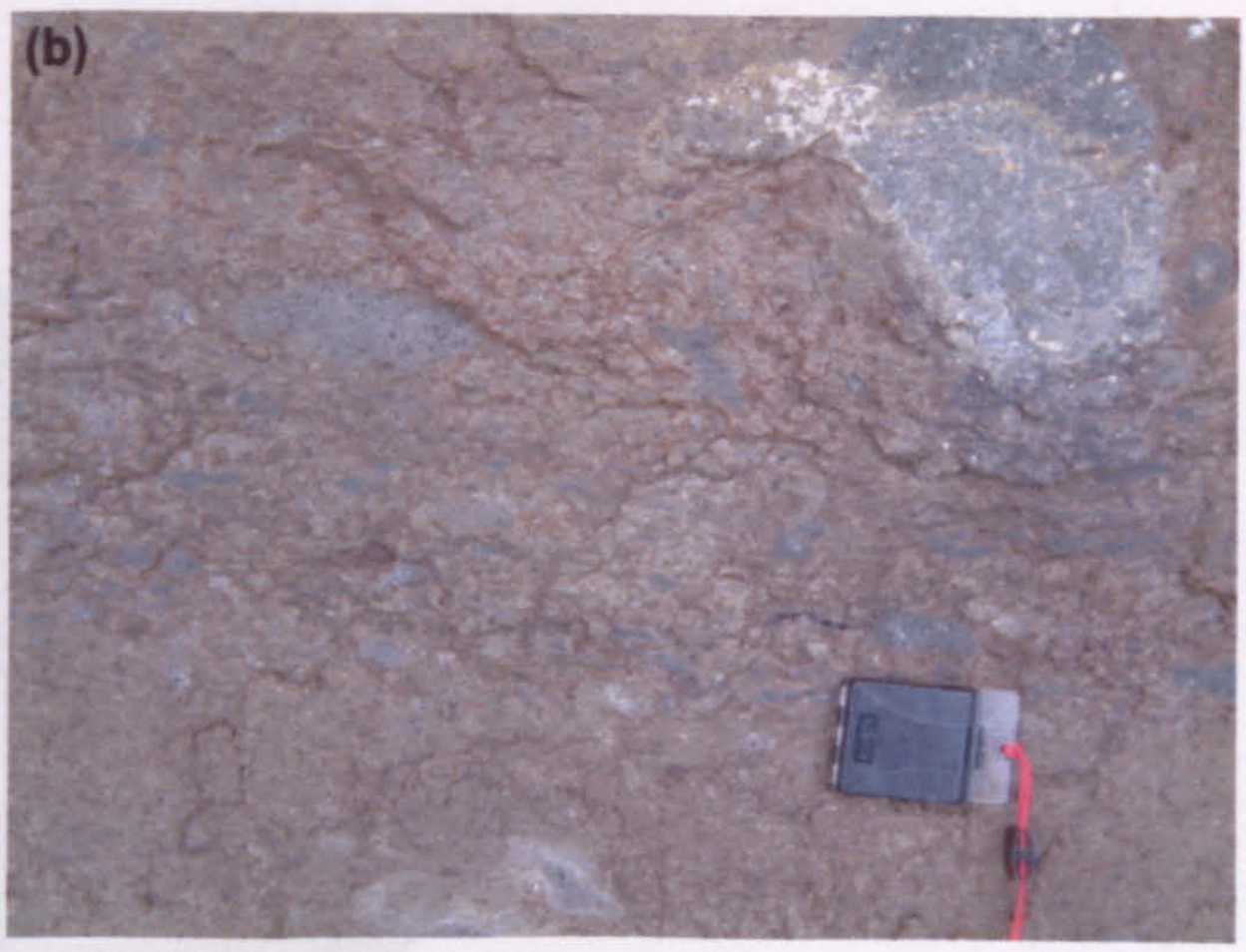

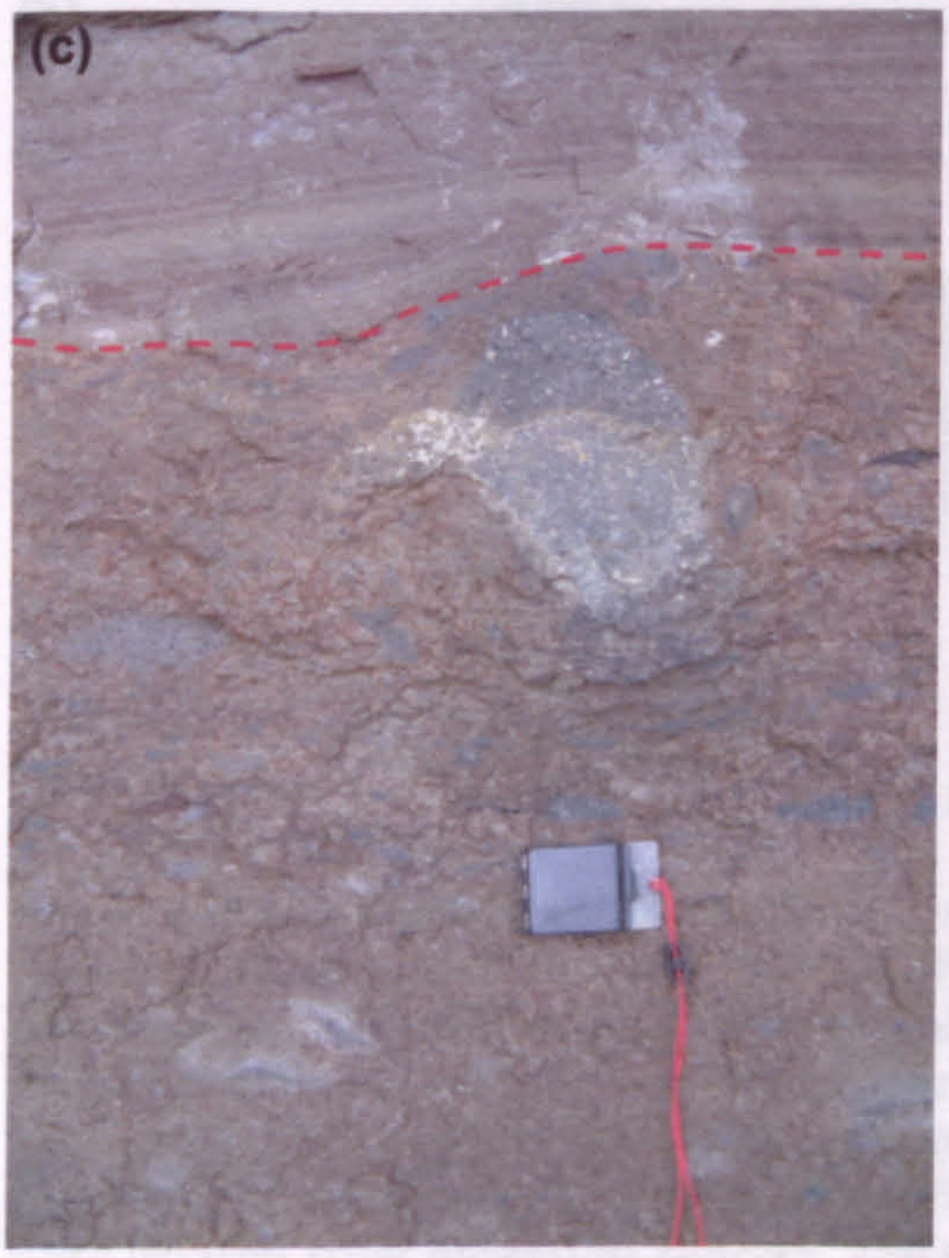

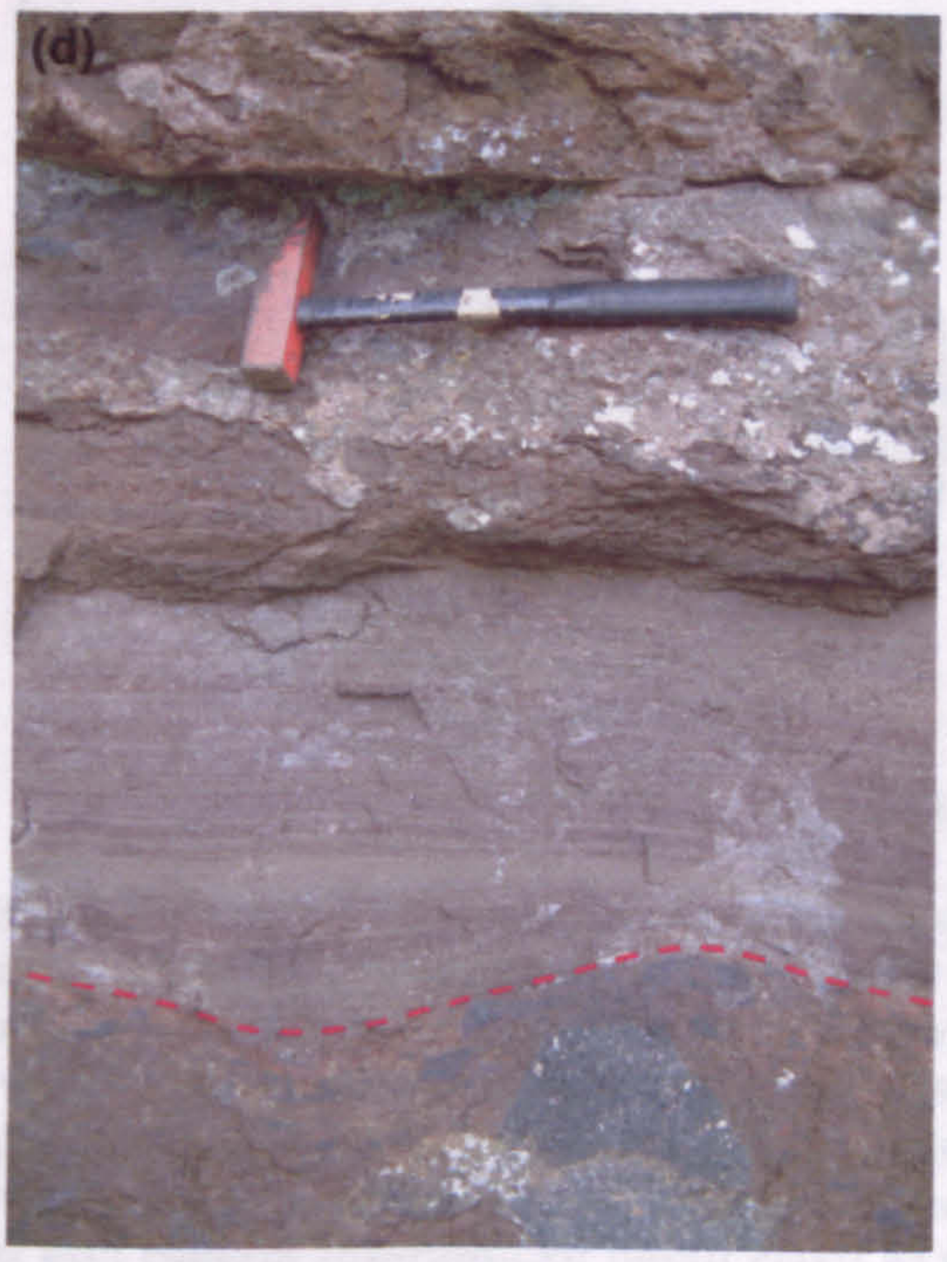

Fig. 5.29. Views of Unit 4, interbedded volcaniclastic conglomerates and sandstones, from sections I and II, Dysjarnar Traverse, *ca.* 2 km N of Tvøroyri, Suðuroy, Faeroe Islands. (a) A conglomerate bed which is overlain by a sandstone bed. The beds are thickly bedded, ranging in thickness from 20 cm up to 50 cm. (b) The conglomerate beds are matrix supported and commonly contain as much as 25 vol.% cobble grade sub-rounded to sub-angular clasts. The clasts have an average size of 7 x 2 cm, with maximum clast sizes reaching 22 x 17 cm. The cobble grade clasts consist of coal, reddened mudstones, and basalt lava. Elongated clasts are commonly aligned parallel to bedding. (c) & (d) The sandstone beds are thickly laminated with alternating reddish and creamy lamina. The majority of the sandstone beds grade normally upwards. The hammer is *ca.* 40 cm long and the compass is *ca.* 10 x 6 cm.

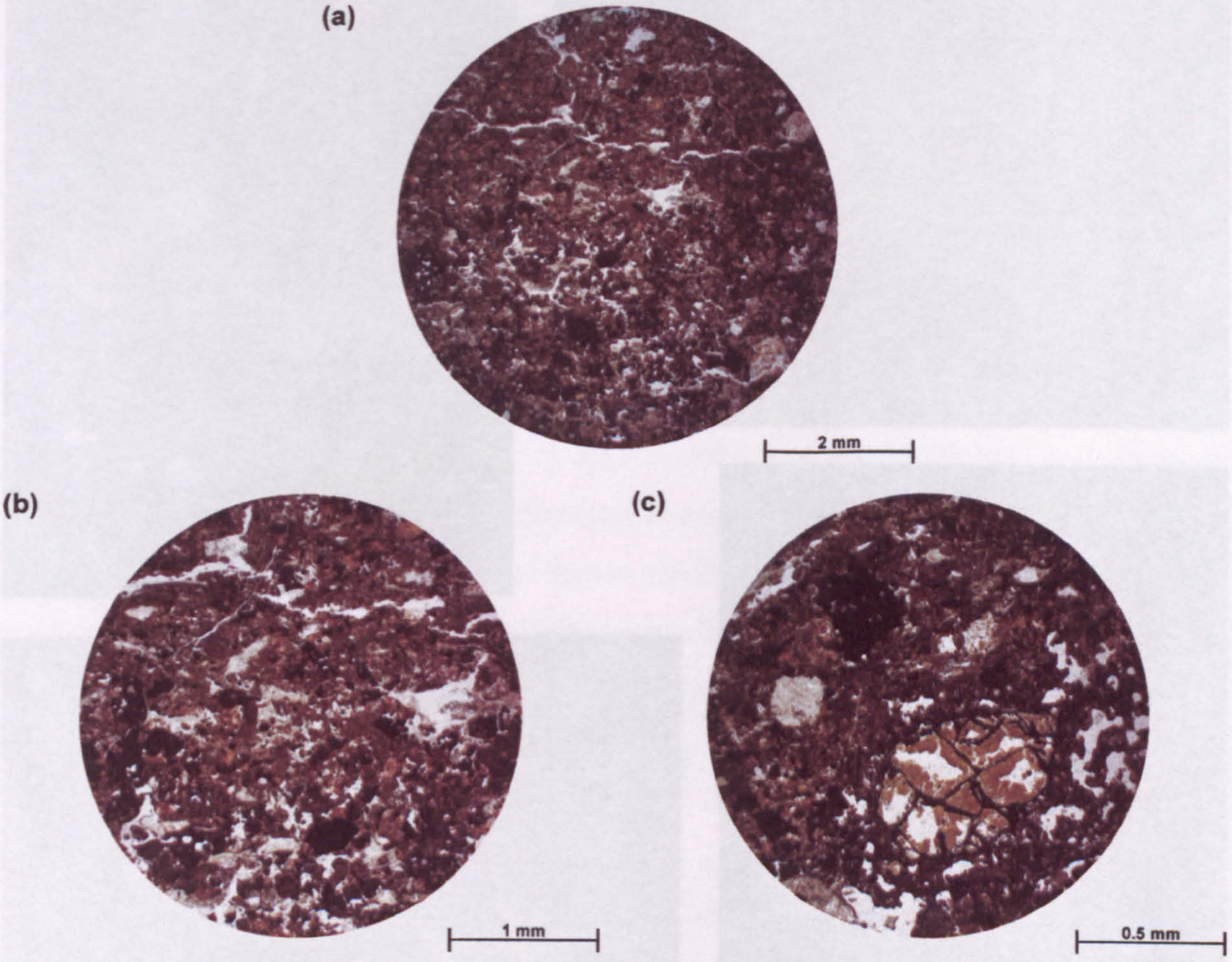

Fig. 5.30. Photomicrographs of the volcaniclastic sandstone beds from Unit 4, sections I and III, Dysjarnar Traverse, *ca.* 2 km N of Tvøroyri, Suðuroy, Faeroe Islands. All of the photomicrographs are under plane-polarised light. (a) & (b) The sandstone beds are poorly sorted, matrix supported and have an average grain size of fine to medium sand. The sandstones are dominated by sub-rounded to angular near opaque and orange palagonitised basaltic glass clasts. The largest of the near opaque clasts are highly vesiculated, suggesting that they are scoria. The variability in colouration of the altered glass clasts suggests that they were derived from numerous sources. The sandstones also contain sub-rounded basalt clasts as well as clasts of volcaniclastic sandstone and mudstone. (c) Some of the basaltic scoria clasts contain serpentinised yellowish euhedral olivine crystals.

Fig. 5.31. Views of Unit 5, partially welded tuff, Dysjarnar Traverse, *ca.* 2 km N of Tvøroyri, Suðuroy, Faeroe Islands. The tuff is very pale orange and is characterised by elongated dark brown flattened basaltic fiamme-like fragments. These fiamme define a planar foliation or eutaxitic texture. Typical sizes of the fiamme are 15 x 5 cm, 10 x 2 cm, and 25 x 8 cm. The welded tuff also contains angular fragments of coal, reddened mudstones, and basalt ranging in size from 0.5 to 10 cm. The hammer is *ca.* 40 cm long and the compass is *ca.* 10 x 6 cm.

average size of medium sand, although shards up to 1 mm are noted (Fig. 5.32). These large shards usually contain yellowish serpentinised euhedral to subhedral olivine crystals. The shards are highly vesiculated and commonly contain laths of plagioclase feldspar 0.1 mm long. The fiamme are morphologically similar to the rest of the tuff except that the glass shards are dark brown-near opaque rather than orange. The boundaries between the orange 'host' tuff and the opaque fiamme are sharp and lobate. The lack of mixing between the two types of glass suggests that the fiamme had formed a cooled crust and behaved plastically at the time of formation. The differences in colouration (opaqueness) between the 'host' tuff and the fiamme may be the consequence of different cooling rates.

Unit 6 is a greyish red (10R 4/2) thickly to very thickly bedded volcaniclastic conglomerate, which is *ca.* 1.6 m thick in Section I and *ca.* 9 m thick in Section III. This conglomerate contains *ca.* 15 vol.% of granule to pebble grade clasts. These consist of angular basalt clasts, which range in size between 1 and 10 cm and sub-rounded coal and reddened tuffaceous sandstone/mudstone clasts, which range in size from 1 to 20 cm. The coal and tuffaceous clasts occur in the lower parts of the conglomerate beds and appear to fine upwards. In thin section, the conglomerate is poorly sorted, generally matrix supported and has an average matrix grain size of fine to medium sand (Fig. 5.33). It contains *ca.* 60 vol.% sub-rounded, near opaque basaltic glass clasts and the largest clasts commonly contain abundant amygdales. The conglomerate also contains *ca.* 20 vol.% sub-rounded dirty yellow to orange palagonitised basaltic glass clasts, which are commonly vesiculated, and some contain laths of plagioclase feldspar. The remaining *ca.* 20 vol.% of the conglomerate is made up of sub-rounded clasts of basalt. These clasts are commonly greyish, very finely crystalline, consisting of rare phenocrysts of plagioclase feldspar in a groundmass of plagioclase feldspar, clinopyroxene and oxides. The top *ca.* 25 cm of the uppermost conglomerate bed has been reddened due to oxidation.

5.3.3.3 Provenance

The VSF lithologies within the Dysjarnar Traverse preserve fragments/clasts from pyroclastic and epiclastic processes. The pyroclastic lithologies all contain palagonitised basaltic glass fragments, most probably derived from a proximal vent, although a source from further a field cannot be totally be ruled out. The epiclastic lithologies are composed of reworked ash and lapilli grade clasts and the range in surface oxidation states of these clasts indicate that numerous pyroclastic fall deposits may have been eroded at the same time. The abundance of reworked glass clasts containing olivine phenocrysts tentatively implies that the basal olivine-phyric vitric tuff was eroded when it was still an

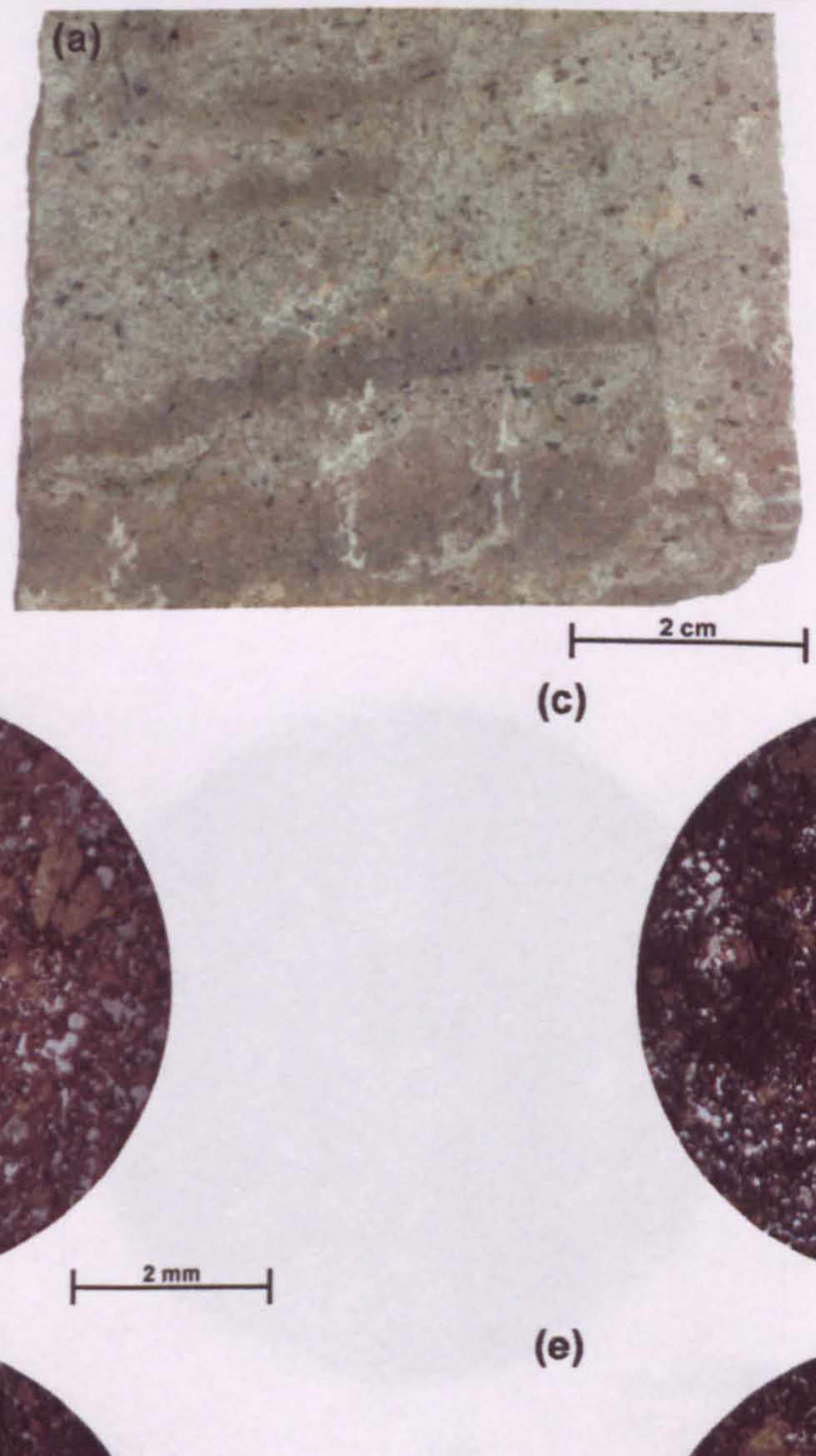

Fig. 5.32. Hand specimen photograph and photomicrographs of Unit 5, partially welded tuff, Dysjarnar Traverse, *ca.* 2 km N of Tvøroyri, Suðuroy, Faeroe Islands. (a) Dark brown fiamme contained within a very pale orange vitric tuff. The tiny (*ca.* 1 mm) black angular crystals observed throughout the vitric tuff are serpentinised olivine crystals. All of the photomicrographs are under plane-polarised light. (b) The tuff is very poorly sorted and clast supported and is composed of >90 vol.% orange palagonitised basaltic cuspate glass shards. The largest glass shards contain yellowish serpentinised euhedral to subhedral olivine crystals. The shards are usually highly vesiculated and commonly contain laths of plagioclase feldspar. (c) The fiamme are morphologically similar to the main orange tuff 'host' except that the glass shards are dark brown-near opaque. (d) & (e) The contact between the orange 'host' tuff and the fiamme is sharp and lobate. The lack of mixing between the two types of glass suggests that the fiamme had formed a cooled crust and behaved plastically at the time of formation. (f) The fiamme contain opaque basaltic glass shards, which commonly contain laths of plagioclase feldspar. (g) The tuff also contains rare reddened angular lithic fragments of volcaniclastic mudstone.

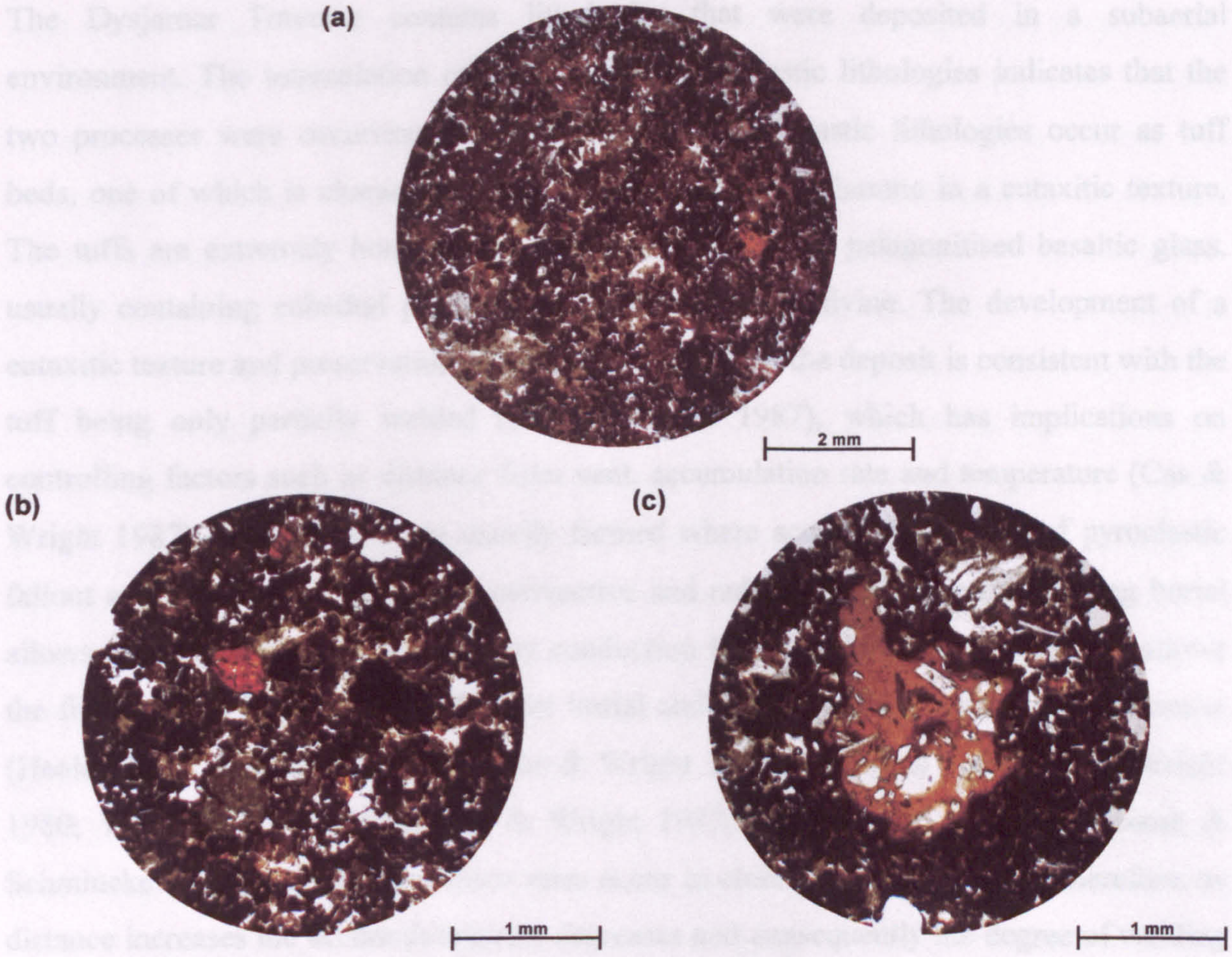

Fig. 5.33. Photomicrographs of Unit 6, volcaniclastic conglomerate, from sections I and III, Dysjarnar Traverse, *ca.* 2 km N of Tvøroyri, Suðuroy, Faeroe Islands. All of the photomicrographs are under plane-polarised light. (a) & (b) The conglomerate is dominated by sub-rounded near opaque basaltic glass clasts and the largest are usually amygdaloidal, filled with zeolitic group minerals, these clasts are most likely scoria. The conglomerate also contains *ca.* 20 vol.% orange palagonitised basaltic clasts. (c) An orange basaltic glass clast that is vesiculated and contains laths of plagioclase feldspar. The clast has cuspate margins, the remains of former bubble walls.

unconsolidated deposit. The coarser volcaniclastic deposits have a greater abundance of basalt clasts and the range in surface oxidation states of these clasts suggests that numerous exposed lava flows were being eroded at the same time. Some of the volcaniclastic lithologies contain clasts of coal and volcaniclastic mudstone, most likely derived from the erosion of the CBF.

5.3.3.4 Environment of Deposition

The Dysjarnar Traverse contains lithologies that were deposited in a subaerial environment. The intercalation of pyroclastic and epiclastic lithologies indicates that the two processes were occurring simultaneously. The pyroclastic lithologies occur as tuff beds, one of which is characteristically welded, containing fiamme in a eutaxitic texture. The tuffs are extremely homogenous, composed entirely of palagonitised basaltic glass, usually containing euhedral phenocrysts of serpentinised olivine. The development of a eutaxitic texture and preservation of the initial porosity of the deposit is consistent with the tuff being only partially welded (Cas & Wright 1987), which has implications on controlling factors such as distance from vent, accumulation rate and temperature (Cas & Wright 1987). Welded tuffs are usually formed where accumulation rates of pyroclastic fallout are high enough to prevent convective and radiative cooling, which during burial allows the fragments to cool slowly by conduction because they are insulated, this allows the fragments to behave plastically after burial and promotes the development of fiamme (Healey 1963; Schmincke 1967; Sparks & Wright 1979; Suthren & Furnes 1980; Wright 1980; Wolff & Wright 1981; Cas & Wright 1987; Calderone *et al.* 1990; Freundt & Schmincke 1995). High accumulation rates occur in close proximity to vents, therefore, as distance increases the accumulation rate decreases and consequently the degree of welding diminishes (Cas & Wright 1987). Consequently, it seems most likely that the partially welded tuff in the Dysjarnar Traverse was formed proximal to the vent, although the exact distance is undeterminable.

The epiclastic lithologies within the Dysjarnar Traverse range from volcaniclastic mudstones through to conglomerates. The deposits are commonly bedded, heterogeneous and poorly sorted, suggesting they were formed by epiclastic processes (cf. Collinson 1996; Talbot & Allen 1996; Tucker 1996a; b). Unit 3, a sequence of interbedded sandstones and mudstones, forms a localised unit within Section II. This alternation of sandstone and mudstone beds implies fluctuating water flow energies (cf. Collinson 1996; Talbot & Allen 1996; Tucker 1996a; b). The sharp-based nature and thicknesses less than 2 m of the sandstone beds coupled with the interbedding of mudstones indicates that the

sequence most likely formed from catastrophic overbank flows on floodplains (cf. Steel & Aasheim 1978; Collinson 1996). This suggests that there was a fluvial channel in close proximity to the deposits and that this channel underwent periods of increased stream flow, most likely the result of increased rainfall (cf. Steel & Aasheim 1978; Collinson 1996). The alternation of sandstone and mudstone beds implies a recurring pattern of flooding episodes most likely reflecting seasonal variations (cf. Collinson 1996; Tucker 1996a; b).

The remaining volcaniclastic lithologies have tabular geometries and a lateral extent of at least 400 m. This coupled with the rocks being generally matrix supported, poorly sorted and having planar laminations/bedding structures suggests that they may represent deposits from a lahar event (cf. Smith 1991; Smith & Lowe 1991). If this is correct, the volcaniclastic rocks were formed by a combination of volcaniclastic debris and hyperconcentrated flow processes (cf. Janda *et al.* 1981; Pierson & Scott 1985; Lowe *et al.* 1986; Naranjo *et al.* 1986; Smith 1986; Rodolfo 1989; Smith & Lowe 1991; Coussot & Meunier 1996; Sohn *et al.* 1999; Kessler & Bédard 2000; Lavigne *et al.* 2000; Lirer *et al.* 2001). The conglomerates most likely represent the volcaniclastic debris flow end of the spectrum (cf. Pierson & Scott 1985; Smith 1986; Smith & Lowe 1991; Bahk & Chough 1996; Coussot & Meunier 1996; Sohn *et al.* 1999; Lirer *et al.* 2001) and the sandstones represent the hyperconcentrated flows (cf. Pierson & Scott 1985; Smith 1986; Smith & Lowe 1991; Bahk & Chough 1996; Coussot & Meunier 1996; Sohn *et al.* 1999; Lirer *et al.* 2001; Kataoka & Nakajo 2002). The occurrence of these volcaniclastic debris and hyperconcentrated flow deposits imply that sedimentation rates were high, most likely due to an increase in pyroclastic debris, suggesting that these deposits were rapidly emplaced during syn-eruption period(s) (cf. Smith 1987b; 1988; Smith & Fritz 1989; Smith 1991; Smith & Lowe 1991; Bahk & Chough 1996). To sustain the lahar(s) abundant surface water was required implying that there was heavy rainfall at the time of the sedimentary event (cf. Smith & Lowe 1991).

5.3.4 Summary

The Hvannhagi–Lónin Traverse preserves a sequence, from the upper section of the LBF, through the CBF and VSF to the MBF. The base of the sequence consists of an agglomerate deposit formed in close proximity to the Stapin Vent, believed to be of LBF age. The vent is mantled by a thin veneer of shales and coals of the CBF. Numerous doleritic sills have disrupted the CBF and VSF and the true thicknesses of the formations in this area cannot be determined. The VSF is at least 26 m thick in the Dysjarnar Traverse and preserves lithologies of pyroclastic and epiclastic origins that were deposited within a

terrestrial environment. The occurrence of a partially welded tuff implies the close proximity of a vent to allow low to moderately high accumulations of pyroclastic fallout to enable the development of a welding fabric. The volcaniclastic lithologies within the traverse record periods of high water discharge, leading to the formation of floodplain and lahar deposits. The volcaniclastic lithologies record an inter-eruption phase consisting of floodplain deposits reflecting fluctuating water flow energies and a low abundance of volcanic debris. The cyclic nature of the floodplain deposits implies wet and relatively dry periods, i.e. seasonal variations. This abruptly changes to a syn-eruption phase that sees a marked influx of coarse volcanic debris deposited as sheet-like bodies during lahar events, i.e. major floods.

5.4 Reyðibarmur–Hvalba Traverse

The traverse is *ca.* 1.8 km long and extends from Reyðibarmur cliff section in the east to the harbour at Hvalba in the west (Fig. 5.1). The traverse dips towards the ENE at a few degrees. Approximately 1.4 km of the traverse east from Hvalba is disrupted by doleritic sills that commonly have apophyses extending into the overlying VSF. The VSF is overlain by, and sometimes transitional with, lava flow units of the MBF (Rasmussen & Noe-Nygaard 1970b). The base of the MBF occurs at a height of 70 m above sea level in this traverse. Good exposure of the VSF occurs at the Reyðibarmur cliff section.

5.4.1 Reyðibarmur Section

5.4.1.1 Overview of Section

The Reyðibarmur cliff section occurs between 1.4 and 1.8 km NE of Hvalba, Suðuroy (Fig. 5.34). The section is *ca.* 40 m thick and dips to the ENE. The base of the section consists of a greenish-grey peperite sequence overlain by reddish lapillistones and tuffs. The west of the section is juxtaposed against a doleritic sill(s).

5.4.1.2 Lithology & Petrography

The base of the section consists of a *ca.* 9 m thick greenish-grey conglomerate-breccia composed of a mixture of basalt and sediment and having features consistent with having formed as a peperite (cf. Brooks *et al.* 1982; Kokelaar 1982; Walker & Francis 1986; Busby-Spera & White 1987; Cas & Wright 1987; McPhie 1993; McPhie *et al.* 1993; Hanson & Hargrove 1999; Rawlings *et al.* 1999; Doyle 2000; White *et al.* 2000; Cas *et al.*

Fig. 5.34. Views of the Reyðibarmur cliff section, *ca.* 1.6 km NE of Hvalba, Suðuroy, Faeroe Islands. The base of the section consists of a greenish-grey peperite sequence overlain by reddish lapillistones and tuffs.

2001; McClintock & White 2002; Skilling *et al.* 2002; Squire & McPhie 2002). The contact between the doleritic sill(s) and the peperite sequence is not observed due to steep inaccessible, vegetated cliffs. However, moving eastwards away from the coherent sill domain, the peperite sequence goes from being a close-packed blocky to a dispersed blocky-fluidal peperite. The close-packed blocky breccia is at least several metres thick and consists of dominantly fragment supported, hence the term close-packed, angular basaltic fragments, which have a maximum size of *ca.* 16 cm and an average size of *ca.* 4 cm (Fig. 5.35). The blocky fragments do not form a jigsaw-fit pattern and are randomly orientated and are set in a matrix of more highly comminuted basalt.

The close-packed blocky peperite is transitional with the dispersed blocky-fluidal peperite. The dispersed blocky-fluidal peperite is poorly sorted and has a maximum fragment size of a few metres. This peperite consists of a mixture of basaltic and sedimentary fragments, which are not fragment supported and hence the use of the term dispersed. The basalt fragments have blocky, platy and fluidal shapes (cf. Skilling *et al.* 2002) (Fig. 5.36a-c) and have a maximum size of 1.0 x 0.5 m and an average size of lapilli. The fragments range from massive to vesicular-/amygdaloidal-rich basalt. A few fluidal fragments are zoned, having a highly vesiculated rim and vesicle-poor core (Fig. 5.36a). The sedimentary fragments consist of coal and volcaniclastic claystone fragments. The claystone fragments are harder to identify because of their basaltic composition, which makes them resemble basaltic fragments on first appearance. However, one such volcaniclastic claystone fragment (*ca.* 40 x 40 cm) is identified by its alternating green/grey layers, interpreted here to represent original bedding (Fig. 5.36d). The coal fragments are found within a 3 m thick section of the dispersed blocky-fluidal peperite (Figs. 5.37 & 5.38). The coal fragments have a maximum size of 2.5 x 0.7 m and range from reddish-brown shaly material to black vitreous coal. The fragments are usually tabular in shape, commonly flat-lying and are aligned parallel to each other, most likely representing the original bedding orientation. Four tabular coal fragments form what appears to be a *ca.* 9 m long near-horizontal, discontinuous coal seam, but with *ca.* 2.5 m of missing coal. The margins to the coal fragments appear to be invaded by dykes of basalt. In addition, 'dykes' of coal invade the matrix of comminuted basalt, coal and volcaniclastic claystone (Fig. 5.37e-h). Other shaly-coal fragments have the appearance of having been stretched and deformed; one such fragment forms a sinuous shape *ca.* 1 m long, with the upper corner hinged around a fluidal basaltic fragment (Fig. 5.38d).

Overlying the dispersed blocky-fluidal peperite are light brown (5YR 5/6) lapillistones and tuffs with a thickness of at least 20-30 m (Fig. 5.39). The lapillistones and tuffs are poorly

Fig. 5.35. Views of the close-packed blocky peperite from the Reyðibarmur cliff section, *ca.* 1.6 km NE of Hvalba, Suðuroy, Faeroe Islands. The blocky peperite consists of basaltic fragments, which have a maximum size of *ca.* 16 cm and an average of *ca.* 4 cm. The blocky fragments do not form a jigsaw-fit pattern and are set in a matrix of more highly comminuted basalt. The hammer is *ca.* 40 cm long and the pens are *ca.* 16 cm in length.

Fig. 5.36. Views of the dispersed blocky-fluidal peperite from the Reyðibarmur cliff section, *ca.* 1.6 km NE of Hvalba, Suðuroy, Faeroe Islands. (a) Basaltic fragments within the peperite, which have blocky, platy and fluidal shapes. One of the fluidal fragments (highlighted in yellow) has a highly vesiculated rim and a vesicle poor core. The peperite also contains a reddened volcaniclastic mudstone clast (VM). (b) A platy basaltic fragment. (c) A highly vesiculated fluidal basaltic fragment. (d) A volcaniclastic claystone fragment (highlighted in yellow) that is *ca.* 40 x 40 cm. The fragment is identified as a claystone because of the alternating green/grey layers, representing original bedding. The compass is *ca.* 10 x 6 cm.

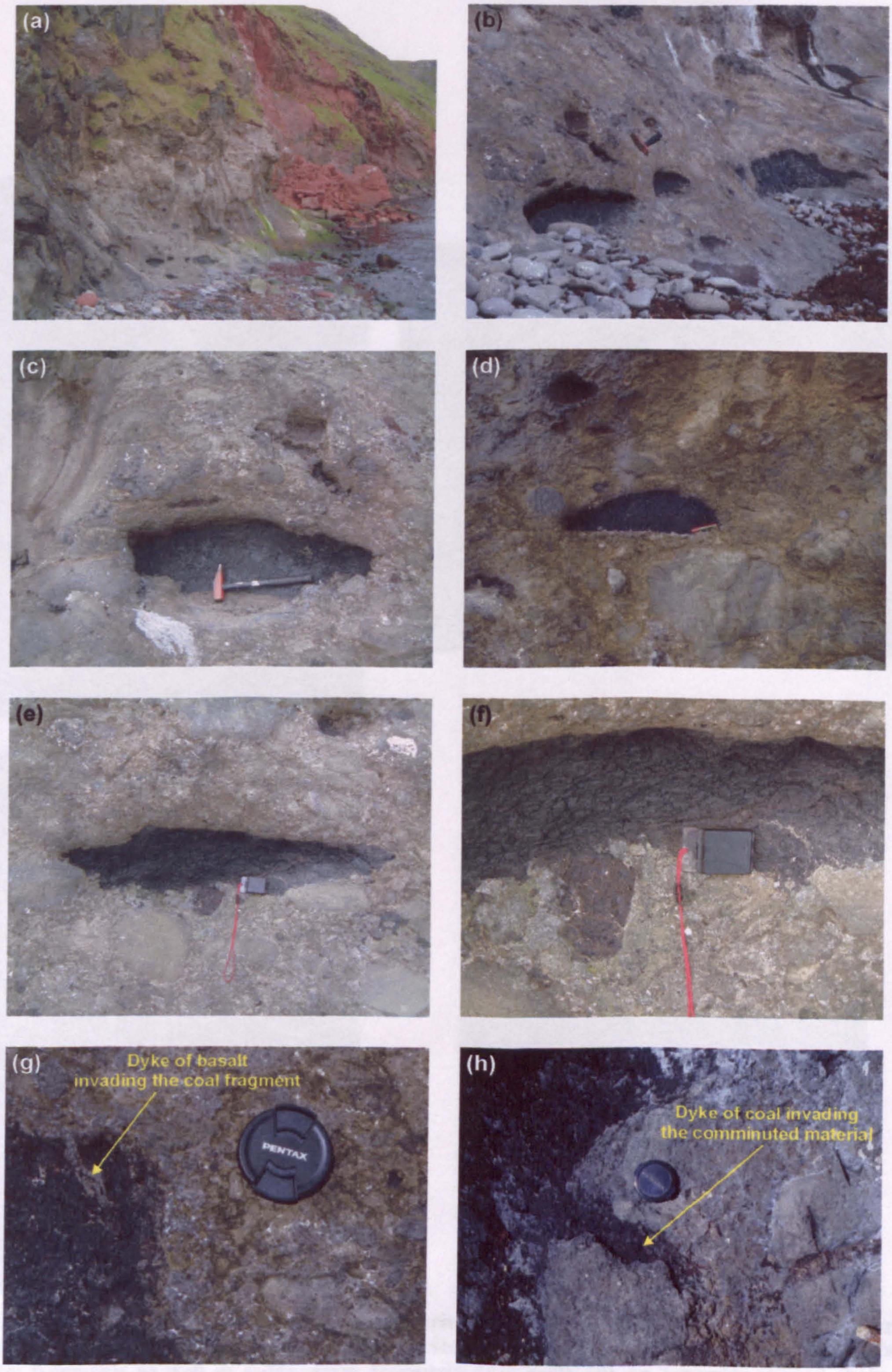

Fig. 5.37. Views of the dispersed blocky-fluidal peperite from the Reyðibarmur cliff section, *ca.* 1.6 km NE of Hvalba, Suðuroy, Faeroe Islands. (a) to (e) Coal fragments are found within the lower 3 m of the dispersed peperite. The fragments have a maximum size of 2.5 x 0.7 m and range from reddish-brown shaly material to black coal. The coal fragments are tabular in shape and are commonly aligned parallel to each other, possibly representing the original bedding orientation. (f) to (h) Dykes of fluidal basalt invading the coal fragments and 'dykes' of coal invading the comminuted basalt, coal and claystone matrix. The hammer is *ca.* 40 cm long, the pens are *ca.* 16 cm long, the compass is *ca.* 10 x 6 cm and the lens cap is *ca.* 6 cm across.

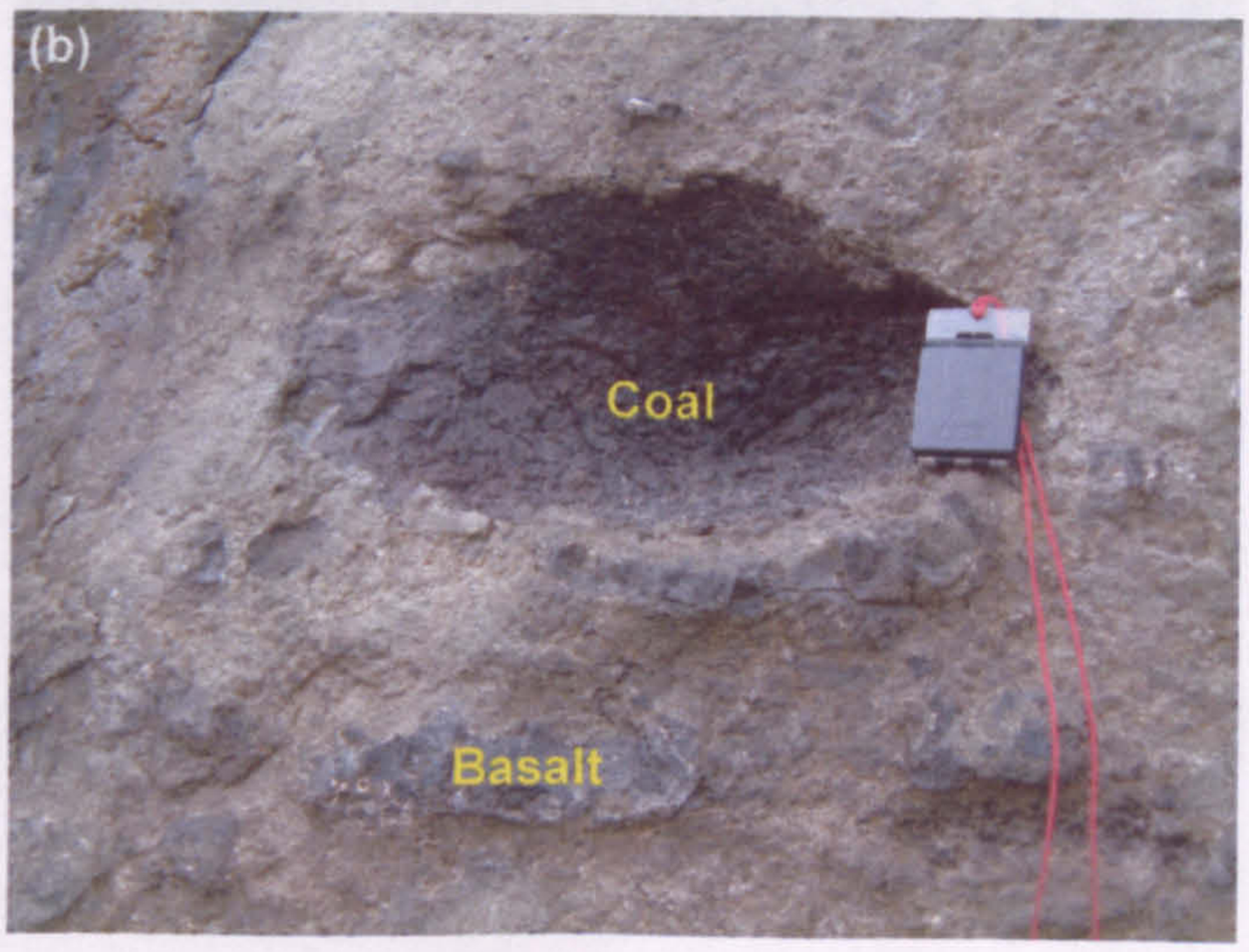

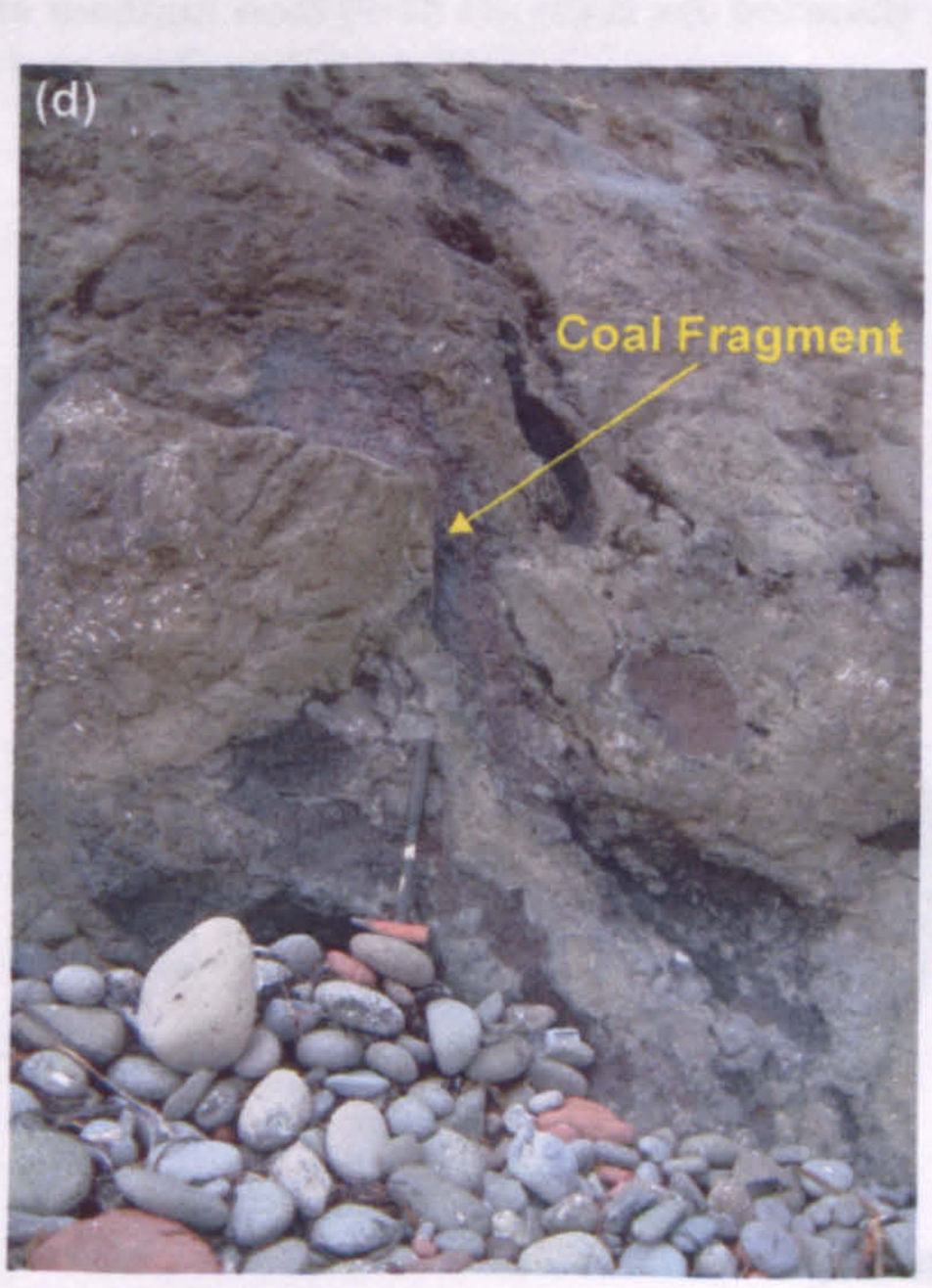

Fig. 5.38. Views of the dispersed blocky-fluidal peperite from the Reyðibarmur cliff section, *ca.* 1.6 km NE of Hvalba, Suðuroy, Faeroe Islands. (a) to (c) The dispersed peperite contains blocky, platy and fluidal basaltic fragments as well as sedimentary fragments (e.g. coal). (d) An irregular shaped shaly-coal fragment, which is *ca.* 1 m long. The hammer is *ca.* 40 cm long and the compass is *ca.* 10 x 6 cm.

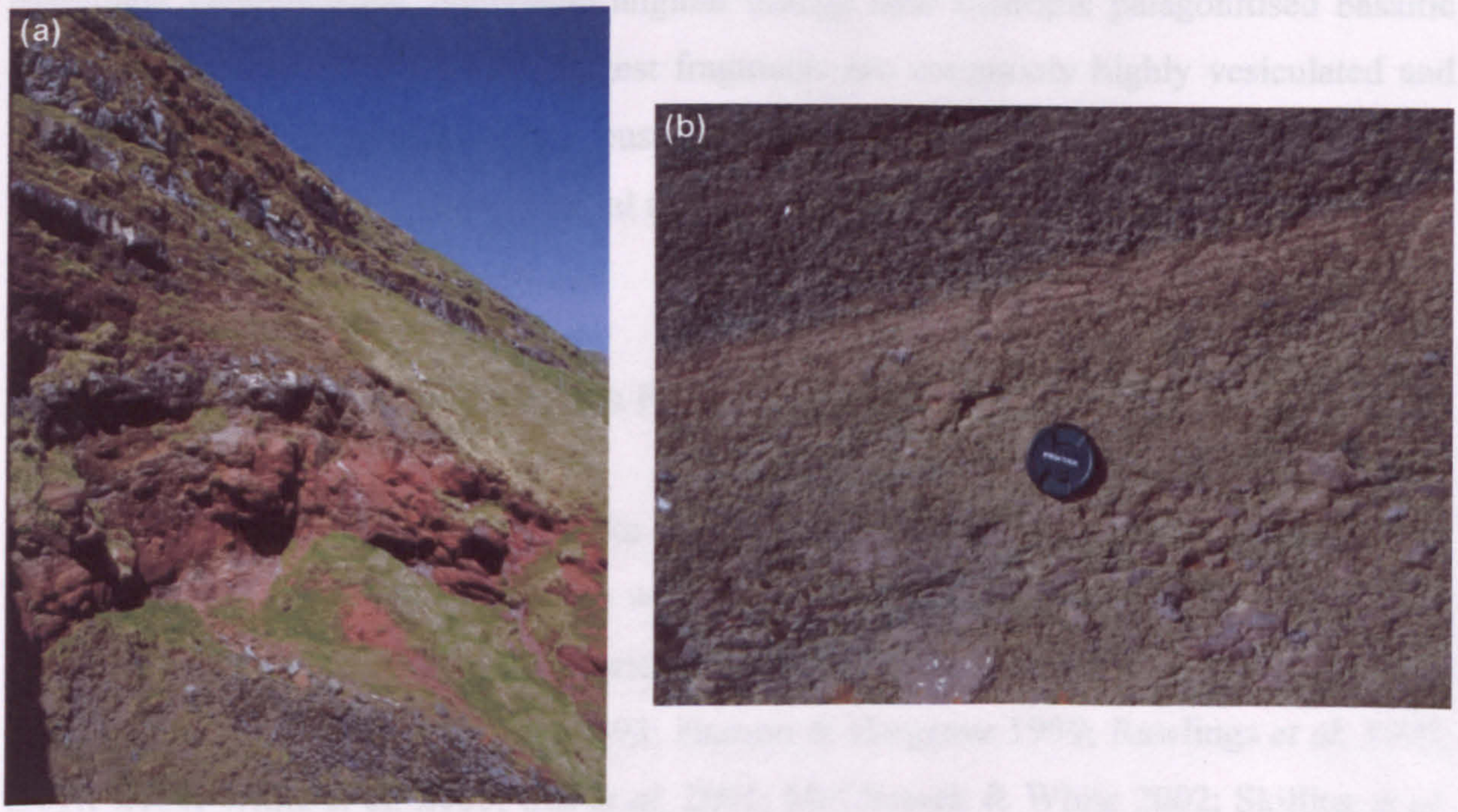

Fig. 5.39. Views of reddened lapillistones and tuffs from the Reyðibarmur cliff section, *ca.* 1.6 km NE of Hvalba, Suðuroy, Faeroe Islands. (a) The lapillistones and tuffs are poorly exposed and are between 20 and 30 m thick. (b) The lapillistones and tuffs form thin to medium beds (4-15 cm) that are normally graded and have a maximum fragment size of 12 x 10 cm. The lens cap is *ca.* 6 cm across.

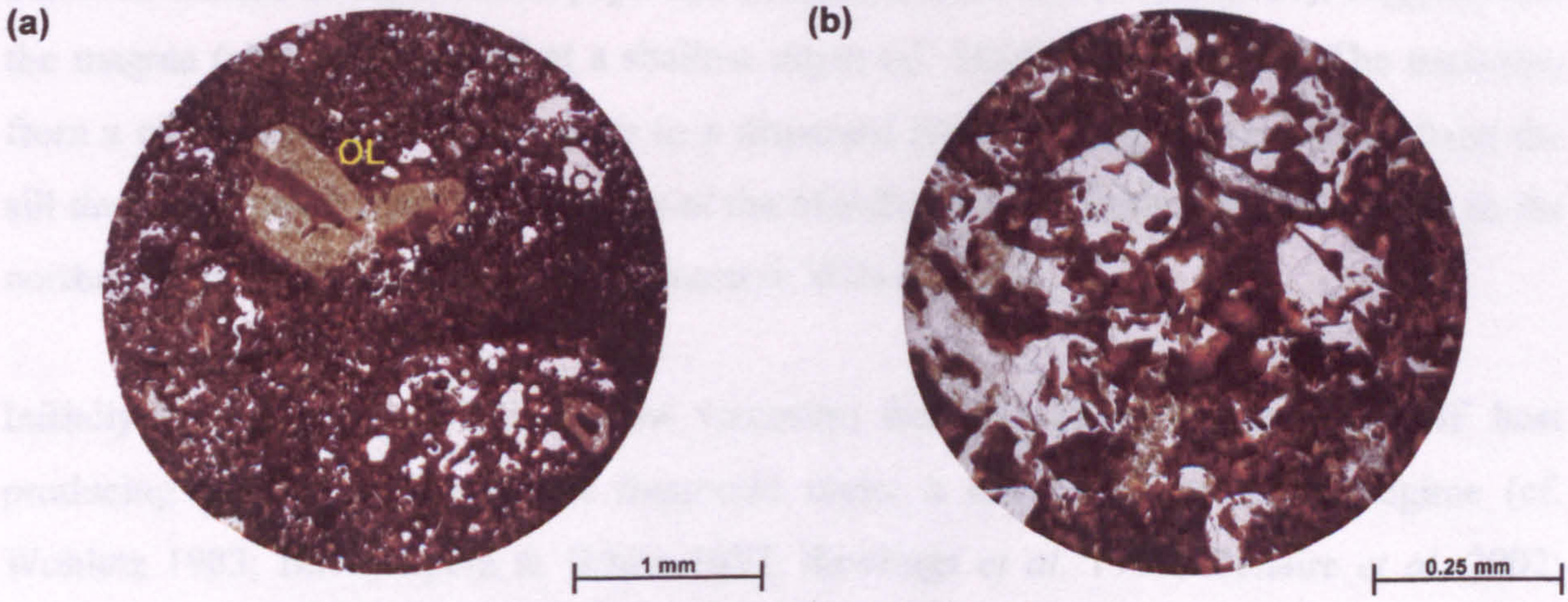

Fig. 5.40. Photomicrographs of a tuff from the Reyðibarmur cliff section, *ca.* 1.6 km NE of Hvalba, Suðuroy, Faeroe Islands. Both photomicrographs are under plane-polarised light. (a) The tuffs are extremely homogeneous containing angular orange near isotropic palagonitised basaltic glass shards. Larger fragments are amygdaloidal and sometimes contain greenish euhedral-subhedral needle shaped serpentinised olivine crystals (OL). (b) The smaller glassy shards have cuspate margins, the remains of bubble walls.

exposed due to the steep vegetated cliffs. Where these units are exposed they consist of poorly sorted thin to medium beds (4-15 cm), which are normally graded and have a maximum fragment size of 12 x 10 cm. In thin section, the lapillistones and tuffs are extremely homogeneous, containing angular orange near isotropic palagonitised basaltic glass fragments (Fig. 5.40). The largest fragments are commonly highly vesiculated and the smaller angular fragments have cuspate margins. Rare (*ca.* 5 vol.%) glass fragments containing greenish euhedral-subhedral needle shaped altered olivine crystals are dispersed throughout the unit.

5.4.1.3 Mode of Formation of the Peperite Sequence

The peperite sequence at the base of the section has features consistent with having formed by the intrusion of magma (a sill) into wet poorly consolidated sediments (cf. Brooks *et al.* 1982; Kokelaar 1982; Walker & Francis 1986; Busby-Spera & White 1987; Cas & Wright 1987; McPhie 1993; McPhie *et al.* 1993; Hanson & Hargrove 1999; Rawlings *et al.* 1999; Doyle 2000; White *et al.* 2000; Cas *et al.* 2001; McClintock & White 2002; Skilling *et al.* 2002; Squire & McPhie 2002). The presence of coal and volcaniclastic claystone fragments within the peperite suggests that the host sedimentary unit belongs to the CBF. The peperite has formed by the disintegration or fragmentation of the invading sill to form juvenile fragments and their mingling with the CBF host. The presence of vesiculated juvenile fragments of basalt, the majority of which are found in the dispersed peperite, a common feature of the Permian peperites of Kiama, Australia (Doyle 2000), suggests that the magma (sill) was intruded at a shallow depth (cf. Skilling *et al.* 2002). The transition from a close-packed blocky peperite to a dispersed blocky-fluidal peperite away from the sill domain is noted from the peperites of the Middle Jurassic Tuttle Lake Formation in the northern Sierra Nevada, California (Hanson & Wilson 1993).

Initially the magma (*ca.* 1200°C, low viscosity) from the sill(s) invaded the CBF host producing fluidal juvenile basalt fragments under a ductile fragmentation regime (cf. Wohletz 1983; Busby-Spera & White 1987; Rawlings *et al.* 1999; Donaire *et al.* 2002; Skilling *et al.* 2002; Squire & McPhie 2002; Wohletz 2002). To maintain the high temperatures of the invading magma, the prevention of direct contact with the pore fluids is essential. This requires the formation of stable insulating vapour films at the magma-host sediment interface (Kokelaar 1982). Vapour films are produced above a certain critical temperature, where film boiling occurred along the contact surfaces of the invading magma (Mills 1984). These insulating vapour films will prevent direct magma-pore fluid contact and promote ductile behaviour of the intruding magma.

As the insulated magma invaded the CBF host it eventually came into contact with coal seams. The coal is thermally unstable and would have reacted differently to the magma than the volcaniclastic claystones. Rapid heating of the coal by the magma would have promoted devolatilisation and dewatering which would have contributed to the thermal metamorphism and rank elevation of coal compared to coal elsewhere in the CBF (cf. McClintock & White 2002). As the coal was heated above temperatures of *ca.* 300°C (cf. Stach *et al.* 1975) it progressively devolatilised, resulting in a softening of the coal whilst maintaining a high viscosity (cf. Lumsden 1967; Nomura *et al.* 1999). A decrease in the volatile content and/or higher heating rates led to the coal having a lower viscosity (cf. Stach *et al.* 1975). The permeability of the coal was dependant upon the level of stress exerted upon it, the higher the stress the higher the permeability, which in turn hinders devolatilisation (cf. Thomas 1992). Therefore, the coal underwent rapid and/or prolonged heating, with accompanying devolatilisation, under relatively low stresses, which resulted in the coal behaving plastically (cf. McClintock & White 2002). Consequently, this process has led to the mutual injection of fluidal basalt into the coal fragments and *vice versa*, as seen in the dispersed peperite at Reyðibarmur.

The blocky fragments have formed as a result of brittle fragmentation (cf. Skilling *et al.* 2002, and references therein). This type of fragmentation is generated by a combination of quenching, mechanical stresses, and by hydromagmatic explosions, where insulating vapour films did not develop and consequently allowed the rapid transfer of magmatic heat to the pore fluid (cf. Kokelaar 1982). The vapour films will not develop where the magma has cooled sufficiently below the critical temperature (Mills 1984). Quenching commonly involves the *in situ* brittle fragmentation as a consequence of thermal stresses induced by cooling contraction (Kokelaar 1986). Quench fragmentation is associated with jigsaw fit blocky peperites (Skilling *et al.* 2002, and references therein). Mechanical stresses lead to brittle fragmentation of more viscous parts of an intrusion in response to the injection of fresh magma (Kokelaar 1986). Hydromagmatic explosions occur where magma engulfs pore fluid-sediment mixtures, which results in the magma fragmenting and being dispersed by the rapidly expanding super-heated pore fluid (cf. Kokelaar 1986). This process is known as 'bulk interaction steam explosion' by Kokelaar (1986) or 'clast blocking' by Busby-Spera & White (1987).

The mixture of juvenile basalt fragment shapes (blocky, platy and fluidal) in the dispersed peperite is also a common feature associated with peperites (Brooks *et al.* 1982; Kokelaar 1982; Busby-Spera & White 1987; McPhie 1993; Hanson & Hargrove 1999; Doyle 2000; Skilling *et al.* 2002; Squire & McPhie 2002). As the blocky fragments form at lower

temperatures it suggests that they formed after the fluidal fragments (cf. Squire & McPhie 2002). The presence of blocky fragments in the dispersed peperite may be the consequence of the propagation of cooler lobes, which fragmented in a brittle fashion. Hydromagmatic explosions may also have produced and distributed the blocky fragments; this may have been aided by the devolatilisation of the coal fragments (cf. Kokelaar 1986; Busby-Spera & White 1987; Hanson & Hargrove 1999; Squire & McPhie 2002).

The lack of a jigsaw fit texture in the close-packed blocky peperite suggests that the fragments were not formed by quenching but by mechanical stresses or hydromagmatic explosions (cf. Squire & McPhie 2002). The blocky fragments in the close-packed peperite may have formed by the later brecciation of previously formed ductile fragments. It is unlikely that one process led to the formation of the close-packed blocky peperite, but more likely a combination of the processes.

5.4.1.4 Provenance

The Reyðibarmur Section consists predominantly of coal and volcaniclastic claystone fragments derived from the CBF. The compact basalt fragments are presumed to be from the brecciation of the sill located to the west of the section rather than from the brecciation of lava flows. The tuffs and lapillistones overlying the peperite sequence consist of angular palagonitised basaltic glass fragments inferred to be derived from a localised vent due to the coarseness of the deposits.

5.4.1.5 Environment of Deposition

The Reyðibarmur Section consists of pyroclastic rocks formed by different processes. The peperite sequence is the result of magma, in the form of a sill, invading an unlithified sequence from the CBF. The range of brecciation textures observed within the peperite suggests that the sill was intruded at shallow depths into water-saturated coal seams and claystones. The peperites are overlain by pyroclastic fallout deposits that have not been invaded by the sill(s), indicating that the peperite formation, i.e. the intrusion of the sill(s), took place before the deposition of the lapillistones and tuffs. The pyroclastic fallout deposits have been deposited in a subaerial environment and have been unaffected by the process of water. This is supported by the lack of sideromelane and quench-type textures (Fisher & Schmincke 1984; Cas & Wright 1987; McPhie *et al.* 1993).

5.5 Synthesis

The Volcaniclastic Sandstone Formation comprises both pyroclastic and epiclastic lithologies that were deposited in a terrestrial environment (Fig. 5.41). Three traverses were investigated in detail on Suðuroy and six pyroclastic and sedimentary sequences were identified. Figure 5.42 is a correlation of the idealised sections from the Reyðibarmur Section, the Svalbarðaá-Myllá Traverse, and the Dysjarnar Traverse. At the base of all three is Unit 1, a sequence of pyroclastic fall deposits consisting of tuffs and lapillistones, dominated by olivine-phyric, palagonitised basaltic glass. These deposits were subsequently reworked by fluvial systems and also occur as clasts within the overlying units of the VSF.

Units 2, 4, and 6, overlying the tuffs and lapillistones of Unit 1, range from mudstones through to polylithic conglomerates and are predominantly composed of rounded ash and lapilli clasts. The conglomerates also contain clasts of coal, volcaniclastic mudstone and basalt. These lithologies are interpreted as having been deposited as laterally extensive sheets from lahar events (cf. Smith 1991; Smith & Lowe 1991). The development of planar laminations, the degree of rounding of the clasts, the poorly sorted and matrix supported nature of the deposits suggest that they were deposited from a combination of volcaniclastic debris and hyperconcentrated flow processes (cf. Janda *et al.* 1981; Pierson & Scott 1985; Lowe *et al.* 1986; Naranjo *et al.* 1986; Smith 1986; Rodolfo 1989; Smith & Lowe 1991; Coussot & Meunier 1996; Sohn *et al.* 1999; Kessler & Bédard 2000; Lavigne *et al.* 2000; Lirer *et al.* 2001). The abundance of coarse volcanic debris within these deposits suggests that deposition occurred during syn-eruption periods when pyroclastic activity was rapidly adding debris to the surrounding land surface (cf. Smith 1987a; b; 1988; Smith & Fritz 1989; Smith 1991; Bahk & Chough 1996). If, the bulking of the volcanic debris and the destabilisation of the land surface, by the destruction of vegetation during volcanic activity, was coupled with high rainfall/surface water then mobilisation of the debris would have resulted in high aggradation rates producing turbulent flood surges (sheet floods) through volcaniclastic debris and hyperconcentrated flow processes (cf. Smith 1986; 1987a; b; 1988; Smith & Fritz 1989; Smith 1991; Smith & Lowe 1991; Haughton 1993; Bahk & Chough 1996; Nakayama & Yoshikawa 1997).

Unit 3 consists of sharp-based sandstones and mudstones. The sandstone beds have thicknesses of less than 2 m and are intercalated with mudstones, which are features commonly associated with floodplain deposits (cf. Steel & Aasheim 1978; Collinson 1996)

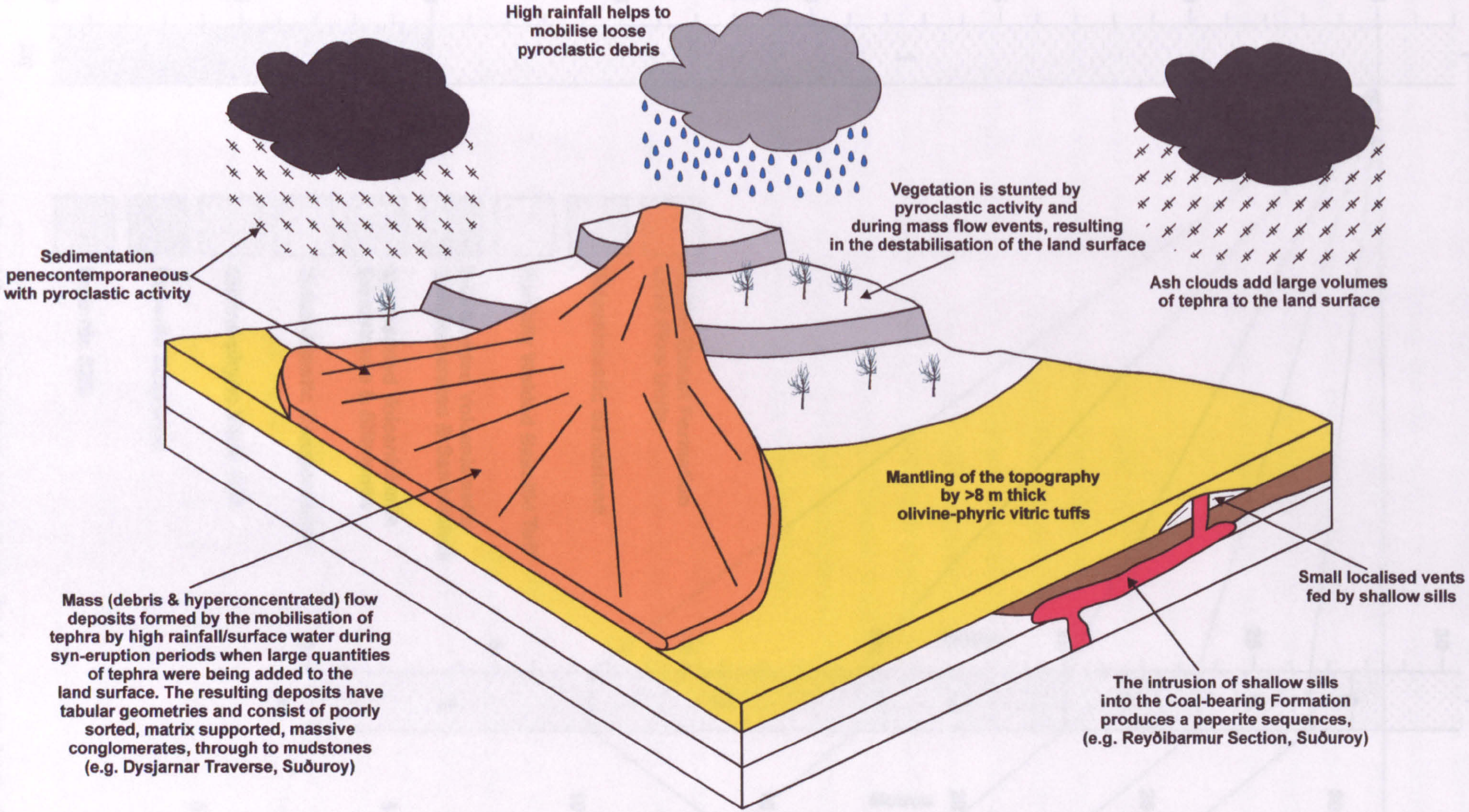

Fig. 5.41. Schematic palaeogeographical block diagram for the Volcaniclastic Sandstone Formation with the main elements highlighted. The formation records a period of simultaneous pyroclastic and sedimentary deposition. Length of each horizontal dimension of the figure is very approximately 1-1.5 km.

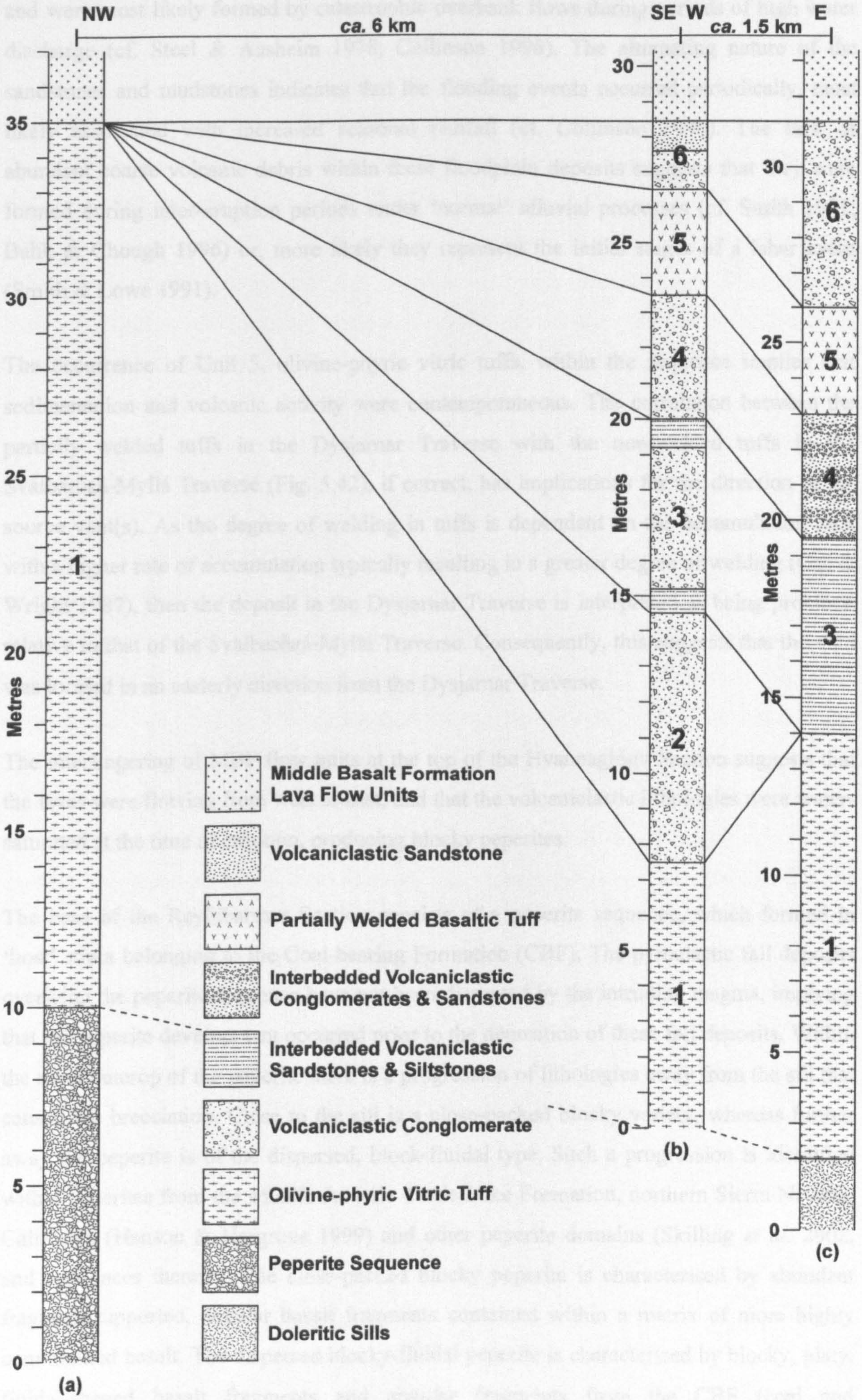

Fig. 5.42. Idealised correlation of the Volcaniclastic Sandstone Formation between (a) the Reyðibarmur Section, (b) the Svalbarðaá-Myllá Traverse, and (c) the Dysjarnar Traverse; Suðuroy, Faeroe Islands.

and were most likely formed by catastrophic overbank flows during periods of high water discharge (cf. Steel & Aasheim 1978; Collinson 1996). The alternating nature of the sandstones and mudstones indicates that the flooding events occurred periodically, most likely associated with increased seasonal rainfall (cf. Collinson 1996). The lack of abundant coarse volcanic debris within these floodplain deposits suggests that they were formed during inter-eruption periods under 'normal' alluvial processes (cf. Smith 1991; Bahk & Chough 1996) or, more likely they represent the initial stages of a lahar event (Smith & Lowe 1991).

The occurrence of Unit 5, olivine-phyric vitric tuffs, within the sequence implies that sedimentation and volcanic activity were contemporaneous. The correlation between the partially welded tuffs in the Dysjarnar Traverse with the non-welded tuffs in the Svalbarðaá-Myllá Traverse (Fig. 5.42), if correct, has implications for the direction of the source vent(s). As the degree of welding in tuffs is dependant on the accumulation rate, with a higher rate of accumulation typically resulting in a greater degree of welding (Cas & Wright 1987), then the deposit in the Dysjarnar Traverse is interpreted as being proximal relative to that of the Svalbarðaá-Myllá Traverse. Consequently, this suggests that the vent was located in an easterly direction from the Dysjarnar Traverse.

The interfingering of MBF flow units at the top of the Hvannagjógv Section suggests that the lavas were flowing from west to east, and that the volcaniclastic lithologies were water-saturated at the time of eruption, producing blocky peperites.

The base of the Reyðibarmur Section consists of a peperite sequence, which formed in 'host' strata belonging to the Coal-bearing Formation (CBF). The pyroclastic fall deposits overlying the peperite sequence have not been disrupted by the intruding magma, implying that the peperite development occurred prior to the deposition of these fall deposits. Within the main outcrop of the peperite there is a progression of lithologies away from the sill that caused the brecciation. Close to the sill is a close-packed blocky variety, whereas further away the peperite is of the dispersed, block-fluidal type. Such a progression is identified within peperites from the Middle Jurassic Tuttle Lake Formation, northern Sierra Nevada, California (Hanson & Hargrove 1999) and other peperite domains (Skilling *et al.* 2002, and references therein). The close-packed blocky peperite is characterised by abundant fragment-supported, angular basalt fragments contained within a matrix of more highly comminuted basalt. The dispersed blocky-fluidal peperite is characterised by blocky, platy, fluidal-shaped basalt fragments and angular fragments from the CBF (coal and

volcaniclastic claystone), which are supported by a matrix of highly comminuted basalt and sediment.

Initially, the sill invaded the CBF 'host' under a ductile fragmentation regime, producing fluidal fragments which were achieved by the development of insulating vapour films (cf. Kokelaar 1982; Wohletz 1983; Mills 1984; Busby-Spera & White 1987; Rawlings *et al.* 1999; Donaire *et al.* 2002; Skilling *et al.* 2002; Squire & McPhie 2002; Wohletz 2002). When the insulated apophyses of the sill came in contact with the coal within the CBF 'host', the coal acted plastically because it rapidly devolatised due to it being thermally unstable (cf. Lumsden 1967; Stach *et al.* 1975; Thomas 1992; Nomura *et al.* 1999; McClintock & White 2002). This led to the mutual injection of fluidal basalt into the coal and *vice versa,* similar to the coal peperites observed at Coombs Hills, Antarctica (McClintock & White 2002).

Once the sill had cooled sufficiently, vapour films were unable to further develop, leading to the brittle fragmentation of newly emerging sill apophyses, thus producing angular basalt fragments. The lack of jigsaw fit blocky peperites implies that the brittle fragmentation did not form through quenching (cf. Skilling *et al.* 2002, and references therein), and therefore more likely occurred through the process of bulk interaction steam explosions (also known as clast blocking) and mechanical stresses (cf. Kokelaar 1986; Busby-Spera & White 1987). The bulk interaction steam explosion process required the engulfing of water-saturated 'host' sediment, which would have rapidly devolatised, causing the fragmentation of the engulfing magma and dispersing the resulting angular fragments throughout the 'host' sediment (cf. Kokelaar 1982; 1986; Busby-Spera & White 1987). This process may have been enhanced by the devolatilisation of the coal fragments (cf. Kokelaar 1986; Busby-Spera & White 1987; Hanson & Wilson 1993; Squire & McPhie 2002).

6 Middle Basalt Formation

In this chapter, the facies architectures are described and interpreted for the lava flows of the Middle Basalt Formation (MBF) and environments of eruption are proposed. As with the Lower and Upper basalt formations previous work has concentrated on the petrology and geochemistry of the lavas and little attention has been given to the interlava lithologies. Five new sections containing volcaniclastic lithologies are described and interpreted and environments of deposition are presented. The interaction between the lava flows and the volcaniclastics is also examined. The lithologies of an accessible 'vent' locality of Rasmussen & Noe-Nygaard (1969; 1970b) is re-evaluated using current volcaniclastic classification schemes and this work shows that the 'vent' is better described as a volcaniclastic conglomerate of epiclastic origin.

6.1 Distribution

The Middle Basalt Formation (MBF) reaches a maximum stratigraphic thickness of *ca.* 1,400 m in the vicinity of Vestmanna, Streymoy (Rasmussen & Noe-Nygaard 1970b; Waagstein 1988). The MBF crops out on all the islands except Mykines, Nólsoy, Svínoy, and Fugloy (Figs. 1.3, 6.1 & 6.2). To the west and south of the archipelago, the MBF overlies the Coal-bearing Formation (CBF) and locally the Volcaniclastic Sandstone Formation (VSF), which it is sometimes transitional with. In the eastern part of the archipelago, the base of the MBF is not exposed. Waagstein (1988) showed that the MBF lavas dip towards the E and NE with an inclination between 2.2 and 3.9°.

6.2 Lava Flows

6.2.1 Petrology & Geochemistry

Petrologically, the lower *ca.* 450 m of the MBF is composed of olivine-phyric flows which progress up sequence to aphyric flows (Figs. 6.3a-d) (Waagstein & Hald 1984; Waagstein 1988; Larsen *et al.* 1999). The upper *ca.* 960 m of the MBF is dominated by plagioclase-phyric flows (Figs. 6.3e-h) (Waagstein & Hald 1984; Waagstein 1988; Larsen *et al.* 1999). Plagioclase feldspar phenocrysts can reach *ca.* 1 cm in size (Rasmussen & Noe-Nygaard 1970b). The progression from the lower 450 m to the upper 960 m lava flows is transitional.

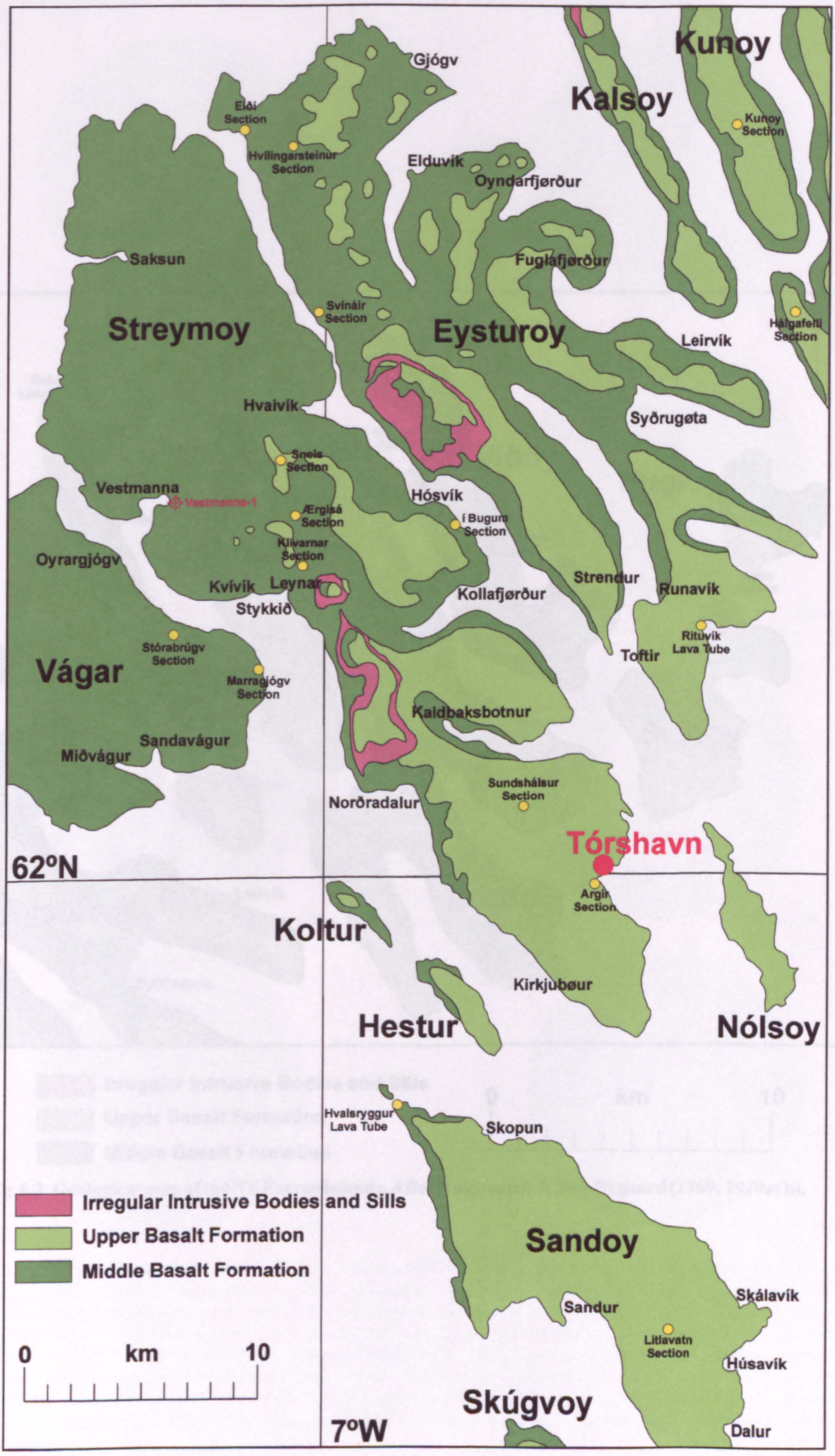

Fig. 6.1. Geological map of the central Faeroe Islands. After Rasmussen & Noe-Nygaard (1969; 1970a; b).

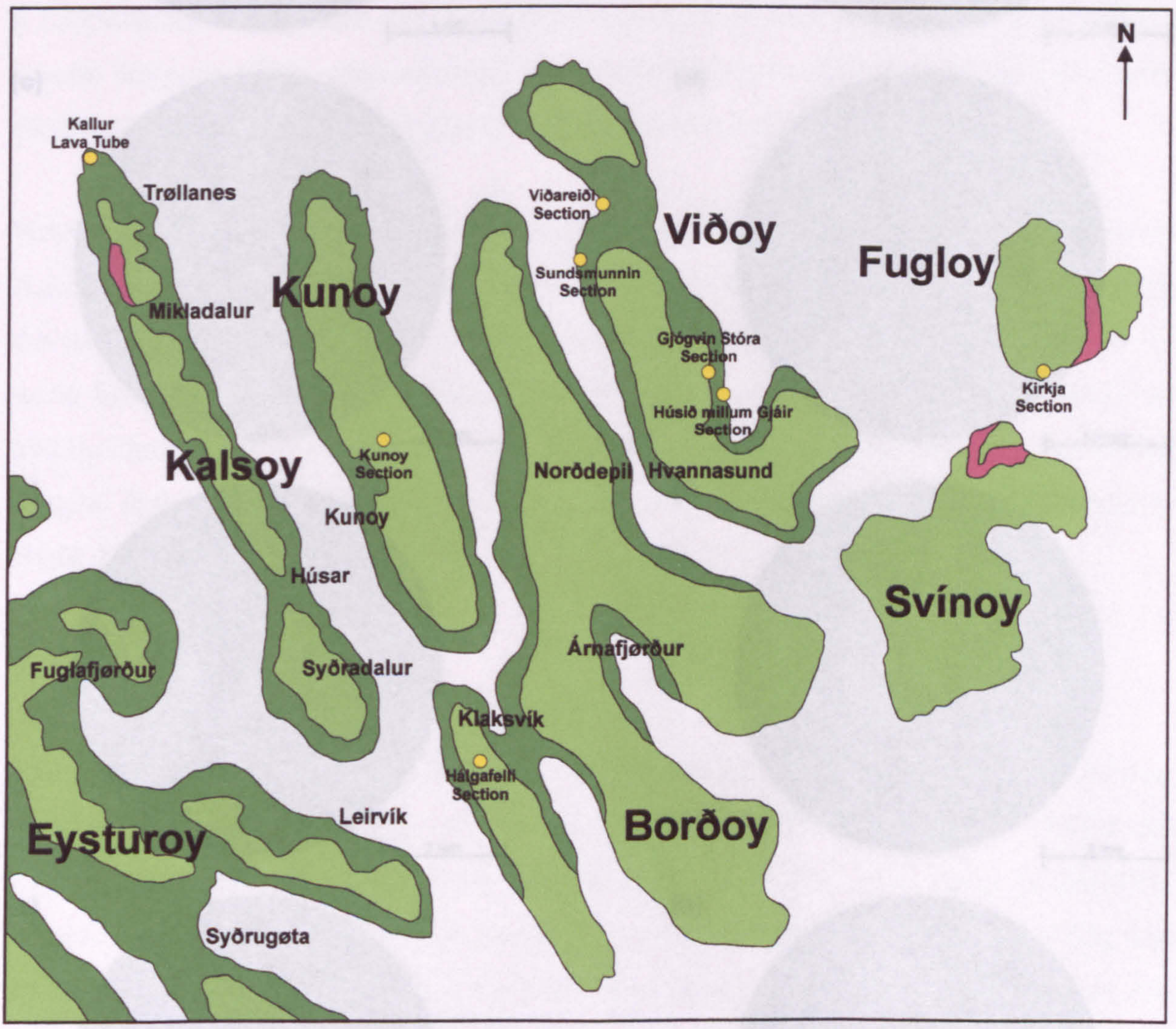

Fig. 6.2. Geological map of the NE Faeroe Islands. After Rasmussen & Noe-Nygaard (1969; 1970a; b).

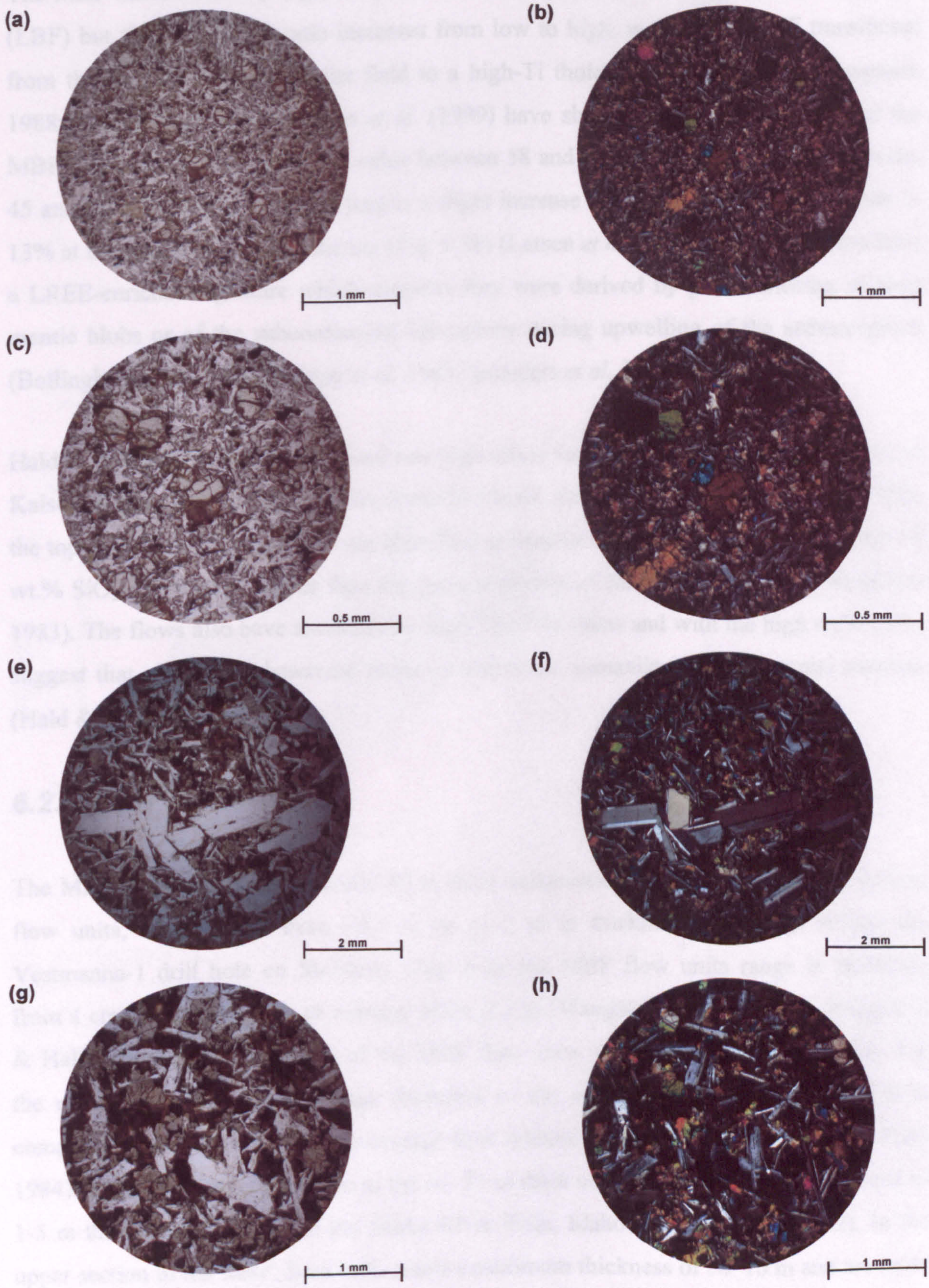

Fig. 6.3. Photomicrographs of Middle Basalt Formation lava flow units from a disused quarry at Selgjógv, *ca.* 3.5 km NW of Hvannasund, Viðoy, Faeroe Islands. (a) & (c) A lava flow unit that is an aphyric finely crystalline basalt displaying an intergranular texture. The basalt consists of laths of plagioclase feldspar, clinopyroxenes, oxides ± olivines. The photomicrographs are under plane polarised light. (b) & (d) The same views as in (a) & (c) but under cross-polarised light. (e) & (g) A lava flow unit that is a plagiocalse-phyric basalt. Phenocrysts of plagioclase feldspar have a maximum length of *ca.* 2 mm set in a finely-medium crystalline groundmass consisting of plagioclase feldspar laths, clinopyroxenes, oxides ± olivines. The photomicrographs are under plane polarised light. (f) & (h) The same views as in (e) & (g) but under cross-polarised light.

The MBF has a relatively high TiO_2/FeO^T ratio compared to the Lower Basalt Formation (LBF) but the FeO^T/MgO ratio increases from low to high, making the MBF transitional from the high-Ti olivine tholeiite field to a high-Ti tholeiite field (Fig. 6.4) (Waagstein 1988; Larsen *et al.* 1999). Larsen *et al.* (1999) have shown that the Mg # value for the MBF decreases up section from a value between 58 and 80 at the base, to a value between 45 and 55 at the top (Fig. 6.5). There is a slight increase up section in wt.% FeO^T from 9-13% at the base to 12-15% at the top (Fig. 6.5b) (Larsen *et al.* 1999). The MBF flows have a LREE-enriched signature which suggests they were derived by partial melting of deep mantle blobs or of the subcontinental lithosphere during upwelling of the asthenosphere (Bollingberg *et al.* 1975; Gariépy *et al.* 1983; Saunders *et al.* 1997).

Hald & Waagstein (1983) recognised two high silicic basalt lavas, the Klaksvík (occurs on Kalsoy, Kunoy and Borðoy) and the Sneis-14 (Sneis, Streymoy) lava flows, *ca.* 80 m from the top of the MBF. These flows are classified as basaltic andesites and have an average 54 wt.% SiO_2, *ca.* 6 wt.% higher than the main sequence of MBF lavas (Hald & Waagstein 1983). The flows also have anomalously high $^{87}Sr/^{86}Sr$ ratios and with the high wt.% SiO_2, suggest that continental basement rocks or sediments contaminated the parental magmas (Hald & Waagstein 1983).

6.2.2 Flow Thicknesses

The MBF is dominated by typically 20 m thick compound lava flows made up of thinner flow units, which range from <0.5 m up to 2 m in thickness (Fig. 6.6). Within the Vestmanna-1 drill hole on Streymoy (Fig. 6.1), the MBF flow units range in thickness from 4 cm up to 14 m, with an average of *ca.* 2.2 m (Waagstein & Hald 1984). Waagstein & Hald (1984) recognised 70% of the MBF flow units in Vestmanna-1 as pahoehoe and the remainder as a'a. The average thickness of the pahoehoe flow units is *ca.* 1.8 m compared to the a'a flows with an average flow thickness of *ca.* 3.2 m (Waagstein & Hald 1984). These data are comparable to the *ca.* 35 m thick compound lava flows composed of 1-5 m thick flow units within the Snake River Plain, Idaho (Greeley 1977; 1982). In the upper section of the MBF, flow units reach a maximum thickness of *ca.* 10 m and are more akin to tabular-classic lava flows.

6.2.3 Morphology

The MBF lava flows, or lava fields, are compound in structure and commonly form very flat shield areas having slope angles less than 0.5° (Noe-Nygaard 1968). Noe-Nygaard

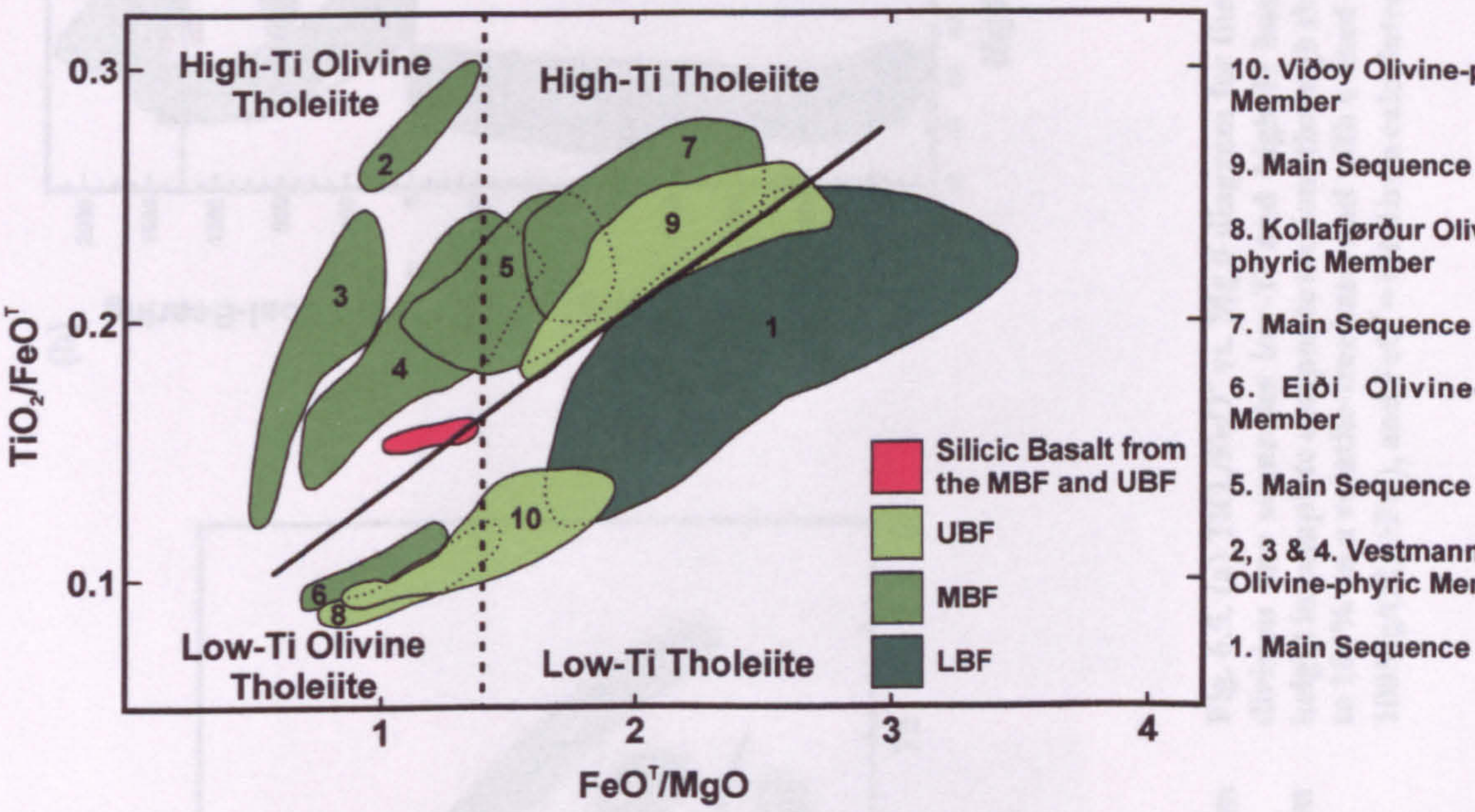

Fig. 6.4. TiO_2/FeO^T vs. FeO^T/MgO diagram for basalt lavas from the Faeroe Plateau Lava Group, Faeroe Islands (FeO^T = total iron recalculated as FeO). The oblique full line and the vertical stippled line mark the proposed boundaries between high-Ti olivine tholeiites, high-Ti tholeiites, low-Ti olivine tholeiites, and low-Ti tholeiites. LBF = Lower Basalt Formation, MBF = Middle Basalt Formation, UBF = Upper Basalt Formation. After Waagstein (1988).

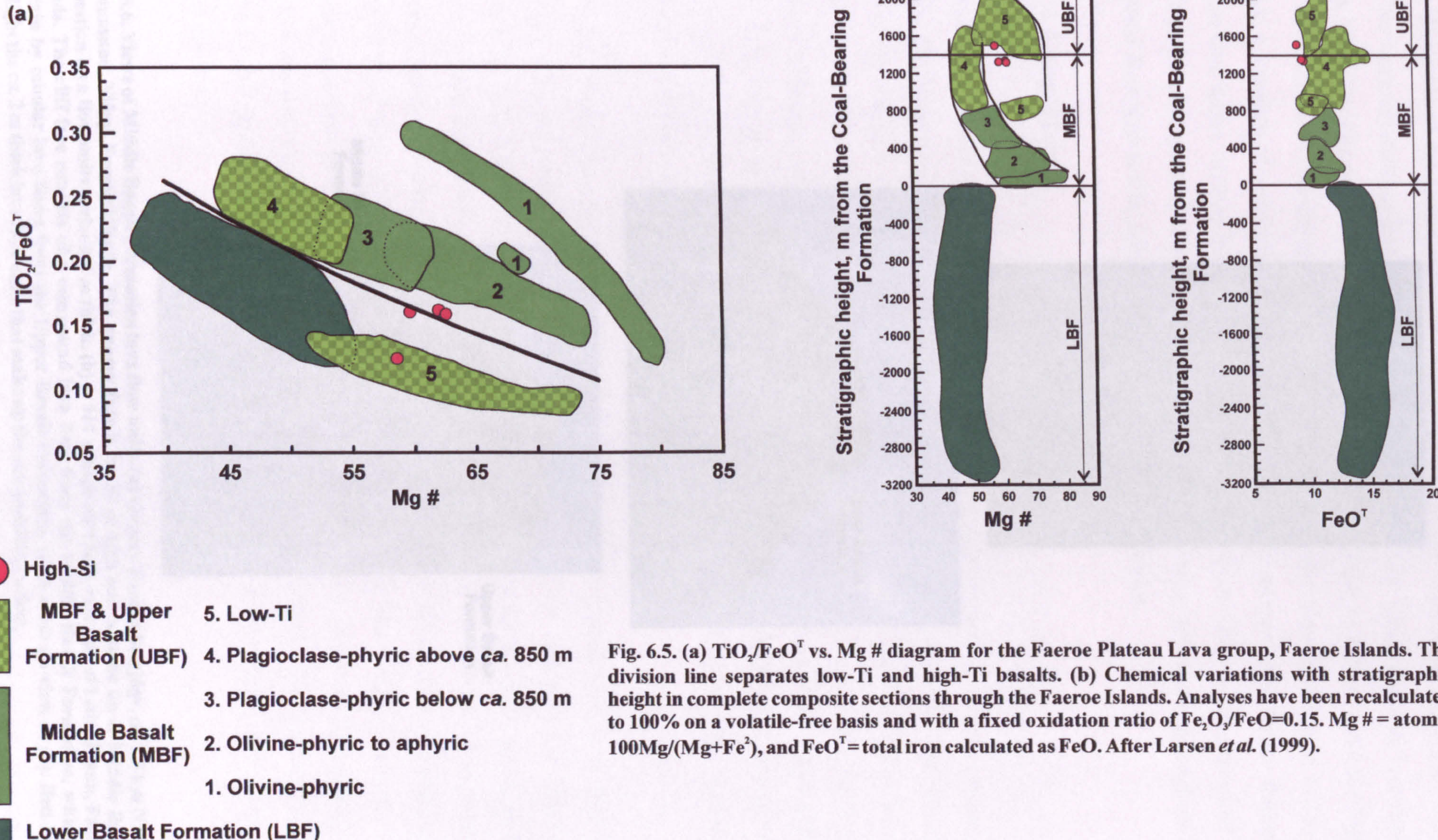

Fig. 6.5. (a) TiO_2/FeO^T vs. Mg # diagram for the Faeroe Plateau Lava group, Faeroe Islands. The division line separates low-Ti and high-Ti basalts. (b) Chemical variations with stratigraphic height in complete composite sections through the Faeroe Islands. Analyses have been recalculated to 100% on a volatile-free basis and with a fixed oxidation ratio of Fe_2O_3/FeO=0.15. Mg # = atomic $100Mg/(Mg+Fe^2)$, and FeO^T = total iron calculated as FeO. After Larsen *et al.* (1999).

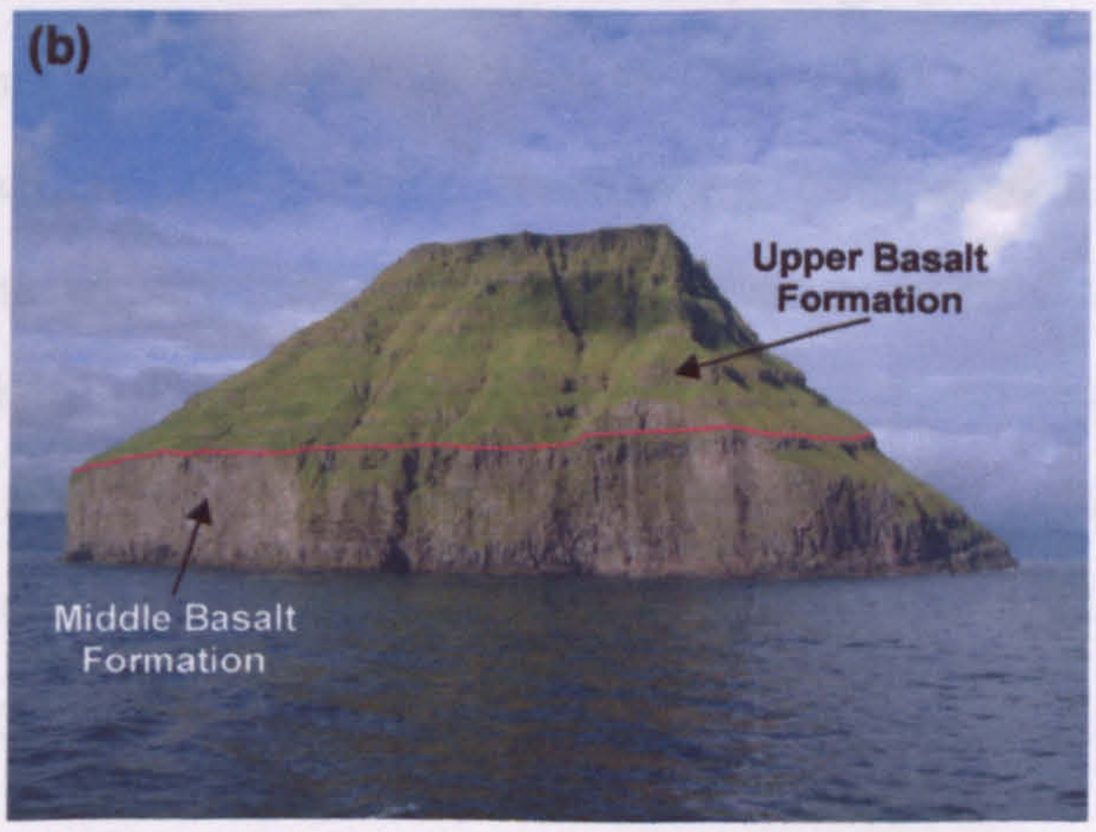

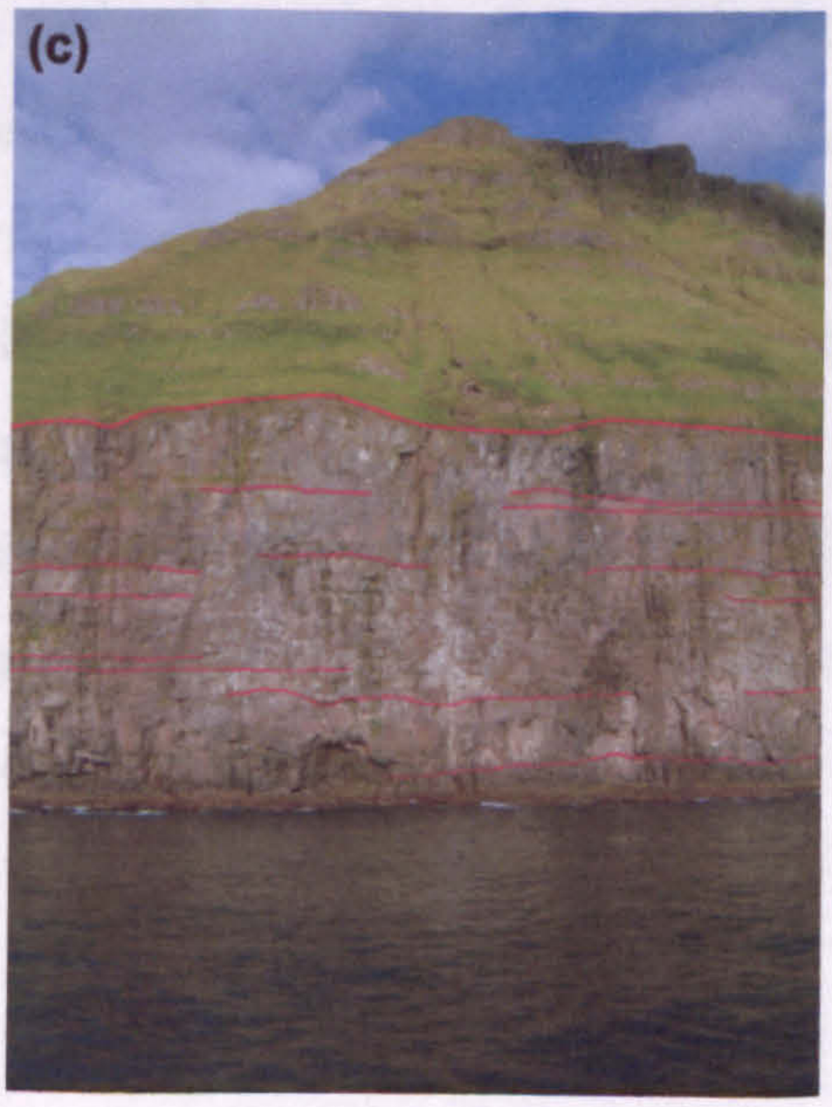

Fig. 6.6. Views of Middle Basalt Formation lava flow units. (a) Quarry Face at Selgjógv, *ca.* 3.5 km NW of Hvannasund, Viðoy, Faeroe Islands. The quarry face is *ca.* 22 m high and is made up of Middle Basalt Formation lava flow units each *ca.* 2 m thick. (b) A 414 m high cliff face, east side of Lítla Dímun, Faeroe Islands. The cliff face consists of a compound lava flow from the Middle Basalt Formation, which is overlain by tabular lava flows from the Upper Basalt Formation. (c) A close up view of (b). Red lines highlight the *ca.* 2 m thick lava flow units that make up the compound lava flow.

(1968) termed these flat shield areas as scutulum type and showed that they commonly have diameters of *ca.* 15 km and volumes of less than 7 km^3. The scutulum type of shield area has been renamed as low shields by Greeley (1977; 1982). The compound lava flows of the MBF are akin to subaerial compound pahoehoe lava fields on Hawai`i, but the MBF lava flows are *ca.* 4 times thicker. The MBF lava fields are pahoehoe in character and they exhibit a number of regional- to small-scale features that support this. These features include lava tubes, surface features and internal structures; these features are described in detail in the subsequent sections. The lava fields have planar tops, which are highlighted by reddened flow tops and by rare volcaniclastic interlava lithologies.

6.2.4 Lava Tubes

Infilled lava tubes are evident throughout the MBF, ranging in size from master tubes to smaller distributary tubes (cf. Rowland & Walker 1990). The master tubes form prominent, stand-alone features, which have resisted weathering, compared to the flow fields within which they formed. The largest master lava tube observed forms a *ca.* 100 m long by *ca.* 10-20 m wide spit of land off the NW coastline of Sandoy, known as Hvalsryggur (Figs. 6.1 & 6.7). This gives a cross-sectional area of *ca.* 160 m^2 and an estimated volume of *ca.* 15,700 m^3. The tube outline is also observed on Trøllhøvdi Island, to the NW, extending the length of the tube by *ca.* 140 m.

Other lava tubes that have resisted erosion are seen on the coastal section at Rituvík, Eysturoy (Fig. 6.1) and along the coastline at Sundsmunnin, *ca.* 800 m S of Viðareiði, Viðoy (Fig. 6.2). The Rituvík lava tube is found sitting on top on the MBF lavas, which appear to have been thermally altered (Fig. 6.8). The lava tube forms a *ca.* 15-20 m long sinuous elliptical cylinder *ca.* 1.1 m high and *ca.* 3.2 m wide, giving a cross-sectional area of *ca.* 2.8 m^2 and volumes between *ca.* 41 and 55 m^3 for the exposed length. The Sundsmunnin lava tube is *ca.* 3 m high and *ca.* 5 m wide, with a cross-sectional area of 12 m^2, and is found within a volcaniclastic conglomerate (Figs. 6.9a-b). The jointing within the lava tube appears to be concentrically zoned, originating from a point within the top left of the tube.

A master lava tube observed in its original state, i.e. within a MBF lava flow field, is located along the coastline at Froðbiarbotnur, *ca.* 3 km NE of Tvøroyri, Suðuroy (Fig. 6.9c). The lava tube is *ca.* 5 m high and *ca.* 9 m wide, with a cross-sectional area of *ca.* 35 m^2. The lava tube is highlighted by its darker colour compared to the planar lava flow units surrounding it. Apophyses of lava are observed extending out of the top of the lava tube.

Fig. 6.7. Views of the lava tube forming Hvalsryggur spit, NW coastline of Sandoy. The lava tube *ca.* 100 m long by *ca.* 10-20 m wide. The tube outline is observed on Trøllhøvdi Island, to the NW, extending the length of the tube by *ca.* 140 m. The tube outline gives a cross-sectional area of *ca.* 160 m^2.

West

East

Fig. 6.8. Middle Basalt Formation lava tube at Rituvík, Eysturoy. The lava tube forms a 15-20 m long sinuous elliptical cylinder *ca.* 1.1 m high and *ca.* 3.2 m wide. The tube has a cross-sectional area of *ca.* 2.8 m^2 and volumes for the exposed length range between *ca.* 41 and 55 m^3.

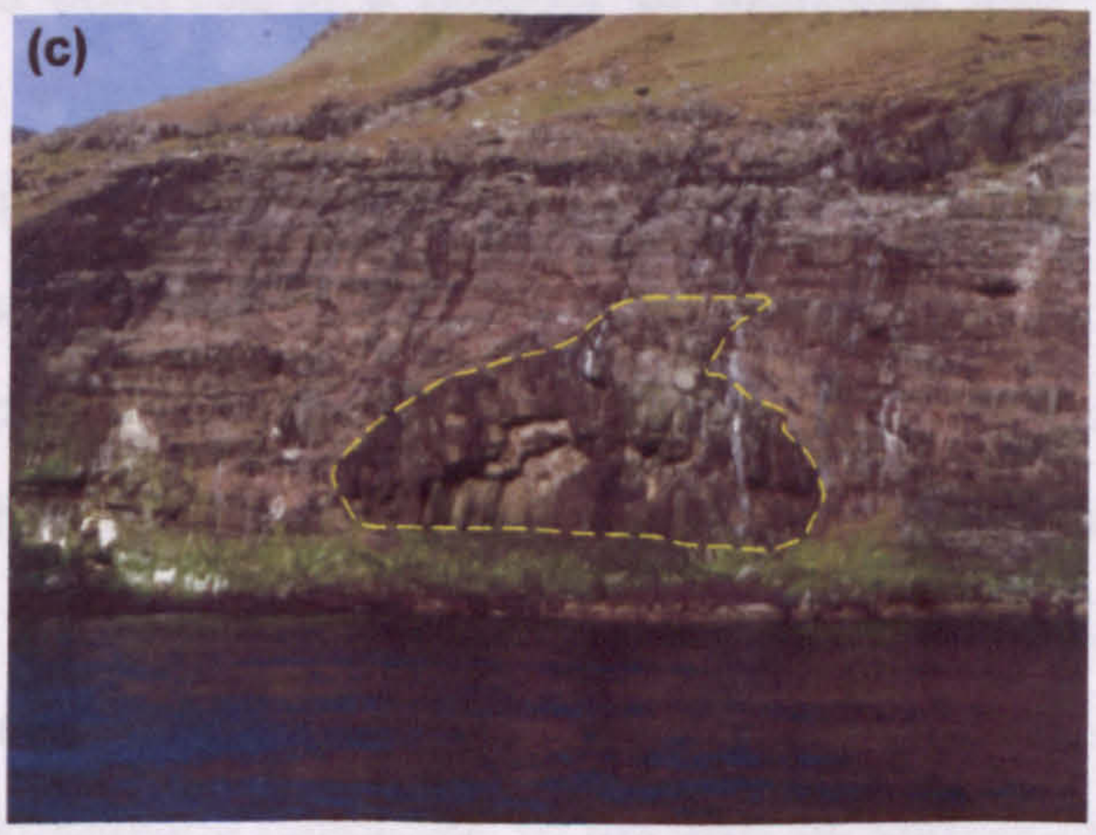

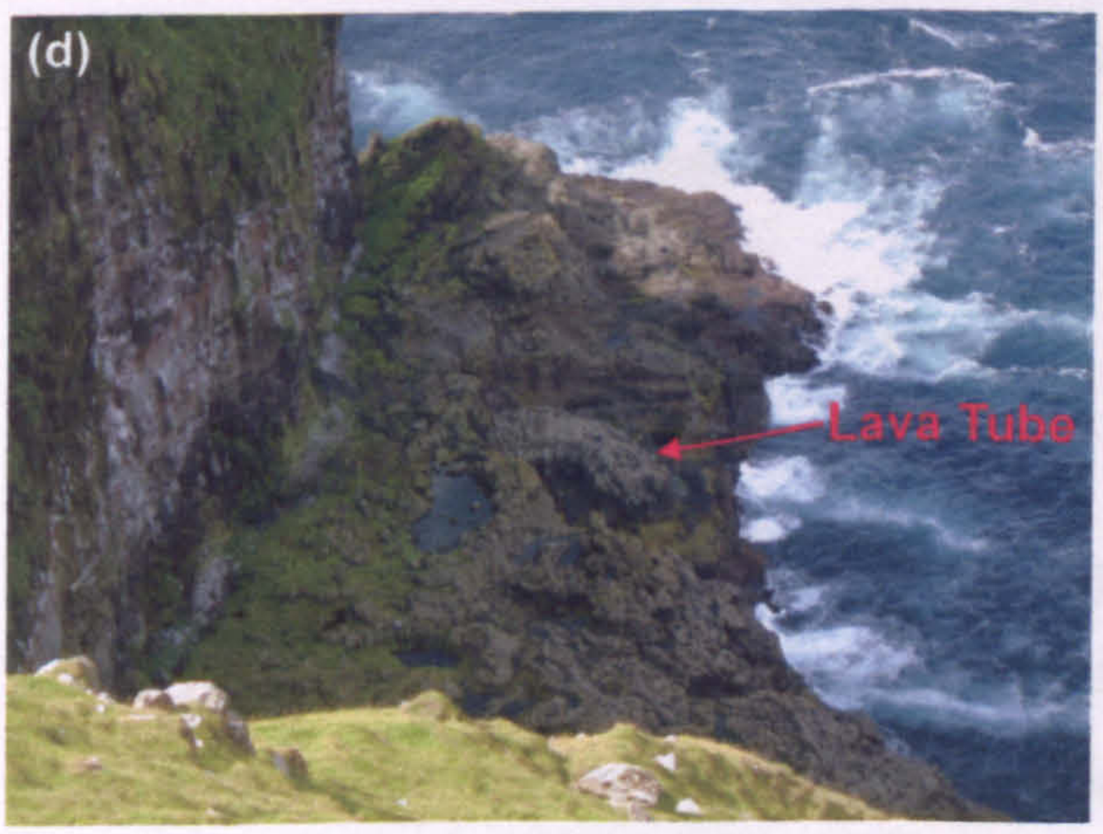

Fig. 6.9. Views of lava tubes from the Middle Basalt Formation. (a) & (b) Sundsmunnin lava tube, *ca.* 800 m S of Viðareiði, Viðoy, Faeroe Islands. The lava tube is *ca.* 3 m high and *ca.* 5 m wide, giving a cross-sectional area of *ca.* 12 m^2. The fracturing within the tube appears to be concentrically zoned, originating from a point in the top left of the tube. (c) A lava tube in the cliff section at Froðbiarbotnur, *ca.* 3 km NE of Tvøroyri, Suðuroy, Faeroe Islands. The lava tube is *ca.* 5 m high and *ca.* 9 wide, a cross-sectional area of *ca.* 35 m^2. (d) A possible master lava tube at Kallur, *ca.* 1 km NW of Trøllanes, Kalsoy, Faeroe Islands. (e) A distributary lava tube at Viðareiði, Viðoy. The lava tube has a cross-sectional area of *ca.* 0.14 m^2. The compass is *ca.* 10 x 6 cm.

Another possible master lava tube is observed at Kallur, *ca.* 1 km NW of Trøllanes, Kalsoy (Figs. 6.2 & 6.9d).

A distributary lava tube with a cross-sectional area *ca.* 0.14 m^2, akin to those described by Rowland & Walker (1990) is observed within a lava flow field at Viðareiði, Viðoy (Figs. 6.2 & 6.9e). The lava tube is lobate in shape and is similar in form to pillow lava. The tube is located within pahoehoe lava flow units. The overlying flow unit exhibits pipe amygdales off the base of the flow, which are aligned perpendicular to the curved contact with the lava tube.

6.2.5 Surface Features

The commonest surface feature observed throughout the MBF is rope structures or surface wrinkles. Ropy lava is observed at a number of localities, although the best-preserved examples are found at Viðareiði, Viðoy (Fig. 6.2) and in the area of Marragjógv, Vágar (Fig. 6.1). At Viðareiði, Viðoy, lava ropes are observed on the upper and lower surfaces of the flow units. Large-scale convex ropes are observed covering an area *ca.* 3 x 2 m (Fig. 6.10a). The convex nature of the ropy lava in this area tentatively suggests a flow direction to the WNW. Within the same coastal area, small-scale ropy lava is observed on the upper surface of a flow front in an area *ca.* 40 x 40 cm (Figs. 6.10b-c). Each rope is *ca.* 1-3 cm thick and has the appearance of twisted bread sticks, producing a braided pattern. The ropes also have an anastomosing character. In the area of Marragjógv, Vágar the ropy lava is preserved on the upper surfaces of lava tongues *ca.* 30 x 30 cm. The convex nature of the ropy lava in this area suggests a tentative flow direction to the NE.

6.2.6 Internal Structure

P-type (pipe-bearing) and S-type (spongy) pahoehoe flow units are both observed within the MBF, but P-type flow units are dominant. The P-type flow units can be separated into a number of separate zones based on amygdale distribution patterns. Figure 6.11 shows a typical P-type flow unit from Viðareiði, Viðoy that can be separated into three zones. The flow unit is *ca.* 1.6 m thick and is separated into basal crust, lava core, and upper crust. The basal crust is *ca.* 10 cm thick and is characterised by pipe amygdales with a maximum length of *ca.* 8 cm that start a few centimetres off the base of the flow unit. The pipe amygdales are sometimes curved in the assumed direction of flow. The lava core is a compact, massive zone with irregular jointing and lacks vesicle/amygdale cylinders. The upper crust is on average *ca.* 25 cm thick and is dominated by elliptical amygdales that

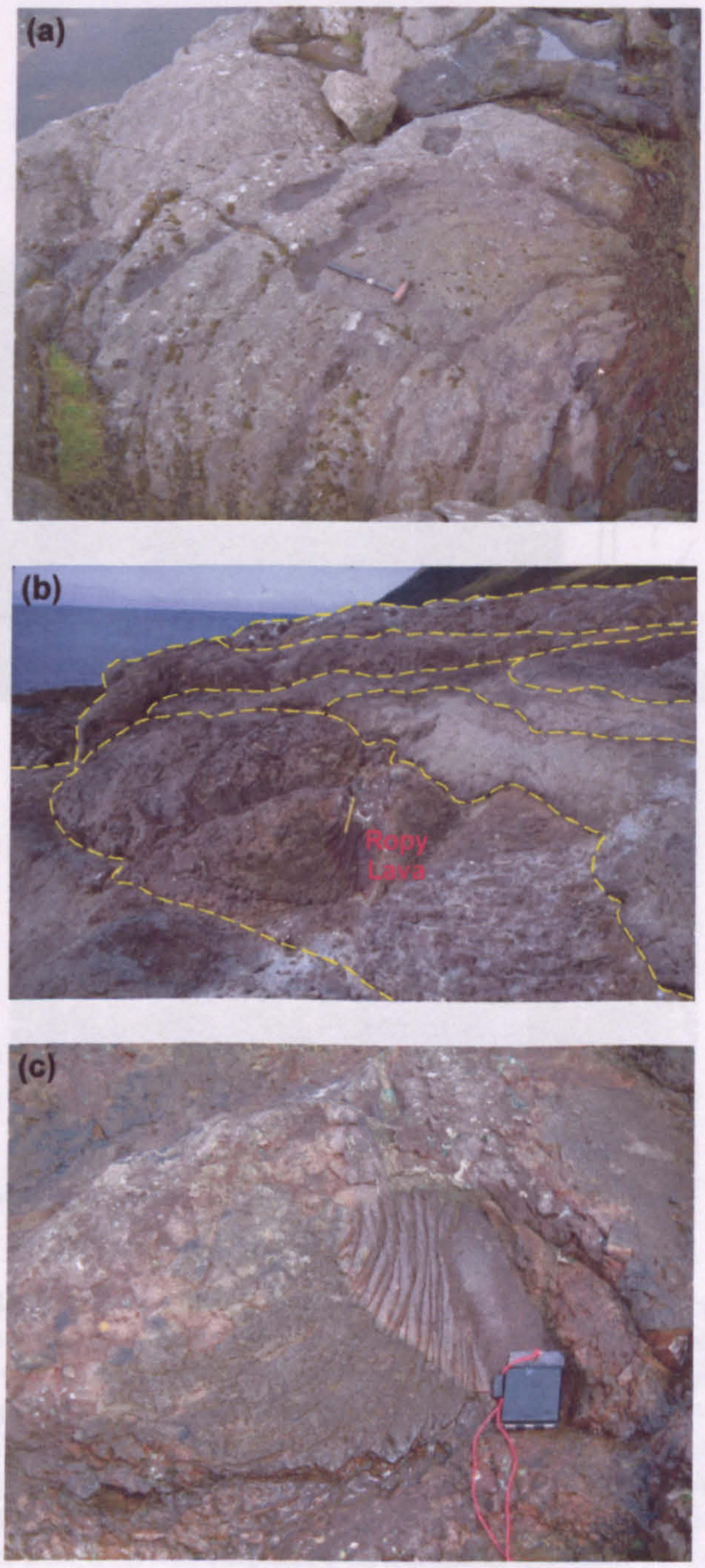

Fig. 6.10. Views of ropy lava from the Middle Basalt Formation (a) Large-scale convex ropes are observed covering an area *ca.* 3 x 2 m at Viðareiði, Viðoy, Faeroe Islands. The convex nature of the ropy lava tentatively suggests a flow direction to the WNW. The hammer is *ca.* 40 cm long and is aligned in the direction of flow. (b) Middle Basalt Formation lava flow units at Viðareiði, Viðoy, Faeroe Islands. On the surface of one of these lava flow units small-scale ropy lava is observed. (c) A close up of the ropy lava observed in (b). The ropes have the appearance of twisted bread sticks and are *ca.* 1-3 cm thick. The ropes cover an area of *ca.* 0.16 m^2. The compass is *ca.* 10 x 6 cm.

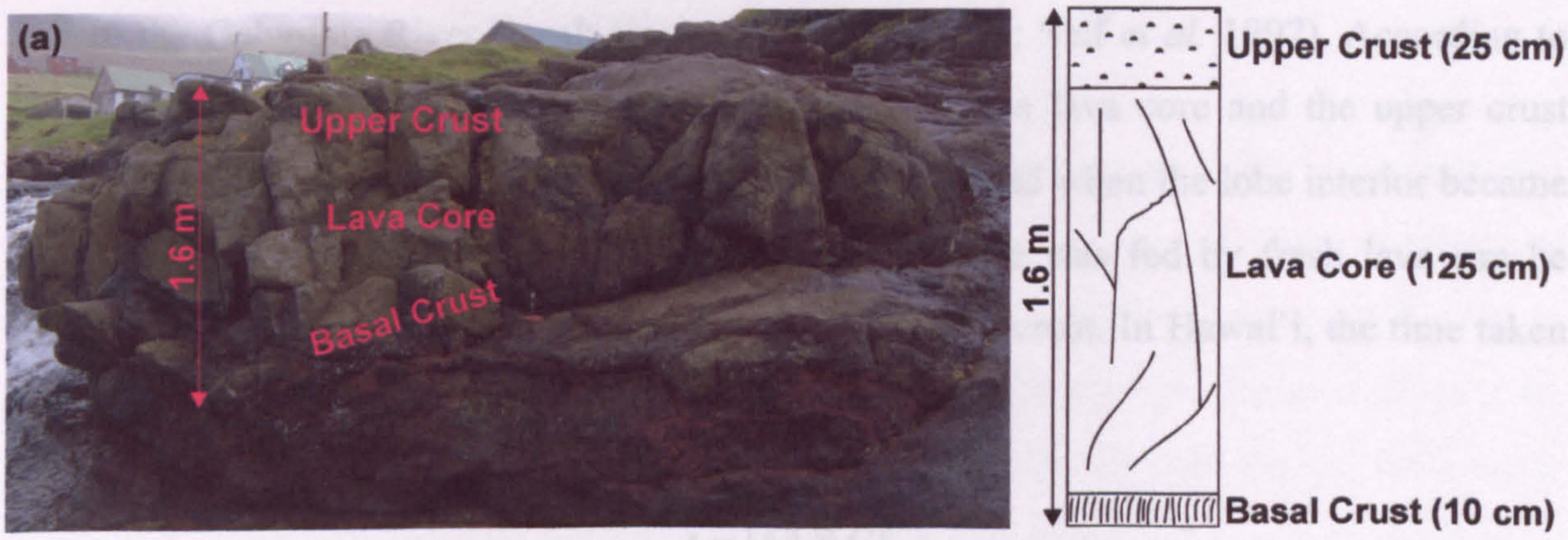

Fig. 6.11. Views of a Middle Basalt Formation P-type pahoehoe lava flow unit at Viðareiði, Viðoy, Faeroe Islands. (a) The P-type pahoehoe lava flow unit is *ca.* 1.6 m thick and is separated into three distinguishable zones: basal crust, lava core, and upper crust. The upper crust is *ca.* 25 cm thick and is dominated by oval amygdales with a maximum diameter of *ca.* 2 cm. The lava core is a compact, massive zone with irregular jointing. The basal crust is *ca.* 10 cm thick and is characterised by containing pipe amygdales. The hammer is *ca.* 40 cm long. (b) A close up of the basal crust. Pipe amygdales reaching a maximum size of *ca.* 8 cm are observed. Some of the pipe amygdales are curved in the direction of flow. The presence of the pipe amygdales suggests that the flow unit was emplaced on a slope of less than 4°. Using the equation of Hon *et al.* (1994) it is suggested that this flow unit was active for *ca.* 10 hours. The compass is *ca.* 10 x 6 cm.

have a maximum diameter of *ca.* 2 cm. The amygdales contain zeolites and calcite. A similar zonal pattern is observed for flow units encountered in the Vestmanna-1 drill hole. Waagstein & Hald (1984) showed that the average flow unit in Vestmanna-1 is *ca.* 2.2 m thick and is separated into basal crust (0.19 m), compact lava core (0.88 m) and upper crust (1.17 m).

The amygdale distribution patterns observed in the P-type flow units described above are similar to those described for inflating pahoehoe lava flows of Hawai`i (Hon *et al.* 1994) and in the Columbia River Basalt Group (Self *et al.* 1996; Self *et al.* 1997). According to the work of Hon *et al.* (1994), the boundary between the lava core and the upper crust marks the end of the injection of fresh lava into the lobe and when the lobe interior became stagnant. An estimate of the amount of time a lava lobe was fed by fresh lava can be obtained by working out the time taken to form the upper crust. In Hawai`i, the time taken to form the upper crust conforms to the empirical equation:

$$t = 164.8\,C^2$$

where t is the time in hours, 164.8 is an empirically determined constant, and C is the upper crust thickness in metres (Hon *et al.* 1994). Time differences (i.e. cooling rates) between the Faeroese MBF flow units and Hawaiian lavas are expected due to differences in rainfall and thermal properties (heat capacity, diffusivity, and latent heat of crystallisation). Assuming that the above equation applies to the flow units of the MBF as well as those in Hawai`i, the flow unit at Viðareiði, Viðoy would have been active for *ca.* 10.3 hours and the average flow unit in the Vestmanna-1 drill hole would have been active for *ca.* 9.4 days.

6.3 Interlava Lithologies

6.3.1 Occurrence

Volcaniclastic rocks are insignificant and seldom seen in the lower section of the MBF, but become commoner in the upper section. The volcaniclastic rocks in the upper section are usually several metres in thickness and consist of tuffaceous and volcaniclastic (epiclastic) sandstones. A number of volcaniclastic sandstone lithologies shall be described collectively due to their poor exposure and similar characteristics. There are a number of localities that have very good exposures or interesting lithologies and shall be described in

the subsequent sections. These localities are: (i) Klivarnar Section, on the SE side of Leynavatn, *ca.* 1.5 km NE of Leynar, Streymoy (Fig. 6.1) (ii) Ærgisá Section, *ca.* 2.5 km N of Leynar, Streymoy (Fig. 6.1); (iii) í Bugum Section, *ca.* 2 km ESE of Hósvík, Streymoy (Fig. 6.1); (iv) Eiði Section, *ca.* 300 m E of Eiði, Eysturoy (Fig. 6.1); and (v) Viðareiði Section, Viðoy (Fig. 6.2).

6.3.2 Lithology & Petrography

6.3.2.1 Volcaniclastic Sandstones

A number of volcaniclastic sandstones have limited exposures and similar characteristics and shall be described collectively for simplicity. The volcaniclastic sandstones observed inbetween MBF lava flow units range from being pale reddish brown (10R 5/4) to moderate reddish brown (10R 4/6). The sandstones have an average thickness of *ca.* 1 m, although they can range from 50 cm up to 1.5 m (Fig. 6.12). They commonly have sharp lower and upper contacts and tabular geometries. The sandstones are poorly to moderately sorted and are dominated by angular to sub-rounded opaque to orange to greenish yellow palagonitised basaltic glass clasts (Fig. 6.13). The clast edges have been obscured due to the hydration process. Some of the sandstones contain minor amounts of basalt, derived from lava flows, which range in texture from equigranular to plagioclase-phyric.

6.3.2.2 Klivarnar Section

The Klivarnar Section consists of a channel infilled by a moderate reddish brown (10R 4/6) volcaniclastic sandstone (Fig. 6.14). This sandstone overlies a *ca.* 1.2 m thick plagioclase-phyric basalt lava flow unit with a hummocky upper surface. The thickness of the sandstone ranges from *ca.* 1 m in the centre of the channel to *ca.* 0.6 m at the margins and it eventually tapers out away from the channel. This sandstone is poorly sorted, clast supported and is dominated by sub-angular to sub-rounded opaque to orange palagonitised basaltic glass clasts (Fig. 6.15). Vesiculated and non-vesiculated varieties of glassy clasts occur. Minor amounts of basalt clasts, usually equigranular, although plagioclase-phyric varieties do occur, are contained within the sandstone. The overlying lava flow has curved lower and upper surfaces a consequence of the lava flow infilling the top of the channel. The base of the lava flow is brecciated producing a blocky peperite along the length of the channel structure.

Fig. 6.12. Views of a *ca.* 1 m thick pale reddish brown volcaniclastic sandstone at Hvílingagarsteinur, *ca.* 1.6 km SW of Slættaratindur and *ca.* 300 m NE of Eiðisvatn, Eysturoy, Faeroe Islands. The unit is thinly to medium bedded and is found inbetween two compound lava flows of the Middle Basalt Formation. The hammer is *ca.* 40 cm long.

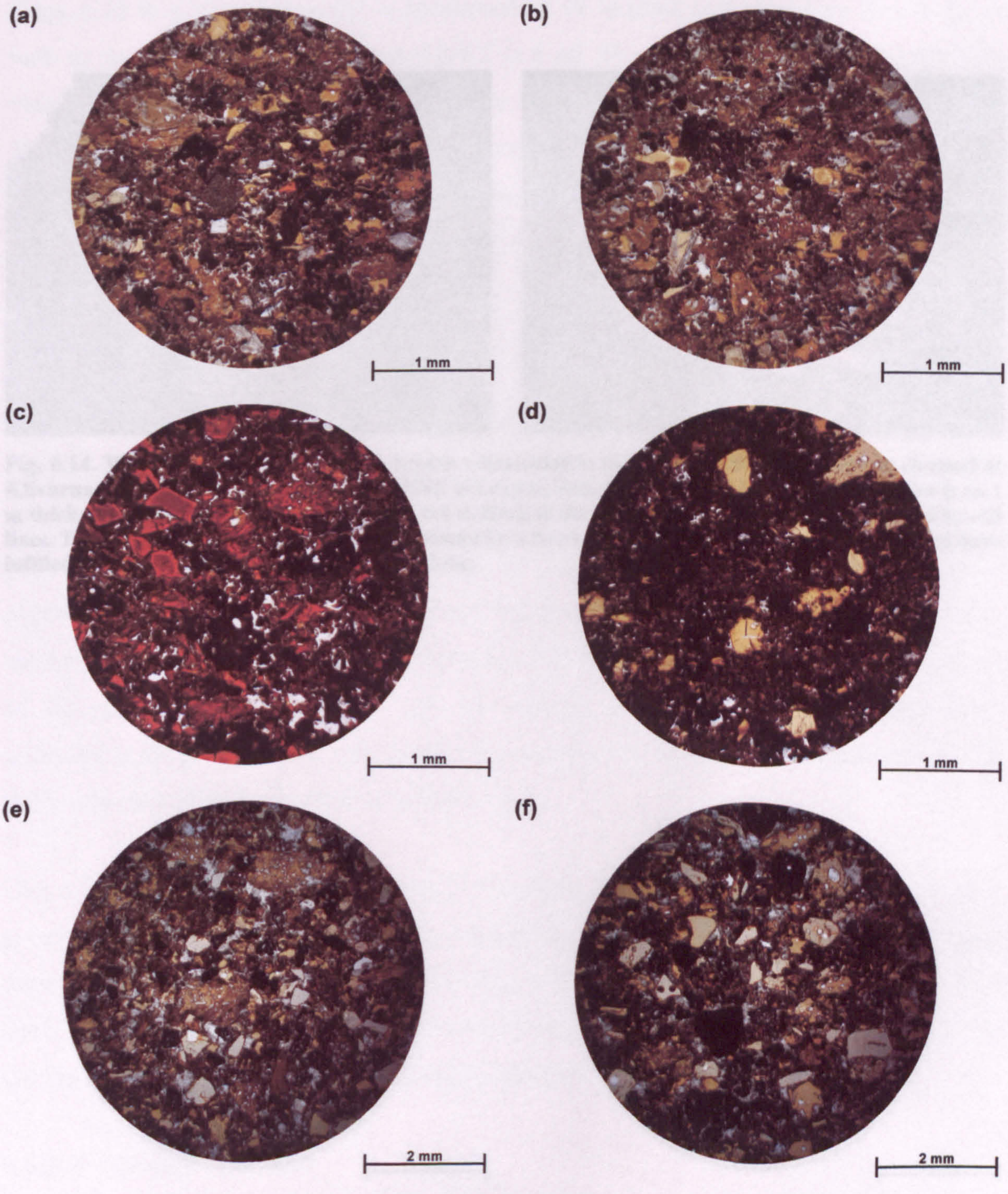

Fig. 6.13. Photomicrographs of a range of volcaniclastic sandstones from the Middle Basalt Formation. All of the photomicrographs are under plane-polarised light. The sandstones are poorly to moderately sorted and are dominated by angular to sub-rounded opaque to orange to greenish yellow palagonitised basaltic glass clasts. The clast edges have been obscured due to the hydration process. Some of the sandstones contain minor amounts of basalt, derived from lava flows, which range in texture from equigranular to plagioclase-phyric. (a) & (b) Volcaniclastic sandstone from Stórabrugv, *ca.* 3.2 km SE of Oyragjógv, Vágar, Faeroe Islands. (c) & (d) Volcaniclastic sandstone from Eiði roadside cutting, *ca.* 300 m E of Eiði, Eysturoy, Faeroe Islands. (e) & (f) Volcaniclastic sandstone from the disused quarry and culvert, *ca.* 600 m N of Svínáir, Eysturoy, Faeroe Islands.

Fig. 6.14. Views of a moderate reddish brown volcaniclastic sandstone infilling a low-lying channel at Klivarnar, SE side of Leynavatn, *ca.* 1 km NNE of Leynar, Streymoy, Faeroe Islands. The sandstone is *ca.* 1 m thick in the centre of the channel and *ca.* 0.6 m thick at the margins. The channel is highlighted by red lines. The tuff is located inbetween two compound lava flows of the Middle Basalt Formation, which have infilled the channel. The hammer is *ca.* 40 cm long.

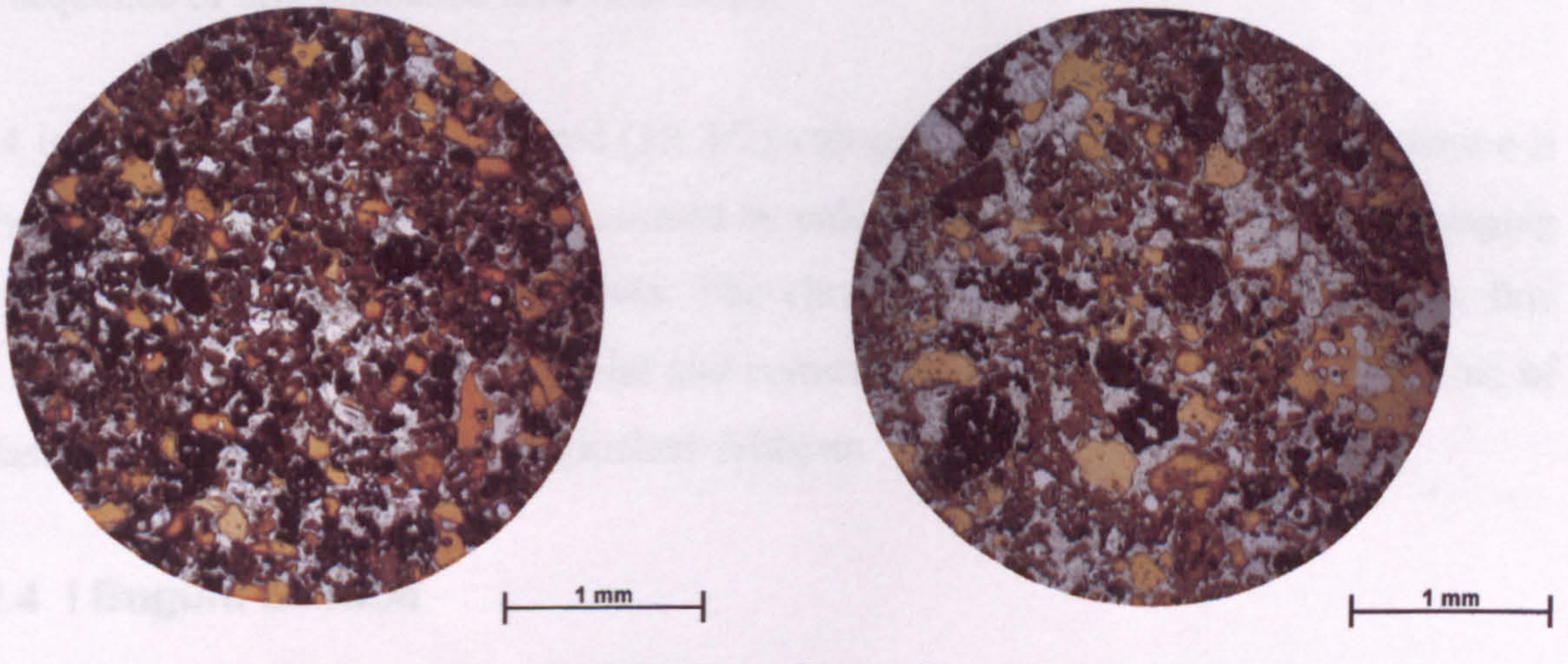

Fig. 6.15. Photomicrographs of the volcaniclastic sandstone from the Middle Basalt Formation at Klivarnar, SE side of Leynavatn, *ca.* 1 km NNE of Leynar, Streymoy, Faeroe Islands. Both photomicrographs are under plane-polarised light. The sandstone is poorly sorted, clast supported and is dominated by sub-angular to sub-rounded opaque to orange palagonitised basaltic glass clasts. Vesiculated and non-vesiculated varieties of glassy clasts occur. Minor amounts of basalt clasts, usually equigranular, although plagioclase-phyric varieties do occur, are contained within the sandstone.

6.3.2.3 Ærgisá Section

The Ærgisá Section consists of a *ca.* 20 m thick sequence straddling the 100 m contour (Figs. 6.16 & 6.17). The section is dominated by <1 m thick pahoehoe lava flow units, as well as four volcaniclastic deposits. Unit 1 is a *ca.* 40 cm thick greyish olive (10Y 4/2) volcaniclastic sandstone and has sharp upper and lower contacts with the lava flow units. This sandstone is poorly sorted and has an average grain size of very fine sand. Angular to sub-rounded opaque to greenish brown palagonitised basaltic glass clasts account for *ca.* 90 vol.% of the sandstone. The remaining *ca.* 10 vol.% of the sandstone is made up of basalt clasts with an average size of 100 μm. Two thin lava flow units overlie the sandstone.

Unit 2 is a *ca.* 80 cm thick greyish olive (10Y 4/2) volcaniclastic sandstone (Fig. 6.18). This sandstone is made up of the same clasts in the same proportions as Unit 1. The only difference is that Unit 2 is moderately sorted. Unit 3 is a *ca.* 95 cm thick greyish red (5R 4/2) volcaniclastic sandstone (Fig. 6.18). This sandstone is moderately sorted, matrix supported and is dominated by blackish red palagonitised basaltic glass clasts. These clasts are angular to sub-rounded and have an average grain size of fine to medium sand. Some of the clasts contain plagioclase feldspar crystals. The clasts are fresher than those observed in the previous two units. Unit 3 has a sharp contact and is overlain by a *ca.* 12 m thick sequence of thin pahoehoe lava flow units.

Unit 4 is a *ca.* 80 cm thick greyish red (5R 4/2) volcaniclastic sandstone. This sandstone is poorly to moderately sorted and is dominated by palagonitised basaltic glass clasts, ranging from near opaque to dirty yellow-brown. The clasts have and average size of very fine sand. The fresher glass clasts are angular and commonly exhibit cuspate margins. Some of the clasts contain phenocrysts of plagioclase feldspar.

6.3.2.4 í Bugum Section

The í Bugum Section consists of a *ca.* 1.5 m thick light olive grey (5Y 5/2) volcaniclastic sandstone inbetween two amygdaloidal lava flow units (Fig. 6.19a). The basal contact is hummocky, with the lower *ca.* 1 m of the sandstone being very thinly to thinly bedded. At approximately 1 to 1.2 m from the base of the sandstone, black carbonaceous material is preserved, which is the fossil remains of leaves and they form thin elongate bands up to 4.5 cm long (Fig. 6.19b). This sandstone is poorly to moderately sorted, on the whole matrix supported and comprises *ca.* 70 vol.% creamy-orange, angular to sub-rounded,

Fig. 6.16. View of a *ca.* 20 m thick sequence consisting of four volcaniclastic sandstones inbetween Middle Basalt Formation pahoehoe lava flow units, Ærgisá stream section, *ca.* 2.5 km N of Leynar, Streymoy, Faeroe Islands.

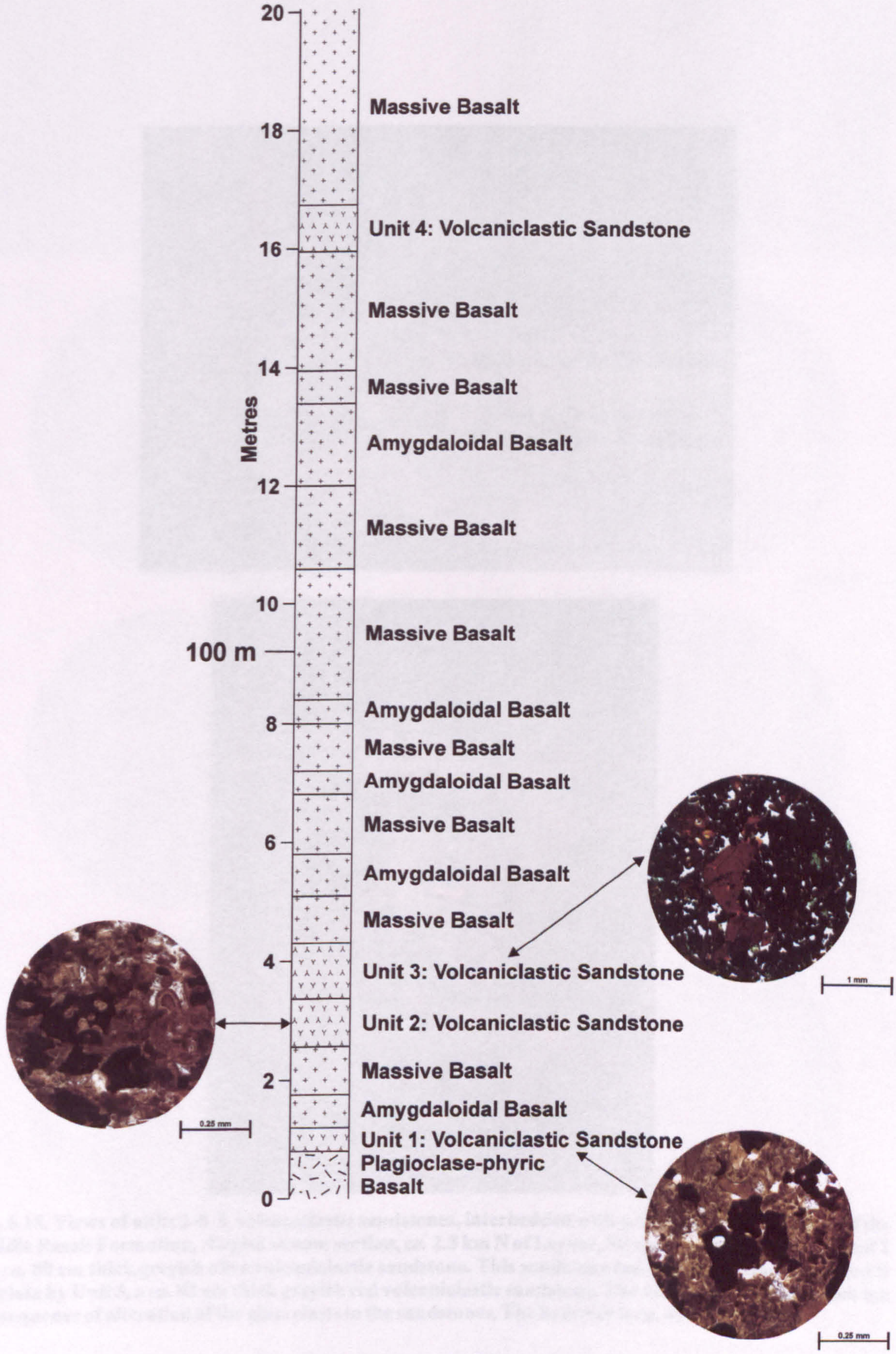

Fig. 6.17. A graphic log for a *ca.* 20 m thick section of the Middle Basalt Formation straddling the 100 m contour at Ærgisá stream section, *ca.* 2.5 km N of Leynar, Streymoy, Faeroe Islands. The two lowermost volcaniclastic sandstones (units 1 & 2) are greyish olive and more highly altered than the two upper greyish red volcaniclastic sandstones (units 3 & 4). The sandstones are interbedded with pahoehoe lava flow units.

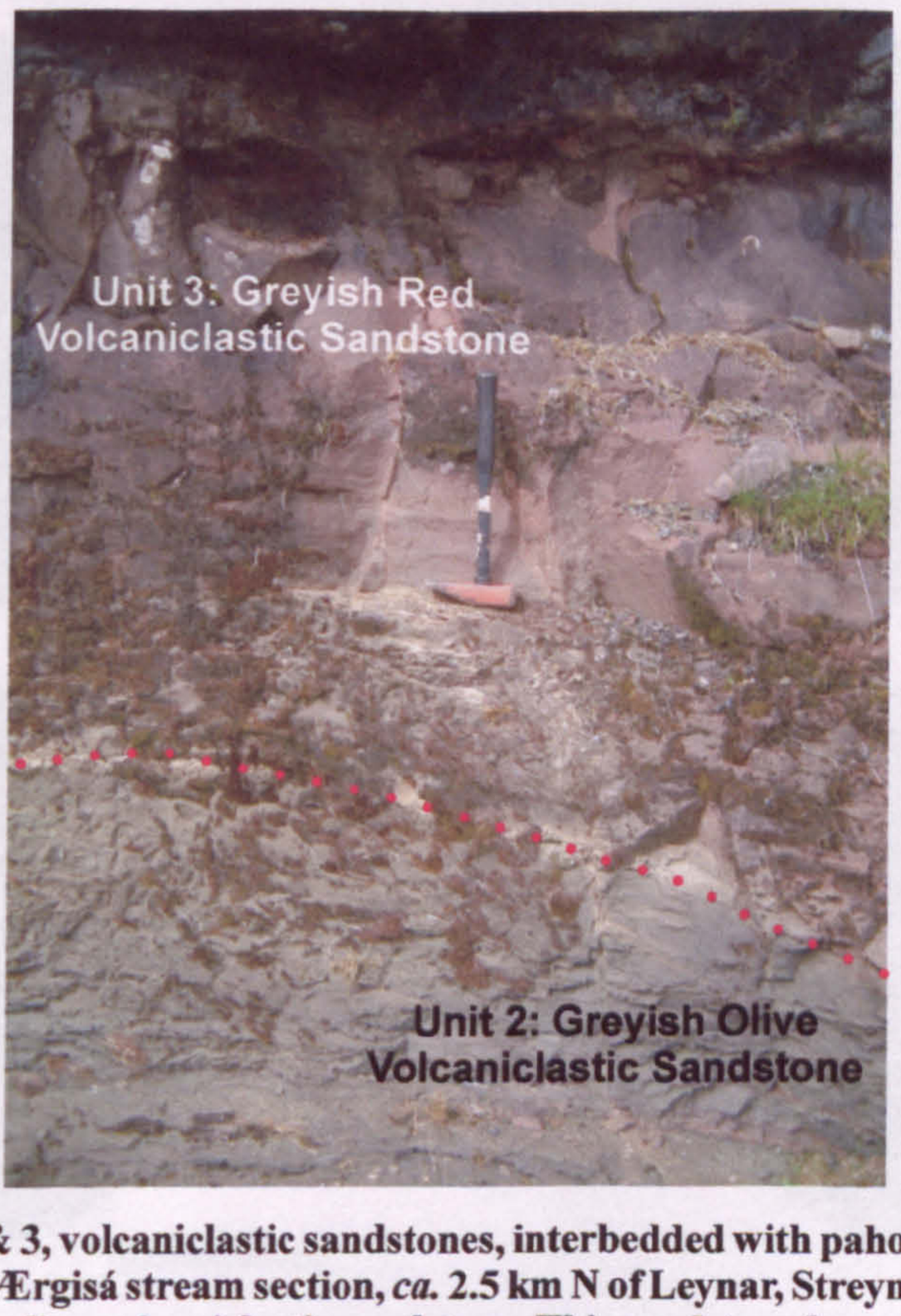

Fig. 6.18. Views of units 2 & 3, volcaniclastic sandstones, interbedded with pahoehoe lava flow units of the Middle Basalt Formation, Ærgisá stream section, *ca.* 2.5 km N of Leynar, Streymoy, Faeroe Islands. Unit 2 is a *ca.* 80 cm thick greyish olive volcaniclastic sandstone. This sandstone has a sharp contact with, and is overlain by Unit 3, a *ca.* 95 cm thick greyish red volcaniclastic sandstone. The difference in colouration is a consequence of alteration of the glass clasts in the sandstones. The hammer is *ca.* 40 cm long.

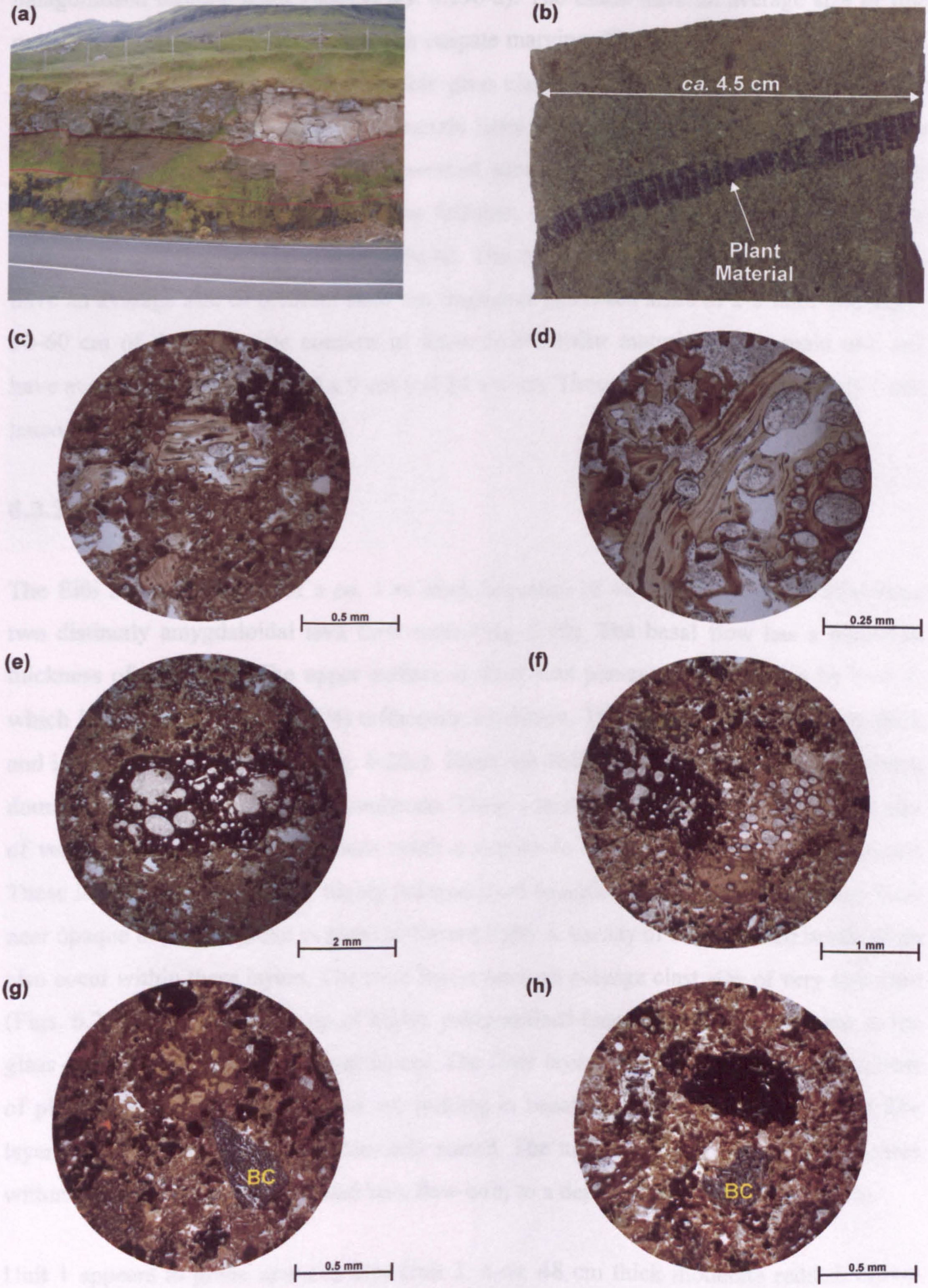

Fig. 6.19. Views and photomicrographs of the í Bugum roadside cutting, *ca.* 2 km ESE of Hósvík, Streymoy, Faeroe Islands. (a) A *ca.* 1.5 m thick light olive grey volcaniclastic sandstone. (b) A leaf imprint *ca.* 4.5 cm long, found on a bedding surface *ca.* 1 to 1.2 m from the base of the sandstone. All of the photomicrographs are under plane-polarised light. (c) & (d) Angular to sub-rounded creamy-orange palagonitised basaltic glass clasts. The clasts have an average size of fine sand, are typically vesiculated and have cuspate margins. (e) & (f) Photomicrographs that show highly vesiculated glass clasts. The near opaque palagonitised basaltic glass clasts are most likely reworked scoria. (g) & (h) Photomicrographs that contain sub-rounded basalt clasts (BC) that are equigranular and consist of plagioclase feldspar laths, clinopyroxenes and oxides. These basalt clasts account for less than 10 vol.% of the sandstone and are most likely derived from lava flows.

palagonitised basaltic glass clasts (Figs. 6.19c-d). The clasts have an average size of fine sand, are typically vesiculated and have cuspate margins. This sandstone also contains *ca.* 20 vol.% of opaque palagonitised basaltic glass clasts that are sub-rounded to sub-angular (Figs. 6.19e-f). Some of these clasts contain laths of plagioclase feldspar, whereas others are highly vesiculated, most likely reworked scoria. Sub-rounded to sub-angular basalt clasts, consisting of laths of plagioclase feldspar, clinopyroxenes and oxides account for <10 vol.% of the sandstone (Figs. 6.19g-h). The opaque glass clasts and the basalt clasts have an average size of medium sand but fragments can reach sizes of 2-3 mm. The upper 50-60 cm of the sandstone consists of lensoids of similar material as the main unit and have average dimensions of 20 x 9 cm and 14 x 6 cm. These lensoids form extremely crude lensoidal bedding.

6.3.2.5 Eiði Section

The Eiði Section consists of a *ca.* 1 m thick sequence of volcaniclastic strata inbetween two distinctly amygdaloidal lava flow units (Fig. 6.20). The basal flow has a minimum thickness of *ca.* 1.8 m. The upper surface is sharp and planar and is overlain by Unit 1, which is a dusky yellow (5Y 6/4) tuffaceous sandstone. This sandstone is *ca.* 50 cm thick and is thinly bedded (2-3 cm) (Fig. 6.20c). There are distinctly darker coarser layers, which dominate the lower 20 cm of the sandstone. These coarser layers have an average clast size of very coarse sand, although clasts reach a maximum of *ca.* 3 mm (i.e. granule grade). These layers are dominated by highly palagonitised basaltic glass clasts, which range from near opaque to yellow-green in plane-polarised light. A variety of sub-rounded basalt clasts also occur within these layers. The finer layers have an average clast size of very fine sand (Figs. 6.21a-d) and are made up of highly palagonitised basaltic glass clasts similar to the glass clasts observed in the coarser layers. The finer layers also contain angular fragments of plagioclase feldspar crystals but are lacking in basalt clasts. Both the coarse and fine layers are clast supported and moderately sorted. The tuffaceous sandstone infills fissures within the underlying amygdaloidal lava flow unit, to a depth of *ca.* 25 cm (Fig. 6.20b).

Unit 1 appears to grade upwards into Unit 2, a *ca.* 48 cm thick moderate reddish brown (10R 4/6) volcaniclastic sandstone (Figs. 6.21e-h). This sandstone is thinly bedded (2-3 cm), grain supported and poorly to moderately sorted. The layers of fine-grained material have an average grain size of very fine sand whereas the coarser layers have an average grain size of coarse to very coarse sand. Both coarse and fine layers are compositional similar in that they are dominated by angular to sub-rounded orange to opaque palagonitised basaltic glass clasts at various stages of alteration. The clasts are vesicular to

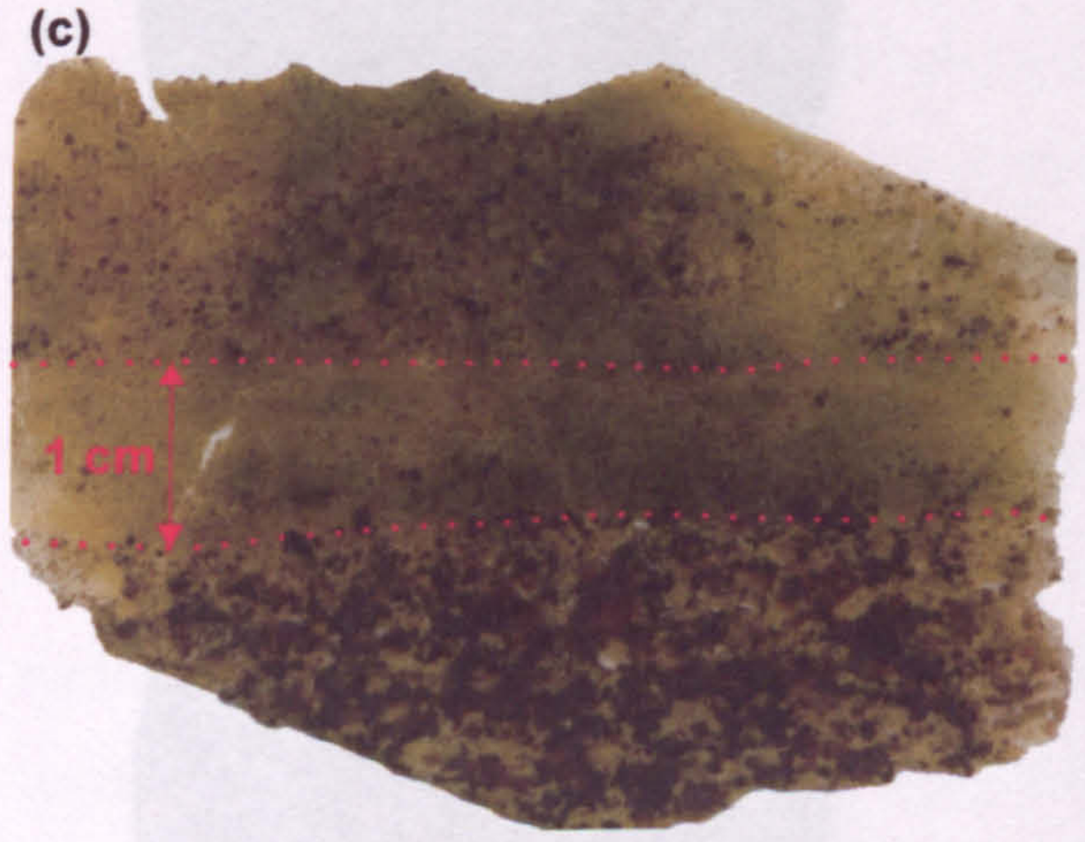

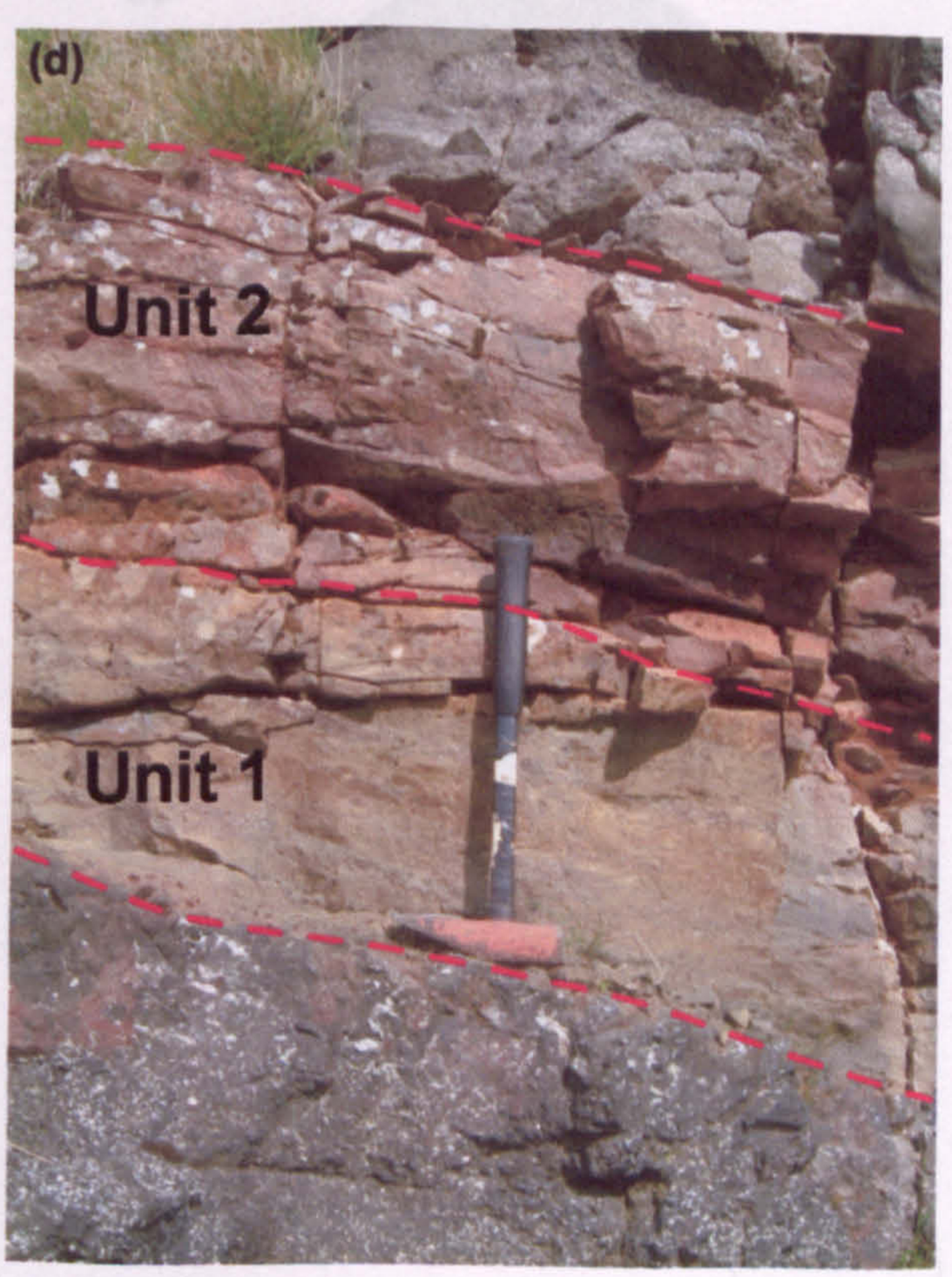

Fig. 6.20. Views and thin section photograph of the volcaniclastic sequence from the Eiði roadside cutting, *ca.* 300 m E of Eiði, Eysturoy, Faeroe Islands. (a) A *ca.* 1 m thick interlava unit inbetween Middle Basalt Formation flow units. (b) The basal dusky yellow tuffaceous sandstone (Unit 1) infills fissures within the underlying amygdaloidal flow unit to a depth of *ca.* 25 cm. (c) Unit 1, tuffaceous sandstone, is distinctly thinly bedded (2-3 cm). (d) The tuffaceous sandstone is overlain by Unit 2, a *ca.* 48 cm moderate reddish brown volcaniclastic sandstone. The hammer is *ca.* 40 cm long.

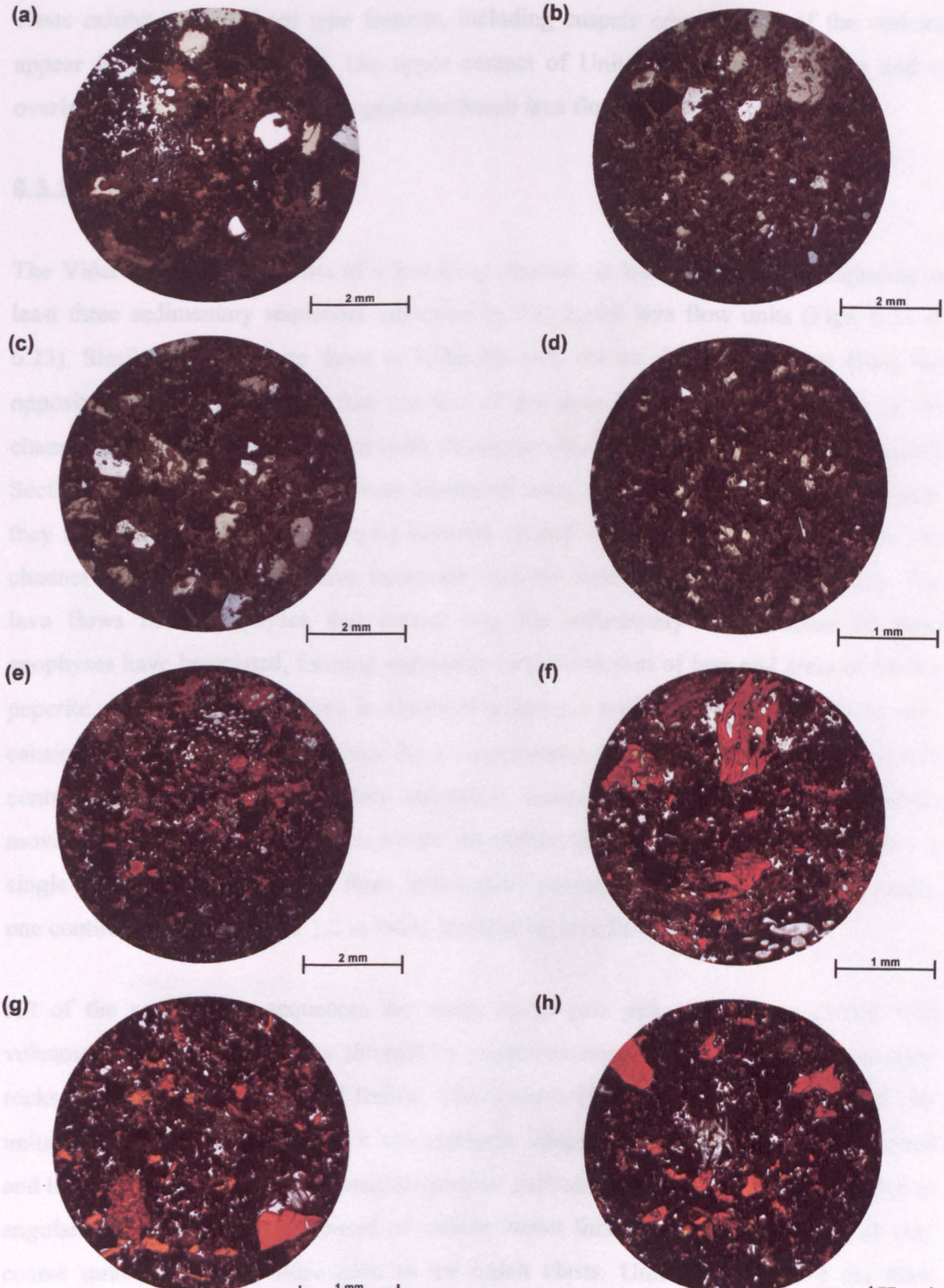

Fig. 6.21. Photomicrographs from the Eiði roadside cutting, *ca.* 300 m E of Eiði, Eysturoy, Faeroe Islands. All of the photomicrographs are under plane-polarised light. (a) to (d) Photomicrographs of Unit 1, a *ca.* 50 cm thick dusky yellow tuffaceous sandstone. The sandstone has an average clast size of very fine sand and is dominated by highly palagonitised basaltic glass clasts. Unit 1 also contains plagioclase feldspar crystal fragments. (e) to (h) Photomicrographs of Unit 2, a *ca.* 48 cm thick moderate reddish brown volcaniclastic sandstone. The sandstone has an average clast size of very fine sand and is dominated by angular to sub-rounded orange to opaque palagonitised basaltic glass clasts. These glass clasts sometimes exhibit shard-type textures including cuspate margins.

non-vesicular and sometimes contain phenocrysts of plagioclase feldspar. Some of the clasts exhibit typical shard type features, including cuspate edges. Some of the vesicles appear flattened and sheared. The upper contact of Unit 2 is sharp and planar and is overlain by a *ca.* 60 cm thick amygdaloidal basalt lava flow unit.

6.3.2.6 Viðareiði Section

The Viðareiði Section consists of a low-lying channel, at least 20 m deep, comprising at least three sedimentary sequences separated by thin basalt lava flow units (Figs. 6.22 & 6.23). Similar lithologies to those at Viðareiði crop out *ca.* 1.5 km due east along the opposite coastline, suggesting they are part of the same lithofacies. The infilling of the channel by the lava flow units can quite clearly be observed to the north of the Viðareiði Section, where the flow units are near horizontal away from the channel but at the margin they are mantling the slope at angles between 20 and 30° (Fig. 6.24). At the base of the channel the lava flow units have interacted with the sedimentary rocks (Fig. 6.25). The lava flows have apophyses that extend into the sedimentary rocks. Some of these apophyses have brecciated, forming apparently isolated masses of lava and areas of blocky peperite. One apophysis of lava is observed splitting a sedimentary sequence in to two, causing the bifurcation of the strata. As a consequence, some of the exposures appear to contain two individual sedimentary sequences separated by a flow unit(s), however, moving laterally away from the exposure the sedimentary sequences combine to form a single sequence. Therefore, the three sedimentary packages described below are actually one continuous sequence, *ca.* 1.2 m thick, intruded by lava flow units.

All of the sedimentary sequences are made up of pale yellowish brown (10YR 6/2) volcaniclastic units, mudstones through to conglomerates (Fig. 6.26). The sedimentary rocks are all poorly lithified and friable. The lower sedimentary package consists of two units. Unit 1a is a *ca.* 24 cm thick volcaniclastic conglomerate that is moderately sorted and has an average grain size of small to medium pebbles (6-10 mm), which are rounded to angular. The pebbles are composed of various basalt lithologies set in a matrix of very coarse sand of similar composition to the basalt clasts. Unit 1b is a *ca.* 9 cm thick volcaniclastic mudstone, which is thickly laminated. This mudstone is overlain by *ca.* 3 m thick sequence of four basalt lava flow units.

Overlying the flow units is Unit 2a, a *ca.* 20 cm thick volcaniclastic sandstone that is poorly sorted and on the whole clast supported (Figs. 6.27a-c). This sandstone is thickly to very thickly laminated and has an average clast size of medium sand, although granule

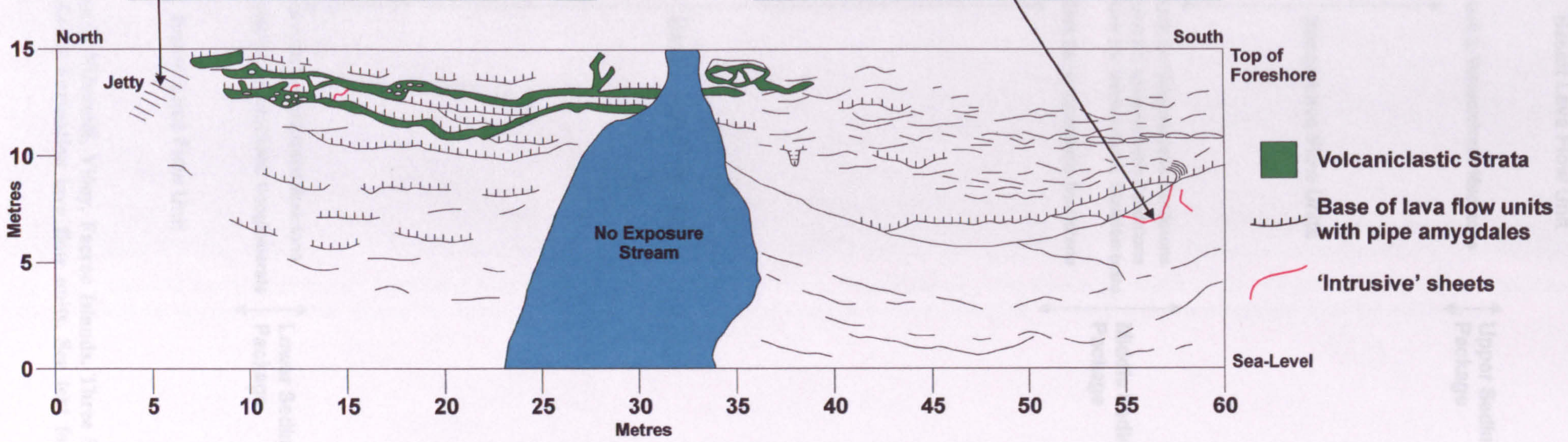

Fig. 6.22. Cross-section along the coast at Viðareiði, Viðoy, Faeroe Islands. A *ca.* 1.2 m thick sedimentary sequence of volcaniclastic conglomerates to mudstones has been invaded by Middle Basalt Formation pahoehoe lava flow units.

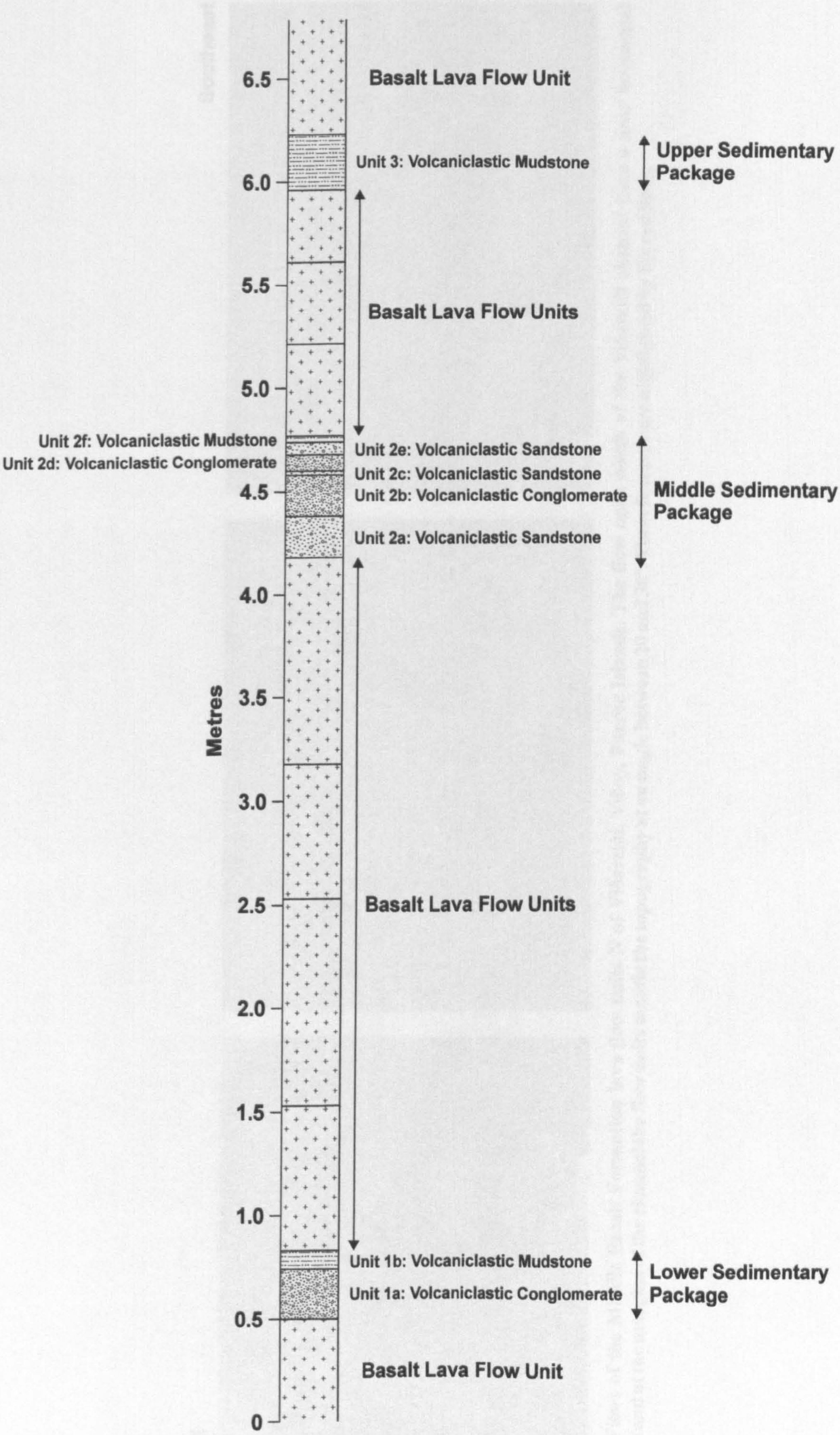

Fig. 6.23. Graphic log for the coastal section at Viðareiði, Viðoy, Faeroe Islands. Three Sedimentary packages are observed inbetween Middle Basalt Formation lava flow units. See text for a detailed discussion.

Northwest

Southeast

Fig. 6.24. Views of the Middle Basalt Formation lava flow units N of Viðareiði, Viðoy, Faeroe Islands. The flow units north of the Viðareiði channel have a near horizontal orientation and at the margins of the channel the flow units mantle the topography at an angle between 20 and 30°. These features are highlighted by the red lines.

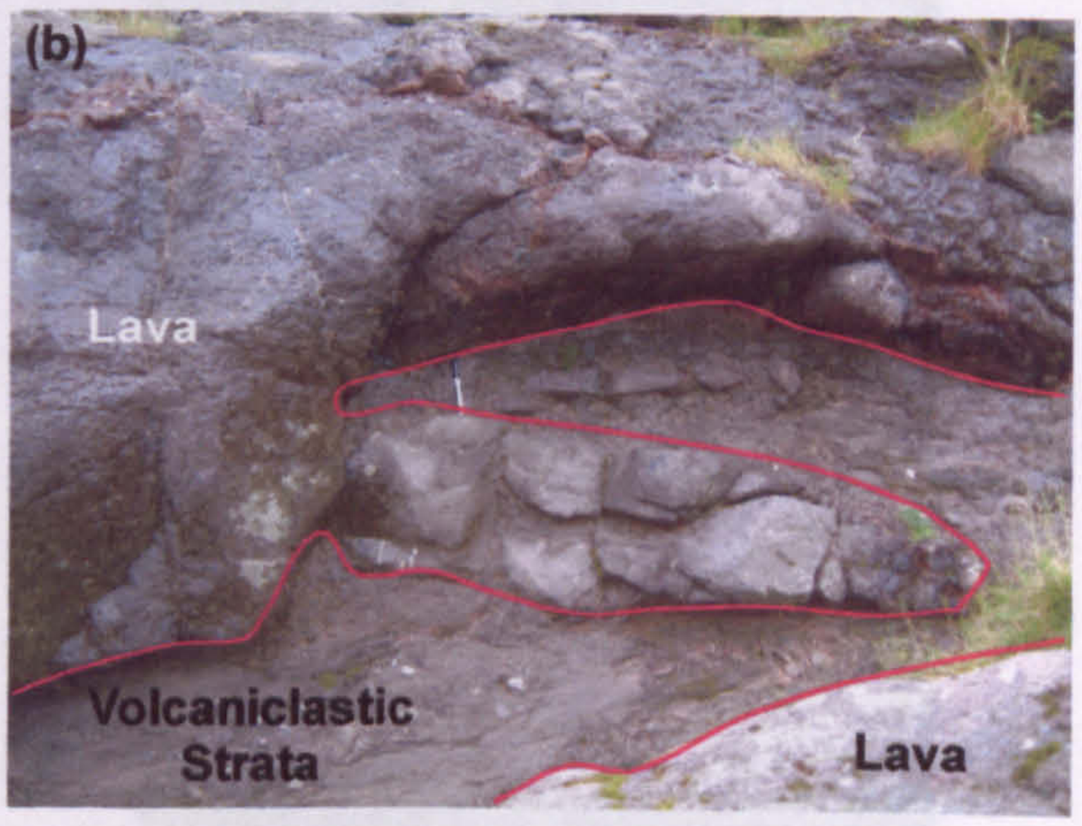

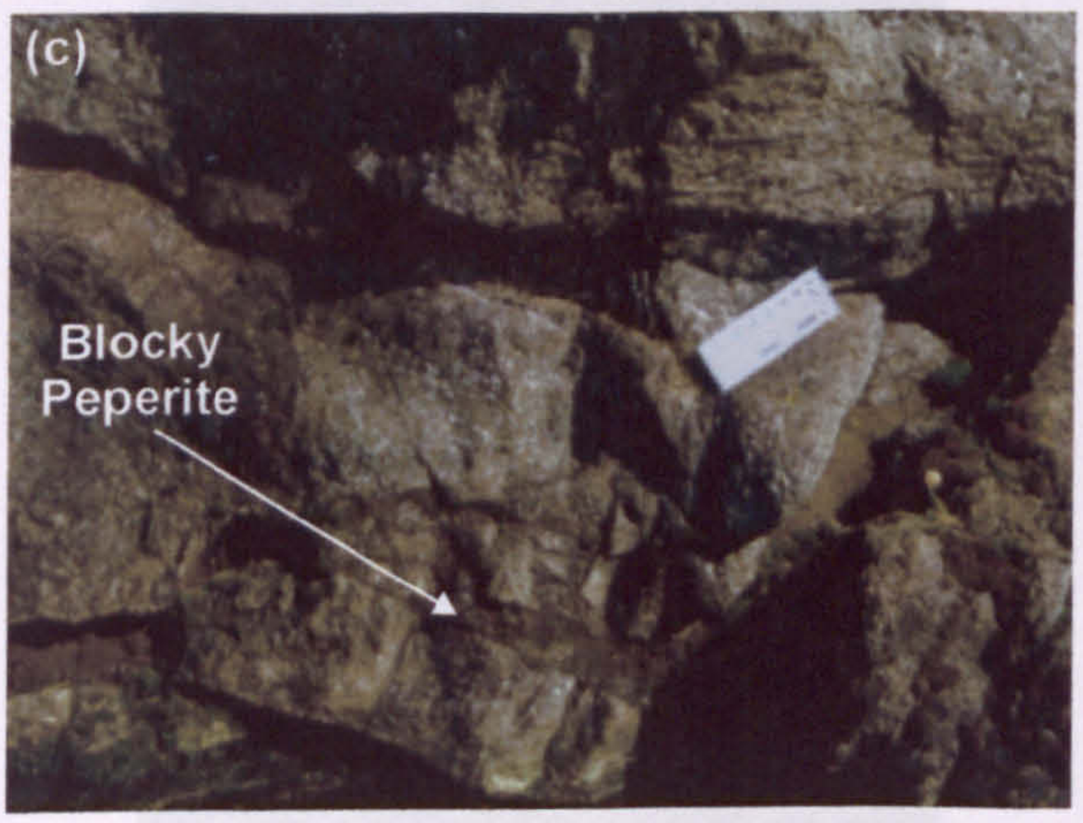

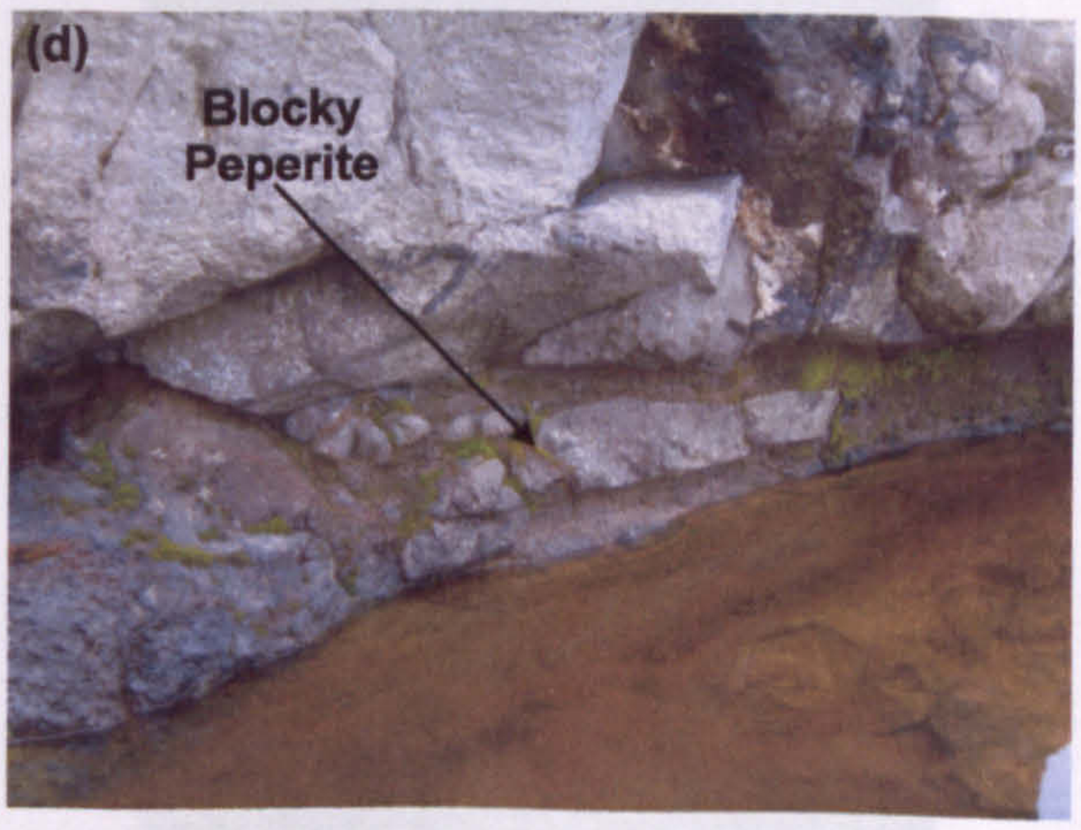

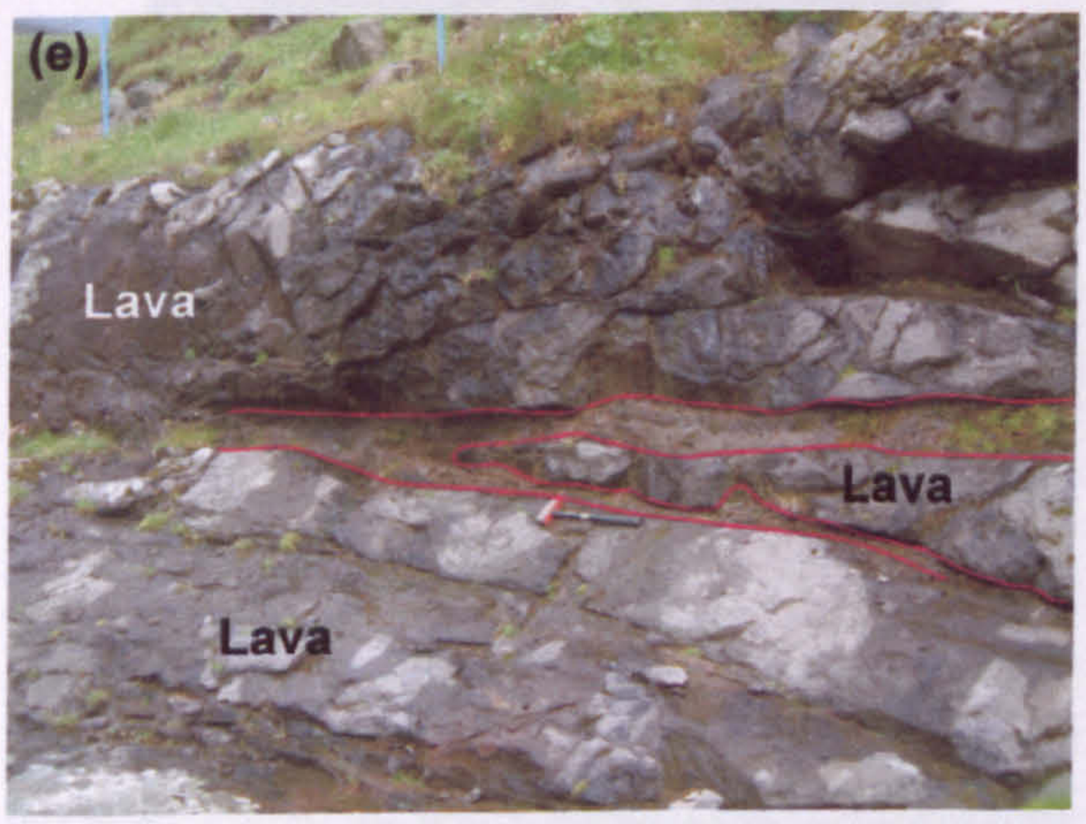

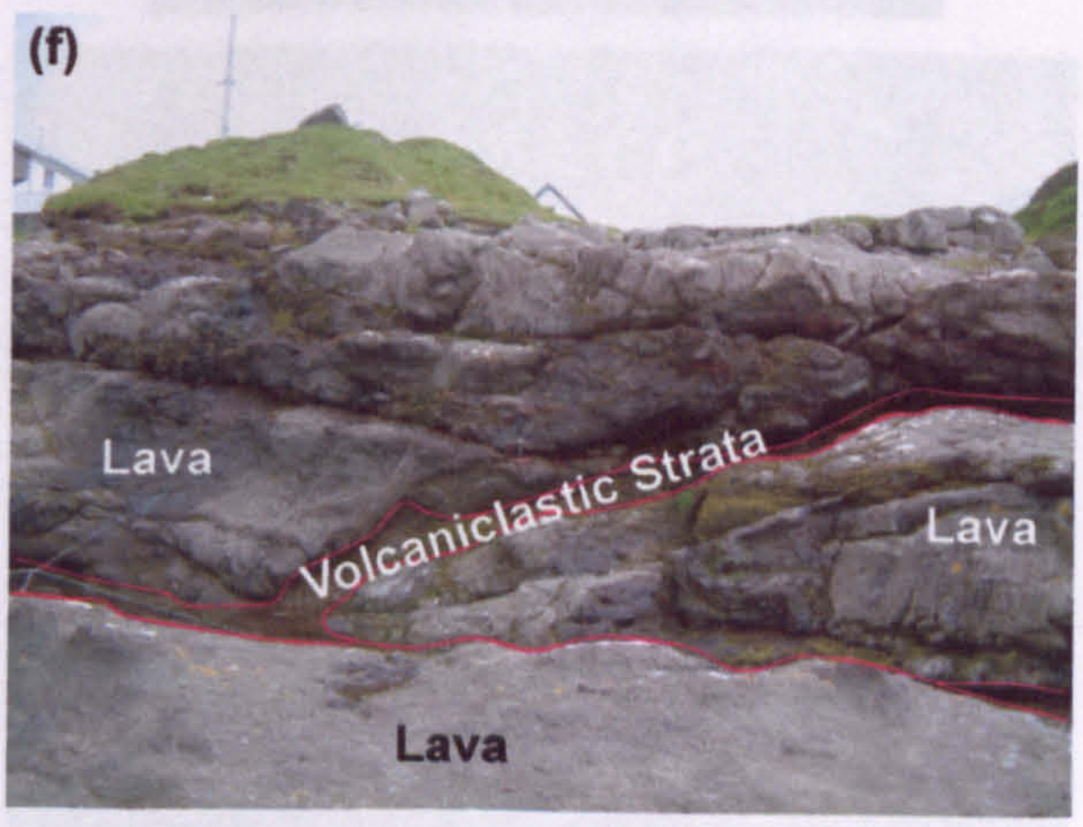

Fig. 6.25. Views of lava-sediment relationships at Viðareiði, Viðoy, Faeroe Islands. (a) & (b) Apophyses of lava have invaded the volcaniclastic strata. (c) & (d) Lava that has invaded the volcaniclastic strata has brecciated, forming a poorly developed blocky peperite. (e) An apophysis of lava is observed splitting a sedimentary sequence in to two, causing the bifurcation of the strata. (f) A single volcaniclastic sequence has been invaded by a lava flow unit and an arm of the sequence is observed 'riding up' over the invading flow. The white card is *ca.* 16 x 6 cm, the pen is *ca.* 14 cm in length and the hammer is *ca.* 40 cm long.

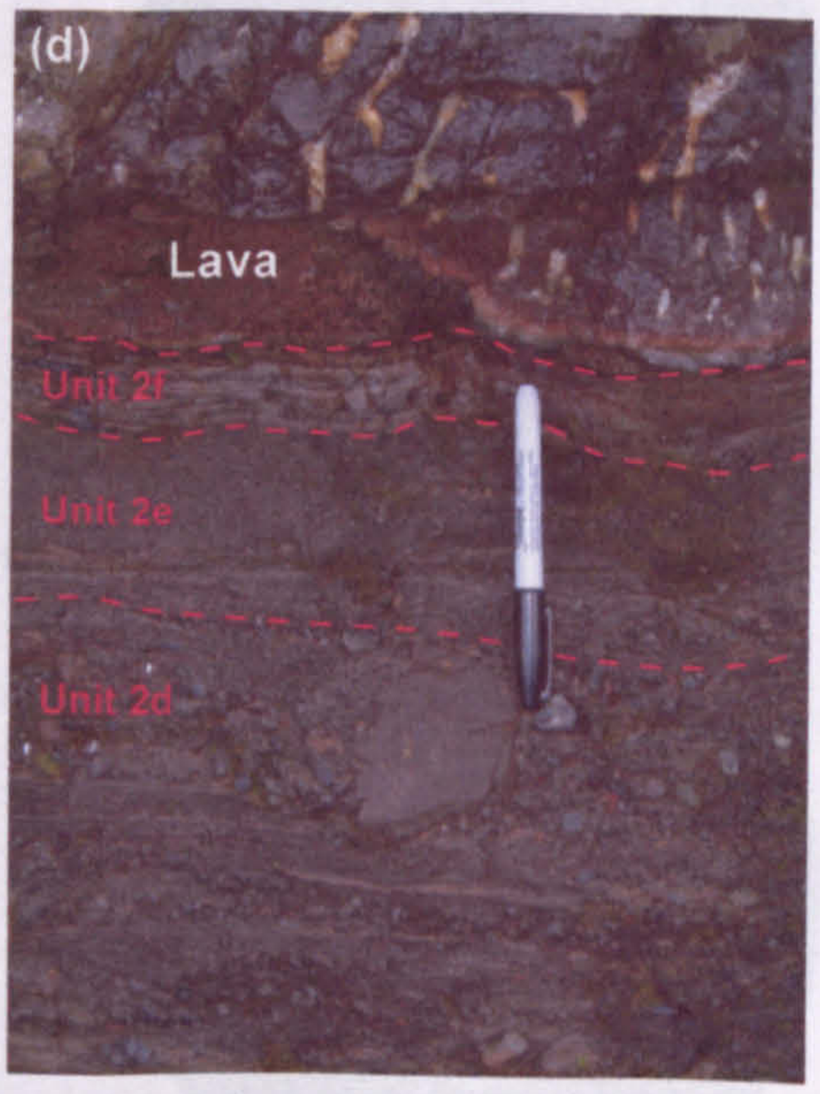

Fig. 6.26. Views of the volcaniclastic strata from the coastal section at Viðareiði, Viðoy, Faeroe Islands. (a) Volcaniclastic conglomerate (Unit 1a) that has an average clast size of small to medium pebbles. The majority of the pebbles have a high degree of rounding. (b) Thickly laminated volcaniclastic mudstone (Unit 1b). (c) & (d) Volcaniclastic strata from the *ca.* 60 cm thick middle sedimentary package. A volcaniclastic conglomerate (Unit 2d) can be seen in the middle part of the photographs. The conglomerate has an average clast size of large pebbles (20-25 mm), but pebbles can reach a maximum size of 80 mm. The conglomerate is overlain by a *ca.* 6 cm thick medium grained volcaniclastic sandstone (Unit 2e), which in turn is overlain by a *ca.* 3 cm thick medium to thickly laminated volcaniclastic mudstone (Unit 2f). The mudstone is overlain by a pahoehoe lava flow unit. (e) & (f) Volcaniclastic mudstone (Unit 3) *ca.* 27 cm thick from the upper sedimentary package, which is very thickly laminated and contains thin layers of sandstone and conglomerate. Lobes from the overlying lava flow unit have nosed into the mudstone and have deformed the laminations. The white card is *ca.* 16 x 6 cm, the compass is *ca.* 10 x 6 cm and the pen is *ca.* 14 cm long.

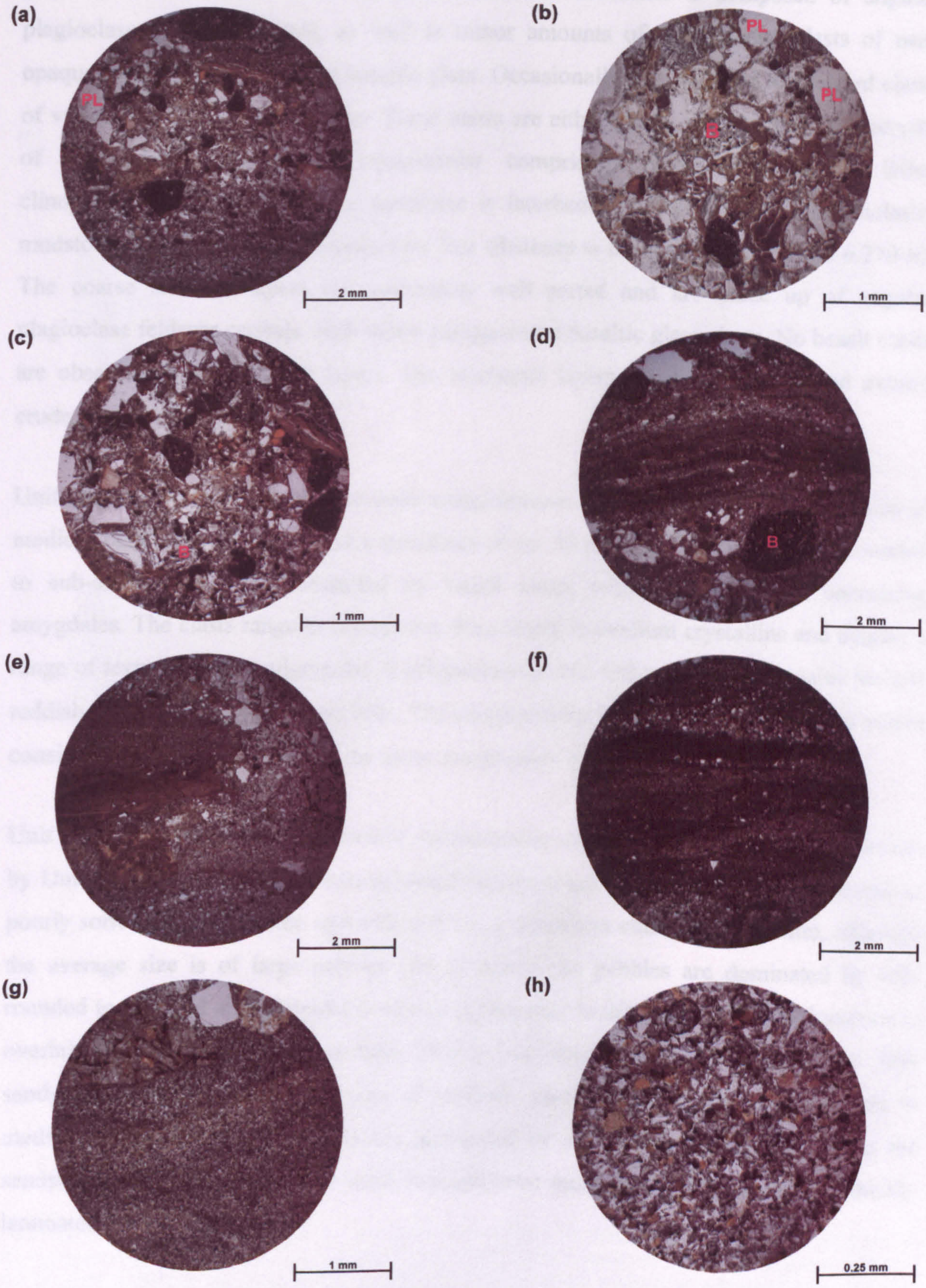

Fig. 6.27. Photomicrographs of Unit 2a, volcaniclastic sandstone with interbedded siltstone layers, of the middle sedimentary package, Viðareiði Section, Viðoy, Faeroe Islands. All of the photomicrographs are under plane-polarised light. (a) to (c) The sandstone is composed of angular plagioclase feldspar crystals (PL), as well as minor amounts of sub-rounded clasts of near opaque to orange palagonitised basaltic glass. Occasionally, sub-rounded to rounded clasts of various basalt (B) lithologies occur. These clasts are either glassy with distinct phenocrysts of plagioclase feldspar, or equigranular comprising plagioclase feldspar laths, clinopyroxenes and oxides. (d) to (f) Thin volcaniclastic siltstone layers inbetween the coarser sandstone layers. (g) & (h) Coarse siltstone layers are moderately well sorted and are made up of angular plagioclase feldspar crystals, with minor palagonitised basaltic glass clasts.

grade (1-3 mm) clasts occur. In thin section, the sandstone is composed of angular plagioclase feldspar crystals, as well as minor amounts of sub-rounded clasts of near opaque to orange palagonitised basaltic glass. Occasionally, sub-rounded to rounded clasts of various basalt lithologies occur. These clasts are either glassy with distinct phenocrysts of plagioclase feldspar, or equigranular comprising plagioclase feldspar laths, clinopyroxenes and oxides. The sandstone is interbedded with layers of volcaniclastic mudstones, ranging from claystones/very fine siltstones to coarse siltstones (Figs. 6.27d-h). The coarse siltstone layers are moderately well sorted and are made up of angular plagioclase feldspar crystals, with minor palagonitised basaltic glass clasts. No basalt clasts are observed in the siltstone layers. The mudstone layers are discontinuous and exhibit crude flaser bedding.

Unit 2b a *ca.* 20 cm thick volcaniclastic conglomerate, which has an average clast size of medium pebbles (10-15 mm) and a maximum of *ca.* 30 mm. The pebbles are sub-rounded to sub-angular and are dominated by basalt clasts with some of them containing amygdales. The clasts range in crystal size from finely to medium crystalline and display a range of textures from equigranular to plagioclase-phyric. Other pebble lithologies include reddish tuffaceous sandstone and bole. The conglomerate is poorly sorted and has a matrix consisting of very coarse sand of the same composition to the pebble sized clasts.

Unit 2c is a *ca.* 2 cm thick very coarse volcaniclastic sandstone, which in turn is overlain by Unit 2d, a *ca.* 8 cm volcaniclastic conglomerate (Figs. 6.26c-d). This conglomerate is poorly sorted, appears to fine upwards and has a maximum clast size of 80 mm, although the average size is of large pebbles (20-25 mm). The pebbles are dominated by sub-rounded to rounded amygdaloidal to non-amygdaloidal basalt clasts. The conglomerate is overlain by Unit 2e, a *ca.* 6 cm thick, thickly laminated, volcaniclastic sandstone. This sandstone has an average clast size of medium sand, although occasionally small to medium pebbles occur. The clasts are dominated by sub-rounded basalt. Overlying the sandstone is Unit 2f, a *ca.* 3 cm thick volcaniclastic mudstone that is medium to thickly laminated.

This middle sedimentary package is overlain by *ca.* 1.2 m thick sequence of compound lava flow units. Overlying these flow units is Unit 3, a *ca.* 27 cm thick volcaniclastic siltstone (Figs. 6.26e-f). This siltstone is very thickly laminated with two or three layers made up of very coarse sandstone and conglomerate (Fig. 6.28). The siltstone is well sorted, has an average clast size of very coarse silt and is dominated by angular plagioclase feldspar grains. The siltstone also contains near opaque palagonitised basaltic glass clasts.

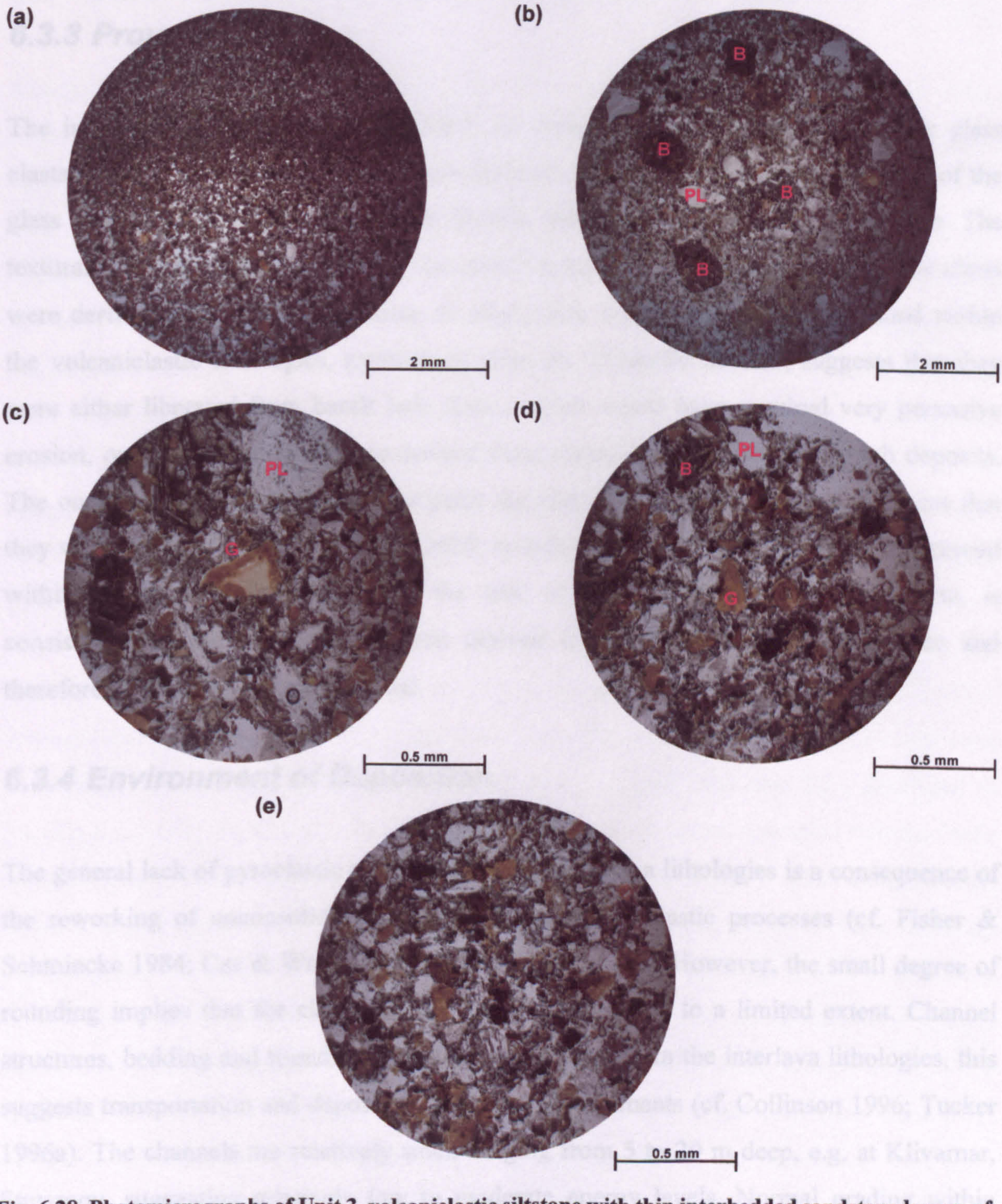

Fig. 6.28. Photomicrographs of Unit 3, volcaniclastic siltstone with thin interbedded sandstone layers. of the upper sedimentary package, Viðareiði Section, Viðoy, Faeroe Islands. All of the photomicrographs are under plane-polarised light. (a) The base of the photomicrograph consists of a layer of volcaniclastic sandstone overlain by a volcaniclastic siltstone with an average clast size of coarse silt. (b) to (e) Volcaniclastic sandstone layer containing angular, colourless, plagioclase feldspar (PL) fragments and near opaque to orange palagonitised basaltic glass (G) clasts. The sandstone layers also contain minor amounts of basalt (B) clasts.

The very coarse sandstone and conglomerate layers are compositionally similar to the siltstone but contain a higher proportion of basalt lithoclasts and the conglomerate layers have a maximum grain size of *ca.* 13 mm (medium pebbles).

6.3.3 Provenance

The interlava lithologies within the MBF are dominated by palagonitised basaltic glass clasts derived from the reworking of ash deposits. The varying degree of alteration of the glass clasts implies that numerous ash deposits were being eroded at the same time. The textural immaturity of the clasts, e.g. the small degree of rounding, indicates that the clasts were derived locally. The abundance of plagioclase feldspar fragments contained within the volcaniclastic lithologies, particularly from the Viðareiði Section, suggests that they were either liberated from basalt lava flows, which would have required very pervasive erosion, or more likely, they were derived from crystal (plagioclase-phyric) ash deposits. The occurrence of basalt clasts, principally the plagioclase-phyric varieties, indicates that they were derived from the erosion of MBF lava flow units. The clast lithologies preserved within the interlava lithologies and the lack of external clasts/grains, e.g. quartz, is consistent with the clasts having been derived from within the depositional area and therefore, they are all intraformational.

6.3.4 Environment of Deposition

The general lack of pyroclastic textures within the interlava lithologies is a consequence of the reworking of unconsolidated ash deposits under epiclastic processes (cf. Fisher & Schmincke 1984; Cas & Wright 1987; McPhie *et al.* 1993). However, the small degree of rounding implies that the clasts have only been transported to a limited extent. Channel structures, bedding and rounding of clasts is common within the interlava lithologies, this suggests transportation and deposition in fluvial environments (cf. Collinson 1996; Tucker 1996a). The channels are relatively small ranging from 5 to 20 m deep, e.g. at Klivarnar, Streymoy, suggesting relatively low to moderate energy levels. Normal grading within some of the sedimentary sequences, particularly at Viðareiði, Viðoy, suggests waning water flow energy levels, possibly associated with (seasonal) flooding events. The general lack of brecciation of lava flows in contact with the sedimentary lithologies suggests that the sedimentary rocks were water-poor at the time of lava emplacement, if the sedimentary rocks were water-rich hyaloclastite and blocky peperite pockets would be expected (cf. Jerram *et al.* 2000; Skilling *et al.* 2002). Minor occurrences of blocky peperites are

recorded at the Klivarnar and Viðareiði sections suggesting that some of the volcaniclastic lithologies were locally wet at the time of lava emplacement.

6.4 'Vent' Lithologies associated with the MBF

Rasmussen & Noe-Nygaard (1970b) identified what they interpreted as ten vents distributed throughout the MBF. Many of these 'vent' localities have been interpreted as vents solely on the basis of the presence of 'agglomerate'. As outlined in Section 2.2 the term agglomerate has been misused in the past and many of the agglomerates are actually volcaniclastic conglomerates of epiclastic origin. It is therefore important to re-evaluated the so called 'vent' localities to see if they are actually composed of agglomerate lithologies or if they have formed from epiclastic processes. Some of the 'vent' localities were only observed from the sea and access to these localities is hazardous and therefore was not attempted. The 'vent' locality on the eastside of Viðoy, between Gjógvin Stóra and Gjógvin Lítla, is associated with the UBF and is described in Section 7.5. One 'vent' locality from the MBF that was accessed is at Sundsmunnin, *ca.* 800 m SW of Viðareiði, Viðoy.

The outcrop is *ca.* 50 m across and *ca.* 30 m high (Fig. 6.29), with irregular vertical contacts with near horizontal MBF lava flow units (Fig. 6.29a). The lava flow units have an average thickness of *ca.* 70 cm. The unit also surrounds the lava tube described in Section 6.2.4 (Fig. 6.29b). The outcrop comprises a poorly sorted reddened volcaniclastic conglomerate, which appears to be crudely layered (Fig. 6.29e). This conglomerate consists of sub-angular to sub-rounded clasts up to 10s of cms in diameter (Figs. 6.29c-d). The conglomerate contains blackish grey amygdaloidal and non-amygdaloidal basalt clasts as well as reddish tuffaceous sandstone and bole clasts. The conglomerate is matrix supported by reddened sand to pebble grade material of similar composition to the clasts described above. The conglomerate is overlain by near horizontal lava flow units (Fig. 6.29f). A thin vertical dyke intrudes the conglomerate at the unit's southern end (Fig. 6.29f). The lack of any volcanic bombs (e.g. shaped or breadcrust types), high degree of heterogeneity of clast types and the rounding of the clasts suggest that the unit is a volcaniclastic conglomerate of epiclastic origin (cf. Fisher & Schmincke 1984; Cas & Wright 1987; McPhie *et al.* 1993).

If the locality was the site of a vent not only would the lava flow units have been destroyed but also the lava tube. However, the lava tube is intact and surrounded by the volcaniclastic conglomerate. As outlined in Section 6.2.4 the lava tubes observed throughout the MBF

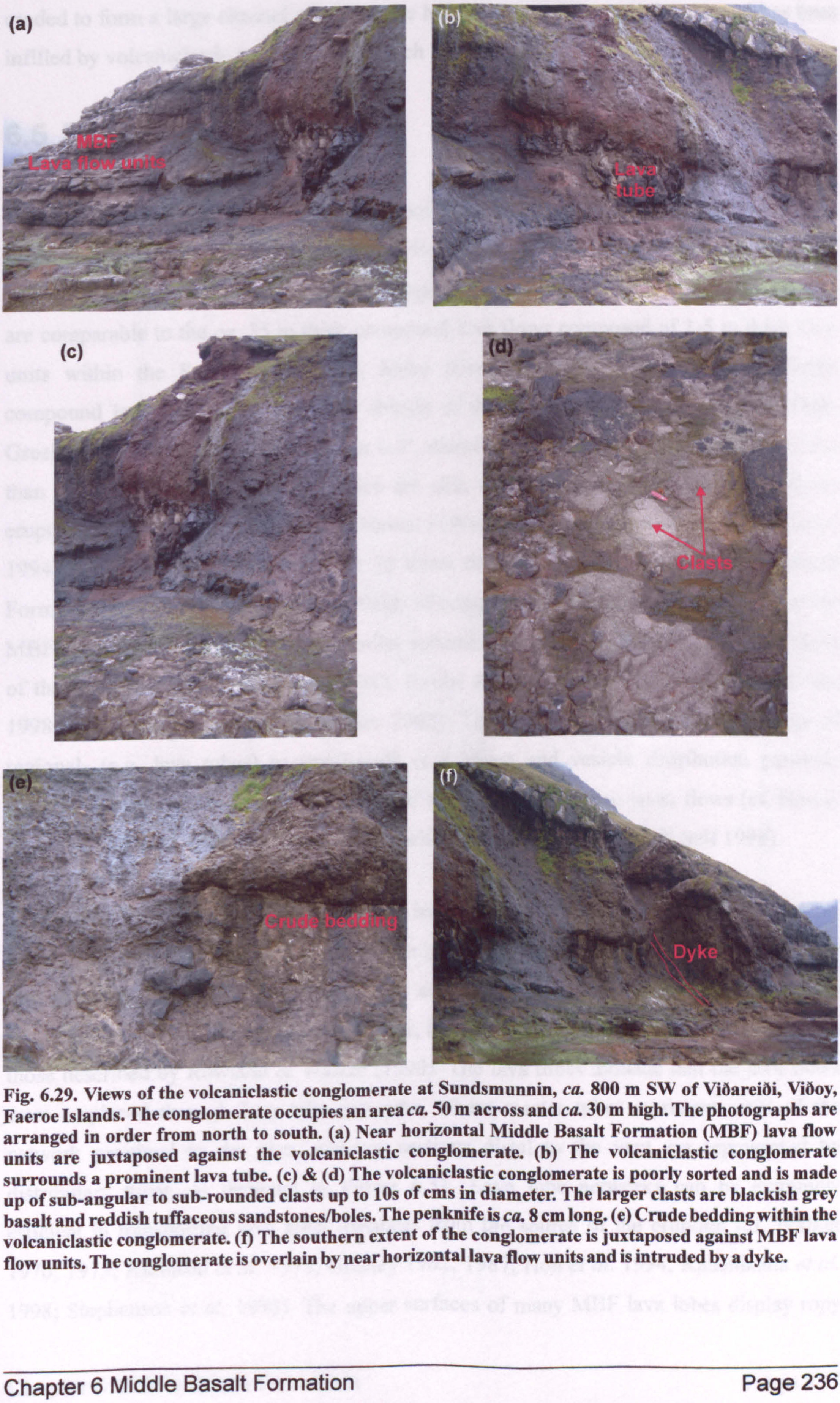

Fig. 6.29. Views of the volcaniclastic conglomerate at Sundsmunnin, *ca.* 800 m SW of Viðareiði, Viðoy, Faeroe Islands. The conglomerate occupies an area *ca.* 50 m across and *ca.* 30 m high. The photographs are arranged in order from north to south. (a) Near horizontal Middle Basalt Formation (MBF) lava flow units are juxtaposed against the volcaniclastic conglomerate. (b) The volcaniclastic conglomerate surrounds a prominent lava tube. (c) & (d) The volcaniclastic conglomerate is poorly sorted and is made up of sub-angular to sub-rounded clasts up to 10s of cms in diameter. The larger clasts are blackish grey basalt and reddish tuffaceous sandstones/boles. The penknife is *ca.* 8 cm long. (e) Crude bedding within the volcaniclastic conglomerate. (f) The southern extent of the conglomerate is juxtaposed against MBF lava flow units. The conglomerate is overlain by near horizontal lava flow units and is intruded by a dyke.

are stand-alone features that have resisted erosion and this would seem to be the case for the lava tube at Sundsmunnin. The lava flow units surrounding the lava tube have been eroded to form a large channel, the lava tube has resisted erosion and the channel has been infilled by volcaniclastic conglomerate, which has encased the lava tube.

6.5 Synthesis

The Middle Basalt Formation (MBF) is dominated by up to 20 m thick compound lava flows that were erupted into a terrestrial environment (Fig. 6.30). The lavas are made up of numerous thinner flow units (lobes) that range in thickness from <0.5 to 2 m. These data are comparable to the *ca.* 35 m thick compound lava flows composed of 1-5 m thick flow units within the Snake River Plain, Idaho (Greeley 1976; 1977; 1982). The MBF compound lava flow fields form low shields of the scutulum type (Noe-Nygaard 1968; Greeley 1982) with slopes of less than 0.5°, diameters of *ca.* 15 km and volumes of less than 7 km^3 (Noe-Nygaard 1968), which are akin to the compound pahoehoe lava flows erupted under subaerial conditions on Hawai`i (Wentworth & Macdonald 1953; Hon *et al.* 1994). The MBF lava flow units are 10 times thinner than those of the Lower Basalt Formation (LBF), but form lava flow fields of comparable thicknesses, suggesting that the MBF flow units were erupted with similar volumes but at lower effusion rates than those of the LBF lava flows (cf. Greeley 1982; Reidel & Tolan 1992; Self *et al.* 1996; Reidel 1998; Thordarson & Self 1998; Jerram 2002). The MBF lava flows have a number of regional- (e.g. lava tubes) to small-scale (e.g. ropes and vesicle distribution patterns) features consistent with having been erupted as inflating pahoehoe lavas flows (cf. Hon *et al.* 1994; Self *et al.* 1996; Self *et al.* 1997; Self *et al.* 1998; Thordarson & Self 1998).

Lava tubes form stand-alone features that have resisted erosion and range in size from master to smaller distributary tubes (cf. Rowland & Walker 1990). The master tubes have cross-sectional areas that range between 3 and 160 m^2. The distributary lava tubes, for example those preserved at Viðareiði, Viðoy, have cross-sectional areas of 0.14 m^2, akin to those described by Rowland & Walker (1990). The lava tubes indicate that the lava flows were emplaced through lava tube networks, where master tubes represent areas of the network proximal to the vent, whereas sections distal to the vent are represented by distributary tubes, as depicted in Figure 6.31. Lava tube networks can be extremely efficient in transporting lava great distances from the source of the eruption (cf. Walker 1970; 1973; Atkinson *et al.* 1975; Greeley 1982; 1987; Hon *et al.* 1994; Kauahikaua *et al.* 1998; Stephenson *et al.* 1998). The upper surfaces of many MBF lava lobes display ropy

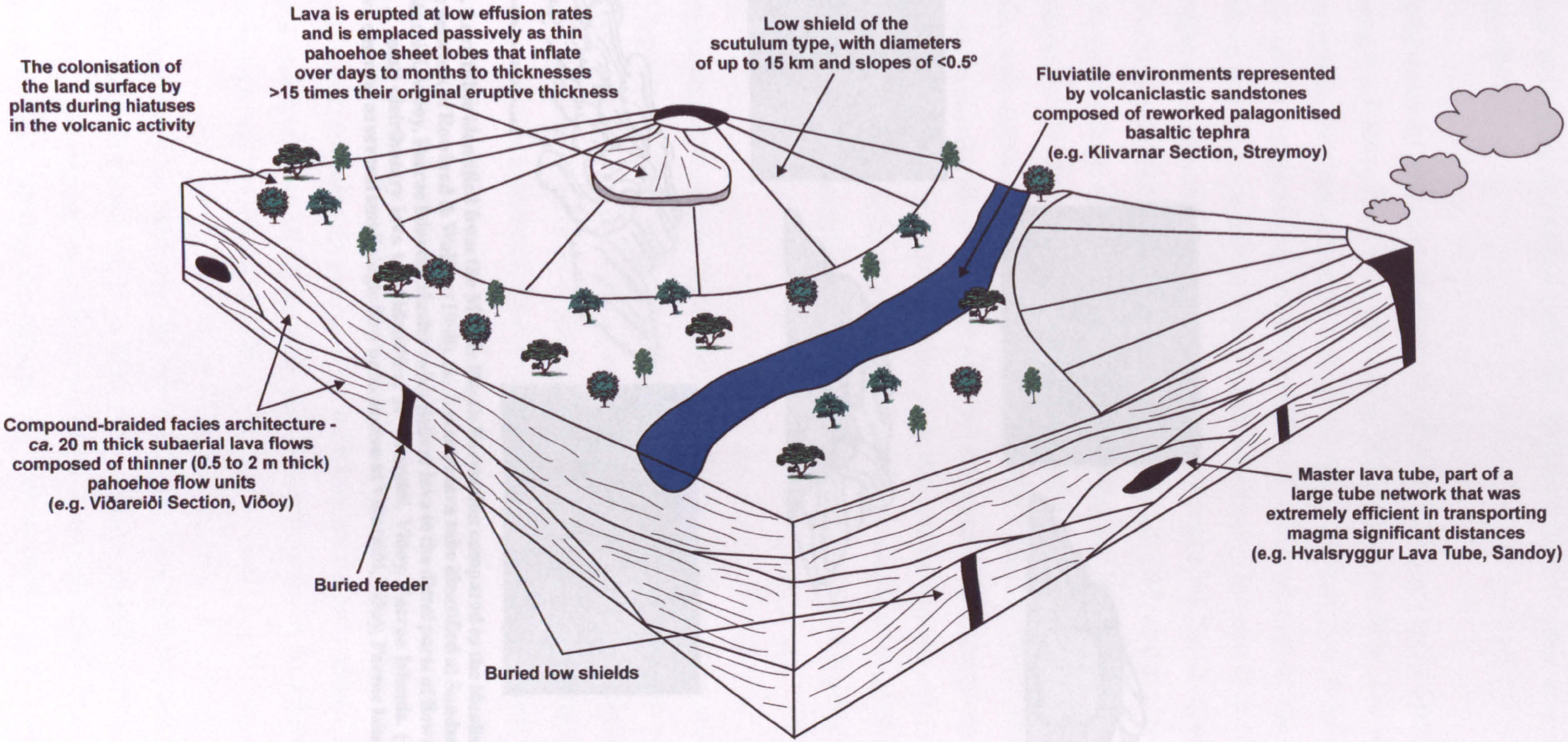

Fig. 6.30. Schematic palaeogeographical block diagram for the Middle Basalt Formation with the main elements highlighted. Length of each horizontal dimension of the figure is very approximately 12-15 km. Lava tubes have been exaggerated in the diagram to highlight them.

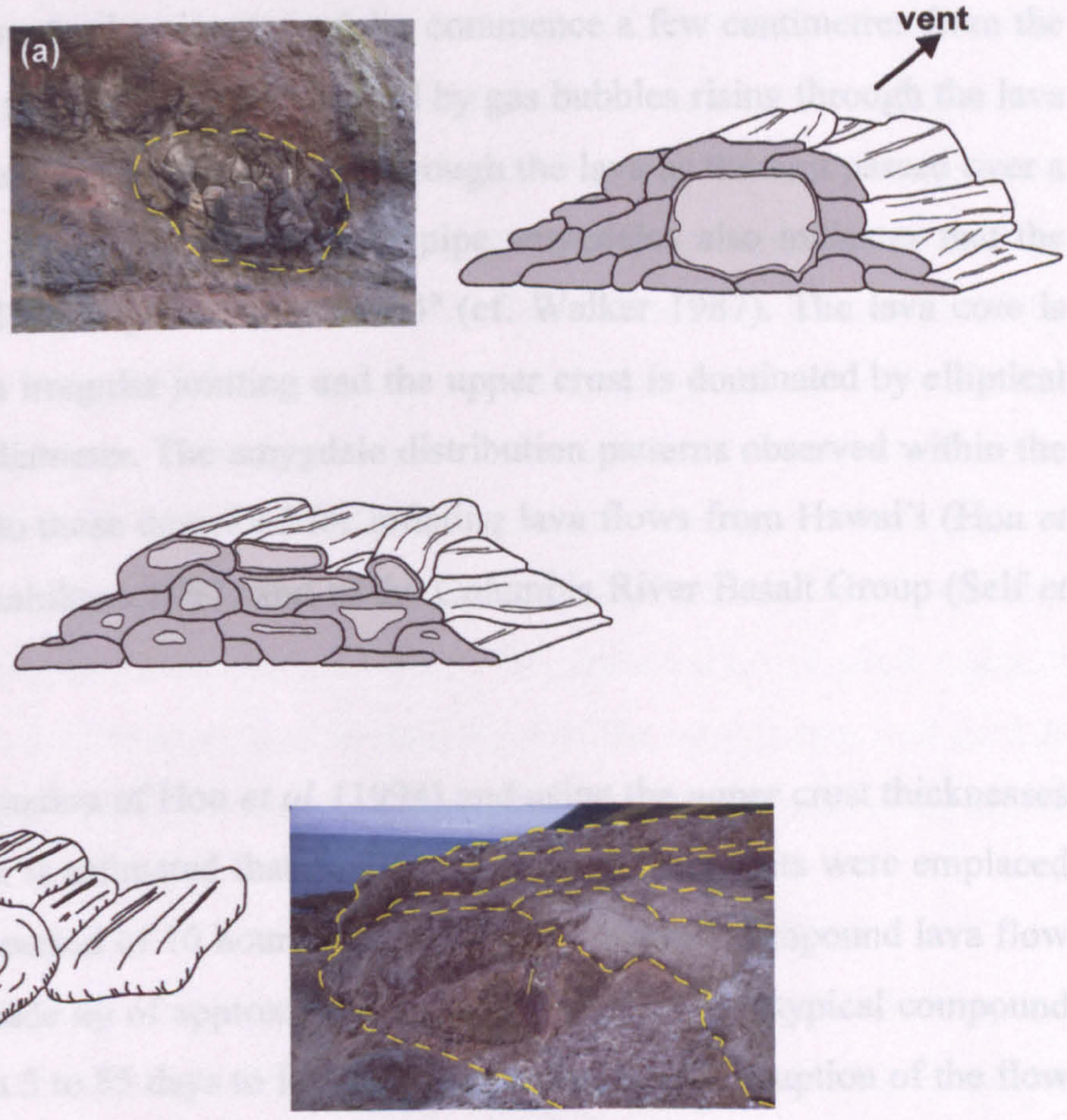

Fig. 6.31. Lava tubes identified from the Middle Basalt Formation compared to the idealised sections of a lava tube network of Rowland & Walker (1990). (a) A master lava tube identified at Sundsmunnin, *ca.* 800 m S of Viðareiði, Viðoy, Faeroe Islands. Master tubes deliver lava to the distal parts of flows away from the vent. (b) A small distributary lava tube identified at Viðareiði, Viðoy, Faeroe Islands. (c) A flow front where lava emerges as several small single flow units as seen at Viðareiði, Viðoy, Faeroe Islands.

structures indicative of being emplaced as pahoehoe lava flows (cf. Wentworth & Macdonald 1953; Fink & Fletcher 1978; Cas & Wright 1987; McPhie *et al.* 1993; Crown & Baloga 1999).

P-type (pipe-bearing) pahoehoe flow units are dominant throughout the MBF, although S-type (spongy) pahoehoe flow units also occur. The P-type pahoehoe flow units have the classic amygdale distribution patterns associated with such units (cf. Wilmoth & Walker 1993) and can be separated into a basal crust, lava core and upper crust. The basal crust is characterised by pipe amygdales that begin a few centimetres from the base of the flow and have lengths of up to 8 cm. As the pipe amygdales commence a few centimetres from the base of the flow unit, this suggests that they formed by gas bubbles rising through the lava at a relatively late stage, rather than steam rising through the lava as the unit passed over a wet substrate (cf. Walker 1987). The presence of pipe amygdales also indicates that the flow units were emplaced on slopes of less than 4° (cf. Walker 1987). The lava core is compact and massive with irregular jointing and the upper crust is dominated by elliptical amygdales up to 2 cm in diameter. The amygdale distribution patterns observed within the MBF flow units are akin to those described for inflating lava flows from Hawai`i (Hon *et al.* 1994; Cashman & Kauahikaua 1997) and in the Columbia River Basalt Group (Self *et al.* 1996; Self *et al.* 1997).

Applying the empirical equation of Hon *et al.* (1994) and using the upper crust thicknesses of the P-type flow units, it is estimated that the MBF pahoehoe flow units were emplaced as inflating bodies over a period of 10 hours to 9 days. If the average compound lava flow is *ca.* 20 m thick and is made up of approximately 10 flow units, then a typical compound lava flow would take from 5 to 85 days to form. This assumes that the eruption of the flow units was continuous and does not take into consideration other external factors e.g. effects of rainfall and thermal properties. Assuming similar low discharge and low volumetric flow rates akin to the pahoehoe lavas of Hawai`i (Rowland & Walker 1990; Hon *et al.* 1994), it is postulated that a flow front of an MBF lava would have taken a few months to just over a year to advance *ca.* 10 km away from a fissure vent with flow front velocities in the order of 1-10 m h^{-1} (cf. Kent *et al.* 1998).

The upper section of the MBF sees the introduction of tabular-classic facies architecture lava flows. These flows are *ca.* 10 m thick rubbly-topped sheet-like bodies and may, in fact, belong to the lower section of the Upper Basalt Formation (UBF). The tabular-classic flows are most likely infilling the topographic lows produced by the low shields. The sheet-like flows appear to form laterally continuous bodies, but are actually confined

within extremely low-lying basins/small depressions. Gradually, the flows infilled the topography, leading to the more laterally continuous flows of the UBF. The drowning of a lava topography by younger flows is also noted from excellently preserved examples in the Snake River Plain, Idaho (Greeley 1976; 1977; 1982).

The relatively rare interlava lithologies within the MBF generally have limited lateral extent and are commonly confined to channel-like structures. The lithologies are predominantly volcaniclastic sandstones, although mudstones and conglomerates also occur. The units are generally bedded and clasts have a degree of rounding suggesting transportation and deposition within a fluvial environment (cf. Collinson 1996; Tucker 1996a). Normal grading of some of the fluvial deposits indicates cycles of waning water flow energy, most likely formed during seasonal flooding episodes. The siltstones, sandstones and conglomerates are poorly sorted and clast to matrix supported. The clasts are intraformational, with no evidence of any external sources. The units are dominated by an abundance of reworked ash grade material, now extremely palagonitised. Rare coarser deposits, particularly at Viðareiði, Viðoy, record an influx of basalt lithoclasts, derived from lava flows, as well as clasts of volcaniclastic mudstone. The basalt clasts show a variation in the degree of surface oxidation, indicating that numerous exposed flows were being eroded within the contemporaneous lava field. The preservation of plant material within the sandstones from the í Bugum Section indicates that the surrounding land surface was vegetated, thus aiding the surface weathering of the volcanic lithologies (cf. Berner & Cochran 1998).

The lack of interlava lithologies in the lower section of the MBF suggests that the eruption of the compound lavas was fairly continuous. Waning volcanic activity in the upper section of the MBF allowed time for the development of fluvial environments within which the volcaniclastic sandstones and conglomerates were deposited (Cas & Wright 1987; Smith 1991; McPhie *et al.* 1993; Reading 1996). The overall lack of basalt clasts within the majority of the fluvial deposits suggests that erosion rates were low or that there was a change in the volcanic style, where pyroclastic debris could have blanketed the land surface and restricted erosion of the flows, otherwise there would be an abundance of lava clasts similar to the amount observed in the LBF. As the rate of erosion is in part determined by climate (Collinson 1996), it is suggested here that there was a deficiency in surface water and low levels of rainfall to aid the high rates of erosion inferred for the LBF.

Furthermore, the general lack of brecciation of the basal crust of the flow units suggests that the land surface was relatively dry at the time of emplacement. If the land surface had pools and/or water-saturated deposits at the time of eruption, hyaloclastite and blocky peperite pockets would have be expected at the base of the flow units, similar to those observed in the LBF and in other lava provinces (Jerram *et al.* 2000; Carr & Jones 2001; Jerram & Stollhofen 2002).

Sedimentary structures within the volcaniclastic mudstones, sandstones and conglomerates at Viðareiði, Viðoy have not been destroyed or significantly modified by the overlying and invasive flow units, which suggests that the magma was emplaced relatively passively (cf. Jerram *et al.* 2000; Jerram & Stollhofen 2002). This may indicate why the volcaniclastic rocks are apparently poorly lithified at Viðareiði, Viðoy, as the flow units have protected them, just as the aeolian sands have been preserved in Namibia, Brazil and South Greenland by passively emplaced flow units (Clemmensen 1988; Jerram *et al.* 2000; Jerram & Stollhofen 2002; Scherer 2002).

7 Upper Basalt Formation

This chapter, through the description of the facies architecture of the lava flows of the Upper Basalt Formation (UBF), proposes the environments of eruption throughout this formation. As with the other basalt formations, previous work has focused on the petrology and geochemistry of the lavas and the interlava lithologies have received little consideration. Here, seven sections containing volcaniclastic lithologies are described and interpreted to understand their modes and environments of deposition. The volcaniclastic lithologies from the Sneis Section are given special attention because they occur at the boundary between the Middle and Upper basalt formations. Lastly, a so-called 'vent' locality is re-examined using current classification schemes to determine whether it is pyroclastic or epiclastic in origin.

7.1 Distribution

The Upper Basalt Formation (UBF) has a preserved stratigraphic thickness of *ca.* 900 m, as an unknown thickness has been eroded from the top of the formation. The amount of missing strata has been estimated from zeolite studies to be of the order of a few hundred metres (Waagstein 1988; Ellis *et al.* 2002). The UBF crops out on all of the islands except Suðuroy, Vágar, Tindhólmur and Mykines (Figs. 1.3, 7.1 & 7.2). The UBF does not occur on northern Streymoy and is sporadic in the NW of Eysturoy. The UBF is always found overlying the Middle Basalt Formation (MBF) and the lavas dip between the NE and SE with an inclination of between 1.7 and 2.9° (Waagstein 1988).

7.2 Lava Flows

7.2.1 Petrology & Geochemistry

The base of the UBF is represented by a plagioclase-phyric flow sequence, *ca.* 300 m thick, in the central Faeroe Islands situated around Sandoy (Waagstein 1988). However, in the NE of the archipelago the base of the UBF is represented by near-aphyric to olivine-phyric flows (Kollafjørdur Member), which are overlain by the dominant plagioclase-phyric flows (Waagstein 1988). The plagioclase-phyric flows in the NE of the Faeroe Islands are overlain by near-aphyric (Fig. 7.3) to olivine-phyric flows (Viðoy Member), which have an aggregate thickness of *ca.* 500-600 m (Waagstein 1988).

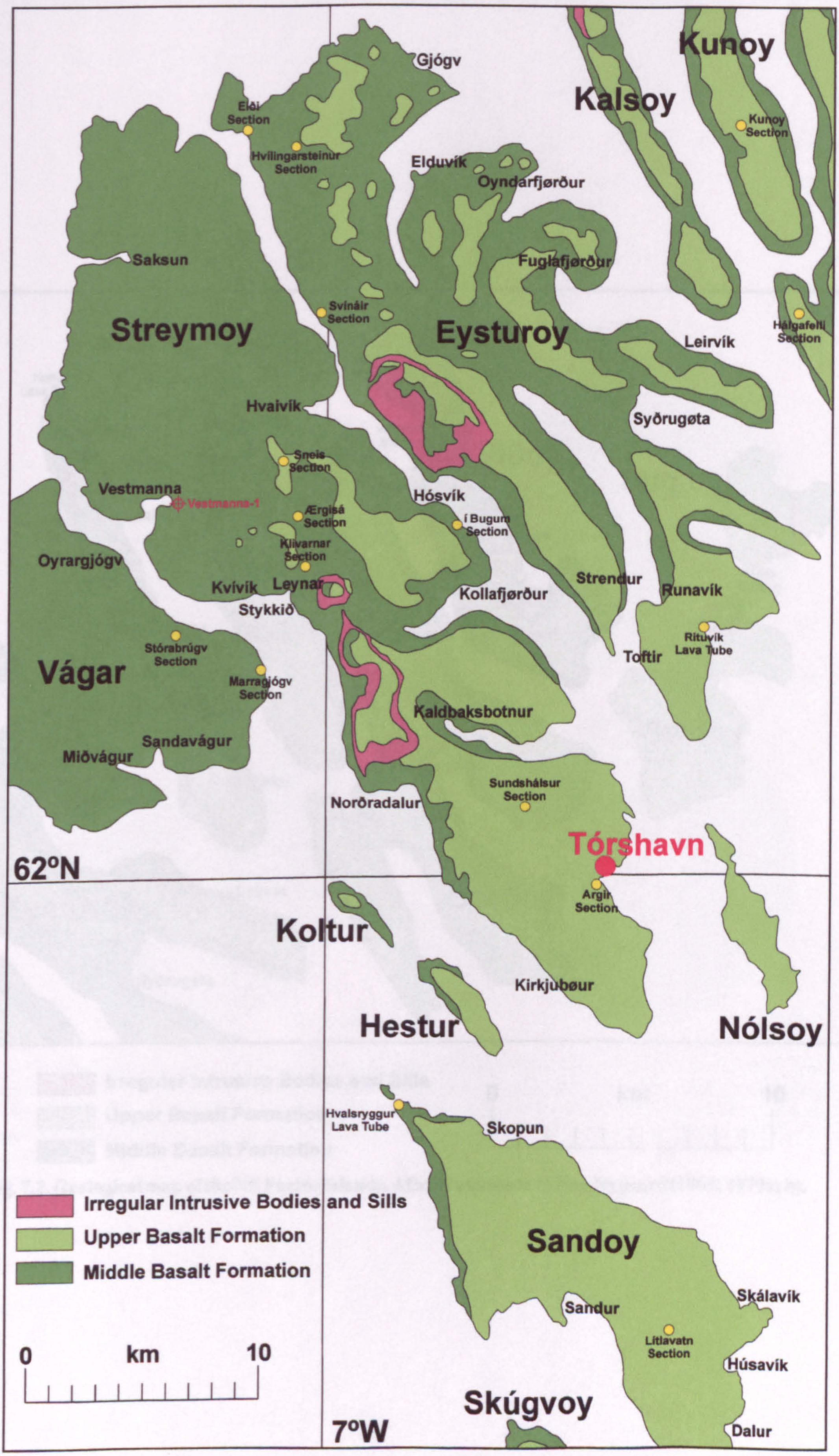

Fig. 7.1. Geological map of the central Faeroe Islands. After Rasmussen & Noe-Nygaard (1969; 1970a; b).

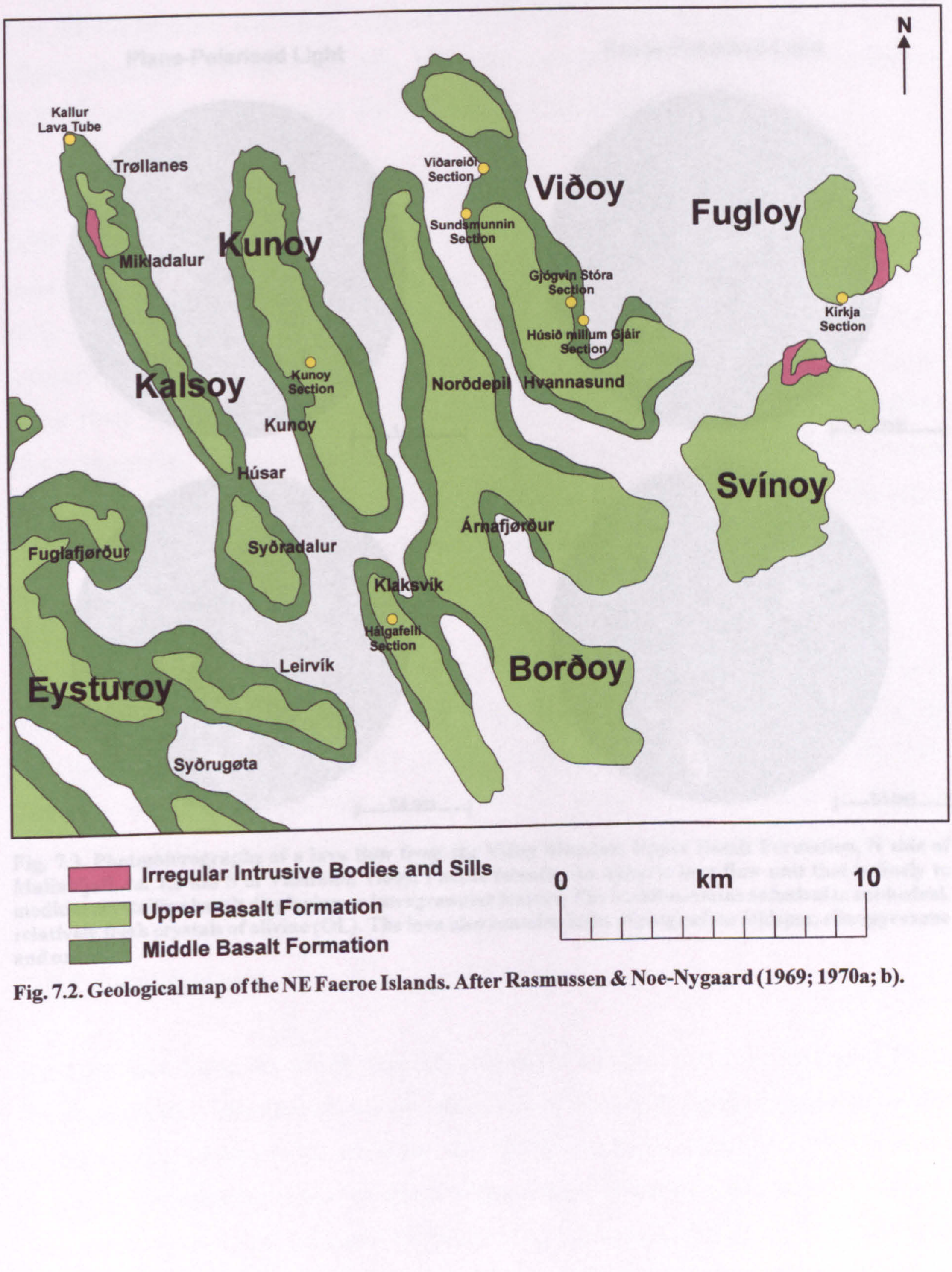

Fig. 7.2. Geological map of the NE Faeroe Islands. After Rasmussen & Noe-Nygaard (1969; 1970a; b).

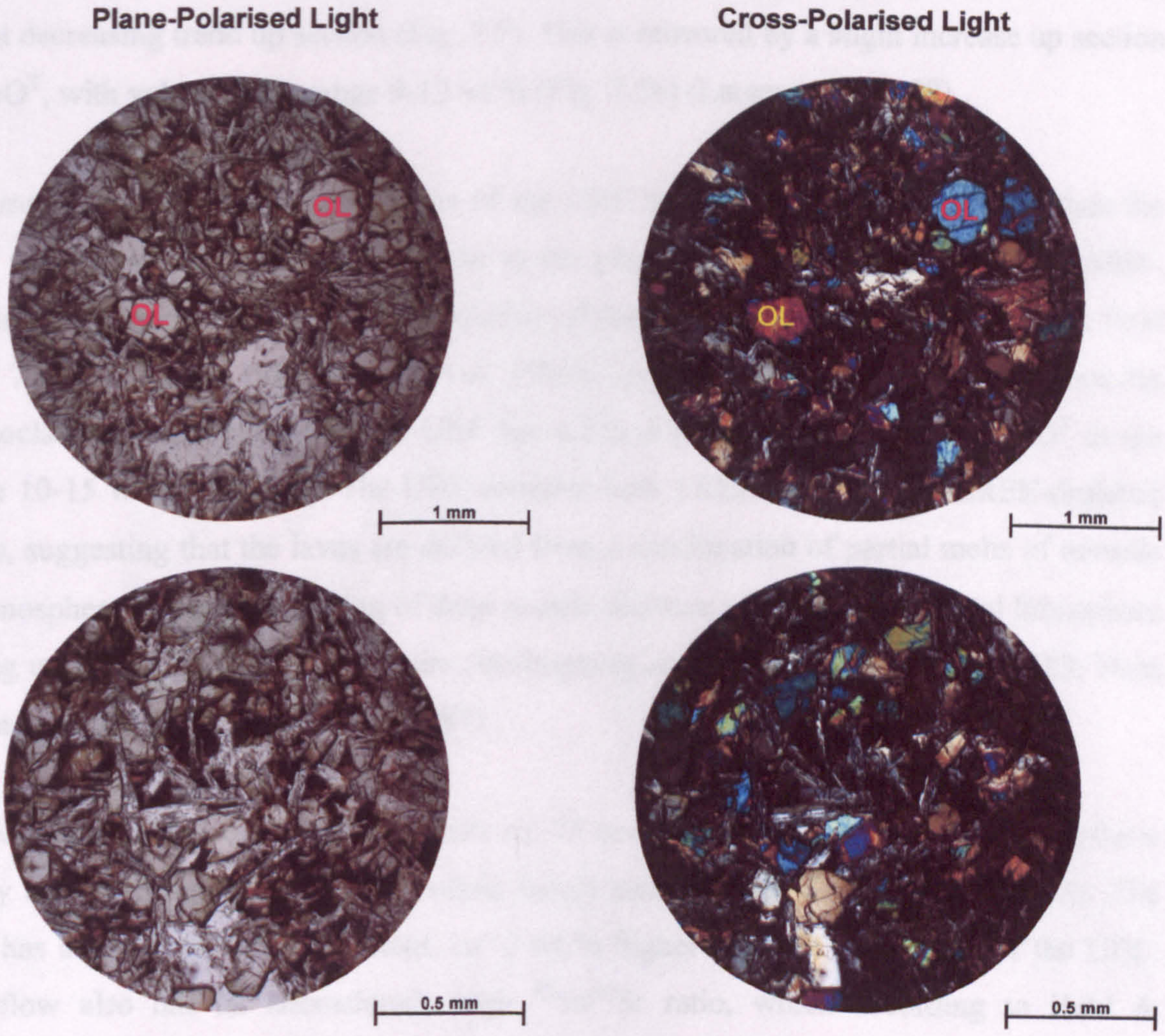

Fig. 7.3. Photomicrographs of a lava flow from the Viðoy Member, Upper Basalt Formation, N side of Malinsfjall, *ca.* 1.5 km S of Viðareiði, Viðoy, Faeroe Islands. An aphyric lava flow unit that is finely to medium crystalline basalt displaying an intergranular texture. The basalt contains anhedral to subhedral, relatively fresh crystals of olivine (OL). The lava also contains laths of plagioclase feldspar, clinopyroxene and oxides.

The Kollafjørdur and Viðoy members of the UBF have a low TiO_2/FeO^T ratio compared to the Lower Basalt Formation (LBF) and the MBF, but the FeO^T/MgO ratio ranges between 0.6 and 2, making the Kollafjørdur and Viðoy members transitional from the low-Ti olivine tholeiite field to the low-Ti tholeiite field (Fig. 7.4) (Waagstein 1988; Larsen *et al.* 1999). The combination of these two low ratios and depletion in Ti, P, K and other incompatible elements make the Kollafjørdur and Viðoy members MORB-like (Mid-Ocean Ridge Basalt) (Waagstein 1988; Larsen *et al.* 1999). Larsen *et al.* (1999) showed that the Kollafjørdur and Viðoy members have a Mg #, in the range 50-73, and shows a slight decreasing trend up section (Fig. 7.5). This is mirrored by a slight increase up section in FeO^T, with values in the range 9-12 wt.% (Fig. 7.5b) (Larsen *et al.* 1999).

The main plagioclase-phyric sequence of the UBF has a higher TiO_2/FeO^T ratio than the LBF and has a FeO^T/MgO ratio similar to the plagioclase-phyric sequence of the MBF, causing the plagioclase-phyric main sequence of the UBF occupy the high-Ti tholeiite field (Fig. 7.5) (Waagstein 1988; Larsen *et al.* 1999). Larsen *et al.* (1999) have shown that the plagioclase-phyric sequence of the UBF has a Mg # in the range 42-54 and FeO^T in the range 10-15 wt.% (Fig. 7.5). The UBF contains both LREE-enriched and LREE-depleted flows, suggesting that the lavas are derived from a combination of partial melts of oceanic asthenosphere and partial melting of deep mantle blobs or of the subcontinental lithosphere during upwelling of the asthenosphere (Bollingberg *et al.* 1975; Gariépy *et al.* 1983; Hald & Waagstein 1983; Saunders *et al.* 1997).

The Villingadalsfjall-6 Lava Flow occurs *ca.* 75 m above the base of the UBF on northern Viðoy and is recognised as a high silicic basalt lava by Hald & Waagstein (1983). The flow has a 52.55 wt.% SiO_2 content, *ca.* 5 wt.% higher than the main lavas of the UBF. The flow also has an anomalously high $^{87}Sr/^{86}Sr$ ratio, which according to Hald & Waagstein (1983) imply that the parental magma was contaminated by continental basement rocks or sediments.

7.2.2 Morphology

The UBF lava flows are morphologically similar to the lava flows of the Lower Basalt Formation (LBF). The UBF flows are laterally extensive, with sheet-like geometries, and are commonly massive with vesicular and rubbly top zones (Fig. 7.6). The lavas are frequently separated by minor reddened volcaniclastic lithologies and, together with the reddened flow tops, this highlights the planar upper surfaces to the flows. This layer cake appearance and associated terraced terrain is characteristic of tabular-classic facies lava

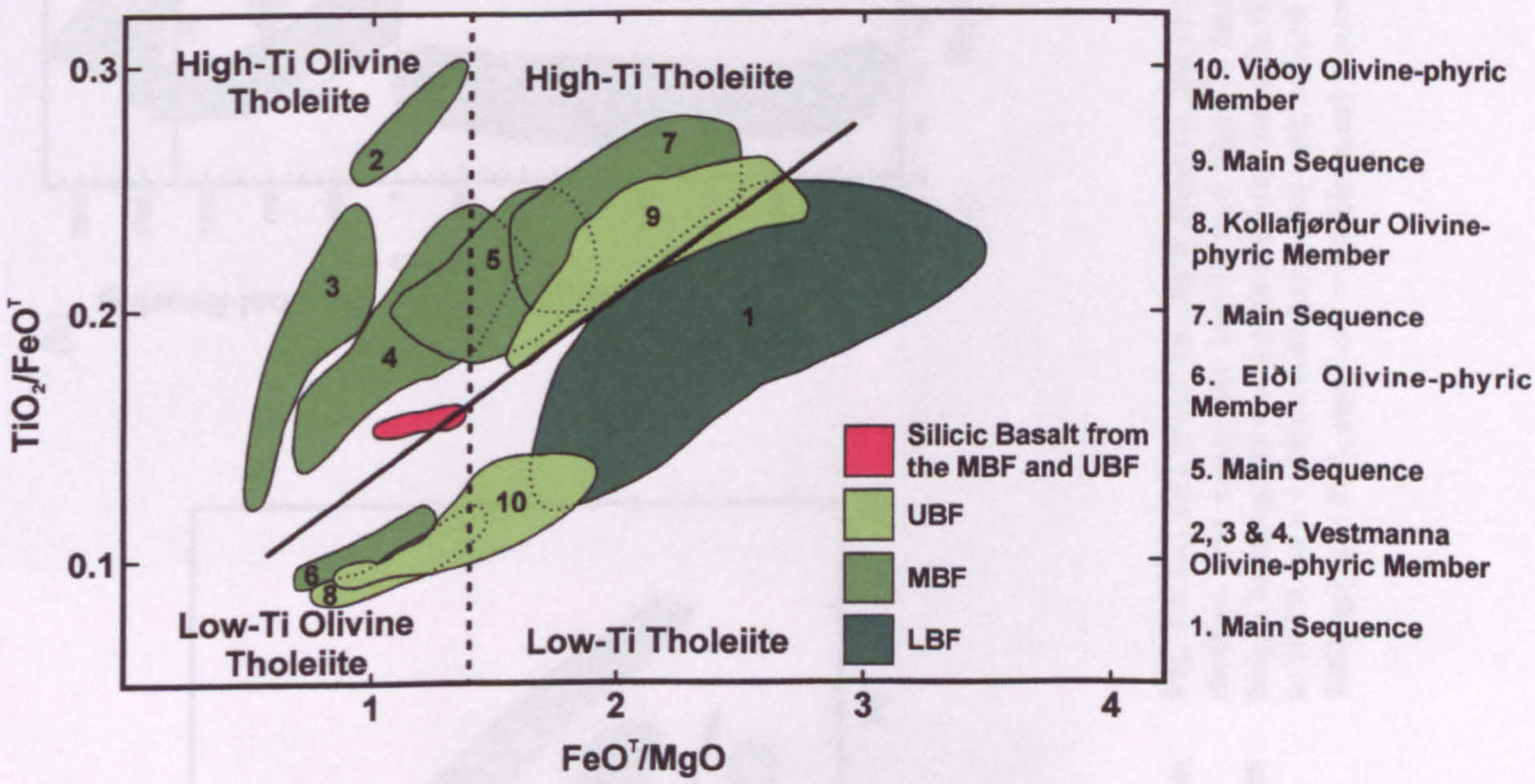

Fig. 7.4. TiO_2/FeO^T vs. FeO^T/MgO diagram for basalt lavas from the Faeroe Plateau Lava Group, Faeroe Islands (FeO^T = total iron recalculated as FeO). The oblique full line and the vertical stippled line mark the proposed boundaries between high-Ti olivine tholeiites, high-Ti tholeiites, low-Ti olivine tholeiites, and low-Ti tholeiites. LBF = Lower Basalt Formation, MBF = Middle Basalt Formation, UBF = Upper Basalt Formation. After Waagstein (1988).

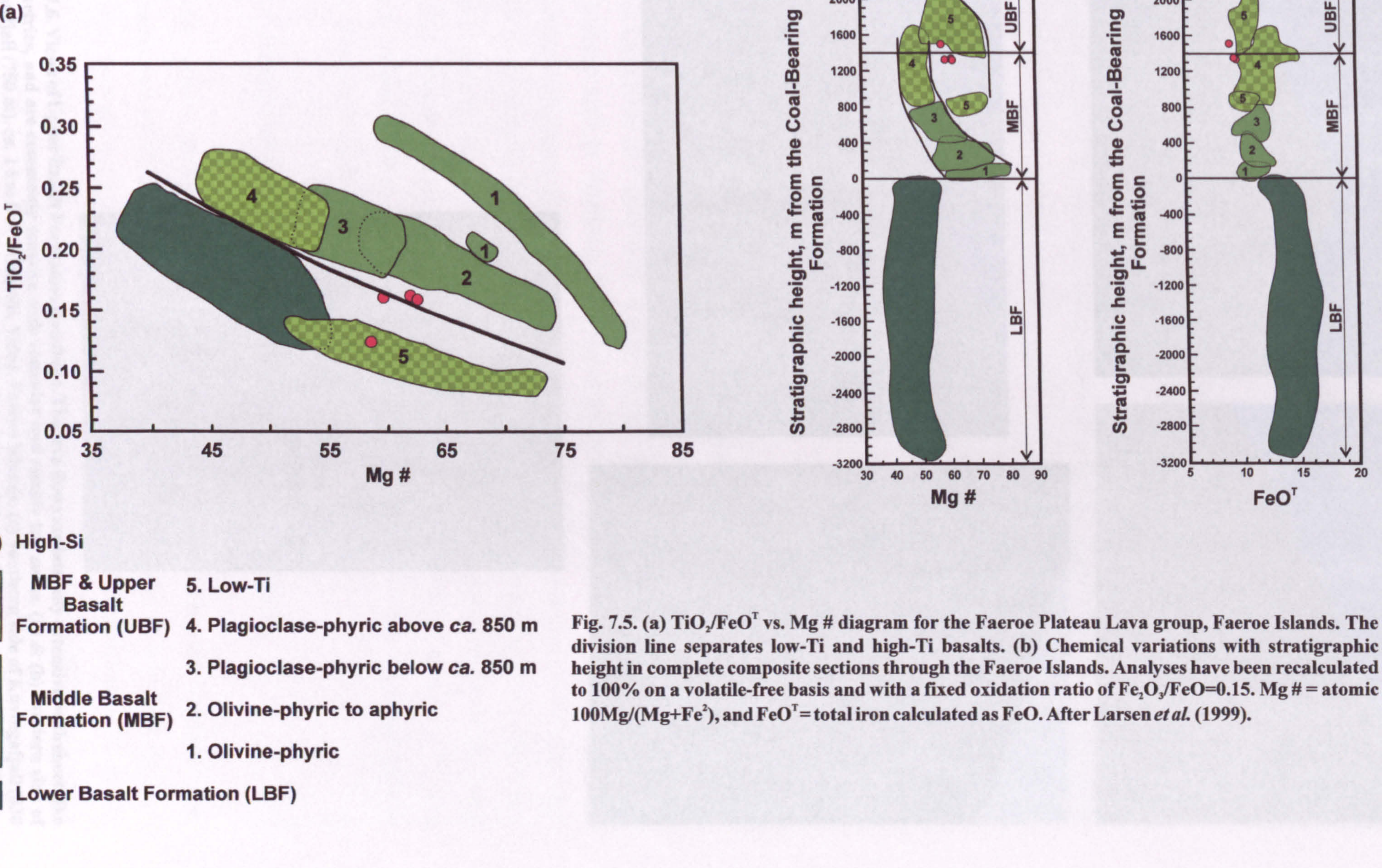

Fig. 7.5. (a) TiO_2/FeO^T vs. Mg # diagram for the Faeroe Plateau Lava group, Faeroe Islands. The division line separates low-Ti and high-Ti basalts. (b) Chemical variations with stratigraphic height in complete composite sections through the Faeroe Islands. Analyses have been recalculated to 100% on a volatile-free basis and with a fixed oxidation ratio of $Fe_2O_3/FeO=0.15$. Mg # = atomic $100Mg/(Mg+Fe^2)$, and FeO^T = total iron calculated as FeO. After Larsen *et al.* (1999).

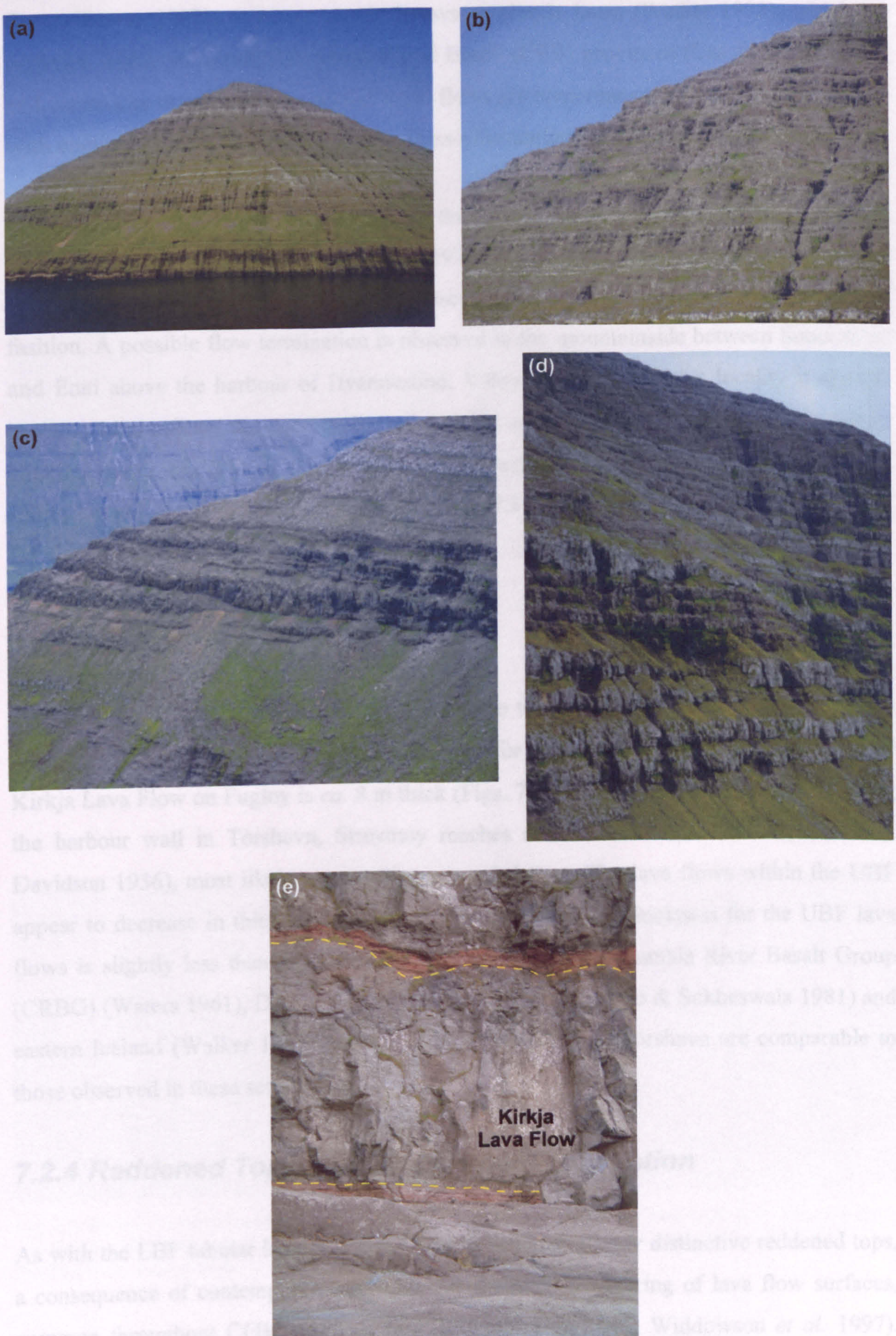

Fig. 7.6. Views of Upper Basalt Formation lava flows. The lava flows are laterally extensive, with sheet-like geometries, and are commonly massive with vesicular and rubbly top zones. (a) & (b) Western side of Malinsfjall (750 m), *ca.* 1 km S of Viðareiði, Viðoy, Faeroe Islands. (c) Southern side of Kúvingafjall (830 m), *ca.* 2 km N of Kunoy, Kunoy, Faeroe Islands. (d) Mountain wall E of Lítlidalur, *ca.* 1.5 km NE of Kunoy, Kunoy, Faeroe Islands. (e) The Kirkja Lava Flow, *ca.* 50 m E of Kirkja harbour, Fugloy, Faeroe Islands. The flow is *ca.* 8 m thick.

flows (Jerram 2002), more commonly known as simple lavas (Walker 1973), which are common within subaerial Continental Flood Basalt (CFB) provinces (Cas & Wright 1987, and references therein). These tabular lavas flows are sometimes transitionally interbedded with compound lava flows of the Middle Basalt Formation (MBF) at the base of the UBF.

Flow edges are difficult to observe due to the abundance of vegetation cover throughout the UBF, but Rasmussen & Noe-Nygaard (1970b) noted that some lava flows terminate by gradually thinning out, whereas plagioclase-phyric flows terminate in a more abrupt fashion. A possible flow termination is observed in the mountainside between Sundsskarð and Enni above the harbour of Hvannasund, Viðoy (Fig. 7.7). At this locality it appears that two tabular flows are overlapping one another and terminating. On the western side of Klakkur, *ca.* 2 km NW of Klaksvík, Borðoy a large tabular lava flow is interpreted as riding up and forming an inverted v-shape (Fig. 7.8), which may be the result of the lava flowing over a palaeo-high.

7.2.3 Flow Thicknesses

The UBF lava flows have an average thickness in the range 8-11 m (Rasmussen & Noe-Nygaard 1970b), half the average flow thickness for similar type flows from the LBF. The Kirkja Lava Flow on Fugloy is *ca.* 8 m thick (Figs. 7.2 & 7.9). However, a lava flow along the harbour wall in Tórshavn, Streymoy reaches a thickness of *ca.* 30 m (Walker & Davidson 1936), most likely representing a ponded flow. The lava flows within the UBF appear to decrease in thickness up section. The average flow thickness for the UBF lava flows is slightly less than those observed for CFBs in the Columbia River Basalt Group (CRBG) (Waters 1961), Deccan Traps (Choubey 1973; Subbarao & Sukheswala 1981) and eastern Iceland (Walker 1963), but the thick flows found at Tórshavn are comparable to those observed in these settings.

7.2.4 Reddened Tops and Environment of Eruption

As with the LBF tabular lava flows, the UBF flows also display distinctive reddened tops, a consequence of contemporaneous subaerial chemical weathering of lava flow surfaces, common throughout CFB provinces (e.g. Wilkins *et al.* 1994; Widdowson *et al.* 1997). However, these reddened tops are not as prevalent or as well developed throughout the UBF as they are in the LBF and consequently soil profiles are similarly lacking. This may be linked to the abundance of volcaniclastic units separating the lava flows and restricting

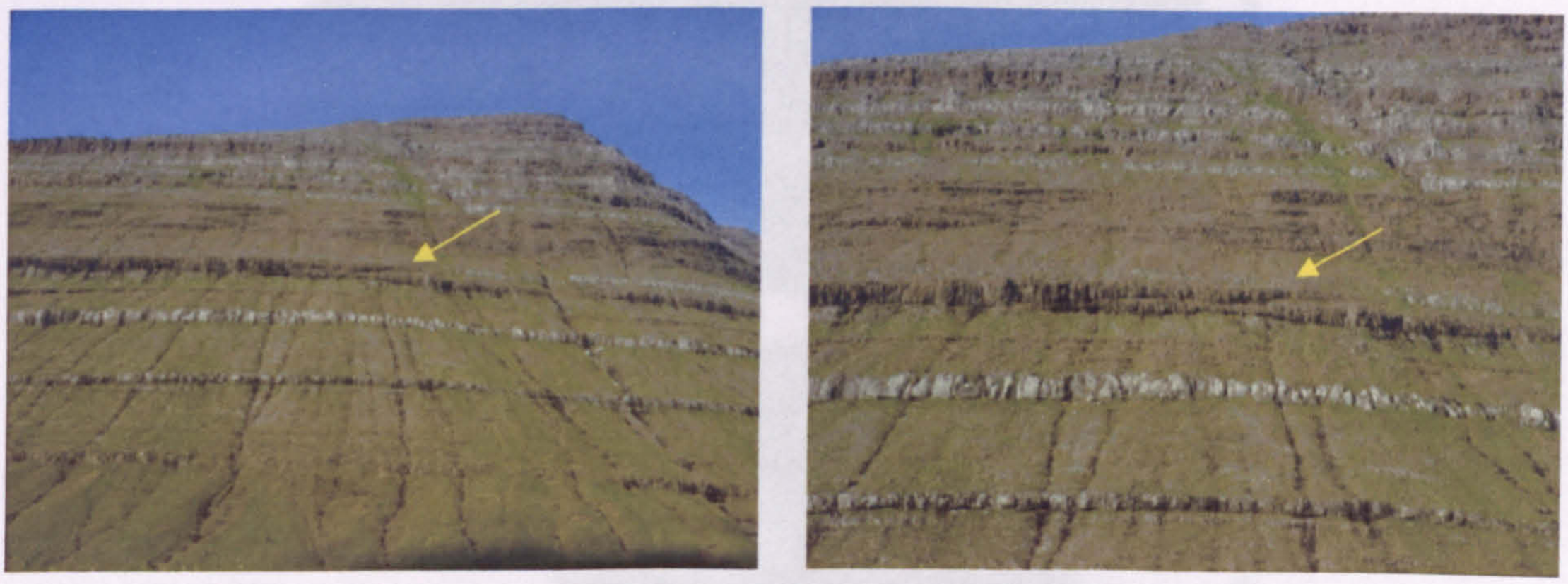

Fig. 7.7. Views of two overlapping tabular lava flows along the mountainside inbetween Sundsskarð and Enni above the harbour of Hvannasund, Viðoy, Faeroe Islands.

Fig. 7.8. On the western side of Klakkur (413 m), *ca.* 2 km NW of Klaksvík, Borðoy, Faeroe Islands a large tabular lava flow is observed riding up and forming an inverted v-shape. This may be the result of the lava flowing over a palaeo-high.

Fig. 7.9. Views of the Kirkja Lava Flow, which is *ca.* 8 m thick and crops out inbetween reddened interlava lithologies. The flow displays indistinct prismatic jointing and occurs *ca.* 50 m E of the Kirkja harbour, Fugloy, Faeroe Islands.

the process of subaerial chemical weathering on the upper surfaces of the lava flows or that the eruption frequency was higher restricting the time available for subaerial weathering.

7.2.5 Development of Prismatic and Columnar Jointing

Columnar jointing is absent throughout the UBF, although poorly developed or prismatically jointed lava flows are common. However, compared to the prismatically jointed lava flows of the LBF they are not as well developed. The jointing in the Kirkja Lava Flow on Fugloy is a typical example of prismatic jointing within the UBF (Fig. 7.9). The joints within the Kirkja flow are very indistinct and from some viewpoints appear to be absent. Another feature associated with the prismatically jointed lava flows of the LBF but are absent from the UBF are hyaloclastite and blocky peperite pockets at the base of the flows. The absence of columnar jointing, hyaloclastite and blocky peperite pockets suggests that the lava flows were erupted onto a dry land surface (cf. Saemundsson 1970; Busby-Spera & White 1987; Lyle 2000; Campbell *et al.* 2001; Jerram 2002; Skilling *et al.* 2002).

A form of lava flow identified by Rasmussen & Noe-Nygaard (1970b) as an agglutinate forms a distinctive feature throughout the UBF. These lava flows are relatively thin, typically no more than 8 m thick, and commonly overlie volcaniclastic lithologies. One such lava flow occurs *ca.* 200 m SE of Hálgafelli summit, *ca.* 420-430 m above sea level, *ca.* 1 km SW of Klaksvík, Borðoy (Figs. 7.2 & 7.10). The lava flow is *ca.* 8 m thick and overlies a *ca.* 4.7 m thick volcaniclastic sequence of sandstones and mudstones (see Section 7.4.2.3). The lava flow is pale grey and densely vesiculated. The surface of the flow is jagged and bumpy having the appearance of a breccia (Fig. 7.10). In thin section, the lava flow consists of phenocryst glomerocrysts (*ca.* 5 vol.%) set in a very finely crystalline groundmass made up of plagioclase feldspar, clinopyroxene and oxides (Fig. 7.11). The glomerocrysts consist of laths of plagioclase feldspar with a maximum size of *ca.* 3 mm and altered subhedral crystals of olivine with a maximum size of *ca.* 1 mm. The basalt lava flow does not appear to be brecciated in thin section suggesting that the lava has been welded together. As much as 25 vol.% of the lava flow is vesiculated. The vesicles are lined by secondary minerals such as zeolites and calcite but are not filled.

7.2.6 Internal Structure

Apart from the agglutinated lava flows that are highly vesiculated (see Section 7.2.5) the tabular lava flows of the UBF are massive, with a uniform and disperse vesicular pattern.

Fig. 7.10. Views of an agglutinated lava flow that occurs *ca.* 200 m SE of Hálgafelli summit, *ca.* 420-430 m above sea level, *ca.* 1 km SW of Klaksvík, Borðoy, Faeroe Islands. The lava flow is *ca.* 8 m thick and overlies a *ca.* 4.7 m thick volcaniclastic sequence of sandstones and mudstones. The lava flow is pale grey and densely vesiculated. The surface of the flow is jagged and bumpy having the appearance of a breccia. The hammer is *ca.* 40 cm long and the lens cap is *ca.* 6 cm across.

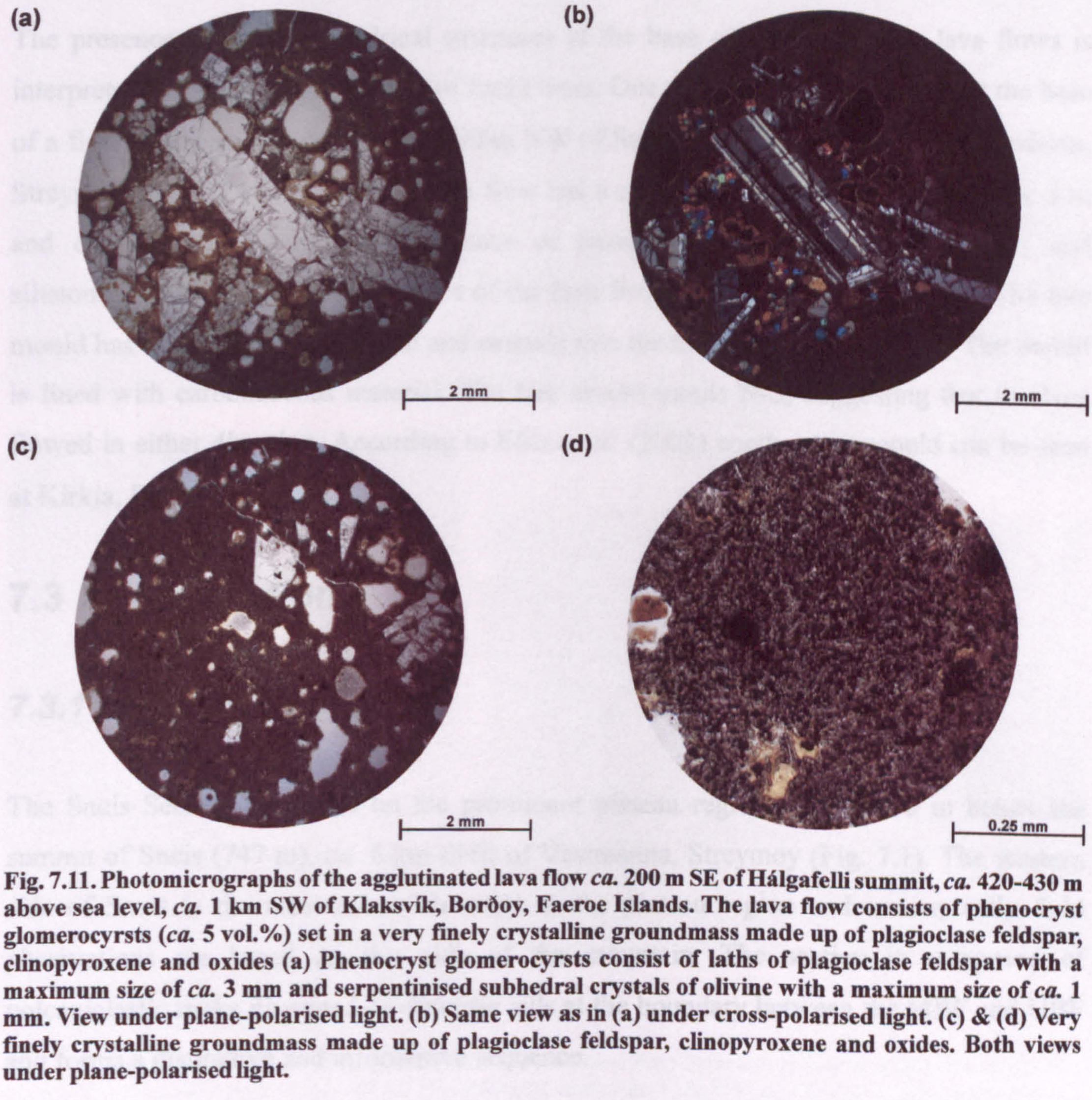

Fig. 7.11. Photomicrographs of the agglutinated lava flow *ca.* 200 m SE of Hálgafelli summit, *ca.* 420-430 m above sea level, *ca.* 1 km SW of Klaksvík, Borðoy, Faeroe Islands. The lava flow consists of phenocryst glomerocyrsts (*ca.* 5 vol.%) set in a very finely crystalline groundmass made up of plagioclase feldspar, clinopyroxene and oxides (a) Phenocryst glomerocyrsts consist of laths of plagioclase feldspar with a maximum size of *ca.* 3 mm and serpentinised subhedral crystals of olivine with a maximum size of *ca.* 1 mm. View under plane-polarised light. (b) Same view as in (a) under cross-polarised light. (c) & (d) Very finely crystalline groundmass made up of plagioclase feldspar, clinopyroxene and oxides. Both views under plane-polarised light.

The tabular lava flows have densely populated vesicular and rubbly flow tops that are generally 1-2 m thick. As with the LBF lava flows, pipe vesicles are rare or absent from the base of the tabular lava flows of the UBF. There is also a lack of vesicles within the lower and middle sections of the tabular lava flows from the UBF. Horizontal vesicle sheets and vertical vesicle cylinders are similarly lacking from the UBF lava flows.

7.2.7 Fossil Trees

The presence of empty cylindrical structures at the base of several tabular lava flows is interpreted to represent the moulds of fossil trees. One such tree mould is found at the base of a flow in a road side cutting, *ca.* 900 m NW of Sundshálsur, *ca.* 5 km NW of Tórshavn, Streymoy (Figs. 7.1 & 7.12). The lava flow has a minimum exposed thickness of *ca.* 3 m and overlies *ca.* 1.2 m thick sequence of cross-laminated fluviatile sandstones and siltstones (Ellis *et al.* 2002). The base of the lava flow is hummocky and uneven. The tree mould has a diameter of *ca.* 30 cm and extends into the lava flow for *ca.* 76 cm. The mould is lined with carbonaceous material. The tree mould trends N-S, suggesting that the lava flowed in either direction. According to Ellis *et al.* (2002) another tree mould can be seen at Kirkja, Fugloy.

7.3 Sneis Section

7.3.1 Summary of Section

The Sneis Section crops out on the prominent plateau region, *ca.* 60-100 m below the summit of Sneis (747 m), *ca.* 6 km ENE of Vestmanna, Streymoy (Fig. 7.1). The western side of Sneis is the most accessible route to the plateau region and consequently field observations are based on this side of the mountain. The section is composed of volcaniclastic rocks disrupted by doleritic sills at the boundary between the MBF and UBF and forms a distinctive and informative sequence.

7.3.2 Lithology & Petrography

Middle Basalt Formation plagioclase-phyric basalt lava flows of a compound nature crop out on the western side of Sneis. Overlying the MBF lava flows towards the top of the slope leading to the plateau region is Unit 1, a prominent *ca.* 2 m thick interval of scree composed of moderate reddish brown (10R 4/6) volcaniclastic sandstone. This sandstone is

Fig. 7.12. Views of a tree mould at the base of a tabular lava flow from the Upper Basalt Formation that occurs in a road side cutting, *ca.* 900 m NW of Sundshálsur, *ca.* 5 km NW of Tórshavn, Streymoy, Faeroe Islands. The tree mould has a diameter of *ca.* 30 cm and extends into the lava flow for *ca.* 76 cm. The mould is lined with carbonaceous material. The tree mould trends N-S, suggesting that the lava flowed in either direction. The lava flow overlies *ca.* 1.2 m thick sequence of cross-laminated fluviatile sandstones and siltstones. The hammer is *ca.* 40 cm long.

poorly sorted, has an average clast size of fine sand and is matrix supported (Fig. 7.13). Angular to sub-rounded, near opaque to orange palagonitised basaltic glass clasts (>95 vol.%) dominate the sandstone. High proportions of these clasts are highly vesiculated or exhibit cuspate margins. Clasts that contain large phenocrysts of plagioclase feldspar, account for no more than 10 vol.% of the sandstone. Unit 1 is overlain by a doleritic sill (see Section 7.3.5), which disrupts the sequence.

Unit 2 is a dusky red (5R 3/4) to greyish red (10R 4/2) volcaniclastic conglomerate that crops out on the plateau region around Sneis (Fig. 7.14). This conglomerate is poorly sorted and clast size ranges from <1 mm up to 26 cm, with an average clast size of *ca.* 6 cm (very coarse pebble grade). The clasts are sub-rounded to angular and the conglomerate is on the whole matrix supported (Fig. 7.15). Some of the clasts are comprised of laths of plagioclase feldspar, averaging 63-125 μm in length, contained within a very finely to finely crystalline groundmass of plagioclase feldspar, clinopyroxene and oxides. Other clasts consist of phenocrysts of plagioclase feldspar, averaging 63-125 μm in length, in an opaque glassy groundmass. Both clast types have highly irregular edges, ranging from u-shaped protrusions to very angular v-shaped incisions. Euhedral to subhedral crystals of serpentinised olivine occur in a small proportion of the clasts (<10 vol.%). The olivine crystals, with or without plagioclase feldspar, generally form a glomerophyric texture within the clasts. Some of the clasts appear to be cemented together by a brownish green zeolitic cement. The upper section of the volcaniclastic conglomerate is thickly laminated (*ca.* 1-3 cm) and is moderate reddish brown (10R 4/6) due to the presence of abundant angular near opaque to orange palagonitised basaltic glass clasts (Fig. 7.16), which do not occur in the lower section of the conglomerate. These glassy clasts range in size from <63 up to 500 μm and are commonly vesiculated and display cuspate margins.

Unit 3 is a dark yellowish orange (10YR 6/6) volcaniclastic sandstone. This poorly sorted and clast supported sandstone is obscured by scree but has a minimum thickness of *ca.* 2 m (Fig. 7.17). It is dominated by very angular to sub-rounded highly palagonitised near opaque to brownish to creamy yellow basaltic glass (>95 vol.%), which ranges in size from very fine to fine sand (63 to 250 μm). Some of the clasts are vesiculated and display cuspate margins. The sandstone also contains sub-rounded clasts of equigranular basalt consisting of laths of plagioclase feldspar, clinopyroxene and oxides (Figs. 7.17a & c). These clasts account for *ca.* 5 vol.% of the sandstone and have a maximum size of *ca.* 0.5 mm. The sandstone has very little zeolitic cement. Overlying Unit 3 is a tabular lava flow *ca.* 6-10 m thick from the UBF.

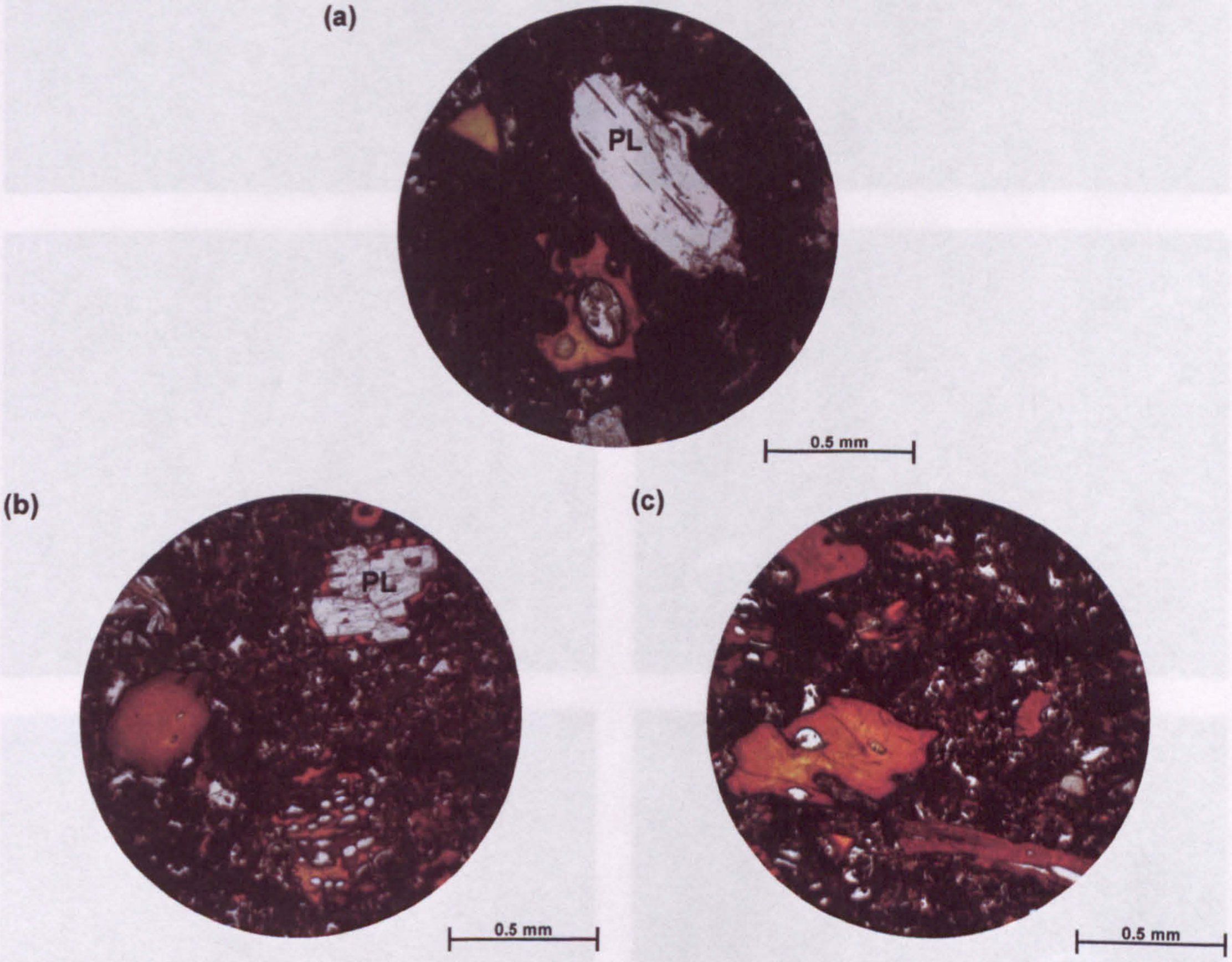

Fig. 7.13. Photomicrographs of Unit 1, a moderate reddish brown volcaniclastic sandstone that crops out *ca.* 800 m NW from the summit of Sneis (747 m), *ca.* 6 km ENE of Vestmanna, Streymoy, Faeroe Islands. All of the photomicrographs are under plane-polarised light. (a) to (c) The sandstone is poorly sorted, has an average clast size of fine sand and is matrix supported. Angular to sub-rounded, near opaque to orange palagonitised basaltic glass clasts (>95 vol.%) dominate the sandstone. High proportions of these clasts are highly vesiculated or exhibit cuspate margins. Clasts that contain large phenocrysts of plagioclase feldspar (PL), account for no more than 10 vol.% of the sandstone.

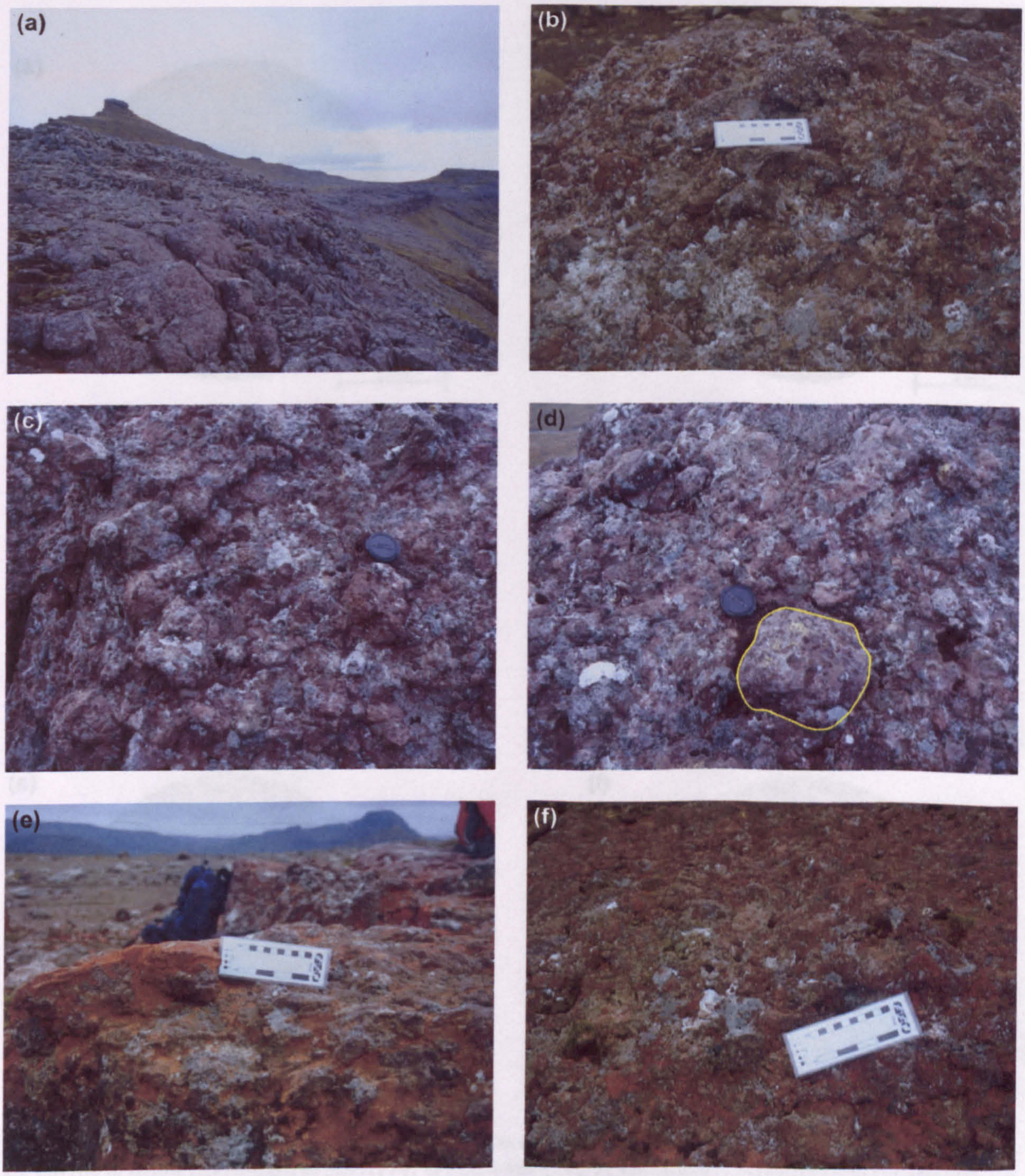

Fig. 7.14. Views of Unit 2, volcaniclastic conglomerate, that crops out on the plateau region, *ca.* 60-100 m below the summit of Sneis (747 m), *ca.* 6 km ENE of Vestmanna, Streymoy, Faeroe Islands. (a) to (d) The conglomerate is poorly sorted and clast size ranges from <1 mm up to 26 cm, with an average clast size of *ca.* 6 cm (very coarse pebble grade). The clasts are sub-rounded to angular and the conglomerate is on the whole matrix supported. The clasts are composed of various forms of basalt. (e) & (f) The upper section of the volcaniclastic conglomerate is thickly laminated (*ca.* 1-3 cm) and is moderate reddish brown due to the presence of abundant angular near opaque to orange palagonitised basaltic glass clasts, which do not occur in the lower section of the conglomerate. The white card is *ca.* 16 x 6 cm and the lens cap is *ca.* 6 cm across.

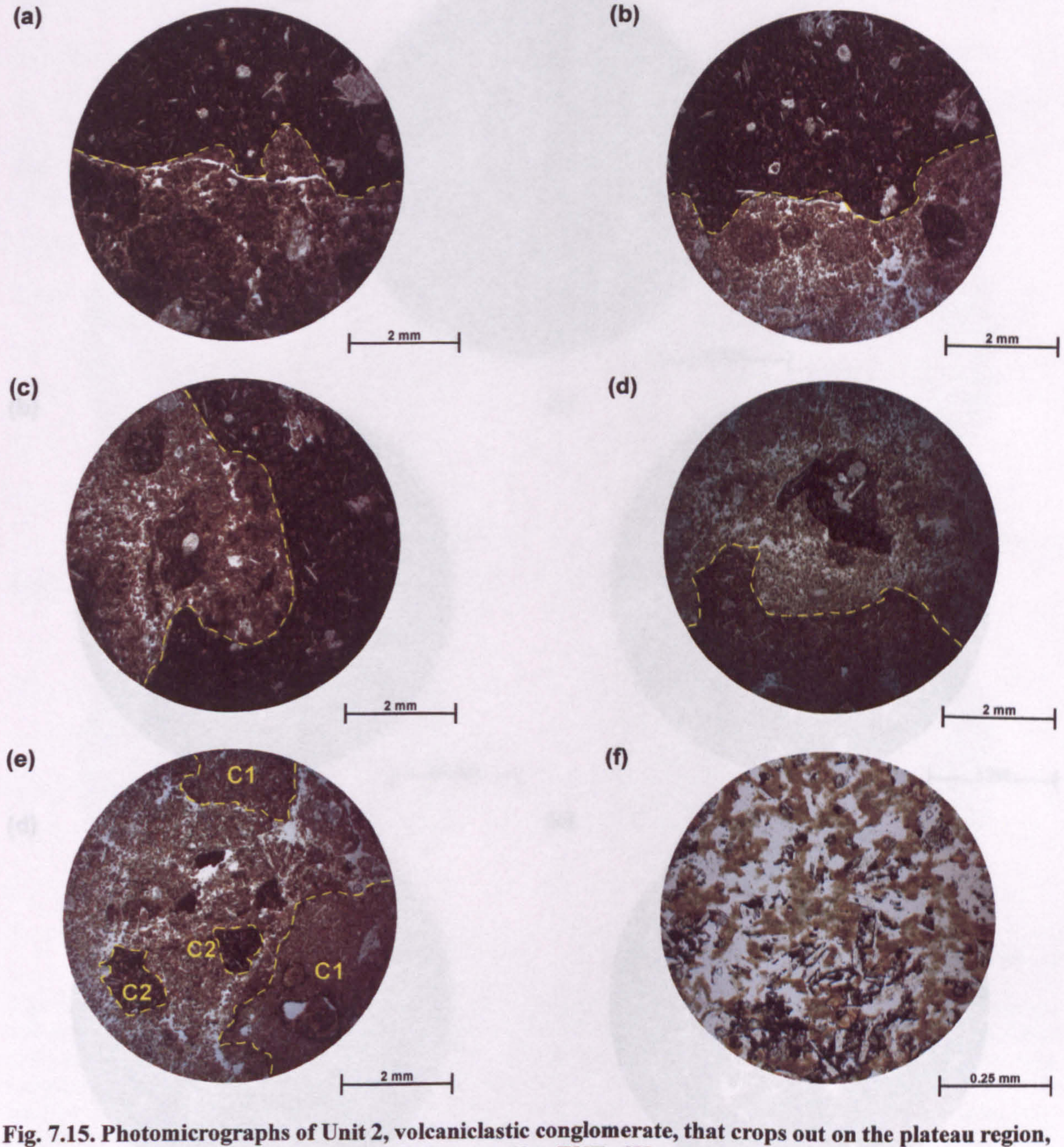

Fig. 7.15. Photomicrographs of Unit 2, volcaniclastic conglomerate, that crops out on the plateau region, *ca.* 60-100 m below the summit of Sneis (747 m), *ca.* 6 km ENE of Vestmanna, Streymoy, Faeroe Islands. All of the photomicrographs are under plane-polarised light. (a) to (d) The basalt clasts are sub-rounded to angular and the conglomerate is on the whole matrix supported. Clasts have highly irregular edges, ranging from u-shaped protrusions to very angular v-shaped incisions. (e) Some of the clasts are comprised of laths of plagioclase feldspar, averaging 63-125 μm in length, contained within a very finely to finely crystalline groundmass of plagioclase feldspar, clinopyroxene and oxides (C1). Other clasts consist of phenocrysts of plagioclase feldspar, averaging 63-125 μm in length, in an opaque glassy groundmass (C2). (f) Some of the clasts appear to be cemented together by a brownish green zeolitic cement.

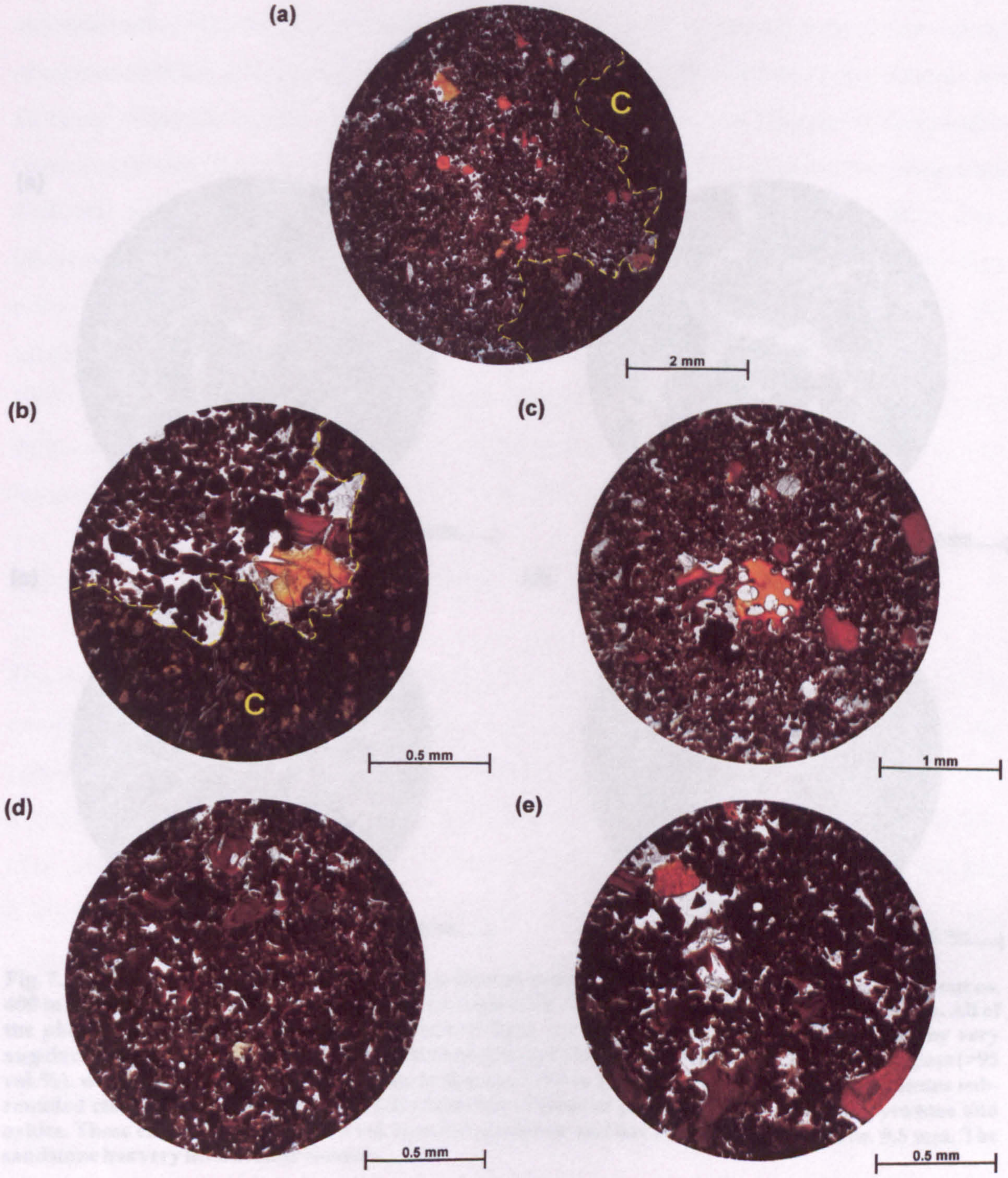

Fig. 7.16. Photomicrographs of the upper section of Unit 2, volcaniclastic conglomerate, that crops out on the plateau region, *ca.* 60-100 m below the summit of Sneis (747 m), *ca.* 6 km ENE of Vestmanna, Streymoy, Faeroe Islands. All of the photomicrographs are under plane-polarised light. (a) & (b) The large irregular shaped basalt clasts (C) are set in a matrix of angular near opaque to orange palagonitised basaltic glass clasts. (c) to (e) These near opaque to orange palagonitised glassy clasts range in size from <63 up to 500 μm and are commonly vesiculated and display cuspate margins, the remains of former bubble walls.

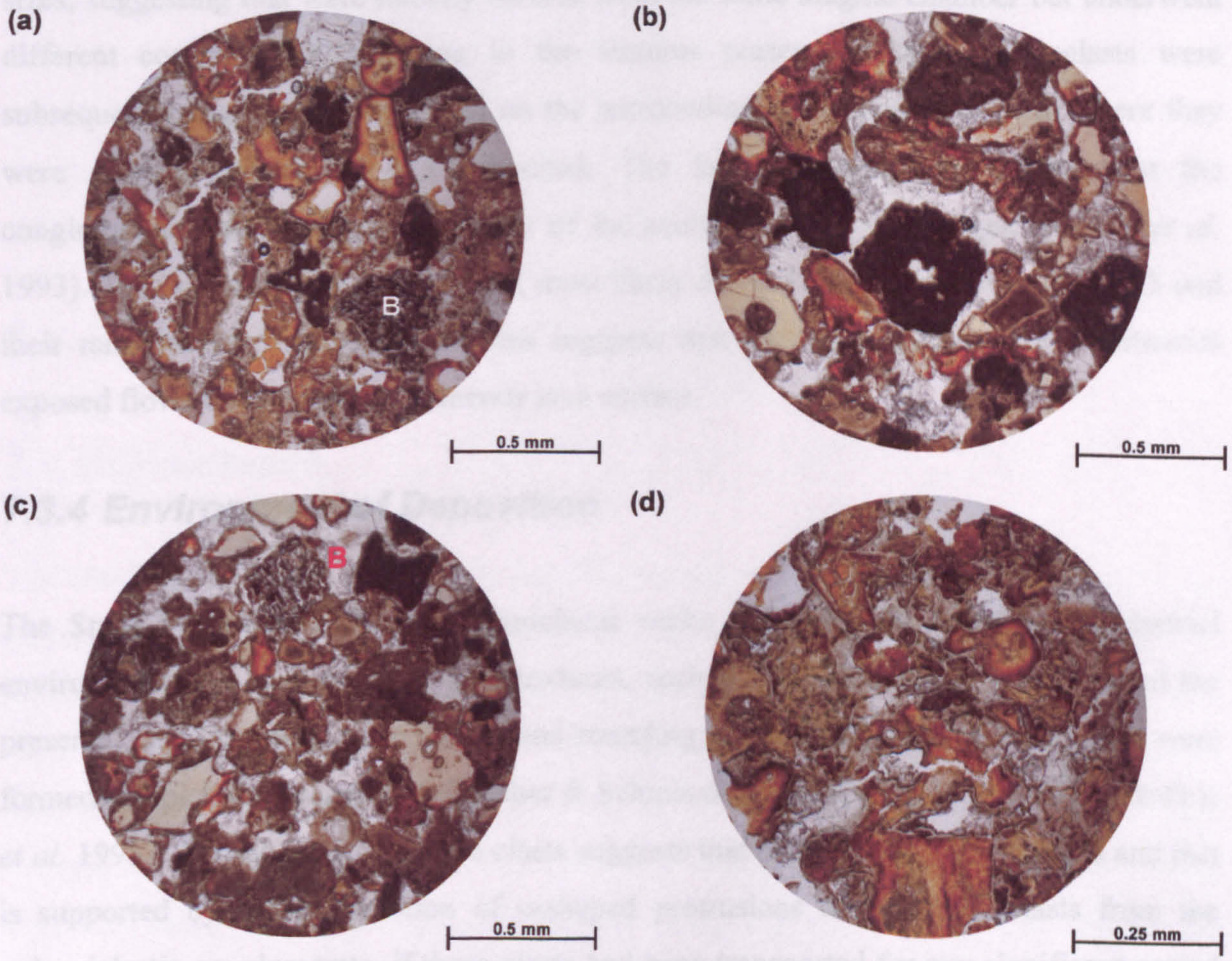

Fig. 7.17. Photomicrographs of Unit 3, a dark yellowish orange volcaniclastic sandstone, that crops out *ca.* 400 m NW from the summit of Sneis (747 m), *ca.* 6 km ENE of Vestmanna, Streymoy, Faeroe Islands. All of the photomicrographs are under plane-polarised light. (a) to (d) The sandstone is dominated by very angular to sub-rounded highly palagonitised near opaque to brownish to creamy yellow basaltic glass (>95 vol.%), which ranges in size from very fine to fine sand (63 to 250 μm). The sandstone also contains sub-rounded clasts of equigranular basalt (B) consisting of laths of plagioclase feldspar, clinopyroxene and oxides. These clasts account for *ca.* 5 vol.% of the sandstone and have a maximum size of *ca.* 0.5 mm. The sandstone has very little zeolitic cement.

7.3.3 Provenance

All of the volcaniclastic rocks from the Sneis Section consist of clasts derived from sources within the depositional area. A common clast type observed in all three of the volcaniclastic rocks is palagonitised basaltic glass, which were derived from the reworking of unconsolidated ash deposits. The phenoclasts from the volcaniclastic conglomerate are all compositionally similar and contain phenocrysts of plagioclase feldspar of comparable sizes, suggesting that were initially derived from the same magma chamber but underwent different cooling rates, resulting in the textures preserved. These phenoclasts were subsequently erupted and deposited on the surrounding volcanic edifice from where they were eroded, transported and deposited. The lack of clast type variation in the conglomerate reflects the homogeneity of the source volcanic edifice (cf. McPhie *et al.* 1993). The occurrence of basalt clasts, most likely derived from lava flows, in Unit 3 and their range in surface oxidation states suggests that they were derived from numerous exposed flows on the contemporaneous lava surface.

7.3.4 Environment of Deposition

The Sneis Section consists of volcaniclastic rocks that were deposited in a terrestrial environment. The lack of pyroclastic textures, such as glass shards and welding, and the preservation of bedding, poor sorting and rounding of clasts indicates that the rocks were formed by epiclastic processes (cf. Fisher & Schmincke 1984; Cas & Wright 1987; McPhie *et al.* 1993). Partial rounding of the clasts suggests that transportation was limited and this is supported by the preservation of u-shaped protrusions on the phenoclasts from the volcaniclastic conglomerate, if these clasts had been transported for any significant period of time these u-shaped protrusions would have been worn down or broken off. The conglomerate is poorly sorted, non-graded, matrix supported, and has a tabular geometry, which indicates that the rock was transported and deposited as a type of epiclastic mass flow (cf. Cas & Wright 1987; Smith & Lowe 1991; McPhie *et al.* 1993). The lack of megablocks, greater than 10 m in size, and fracturing of clasts suggests that the conglomerate is a volcaniclastic debris flow (cf. Yarnold 1993). The inclusion of basaltic glass fragments in the upper section of the volcaniclastic conglomerate implies that an eruption had begun before the debris flow became stagnant and according to Smith (1991) volcaniclastic debris flows are commonly deposited during syn-eruption periods.

7.3.5 Intrusive Lithologies

The volcaniclastic lithologies between the MBF and the UBF on Sneis have has been disrupted by a dark grey (N3) finely crystalline basaltic sill (Figs. 7.18 & 7.19). The sill exhibits a foliation in hand specimen, due to the alignment of plagioclase feldspar in the groundmass. The orientation of this foliation indicates locally the direction in which the sill was travelling. Where the foliation is in a vertical orientation it suggests that this part of the sill represents a vertical conduit flowing towards the surface. Where the sill is in contact with the volcaniclastic conglomerate the foliation is commonly in a horizontal orientation, suggesting that the sill spread laterally into the poorly lithified volcaniclastic conglomerate. The sill is equigranular and consists of laths of plagioclase feldspar, subhedral crystals of clinopyroxene and olivine, and angular oxides (Fig. 7.19).

7.4 Interlava Lithologies

7.4.1 Occurrence

The interlava lithologies observed in the UBF consist primarily of volcaniclastic lutites to rudites. Volcaniclastic sandstones are by far the most common interlava lithology. A number of localities are described below giving an overall picture of the volcaniclastic rocks observed throughout the UBF. From east to west the localities described are as follows: (i) Kirkja Section, *ca.* 50 m E of the Kirkja harbour, Fugloy (Fig. 7.2); (ii) Gjógvin Stóra Section, *ca.* 100-150 m above sea level, *ca.* 5 km SE of Viðareiði, Viðoy (Fig. 7.2); (iii) Hálgafelli Section, *ca.* 400-430 m above sea level, *ca.* 200 m SE from the summit of Hálgafelli, *ca.* 1 km SW of Klaksvík, Borðoy (Fig. 7.2); (iv) Kunoy Section, *ca.* 500-780 m above sea level, *ca.* 800 m S from the summit of Middagsfjall, *ca.* 1.5 km NE of Kunoy, Kunoy (Fig. 7.2); (v) Lítlavatn Section, a roadside cutting between Sandur and Skálavík, *ca.* 400 m N of Lítlavatn, Sandoy (Fig. 7.1); and (vi) Argir Section, a roadside cutting, *ca.* 600 m E of Itróttavøllur, *ca.* 1 km W of Argir, Streymoy (Fig. 7.1).

7.4.2 Lithology & Petrography

7.4.2.1 Kirkja Section

The Kirkja Section consists of a sequence of two volcaniclastic sandstones inbetween tabular lava flows of the UBF (Fig. 7.20). The basal lava flow is a plagioclase-phyric basalt

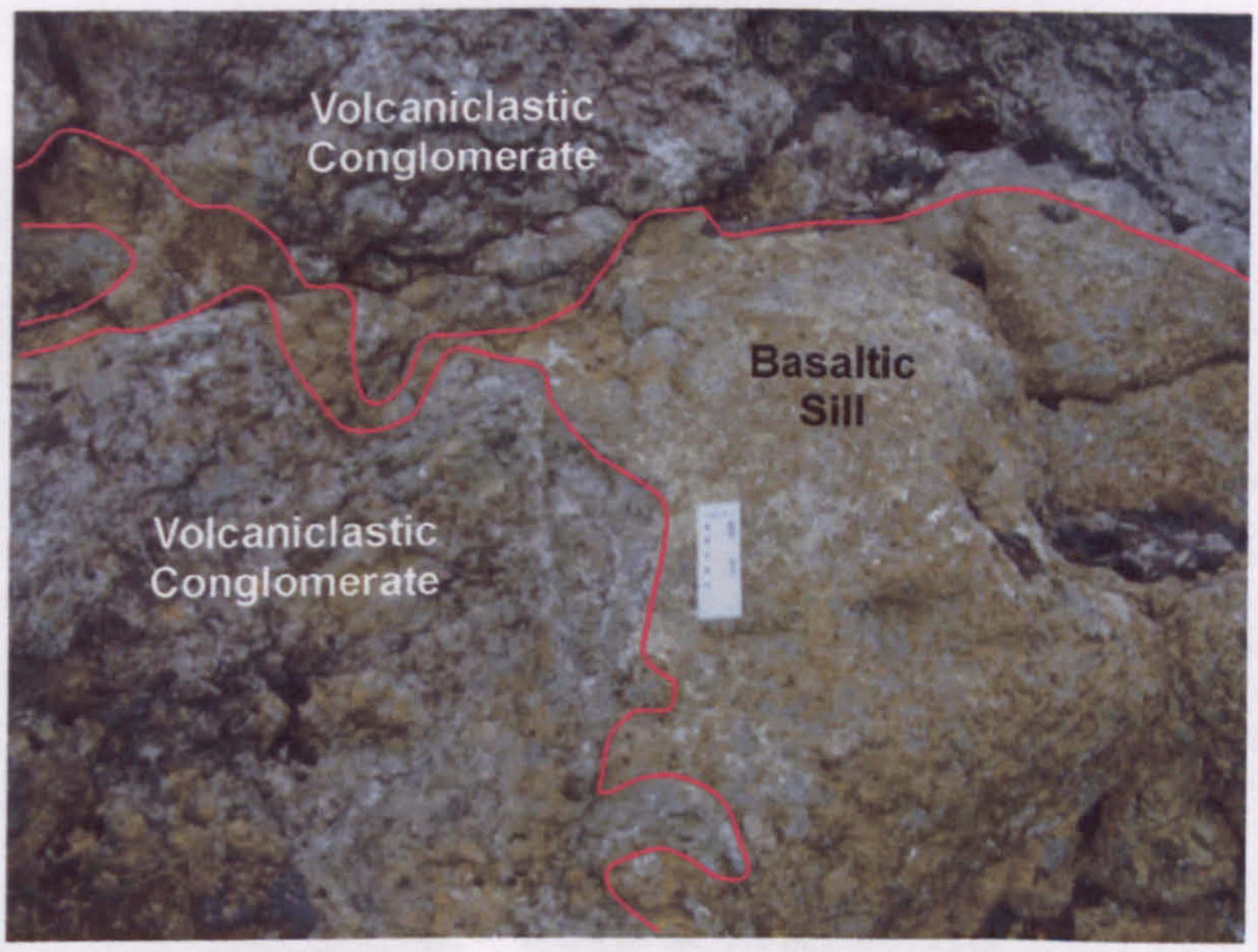

Fig. 7.18. View of the finely crystalline basaltic sill that crops out on the plateau region, *ca.* 60-100 m below the summit of Sneis (747 m), *ca.* 6 km ENE of Vestmanna, Streymoy, Faeroe Islands. The sill has intruded a poorly lithified volcaniclastic conglomerate.

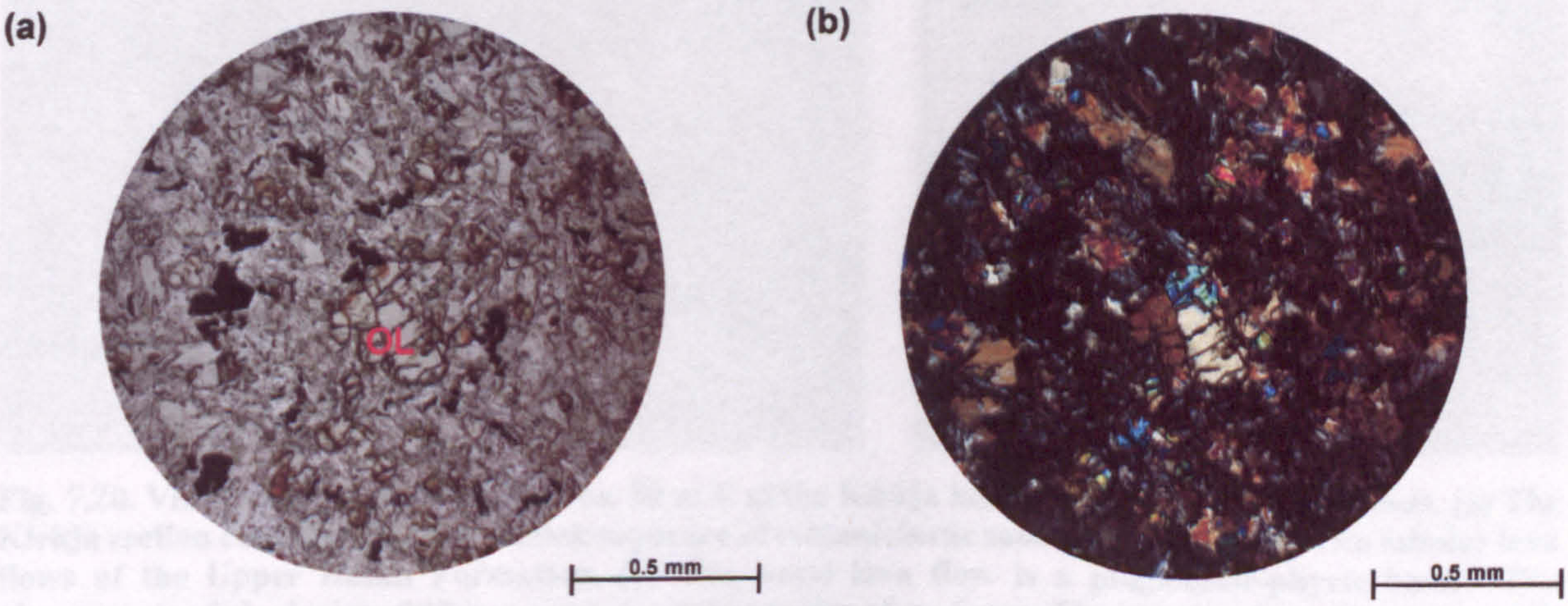

Fig. 7.19. Photomicrographs of the finely crystalline basaltic sill that crops out on the plateau region, *ca.* 60-100 m below the summit of Sneis (747 m), *ca.* 6 km ENE of Vestmanna, Streymoy, Faeroe Islands. (a) The sill is equigranular and consists of laths of plagioclase feldspar, subhedral crystals of clinopyroxene and olivine (OL), and angular oxides. The photomicrograph is under plane-polarised light. (b) Same as in (a) but under cross-polarised light.

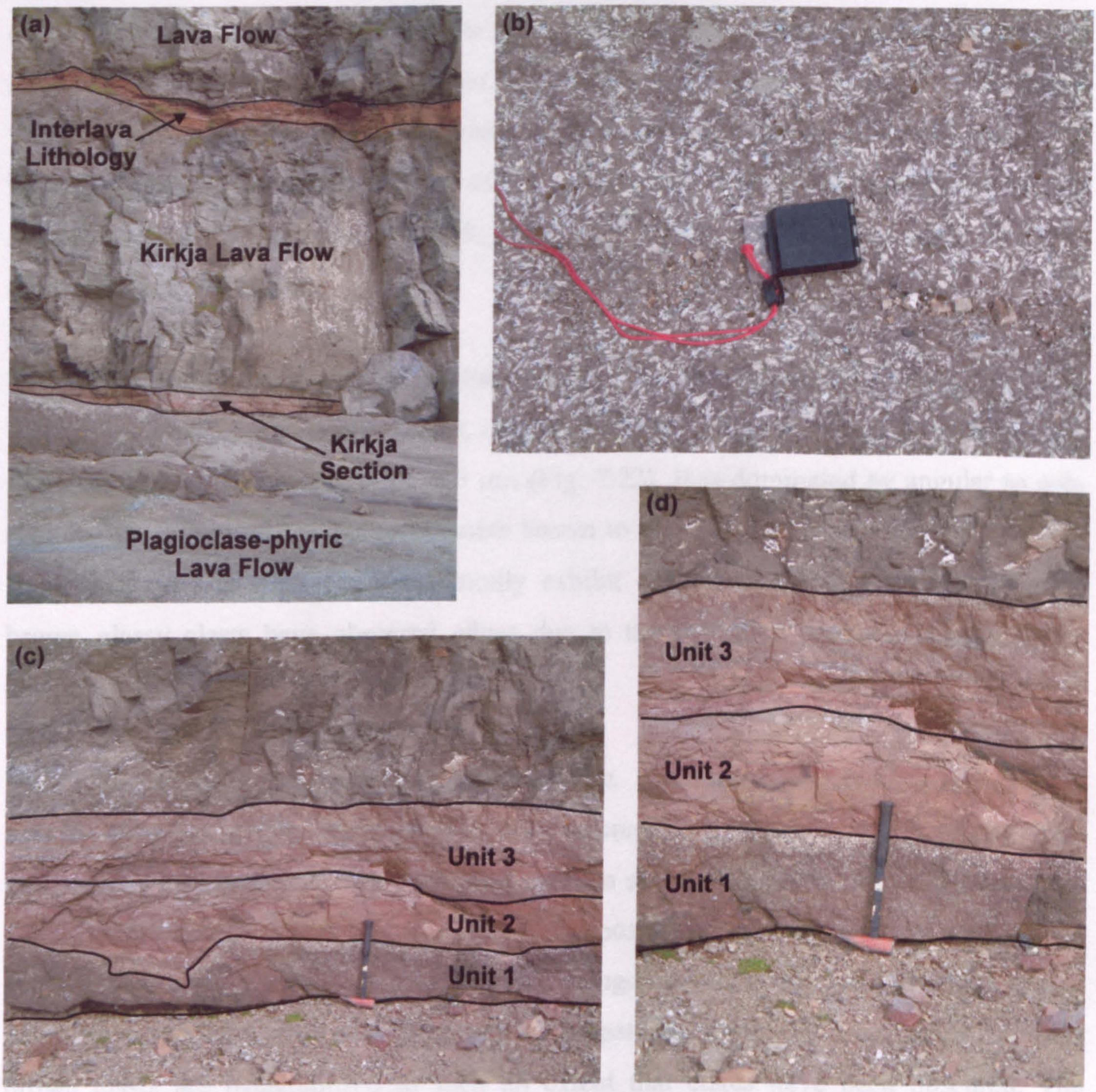

Fig. 7.20. Views of the Kirkja Section, *ca.* 50 m E of the Kirkja harbour, Fugloy, Faeroe Islands. (a) The Kirkja section consists of a *ca.* 1 m thick sequence of volcaniclastic sandstones inbetween two tabular lava flows of the Upper Basalt Formation. (b) The basal lava flow is a plagioclase-phyric basalt. The phenocrysts of plagioclase feldspar reach a maximum size of *ca.* 6 mm. The compass is *ca.* 10 x 6 cm. (c) & (d) The Kirkja Section consists of three volcaniclastic sandstone units: 1, 2, and 3. Unit 1 is a *ca.* 20 cm thick, Unit 2 is a *ca.* 23 cm thick and Unit 3 is a *ca.* 25 cm thick. The hammer is *ca.* 40 cm long.

(Fig. 7.20b), with phenocrysts of plagioclase feldspar reaching a maximum size of *ca.* 6 mm. The upper *ca.* 8 cm of the lava is mauve coloured and vesicle rich. Overlying the lava is Unit 1, a *ca.* 20 cm thick moderate reddish brown (10R 5/4) volcaniclastic sandstone (Fig. 7.20). This sandstone is poorly sorted, matrix supported, with an average clast size of very fine to fine sand and a maximum size of 500 μm (Fig. 7.21). It is dominated by angular to sub-rounded palagonitised opaque to orange basaltic glass clasts. Some of the clasts exhibit shard textures and cuspate margins. The opaque clasts are usually vesiculated and contain laths of plagioclase feldspar. Plagioclase-bearing clasts account for less than 5 vol.% of the sandstone. The finer grained clasts have edges that are obscured due to the hydration process. Less than 5 vol.% of the sandstone is made up of sub-angular to sub-rounded clasts of equigranular basalt, which consist of laths of plagioclase feldspar, clinopyroxene and oxides.

Unit 2 is a *ca.* 23 cm thick pale reddish brown (10R 5/4) volcaniclastic sandstone (Fig. 7.20). This sandstone is poorly sorted, clast supported, with an average clast size of very fine sand and a maximum size of 300 μm (Fig. 7.22). It is dominated by angular to sub-rounded palagonitised opaque to greenish brown to pale yellow basaltic glass clasts. The larger pale yellow glass clasts commonly exhibit cuspate margins. The finer greenish brown glassy clasts have obscured edges due to the hydration process. The sandstone contains <5 vol.% of zeolitic cement.

Unit 3 is a *ca.* 25 cm thick, thickly laminated (*ca.* 10-20 mm), pale reddish brown (10R 5/4) to pale yellowish brown (10YR 6/2) volcaniclastic sandstone (Fig. 7.20). This sandstone is poorly sorted, clast supported, with an average clast size of medium sand and a maximum size of 0.8 mm (Fig. 7.23). It is composed entirely of angular to sub-rounded palagonitised opaque to reddish brown to pale orange basaltic glass clasts. The pale orange glass clasts exhibit shard textures as well as cuspate margins. The finer grained reddish brown clasts are palagonitised to such an extent that edges have been obscured. The sandstone is overlain by an 8 m thick tabular lava flow (Fig. 7.20), the lower *ca.* 40 cm of which displays vesicles with a maximum size of *ca.* 6 cm. The lava flow is in turn overlain by another *ca.* 1 m thick volcaniclastic sequence. Unfortunately, the exposure is inaccessible and unable to be examined.

7.4.2.2 Gjógvin Stóra Section

The Gjógvin Stóra Section consists of a sequence through the UBF above the first tabular lava flow of the UBF (Fig. 7.24). The good exposure at Gjógvin Stóra is a consequence of

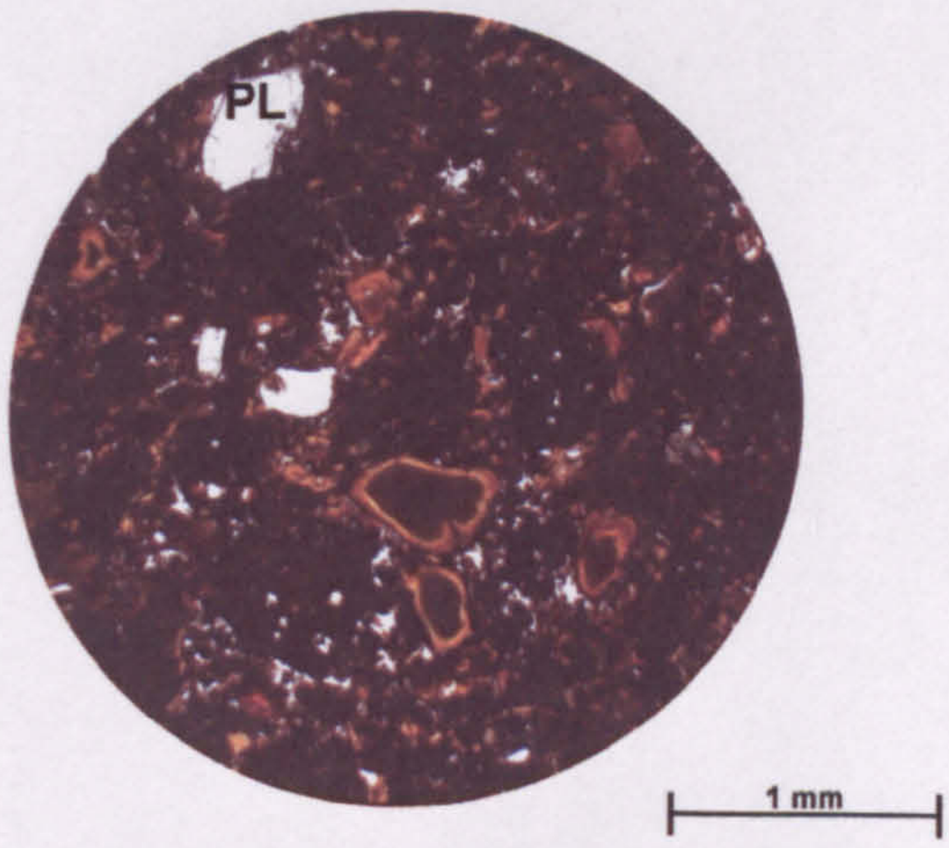

Fig. 7.21. Photomicrograph of Unit 1, volcaniclastic sandstone, Kirkja Section, *ca.* 50 m E of the Kirkja harbour, Fugloy, Faeroe Islands. The photomicrograph is under plane-polarised light. The sandstone is poorly sorted, matrix supported, with an average clast size of very fine to fine sand and a maximum size of 500 μm. It is dominated by angular to sub-rounded palagonitised opaque to orange basaltic glass clasts. Some of the clasts exhibit shard textures and cuspate margins. The opaque clasts are usually vesiculated and contain laths of plagioclase feldspar (PL). Plagioclase-bearing clasts account for less than 5 vol.% of the sandstone. The finer grained clasts have edges that are obscured due to the hydration process. Less than 5 vol.% of the sandstone is made up of sub-angular to sub-rounded clasts of equigranular basalt, which consist of laths of plagioclase feldspar, clinopyroxene and oxides.

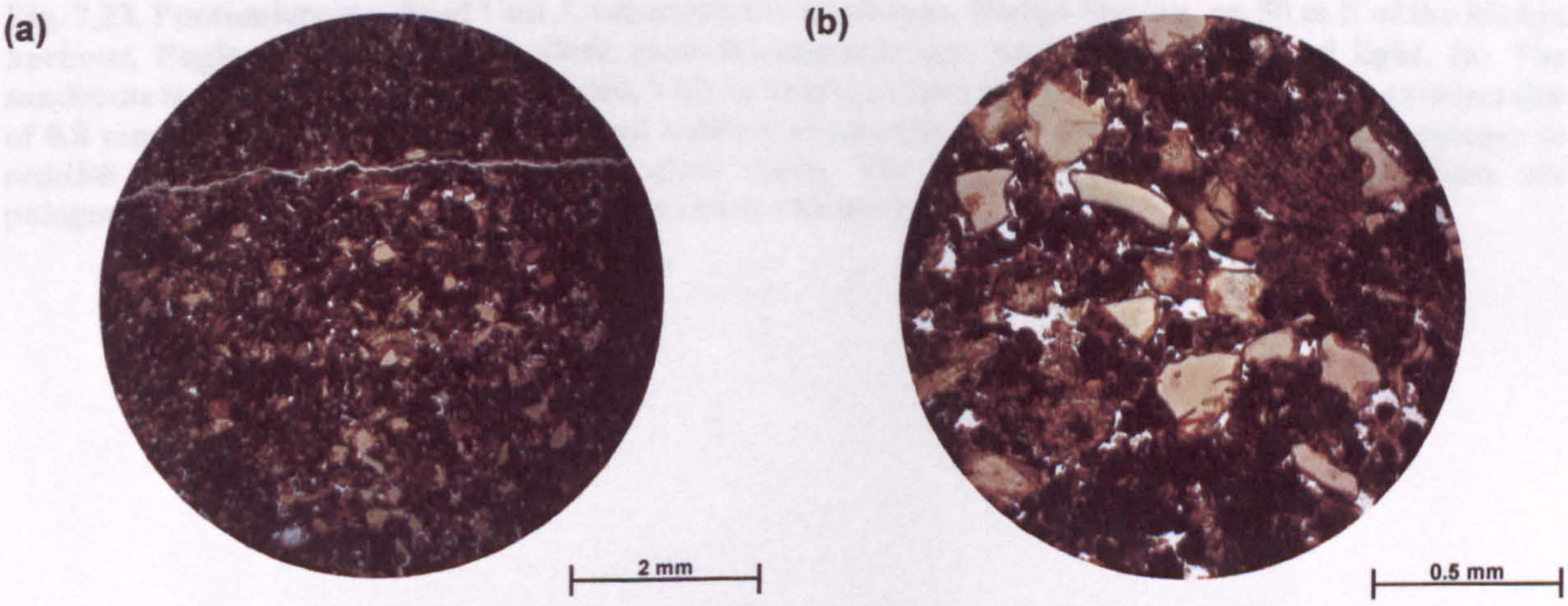

Fig. 7.22. Photomicrographs of Unit 2, volcaniclastic sandstone, Kirkja Section, *ca.* 50 m E of the Kirkja harbour, Fugloy, Faeroe Islands. Both photomicrographs are under plane-polarised light. (a) The sandstone is poorly sorted, clast supported, with an average clast size of very fine sand and a maximum size of 300 μm. (b) The sandstone is dominated by angular to sub-rounded palagonitised opaque to greenish brown to pale yellow basaltic glass clasts. The finer greenish brown glassy clasts have obscured edges due to the hydration process. The sandstone contains <5 vol.% of zeolitic cement.

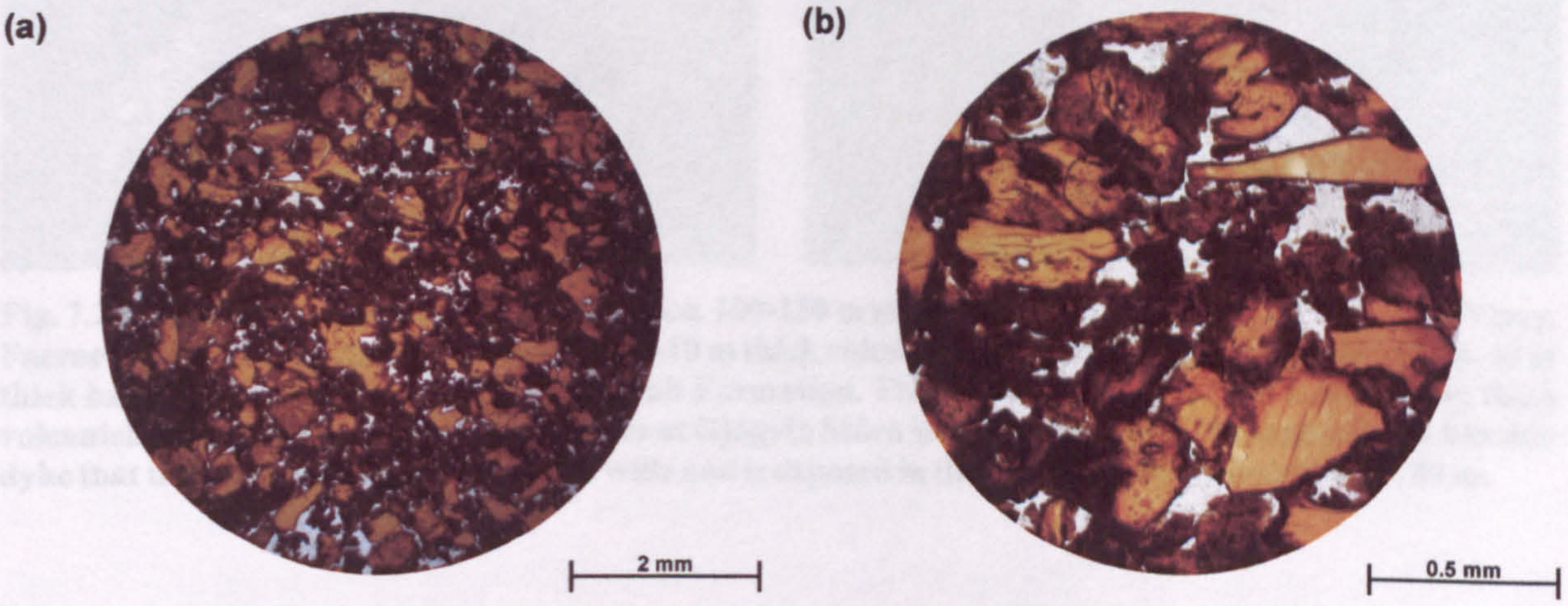

Fig. 7.23. Photomicrographs of Unit 3, volcaniclastic sandstone, Kirkja Section, *ca.* 50 m E of the Kirkja harbour, Fugloy, Faeroe Islands. Both photomicrographs are under plane-polarised light. (a) The sandstone is poorly sorted, clast supported, with an average clast size of medium sand and a maximum size of 0.8 mm. (b) The sandstone is composed entirely of angular to sub-rounded palagonitised opaque to reddish brown to pale orange basaltic glass clasts. The finer grained reddish brown clasts are palagonitised to such an extent that edges have been obscured.

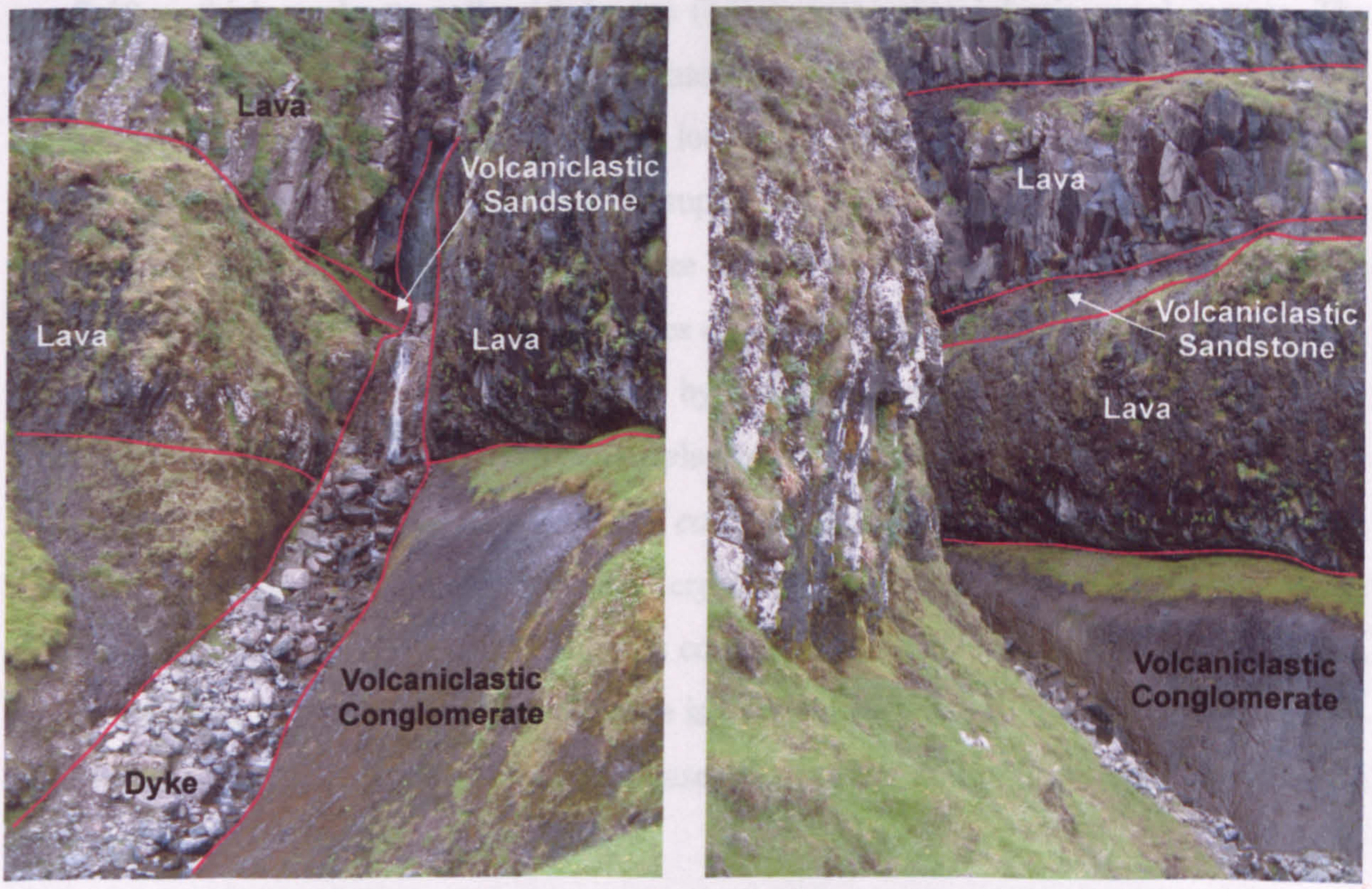

Fig. 7.24. Views of the Gjógvin Stóra Section, *ca.* 100-150 m above sea level, *ca.* 5 km SE of Viðareiði, Viðoy, Faeroe Islands. The section consists of a *ca.* 7-10 m thick volcaniclastic conglomerate overlain by a *ca.* 10 m thick basaltic lava flow from the Upper Basalt Formation. The lava flow is overlain by a *ca.* 0.6-2 m thick volcaniclastic sandstone. The good exposure at Gjógvin Stóra is a consequence of the presence of a basaltic dyke that trends E-W. The dyke is *ca.* 3 m wide and is exposed in the gully wall over a height of *ca.* 80 m.

Fig. 7.25. View of the volcaniclastic conglomerate from the Gjógvin Stóra Section, *ca.* 100-150 m above sea level, *ca.* 5 km SE of Viðareiði, Viðoy, Faeroe Islands. The conglomerate is poorly sorted, matrix supported, with an average clast size of coarse pebbles (*ca.* 2.5 x 3 cm) and a maximum size of *ca.* 15 x 12 cm. The penknife is *ca.* 8 cm in length.

the presence of a basaltic dyke that trends E-W. The dyke is *ca.* 3 m wide and is exposed in the gully wall over a height of *ca.* 80 m. The basal *ca.* 30 m thick lava flow is overlain by *ca.* 7-10 m thick moderate yellowish brown (10YR 5/4) volcaniclastic conglomerate. The contact between the lava and the conglomerate is not exposed. The conglomerate crops out for a distance of *ca.* 500 m to the N of this locality, before it is lost due to poor exposure. The conglomerate is poorly sorted, matrix supported, with an average clast size of coarse pebbles (*ca.* 2.5 x 3 cm) and a maximum size of *ca.* 15 x 12 cm (Fig. 7.25). The clasts are primarily sub-rounded, although angular ones do occur. In thin section, the conglomerate is homogenous in clast type, being dominated by plagioclase-phyric basalt clasts (Fig. 7.26). The clasts are comprised of phenocrysts of plagioclase feldspar, averaging *ca.* 100-200 μm in length and having a maximum length of *ca.* 1 cm, and are contained within an opaque glassy groundmass. Occasionally, anhedral crystals of clinopyroxene are observed and are less than 200 μm in size. Some of the clasts contain amoeboidal-shaped amygdales infilled by zeolites. The volcaniclastic conglomerate is overlain by a *ca.* 10 m thick lava flow with poorly developed prismatic jointing at its base. The middle and upper sections of the lava flow appear brecciated and agglutinated.

The lava flow is overlain by a moderate reddish brown (10R 4/6) volcaniclastic sandstone. This sandstone has a thickness between *ca.* 0.6 and 2 m and can be traced for at least 600 m S of Gjógvin Stóra. It is poorly sorted, clast supported, with an average clast size of very fine to fine sand and a maximum size of 500 μm (Fig. 7.27). The sandstone is wholly composed of angular to sub-rounded palagonitised opaque and orange basaltic glass clasts. Some of the clasts exhibit shard textures, vesicles and cuspate margins. Phenocrysts of plagioclase feldspar are observed in a small proportion of the clasts (<5 vol.%). The pore space of the sandstone has been partially infilled by zeolitic material. The sandstone is overlain by a *ca.* 10 m thick tabular lava flow, which displays a brecciated base.

7.4.2.3 Hálgafelli Section

The Hálgafelli Section consists of a *ca.* 4.7 m thick sequence of volcaniclastic siltstones and sandstones (Figs. 7.28 & 7.29). The section crops out *ca.* 6 m above a tabular lava flow of the UBF. Unit 1 consists of a moderate yellowish brown (10YR 5/4) highly altered volcaniclastic sandstone. This sandstone has a minimum thickness of *ca.* 1.8 m, is poorly sorted and clast supported (Fig. 7.30). The average clast size of the sandstone is medium to coarse sand, although clasts up to 3 mm occur. Approximately 20 vol.% of the sandstone consists of sub-rounded opaque basaltic glass clasts, characterised by an abundance of vesicles infilled by zeolitic material. The remainder of the sandstone consists of sub-

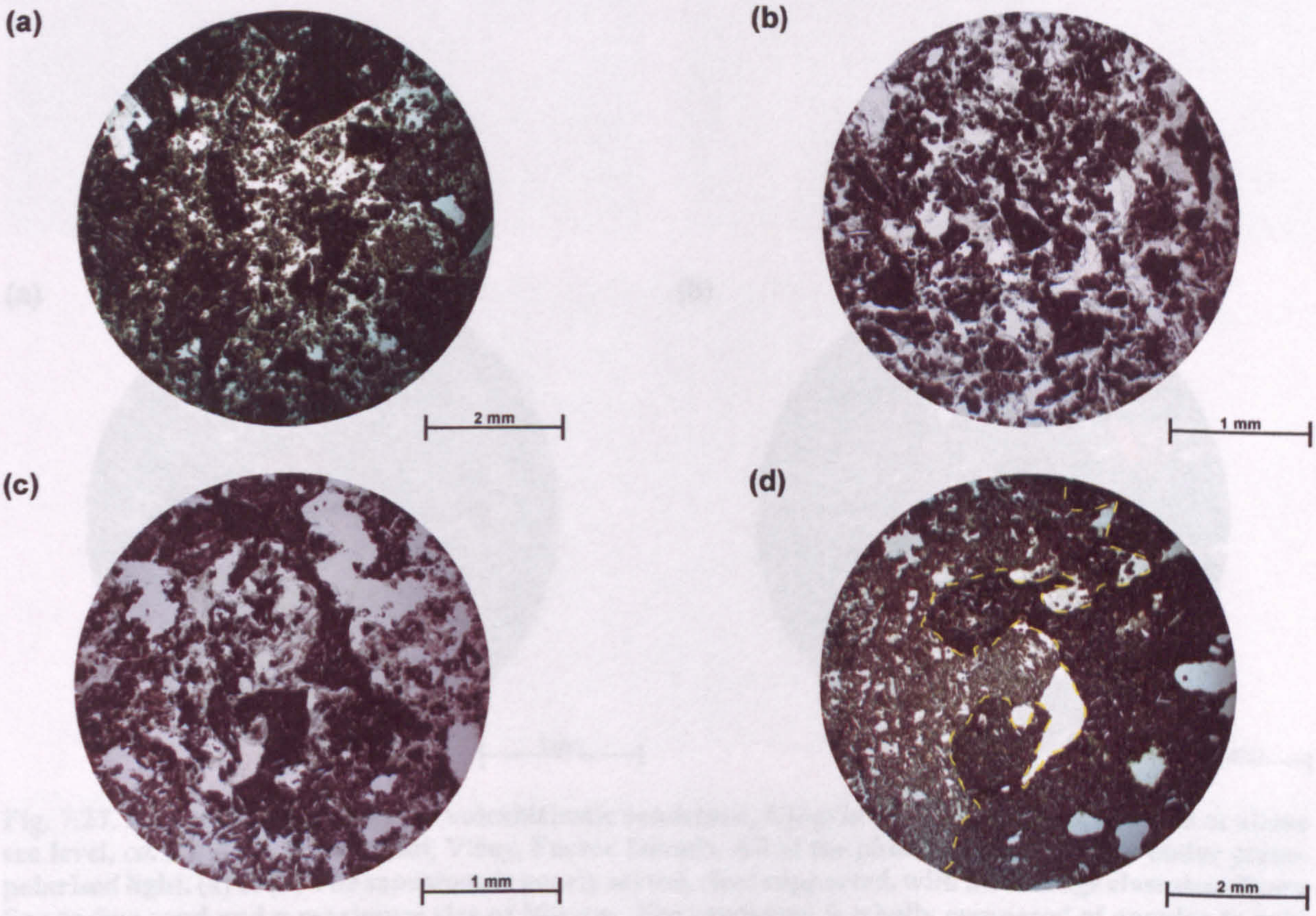

Fig. 7.26. Photomicrographs of the volcaniclastic conglomerate, Gjógvin Stóra Section, *ca.* 100-150 m above sea level, *ca.* 5 km SE of Viðareiði, Viðoy, Faeroe Islands. All of the photomicrographs are under plane-polarised light. (a) to (c) The conglomerate is poorly sorted, matrix supported, with an average clast size of coarse pebbles (*ca.* 2.5 x 3 cm) and a maximum size of *ca.* 15 x 12 cm. The clasts are primarily sub-rounded, although angular ones do occur. (d) Some of the clasts have irregular edges, ranging from u-shaped protrusions to v-shaped incisions. Clast type is very homogenous, being dominated by plagioclase-phyric basalt clasts. The clasts are comprised of phenocrysts of plagioclase feldspar, averaging *ca.* 100-200 μm in length and having a maximum length of *ca.* 1 cm, and are contained within an opaque glassy groundmass.

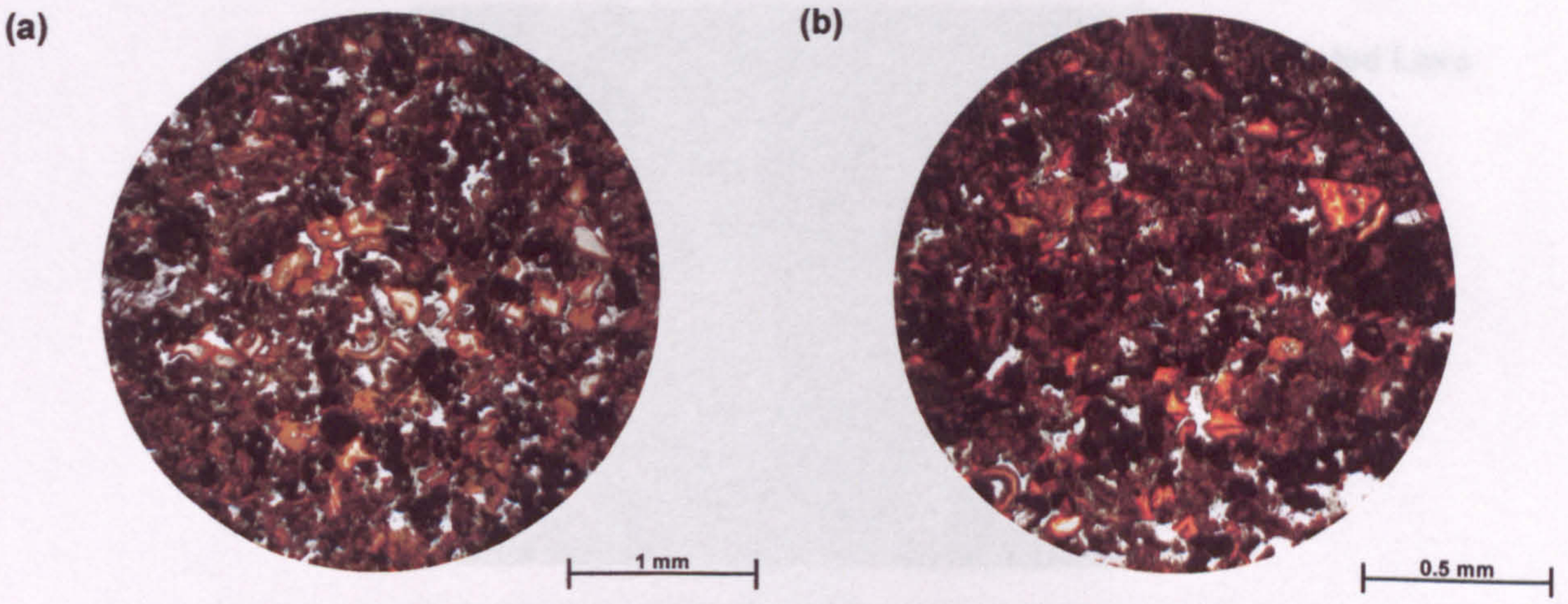

Fig. 7.27. Photomicrographs of the volcaniclastic sandstone, Gjógvin Stóra Section, *ca.* 100-150 m above sea level, *ca.* 5 km SE of Viðareiði, Viðoy, Faeroe Islands. All of the photomicrographs are under plane-polarised light. (a) & (b) The sandstone is poorly sorted, clast supported, with an average clast size of very fine to fine sand and a maximum size of 500 μm. The sandstone is wholly composed of angular to sub-rounded palagonitised opaque and orange basaltic glass clasts.

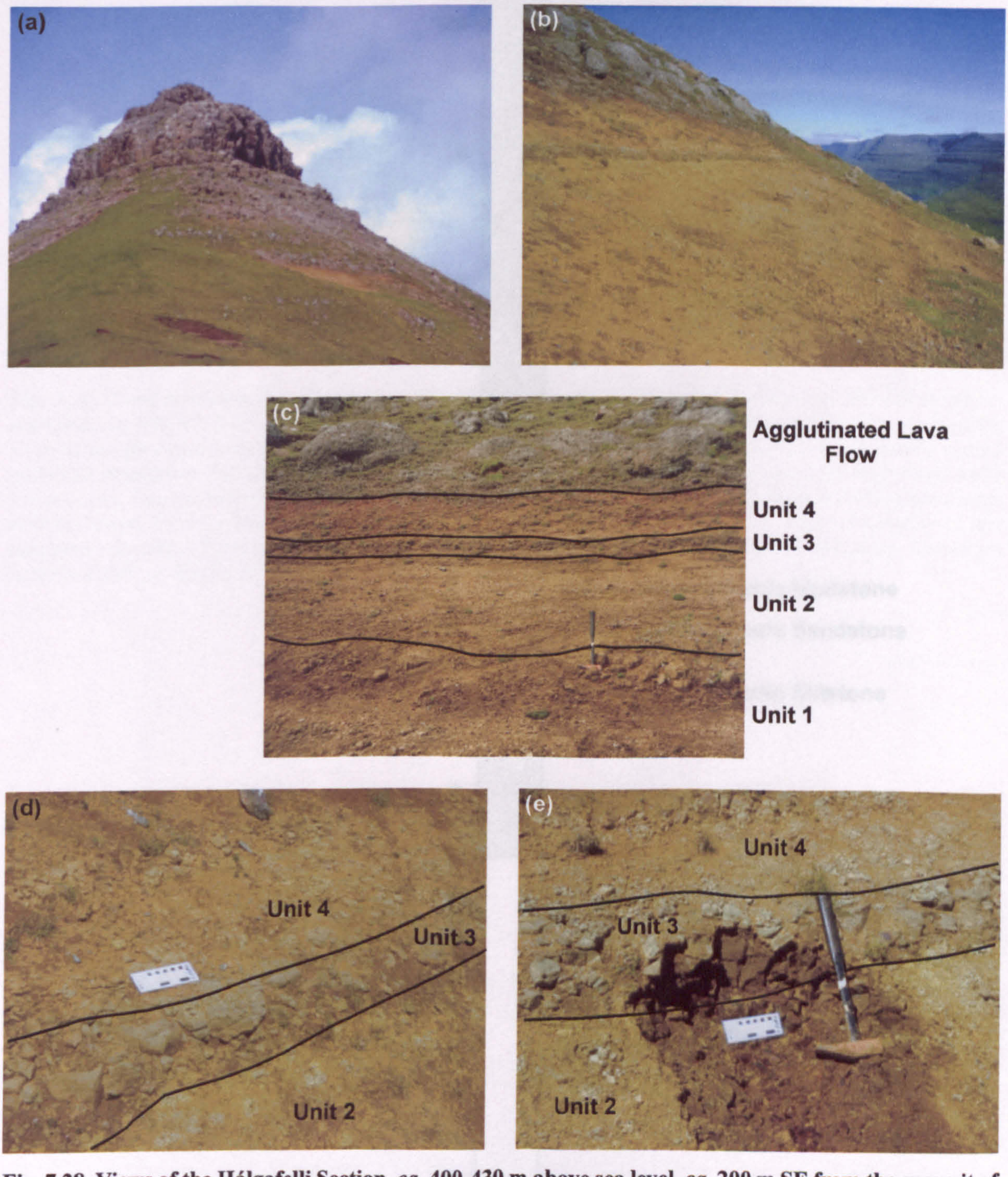

Fig. 7.28. Views of the Hálgafelli Section, *ca.* 400-430 m above sea level, *ca.* 200 m SE from the summit of Hálgafelli, *ca.* 1 km SW of Klaksvík, Borðoy, Faeroe Islands. (a) & (b) The section is *ca.* 4.7 m thick and consists of a sequence of volcaniclastic siltstones and sandstones below an agglutinated lava flow. (c) to (e) The sequence can be subdivided into 4 units: unit 1 is a *ca.* 1.8 m thick volcaniclastic sandstone, unit 2 is a *ca.* 1.6 m thick volcaniclastic siltstone, unit 3 is a *ca.* 30 cm thick volcaniclastic sandstone, and unit 4 is a *ca.* 1 m thick volcaniclastic mudstone. The white card is *ca.* 16 x 6 cm and the hammer is *ca.* 40 cm long.

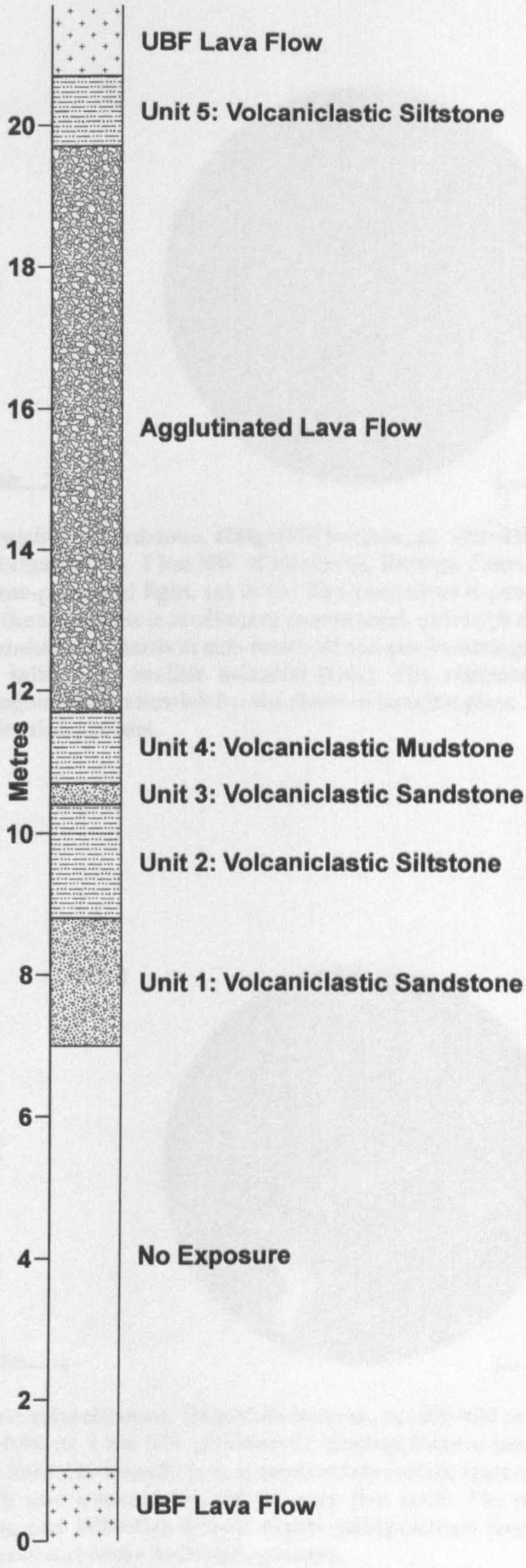

Fig. 7.29. A graphic log for a *ca.* 20 m thick Hálgafelli Section through the Upper Basalt Formation (UBF), *ca.* 400-430 m above sea level, *ca.* 200 m SE from the summit of Hálgafelli, *ca.* 1 km SW of Klaksvík, Borðoy, Faeroe Islands.

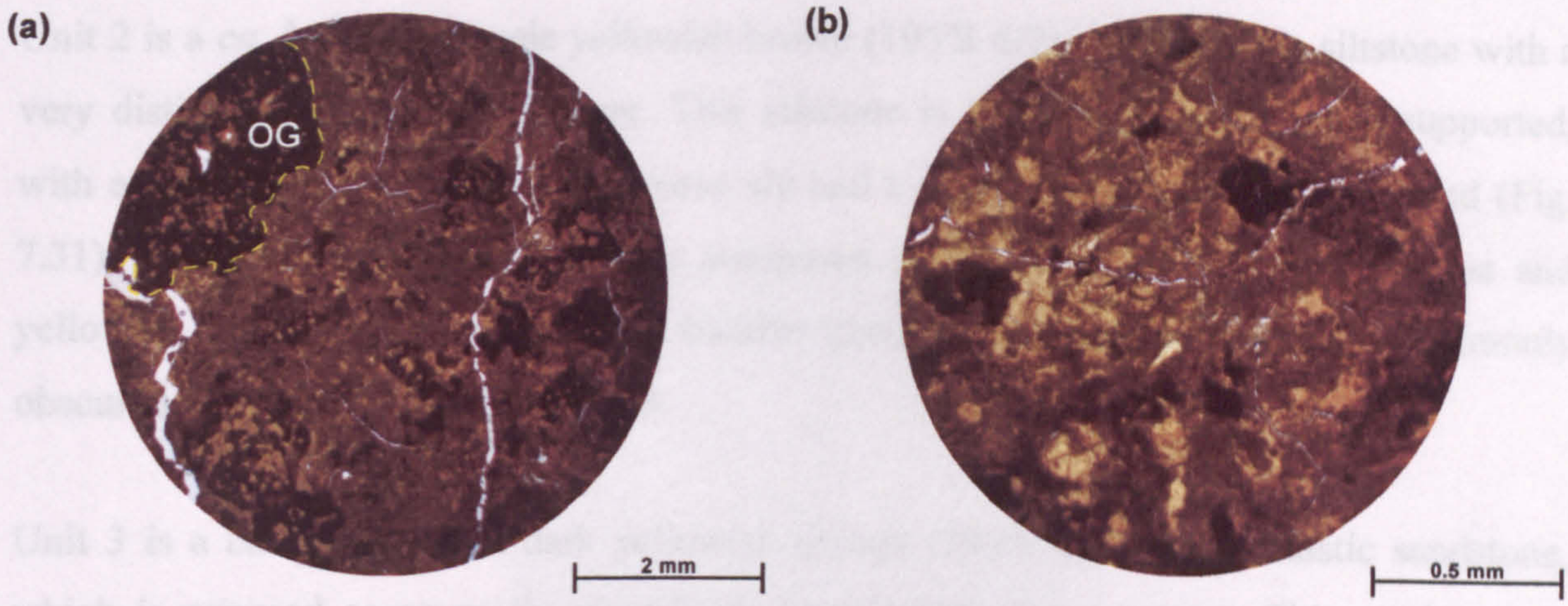

Fig. 7.30. Photomicrographs of Unit 1, volcaniclastic sandstone, Hálgafelli Section, *ca.* 400-430 m above sea level, *ca.* 200 m SE from the summit of Hálgafelli, *ca.* 1 km SW of Klaksvík, Borðoy, Faeroe Islands. Both of the photomicrographs are under plane-polarised light. (a) & (b) The sandstone is poorly sorted and clast supported. The average clast size of the sandstone is medium to coarse sand, although clasts up to 3 mm occur. Approximately 20 vol.% of the sandstone consists of sub-rounded opaque basaltic glass clasts, characterised by an abundance of vesicles infilled by zeolitic material (OG). The remainder of the sandstone consists of sub-rounded highly palagonitised yellowish brown clasts of basaltic glass. The edges to these clasts are highly diffuse due to the hydration process.

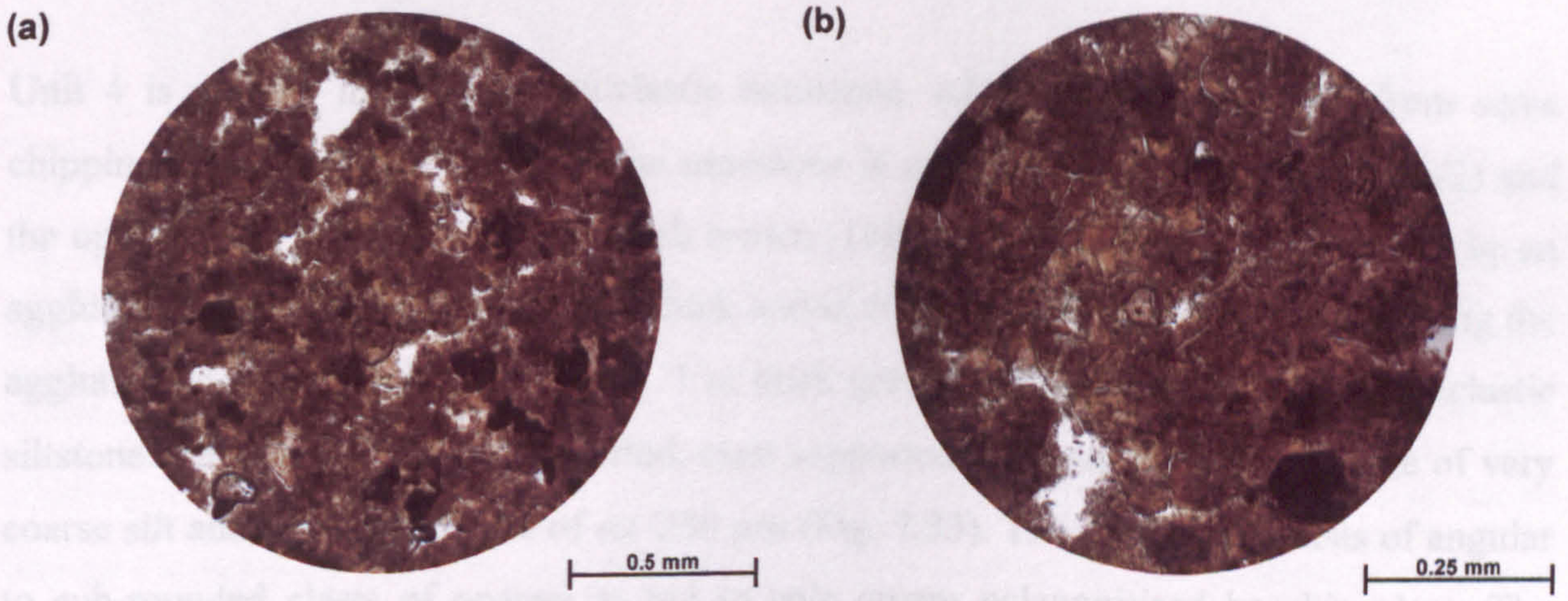

Fig. 7.31. Photomicrographs of Unit 2, volcaniclastic siltstone, Hálgafelli Section, *ca.* 400-430 m above sea level, *ca.* 200 m SE from the summit of Hálgafelli, *ca.* 1 km SW of Klaksvík, Borðoy, Faeroe Islands. Both photomicrographs are under plane-polarised light. (a) The siltstone is moderately sorted, clast supported, with an average clast size of very coarse silt and a maximum size of very fine sand. The siltstone is composed of angular to sub-rounded opaque and yellowish brown highly palagonitised basaltic glass clasts. (b) The clast edges are commonly obscured due to the hydration process.

rounded highly palagonitised yellowish brown clasts of basaltic glass. The edges to these clasts are highly diffuse due to the hydration process and sometimes contain vesicles infilled by zeolitic material.

Unit 2 is a *ca.* 1.6 m thick pale yellowish brown (10YR 6/2) volcaniclastic siltstone with a very distinctive conchoidal fracture. This siltstone is moderately sorted, clast supported, with an average clast size of very coarse silt and a maximum size of very fine sand (Fig. 7.31). In thin section, the siltstone is composed of angular to sub-rounded opaque and yellowish brown highly palagonitised basaltic glass clasts. The clast edges are commonly obscured due to the hydration process.

Unit 3 is a *ca.* 30 cm thick dark yellowish orange (10YR 6/6) volcaniclastic sandstone, which is exposed as an easily identifiable band within the exposure. This sandstone is poorly sorted, matrix supported, with an average clast size of medium to coarse sand and a maximum size of 1.5 mm (Fig. 7.32). In thin section, the sandstone is dominated by angular to sub-rounded opaque to greenish brown palagonitised basaltic glass clasts. The clasts commonly contain highly altered 'broken' phenocrysts of plagioclase feldspar, which have a maximum size of *ca.* 1 mm. Some of the least altered clasts contain vesicles and exhibit cuspate margins. The sandstone contains sub-rounded clasts of equigranular basalt that have a maximum size of *ca.* 1 mm (<5 vol.%) and are composed of laths of plagioclase feldspar, clinopyroxene and oxides.

Unit 4 is a *ca.* 1 m thick volcaniclastic mudstone, which is only identified from scree chippings. The basal *ca.* 60 cm of the mudstone is pale yellowish brown (10YR 6/2) and the upper *ca.* 40 cm is moderate reddish brown (10R 4/6). This mudstone is overlain by an agglutinated lava flow that is *ca.* 8 m thick and is discussed in Section 7.2.5. Overlying the agglutinated lava flow is Unit 5, a *ca.* 1 m thick greyish orange (10YR 7/4) volcaniclastic siltstone. This siltstone is poorly sorted, clast supported, with an average clast size of very coarse silt and a maximum size of *ca.* 250 μm (Fig. 7.33). The siltstone consists of angular to sub-rounded clasts of opaque to red to pale cream palagonitised basaltic glass. The majority of the clasts exhibit cuspate margins and the largest ones contain vesicles. The siltstone is overlain by a tabular lava flow from the UBF.

7.4.2.4 Kunoy Section

The Kunoy Section consists of 5 separate volcaniclastic sandstones inbetween tabular lava flows over a thickness of *ca.* 300 m (Fig. 7.34). Unit 1 crops out *ca.* 500 m above sea level

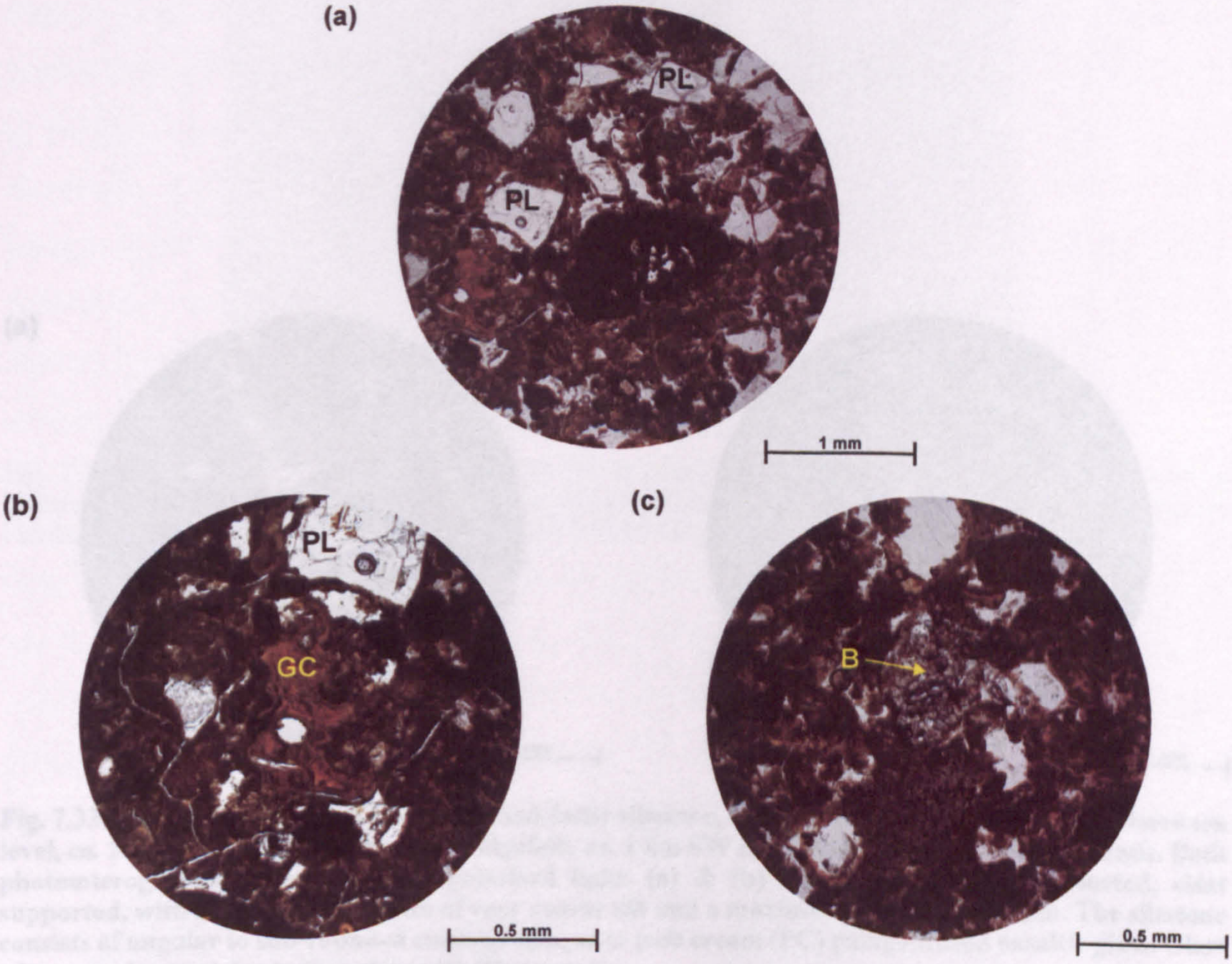

Fig. 7.32. Photomicrographs of Unit 3, volcaniclastic sandstone, Hálgafelli Section, *ca.* 400-430 m above sea level, *ca.* 200 m SE from the summit of Hálgafelli, *ca.* 1 km SW of Klaksvík, Borðoy, Faeroe Islands. All of the photomicrographs are under plane-polarised light. (a) The sandstone is poorly sorted, matrix supported, with an average clast size of medium to coarse sand and a maximum size of 1.5 mm. The sandstone is dominated by angular to sub-rounded opaque to greenish brown palagonitised basaltic glass clasts. The clasts commonly contain highly altered 'broken' phenocrysts of plagioclase feldspar (PL), which have a maximum size of *ca.* 1 mm. (b) Some of the least altered glassy clasts (GC) contain vesicles and exhibit cuspate margins. (c) The sandstone contains sub-rounded clasts of equigranular basalt (B) that have a maximum size of *ca.* 1 mm (<5 vol.%) and are composed of laths of plagioclase feldspar, clinopyroxene and oxides.

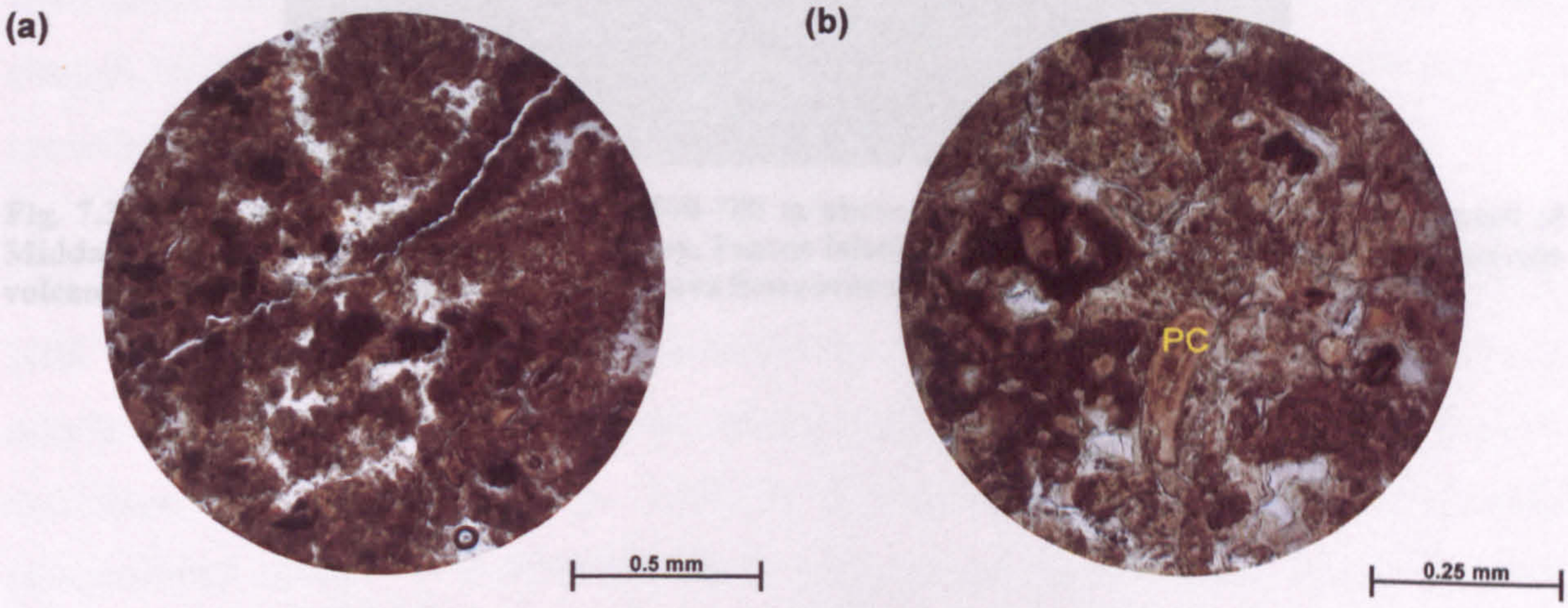

Fig. 7.33. Photomicrographs of Unit 5, volcaniclastic siltstone, Hálgafelli Section, *ca.* 400-430 m above sea level, *ca.* 200 m SE from the summit of Hálgafelli, *ca.* 1 km SW of Klaksvík, Borðoy, Faeroe Islands. Both photomicrographs are under plane-polarised light. (a) & (b) The siltstone is poorly sorted, clast supported, with an average clast size of very coarse silt and a maximum size of *ca.* 250 μm. The siltstone consists of angular to sub-rounded clasts of opaque to pale cream (PC) palagonitised basaltic glass. Clast edges are obscured due to the palagonitisation process.

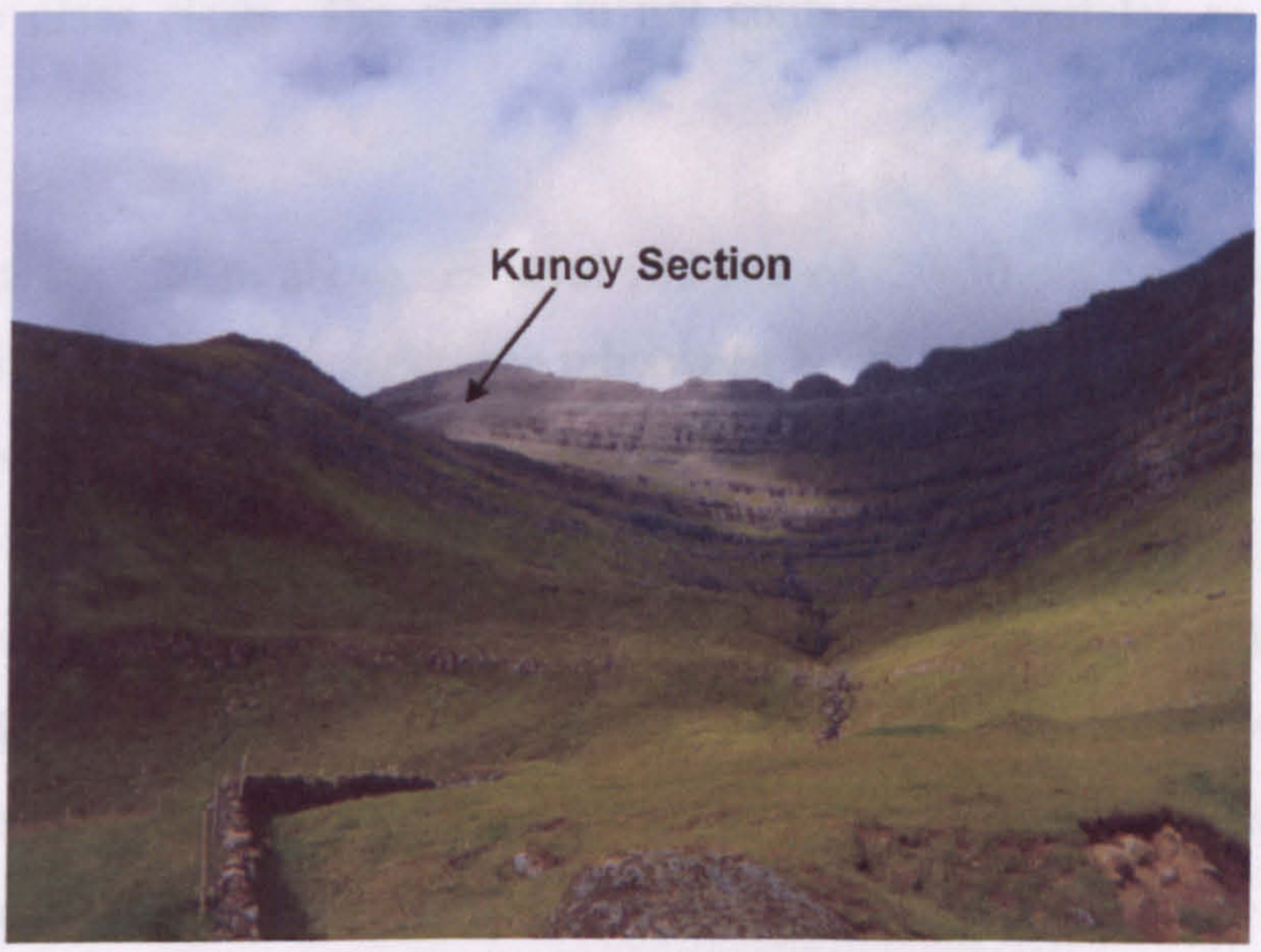

Fig. 7.34. View of the Kunoy Section, *ca.* 500-780 m above sea level, *ca.* 800 m S from the summit of Middagsfjall, *ca.* 1.5 km NE of Kunoy, Kunoy, Faeroe Islands. The Kunoy Section consists of 5 separate volcaniclastic sandstones inbetween tabular lava flows over a thickness of *ca.* 300 m.

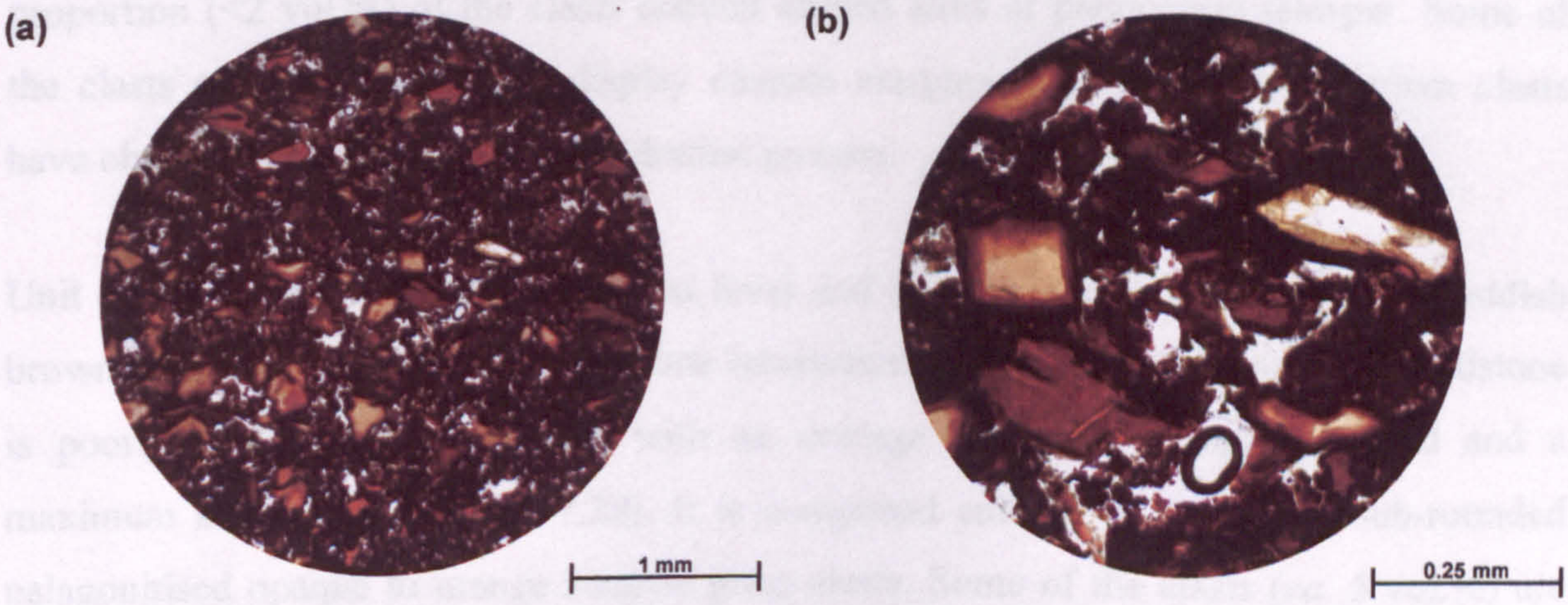

Fig. 7.35. Photomicrographs of Unit 1, volcaniclastic sandstone, Kunoy Section, *ca.* 500 m above sea level, *ca.* 800 m S from the summit of Middagsfjall, *ca.* 1.5 km NE of Kunoy, Kunoy, Faeroe Islands. Both photomicrographs are under plane-polarised light. (a) The sandstone is poorly sorted and clast supported. It has an average clast size of very fine sand and a maximum size of 400 μm. (b) The sandstone is wholly composed of sub-angular to sub-rounded palagonitised opaque to orange basaltic glass clasts.

and is a *ca.* 1 m thick moderate reddish brown (10R 6/6) volcaniclastic sandstone. This sandstone is thinly to medium laminated (1-10 mm), poorly sorted and clast supported (Fig. 7.35). It has an average clast size of very fine sand and a maximum size of 400 μm. The sandstone is wholly composed of sub-angular to sub-rounded palagonitised opaque to orange basaltic glass clasts. The clasts do not contain any vesicles or display cuspate margins.

Unit 2 crops out *ca.* 520 m above sea level and is a *ca.* 20-30 cm thick moderate reddish brown (10R 6/6) volcaniclastic sandstone inbetween two tabular lava flows. This sandstone is poorly sorted, clast supported, with an average clast size of medium sand and a maximum size of 400 μm (Fig. 7.36). It is dominated by angular to sub-rounded palagonitised opaque to orange basaltic glass clasts. Some of the clasts are highly vesiculated and display cuspate margins. A small proportion (<2 vol.%) of the clasts contain highly altered laths of plagioclase feldspar, with a maximum size of 300 μm. The sandstone has *ca.* 10 vol.% zeolitic cement.

Unit 3 crops out *ca.* 600 m above sea level and is a *ca.* 2 m thick moderate reddish brown (10R 6/6) volcaniclastic sandstone inbetween two tabular lava flows. This sandstone is poorly sorted, clast supported, with an average clast size of fine to medium sand and a maximum size of 0.6 mm (Fig. 7.37). It is dominated by sub-angular to rounded palagonitised opaque to reddish brown to pale orange basaltic glass clasts. A small proportion (<2 vol.%) of the clasts contain altered laths of plagioclase feldspar. Some of the clasts contain vesicles and display cuspate margins. The finer reddish brown clasts have obscured margins due to the hydration process.

Unit 4 crops out *ca.* 730 m above sea level and is a *ca.* 1-2 m thick moderate reddish brown (10R 6/6) volcaniclastic sandstone inbetween two tabular lava flows. This sandstone is poorly sorted, clast supported, with an average clast size of medium sand and a maximum size of 1 mm (Fig. 7.38). It is comprised entirely of angular to sub-rounded palagonitised opaque to orange basaltic glass clasts. Some of the clasts (*ca.* 5 vol.%) are vesiculated, which are usually infilled with zeolitic material. The finer grained more altered clasts have obscured edges due to the hydration process. Approximately 20 vol.% of the sandstone consists of 'broken' laths of altered plagioclase feldspar, with an average size of *ca.* 0.5 mm.

Unit 5 crops out *ca.* 780 m above sea level and is a *ca.* 1 m thick moderate reddish brown (10R 6/6) volcaniclastic sandstone inbetween two tabular lava flows. This sandstone is

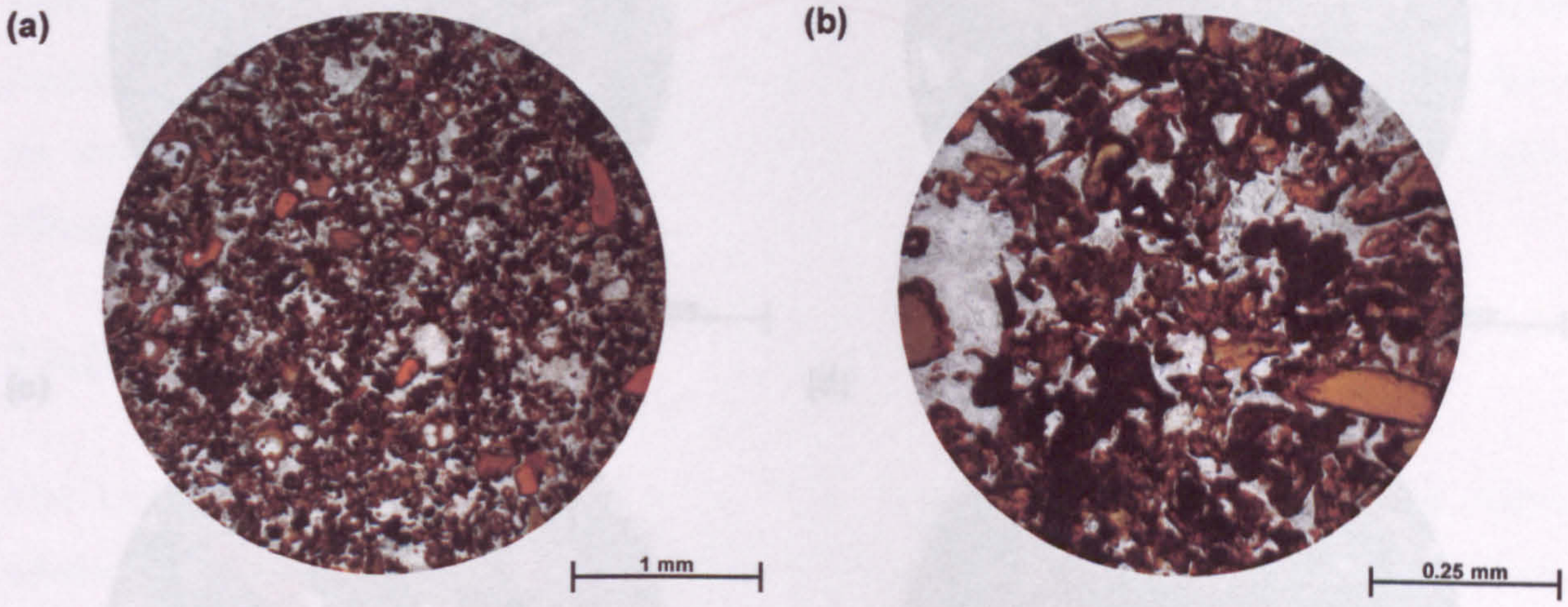

Fig. 7.36. Photomicrographs of Unit 2, volcaniclastic sandstone, Kunoy Section, *ca.* 520 m above sea level, *ca.* 800 m S from the summit of Middagsfjall, *ca.* 1.5 km NE of Kunoy, Kunoy, Faeroe Islands. Both photomicrographs are under plane-polarised light. (a) The sandstone is poorly sorted, clast supported, with an average clast size of medium sand and a maximum size of 400 μm. (B) The sandstone is dominated by angular to sub-rounded palagonitised opaque to orange basaltic glass clasts.

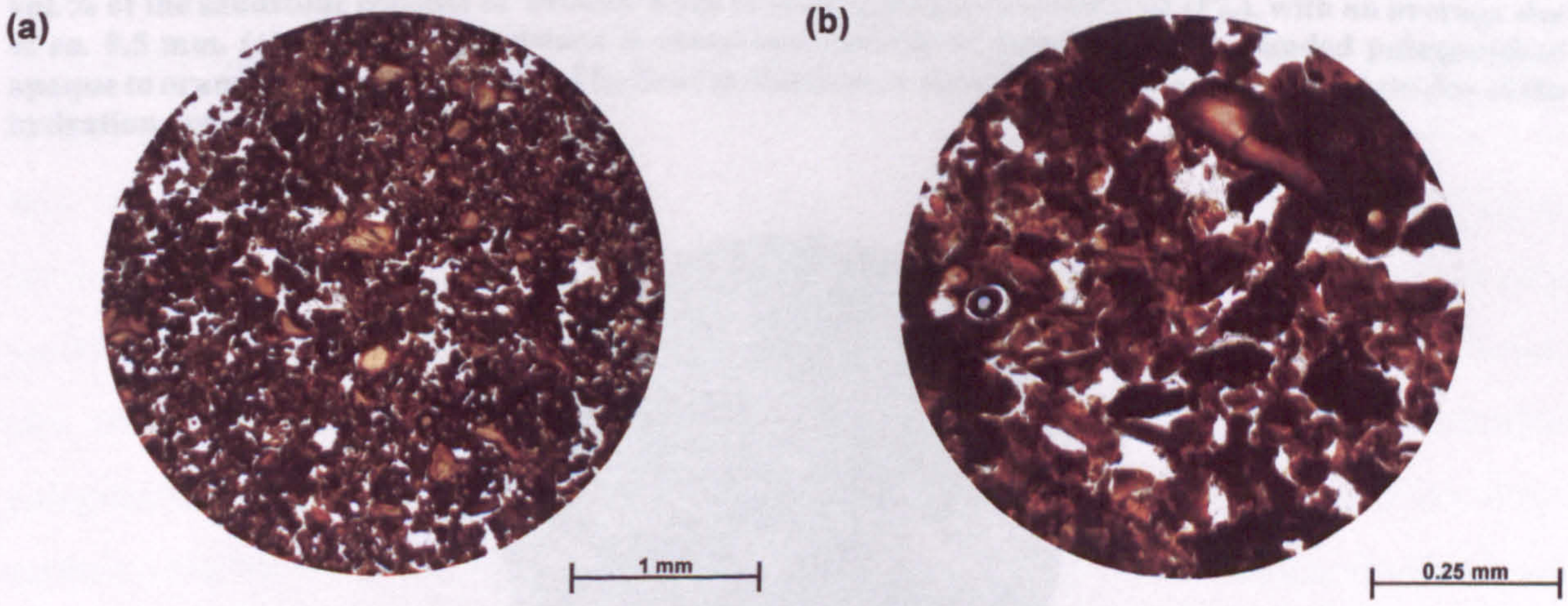

Fig. 7.37. Photomicrographs of Unit 3, volcaniclastic sandstone, Kunoy Section, *ca.* 600 m above sea level, *ca.* 800 m S from the summit of Middagsfjall, *ca.* 1.5 km NE of Kunoy, Kunoy, Faeroe Islands. Both photomicrographs are under plane-polarised light. (a) The sandstone is poorly sorted, clast supported, with an average clast size of fine to medium sand and a maximum size of 0.6 mm. (b) It is dominated by sub-angular to rounded palagonitised opaque to reddish brown to pale orange basaltic glass clasts. The finer reddish brown clasts have obscured margins due to the hydration process.

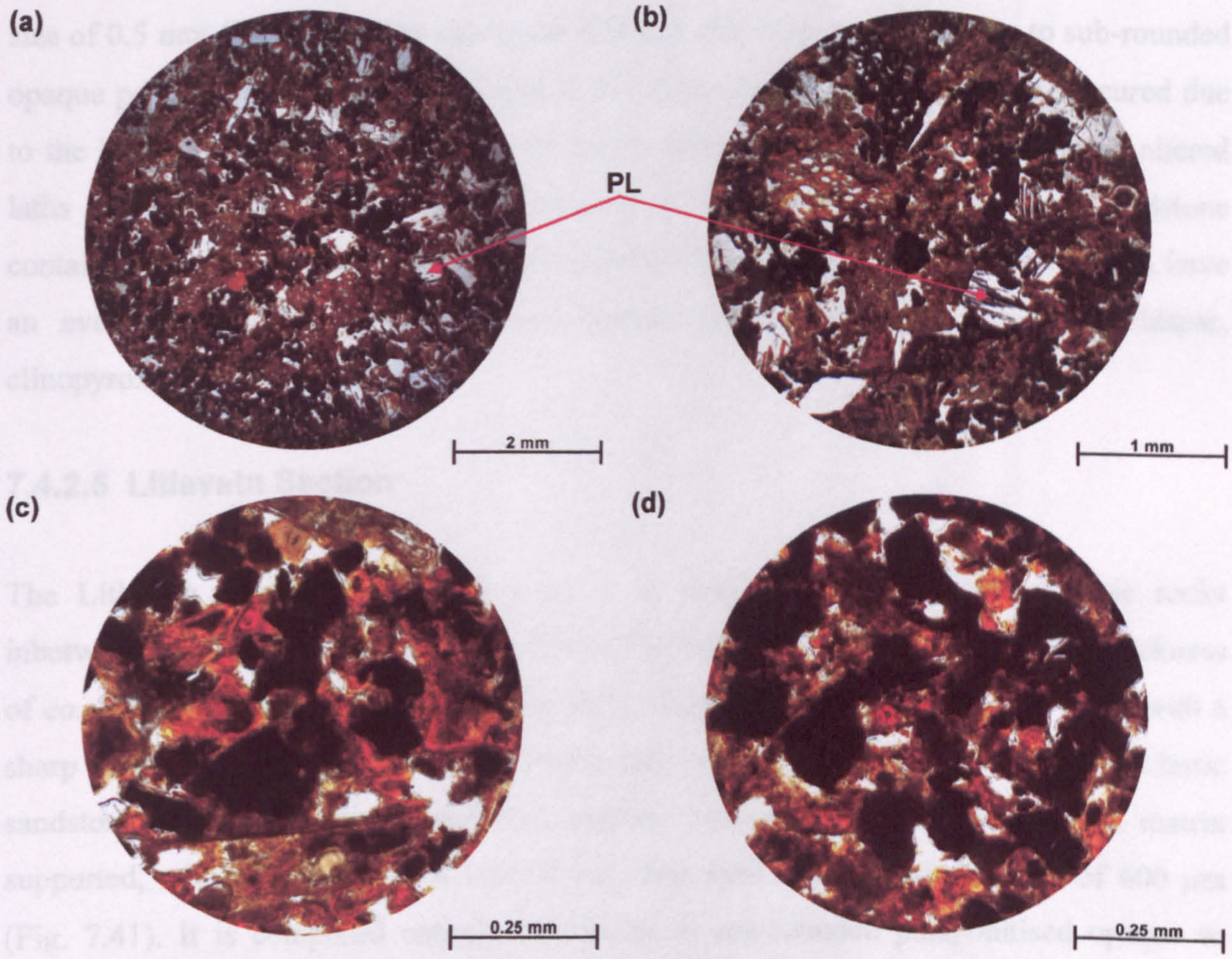

Fig. 7.38. Photomicrographs of Unit 4, volcaniclastic sandstone, Kunoy Section, *ca.* 730 m above sea level, *ca.* 800 m S from the summit of Middagsfjall, *ca.* 1.5 km NE of Kunoy, Kunoy, Faeroe Islands. All of the photomicrographs are under plane-polarised light. (a) & (b) The sandstone is poorly sorted, clast supported, with an average clast size of medium sand and a maximum size of 1 mm. Approximately 20 vol.% of the sandstone consists of 'broken' laths of altered plagioclase feldspar (PL), with an average size of *ca.* 0.5 mm. (c) & (d) The sandstone is comprised entirely of angular to sub-rounded palagonitised opaque to orange basaltic glass clasts. The finer grained more altered clasts have obscured edges due to the hydration process.

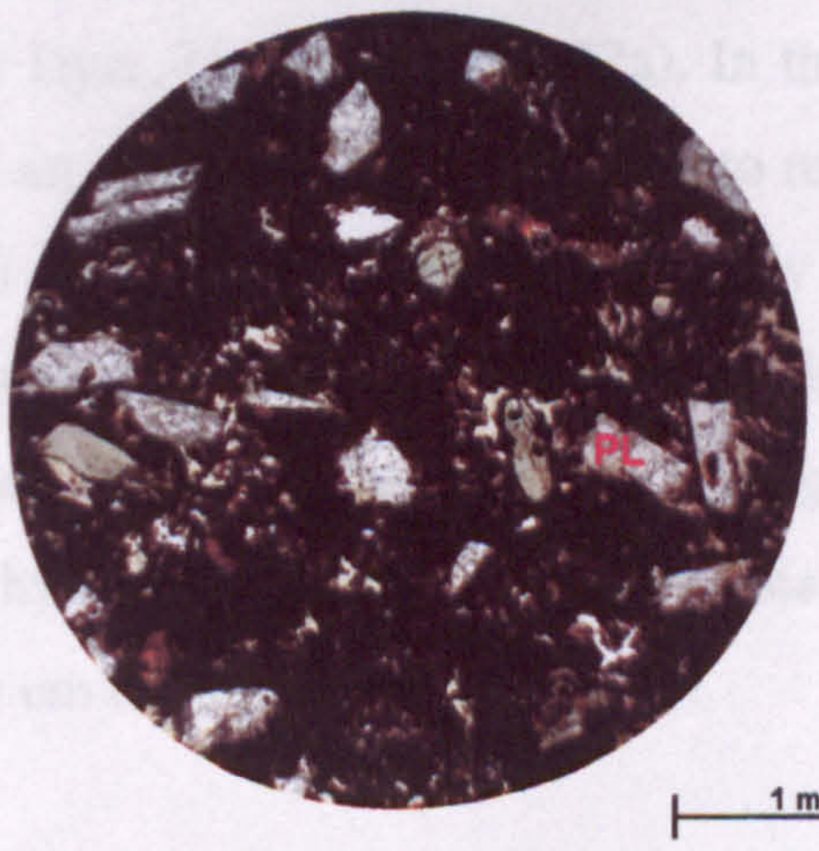

Fig. 7.39. Photomicrograph of Unit 5, volcaniclastic sandstone, Kunoy Section, *ca.* 780 m above sea level, *ca.* 800 m S from the summit of Middagsfjall, *ca.* 1.5 km NE of Kunoy, Kunoy, Faeroe Islands. The photomicrographs is under plane-polarised light. The sandstone is poorly sorted, clast supported, with an average clast size of medium sand and a maximum size of 0.5 mm. The sandstone is dominated by near sub-angular to sub-rounded opaque palagonitised basaltic glass clasts. The edges to the clasts are highly obscured due to the hydration process. Approximately 20-30 vol.% of the sandstone consists of altered laths of plagioclase feldspar (PL), which have an average size of 0.4 mm.

poorly sorted, clast supported, with an average clast size of medium sand and a maximum size of 0.5 mm (Fig. 7.39). The sandstone is dominated by near sub-angular to sub-rounded opaque palagonitised basaltic glass clasts. The edges to the clasts are highly obscured due to the hydration process. Approximately 20-30 vol.% of the sandstone consists of altered laths of plagioclase feldspar, which have an average size of 0.4 mm. The sandstone contains <2 vol.% of sub-angular to sub-rounded clasts of equigranular basalt, which have an average size of *ca.* 0.4 mm and contain altered laths of plagioclase feldspar, clinopyroxene and oxides.

7.4.2.5 Lítlavatn Section

The Lítlavatn Section consists of a *ca.* 1 m thick sequence of volcaniclastic rocks inbetween two tabular lava flows (Fig. 7.40). The basal lava flow has an exposed thickness of *ca.* 1.2 m and is characterised by abundant amygdales. Overlying the lava flow, with a sharp contact, is Unit 1, a *ca.* 30 cm thick pale reddish brown (10R 5/4) volcaniclastic sandstone with a distinctive conchoidal fracture. This sandstone is poorly sorted, matrix supported, with an average clast size of very fine sand and a maximum size of 400 μm (Fig. 7.41). It is composed entirely of angular to sub-rounded palagonitised opaque to brownish basaltic glass clasts, with edges that are extremely diffuse due to the hydration process.

Unit 2 is a *ca.* 19 cm thick pale reddish brown (10R 5/4) volcaniclastic sandstone, which is thickly laminated and faintly cross-bedded with a flow direction to the WNW (*ca.* 300°). In thin section, the sandstone contains two layers separated by a sharp contact, the lower layer, Unit 2a and the upper layer, Unit 2b (Fig. 7.42a). In thin section, Unit 2a is poorly sorted, clast supported, with an average clast size of fine to medium sand and a maximum size of 1 mm (Figs. 7.42b & c). It is composed entirely of angular to sub-rounded palagonitised opaque to brownish orange to orange basaltic glass clasts. Some of the clasts contain vesicles as well as having cuspate margins. The finer grained clasts have edges that are obscured due to the hydration process. Lithic clasts from Unit 2a have been incorporated into the lower 1 cm of the overlying Unit 2b.

The upper sandstone layer, Unit 2b, is poorly sorted, clast supported, with an average clast size of fine sand and a maximum size of 300 μm (Figs. 7.42d & e). It is composed entirely of angular to sub-rounded palagonitised opaque to brownish orange to pale yellow basaltic glass clasts. A small proportion (<5 vol.%) of the clasts contain vesicles and have cuspate margins. Some of the clasts (<5 vol.%) contain altered phenocrysts of plagioclase feldspar,

Fig. 7.40. Views of the Lítlavatn Section, roadside cutting between Sandur and Skálavík, *ca.* 400 m N of Lítlavatn, Sandoy, Faeroe Islands. The sequence of volcaniclastic rocks inbetween two tabular lava flows of the Upper Basalt Formation (UBF). The sequence can be separated into 3 units. The hammer is *ca.* 40 cm long.

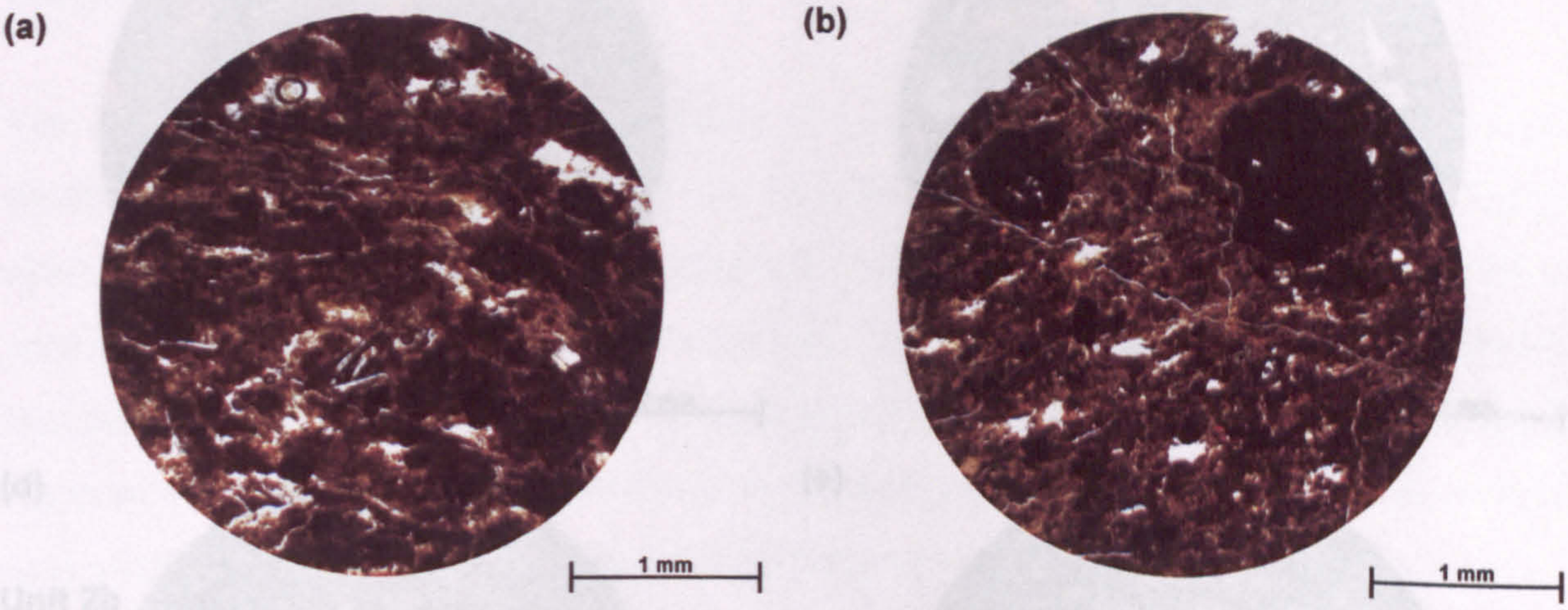

Fig. 7.41. Photomicrographs of Unit 1, volcaniclastic sandstone, Lítlavatn Section, roadside cutting between Sandur and Skálavík, *ca.* 400 m N of Lítlavatn, Sandoy, Faeroe Islands. Both photomicrographs are under plane-polarised light. (a) & (b) The sandstone is poorly sorted, matrix supported, with an average clast size of very fine sand and a maximum size of 400 µm. It is composed entirely of angular to sub-rounded palagonitised opaque to brownish basaltic glass clasts, with edges that are extremely diffuse due to the hydration process.

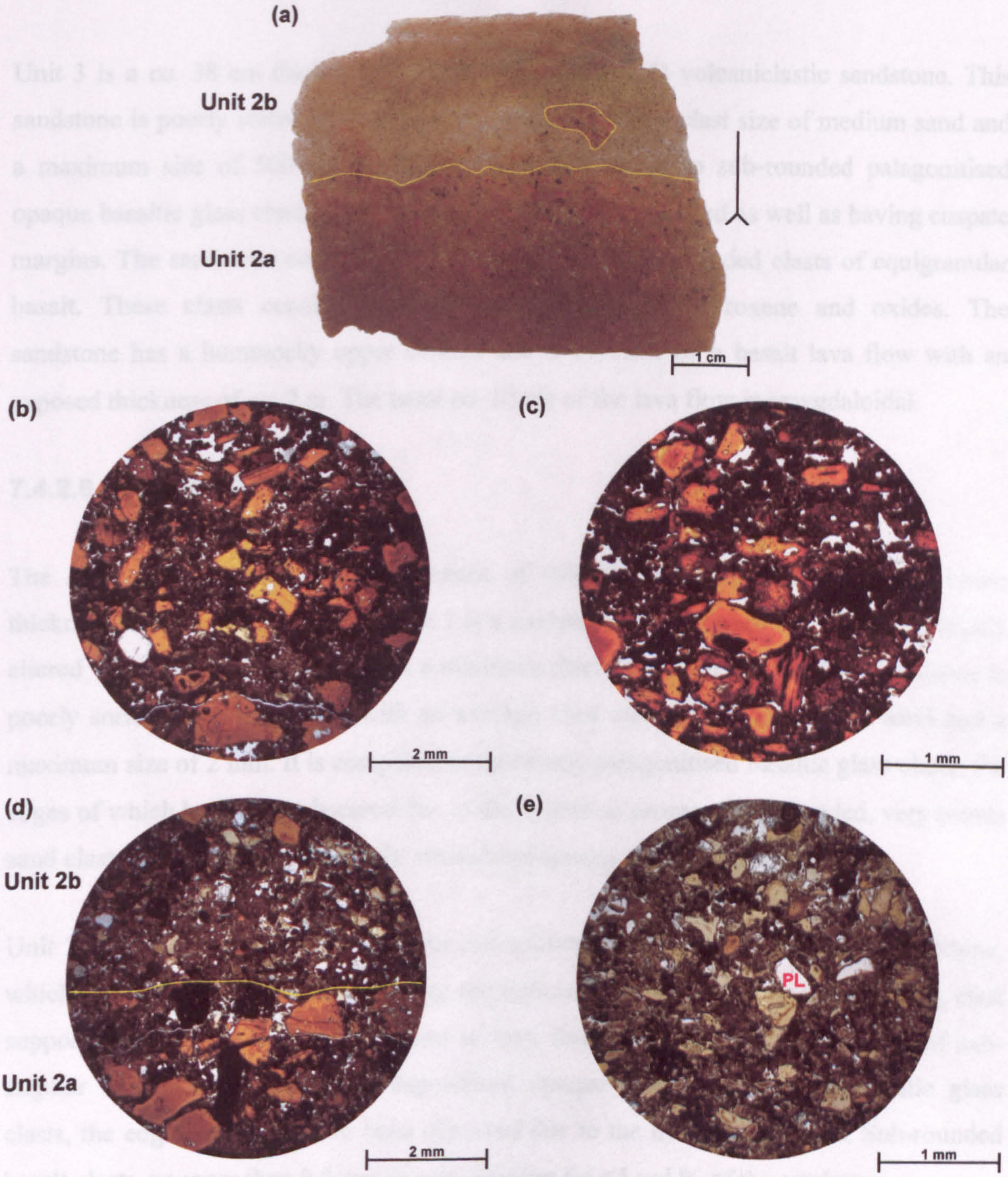

Fig. 7.42. Thin section photography and photomicrographs of Unit 2, volcaniclastic sandstone, Lítlavatn Section, roadside cutting between Sandur and Skálavík, *ca.* 400 m N of Lítlavatn, Sandoy, Faeroe Islands. All of the photomicrographs are under plane-polarised light. (a) The sandstone is thickly laminated and the thin section slide can be separated into two layers (units 2a & 2b) by a sharp contact. Lithic clasts (yellow circle) from Unit 2a have been incorporated into the lower 1 cm of the overlying Unit 2b. (b) & (c) Photomicrographs of Unit 2a. The sandstone is poorly sorted, clast supported, with an average clast size of fine to medium sand and a maximum size of 1 mm. It is composed entirely of angular to sub-rounded palagonitised opaque to brownish orange to orange basaltic glass clasts. The finer grained clasts have edges that are obscured due to the hydration process. (d) & (e) Photomicrographs of unit 2b. The sandstone is poorly sorted, clast supported, with an average clast size of fine sand and a maximum size of 300 μm. It is composed entirely of angular to sub-rounded palagonitised opaque to brownish orange to pale yellow basaltic glass clasts. Some of the clasts (<5 vol.%) contain altered phenocrysts of plagioclase feldspar (PL), which have an average size of 100-200 μm. Finer grained clasts have edges that have been obscured due to the hydration process.

which have an average size of 100-200 μm. Finer grained clasts have edges that have been obscured due to the hydration process.

Unit 3 is a *ca.* 38 cm thick pale reddish brown (10R 5/4) volcaniclastic sandstone. This sandstone is poorly sorted, clast supported, with an average clast size of medium sand and a maximum size of 500 μm. It is dominated by angular to sub-rounded palagonitised opaque basaltic glass clasts. The clasts are commonly vesiculated as well as having cuspate margins. The sandstone contains <5 vol.% sub-rounded to rounded clasts of equigranular basalt. These clasts consist of plagioclase feldspar, clinopyroxene and oxides. The sandstone has a hummocky upper contact and is overlain by a basalt lava flow with an exposed thickness of *ca.* 2 m. The basal *ca.* 10 cm of the lava flow is amygdaloidal.

7.4.2.6 Argir Section

The Argir Section consists of a sequence of volcaniclastic rocks that has a minimum thickness of *ca.* 3.3 m (Fig. 7.43). Unit 1 is a moderate yellowish brown (10YR 5/4) highly altered volcaniclastic sandstone with a minimum thickness of *ca.* 20 cm. This sandstone is poorly sorted, clast supported, with an average clast size of fine to medium sand and a maximum size of 2 mm. It is composed of extremely palagonitised basaltic glass clasts, the edges of which have been obscured due to the hydration process. Sub-rounded, very coarse sand clasts generally occur as highly vesiculated opaque basaltic glass.

Unit 2 is a *ca.* 1.15 m thick pale yellowish brown (10YR 6/2) volcaniclastic sandstone, which has very distinct lenses occurring throughout. This sandstone is poorly sorted, clast supported and has an average clast size of very fine to fine sand. It is composed of sub-angular to sub-rounded highly palagonitised opaque to greenish yellow basaltic glass clasts, the edges of which have been obscured due to the hydration process. Sub-rounded basalt clasts, no more than 0.5 mm in size, account for <5 vol.% of the sandstone.

Unit 3 is a *ca.* 35 cm thick highly altered moderate yellowish brown (10YR 5/4) volcaniclastic siltstone, which has a distinctive conchoidal fracture. This siltstone is poorly sorted, clast supported and is dominated by angular to sub-rounded opaque to greenish yellow to orange palagonitised basaltic glass clasts. Clast margins are obscured due to the palagonitisation process.

Unit 4 is a *ca.* 1.6 m thick moderate reddish brown (10R 4/6) cross-bedded volcaniclastic sandstone. This sandstone is poorly sorted, clast supported and has an average clast size of

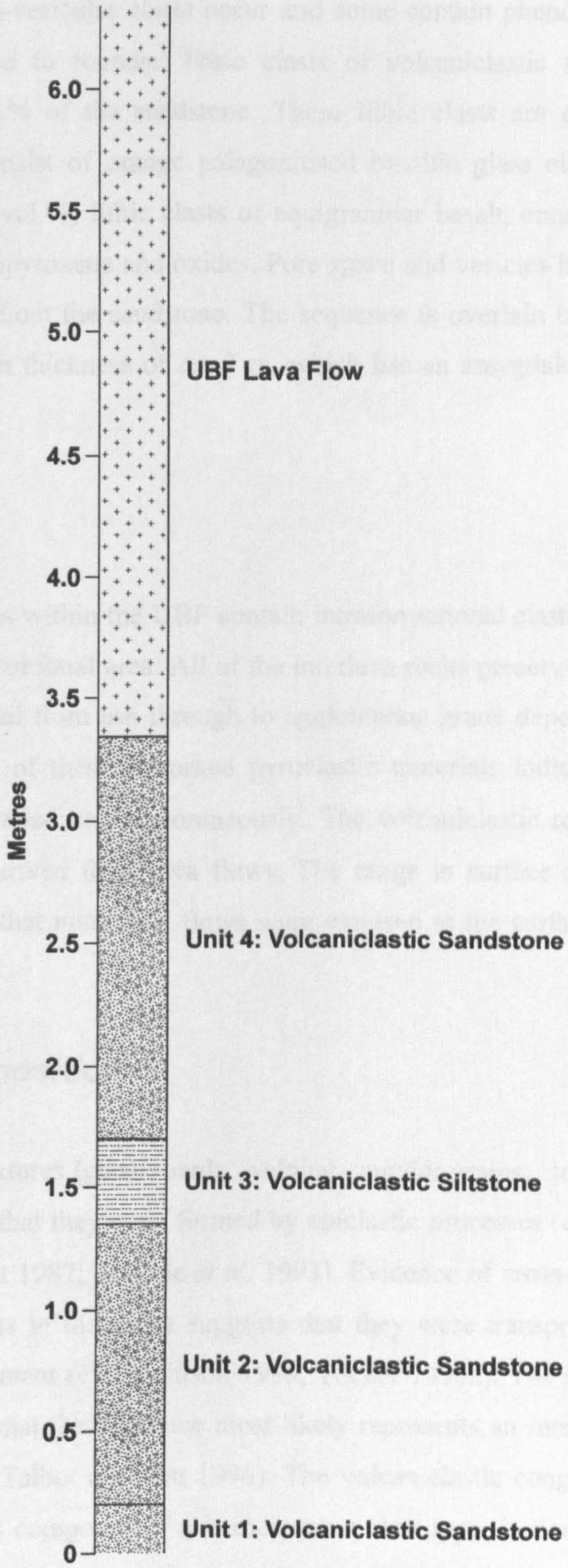

Fig. 7.43. Graphic log for the *ca.* 6.3 m thick sequence through the Upper Basalt Formation (UBF) at the Argir roadside cutting, *ca.* 600 m E of Itróttavøllur, *ca.* 1 km W of Argir, Streymoy, Faeroe Islands.

coarse sand (*ca.* 0.5 mm), although clasts up to 5 mm do occur (Fig. 7.44). It is composed of very angular to sub-rounded opaque to orange palagonitised basaltic glass clasts. Vesicular (*ca.* 40 vol.%) and non-vesicular clasts occur and some contain phenocrysts of plagioclase feldspar. Sub-rounded to rounded lithic clasts of volcaniclastic mudstone account for no more than 2 vol.% of the sandstone. These lithic clasts are extremely homogenous, well sorted and consist of orange palagonitised basaltic glass clasts. The sandstone also contains rare (<2 vol.%) lithic clasts of equigranular basalt, consisting of laths of plagioclase feldspar, clinopyroxene and oxides. Pore space and vesicles have been infilled by zeolitic cement throughout the sandstone. The sequence is overlain by a UBF tabular lava flow with a minimum thickness of *ca.* 3 m, which has an amygdaloidal rich base.

7.4.3 Provenance

All of the volcaniclastic lithologies within the UBF contain intraformational clasts derived from sources within the UBF depositional area. All of the interlava rocks preserved within the UBF contain reworked material from ash through to agglomerate grade deposits. The range in surface oxidation states of these reworked pyroclastic materials indicates that numerous deposits were being eroded contemporaneously. The volcaniclastic rocks also contain eroded clasts of basalt derived from lava flows. The range in surface oxidation states of the lava clasts suggests that numerous flows were exposed at the surface at the time of active erosion.

7.4.4 Environment of Deposition

The general lack of pyroclastic textures (glass shards, welding, angular grains, etc.) within the interlava lithologies indicates that they were formed by epiclastic processes (cf. Fisher & Schmincke 1984; Cas & Wright 1987; McPhie *et al.* 1993). Evidence of cross-bedding, laminations and rounding of clasts in the rocks suggests that they were transported and deposited within a fluvial environment (cf. Collinson 1996; Tucker 1996a). The siltstones of the Hálgafelli Section implies that the sequence most likely represents an interchannel lake deposit (cf. Collinson 1996; Talbot & Allen 1996). The volcaniclastic conglomerate that crops out at Gjógvin Stóra is composed of a homogenous clast type, is non-graded, poorly sorted, matrix supported and has a tabular geometry consistent with having been formed as a volcaniclastic debris flow (cf. Cas & Wright 1987; Smith 1991; Smith & Lowe 1991; McPhie *et al.* 1993; Yarnold 1993). Smith (1991) has demonstrated that

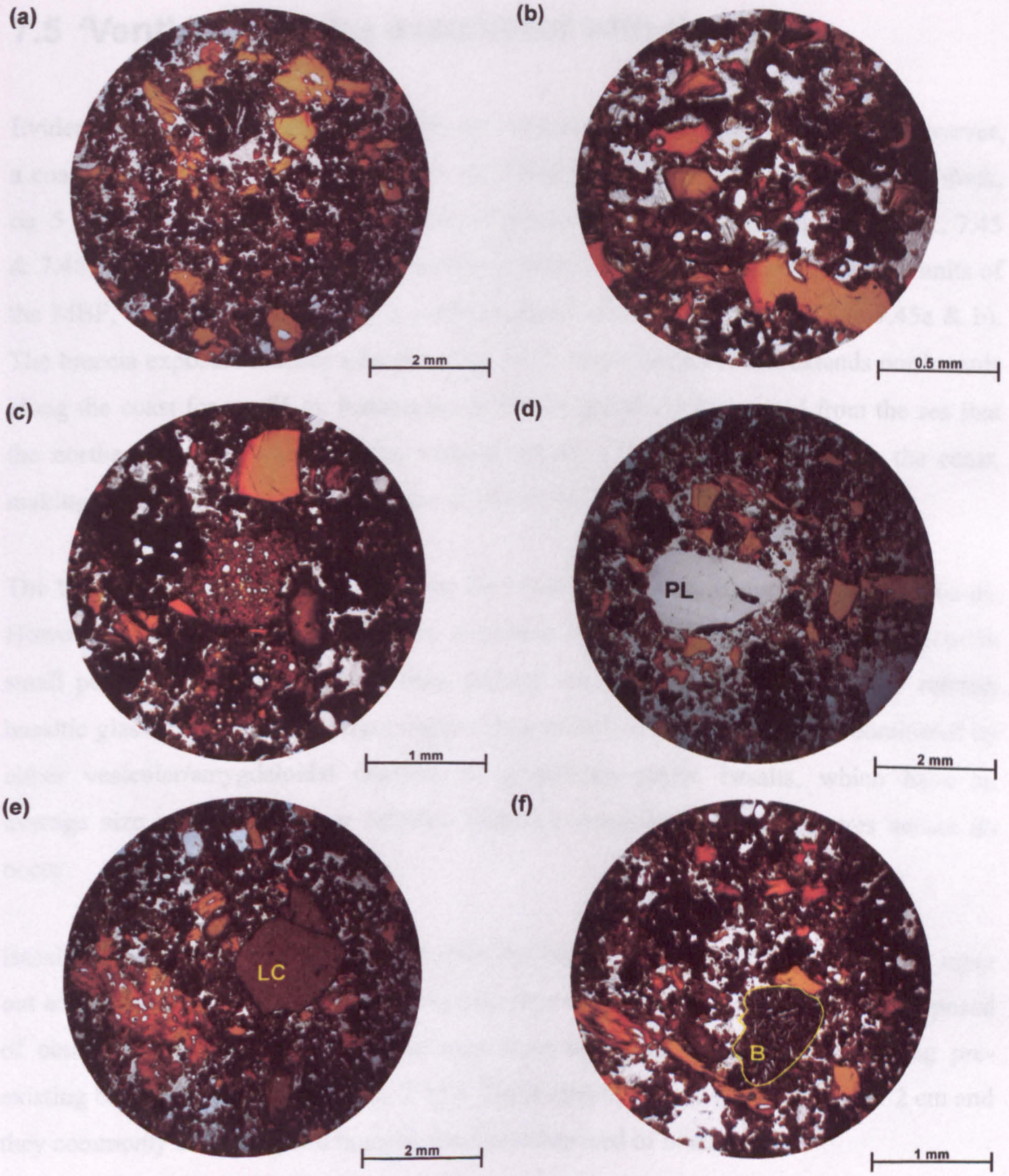

Fig. 7.44. Photomicrographs of Unit 4, volcaniclastic sandstone, Argir roadside cutting, *ca.* 600 m E of Itróttavøllur, *ca.* 1 km W of Argir, Streymoy, Faeroe Islands. All of the photomicrographs are under plane-polarised light. (a) The sandstone is poorly sorted, clast supported and has an average clast size of coarse sand (*ca.* 0.5 mm), although clasts up to 5 mm do occur. (b) The sandstone is composed of very angular to sub-rounded opaque to orange palagonitised basaltic glass clasts. (c) & (d) Vesicular (*ca.* 40 vol.%) and non-vesicular clasts occur and some contain phenocrysts of plagioclase feldspar (PL). (e) Sub-rounded to rounded lithic clasts of volcaniclastic mudstone (LC) account for no more than 2 vol.% of the sandstone. These lithic clasts are extremely homogenous, well sorted and consist of orange palagonitised basaltic glass clasts. (f) The sandstone also contains rare (<2 vol.%) lithic clasts of equigranular basalt (B), consisting of laths of plagioclase feldspar, clinopyroxene and oxides.

volcaniclastic debris flows are commonly formed under syn-eruption conditions compared to fluvial deposits that are formed during hiatuses (inter-eruption) in volcanic activity.

7.5 'Vent' Lithologies associated with the UBF

Evidence of so-called 'vent' lithologies are extremely rare throughout the UBF. However, a coastal section at Húsið millum Gjáir, *ca.* 250 m S of Gjógvin Stóra, W side of Viðvík, *ca.* 5 km SE of Viðareiði, Viðoy consists of an associated 'vent' lithology (Figs. 7.2, 7.45 & 7.46). The southern extent of the section is represented by near horizontal flow units of the MBF, which are truncated by a vertical contact with a breccia unit (Figs. 7.45a & b). The breccia exposure reaches a height of *ca.* 20 m above sea level and extends northwards along the coast for *ca.* 75 m. Rasmussen & Noe-Nygaard (1970b) noted from the sea that the northern contact, which is also vertical, occurs a further *ca.* 70 m along the coast, making the lateral extent of the breccia *ca.* 145 m wide.

The breccia is very poorly sorted and on the whole is fragment supported (Figs. 7.46a-d). However, areas of reddish very coarse sandstone devoid of large fragments do occur in small pockets (Fig. 7.46e). These finer grained areas are composed of angular reddish basaltic glass fragments. The larger angular fragments within the breccia are dominated by either vesicular/amygdaloidal compact or plagioclase-phyric basalts, which have an average size of small to large cobbles, although megablocks several metres across do occur.

Basaltic dykes transect and taper out within the breccia. The ends of the dykes that taper out are highly brecciated, forming blocky peperites of angular fragments that are composed of compact basalt. Amoeboidal apophyses from the dykes are observed splitting pre-existing basalt fragments apart (Fig. 7.46f). These apophyses can be as thin as *ca.* 2 cm and they commonly exhibit chilled margins that are composed of black glass.

The sharp vertical contacts at the extremities of the breccia exposure suggest that they have formed by explosive rather than erosive processes and the abundance of angular lava fragments from the MBF within the breccia supports this. The amoeboid apophyses observed splitting pre-existing basalt fragments apart indicates that the brecciation was the direct result of the basaltic dykes intruding the sequence. The extent of brecciation implies a multiphase process, involving numerous injections of magma. The highly vesicular nature of the dykes and their blocky fragments suggests that the brecciation occurred at shallow levels. The pockets of reddish volcaniclastic sandstone indicate that the MBF

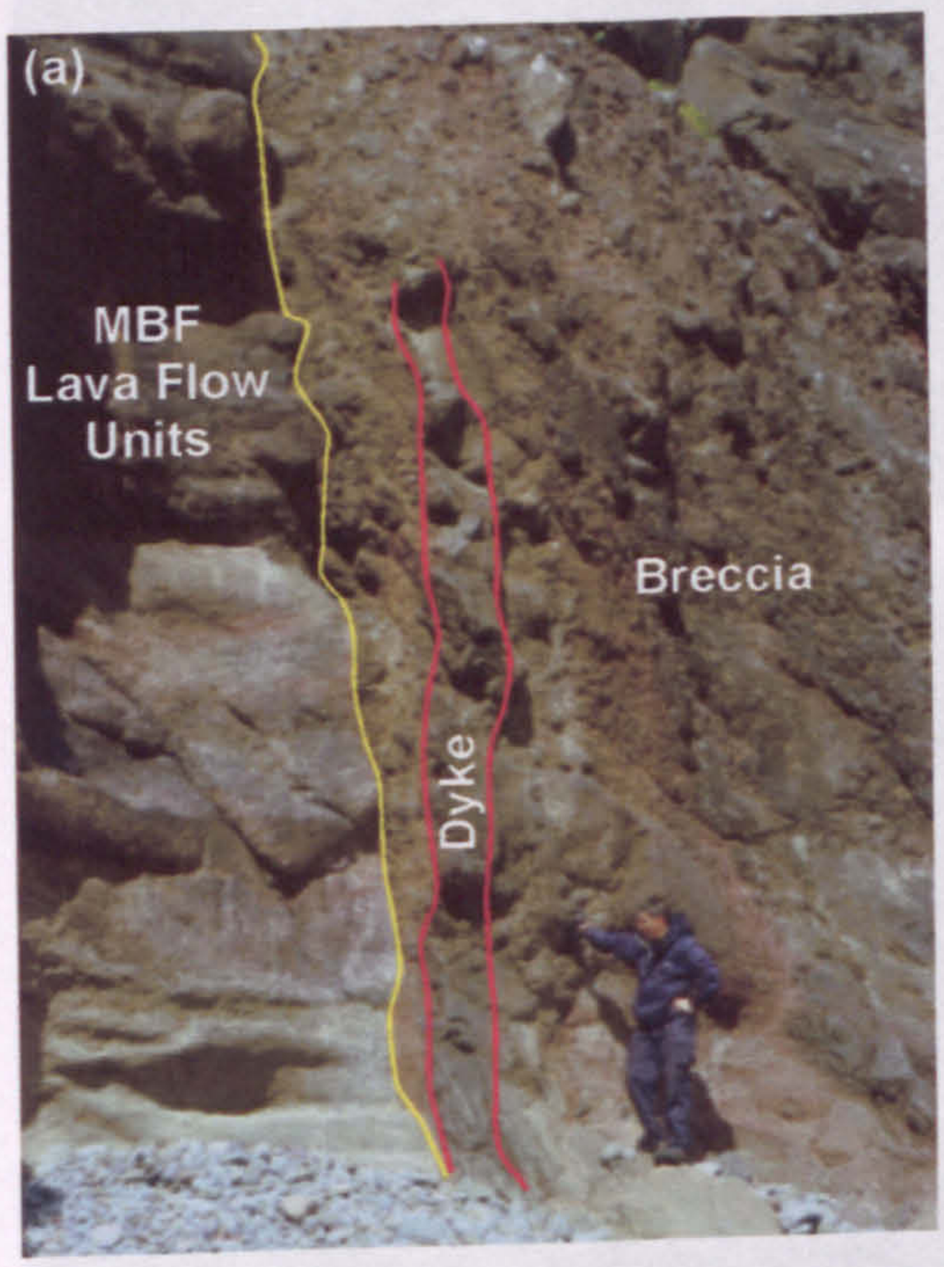

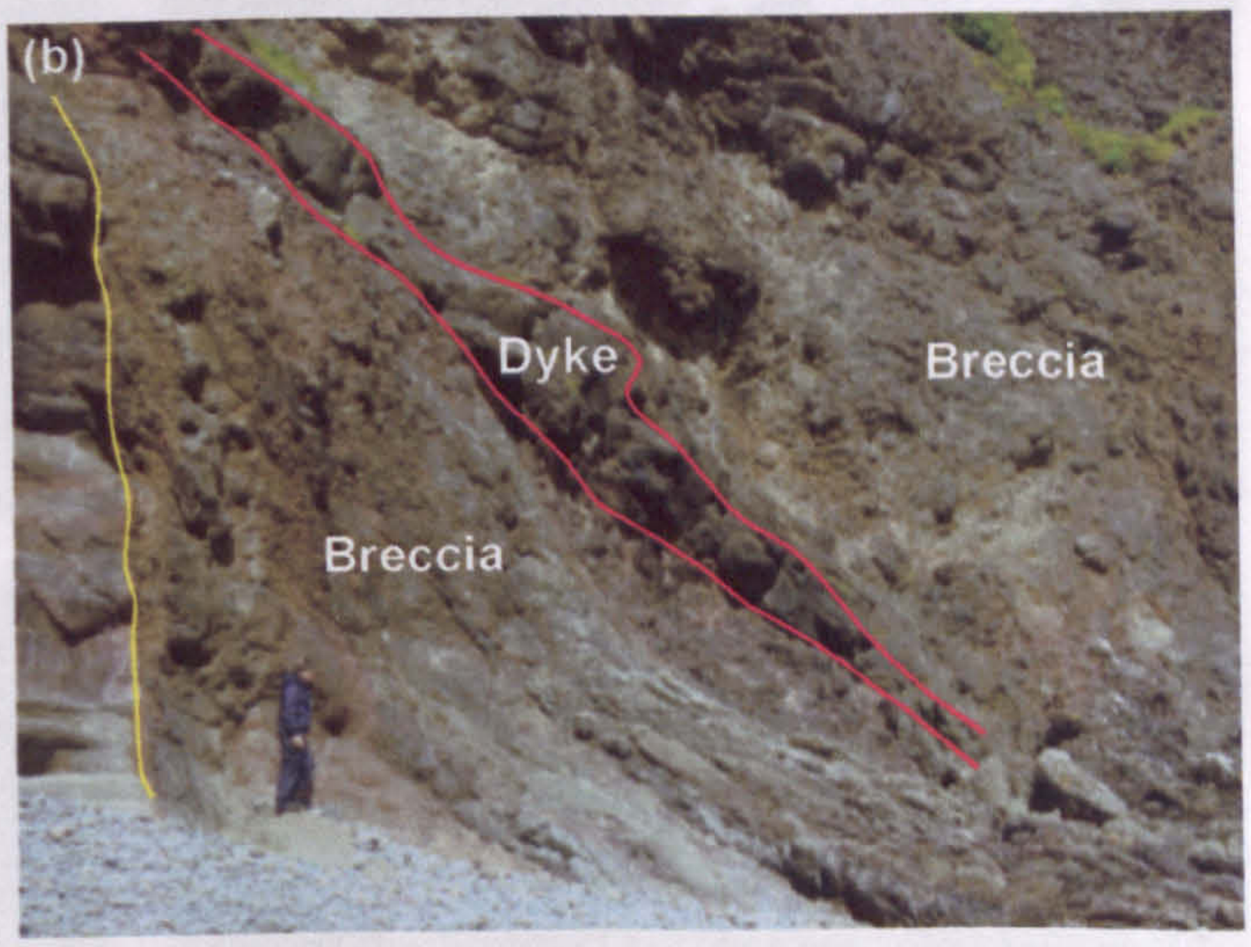

Fig. 7.45. Views of the pyroclastic breccia at Húsið millum Gjáir, *ca.* 250 m S of Gjógvin Stóra, W side of Viðvík, *ca.* 5 km SE of Viðareiði, Viðoy, Faeroe Islands. (a) & (b) The southern extent of the section is represented by near horizontal flow units of the Middle Basalt Formation (MBF), which are truncated by a vertical contact with a breccia unit. Basaltic dykes transect and taper out within the breccia. (c) & (d) The breccia exposure reaches a height of *ca.* 20 m.

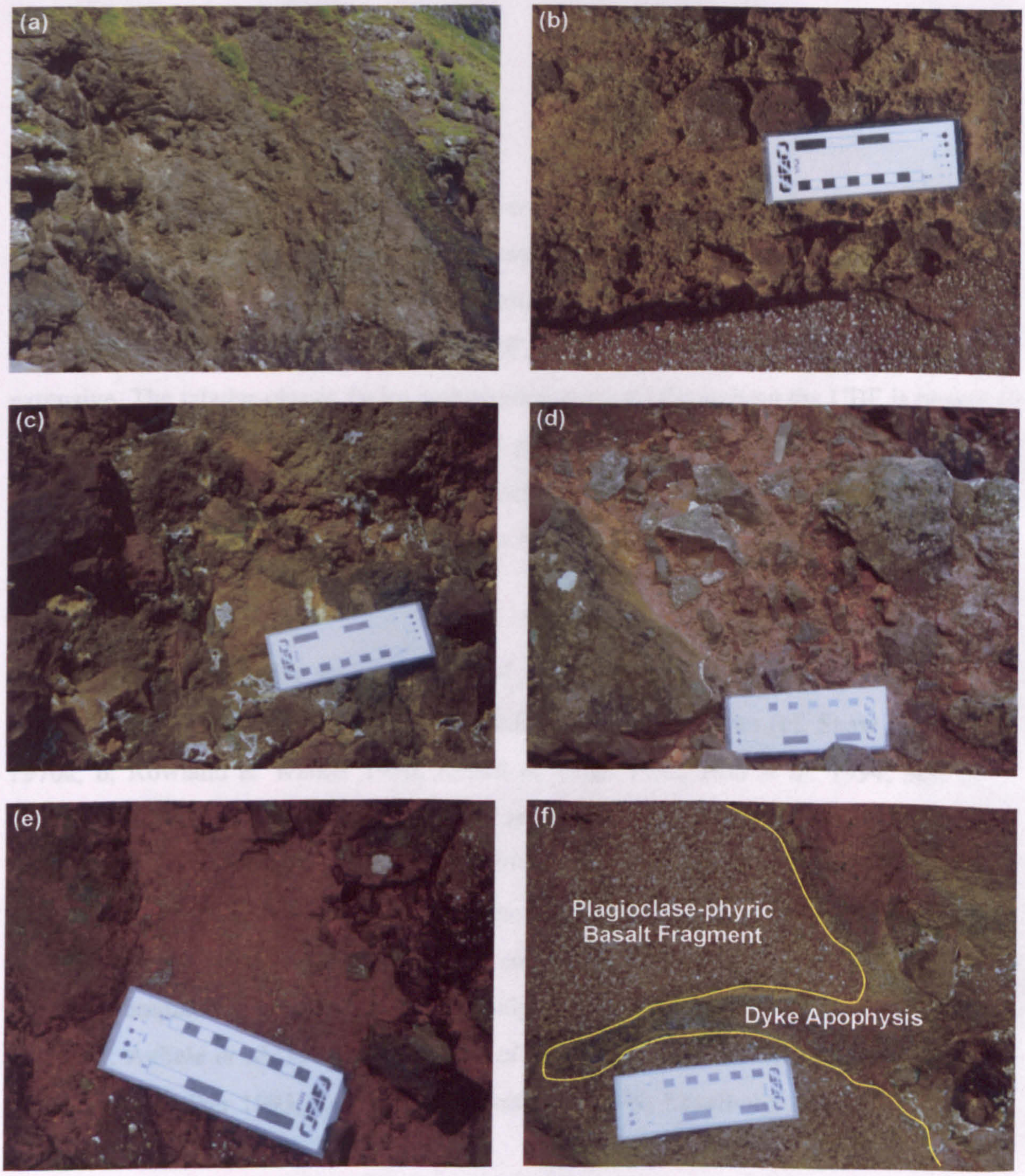

Fig. 7.46. Views of the pyroclastic breccia from the coastal section at Húsið millum Gjáir, *ca.* 250 m S of Gjógvin Stóra, W side of Viðvík, *ca.* 5 km SE of Viðareiði, Viðoy, Faeroe Islands. (a) to (d) The breccia is very poorly sorted and on the whole is fragment supported. The larger angular fragments within the breccia are dominated by either vesicular/amygdaloidal compact or plagioclase-phyric basalts, which have an average size of small to large cobbles, although megablocks several metres across do occur. (e) Areas of reddish very coarse sandstone devoid of large fragments occur in small pockets. These very coarse sandstone areas are composed of angular reddish basaltic glass fragments. (f) An Amoeboidal apophysis from the basaltic dyke is observed splitting a pre-existing basalt fragment apart. These apophyses can be as thin as *ca.* 2 cm and they commonly exhibit chilled margins that are composed of black glass. The white card is *ca.* 16 x 6 cm.

sequence, before brecciation, contained not only basalt lava flows but also volcaniclastic lithologies. The lack of exposure makes it difficult to ascertain whether the dykes intruded the UBF lavas or were the feeders for the first lava flow of the UBF, which is only ten's of metres above the breccia.

7.6 Synthesis

Similar to the lavas of the Lower Basalt Formation (LBF), the Upper Basalt Formation (UBF) flows are typically rubbly-topped sheet-like bodies with significant lateral extents (>6 km) that were emplaced into a subaerial environment (Fig. 7.47). Flow edges are preserved within the UBF, unlike the LBF, suggesting that they are not as laterally extensive. The tabular-classic facies architecture observed throughout the UBF is typical of large volume eruptions common within CFB provinces (Cas & Wright 1987; Walker 1993; Jerram 2002). However, the average flow thickness for the UBF is 8-11 m, half that of the LBF lavas, implying that the UBF eruptions were not as voluminous as those of the LBF (cf. Walker 1970; 1973).

The UBF lava flows, like those of the LBF, have features congruent with having been emplaced rapidly as a'a flows, rather than inflated pahoehoe flows (cf. Shaw & Swanson 1970a; b; Rowland & Walker 1990; Reidel & Tolan 1992; Hon *et al.* 1994; Self *et al.* 1996; Cashman & Kauahikaua 1997; Self *et al.* 1997; Keszthelyi & Self 1998; Reidel 1998; Self *et al.* 1998; Thordarson & Self 1998). This is supported by the rubbly flow tops and the vesicle distribution patterns within the UBF lava flows, which are characterised by vesicle-rich upper crusts and vesicle-poor cores and basal crusts, commonly associated with post-emplacement bubble rise of slowly solidifying ponded, rapidly emplaced a'a flows (cf. Aubele *et al.* 1988; Sahagian *et al.* 1989; Rowland & Walker 1990; Reidel & Tolan 1992; Walker 1993; Cashman & Kauahikaua 1997; Keszthelyi & Self 1998; Reidel 1998).

Columnar jointed flows are absent from the UBF, although indistinct prismatic jointing is relatively common. The occurrence of prismatically jointed flows indicates that they were emplaced into a relatively dry environment (cf. Jerram 2002). However, the presence of highly vesiculated agglutinated lava flows, composed of olivine and plagioclase feldspar glomerocrysts set within a very finely to glassy groundmass, implies that some flows were erupted into a relatively wet environment. This is supported by the overall brecciated appearance of such lava flows and the association with underlying fluvial volcaniclastic

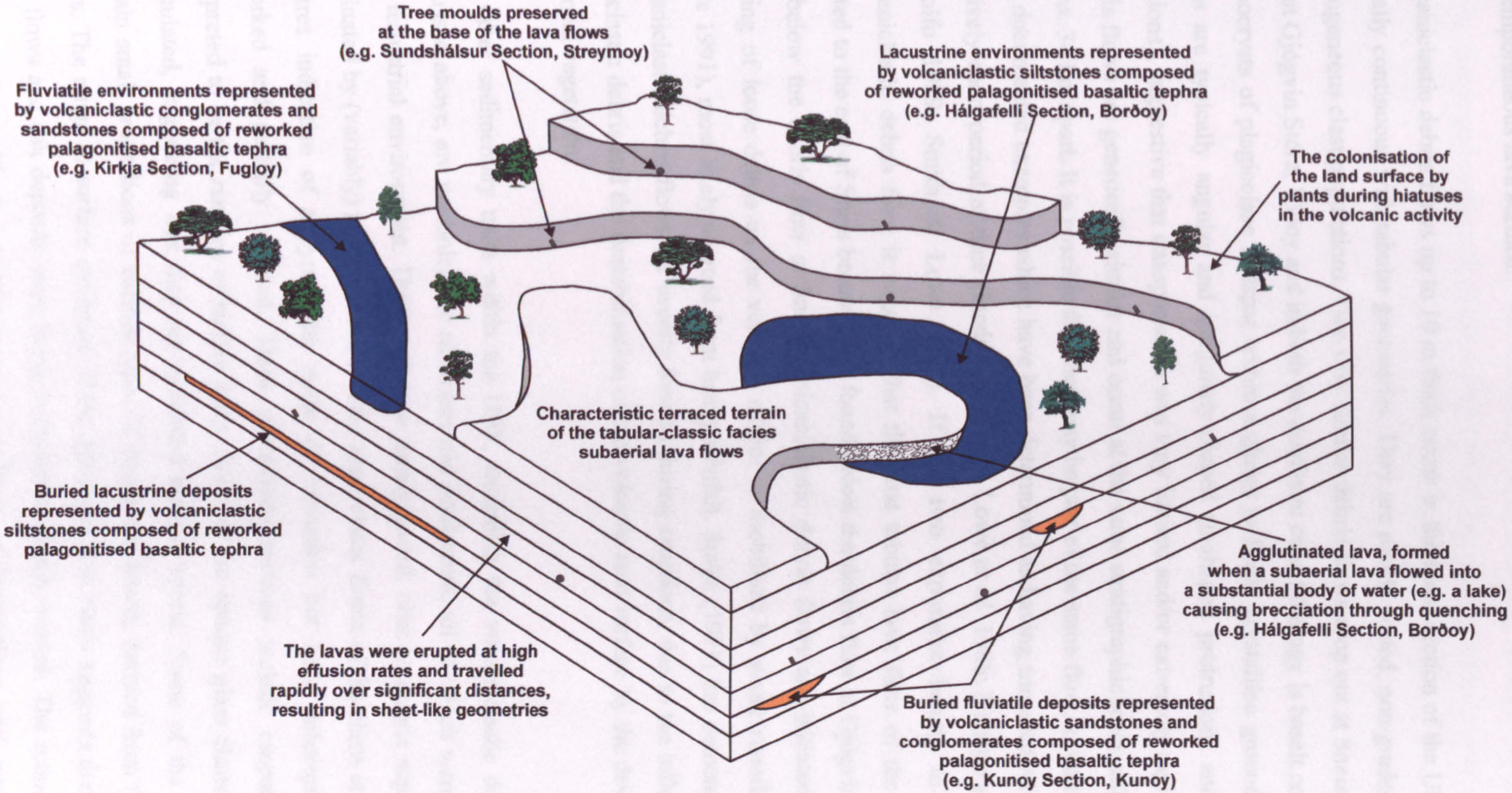

Fig. 7.47. Schematic palaeogeographical block diagram for the Upper Basalt Formation with the main elements highlighted. Length of each horizontal dimension of the figure is very approximately 1-2 km.

strata. These data collectively suggest the presence of surface water on the contemporaneous lava surface.

Volcaniclastic debris flows up to 10 m thick occur in the basal section of the UBF and are laterally continuous with tabular geometries. They are poorly sorted, non-graded and have homogeneous clast populations. Two very similar debris flows crop out at Sneis, Streymoy and at Gjógvin Stóra, Viðoy and in both the dominant clast lithology is basalt composed of phenocrysts of plagioclase feldspar within a glassy to finely crystalline groundmass. The clasts are typically angular and irregularly-shaped (u-shaped protrusions and v-shaped incisions), suggestive that transportation was very limited and/or extremely rapid. The two debris flows are genetically similar and occur at the same stratigraphic level, although they are *ca.* 34 km apart. It is possible that they may be part of the same flow, as there are many well documented examples which have been determined as having travelled >100 km in a relatively short period of time (Janda *et al.* 1981; Lowe *et al.* 1986; Naranjo *et al.* 1986; Rodolfo 1989; Smith & Lowe 1991). If the two exposures belong to the same volcaniclastic debris flow it suggests that the first tabular lava flow of the UBF was erupted to the east of Sneis because it is found below the debris flow at Gjógvin Stóra and not below the debris flow at Sneis. Volcaniclastic debris flows are initiated when the bulking of loose debris on the volcanic edifice is mobilised by water runoff (Smith & Lowe 1991), most likely sourced from heavy rainfall. Smith (1991) has demonstrated that volcaniclastic debris flows are usually formed during eruptions, due to the influx of loose pyroclastic debris and the destabilisation of the volcanic land surface by the devastation of the local vegetation.

The other sedimentary units within the UBF, excluding the volcaniclastic debris flows discussed above, are volcaniclastic siltstones and sandstones, all of which were deposited in a terrestrial environment. These units are poorly sorted, clast to matrix supported and dominated by (variably) palagonitised basaltic glass clasts. Some of the clasts still preserve textures indicative of a pyroclastic mode of formation but have subsequently been reworked and partially rounded. These pyroclastic textures include cuspate margins interpreted to be the remains of bubble walls. Some of the opaque glass clasts are highly vesiculated, suggesting that they are reworked basaltic scoria. Some of the lithologies contain small proportions of various types of crystalline basalt, derived from (older) lava flows. The range of surface oxidation of the glass and lava clasts suggests that numerous lava flows and ash deposits were being contemporaneously eroded. The rounding of the clasts, together with the development of evidence of laminations and cross-bedding, indicates that the volcaniclastic lithologies were deposited in a fluvial environment (cf.

Collinson 1996; Tucker 1996a). Smith (1991) has demonstrated that finer-grained fluvial deposits in a volcanic setting are commonly formed during hiatuses in the volcanic activity, due in part to the lack of loose debris which has already been removed during syn-eruption periods by debris flows and the stabilising of the volcanic land surface by vegetation. Evidence for the establishment of vegetation on the volcanic land surface is preserved at the bases of lava flows in the UBF in the form of tree moulds, for example, at Sundshálsur, Streymoy. Vegetation was destroyed by the eruption of the flows and consequently, led to the destabilisation of the land surface providing loose debris for transportation.

The general lack of palaeosols preserved within the UBF, compared to the LBF, suggests that the eruption frequency was higher in the UBF, which reduced the amount of time available for subaerial chemical weathering. These higher eruption frequencies also hindered the development of fluvial systems, restricting the amount of erosion on the contemporaneous land surface. This is reflected in the overall lack of basalt lava clasts within the volcaniclastic lithologies of the UBF compared to the dominance of lava clasts in the LBF volcaniclastic strata. Where fluvial strata are recorded within the UBF they are commonly associated with plant debris and fossil trees, suggesting that hiatuses in the volcanic activity were prolonged.

8 Faeroe-Shetland Basin

The first half of this chapter is a brief summary of the volcanic lithologies reported in the literature, which are encountered within the Faeroe-Shetland Basin. This includes lavas, pyroclastic rocks, sills and central complexes. The second half of the chapter describes the lithologies from the volcanic interval within Well 214/4-1. Data available for the study consisted of the well log, sidewall core samples and ditch cuttings. Unfortunately, no seismic lines of the Faeroe-Shetland Basin were available for consultation. A geochemical analysis of the igneous material extracted from the ditch cuttings is correlated to the volcanic succession of the Faeroe Islands. Lastly, environments of eruption and deposition for the volcanic interval are proposed for the well and how these relate to the Faeroe Plateau Lava Group of the Faeroe Islands are described.

8.1 Distribution of Volcanic Rocks in the FSB

The Faeroe-Shetland Basin (FSB) is located to the SE of the Faeroe Islands and NW of the Shetland Islands and has an overall NE-SW trend. The FSB and a number of sub-basins are confined to the NE by the Erlend and North Shetland Platforms, to the SE by the Shetland Spine Fault, to the W by the Westray Ridge and to the NW by the Corona Ridge (Fig. 8.1) (Dean *et al.* 1999). Prominent features associated with the Palaeogene interval of the FSB include the Faeroe-Shetland Escarpment to the N and the Wyville-Thomson Ridge to the S (Fig. 8.2). The Wyville-Thomson Ridge marks the transition from the FSB into the North Rockall Trough. A generalised sedimentary sequence for the Palaeogene west of Shetland area is presented in Figure 8.3. The Palaeogene in this area is subdivided into three sedimentary groups: Shetland, Faeroe, and Moray. Each of these groups can be subdivided into formations (Knox *et al.* 1997).

Both extrusive and intrusive igneous rocks occur throughout the FSB (Andersen 1988; Fitch *et al.* 1988; Gibb & Kanaris-Sotiriou 1988; Morton *et al.* 1988; Stoker *et al.* 1988; Hinz *et al.* 1993; Kanaris-Sotiriou *et al.* 1993; Ritchie & Hitchen 1996; Levell & Thompson 1999; Naylor *et al.* 1999; Ritchie *et al.* 1999; Planke 2001; Ellis *et al.* 2002; Jolley & Bell 2002a). Lavas from the Faeroe Plateau Lava Group (FPLG) dominate the area to the NW of the FSB extending back to the Faeroe Islands. There are also localised lavas associated with the Erlend Volcanic Centre (Mitchell & Euwe 1988; Kanaris-Sotiriou *et al.* 1993; Ritchie & Hitchen 1996; Naylor *et al.* 1999; Jolley & Bell 2002b). Tuffs are present within the FSB; in particular the well-documented Balder Formation and the less

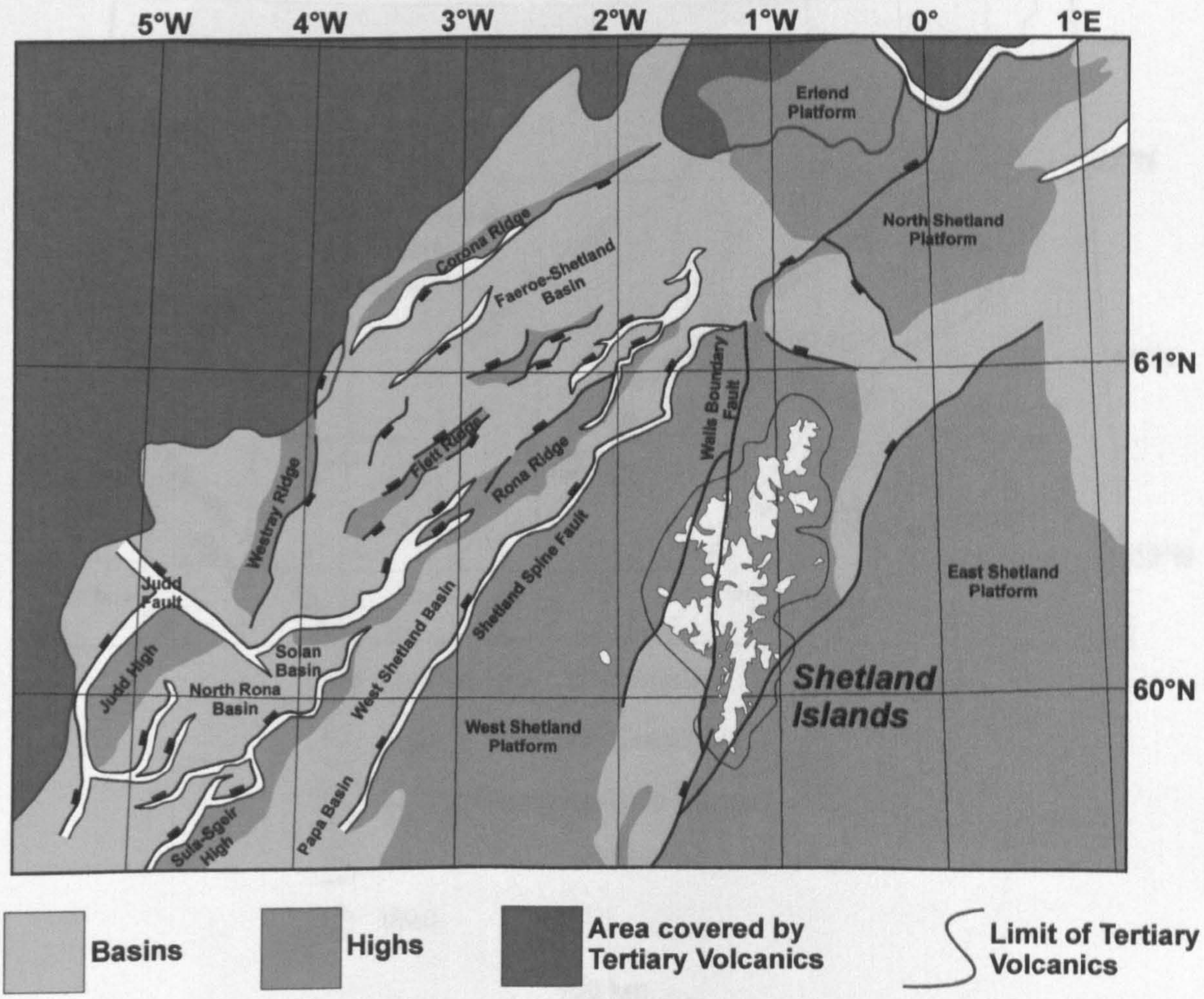

Fig. 8.1. Principle tectonic element map of the Faeroe-Shetland and surrounding basins, NE Atlantic. After Dean *et al.* (1999).

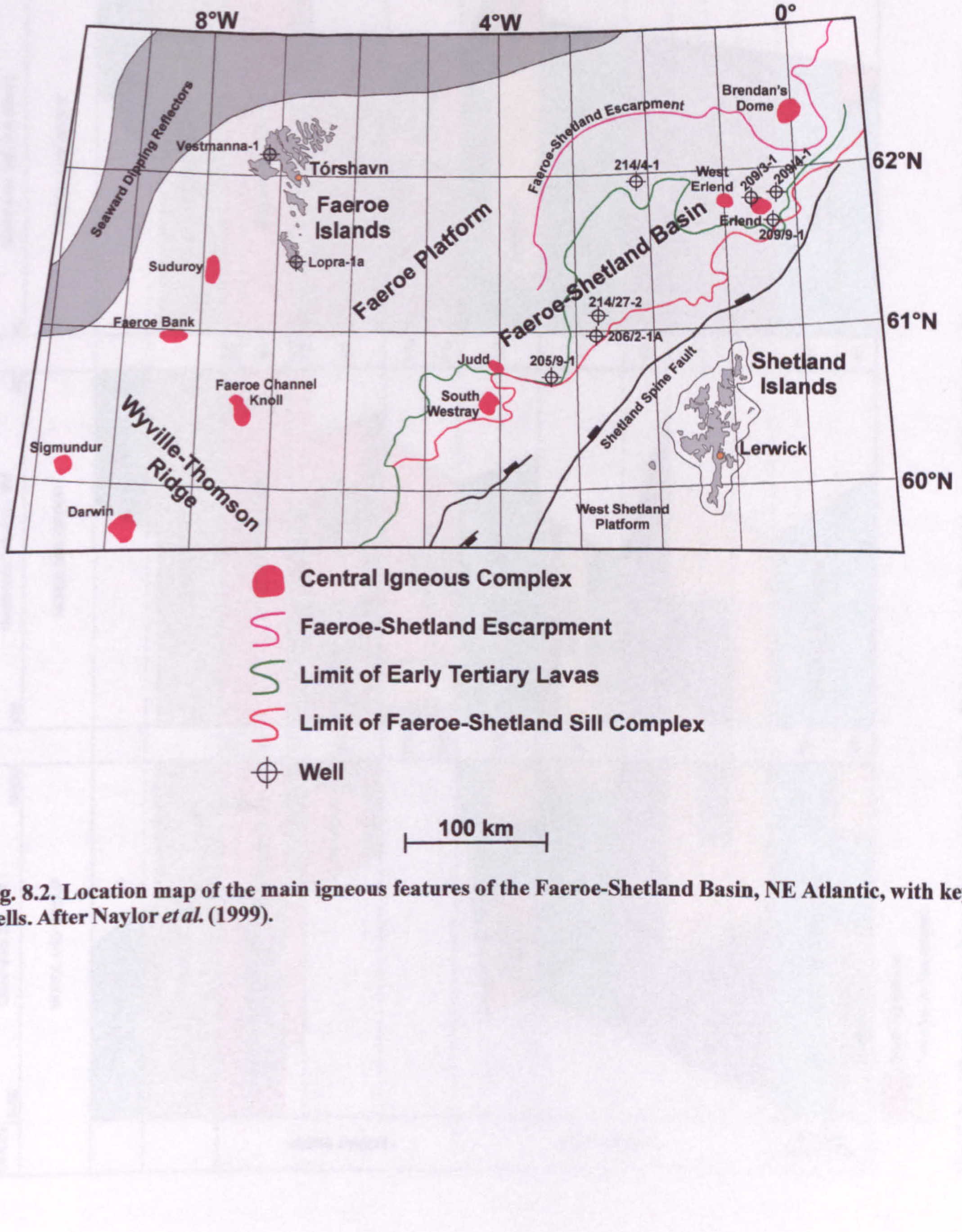

Fig. 8.2. Location map of the main igneous features of the Faeroe-Shetland Basin, NE Atlantic, with key wells. After Naylor *et al.* (1999).

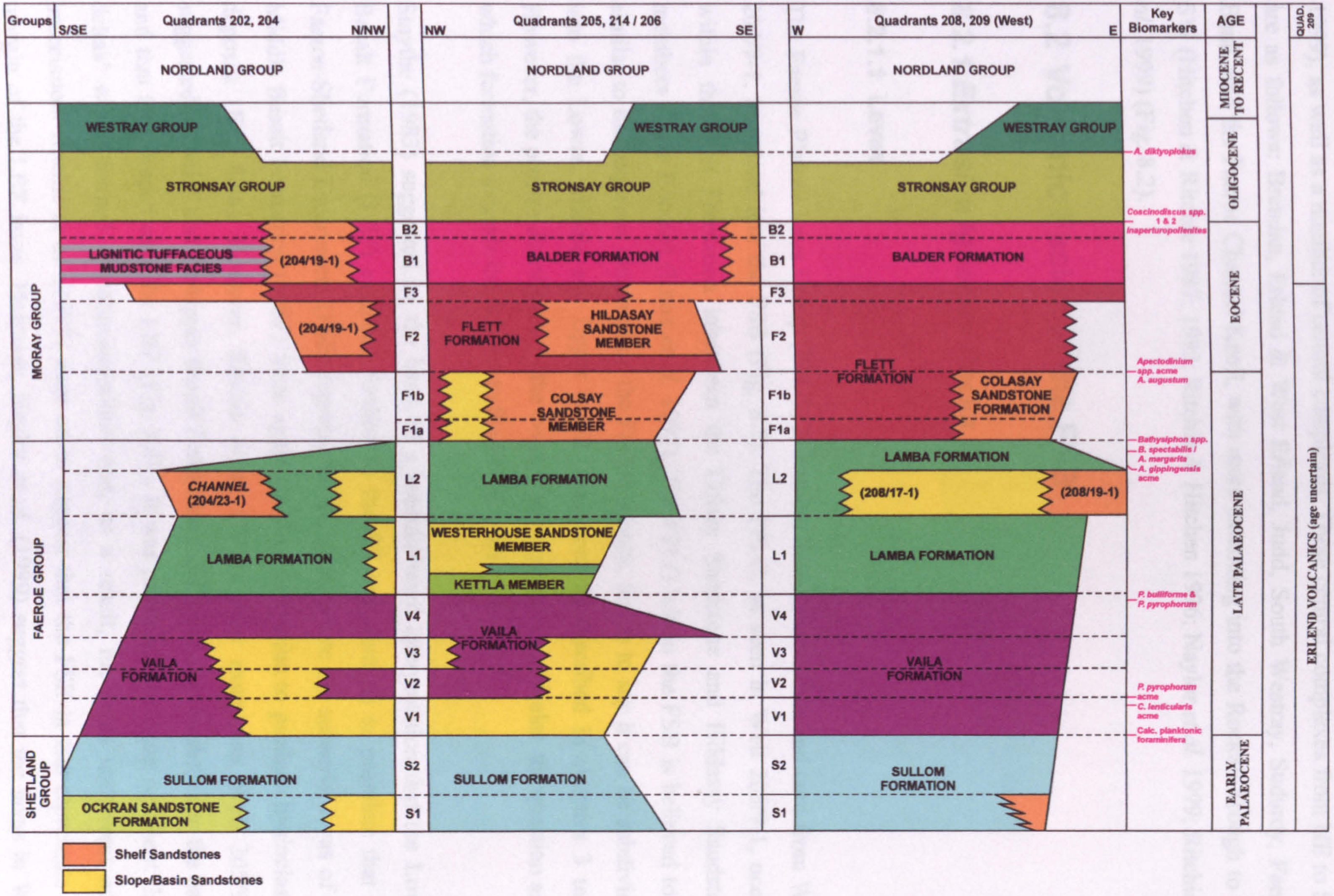

Fig. 8.3. Lithostratigraphic nomenclature for the Palaeogene of the UK west of the Shetland area. After Knox *et al.* (1997).

understood Kettla Member (Knox *et al.* 1997; Naylor *et al.* 1999). Intrusive rocks within the FSB consist of the Faeroe-Shetland Sill Complex (Ridd 1983; Mudge & Rashid 1987; Gibb & Kanaris-Sotiriou 1988; Hitchen & Ritchie 1993; Naylor *et al.* 1999; Ritchie *et al.* 1999), as well as a number of central complexes. These central complexes from NE to SW are as follows: Brendan, Erlend & West Erlend, Judd, South Westray, Suduroy, Faeroe Bank, and the Faeroe Channel Knoll, with more extending into the Rockall Trough to the SW (Hitchen & Ritchie 1987; 1993; Ritchie & Hitchen 1996; Naylor *et al.* 1999; Ritchie *et al.* 1999) (Fig. 8.2).

8.2 Volcanic Facies in the FSB

8.2.1 Extrusive Igneous Rocks

8.2.1.1 Lavas

The Faeroe Plateau Lava Group (FPLG) is known, from seismic data and core from Well 205/9-1, to extend into the FSB (Fig. 8.2). The FPLG, as seen in Well 205/9-1, occurs within the Flett Formation inbetween the Colsay Sandstone and Hildasay Sandstone members (early Eocene) (Knox *et al.* 1997). The FPLG within the FSB is believed to be similar to the sequence observed on the Faeroe Islands, that is to say it can be subdivided into the Lower, Middle and Upper basalt formations as described in chapters 3 to 7. However, the precise distribution of the lavas is in question, in particular, the question as to which formation extends the furthest to the SE (Ritchie *et al.* 1999).

Smythe (1983) suggested on the basis of a seismic-based interpretation that the Lower Basalt Formation (LBF) extended furthest to the SE and went on to postulate that the Faeroe-Shetland Escarpment (FSE) represented the point where the subaerial lavas of the Middle Basalt Formation (MBF) froze against a palaeoshoreline to produce hyaloclastite deposits (Fig. 8.4a). However, Ritchie *et al.* (1999), after examining Well 205/9-1, suggested the MBF and the Upper Basalt Formation (UBF) extended furthest into the basin and that they draped over the LBF (Fig. 8.4b). It was proposed that these represent 'lava deltas' which formed at palaeoshorelines and, as a result, the lavas underwent auto-brecciation. Ritchie *et al.* (1999) went on to suggest that the FSE in fact represents the margin of the LBF lavas. However, Naylor *et al.* (1999) suggest that the lavas in Well 205/9-1 are time equivalent to the top of the LBF or the base of the MBF and Ellis *et al.* (2002) suggest that they correlate to the LBF which were most likely erupted locally. More

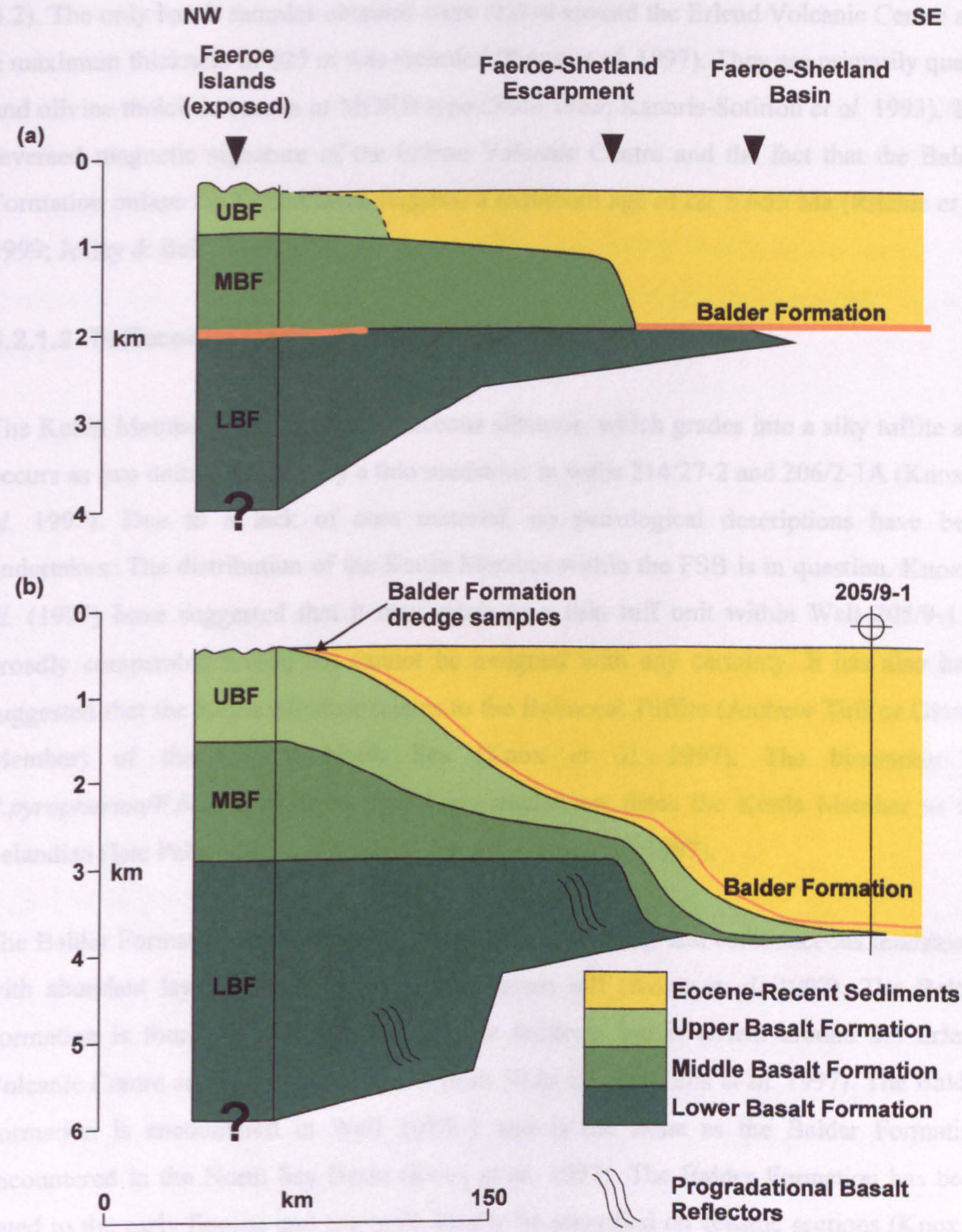

Fig. 8.4. Schematic correlation of the onshore and offshore Faeroe Plateau Lava Group after (a) Smythe (1983) and (b) Ritchie *et al.* (1999). Naylor *et al.* (1999) and Ellis *et al.* (2002) suggest that the lavas in Well 205/9-1 correlate to the Lower Basalt Formation, thus, suggesting that the correlation by Ritchie *et al.* (1999) may be incorrect.

detailed examination of the geochemical and age data is required to precisely correlate the lavas encountered in Well 205/9-1 to the lavas of the FPLG.

The Erlend lavas are associated with the Erlend and West Erlend Volcanic Centres (Fig. 8.2). The only basalt samples obtained were drilled around the Erlend Volcanic Centre and a maximum thickness of 825 m was recorded (Knox *et al.* 1997). They are primarily quartz and olivine tholeiitic basalts of MORB-type (Ridd 1983; Kanaris-Sotiriou *et al.* 1993). The reversed magnetic signature of the Erlend Volcanic Centre and the fact that the Balder Formation onlaps the Erlend lavas suggests a minimum age of *ca.* 57-55 Ma (Ritchie *et al.* 1999; Jolley & Bell 2002b).

8.2.1.2 Tuffaceous Units

The Kettla Member is primarily a tuffaceous siltstone, which grades into a silty tuffite and occurs as two units, separated by a thin mudstone in wells 214/27-2 and 206/2-1A (Knox *et al.* 1997). Due to a lack of core material, no petrological descriptions have been undertaken. The distribution of the Kettla Member within the FSB is in question. Knox *et al.* (1997) have suggested that it may relate to a thin tuff unit within Well 205/9-1 at broadly comparable levels, but cannot be assigned with any certainty. It has also been suggested that the Kettla Member relates to the Balmoral Tuffite (Andrew Tuff or Glamis Member) of the Central North Sea (Knox *et al.* 1997). The biomarker of *P.pyrophorum/P.bulltforne* from underlying mudstones dates the Kettla Member to the Selandian (late Palaeocene (*ca.* 58.9-58.2 Ma)) (Knox *et al.* 1997).

The Balder Formation is characterised by grey, variably silty and carbonaceous mudstones with abundant layers of green-grey to grey-green tuff (Knox *et al.* 1997). The Balder Formation is found in all of the Palaeogene sections, but is absent around the Erlend Volcanic Centre and ranges in thickness from 50 to 150 m (Knox *et al.* 1997). The Balder Formation is encountered in Well 205/9-1 and is the same as the Balder Formation encountered in the North Sea Basin (Knox *et al.* 1997). The Balder Formation has been dated to the early Eocene and can quite clearly be identified on seismic sections (Knox *et al.* 1997).

8.2.2 Intrusive Igneous Rocks

8.2.2.1 Sill Complexes

The Faeroe-Shetland Sill Complex extends from the Wyville-Thomson Ridge in the SW to the Vøring Basin in the NE (Fig. 8.2). The complex is 750 km long by 100 km wide (Ritchie *et al.* 1999) and covers an area of 40,000 km^2 (Naylor *et al.* 1999). The sills within the complex are tholeiitic olivine dolerites with a T-MORB type composition. They are geochemically similar to that of the UBF of the FPLG. The complex has been intruded into strata of predominantly Cretaceous age (Naylor *et al.* 1999). Dating of the complex has produced a wide spectrum of ages ranging from *ca.* 82 to 48 Ma, but a consensus supports an age between *ca.* 55-53 Ma (Ritchie *et al.* 1999).

8.2.2.2 Central Complexes

A number of the central complexes within the FSB have only been recognised by geophysical studies. These complexes include: Brendan, Judd, South Westray, Suduroy, Faeroe Bank, and Faeroe Channel Knoll (Fig. 8.2). As a result they are poorly understood, but all are recognised as being Palaeogene in age (B.R. Bell *pers. comm.*). Drilling has proved the presence of the Erlend Volcanic Centre, which consists of intrusive rocks that are silicic rhyolites and dacites (Naylor *et al.* 1999), which are reversely magnetised (Rumph *et al.* 1993).

8.3 Well 214/4-1

Well 214/4-1 (61°57'54''N, 002°14'01''W) is located *ca.* 237 km E of Tórshavn, Faeroe Islands and *ca.* 210 km NNW of Lerwick, Shetland Islands in the Faeroe-Shetland Basin (FSB) (Figs. 1.2 & 8.2). The well was drilled by Mobil (now part of ExxonMobil) between the 10 April and 14 July 1999 and reached a total depth of *ca.* 14,700 ft (*ca.* 4,480 m). The well drilled through a volcanic interval *ca.* 1,920 ft (*ca.* 585 m) thick from the depth of *ca.* 12,780 ft (*ca.* 3,895 m) to the base of the well (Fig. 8.5). Fifty-one sidewall cores were recovered from the volcanic interval during runs 3a and 3b.

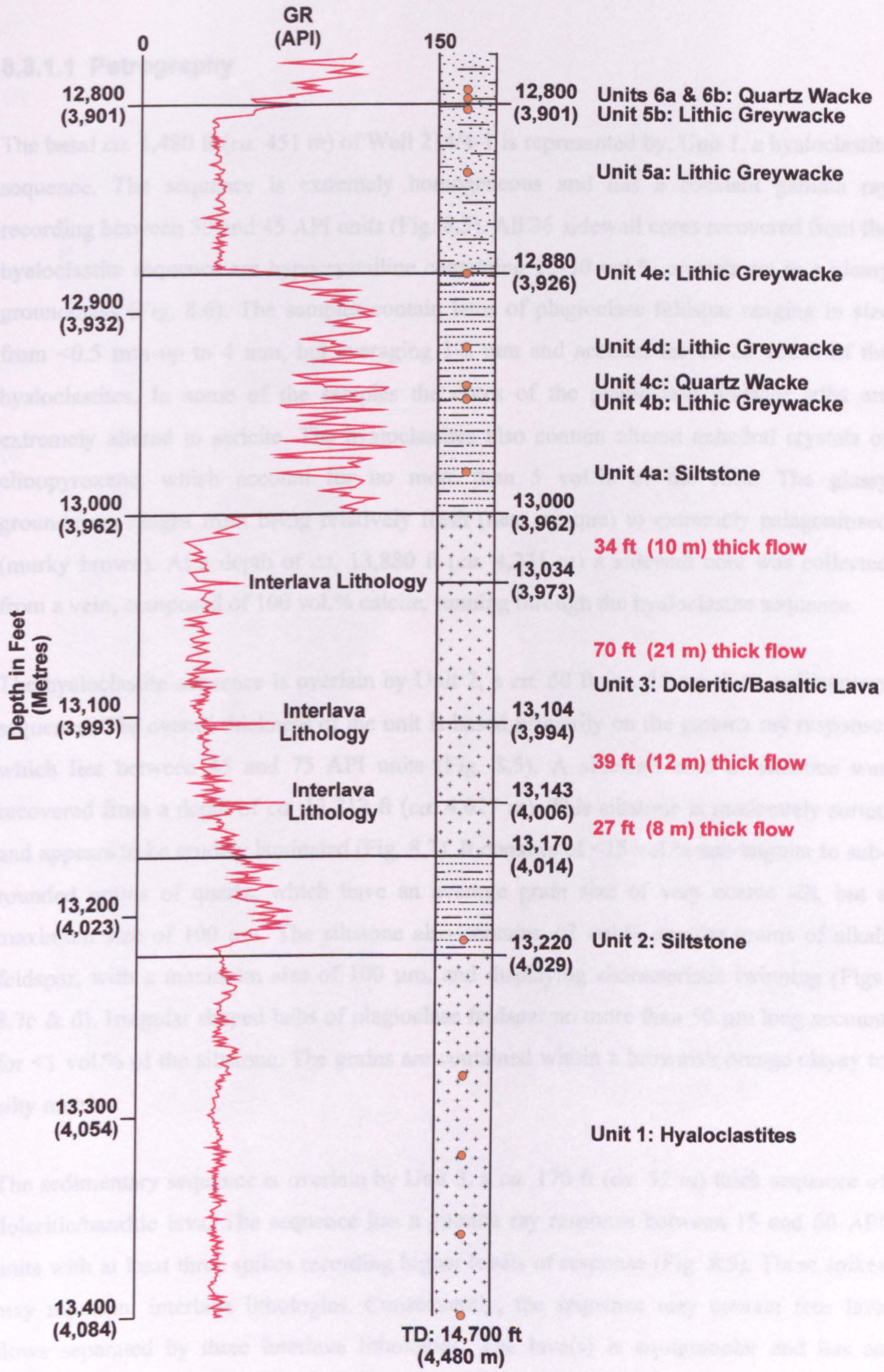

Fig. 8.5. Wireline log for the upper section of the volcanic interval in Well 214/4-1, Faeroe-Shetland Basin. Unit 1 is extremely homogenous and extends to the base of the well. The orange circles represent recovered sidewall cores.

8.3.1 Volcanic Interval

8.3.1.1 Petrography

The basal *ca.* 1,480 ft (*ca.* 451 m) of Well 214/4-1 is represented by, Unit 1, a hyaloclastite sequence. The sequence is extremely homogeneous and has a constant gamma ray recording between 30 and 45 API units (Fig. 8.5). All 36 sidewall cores recovered from the hyaloclastite sequence are hypocrystalline containing 10-30 vol.% crystals set in a glassy groundmass (Fig. 8.6). The samples contain laths of plagioclase feldspar ranging in size from <0.5 mm up to 4 mm, but averaging 1-2 mm and account for 10-25 vol.% of the hyaloclastites. In some of the samples the cores of the plagioclase feldspar laths are extremely altered to sericite. The hyaloclastites also contain altered anhedral crystals of clinopyroxene, which account for no more than 5 vol.% of the rock. The glassy groundmass ranges from being relatively fresh (near opaque) to extremely palagonitised (murky brown). At a depth of *ca.* 13,880 ft (*ca.* 4,231 m) a sidewall core was collected from a vein, composed of 100 vol.% calcite, running through the hyaloclastite sequence.

The hyaloclastite sequence is overlain by Unit 2, a *ca.* 50 ft (*ca.* 15 m) thick sedimentary sequence. The overall thickness of the unit is based primarily on the gamma ray response, which lies between 45 and 75 API units (Fig. 8.5). A sidewall core of siltstone was recovered from a depth of *ca.* 13,212 ft (*ca.* 4,027 m). This siltstone is moderately sorted and appears to be crudely laminated (Fig. 8.7). It consists of <15 vol.% sub-angular to sub-rounded grains of quartz, which have an average grain size of very coarse silt, but a maximum size of 100 µm. The siltstone also contains <2 vol.% angular grains of alkali feldspar, with a maximum size of 100 µm, and displaying characteristic twinning (Figs. 8.7c & d). Irregular shaped laths of plagioclase feldspar no more than 50 µm long account for <1 vol.% of the siltstone. The grains are contained within a brownish orange clayey to silty matrix.

The sedimentary sequence is overlain by Unit 3, a *ca.* 170 ft (*ca.* 52 m) thick sequence of doleritic/basaltic lava. The sequence has a gamma ray response between 15 and 60 API units with at least three spikes recording higher levels of response (Fig. 8.5). These spikes may represent interlava lithologies. Consequently, the sequence may contain four lava flows separated by three interlava lithologies. The lava(s) is equigranular and has an average crystal size 300-500 µm (medium crystalline) (Fig. 8.8). It consists of *ca.* 50 vol.% randomly arranged laths of plagioclase feldspar, which have a maximum size of 1 mm together with *ca.* 40 vol.% anhedral crystals of clinopyroxene, which have a maximum size

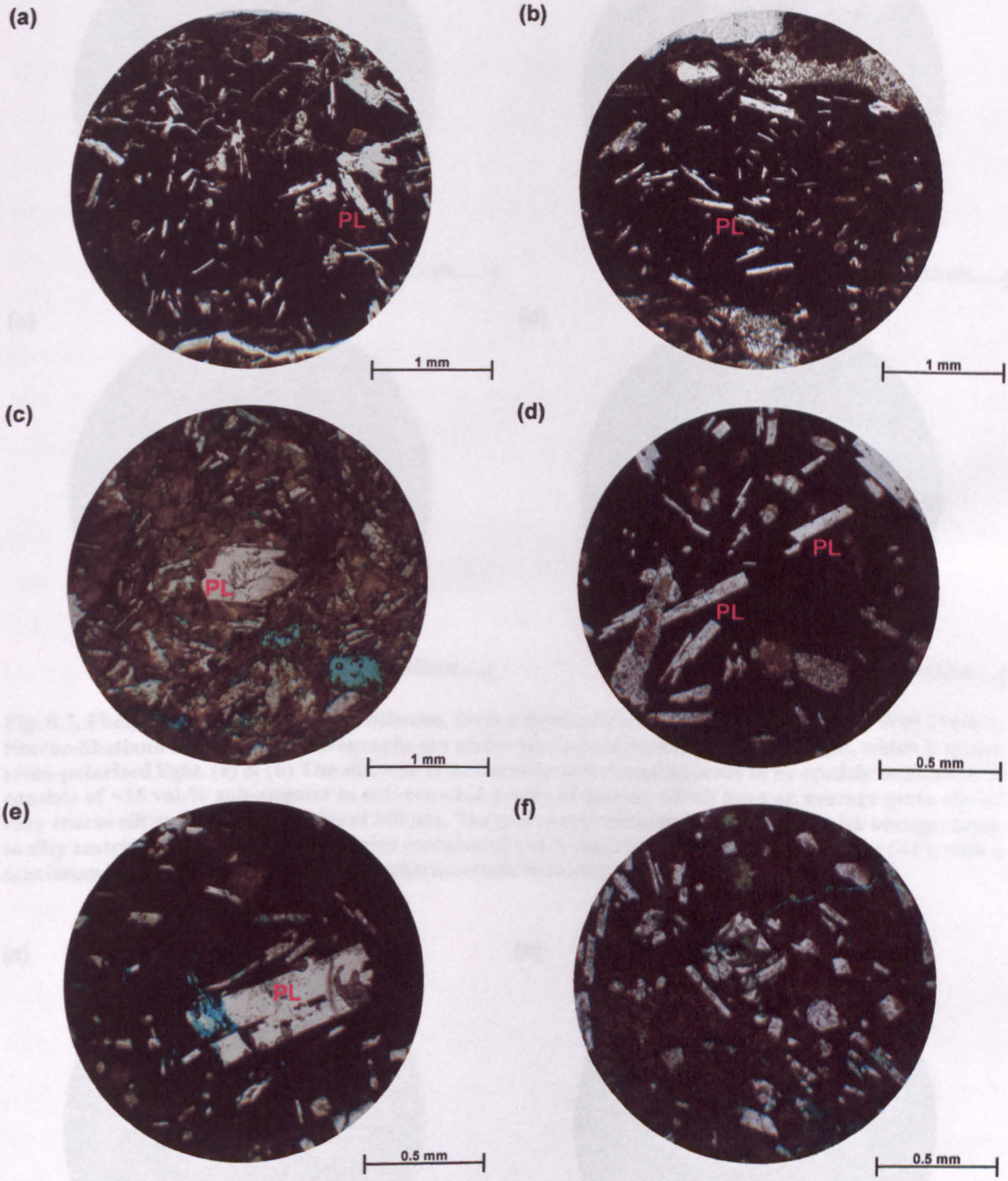

Fig. 8.6. Photomicrographs of Unit 1, hyaloclastite sequence, from Well 214/4-1, Faeroe-Shetland Basin. All of the photomicrographs are under plane-polarised light. The hyaloclastites are hypocrystalline containing 10-30 vol.% crystals set in a glassy groundmass. The samples contain laths of plagioclase feldspar (PL) ranging in size from <0.5 mm up to 4 mm, but averaging 1-2 mm and account for 10-25 vol.% of the hyaloclastites. In some of the samples the cores of the plagioclase feldspar laths are extremely altered to sericite. The hyaloclastites also contain altered anhedral crystals of clinopyroxene, which account for no more than 5 vol.% of the rock. The glassy groundmass ranges from being relatively fresh (near opaque) to extremely palagonitised (murky brown). Sidewall cores from depths of (a) *ca.* 13, 400 ft (*ca.* 4,084 m), (b) *ca.* 13,500 ft (*ca.* 4,115 m), (c) & (d) *ca.* 13,550 ft (*ca.* 4,130 m), (e) *ca.* 13,780 ft (*ca.* 4,200 m) and (f) *ca.* 14,240 ft (*ca.* 4,340 m).

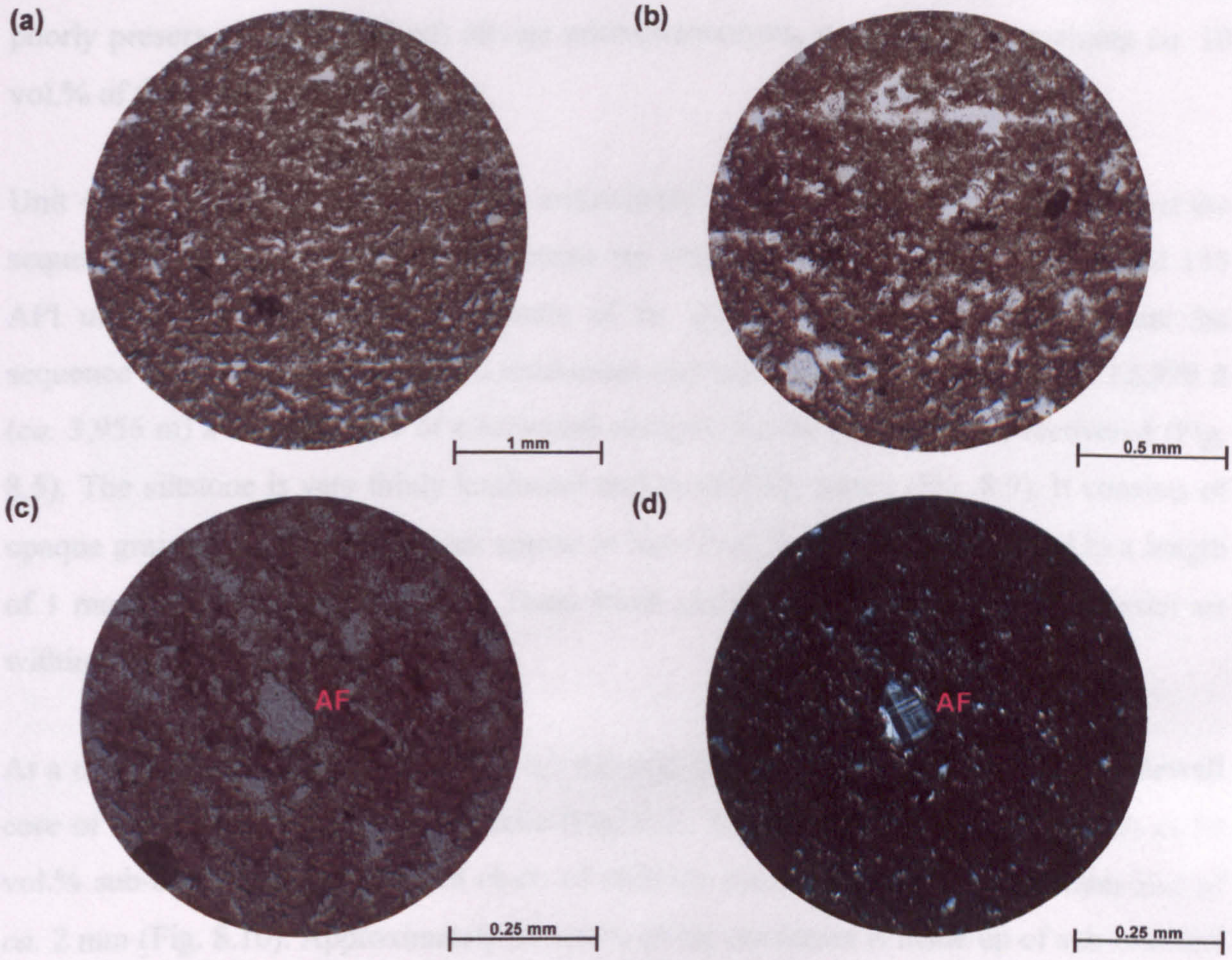

Fig. 8.7. Photomicrographs of Unit 2, siltstone, from a depth of *ca.* 13,212 ft (*ca.* 4,027 m) in Well 214/4-1, Faeroe-Shetland Basin. Photomicrographs are under plane-polarised light except for (d), which is under cross-polarised light. (a) & (b) The siltstone is moderately sorted and appears to be crudely laminated. It consists of <15 vol.% sub-angular to sub-rounded grains of quartz, which have an average grain size of very coarse silt and a maximum size of 100 µm. The grains are contained within a brownish orange clayey to silty matrix. (c) & (d) The siltstone also contains <2 vol.% angular grains of alkali feldspar (AF), with a maximum size of 100 µm, and displaying characteristic twinning.

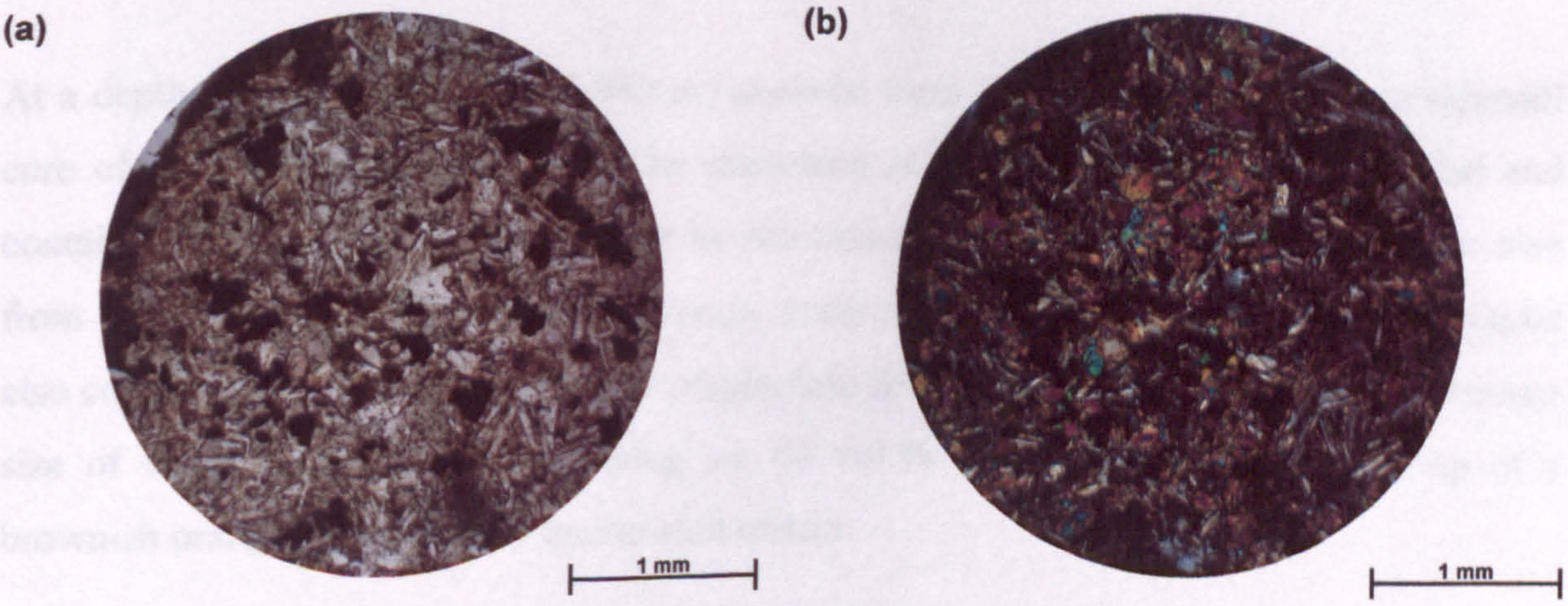

Fig. 8.8. Photomicrographs of Unit 3, doleritic/basaltic lava, from a depth of *ca.* 13,150 ft (*ca.* 4,008 m) in Well 214/4-1, Faeroe-Shetaland Basin. (a) Photomicrograph under plane-polarised light. The lava is equigranular and has an average crystal size 300-500 µm (medium crystalline). It consists of *ca.* 50 vol.% randomly arranged laths of plagioclase feldspar, which have a maximum size of 1 mm together with *ca.* 40 vol.% anhedral crystals of clinopyroxene, which have a maximum size of 300 µm. Irregular shaped oxides with a maximum size of *ca.* 500 µm, together with poorly preserved (serpentinised) olivine microphenocrysts, represent the remaining *ca.* 10 vol.% of the lava. (b) Same view as in (a) but under cross-polarised light.

of 300 µm. Irregular shaped oxides with a maximum size of *ca.* 500 µm, together with poorly preserved (serpentinised) olivine microphenocrysts, represent the remaining *ca.* 10 vol.% of the lava.

Unit 4 is a *ca.* 120 ft (*ca.* 37 m) thick sedimentary sequence. The overall thickness of the sequence is based primarily on the gamma ray response, which lies between 75 and 135 API units (Fig. 8.5). The erratic nature of the gamma ray response suggests that the sequence is made up of intercalated mudstones and sandstones. At a depth of *ca.* 12,979 ft (*ca.* 3,956 m) a sidewall core of a brownish orange siltstone (Unit 4a) was recovered (Fig. 8.5). The siltstone is very thinly laminated and moderately sorted (Fig. 8.9). It consists of opaque grains <100 µm in size that appear to have been flattened and stretched to a length of 1 mm parallel to the lamination. These black grains may be carbonaceous material set within a clayey to silty matrix.

At a depth of *ca.* 12,941 ft (*ca.* 3,944 m) material from Unit 4b was recovered, a sidewall core of a poorly sorted lithic greywacke (Fig. 8.5). The sandstone contains as much as 30 vol.% sub-angular to sub-rounded clasts of doleritic lava, which have a maximum size of *ca.* 2 mm (Fig. 8.10). Approximately 20 vol.% of the sandstone is made up of sub-rounded clasts of brownish orange siltstone, which range in size from 1 to 5 mm. The lithic clasts are contained within a matrix comprising *ca.* 10 vol.% angular to sub-rounded grains of quartz with an average size of very fine sand, although grains with a maximum size of 300 µm have been recorded. The remaining 40 vol.% of the matrix is made up of brownish clayey to silty material.

At a depth of *ca.* 12,933 ft (*ca.* 3,942 m) material from Unit 4c was recovered, a sidewall core of a quartz wacke (Fig. 8.5). The sandstone is poorly sorted, matrix supported and contains as much as 40 vol.% angular to sub-rounded quartz grains, which range in size from 100 to 500 µm, which have an average grain size of fine sand (Fig. 8.11). The wacke also contains <1 vol.% altered angular plagioclase feldspar crystals, which have an average size of very fine sand. The remaining *ca.* 60 vol.% of the sandstone is made up of a brownish orange clayey to silty quartz-rich matrix.

At a depth of *ca.* 12,916 ft (*ca.* 3,937 m) material from Unit 4d was recovered, a sidewall core of a lithic greywacke (Fig. 8.5). The sandstone is poorly sorted, on the whole matrix supported, and consists of *ca.* 30 vol.% sub-angular to sub-rounded clasts of doleritic lava, which range in size from 1 to 5 mm (Fig. 8.12). The sandstone also contains *ca.* 10 vol.% lithic clasts of siltstone, which range in size from 1 to 5 mm. The greywacke also contains

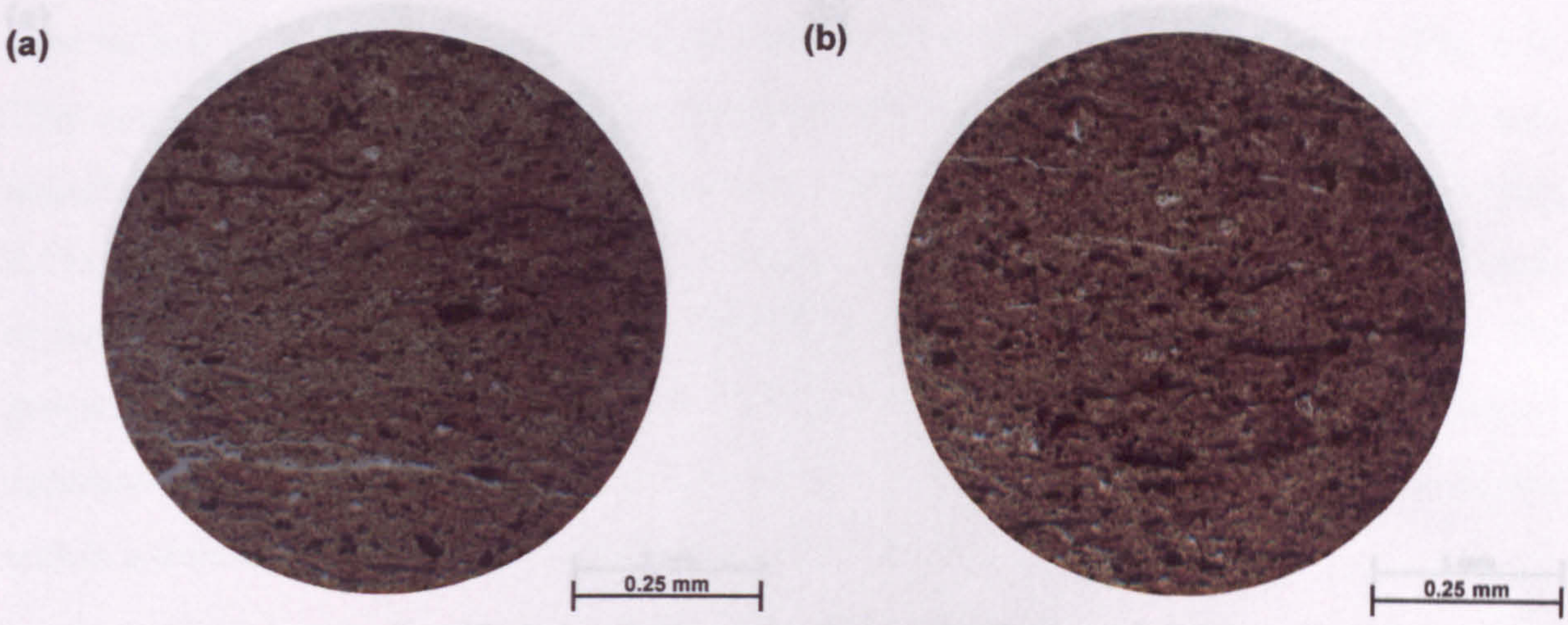

Fig. 8.9. Photomicrographs of Unit 4a, siltstone, from a depth of *ca.* 12,979 ft (*ca.* 3,956 m) in Well 214/4-1, Faeroe-Shetland Basin. Both photomicrographs are under plane-polarised light. (a) & (b) The siltstone is very thinly laminated and moderately sorted. It consists of opaque grains <100 μm in size that appear to have been flattened and stretched to a length of 1 mm parallel to the lamination. These black grains may be carbonaceous material set within a clayey to silty matrix.

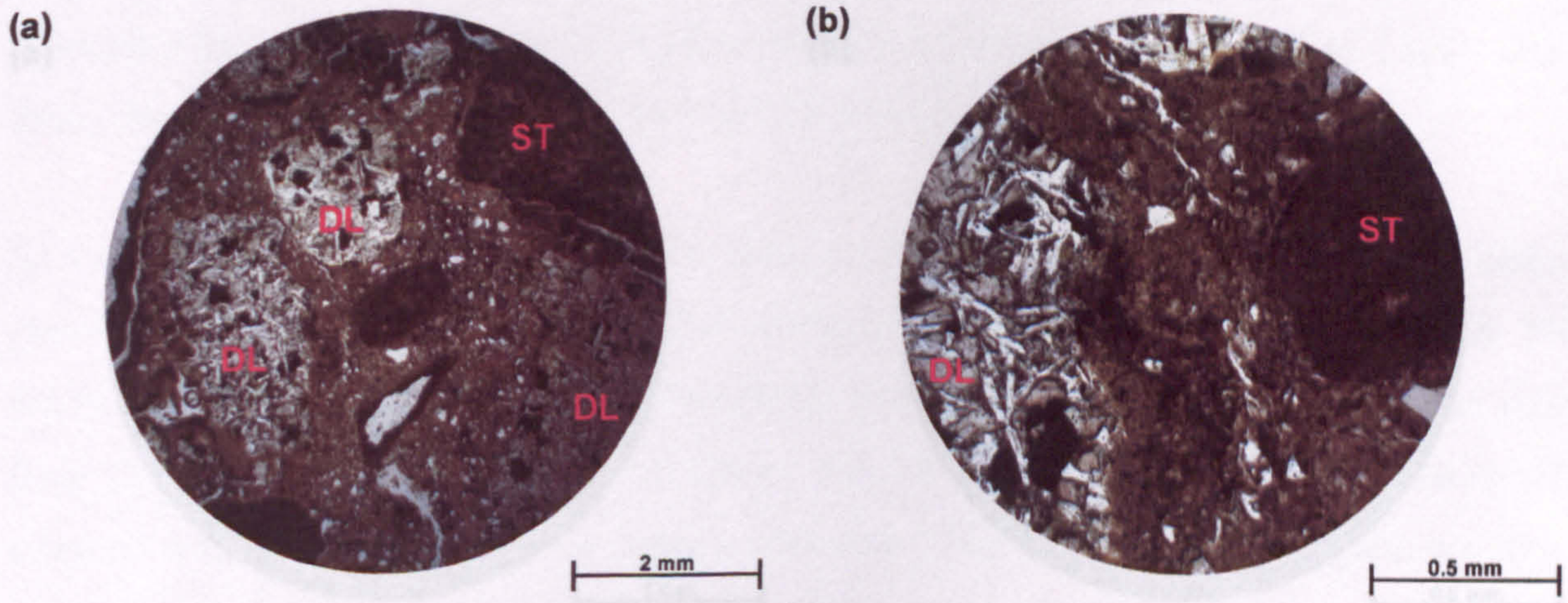

Fig. 8.10. Photomicrographs of Unit 4b, lithic greywacke, from a depth of *ca.* 12, 941 ft (*ca.* 3,944 m) in Well 214/4-1, Faeroe-Shetland Basin. Both photomicrographs are under plane-polarised light. (a) & (b) The sandstone contains as much as 30 vol.% sub-angular to sub-rounded clasts of doleritic lava (DL), which have a maximum size of *ca.* 2 mm. Approximately 20 vol.% of the sandstone is made up of sub-rounded clasts of brownish orange siltstone (ST), which range in size from 1 to 5 mm. The lithic clasts are contained within a matrix comprising *ca.* 10 vol.% angular to sub-rounded grains of quartz with an average size of very fine sand, although grains with a maximum size of 300 μm have been recorded. The remaining 40 vol.% of the matrix is made up of brownish clayey to silty material.

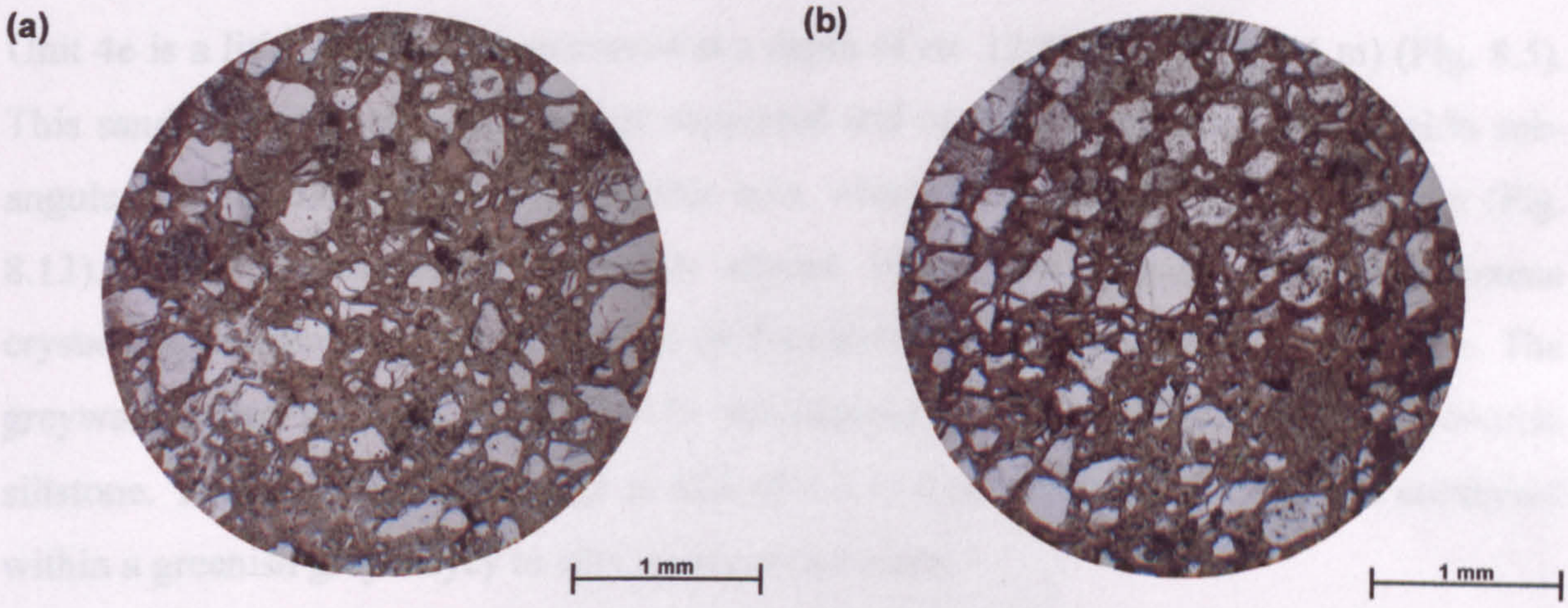

Fig. 8.11. Photomicrographs of Unit 4c, quartz wacke, from a depth of *ca.* 12,933 ft (*ca.* 3,942 m) in Well 214/4-1, Faeroe-Shetland Basin. Both photomicrographs are under plane-polarised light. (a) & (b) The sandstone is poorly sorted, matrix supported and contains as much as 40 vol.% angular to sub-rounded quartz grains, which range in size from 100 to 500 μm with have an average grain size of fine sand. The wacke also contains <1 vol.% altered angular plagioclase feldspar crystals, which have an average size of very fine sand. The remaining *ca.* 60 vol.% of the sandstone is made up of a brownish orange clayey to silty quartz-rich matrix.

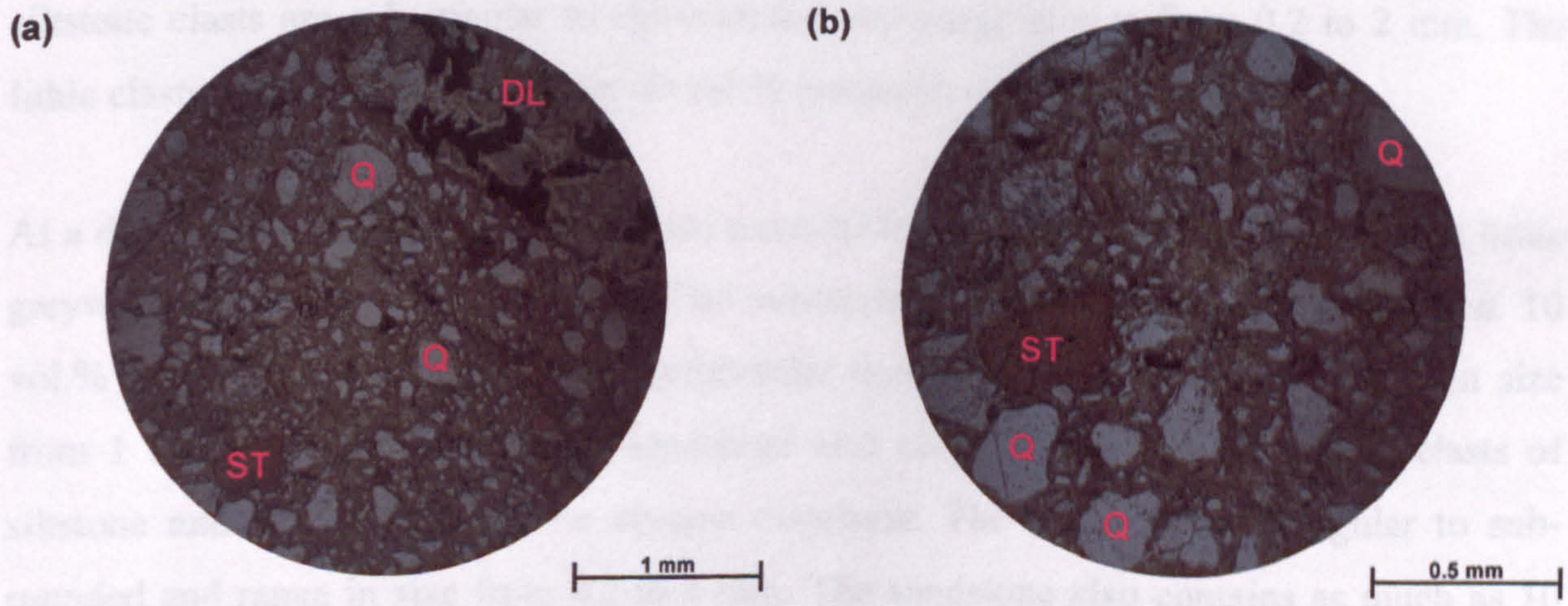

Fig. 8.12. Photomicrographs of Unit 4d, lithic greywacke, from a depth of *ca.* 12,916 ft (*ca.* 3,937 m) in Well 214/4-1, Faeroe-Shetland Basin. Both photomicrographs are under plane-polarised light. (a) & (b) The sandstone is poorly sorted, on the whole matrix supported, and consists of *ca.* 30 vol.% sub-angular to sub-rounded clasts of doleritic lava (DL), which range in size from 1 to 5 mm. The sandstone also contains *ca.* 10 vol.% lithic clasts of siltstone (ST), which range in size from 1 to 5 mm. The greywacke also contains *ca.* 20 vol.% sub-angular to sub-rounded grains of quartz (Q) with an average size of fine sand and a maximum size of 500 μm. The remaining 40 vol.% of the greywacke is composed of a greyish clayey to silty quartz-rich matrix.

ca. 20 vol.% sub-angular to sub-rounded grains of quartz with an average size of fine sand and a maximum size of 500 μm. The remaining 40 vol.% of the greywacke is composed of a greyish clayey to silty quartz-rich matrix.

Unit 4e is a lithic greywacke recovered at a depth of *ca.* 12,880 ft (*ca.* 3,926 m) (Fig. 8.5). This sandstone is poorly sorted, clast supported and consists of as much as 50 vol.% sub-angular to sub-rounded clasts of doleritic lava, which have an average size of 2 mm (Fig. 8.13). Some of these clasts are highly altered. Plagioclase feldspar and clinopyroxene crystals have been liberated from some of the clasts and incorporated into the matrix. The greywacke also contains *ca.* 30 vol.% sub-angular to sub-rounded clasts of brownish siltstone. The siltstone clasts range in size of 0.3 to 4 mm. The lithic clasts are contained within a greenish grey clayey to silty quartz-rich matrix.

Unit 5 is a *ca.* 80 ft (*ca.* 24 m) thick sedimentary sequence. The overall thickness of the sequence and the distinction from the underlying unit is established from the gamma ray log, which is constant throughout the unit, ranging between 30 and 45 API units (Fig. 8.5). At a depth of *ca.* 12,830 ft (*ca.* 3,911 m) material from Unit 5a was recovered, a sidewall core of a lithic greywacke (Fig. 8.5). This sandstone is poorly sorted and contains *ca.* 30 vol.% sub-angular to sub-rounded doleritic lava clasts, which range in size from 1 to 4 mm (Fig. 8.14). The sandstone also contains *ca.* 30 vol.% brownish clasts of siltstone. The siltstone clasts are sub-angular to sub-rounded and range in size from 0.2 to 2 mm. The lithic clasts are contained within *ca.* 40 vol.% brownish clayey to silty matrix.

At a depth of *ca.* 12,802 ft (*ca.* 3,902 m) material from Unit 5b, a sidewall core of a lithic greywacke was recovered (Fig. 8.5). The sandstone is poorly sorted and contains *ca.* 10 vol.% sub-angular to sub-rounded equigranular doleritic lava clasts, which range in size from 1 to 5 mm (Fig. 8.15). The sandstone also contains *ca.* 10 vol.% lithic clasts of siltstone and what appears to be opaque claystone. The clasts are sub-angular to sub-rounded and range in size from 0.2 to 1 mm. The sandstone also contains as much as 10 vol.% sub-angular to sub-rounded grains of quartz, with an average size of fine sand. The remaining *ca.* 70 vol.% of the sandstone consists of a brownish grey quartz-rich silty matrix.

Unit 6 is a sedimentary sequence with a minimum thickness of *ca.* 20 ft (*ca.* 6 m). The gamma ray response ranges between 60 and 120 API units (Fig. 8.5). At a depth of *ca.* 12,793 ft (*ca.* 3,899 m) material from Unit 6a was recovered, a sidewall core of a quartz wacke (Fig. 8.5). The sandstone is poorly sorted, matrix supported and contains <5 vol.%

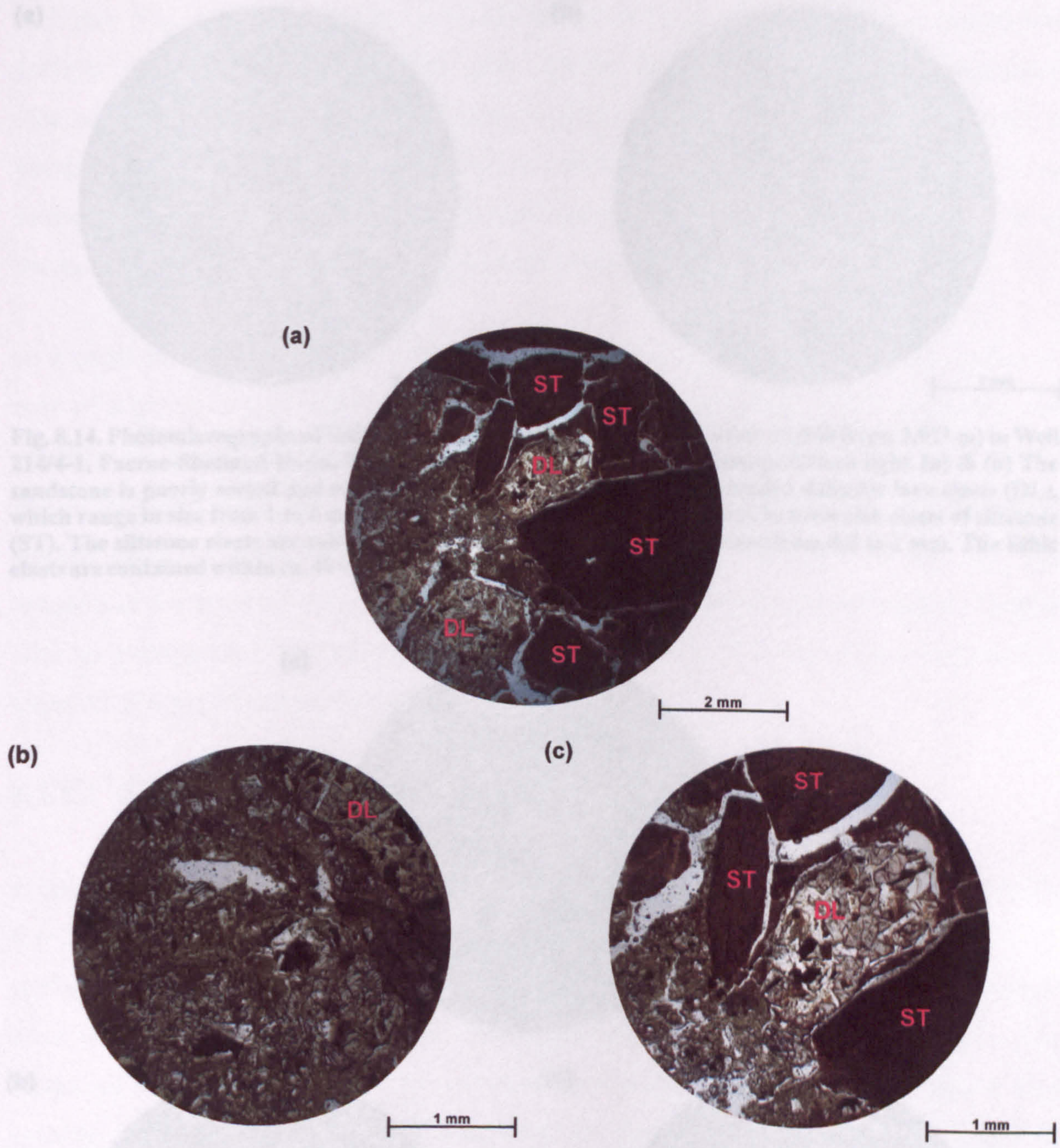

Fig. 8.13. Photomicrographs of Unit 4e, lithic greywacke, from a depth of *ca.* 12,880 ft (*ca.* 3,926 m) in Well 214/4-1, Faeroe-Shetland Basin. All of the photomicrographs are under plane-polarised light. (A) to (c) The sandstone is poorly sorted, clast supported and consists of as much as 50 vol.% sub-angular to sub-rounded clasts of doleritic lava (DL), which have an average size of 2 mm. Some of these clasts are highly altered. Plagioclase feldspar and clinopyroxene crystals have been liberated from some of the clasts and incorporated into the matrix. The greywacke also contains *ca.* 30 vol.% sub-angular to sub-rounded clasts of brownish siltstone (ST), which range in size of 0.3 to 4 mm. The lithic clasts are contained within a greenish grey clayey to silty quartz-rich matrix.

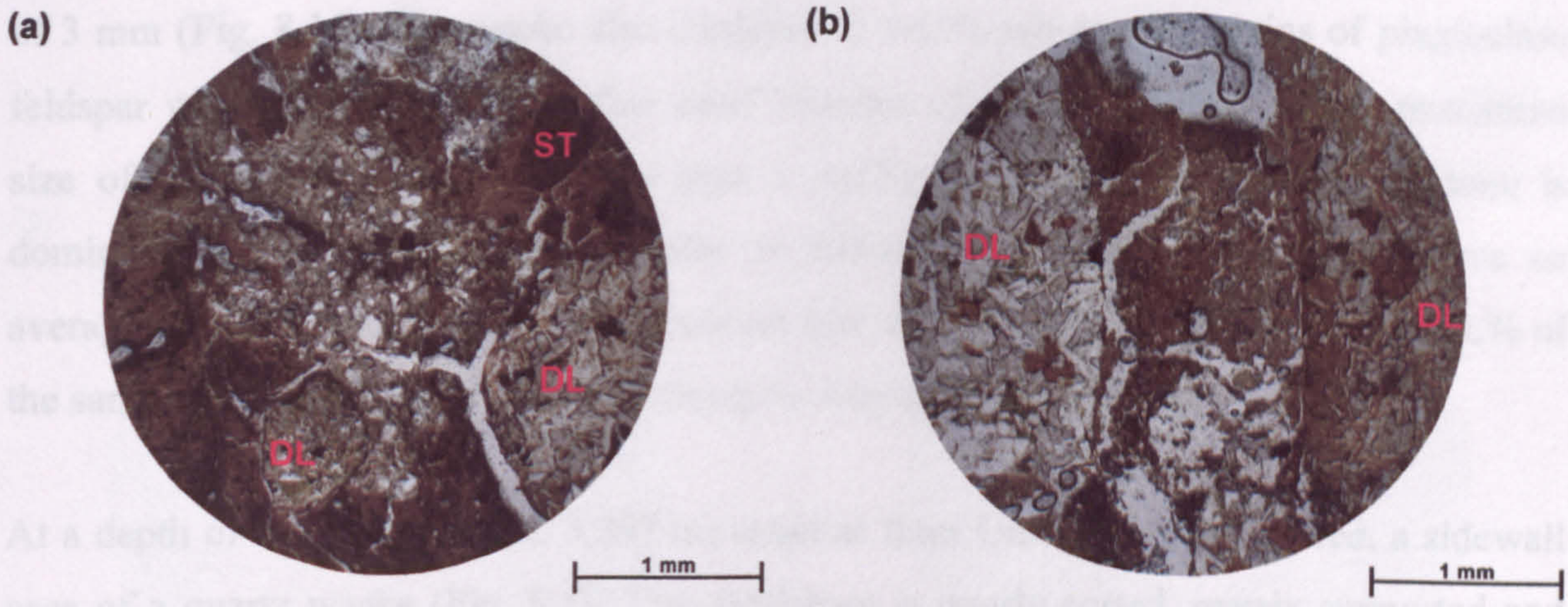

Fig. 8.14. Photomicrographs of Unit 5a, lithic greywacke, from a depth of *ca.* 12,830 ft (*ca.* 3,911 m) in Well 214/4-1, Faeroe-Shetland Basin. Both photomicrographs are under plane-polarised light. (a) & (b) The sandstone is poorly sorted and contains *ca.* 30% sub-angular to sub-rounded doleritic lava clasts (DL), which range in size from 1 to 4 mm. The sandstone also contains *ca.* 30 vol.% brownish clasts of siltstone (ST). The siltstone clasts are sub-angular to sub-rounded and range in size from 0.2 to 2 mm. The lithic clasts are contained within *ca.* 40 vol.% brownish clayey to silty matrix.

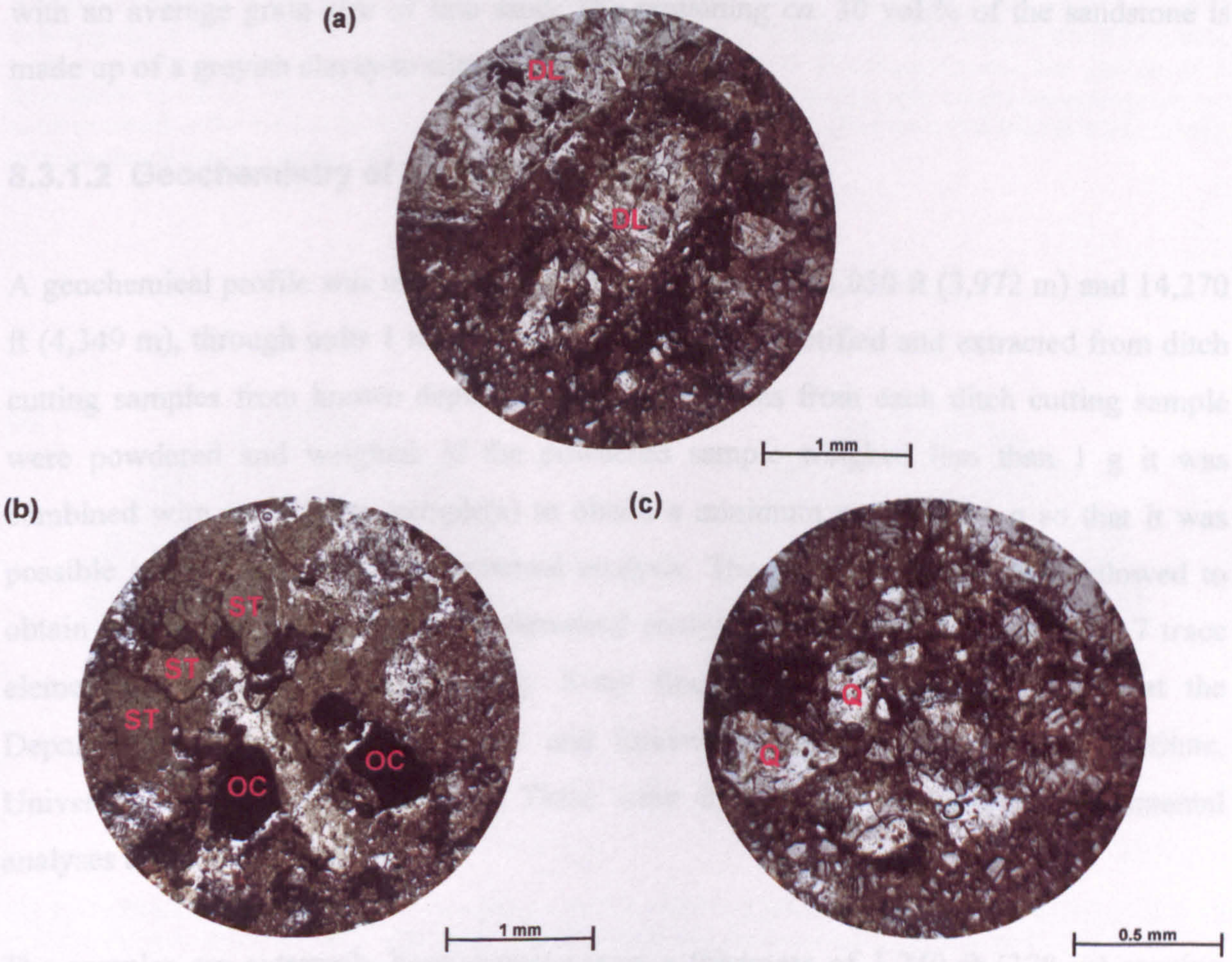

Fig. 8.15. Photomicrographs of Unit 5b, lithic greywacke, from a depth of *ca.* 12,802 ft (*ca.* 3,902 m) in Well 214/4-1, Faeroe-Shetland Basin. All of the photomicrographs are under plane-polarised light. (a) to (c) The sandstone is poorly sorted and contains *ca.* 10 vol.% sub-angular to sub-rounded equigranular doleritic lava clasts (DL), which range in size from 1 to 5. The sandstone also contains *ca.* 10 vol.% lithic clasts of siltstone (ST) and what appears to be opaque claystone (OC). The clasts are sub-angular to sub-rounded and range in size from 0.2 to 1 mm. The sandstone also contains as much as 10 vol.% sub-angular to sub-rounded grains of quartz (Q), with an average size of fine sand. The remaining *ca.* 70 vol.% of the sandstone consists of a brownish grey quartz-rich silty matrix.

lithic clasts of doleritic lava, which are sub-angular to sub-rounded with a maximum size of 3 mm (Fig. 8.16). The wacke also contains <2 vol.% sub-angular grains of plagioclase feldspar with an average size of fine sand. Needles of epidote crystals, with a maximum size of *ca.* 1 mm, account for less than 1 vol.% of the sandstone. The sandstone is dominated by *ca.* 60 vol.% sub-angular to sub-rounded quartz grains, which have an average size of medium sand and a maximum size of 1 mm. The remaining *ca.* 32 vol.% of the sandstone is made up of a greyish clayey to silty quartz-rich matrix.

At a depth of *ca.* 12,787 ft (*ca.* 3,897 m) material from Unit 6b was recovered, a sidewall core of a quartz wacke (Fig. 8.5). This sandstone is poorly sorted, matrix supported and contains *ca.* 65 vol.% sub-angular to sub-rounded grains of quartz with an average grain size of fine sand and a maximum size of 500 μm (Fig. 8.17). It also contains <3 vol.% sub-angular grains of plagioclase feldspar that have a maximum grain size of 300 μm. The wacke also contains <2 vol.% sub-angular to sub-rounded needle-shaped epidote crystals with an average grain size of fine sand. The remaining *ca.* 30 vol.% of the sandstone is made up of a greyish clayey to silty quartz-rich matrix.

8.3.1.2 Geochemistry of the Hyaloclastites & Lavas

A geochemical profile was undertaken between a depth of 13,030 ft (3,972 m) and 14,270 ft (4,349 m), through units 1 to 3. Igneous grains were identified and extracted from ditch cutting samples from known depths. The igneous grains from each ditch cutting sample were powdered and weighed. If the powdered sample weighed less than 1 g it was combined with an adjacent sample(s) to obtain a minimum weight of 1 g so that it was possible to undertake a major elemental analysis. The same procedure was followed to obtain a minimum of 8 g for trace elemental analysis (Table 8.1). 22 major and 7 trace elemental analyses were obtained by X-ray fluorescence spectroscopy (XRF) at the Department of Geology, Geophysics and Environmental Geoscience, Grant Institute, University of Edinburgh, Scotland. There were three major and one trace elemental analyses that were erroneous.

The samples are extremely homogeneous over a thickness of 1,240 ft (378 m) ranging between 47.24 to 48.44 wt.% SiO_2 a difference of only 1.2 wt.% (Table 8.2). The only consistent variation observed between the samples is accentuated in the Harker and Fenner diagrams (Figs. 8.18 & 8.19), where the highest combined sample (13,030 & 13,050 & 13,090 ft) has a noticeably higher concentration of MgO and lower concentrations of FeO^T, TiO_2, and P_2O_5. However, these differences are extremely minor, differing from the other

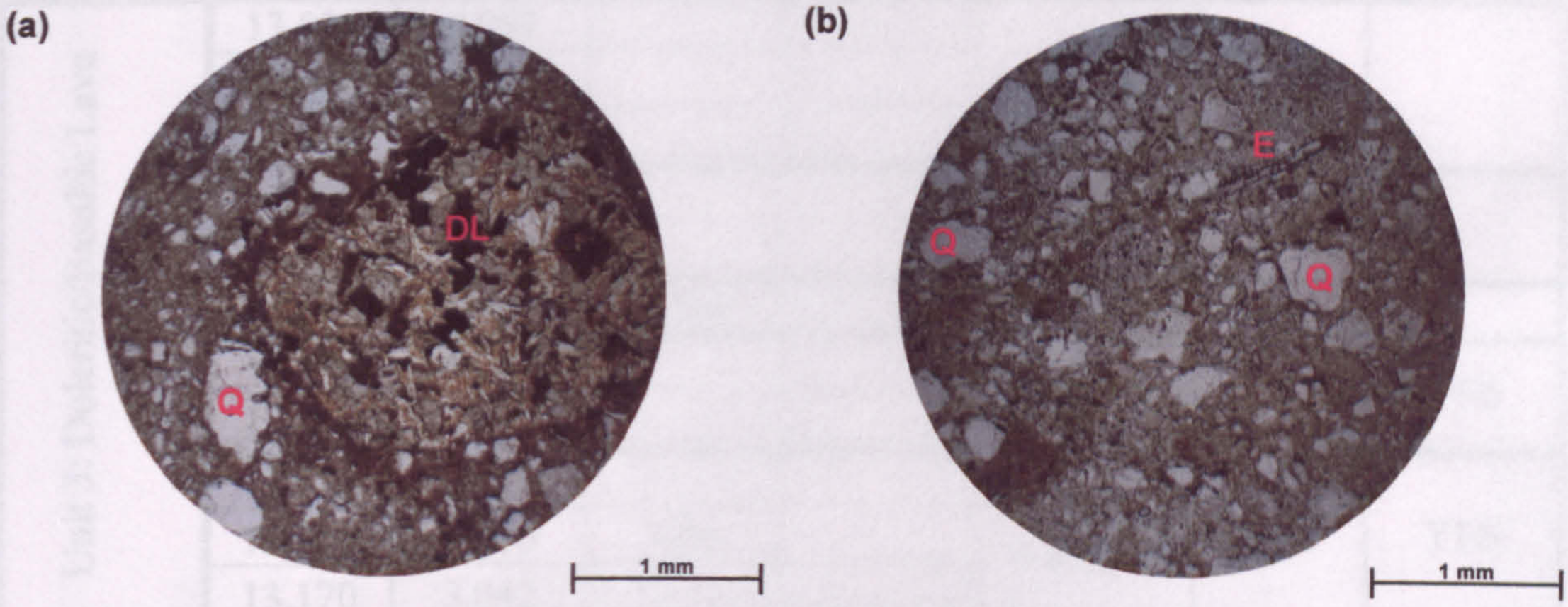

Fig. 8.16. Photomicrographs of Unit 6a, quartz wacke, from a depth of *ca.* 12,793 ft (*ca.* 3,899 m) in Well 214/4-1, Faeroe-Shetland Basin. Both photomicrographs are under plane-polarised light. (a) & (b) The sandstone is poorly sorted, matrix supported and contains <5 vol.% lithic clasts of doleritic lava (DL) which are sub-angular to sub-rounded with a maximum size of 3 mm. The wacke also contains <2 vol.% sub-angular grains of plagioclase feldspar with an average size of fine sand. Needles of epidote (E) crystals, with a maximum size of *ca.* 1 mm, account for less than 1 vol.% of the sandstone. The sandstone is dominated by *ca.* 60 vol.% sub-angular to sub-rounded quartz (Q) grains, which have an average size of medium sand and a maximum size of 1 mm. The remaining *ca.* 32 vol.% of the sandstone is made up of a greyish clayey to silty quartz-rich matrix.

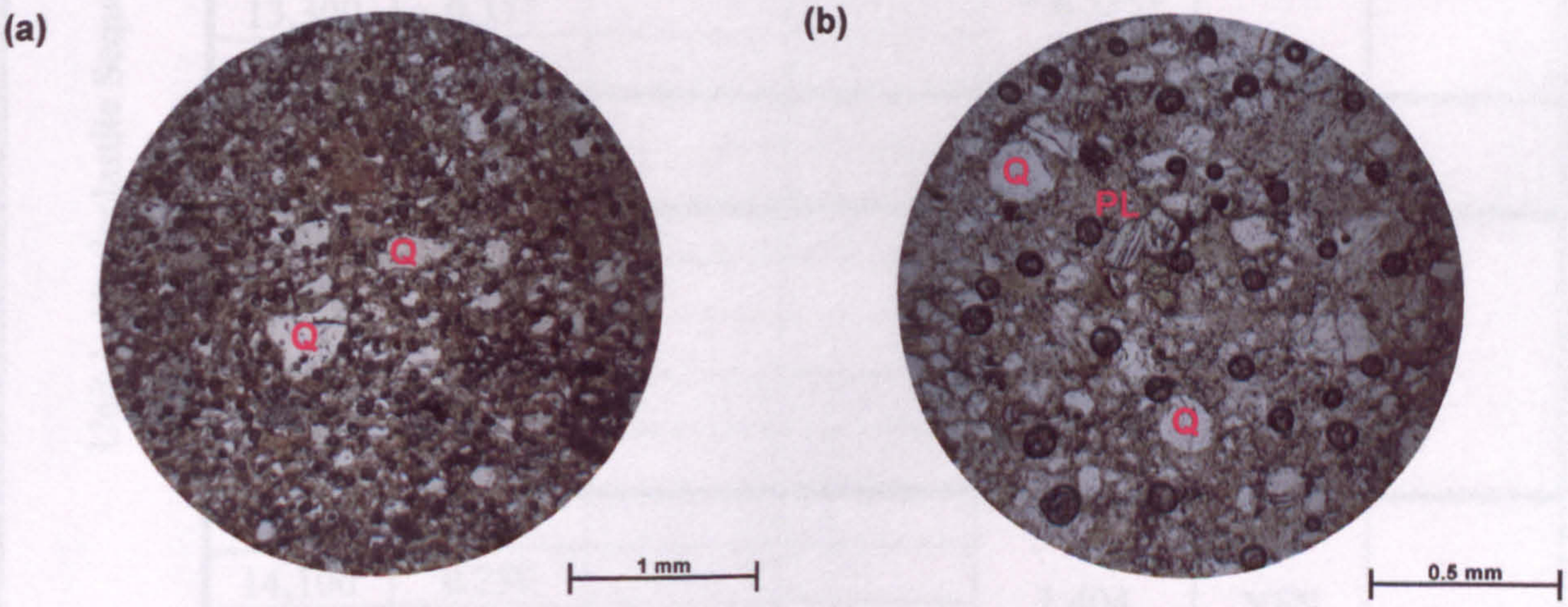

Fig. 8.17. Photomicrographs of Unit 6b, quartz wacke, from a depth of *ca.* 12,787 ft (*ca.* 3,897 m) in Well 214/4-1, Faeroe-Shetland Basin. Both photomicrographs are under plane-polarised light. (A) & (b) The sandstone is poorly sorted, matrix supported and contains *ca.* 65 vol.% sub-angular to sub-rounded grains of quartz (Q) with an average grain size of fine sand and a maximum size of 500 μm. It also contains <3 vol.% sub-angular grains of plagioclase feldspar (PL) that have a maximum grain size of 300 μm. The remaining *ca.* 30 vol.% of the sandstone is made up of a greyish clayey to silty quartz-rich matrix.

Geology	Depth (ft)	Weight (g)	Individual Major Analyses	Individual Trace Analyses	Combined Weights (g)	Combined Major Analyses	Combined Trace Analyses
Unit 3: Doleritic/Basaltic Lava Sequence	13,030	0.084			1.346	YES	
	13,050	0.249					
	13,090	1.013					
	13,100	0.670			1.622	YES	
	13,110	0.952					
	13,120	3.705	YES				
	13,130	4.844			8.868	YES	YES
	13,140	4.024					
	13,150	2.676			9.128 (-1 = 8.128)	YES	YES
	13,160	3.410	YES				
	13,170	3.042					
Unit 2: Sedimentary Sequence	13,180	6.250	YES		11.521 (-2 = 9.521)	YES	YES
	13,190	5.271	YES				
	13,200	10.886	YES	YES			
	13,210	4.008	YES				
	13,220	2.279	YES				
Unit 1: Hyaloclastite Sequence	13,230	3.949	YES		11.991 (-3 = 8.991)	YES	YES
	13,240	3.237	YES				
	13,260	4.805	YES				
	13,270	8.119	YES	YES			
	13,280	3.981			9.535 (-1 = 8.535)	YES	YES
	13,290	4.878	YES				
	13,300	0.351					
	13,350	0.325					
	13,400	0.782			1.154	YES	
	13,440	0.372					
	13,520	0.462			1.452	YES	
	13,600	0.408					
	13,700	0.056					
	13,820	0.215					
	13,900	0.311					
	14,000	0.464			1.404	YES	
	14,100	0.259					
	14,200	0.343					
	14,270	0.338					
Total Analyses			12	2		10	5

Table 8.1. Weights of powdered igneous material extracted from ditch cutting samples from known depths in Well 214/4-1, Faeroe-Shetland Basin. Samples with weights over 1 g were analysed for major elements and samples with weights over 8 g were analysed for trace elements. If the powdered sample weighed less than 1 g it was combined with an adjacent sample(s) to obtain a minimum weight of 1 g so that it was possible to undertake a major elemental analysis. The same procedure was followed to obtain a minimum of 8 g for trace elemental analysis.

Depth, ft	13030 & 13050 & 13090	13100 & 13110	13120	13130 & 13140	13150 & 13160 & 13170	13160	13180	13190	13180 & 13190	13200	13210	13240	13260	13270	13290	13280 & 13290 & 13300 & 13350
SiO_2	47.91	48.31	47.99	48.32	48.44	48.26	48.07	48.11	48.01	48.41	48.32	47.83	47.54	47.24	47.54	47.99
TiO_2	2.14	2.35	2.40	2.38	2.39	2.45	2.37	2.47	2.44	2.44	2.41	2.42	2.37	2.35	2.46	2.41
Al_2O_3	13.72	13.59	13.48	13.62	13.70	13.55	13.72	13.70	13.70	13.70	13.65	13.65	13.51	13.49	13.45	13.71
Fe_2O_3	1.58	1.62	1.67	1.66	1.64	1.65	1.64	1.68	1.65	1.66	1.65	1.63	1.63	1.61	1.62	1.64
FeO	10.50	10.80	11.11	11.05	10.95	10.98	10.94	11.17	11.02	11.08	11.03	10.89	10.87	10.74	10.81	10.90
MnO	0.21	0.21	0.21	0.21	0.20	0.20	0.20	0.21	0.20	0.20	0.21	0.21	0.20	0.20	0.21	0.21
MgO	6.88	6.53	6.63	6.58	6.59	6.53	6.42	6.50	6.44	6.63	6.54	6.32	6.30	6.22	6.23	6.32
CaO	11.18	11.05	10.96	11.07	11.13	11.10	11.04	11.16	11.05	11.17	11.12	11.13	11.04	10.93	11.07	11.12
Na_2O	2.24	2.30	2.25	2.29	2.34	2.31	2.31	2.32	2.32	2.31	2.31	2.34	2.29	2.30	2.30	2.34
K_2O	0.58	0.61	0.63	0.60	0.57	0.56	0.55	0.53	0.54	0.56	0.56	0.52	0.51	0.53	0.54	0.53
P_2O_5	0.19	0.24	0.22	0.22	0.22	0.22	0.22	0.21	0.22	0.23	0.22	0.22	0.22	0.22	0.23	0.23
LOI	1.15	0.74	0.68	0.57	0.54	0.52	0.53	0.32	0.55	0.26	0.38	0.39	0.39	0.29	0.49	0.37
Total	98.28	98.34	98.22	98.57	98.72	98.32	98.00	98.39	98.14	98.65	98.40	97.55	96.87	96.13	96.94	97.77
FeO^T	11.92	12.26	12.61	12.55	12.43	12.46	12.42	12.68	12.50	12.57	12.52	12.36	12.34	12.19	12.27	12.38
Mg #	53.87	51.86	51.54	51.47	51.75	51.46	51.11	50.90	51.03	51.61	51.38	50.85	50.80	50.79	50.67	50.81
FeO^T/MgO	1.73	1.88	1.90	1.91	1.89	1.91	1.93	1.95	1.94	1.90	1.91	1.96	1.96	1.96	1.97	1.96
TiO_2/FeO^T	0.180	0.192	0.190	0.190	0.193	0.197	0.190	0.195	0.195	0.194	0.192	0.196	0.192	0.193	0.200	0.195
Nb				17.30	20.60				22.40	36.40				22.70		34.80
Zr				151.00	146.50				150.80	148.90				149.70		151.00
Y				32.40	31.60				32.10	31.70				32.40		32.40
Sr				239.40	238.80				250.00	245.40				249.80		251.80
Rb				6.50	6.50				6.60	6.70				6.90		6.90
La				10.50	12.10				10.20	12.40				13.00		10.50
Ce				30.60	31.60				33.40	31.20				30.50		32.40
Nd				21.80	19.50				21.80	20.90				20.00		20.90
Zn				108.80	108.70				105.30	105.70				107.40		110.10
Cu				185.70	182.00				181.40	176.30				189.30		182.80
Ni				96.00	96.00				91.50	96.30				95.20		98.60
Cr				181.80	187.90				173.70	180.10				172.50		180.10
V				407.30	405.80				395.70	410.60				399.30		411.50
Ba				102.70	108.60				98.70	91.80				132.20		212.90
Sc				38.00	38.50				36.20	37.30				35.30		38.10

Table 8.2. Major and trace elemental analyses for the igneous-bearing ditch cutting samples from Well 214/4-1, Faeroe-Shetland Basin. The analyses have been recalculated with a fixed oxidation ratio of $Fe_2O_3/FeO = 0.15$. Mg# = atomic $100Mg/(Mg+Fe^2)$, and FeO^T = total iron calculated as FeO (see Appendix B).

Depth, ft	13400 & 13440	13520 & 13600 & 13700 & 13820 & 13900	14000 & 14100 & 14200 & 14270	Minimum	Maximum	Average
SiO_2	47.89	48.29	47.93	47.24	48.44	48.02
TiO_2	2.43	2.45	2.51	2.14	2.51	2.40
Al_2O_3	13.58	13.69	13.61	13.45	13.72	13.62
Fe_2O_3	1.65	1.64	1.63	1.58	1.68	1.64
FeO	10.99	10.91	10.89	10.50	11.17	10.93
MnO	0.21	0.21	0.21	0.20	0.21	0.21
MgO	6.37	6.37	6.28	6.22	6.88	6.46
CaO	11.06	11.18	11.09	10.93	11.18	11.09
Na_2O	2.33	2.41	2.42	2.24	2.42	2.32
K_2O	0.51	0.49	0.51	0.49	0.63	0.55
P_2O_5	0.22	0.23	0.24	0.19	0.24	0.22
LOI	0.41	0.35	0.84	0.26	1.15	0.51
Total	97.65	98.21	98.16	96.13	98.72	97.96
FeO^T	12.47	12.38	12.36	11.92	12.68	12.40
Mg #	50.81	50.99	50.69	50.67	53.87	51.28
FeO^T/MgO	1.96	1.94	1.97	1.73	1.97	1.92
TiO_2/FeO^T	0.195	0.198	0.203	0.18	0.20	0.19
Nb				17.30	36.40	25.70
Zr				146.50	151.00	149.65
Y				31.60	32.40	32.10
Sr				238.80	251.80	245.87
Rb				6.50	6.90	6.68
La				10.20	13.00	11.45
Ce				30.50	33.40	31.62
Nd				19.50	21.80	20.82
Zn				105.30	110.10	107.67
Cu				176.30	189.30	182.92
Ni				91.50	98.60	95.60
Cr				172.50	187.90	179.35
V				395.70	411.50	405.03
Ba				91.80	212.90	124.48
Sc				35.30	38.50	37.23

Table 8.2 continued. Major and trace elemental analyses for the igneous-bearing ditch cutting samples from Well 214/4-1, Faeroe-Shetland Basin. The analyses have been recalculated with a fixed oxidation ratio of $Fe_2O_3/FeO = 0.15$. Mg # = atomic 100Mg/(Mg + Fe^2), and FeO^T = total iron calculated as FeO (see Appendix B).

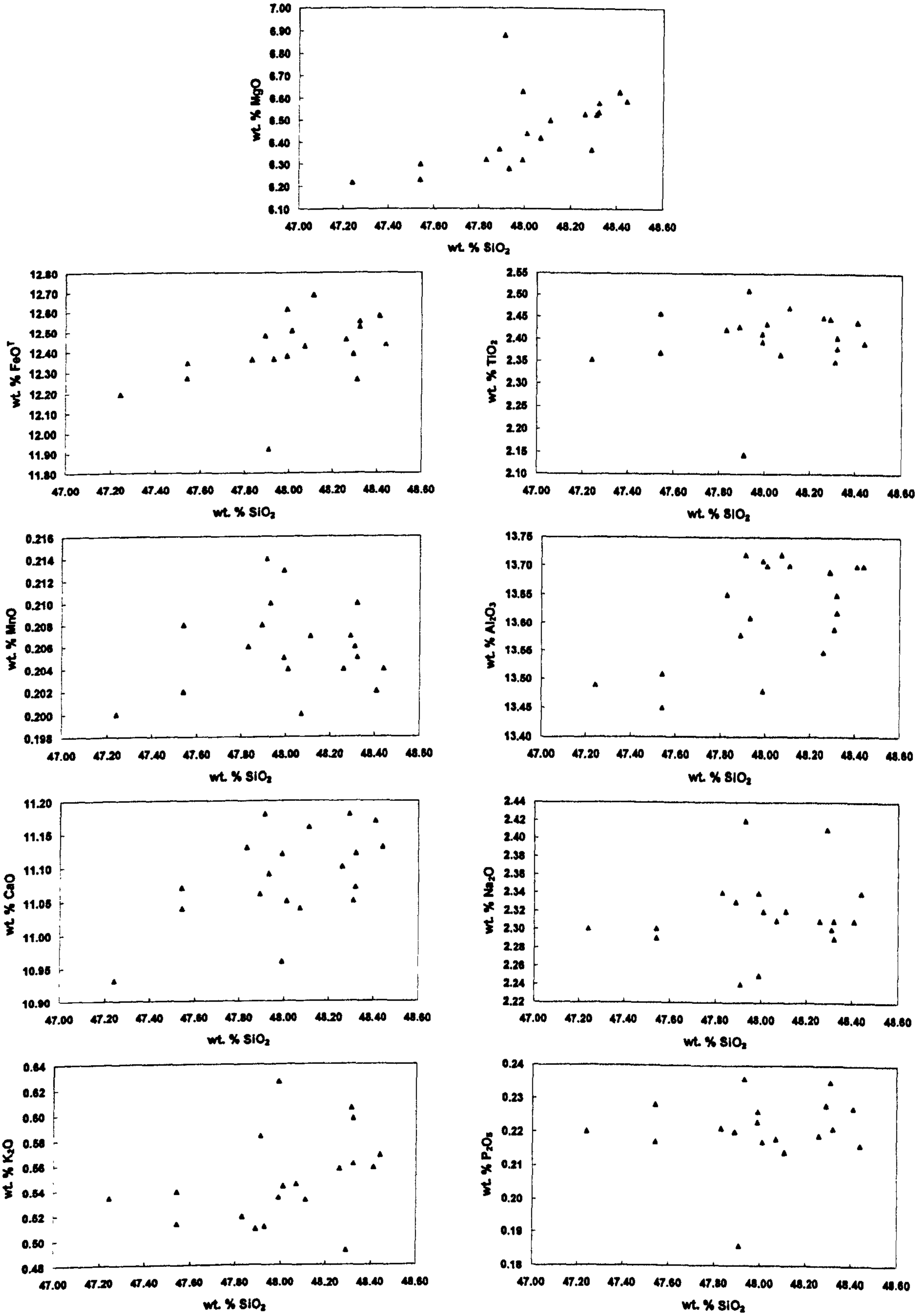

Fig. 8.18. Harker variation diagrams for the igneous-bearing ditch cutting samples analysed from Well 214/4-1, Faeroe-Shetland Basin. The samples are extremely homogeneous over a thickness of 1,240 ft (378 m) ranging between 47.24 to 48.44 wt.% SiO_2 a difference of only 1.2 wt.%. The only consistent variation observed in the diagrams is the highest combined sample (13,030 & 13,050 & 13,090 ft) having a noticeably higher concentration of MgO and lower concentrations of FeO^T, TiO_2, and P_2O_5 than the over samples. However, these differences are extremely minor, differing from the other samples by less than 0.3 wt.%. The analyses have been recalculated with a fixed oxidation ratio of $Fe_2O_3/FeO = 0.15$. FeO^T = total iron calculated as FeO (see Appendix B).

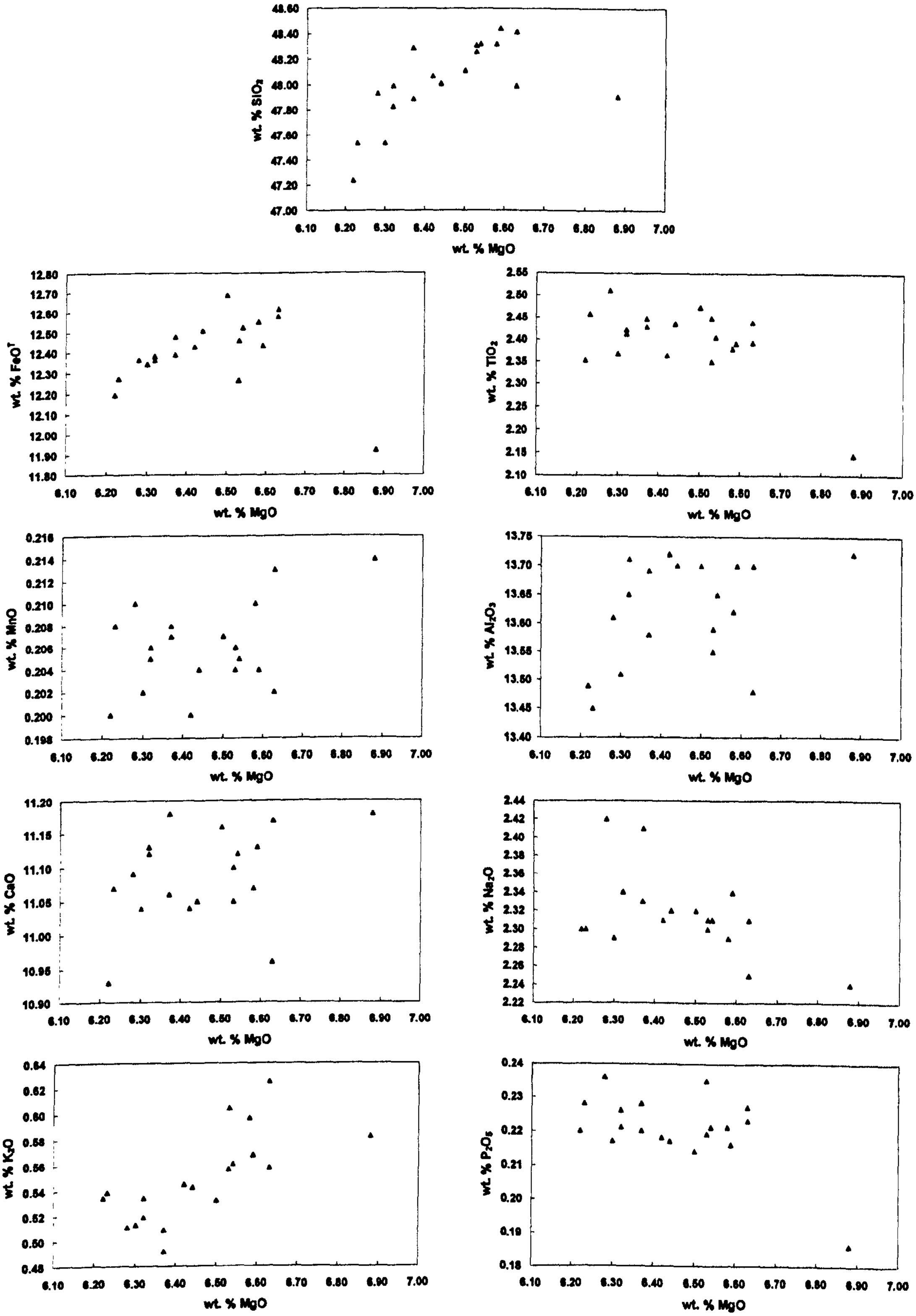

Fig. 8.19. Fenner variation diagrams for the igneous-bearing ditch cutting samples analysed from Well 214/4-1, Faeroe-Shetland Basin. The samples are extremely homogeneous over a thickness of 1,240 ft (378 m) ranging between 6.22 to 6.88 wt.% MgO a difference of only 0.66 wt.%. The only consistent variation observed in the diagrams is the highest combined sample (13,030 & 13,050 & 13,090 ft) having a noticeably higher concentration of MgO and lower concentrations of FeO^T, TiO_2, and P_2O_5 than the other samples. Consequently, two trend lines have been plotted on the diagram including and excluding the highest combined sample (13,030 & 13,050 & 13,090 ft). However, these differences are extremely minor, differing from the other samples by less than 0.3 wt.%. The analyses have been recalculated with a fixed oxidation ratio of $Fe_2O_3/FeO = 0.15$. FeO^T = total iron calculated as FeO (see Appendix B).

samples by less than 0.3 wt.%. The TiO_2 content within the samples analysed vary between 2.14 and 2.51 wt.%. The Mg # ranges between 50.67 and 51.86, a difference of 1.19; this however excludes the highest sample, which has a Mg # of 53.87 (see Appendix B on how the Mg # is calculated). All of the samples plot within the basalt field of the Cox *et al.* (1979) and Le Bas *et al.* (1986) nomenclature diagrams (Figs. 8.20 & 8.21) and they plot between the basalt and ferro-basalt sections of the tholeiitic field of the AFM diagram (Fig. 8.22). From the CIPW calculations it can be seen that the samples are all hypersthene normative basalts (Table 8.3).

8.3.1.3 Correlation with the Faeroe Islands

As outlined in Section 1.3, the Faeroe Plateau Lava Group (FPLG) on the Faeroe Islands have been separated into three formations: Lower, Middle, and Upper. The three formations have quite separate geochemical characteristics, which are highlighted in the diagrams of Waagstein (1988) and Larsen *et al.* (1999) (Figs. 1.6 & 1.7). Larsen *et al.* (1999), with the aid of a large geochemical dataset, were able to correlate the FPLG on the Faeroe Islands to the Nansen Fjord volcanic succession, East Greenland, *ca.* 1,000 km apart. The basaltic samples encountered within Well 214/4-1 have been plotted on the diagrams of Waagstein (1988) and Larsen *et al.* (1999) in an attempt to correlate them with the FPLG on the Faeroe Islands and in turn the Nansen Fjord volcanic succession.

The samples from Well 214/4-1 plot within the low-Ti tholeiite field on the TiO_2/FeO^T vs. FeO^T/MgO diagram of Waagstein (1988) (Fig. 8.23). The samples plot close together except for the highest combined sample (13,030 & 13,050 & 13,090 ft), due to the sample having a slightly higher MgO content. The samples also plot within the Lower Basalt Formation (LBF) field of the TiO_2/FeO^T vs. FeO^T/MgO diagram (Fig. 8.24). The samples plot below the dividing line on the TiO_2/FeO^T v. Mg # diagram of Larsen *et al.* (1999) (Fig. 8.25). Again, the samples plot close to one another except for the highest combined sample (13,030 & 13,050 & 13,090 ft), due to the sample having a slightly higher MgO content. As with the diagram of Waagstein (1988), the samples plot within the LBF field on the TiO_2/FeO^T v. Mg # diagram (Fig. 8.26). Therefore, it seems apparent that the basaltic samples from Well 214/4-1 are geochemically similar to the LBF from the Faeroe Islands (including Lopra-1). From the trans-Atlantic correlation made by Larsen *et al.* (1999) it follows that the basaltic samples from Well 214/4-1 can also be correlated to the East Greenland Nansen Fjord Formation (Fig. 8.27). However, the samples may correlate geochemically but they do not correlate texturally. The basal *ca.* 1,480 ft (*ca.* 451 m) of Well 214/4-1 are represented by hyaloclastites whereas only minor hyaloclastite deposits

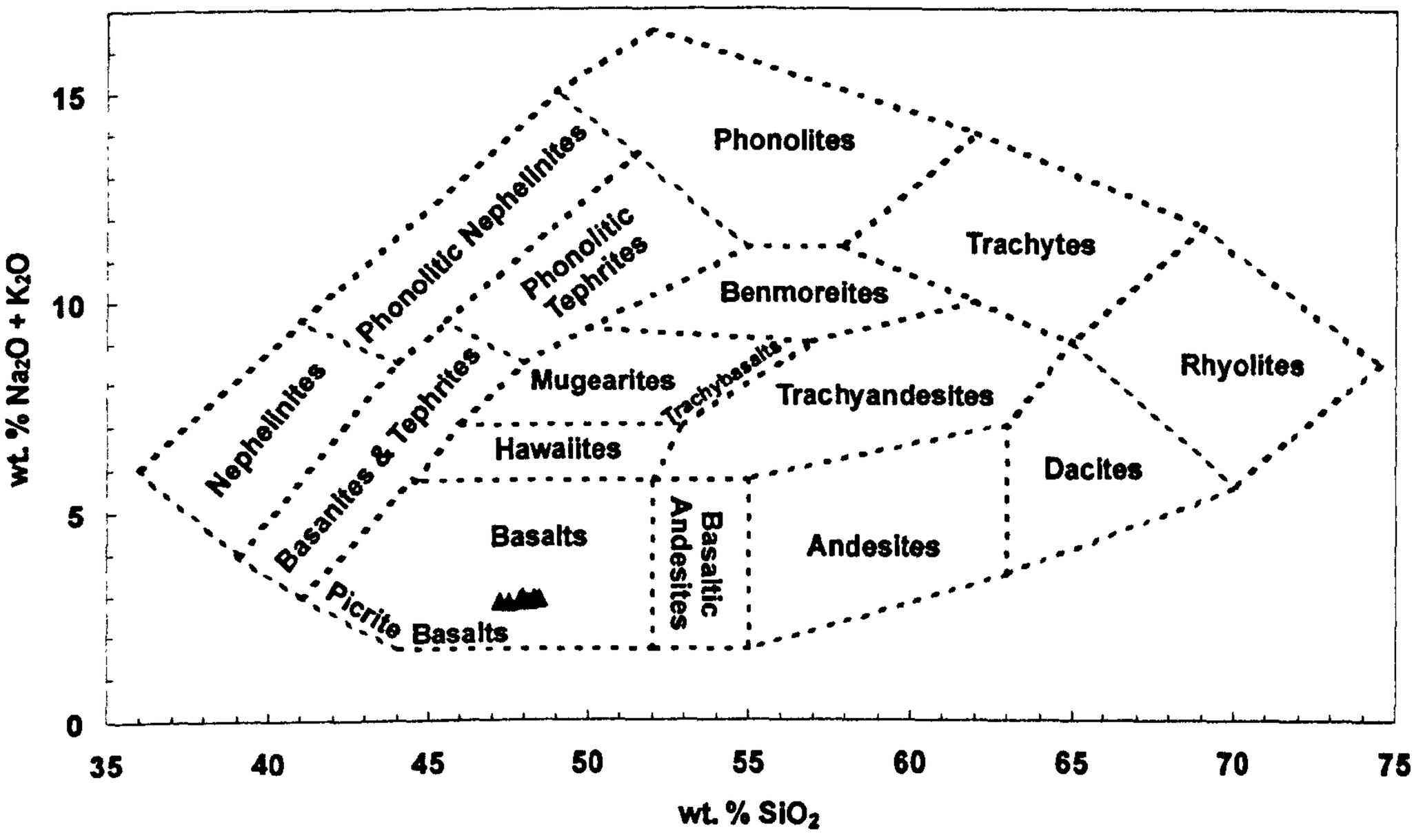

Fig. 8.20. Nomenclature diagram for normal (i.e. non-potassic) volcanic rocks with the igneous-bearing ditch cutting samples from Well 214/4-1, Faeroe-Shetland Basin, plotting within the basalt field. After Cox *et al.* (1979).

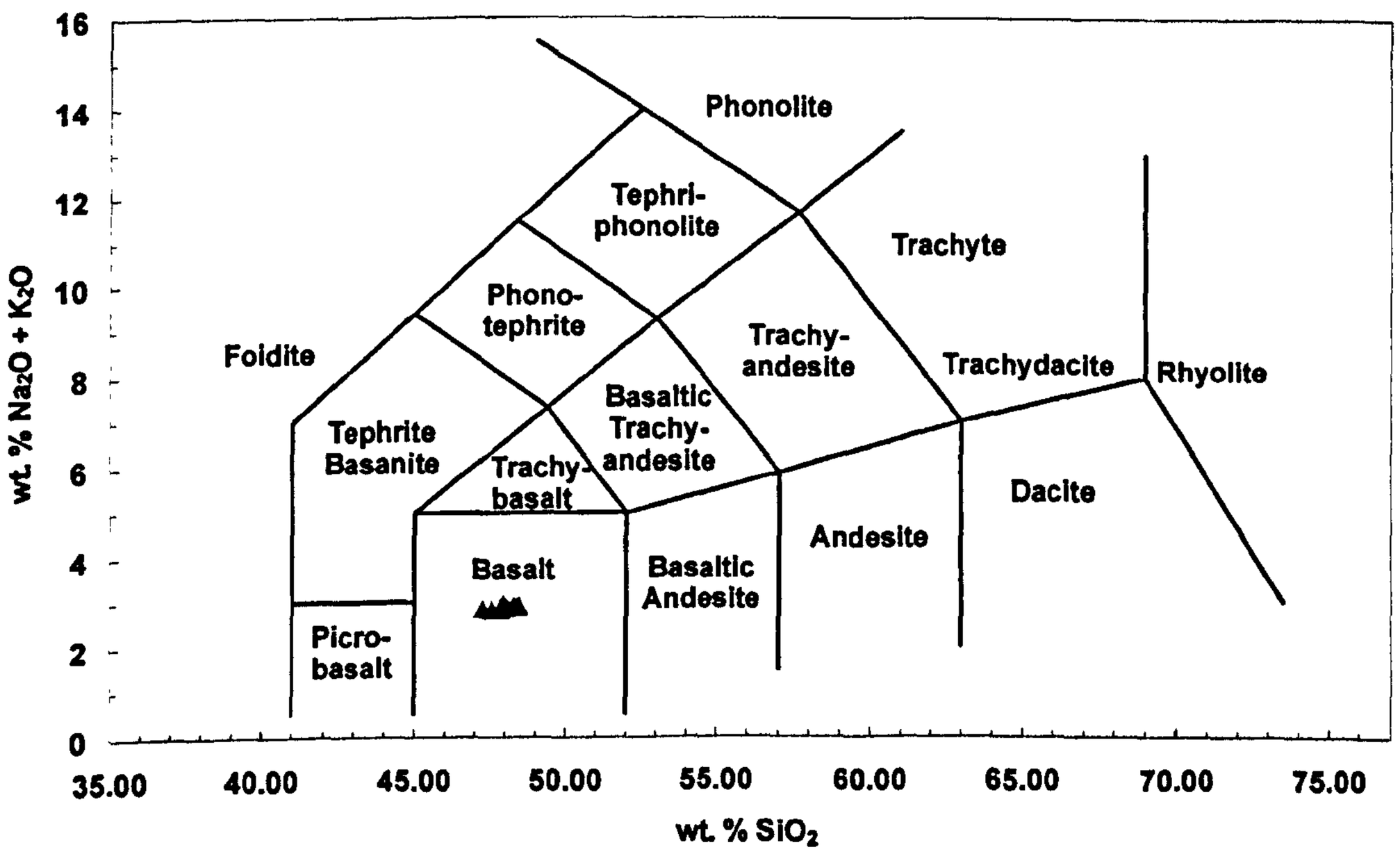

Fig. 8.21. The total alkali-silica (TAS) nomenclature diagram with the igneous-bearing ditch cutting samples from Well 214/4-1, Faeroe-Shetland Basin, plotting within the basalt field. After Le Bas *et al.* (1986).

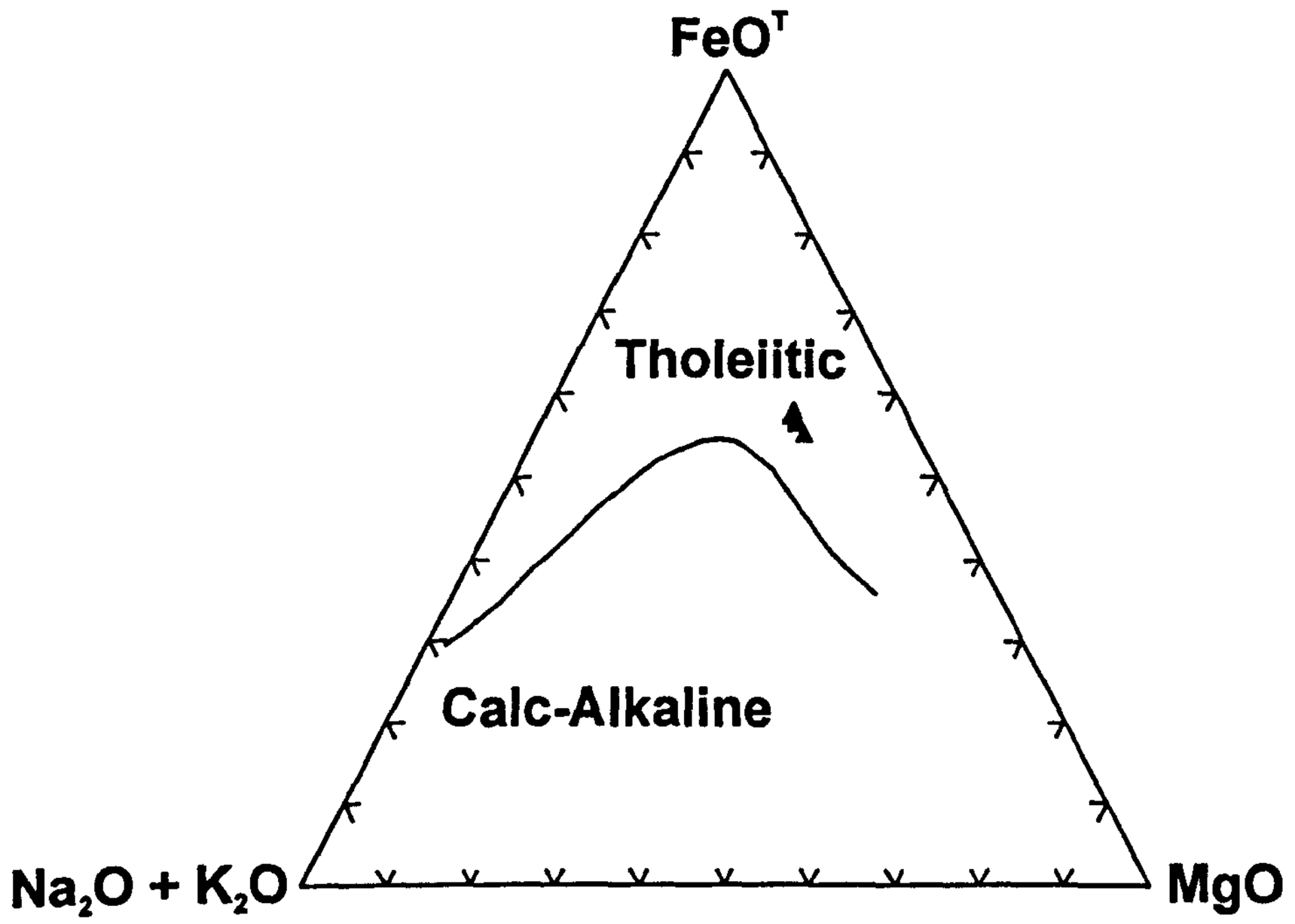

Fig. 8.22. The AFM diagram with the igneous-bearing ditch cutting samples from Well 214/4-1, Faeroe-Shetland Basin, plotting within the tholeiitic field. The analyses have been recalculated with a fixed oxidation ratio of $Fe_2O_3/FeO = 0.15$. FeO^T = total iron calculated as FeO (see Appendix B).

Depth, ft	13030 & 13050 & 13090	13100 & 13110	13120	13130 & 13140	13150 & 13160 & 13170	13160	13180	13190	13180 & 13190	13200	13210	13240	13260	13270	13290
Qz	0.00	0.00	0.00	0.00	0.00	0.00	0.00	0.00	0.00	0.00	0.00	0.00	0.00	0.00	0.00
Or	3.58	3.76	3.89	3.68	3.49	3.45	3.39	3.25	3.33	3.42	3.44	3.22	3.18	3.33	3.37
Ab	21.02	21.54	21.10	21.37	21.78	21.60	21.67	21.65	21.75	21.47	21.55	22.03	21.72	21.95	21.82
An	26.83	26.03	25.93	26.10	26.12	25.99	26.59	26.40	26.49	26.25	26.21	26.43	26.49	26.49	26.19
Ne	0.00	0.00	0.00	0.00	0.00	0.00	0.00	0.00	0.00	0.00	0.00	0.00	0.00	0.00	0.00
Di	23.88	23.61	23.49	23.59	23.71	23.90	23.31	23.77	23.39	23.65	23.70	23.97	23.88	23.70	24.21
Hy	14.78	16.88	16.26	16.40	15.89	16.60	16.49	15.38	16.05	16.10	16.37	15.34	16.26	15.82	16.02
Ol	4.65	2.49	3.54	3.13	3.29	2.64	2.82	3.69	3.16	3.30	2.97	3.21	2.70	2.95	2.46
Mt	1.73	1.77	1.82	1.80	1.78	1.80	1.79	1.83	1.80	1.80	1.79	1.79	1.80	1.79	1.79
Il	3.12	3.41	3.49	3.45	3.45	3.55	3.45	3.58	3.55	3.52	3.49	3.53	3.49	3.48	3.62
Ap	0.42	0.52	0.48	0.48	0.48	0.48	0.48	0.46	0.48	0.50	0.48	0.48	0.49	0.49	0.51

Depth, ft	13280 & 13290 & 13300 & 13350	13400 & 13440	13520 & 13600 & 13700 & 13820 & 13900	14000 & 14100 & 14200 & 14270
Qz	0.00	0.00	0.00	0.00
Or	3.27	3.16	3.01	3.15
Ab	21.97	21.92	22.51	22.74
An	26.51	26.30	26.11	25.93
Ne	0.00	0.00	0.00	0.00
Di	23.70	23.76	24.04	24.02
Hy	15.84	16.15	15.56	14.89
Ol	2.89	2.88	2.93	3.30
Mt	1.79	1.81	1.78	1.78
Il	3.51	3.55	3.55	3.66
Ap	0.50	0.48	0.50	0.53

Table 8.3. CIPW normative analyses for the igneous-bearing ditch cutting samples from Well 214/4-1, Faeroe-Shetland Basin. The CIPW norms are calculated with a fixed oxidation ratio of $Fe_2O_3/FeO = 0.15$.

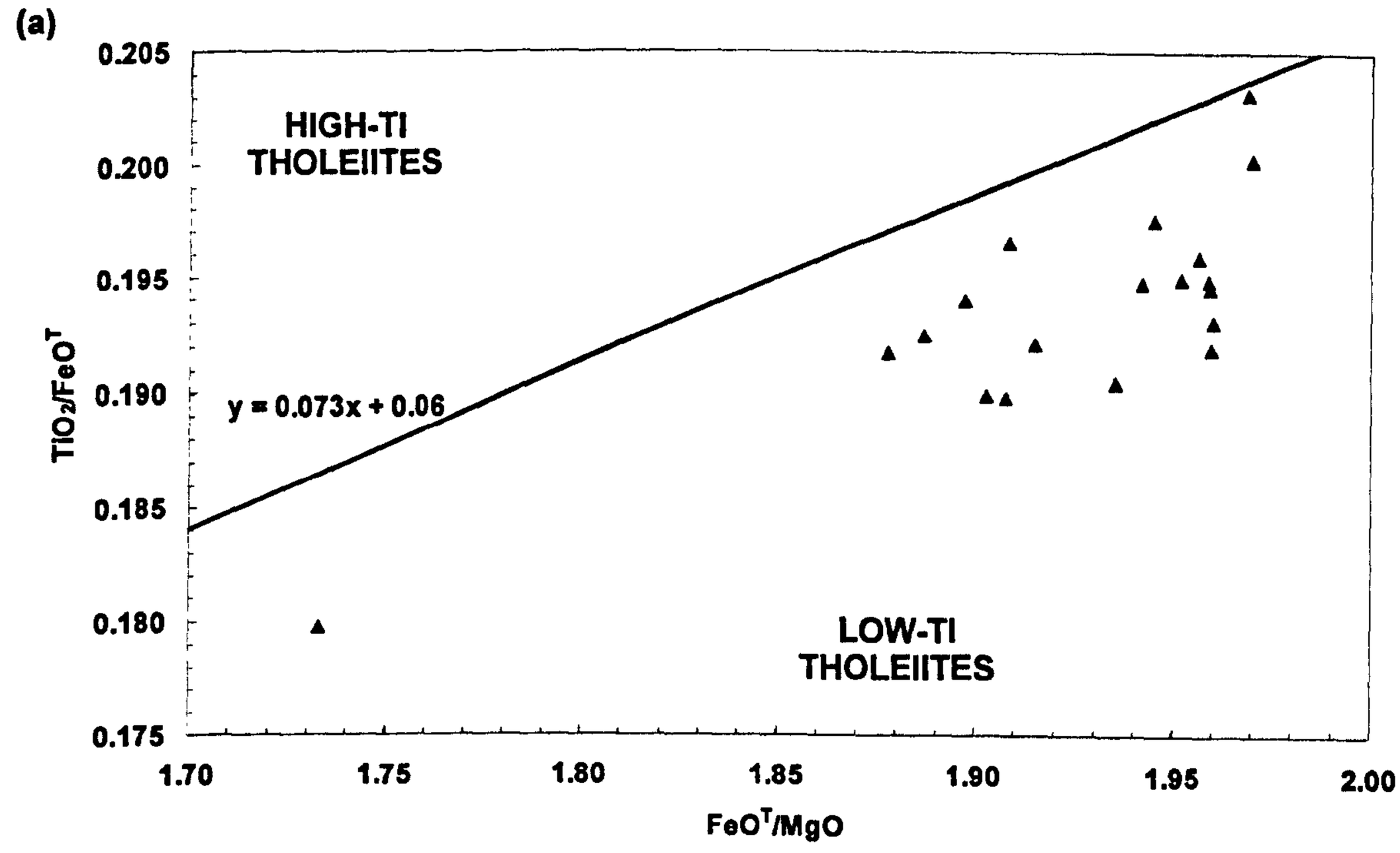

Fig. 8.23. TiO_2/FeO^T vs. FeO^T/MgO diagrams with the igneous-bearing ditch cutting samples from Well 214/4-1, Faeroe-Shetland Basin, plotted with the low-Ti tholeiite field. The oblique full line and the vertical stippled line mark the boundaries between high-Ti olivine tholeiites, high-Ti tholeiites, low-Ti olivine tholeiites, and low-Ti tholeiites. The analyses have been recalculated with a fixed oxidation ratio of $Fe_2O_3/FeO = 0.15$. FeO^T = total iron calculated as FeO (see Appendix B). Divisions after Waagstein (1988).

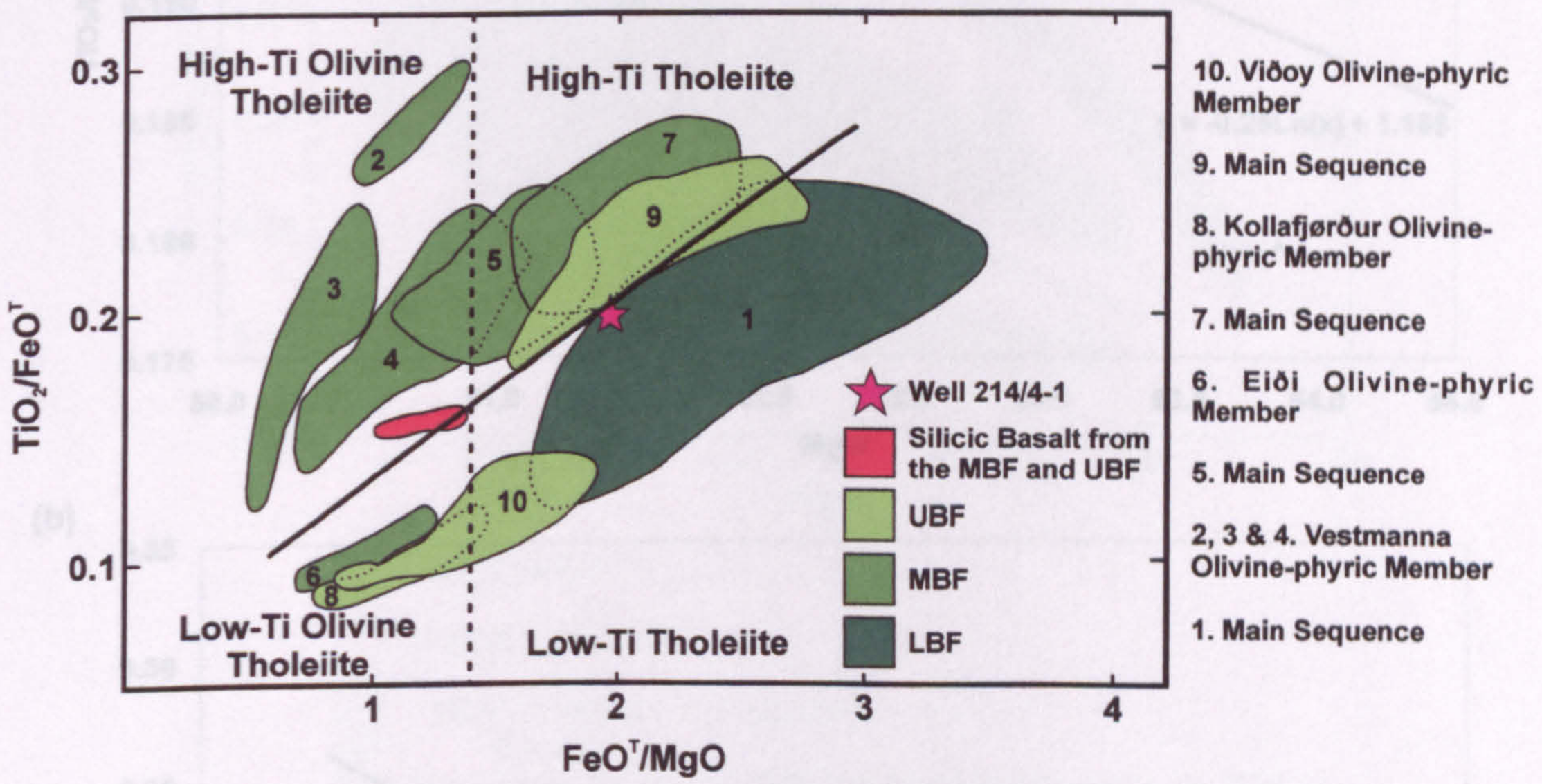

Fig. 8.24. TiO_2/FeO^T vs. FeO^T/MgO diagram for the basalt lavas from the Faeroe Plateau Lava Group on the Faeroe Islands and the igneous-bearing ditch cutting samples from Well 214/4-1, Faeroe-Shetland Basin. The oblique full line and the vertical stippled line mark the boundaries between high-Ti olivine tholeiites, high-Ti tholeiites, low-Ti olivine tholeiites, and low-Ti tholeiites. LBF = Lower Basalt Formation, MBF = Middle Basalt Formation, UBF = Upper Basalt Formation. The analyses have been recalculated with a fixed oxidation ratio of $Fe_2O_3/FeO = 0.15$. FeO^T = total iron calculated as FeO (see Appendix B). The ditch cutting samples from Well 214/4-1 plot within the LBF field. Well 214/4-1 data added to the modified diagram of Waagstein (1988).

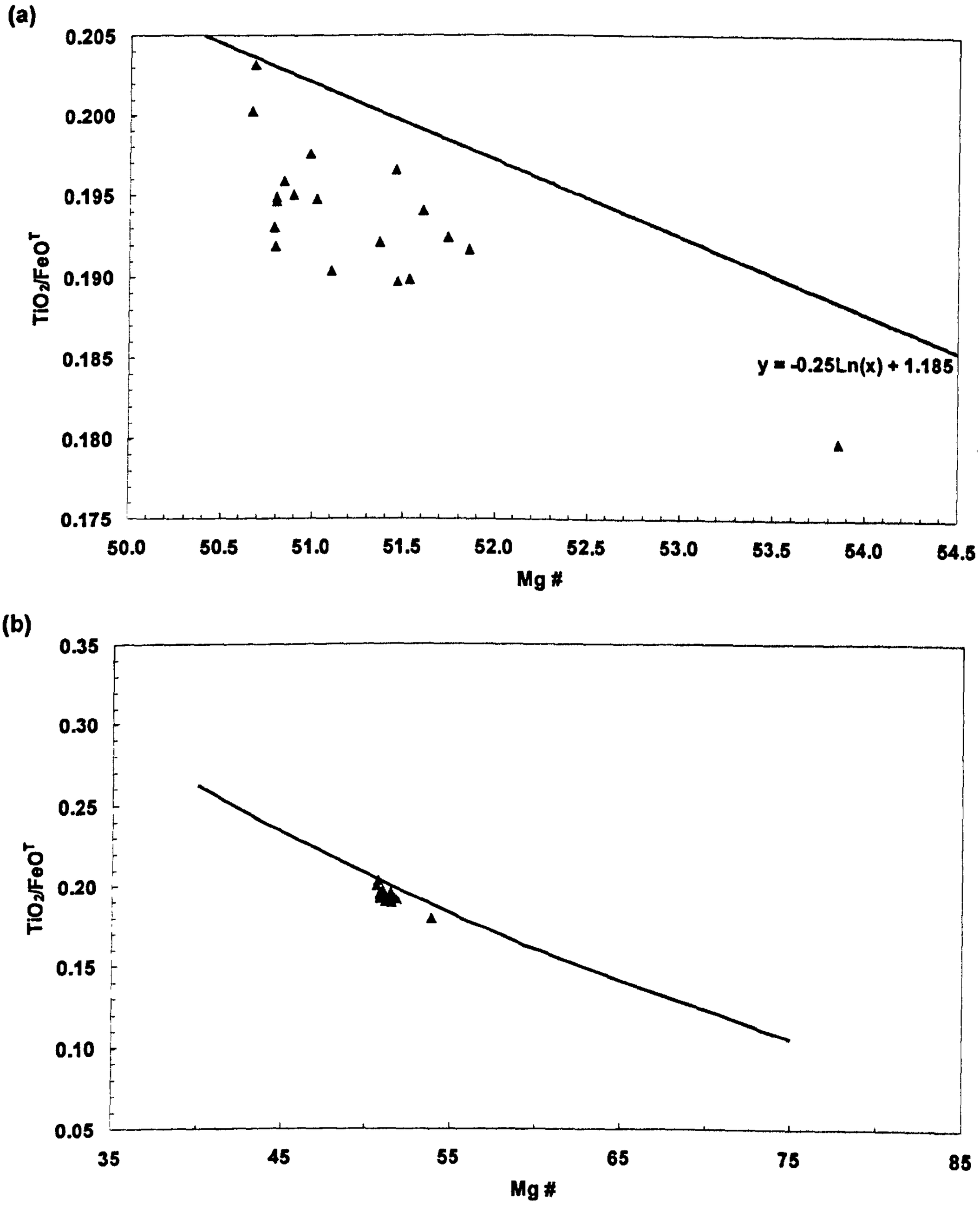

Fig. 8.25. TiO_2/FeO^T vs. Mg # diagrams with the igneous-bearing ditch cutting samples from Well 214/4-1, Faeroe-Shetland Basin. The analyses have been recalculated with a fixed oxidation ratio of $Fe_2O_3/FeO = 0.15$. Mg # = atomic $100Mg/(Mg + Fe^2)$, and FeO^T = total iron calculated as FeO (see Appendix B). Division line after Larsen *et al.* (1999).

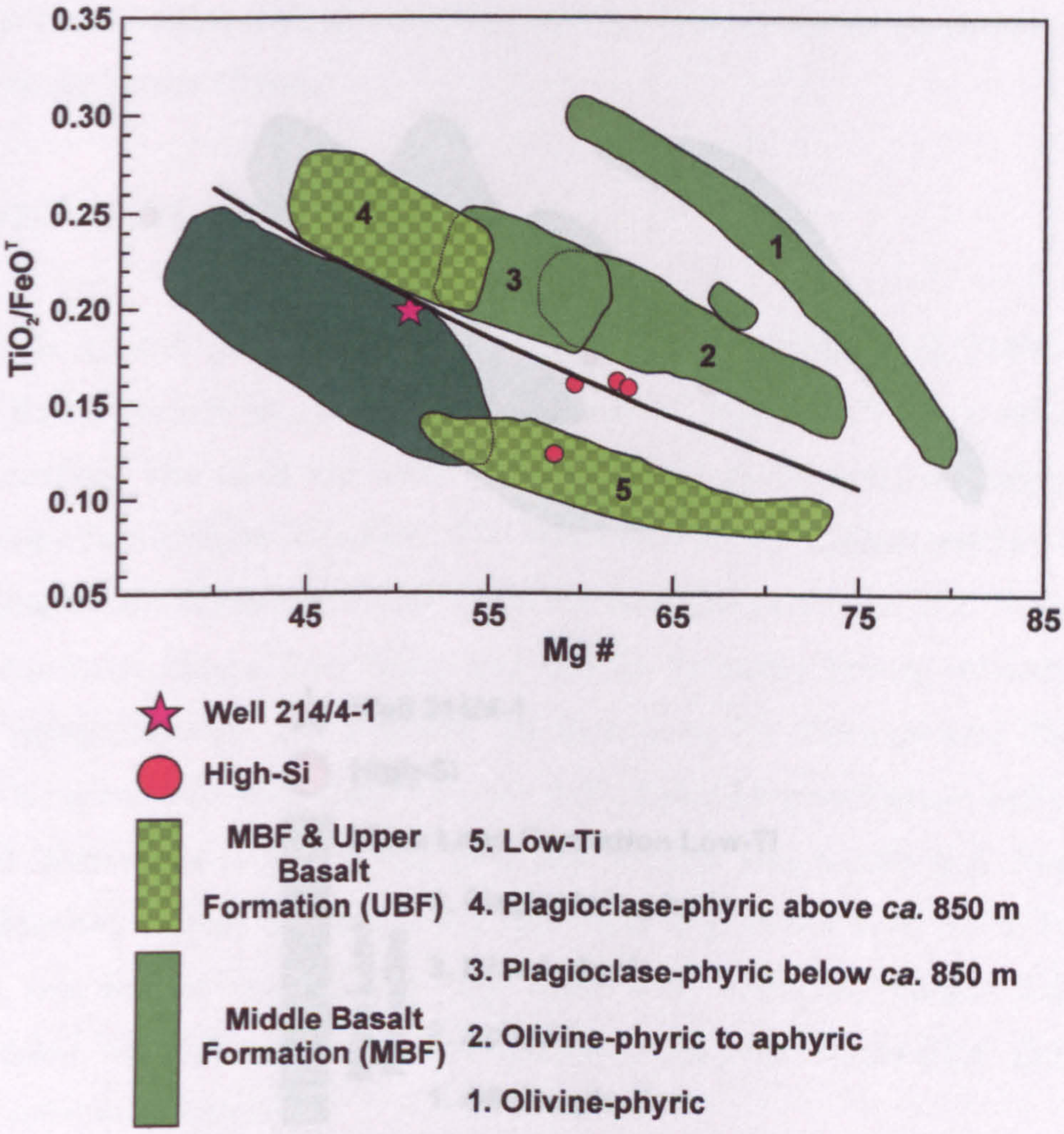

Fig. 8.26. TiO_2/FeO^T vs. Mg # diagram for the basalt lavas of the Faeroe Plateau Lava Group on the Faeroe Islands and the igneous-bearing ditch cutting samples from Well 214/4-1, Faeroe-Shetland Basin. The division line separates low-Ti and high-Ti basalts. The analyses have been recalculated with a fixed oxidation ratio of $Fe_2O_3/FeO = 0.15$. Mg # = atomic $100Mg/(Mg + Fe^2)$, and FeO^T = total iron calculated as FeO (see Appendix B). The ditch cutting samples from Well 214/4-1 plot within the Lower Basalt Formation field. Well 214/4-1 data added to the modified diagram of Larsen *et al.* (1999).

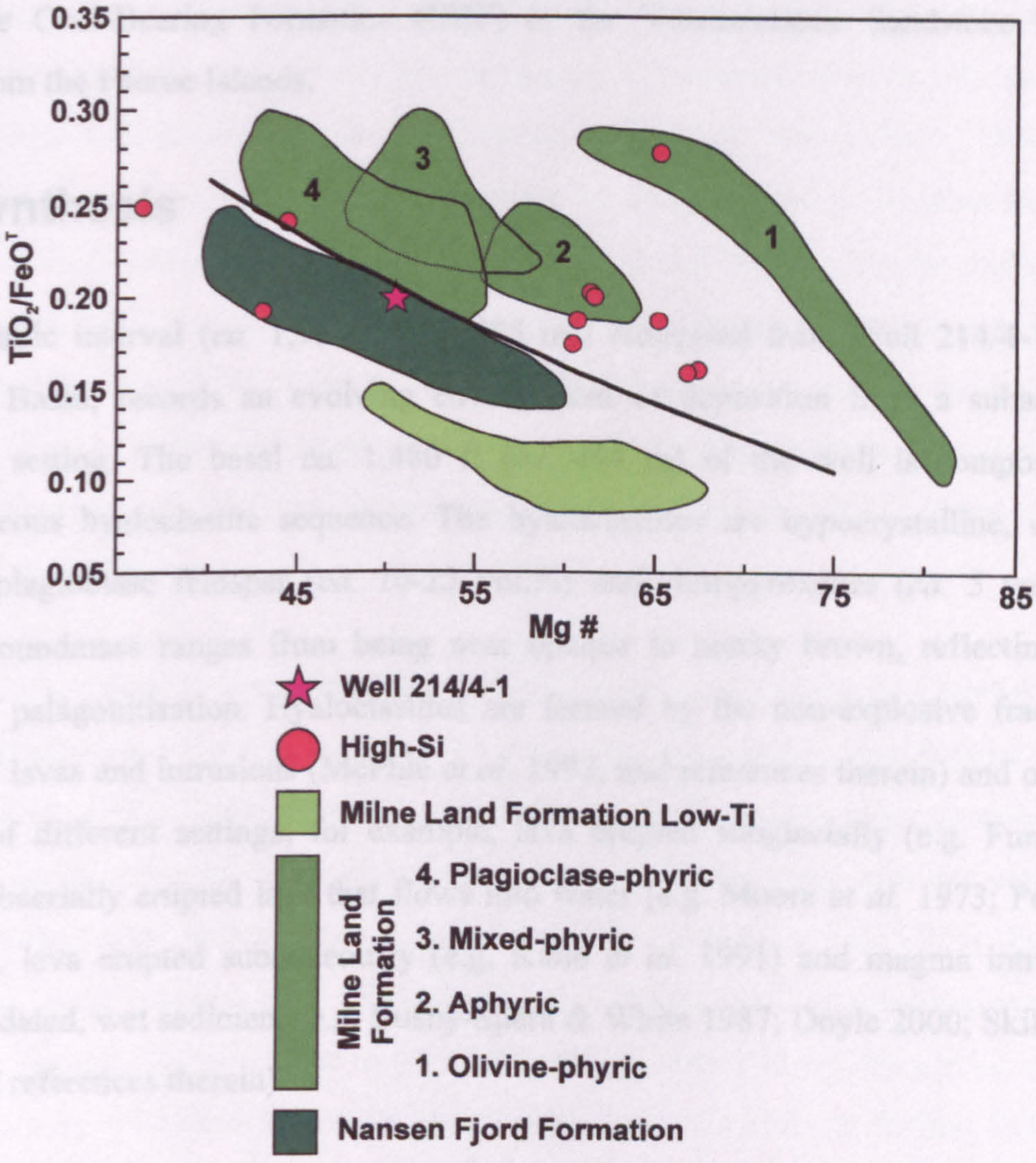

Fig. 8.27. TiO_2/FeO^T vs. Mg # diagram for the basalt lavas of the Nansen Fjord & Milne Land formations in the Nansen Fjord area, E Greenland and the igneous-bearing ditch cutting samples from Well 214/4-1, Faeroe-Shetland Basin. The division line separates low-Ti and high-Ti basalts. The analyses have been recalculated with a fixed oxidation ratio of $Fe_2O_3/FeO = 0.15$. Mg # = atomic $100Mg/(Mg + Fe^2)$, and FeO^T = total iron calculated as FeO (see Appendix B). The ditch cutting samples from Well 214/4-1 plot within the Nansen Fjord Formation field. Well 214/4-1 data added to the modified diagram of Larsen *et al.* (1999).

are recorded from the base of the Nansen Fjord Formation, East Greenland (Larsen *et al.* 1999). To date, no hyaloclastite deposits have been recognised from the *ca.* 4.5 km thick pile of the LBF on the Faeroe Islands, including Lopra-1 & 1A. This can be explained by the type of environment into which the lavas flowed, that is, the lavas may have been erupted into a subaerial environment and flowed into a substantial water body (i.e. the FSB at that time) (see Section 8.4 for detailed discussion). The volcaniclastic greywackes overlying the doleritic lava (Unit 3) in Well 214/4-1 are most likely time equivalent to either the Coal-Bearing Formation (CBF) or the Volcaniclastic Sandstone Formation (VSF) from the Faeroe Islands.

8.4 Synthesis

The volcanic interval (*ca.* 1,920 ft (*ca.* 585 m)) recovered from Well 214/4-1, Faeroe-Shetland Basin, records an evolving environment of deposition from a subaqueous to subaerial setting. The basal *ca.* 1,480 ft (*ca.* 451 m) of the well is composed of an homogeneous hyaloclastite sequence. The hyaloclastites are hypocrystalline, containing laths of plagioclase feldspar (*ca.* 10-25 vol.%) and clinopyroxenes (*ca.* 5 vol.%). The glassy groundmass ranges from being near opaque to murky brown, reflecting various stages of palagonitisation. Hyaloclastites are formed by the non-explosive fracturing of quenched lavas and intrusions (McPhie *et al.* 1993, and references therein) and occurs in a number of different settings, for example, lava erupted subglacially (e.g. Furnes *et al.* 1980), subaerially erupted lava that flows into water (e.g. Moore *et al.* 1973; Pedersen *et al.* 1998), lava erupted subaqueously (e.g. Kano *et al.* 1991) and magma intruded into unconsolidated, wet sediment (e.g. Busby-Spera & White 1987; Doyle 2000; Skilling *et al.* 2002, and references therein).

Approximately 50 ft (*ca.* 15 m) above the hyaloclastite sequence a *ca.* 170 ft (*ca.* 52 m) thick sequence of doleritic/basaltic lava occurs. The sequence consists of 4 lava flows separated by interlava lithologies. The lavas are all holocrystalline, containing plagioclase feldspar (*ca.* 50 vol.%), clinopyroxene (*ca.* 40 vol.%), serpentinised olivine (*ca.* 5 vol.%), and oxides (*ca.* 5 vol.%). The holocrystalline nature of the dolerites/basalts and the occurrence of interbedded clastic lithologies support the premise that these represent subaerial lava flows rather than intrusive bodies (Cas & Wright 1987; McPhie *et al.* 1993). The lava flows are geochemically identical to the hyaloclastites (see below), suggesting that they were erupted from the same magma chamber and possibly under the same

conditions. Therefore, the hyaloclastites most likely represent subaerially erupted lava that flowed into water.

The geochemistry of the hyaloclastite and lava sequences is extremely homogeneous throughout the 1,240 ft (*ca.* 378 m) analysed profile. The geochemical data plotted on the variation diagrams of Waagstein (1988) and Larsen *et al.* (1999) correlate the hyaloclastite and lava sequences from Well 214/4-1 to the Lower Basalt Formation (LBF) of the Faeroe Islands (including Lopra-1 & 1A) and the East Greenland Nansen Fjord Formation. The LBF is represented by a *ca.* 4.5 km thick sequence of subaerial lavas *ca.* 240 km to the W of Well 214/4-1. It is unclear whether the hyaloclastites and lavas in Well 214/4-1 and the LBF of the Faeroe Islands were erupted from the same fissure or whether the volcanic rocks in Well 214/4-1 were erupted locally from a vent with a similar melting source region as the LBF. However, it seems apparent that the hyaloclastites and lavas were erupted to the W or NW of Well 214/4-1 and flowed in an easterly to south-easterly direction. This is tentatively supported by the foreset-bedded hyaloclastites at the Faeroe-Shetland Escarpment (FSE) which prograde to the SE (Smythe 1983; Naylor *et al.* 1999; Ritchie *et al.* 1999).

The FSE is less than 50 km to the NW of Well 214/4-1 and, therefore, it seems likely that the hyaloclastites and lavas in Well 214/4-1 are linked the lava delta that formed at the FSE (Naylor *et al.* 1999). Lava deltas are characterised by foreset-bedding produced by the progradation of subaerial lavas that flowed from land into water and are analogous to alluvial Gilbert-type deltas (Jones & Nelson 1970; Moore *et al.* 1973; Porebski & Gradzinski 1990; Pedersen *et al.* 1998; Planke *et al.* 2000). As the subaerial lavas flow into water they are rapidly cooled due to quenching, which results in the brecciation of the lava to produce hypocrystalline fragments i.e. hyaloclastites (cf. Jones & Nelson 1970; Moore *et al.* 1973; Porebski & Gradzinski 1990; Pedersen *et al.* 1998; Planke *et al.* 2000). Subsequent eruptions of subaerial lavas continually add new hyaloclastites to the front of the advancing delta and the boundaries between the hyaloclastites produce the foreset-bedding (Jones & Nelson 1970; Moore *et al.* 1973; Porebski & Gradzinski 1990; Pedersen *et al.* 1998; Planke *et al.* 2000). The continued progradation of the lava delta advances the shoreline further into the basin, whilst adding new subaerial terrain to the landmass behind (Jones & Nelson 1970; Moore *et al.* 1973; Porebski & Gradzinski 1990; Pedersen *et al.* 1998; Planke *et al.* 2000) (Fig. 8.28).

Therefore, the hyaloclastites and lavas within Well 214/4-1 represent a section through a lava-fed Gilbert-type delta that advanced from the palaeoshoreline to the NW. The

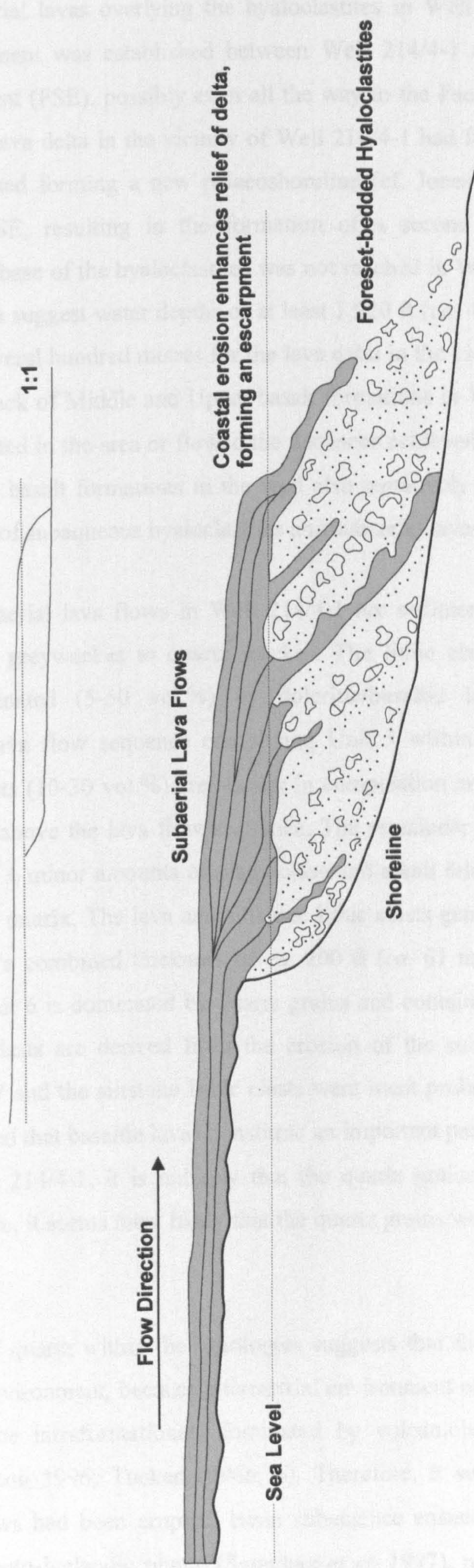

Fig. 8.28. Schematic cross-section illustrating the mode of formation of a lava-fed Gilbert-type delta with foreset-bedded hyaloclastites. After Moore *et al.* (1973).

presence of subaerial lavas overlying the hyaloclastites in Well 214/4-1 suggests that a terrestrial environment was established between Well 214/4-1 and at least the Faeroe-Shetland Escarpment (FSE), possibly even all the way to the Faeroe Islands. This implies that that after the lava delta in the vicinity of Well 214/4-1 had formed subsidence and/or sea level rise ensued forming a new palaeoshoreline (cf. Jones & Nelson 1970) in the vicinity of the FSE, resulting in the formation of a second lava delta (Fig. 8.29). Unfortunately, the base of the hyaloclastites was not reached in Well 214/4-1, although the drilled section does suggest water depths of at least 1,920 ft (*ca.* 451 m). This compares to water depths of several hundred metres for the lava delta in the vicinity of the FSE (Naylor *et al.* 1999). The lack of Middle and Upper basalt formations in Well 214/4-1 implies that they were not erupted in the area or flowed the distances achieved by the LBF. The lack of Middle and Upper basalt formations in the well also tentatively suggests that the FSE is composed entirely of subaqueous hyaloclastites and subaerial lavas of the LBF.

Overlying the subaerial lava flows in Well 214/4-1 are sedimentary strata ranging from siltstones to lithic greywackes to quartz wackes. The lithic clasts contained within the wackes are dominated (5-50 vol.%) by doleritic/basaltic lava comparable to the doleritic/basaltic lava flow sequence comprising Unit 3 within the well. Similarly, the siltstone lithic clasts (10-30 vol.%) are similar in composition and texture to Unit 4a that crops out directly above the lava flow sequence. The remainder of the wackes consist of quartz phenoclasts ± minor amounts of plagioclase and alkali feldspar set within a quartz-rich clayey to silty matrix. The lava and siltstone lithic clasts generally only occur in units 4 and 5 that have a combined thickness of *ca.* 200 ft (*ca.* 61 m) directly above the lava flow sequence. Unit 6 is dominated by quartz grains and contains less than 5 vol.% lithic clasts. The lava clasts are derived from the erosion of the subaerial lava flows, either locally or to the W and the siltstone lithic clasts were most probably eroded locally. As it has been established that basaltic lavas constitute an important part of the Palaeogene strata to the W of Well 214/4-1, it is unlikely that the quartz grains were sourced from this direction. Therefore, it seems most likely that the quartz grains were eroded from basement highs to the E.

The dominance of quartz within the lithologies suggests that the wackes were deposited within a marine environment, because a terrestrial environment on the subaerial lava flows would generally be intraformational, dominated by volcaniclastic sandstones with no quartz (cf. Collinson 1996; Tucker 1996a; b). Therefore, it seems likely that after the subaerial lava flows had been erupted, basin subsidence ensued, possibly related to the deflation of the proto-Icelandic plume (Saunders *et al.* 1997), resulting in sea level rises

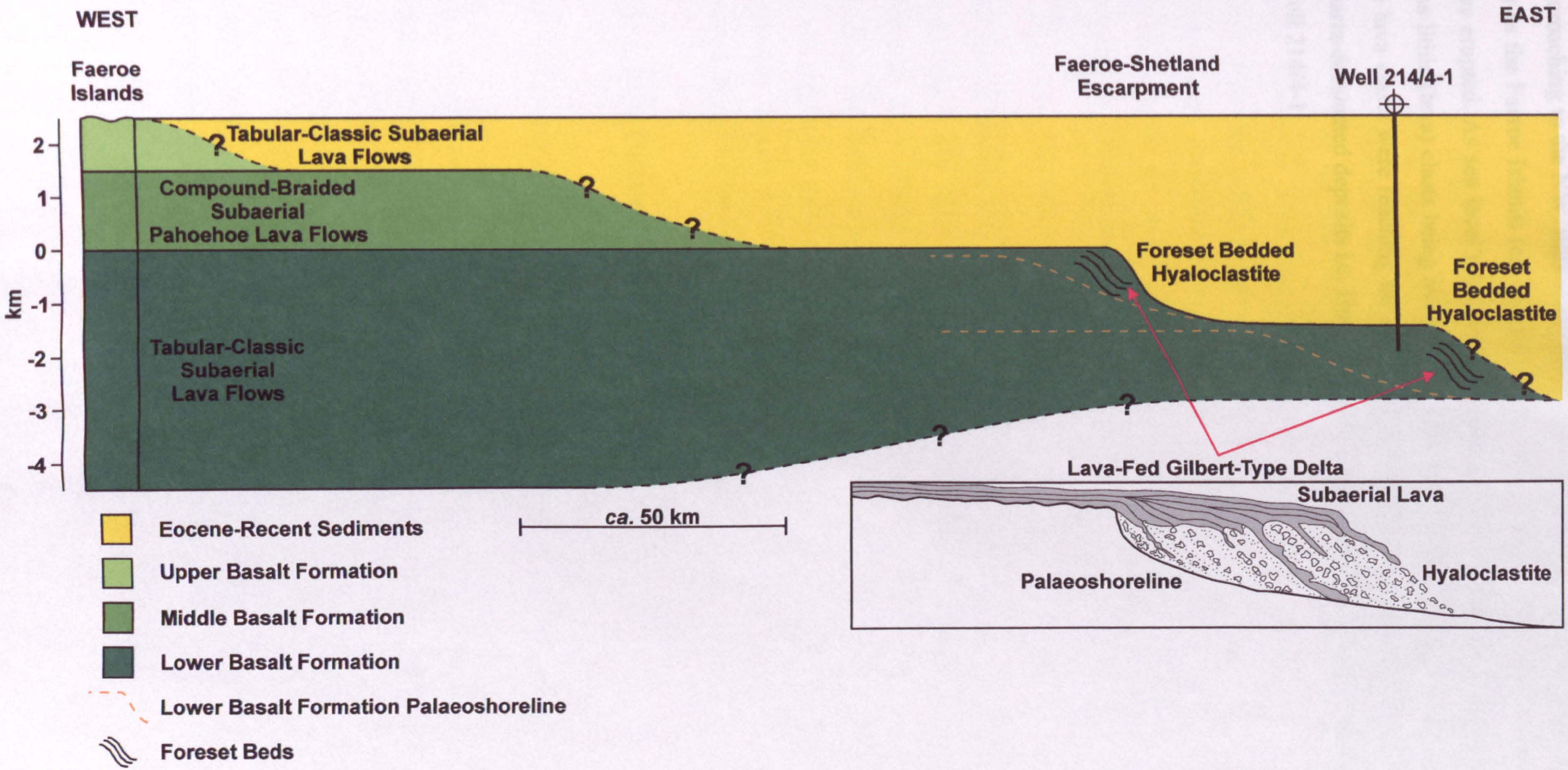

Fig. 8.29. Schematic correlation of the onshore and offshore Faeroe Plateau Lava Group (FPLG). The volcanic interval within Well 214/4-1 is geochemically correlated to the Lower Basalt Formation (LBF) of the Faeroe Islands and is represented by a hyaloclastite delta overlain by subaerial lava flows. These data imply that the Faeroe-Shetland Escarpment represents a second hyaloclastite delta within the LBF, which in turn suggests that basin subsidence was occurring during the FPLG volcanism, resulting in the sea encroaching towards the Faeroe Islands. The lava-fed Gilbert type delta is after Moore *et al.* (1973) and can also be seen in detail in Figure 8.28.

encroaching to the NW. Ellis *et al.* (2002) have demonstrated that sea levels encroached as far as the Faeroe Islands (*ca.* 240 km to the NW) by the time the Upper Basalt Formation was erupted. As sea level rose, erosion of the subaerial lavas was restricted, resulting in less lithic (lava) clasts being incorporated into the overlying deposits. This continued until no lava clasts were reaching the deep sections of the basin, resulting in the deposition of quartz-dominated deposits i.e. Unit 6 *ca.* 200 ft (*ca.* 61 m) above the lava flow sequence in Well 214/4-1.

9 Synthesis

The aim of this thesis has been to re-examine the Faeroe Plateau Lava Group (FPLG) on the Faeroe Islands and within the Faeroe-Shetland Basin, in terms of environment of eruption and deposition of the lava flows and interlava lithologies, respectively, through the evolution of the lava field. The FPLG consists of five formations exposed on the Faeroe Islands (*ca.* 3 km thick) which, in chronological order, are as follows: the Lower Basalt Formation (LBF) (Chapter 3); the Coal-bearing Formation (CBF) (Chapter 4); the Volcaniclastic Sandstone Formation (VSF) (Chapter 5); the Middle Basalt Formation (MBF) (Chapter 6); and, the Upper Basalt Formation (UBF) (Chapter 7). Chapter 8 describes the offshore extension of the LBF within Well 214/4-1 of the Faeroe-Shetland Basin.

The aim of Section 9.1, below, is to compare and contrast the various lava-dominated formations (LBF, MBF & UBF) of the FPLG with lava fields from other volcanic provinces in an attempt to understand their mode of emplacement and environment of eruption. The interlava lithologies from the FPLG are compared and contrasted in Section 9.2 to understand their environment of deposition and how they were affected by the volcanism. Section 9.3 brings together the findings in sections 9.1 and 9.2 to present a coherent model for the evolving lava field of the FPLG.

9.1 Lava Flows

9.1.1 Facies Architecture and Environment of Eruption

The Faeroe Plateau Lava Group (FPLG) has a recorded thickness of *ca.* 6.5 km from the exposed and drilled sections of the Faeroe Islands. The FPLG, based on field (Figs. 1.3, 1.4, 1.5, 3.6 & 7.6) and geochemical data (Figs. 1.6 & 1.7), has been separated into three (basalt) formations: Lower (LBF), Middle (MBF), and Upper (UBF). The LBF & UBF have a tabular-classic facies architecture, which contrasts with the MBF, which has a compound-braided facies architecture (see below). The LBF in the Faeroe-Shetland Basin is represented by both subaerial facies flows and submarine hyaloclastite deposits.

9.1.1.1 Tabular-Classic Facies Architecture

The LBF (Chapter 3) & UBF (Chapter 7) are dominated by subaerially erupted prismatically jointed lava flows that have rubbly and vesicular flow tops. They are laterally extensive, with sheet-like geometries, and the LBF flows have average thicknesses of *ca.* 25 m (max. *ca.* 70 m) (Figs. 3.6 & 3.8), which contrasts with those of the UBF that have average thicknesses of 8-11 m (max. *ca.* 30 m) (Fig. 7.9), most likely a consequence of reduced voluminous eruptions. These characteristics are comparable to the 60 m thick (max.) Tsuhasis Member lava flows, Awahab Formation, Paraná-Etendeka Flood Basalt Province, which have rubbly vesicle-rich flow tops and massive basal/core regions (Jerram *et al.* 1999). These Tsuhasis Member lava flows have been identified as having a tabular-classic facies architecture (Jerram *et al.* 1999; Jerram 2002), similar to that reported here for the lavas of the LBF and the UBF. Tabular-classic facies lava flows, characterised by massive core/basal regions and rubbly vesicular rich flow tops with laterally extensive sheet-like geometries, have also been identified in other Continental Flood Basalt provinces, including the Teepee Butte Member, Grande Ronde Basalt Formation, Columbia River Basalt Group (CRBG) (Reidel & Tolan 1992).

The tabular-classic facies basalt flows of the Teepee Butte Member and the Yakima Basalt Subgroup, CRBG, are predominantly aphyric and a lack of coarse crystallisation over distances of tens to hundreds of kilometres implies that they were rapidly emplaced, from high effusion rate (>0.6 km^3/hr/linear km of fissure, with fissure widths >3 m) eruptions (cf. Shaw & Swanson 1970a; b; Swanson *et al.* 1975; Reidel & Tolan 1992). Consequently, it is proposed here that the voluminous aphyric basalt flows of the LBF & UBF were similarly erupted at high effusion rates, travelled extremely rapidly, and were emplaced over periods of days to weeks. This is supported by the general downward decrease in vesicle size, which is consistent with them having formed during post-emplacement bubble rise (cf. Aubele *et al.* 1988; Sahagian *et al.* 1989; Cashman & Kauahikaua 1997) and is characteristic of other rapidly emplaced lava flows, e.g. Alae lava lake, Hawai`i (Peck 1978; Cashman & Kauahikaua 1997).

However, observations of emplacement mechanisms of lavas on Hawai`i (Hon *et al.* 1994) have led to the identification of the inflation (endogenous) process (Hon *et al.* 1994), which has resulted in the re-evaluation of the emplacement mechanisms of Continental Flood Basalts (CFBs), particularly those of the Columbia River Basalt Group (CRBG) (Self *et al.* 1996; Self *et al.* 1997; Thordarson & Self 1998). As a result, some tabular-classic facies flows have been reinterpreted as forming part of extremely large-scale

compound-braided facies that were emplaced slowly through the inflation process e.g. the Roza Member, CRBG (Self *et al.* 1996; Self *et al.* 1997; Thordarson & Self 1998). However, features characteristic of the inflation process are absent from the LBF & UBF flows, but are observed throughout the MBF (see Section 9.1.1.2). This may be directly related to effusion rate, where the LBF & UBF were erupted with high effusion rates, whereas the MBF flows, with similar volumes, were erupted at lower effusion rates (cf. Walker 1970; Self *et al.* 1997; Self *et al.* 1998; Jerram 2002, and others).

The jointing patterns (prismatic and columnar) preserved within the tabular-classic facies lava flows are directly related to the environment into which the flows were erupted (Jerram 2002). Prismatically and poorly-jointed lava flows are dominant within the lower *ca.* 800 m of the exposed LBF (Fig. 3.9) and throughout the *ca.* 900 m of the UBF (Fig. 7.9), which implies that they were erupted into a relatively dry environment (cf. Jerram 2002). This is supported by the commonness of prismatic joints and the general lack of columnar joints within, for example, the lava flows of the Awahab Formation, Paraná-Etendeka Flood Basalt Province, which were emplaced in an aeolian, arid, subaerial environment (Jerram *et al.* 1999; Jerram *et al.* 2000; Jerram 2002; Jerram & Stollhofen 2002). The aeolian character of this environment implies that there was an overall lack of surface water available to ingress through the cooling surfaces of the lava flows, thus preventing the modification of the internal isotherms, and permitting the development of regular columns (Jerram *et al.* 1999).

Lyle (2000) demonstrated that columnar jointed lava flows from a number of provinces, including: the Palaeogene Antrim and Mull lava fields of Northern Ireland and Scotland, respectively; the Miocene CRBG; and the Quaternary lavas of southern Iceland; are commonly associated with features suggesting that these flows were emplaced within wet subaerial environments. These associated features are outlined in Section 2.1.2.3 and are observed in close association with the well-developed columnar jointed lavas of the upper 100 m of the exposed LBF. Columnar jointed flows (e.g. Kúlugjógv Lava Flow (Figs. 3.13 & 3.14) commonly overlie fluviatile or lacustrine strata, suggesting that significant quantities of surface water were available and capable of ingress through cooling surfaces, and were thus able to disturb the internal isotherms. An example of extreme isothermal modification is preserved at Hov (Fig. 3.12), where a multi-tiered lava flow has an entablature dominated by curvi-columnar columns, characteristic of water ingress through the upper surface of the flow (cf. Saemundsson 1970). This ingress of water implies either high rainfall or surface water sourced from the damming of pre-existing river channels (cf. Saemundsson 1970; Lyle 2000). Evidence for the damming of a river channel is preserved

to the E of Froðba, Suðuroy, where the Kúlugjógv Lava Flow has infilled a channel *ca.* 20 m deep (Fig. 3.13). Some of the lava flows (e.g. the Hvalbiareiði and Skarvatangi lava flows) also have basal pillows, hyaloclastites and blocky peperites, all indicative of lava flowing into/over water saturated sediments or pools of water, respectively (cf. Lyle 2000; Skilling *et al.* 2002).

The lack of columnar jointed lava flows in the UBF suggests that there was a general absence of surface water available to ingress through the cooling surfaces. However, a number of *ca.* 8 m thick agglutinated lava flows, which have the appearance of breccia in outcrop, have been observed overlying fluviatile and lacustrine strata e.g. the Hálgafelli Section, Borðoy (Fig. 7.10). The agglutinated nature of these flows and the association with the underlying sedimentary strata implies that there were localised bodies of water (i.e. lakes) into which the lavas flowed, resulting in their quenching and brecciation (cf. Skilling *et al.* 2002, and references therein).

9.1.1.2 Compound-Braided Facies Architecture

The *ca.* 1.4 km thick MBF consists of lava flow units that range in thickness from <0.5 to 2 m, and which have smooth, sometimes ropy, surfaces, suggesting that they are pahoehoe lavas (cf. Wentworth & Macdonald 1953; MacDonald 1967; Fink & Fletcher 1978; Basaltic Volcanism Study Project 1981; Cas & Wright 1987; Walker 1989; Rowland & Walker 1990; McPhie *et al.* 1993; Walker 1993; Wilmoth & Walker 1993; Self *et al.* 1998; Crown & Baloga 1999) (Fig. 6.10). Two different types of pahoehoe lava have been recognised in the MBF based on their amygdale distribution patterns: S-type (spongy) and P-type (pipe-bearing) (cf. Wilmoth & Walker 1993). Some of the flow units are highly amygdaloidal throughout their thickness, suggesting that they are spongy or S-type pahoehoe flows (cf. Walker 1989; Wilmoth & Walker 1993). The majority, however, can be separated into a basal crust, a lava core and an upper crust, which are characteristic of P-type flows (cf. Wilmoth & Walker 1993) (Fig. 6.11). The basal crust generally consists of pipe amygdales that have a maximum length of 8 cm, and which are sometimes curved in the direction of flow. They commonly occur at least 2 cm off the base of the lava, suggesting that they formed from late-stage bubble rise rather than from steam originating from the heating of surface water, rising through the lava (cf. Walker 1987). The presence of the pipes also suggests that the lava flow units were emplaced on slopes of <4° (cf. Walker 1987). The lava core is typically massive and compact, with irregular jointing, and the upper crust is dominated by elliptical amygdales up to 2 cm in diameter.

The flow units form compound lava flows (i.e. compound-braided facies architecture) with average thicknesses of *ca.* 20 m, which are identified from poorly developed reddened flow tops or sparse interlava lithologies. The compound nature and the dominance of P-type pahoehoe of the MBF is comparable to the 5 m thick flow units of Hawai`i that formed from the inflation (endogenous) process (Fig. 2.6) (Hon *et al.* 1994; Cashman & Kauahikaua 1997). The Hawaiian flow units were erupted at low effusion rates as 20-30 cm thick pahoehoe lavas that thickened to *ca.* 1 m in 1-2 hours and to 4 m after 14 days (Hon *et al.* 1994). Based on these observations, Hon *et al.* (1994) proposed an empirical equation to estimate the time that each flow unit was active. Applying this equation by using the upper crust thickness of the MBF P-type flows, it is estimated that they were active over a period of 10 hours (1.6 m thick flow) to 9 days (2.2 m thick flow), similar to the durations determined by Hon *et al.* (1994) described above. However, this assumes that the MBF lavas were emplaced under the same conditions (for example, temperature) as the Hawaiian flows, and does not take into consideration other external factors, such as the effects of rainfall. If the MBF flow units were erupted continuously to form a compound lava flow *ca.* 20 m thick it follows that the lava flow was emplaced over a period of 5 to 85 days. Pahoehoe formation on Hawai`i is associated with low discharge rates resulting in low volumetric flow rates with flow-front velocities of the order of 1-10 m h^{-1} (cf. Rowland & Walker 1990; Hon *et al.* 1994). Assuming similar velocities for the MBF, it would have taken a few months to just over a year for a flow-front to advance *ca.* 10 km from a fissure vent (cf. Kent *et al.* 1998).

Another feature associated with the development of inflating pahoehoe lavas on Hawai`i is the formation of lava tubes through the coalescence of pahoehoe lobes (Hon *et al.* 1994; Kauahikaua *et al.* 1998). The lava tubes decrease in size, from master tubes through distributary tubes to flow fronts, away from the source fissure/vent (Fig. 6.31) (Rowland & Walker 1990). Master tubes, ranging in cross-sectional area from 3 to 160 m^2, occur throughout the MBF (Figs. 6.7, 6.8 & 6.9) and smaller distributary tubes with cross-sectional areas of <0.15 m^2 also occur, particularly at Viðareiði, Viðoy (Fig. 6.9e). The presence of the lava tubes in the MBF supports the premise that the associated pahoehoe lavas were emplaced through the inflation process (cf. Hon *et al.* 1994) and also implies that lava tube networks were able to transport magma significant distances away from the source vents (cf. Atkinson *et al.* 1975; Greeley 1982; 1987; Hon *et al.* 1994; Peterson *et al.* 1994; Cashman *et al.* 1998; Kauahikaua *et al.* 1998; Stephenson *et al.* 1998).

The MBF compound lava flows form edifices *ca.* 70 m high, 15 km across with slopes of <0.5° and volumes of <7 km^3 (Noe-Nygaard 1968). This type of structure is known as a

low shield of the scutulum type (Noe-Nygaard 1968; Greeley 1982). Greeley (1976; 1977; 1982) compared the MBF lava flows and associated low shields to those of the Snake River Plain, Idaho, and proposed a new style of volcanism referred to as Basaltic Plains Volcanism (Fig. 2.8). This style of volcanic activity has combined features from Continental Flood Basalt provinces (e.g. high volume flows, rift fissures, planar surfaces) and Hawaiian volcanism (e.g. compound pahoehoe lavas, low shields, lava tubes) (Greeley 1976; 1977; 1982). The MBF and Snake River Plain sequences are extremely similar in style and share many characteristic features. First, both provinces are dominated by large volume compound pahoehoe lava flows. The compound flows of the MBF average *ca.* 20 m in thickness, similar to those of the Hell's Half Acre and Wapi fields, Snake River Plains, which have flows with average thicknesses of *ca.* 35 m (Greeley 1982). These thick compound flows are composed of flow units averaging between 1 and 5 m (Greeley 1982), which compares closely to the average thickness of 2 m within the MBF. Second, lava tubes are extremely common in both provinces, implying that they played a major role in transporting lava large distances (see above). A third feature observed is the drowning of the lava topography by tabular-classic facies lava flows. In Idaho, the low shields are partially buried by the King's Bowl Flow, with flow thicknesses of *ca.* 4 m (Greeley 1982), whereas in the Faeroe Islands the top surfaces of the low shields of the MBF are covered by, or interdigitate with, the basal *ca.* 10 m thick tabular-classic UBF flows.

A similar relationship of compound-braided facies lavas overlain by tabular-classic facies flows is observed in the Huab Basin, Paraná-Etendeka Flood Basalt Province, Namibia (Jerram *et al.* 1999; Jerram *et al.* 2000; Jerram & Stollhofen 2002). Here, compound flows of the Tafelkop Inter-dune Member, Awahab Formation, are composed of olivine-phyric pahoehoe lobes up to a few metres thick and are overlain by the thicker tabular-classic Tsuhasis Member flows (Jerram *et al.* 1999; Jerram *et al.* 2000; Jerram & Stollhofen 2002, see above). The Tafelkop Inter-dune Member compound flows were emplaced passively by the inflation process (Jerram *et al.* 1999; Jerram *et al.* 2000; Jerram & Stollhofen 2002), akin to those of Hawai`i and the MBF. Aeolian ergs contained within the Tafelkop flows preserve dune structures that have not been modified or destroyed by the overlying lava flows, suggesting that the lavas were emplaced passively (Jerram *et al.* 1999; Jerram *et al.* 2000; Jerram & Stollhofen 2002). This observation supports the hypothesis that the pahoehoe flows were emplaced over months to years by the inflation process (Jerram *et al.* 1999; Jerram *et al.* 2000; Jerram & Stollhofen 2002). At Viðareiði, Viðoy, fluviatile sedimentary rocks are preserved inbetween pahoehoe flow units of the MBF and the bedform structures (e.g. planar laminations) in the sedimentary strata have not been significantly modified or destroyed (Fig. 6.25), suggesting that the lavas were emplaced

passively, similar to the Tafelkop Inter-dune Member flows. The preservation of sedimentary strata by lava flows is also recorded in the Serra Geral Formation, Paraná-Etendeka Flood Basalt Province, Brazil (Scherer 2002) and in the Mussartût Member, Eriksford Formation, South Greenland (Clemmensen 1988).

Other pahoehoe flow units of similar thickness to those of the MBF, the Snake River Plains and the Tafelkop Inter-dune Member, have been identified from the British Tertiary Igneous Province. The base of the Tertiary sequence consists of 2-5 m thick pahoehoe sheets of simple character (Williamson & Bell 1994; Kent *et al.* 1998), which were emplaced by the inflation process (Kent *et al.* 1998). Associated with these pahoehoe flows is a much larger, 16-30 m thick, pahoehoe unit, which has features suggestive of emplacement through the inflation process (Kent *et al.* 1998). The occurrence of large (*ca.* 30 m thick) inflated pahoehoe units inbetween thinner (0.3 to 3 m thick) units is also observed in the CRBG (Self *et al.* 1996; Self *et al.* 1997; Self *et al.* 1998; Thordarson & Self 1998). The present study has not observed any large, >5 m thick, inflated pahoehoe lava flows in the MBF.

9.1.1.3 Hyaloclastite Facies Architecture

The volcanic interval, which is geochemically equivalent to the LBF on the Faeroe Islands (see Section 8.3.1.3) in Well 214/4-1, Faeroe-Shetland Basin, consists of hypocrystalline basalt fragments forming a *ca.* 450 m thick hyaloclastite sequence, which is overlain by subaerial lava flows with a combined thickness of *ca.* 50 m. The hyaloclastites were formed from the quenching of subaerial lava in water (cf. Cas & Wright 1987; McPhie *et al.* 1993). Seismic data collected from the area around the Faeroe-Shetland Escarpment are characterised by dipping reflectors interpreted as prograding foresets within hyaloclastite sequences (Naylor *et al.* 1999; Ritchie *et al.* 1999; Planke *et al.* 2000). The occurrence of foreset bedded hyaloclastites in the Faeroe-Shetland Basin, at least *ca.* 450 m thick in Well 214/4-1, are similar to the onshore examples of Disko and Nuussuaq, West Greenland (Pedersen *et al.* 1998). Here, hyaloclastite breccias consist of 450 m high, 0.5-2 m thick foresets that laterally grade into and are overlain by subaerial lava flows (Pedersen *et al.* 1998).

Hyaloclastites that grade laterally into, and are commonly overlain by, subaerial lavas have been interpreted to represent the locations of palaeoshorelines, whereby lava flows have travelled from a (dry) land surface into water (Jones & Nelson 1970; Moore *et al.* 1973; Porebski & Gradzinski 1990; Pedersen *et al.* 1998; Planke *et al.* 2000; Carr & Jones 2001).

The prograding foresets of the hyaloclastite sequences are similar to Gilbert-type deltas of sedimentary environments and, consequently, have been referred to as lava-fed Gilbert-type deltas by Porebski & Gradzinski (1990). Consequently, the hyaloclastite sequence and overlying subaerial lava flows in Well 214/4-1 most likely represent a lava delta formed in close proximity to a palaeoshoreline and the angularity of the foresets suggests that the lava delta was prograding from a westerly direction (cf. Porebski & Gradzinski 1990; Pedersen *et al.* 1998; Planke *et al.* 2000). The thickness of hyaloclastite sequences is directly related to water depth (cf. Jones & Nelson 1970; Pedersen *et al.* 1998); therefore, in the vicinity of Well 214/4-1 the basin was at least 450 m deep during hyaloclastite deposition.

9.2 Interlava Lithologies

9.2.1 Environment of Deposition

The interlava lithologies investigated in this study from the FPLG on the Faeroe Islands were deposited onto a terrestrial terrain during hiatuses in the eruption of the basalt lava flows. The interlava lithologies are dominated by epiclastic facies composed of intraformational clasts derived from the reworking of poorly consolidated tephra and the erosion of pre-existing lava flows and volcaniclastic rocks. The study of other continental volcanic terrains and the effect of volcanism on fluvial systems has led to the recognition of two facies sequences: inter- and syn-eruption facies (Smith 1987a; 1988; Smith & Fritz 1989; Runkel 1990; Smith 1991; Cole & Ridgway 1993; Haughton 1993; Bahk & Chough 1996). Inter-eruption facies (Section 9.2.1.1) are characterised by 'normal' terrestrial environments (i.e. fluvial, lacustrine, etc.) whereas syn-eruption facies (Section 9.2.1.2) are unique to volcanic terrains and are dominated by high-sediment-load flood to mass-flow deposits that are different to those formed in non-volcanic settings (Smith 1987a; 1988; Smith & Fritz 1989; Runkel 1990; Smith 1991; Cole & Ridgway 1993; Haughton 1993; Bahk & Chough 1996). Both facies types have been recognised throughout the FPLG on the Faeroe Islands, although the inter-eruption facies are by far the most dominant. For completeness, tuff beds and peperites, which only occur in minor amounts, shall be discussed collectively with the syn-eruption facies (Section 9.2.1.2).

9.2.1.1 Inter-Eruption Facies

The inter-eruption facies of the FPLG are dominated by fluviatile, lacustrine, swamp and palaeosol environments (and associated lithologies) that were formed during hiatuses

between eruptions of the basalt lava flows. Hiatuses in the volcanic activity allowed time for the chemical and physical weathering of the volcanic land surface. However, subsidence rates had to be high enough to allow for the accumulation of the detritus (cf. Smith 1987a; Smith & Fritz 1989; Runkel 1990; Smith 1991; Cole & Ridgway 1993; Haughton 1993; Bahk & Chough 1996). The *ca.* 10 m thick Coal-bearing Formation (CBF) was deposited during a significant hiatus, whereby the time between eruptions (i.e. between the LBF and MBF) was prolonged, thus allowing extensive weathering/erosion of the volcanic terrain and a subsidence rate which was high enough to allow the deposition of the uncommonly thick CBF inter-eruption sequence.

The fluviatile sequences, each no more than 2 m thick, are contained within channel-type structures throughout the FPLG and consist of poorly sorted, clast- to matrix-supported volcaniclastic sandstones, although conglomerates also occur. Channel-type structures range from deep (*ca.* 20 m) relatively narrow channels (e.g. Kúlugjógv Section (Fig. 3.13)) to broad channels no more than 2 m deep (e.g. Klivarnar Section (Fig. 6.14)). The majority of the sandstones are composed of reworked tephra, predominantly coarse ash but also lapilli grade. The tephra exhibits a range of colours, textures and grain sizes, implying that the clasts were derived from numerous poorly consolidated tuff and lapillistone beds, which supports the premise that they represent epiclastic strata (cf. Cas & Wright 1987; McPhie *et al.* 1993). The sandstones also contain variable amounts of lithic clasts derived from pre-existing epiclastic sandstones, mudstones as well as tuffs and basalt lava flows. The degree of rounding of the clasts within the sandstones ranges from angular to sub-rounded, implying that they have only undergone minor transportation. Such lava clast dominated volcaniclastic sandstones are well represented in the upper section of the LBF and within the CBF. These basalt clasts have typically undergone a high degree of reworking and are commonly aligned parallel to bedding, indicating localised river flow directions (e.g. Kúlugjógv Section (Fig. 3.19)). The occurrence of lensoidal bedding in the í Bugum Section (MBF) tentatively suggests that the fluvial system consisted of braided streams (cf. Bahk & Chough 1996). Mudstone lithologies associated with the fluviatile systems most likely represent interchannel environments consisting of swamps and small lakes as well as possibly recording episodes of flooding (cf. Smith 1991; Cole & Ridgway 1993; Haughton 1993; Bahk & Chough 1996; Collinson 1996).

Coals are not preserved in the MBF & UBF, although plant material has been recovered from the í Bugum Section implying that the surrounding land surface was vegetated at the time. This is supported by the presence of tree moulds within the bases of some of the UBF lava flows that are commonly located overlying fluviatile strata. The occurrence of the

plant material, particularly the tree moulds (Fig. 7.12), suggests that the hiatuses in volcanism were prolonged, even though the associated thin fluvial deposits imply relatively short hiatuses. This observation may be explained by low subsidence rates that prevented the accumulation of detritus (cf. Smith 1987a; Smith & Fritz 1989; Smith 1991; Haughton 1993; Bahk & Chough 1996).

The *in situ* subaerial chemical weathering of the volcanic terrain, under a temperate to warm climate with seasonal rainfall (Parra *et al.* 1987; Lund 1989), led to the formation of palaeosols, which are particularly well preserved in the upper section of the LBF and within the CBF. These palaeosols were predominantly derived from the weathering of basalt lava flows (e.g. Parra *et al.* 1987), but also from volcaniclastic rocks (tuffs or epiclastic sandstones) (e.g. Sabine 1971). The palaeosols within the upper section of the LBF are reddened boles (or ferruginous palaeosols) and are composed of ferric iron oxyhydrates (ferrihydrite and goethite) and ferric iron oxides (haematite) and were most likely formed in a well-drained environment (cf. Baas-Becking *et al.* 1960; Retallack 1997; Duchaufour 1998; Retallack 2001). Applying the calculations of Nahon (1991), it is suggested that a 2 m thick bole (derived from the weathering of basalt) from the LBF would have formed within a hiatus of at least 140 kyrs.

The palaeosols of the CBF are dominated by grey gleysols that formed under waterlogged conditions (cf. Baas-Becking *et al.* 1960; Besly & Fielding 1989; Retallack 1994; 1997; Duchaufour 1998; Retallack 2001) and are characterised by an abundance of organic material and siderite spherules no more than 2 mm in diameter. The presence of the organic material implies the surrounding land surface was heavily vegetated. The accumulation and subsequent decomposition of the organic material and associated manganese and iron reduction led to supersaturated levels of bicarbonate, Fe^{2+} and Mn^{2+} in the pore fluids, which were favourable conditions to precipitate the siderite spherules (cf. Berner 1981). The high levels of Fe and Mn were most likely derived directly from water percolating through the surrounding LBF lava flows. The reducing waterlogged land surface and the accumulation of organic material also resulted in the formation of mineable coal seams within the CBF; minor amounts of coal are also preserved within the upper section of LBF, for example on Mykines and Suðuroy. Rasmussen & Noe-Nygaard (1970b) and Lund (1983; 1989) suggested that the coals were formed in a lacustrine setting because, in part, the plant macerals from the coals are partly allochthonous in origin. The occurrence of a semi-gleysol in the Ulingatangi Section of the CBF implies that the palaeosol underwent fluctuating water table levels (cf. Besly & Fielding 1989) at least four times, most likely reflecting seasonal variations.

9.2.1.2 Syn-Eruption Facies

The syn-eruption facies of the FPLG on the Faeroe Islands were deposited by processes ranging from (volcaniclastic) debris flows to hyperconcentrated flows, together with tuffs and peperites. Mass flow deposits form the bulk of the Volcaniclastic Sandstone Formation (VSF) and occur with laterally extensive tuff beds. A debris flow has also been recognised from the base of the UBF in localities up to 34 km apart, and which is interpreted as being a single depositional unit. Peperites are commonly found within the basal crusts of lava flows (sections 9.1.1.1 & 9.1.1.2) and a major peperite sequence is preserved in the Reyðibarmur Section, Suðuroy, where a shallow sill has invaded the CBF.

The mass flows of the VSF range from mudstones through to conglomerates, are no more than a few metres thick, and extend over distances of up to a few kilometres. These flows have tabular geometries and are dominated by reworked ash and lapilli clasts. The coarse deposits are poorly sorted and matrix-supported and contain phenoclasts of coal, volcaniclastic mudstone and basalt. They commonly exhibit a planar lamination and clasts have a high degree of rounding, suggesting that they formed by a combination of volcaniclastic debris and hyperconcentrated flow processes (cf. Janda *et al.* 1981; Pierson & Scott 1985; Lowe *et al.* 1986; Naranjo *et al.* 1986; Smith 1986; Rodolfo 1989; Smith & Lowe 1991; Coussot & Meunier 1996; Sohn *et al.* 1999; Kessler & Bédard 2000; Lavigne *et al.* 2000; Lirer *et al.* 2001). The lack of channel-shaped margins and cross-bedding suggests that deposition occurred on volcaniclastic aprons where streams were not established (cf. Palmer & Walton 1990; Smith 1991; Bahk & Chough 1996; Nakayama & Yoshikawa 1997). The debris and hyperconcentrated flows were most likely initiated in response to an increase in tephra added to the surrounding land surface from renewed eruptions, which was accompanied by high rainfall resulting in high aggradation rates producing turbulent flood surges (sheet floods) (cf. Smith 1986; 1987a; b; 1988; Smith & Fritz 1989; Smith 1991; Smith & Lowe 1991; Haughton 1993; Bahk & Chough 1996; Nakayama & Yoshikawa 1997). This interpretation is supported by an association with tuff beds, together with the incorporation of clasts derived from these units within the mass flow deposits (cf. Smith 1991; Haughton 1993; Bahk & Chough 1996; Nakayama & Yoshikawa 1997). The olivine-phyric vitric tuff beds of the VSF show little compositional variation, both vertically and laterally. These beds have thicknesses of greater than 4 m and have tabular geometries. Welded tuffs towards the top of this sequence are characterised by fiamme and are interbedded with mass flow deposits, thus supporting the premise that sedimentation and volcanic activity were contemporaneous.

The debris flow at the base of the UBF has a tabular geometry and is at least 10 m thick. It is a conglomerate that is characterised by being poorly sorted, non-graded and having an homogenous clast population (Figs. 7.14, 7.15, 7.24 & 7.25). The clasts are dominated by plagioclase-phyric glassy to finely crystalline basalts, which are typically angular with irregular-shaped edges. The absence of any megablocks greater than 10 m in size, together with a lack of fracturing of clasts, suggests that this conglomerate is the product of a volcaniclastic debris flow (cf. Yarnold 1993). The irregular-shaped clast edges suggest that the debris flow travelled either a relatively short distance, or very rapidly. As with the mass flows of the VSF, the debris flow of the UBF was formed when a substantial amount of volcanic debris was deposited on the surrounding land surface, with high rainfall mobilising the debris to produce sheet floods, possibly covering substantial distances. There are many documented examples where debris flows have travelled distances greater than 100 km (e.g. Janda *et al.* 1981; Lowe *et al.* 1986; Naranjo *et al.* 1986; Rodolfo 1989; Smith & Lowe 1991). The incorporation of ash into the top of the debris flow at Sneis implies that an eruption had begun before the mass flow had frozen, suggesting that the flow was contemporaneous with volcanism.

The peperite sequence at the base of the VSF records an episode when sills invaded and mingled with strata from the CBF. The vesicularity of the sills implies that they were emplaced at a relatively shallow level, most likely representing a conduit for a vent, which may have erupted the tuffs of the VSF. As the sill propagated through the CBF strata, vapour-insulated apophyses initially produced a dispersed blocky-fluidal peperite under a ductile fragmentation regime (cf. Kokelaar 1982; Wohletz 1983; Mills 1984; Busby-Spera & White 1987; Rawlings *et al.* 1999; Donaire *et al.* 2002; Skilling *et al.* 2002; Squire & McPhie 2002; Wohletz 2002). When these early-stage apophyses came into contact with the thermally unstable coal, it led to the mutual injection of sill into coal and *vice versa* (cf. Lumsden 1967; Stach *et al.* 1975; Thomas 1992; Nomura *et al.* 1999; McClintock & White 2002). As the sills cooled they could no longer develop vapour films and consequently they entered the brittle fragmentation regime, leading to the formation of a close-packed blocky peperite. The lack of jigsaw-fit clasts within this peperite suggests that it was formed by bulk interaction steam explosions and mechanical stresses, rather than through quenching (cf. Kokelaar 1986; Busby-Spera & White 1987). For a more detailed discussion of the peperite-forming process see Section 5.4.1.3.

9.3 Evolution of the Faeroe Plateau Lava Group

The Faeroe Plateau Lava Group (FPLG) began with the eruption of a pre-break-up succession in the Palaeocene (C27R-C25R (*ca.* 60.56-57.5 Ma)) (Waagstein 1988; Ritchie *et al.* 1999; Ellis *et al.* 2002) and consists of the Lower Basalt Formation (LBF) on the Faeroe Islands and the Nansen Fjord Formation, East Greenland (Larsen *et al.* 1999). The LBF has a recorded stratigraphic thickness of *ca.* 4.5 km in the vicinity of the Faeroe Islands and is entirely composed of subaerial lava flows exhibiting a tabular-classic facies architecture. However, to the east of the Faeroe Islands, moving into the Faeroe-Shetland Basin, the LBF consists of (marine) hyaloclastite sequences overlain by subaerial lava flows (e.g. Well 214/4-1). In comparison with exposed examples of hyaloclastite sequences (for example, Disko and Nuussuaq, West Greenland (Pedersen *et al.* 1998)) it seems likely that the LBF lava flows travelled in an easterly direction from the Faeroe Islands, a distance of at least 240 km. In doing so, they flowed from a subaerial environment into a substantial body of water at least 450 m deep (i.e. the Faeroe-Shetland Basin at that time). The presence of the subaerial lava flows overlying the hyaloclastites indicates that sea level fell and/or uplift occurred and that a terrestrial environment was established to the west, possibly all the way back to the Faeroe Islands.

The identification of the Faeroe-Shetland Escarpment as a hyaloclastite sequence (Ritchie *et al.* 1999) <50 km to the NW of Well 214/4-1 implies that sea level rose and/or subsidence occurred, resulting in the palaeoshoreline moving to the W/NW. Thus, the number of hyaloclastite deltas, which developed within the Faeroe-Shetland Basin, appears to have been under-estimated, and it seems likely that the sea was steadily encroaching to the W/NW (i.e. towards the Faeroe Islands) throughout the period of the volcanism (Fig. 9.1).

The LBF subaerial lavas of the Faeroe Islands were erupted at high effusion rates and travelled rapidly over large distances into a relatively dry environment under a warm and temperate climate (Parra *et al.* 1987; Lund 1989). The lavas were most likely erupted from fissures to the W of the Faeroe Islands (Rasmussen & Noe-Nygaard 1970b; Larsen *et al.* 1999), but point sources may have played a significant role in adding tephra to the developing land surface (cf. Swanson *et al.* 1975). A point source vent is identified at Stapin, Suðuroy and consists of basaltic agglomerate subsequently overlain by coals from the CBF.

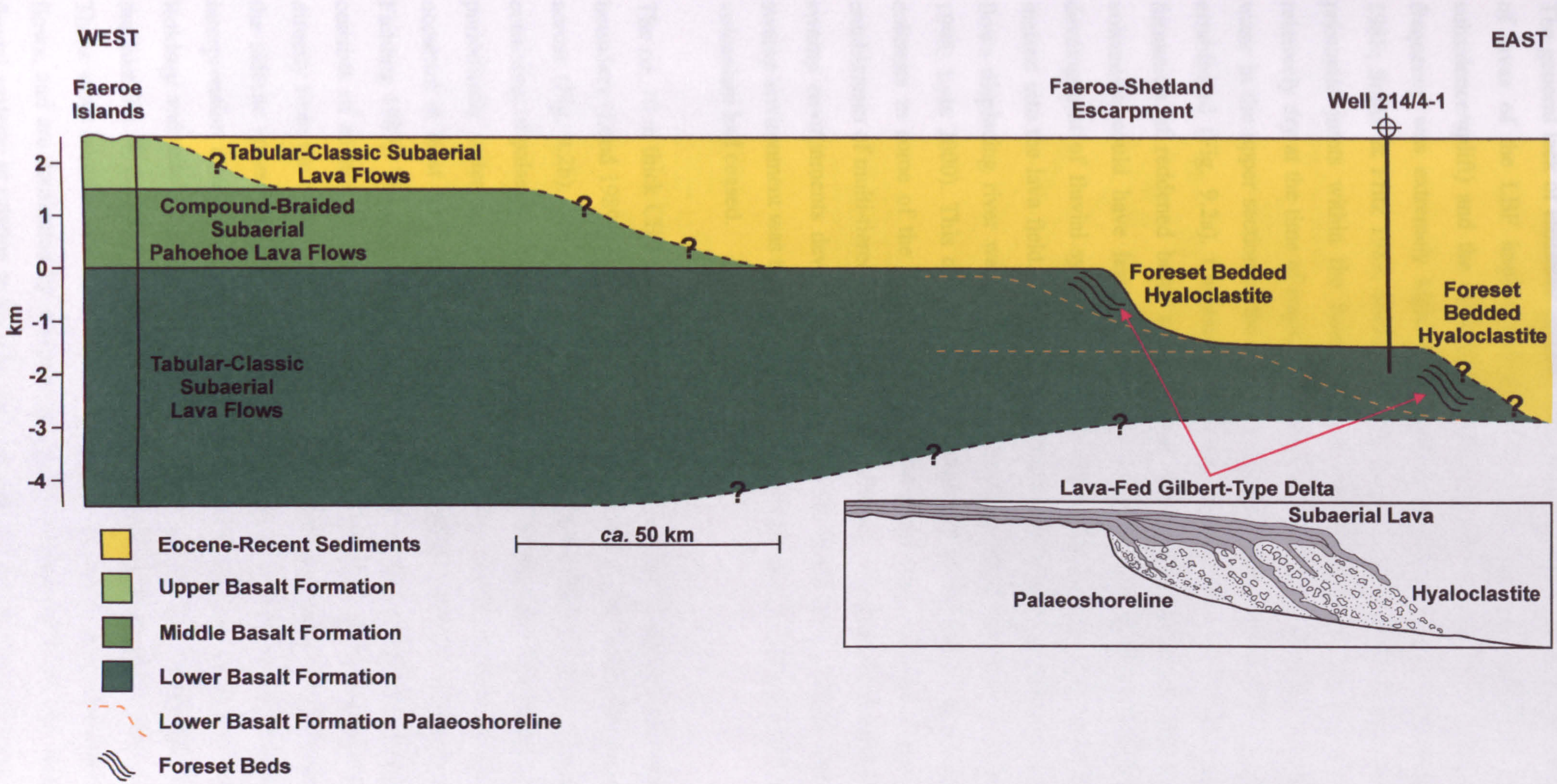

Fig. 9.1. Schematic correlation of the onshore and offshore Faeroe Plateau Lava Group (FPLG). The volcanic interval within Well 214/4-1 is geochemically correlated to the Lower Basalt Formation (LBF) of the Faeroe Islands and is represented by a hyaloclastite delta overlain by subaerial lava flows. These data imply that the Faeroe-Shetland Escarpment represents a second hyaloclastite delta within the LBF, which in turn suggests that basin subsidence was occurring during the FPLG volcanism, resulting in the sea encroaching towards the Faeroe Islands. The lava-fed Gilbert type delta is after Moore *et al.* (1973).

The general lack of erosional surfaces and sedimentary strata within the lowest *ca.* 800 m of lavas of the LBF implies that either the land mass was relatively stable (i.e. no subsidence/uplift) and the climate was relatively dry or, more likely, that the eruption frequency was extremely high, which prevented erosion and sedimentation (cf. Smith 1988; Smith & Fritz 1989; Smith 1991; Smith *et al.* 2002, and others). The presence of prismatic joints within the lavas supports the premise that the volcanic terrain was relatively dry at the time of emplacement (cf. Jerram 2002). However, volcanism began to wane in the upper section of the LBF and, during hiatuses, terrestrial environments were established (Fig. 9.2a). Chemical weathering of the basalt lava flows resulted in the formation of reddened boles no more than 2 m thick, suggesting that hiatuses in the volcanism could have lasted for periods of up to 140 kyrs (cf. Nahon 1991). The development of fluvial systems led to the erosion of the lava flows and channels were incised into the lava field. Some of the channels were subsequently dammed by later lava flows displacing river water and possibly forming ephemeral lakes (cf. Lyle & Preston 1998; Lyle 2000). This displaced surface water led to the formation of well-developed columns in some of the lava flows (e.g. Kúlugjógv Lava Flow) and curvi-columns in entablatures of multi-tiered flows (e.g. Hov, Suðuroy). A vegetated landscape emerged and swamp environments developed which led to the formation of minor coal seams. This swamp environment was the precursor to the Coal-bearing Formation (CBF) once the LBF volcanism had ceased.

The *ca.* 10 m thick CBF on Suðuroy was deposited at the Palaeocene-Eocene (*ca.* 57 Ma) boundary (Lund 1989; Jolley 1997) and is dominated by a lake environment at least 10 km across (Fig. 9.2b). The margin of the lake is characterised by the Ulingatangi Section, consisting of palaeosols formed under well-drained through to waterlogged conditions. The periodically waterlogged palaeosols (semi-gleysols) record water-level fluctuations that occurred at least four times, most likely representing seasonal variations (cf. Besly & Fielding 1989). The lake centre was located in the vicinity of the Rokhagi Section, which consists of an ironstone bed composed almost entirely of siderite spherules precipitated directly from the hypolimnion. This contrasts to the Ulingatangi clay ironstone bed where the siderite spherules were precipitated from pore fluids within the palaeosols. Such an interpretation is supported by the presence of two thick coal seams (*ca.* 1.7 m thick) at Rokhagi and only a thin discontinuous coal seam (<0.7 m) at Ulingatangi. To the west of the lake (i.e. W Suðuroy), fluviatile sandstones and conglomerates overlie the coal seams. These strata contain sub-rounded clasts of basalt, derived from the surrounding LBF lava flows, and are dominated by reworked ash grade volcanic material. The location of these fluvial systems in relation to the lake indicates that the streams were flowing from west to

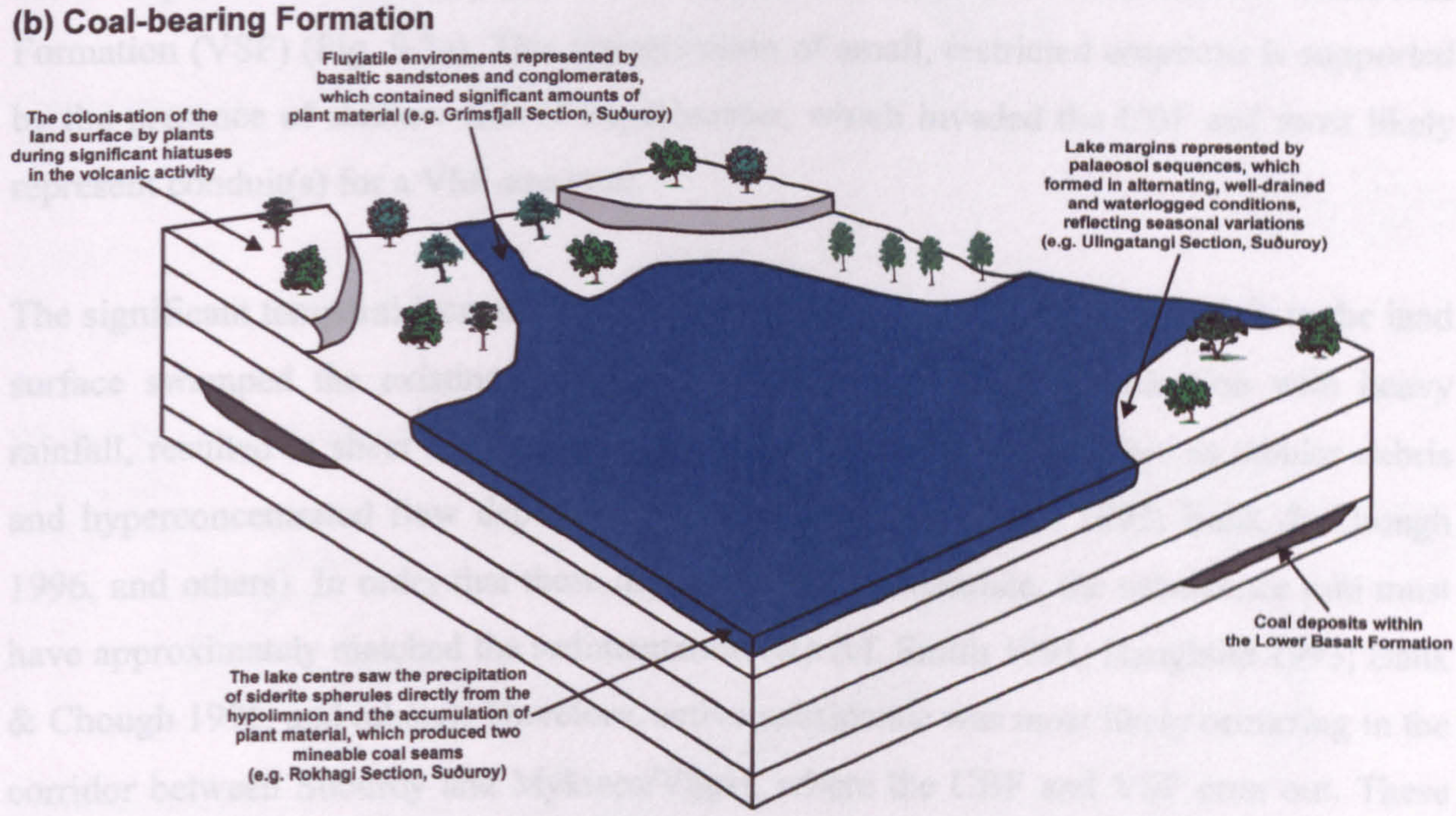

Fig. 9.2. Schematic palaeogeographical block diagrams for (a) the Lower Basalt Formation and (b) the Coal-bearing Formation. The length of each horizontal dimension in figure (a) is very approximately 1-2 km and in (b) is very approximately 4-5 km.

east and were also transporting plant material into the lacustrine environment. This model tentatively implies that there was high ground to the west of Suðuroy.

Volcanism on the Faeroe Islands recommenced penecontemporaneously with the initial stages of the opening of the NE Atlantic and is marked by the localised eruption of a >8 m thick sequence of olivine-phyric tuffs at the base of the Volcaniclastic Sandstone Formation (VSF) (Fig. 9.3a). This interpretation of small, restricted eruptions is supported by the presence of shallow sills at Reyðibarmur, which invaded the CBF and most likely represent conduit(s) for a VSF-age vent.

The significant temporal increase in the relative proportion of pyroclastic debris to the land surface swamped the existing fluvial system and, possibly in combination with heavy rainfall, resulted in sheet floods (lahar events) covering the land surface as tabular debris and hyperconcentrated flow deposits (cf. Smith 1991; Haughton 1993; Bahk & Chough 1996, and others). In order that these deposits could accumulate, the subsidence rate must have approximately matched the sedimentation rate (cf. Smith 1991; Haughton 1993; Bahk & Chough 1996, and others). Therefore, active subsidence was most likely occurring in the corridor between Suðuroy and Mykines/Vágar, where the CBF and VSF crop out. These mass flow deposits are interbedded with olivine-phyric tuff beds, supporting the premise that the deposits represent a syn-eruption facies (cf. Smith 1991).

The Middle Basalt (MBF) and the Upper Basalt (UBF) formations represent a syn-break-up succession, along with the Milne Land Formation of East Greenland (Larsen *et al.* 1999), which were emplaced during the earliest Ypresian (Waagstein 1988; Larsen *et al.* 1999; Ritchie *et al.* 1999). The MBF lava flows were subaerially erupted through low shield volcanoes that were locally situated around the Faeroe Islands (Fig. 9.3b). These shields are of the scutulum type and have diameters of *ca.* 15 km and heights no more than 100 m (Noe-Nygaard 1968). The MBF lava flows were erupted at lower effusion rates than the LBF and UBF, which resulted in a compound-braided facies architecture (cf. Walker 1970; Hon *et al.* 1994; Self *et al.* 1997; Self *et al.* 1998). The MBF is *ca.* 1.4 km thick and is composed of lava flows that are *ca.* 20 m thick, which in turn are made up of thinner flow units *ca.* 2 m thick. These flows were emplaced on slopes of <4° through an inflation (endogenous) process over many months to years (cf. Hon *et al.* 1994; Self *et al.* 1996) and were also transported through very efficient lava tube networks. The MBF is very similar to the Basaltic Plains Volcanism of the Snake River Plains, Idaho, identified by Greeley (1976; 1977; 1982). Hiatuses between eruptions are represented by fluvial system sandstones comprising reworked ash grade clasts and containing plant material, implying

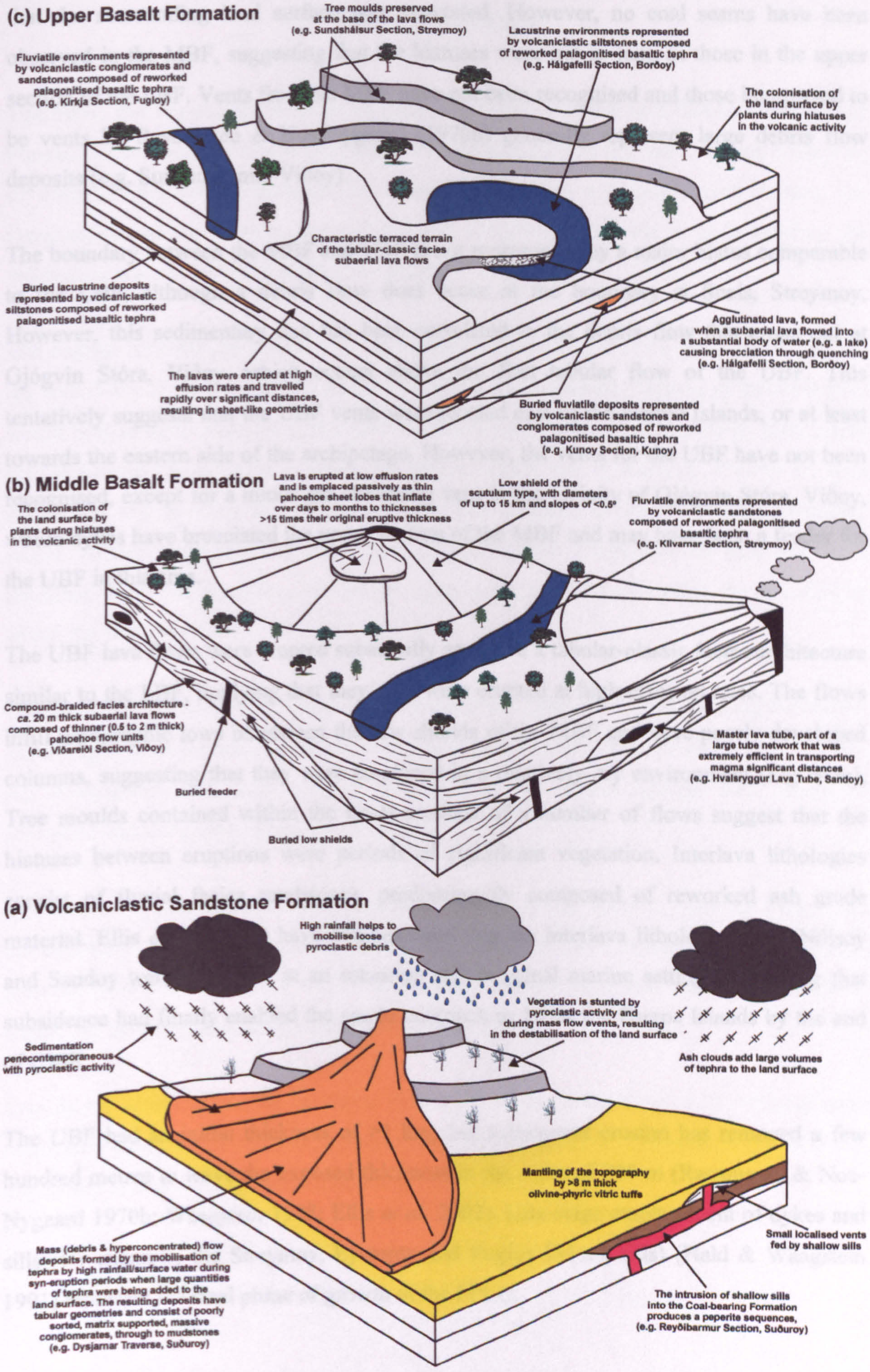

Fig. 9.3. Schematic palaeogeographical block diagrams for (a) the Volcaniclastic Sandstone Formation, (b) the Middle Basalt Formation and (c) the Upper Basalt Formation. The length of each horizontal dimension in figure (a) is very approximately 1-1.5 km, in (b) is very approximately 12-15 km and in (c) is very approximately 1-2 km. The Lava tubes in (b) have been exaggerated to highlight them.

that the surrounding land surface was vegetated. However, no coal seams have been observed in the MBF, suggesting that the hiatuses were not as long as those in the upper section of the LBF. Vents from the MBF have not been recognised and those interpreted to be vents by Rasmussen & Noe-Nygaard (1970b) generally represent large debris flow deposits (e.g. Sundsmunnin, Viðoy).

The boundary between the MBF and UBF is not represented by a major hiatus comparable to the CBF, although a debris flow does occur at the boundary at Sneis, Streymoy. However, this sedimentary unit has been correlated to the debris flow that crops out at Gjógvin Stóra, Viðoy, which occurs above the first tabular flow of the UBF. This tentatively suggests that the UBF vents were located east of the Faeroe Islands, or at least towards the eastern side of the archipelago. However, the vents for the UBF have not been recognised, except for a minor gas streaming vent in the vicinity of Gjógvin Stóra, Viðoy, where dykes have brecciated the upper section of the MBF and may have been a feeder for the UBF in this area.

The UBF lava flows were erupted subaerially and have a tabular-classic facies architecture similar to the LBF, implying that they, too, were erupted at high effusion rates. The flows infill topographic lows inbetween the low shields of the MBF and have poorly-developed columns, suggesting that they were emplaced in a relatively dry environment (Fig. 9.3c). Tree moulds contained within the basal sections of a number of flows suggest that the hiatuses between eruptions were periods of significant vegetation. Interlava lithologies consist of fluvial facies sandstones, predominantly composed of reworked ash grade material. Ellis *et al.* (2002) have demonstrated that the interlava lithologies from Nólsoy and Sandoy were deposited in an estuarine and marginal marine setting, suggesting that subsidence had finally enabled the sea to encroach as far as the Faeroe Islands by the end of C24R.

The UBF had an initial thickness of >1 km, but subsequent erosion has removed a few hundred metres to leave the exposed thickness in the order of 900 m (Rasmussen & Noe-Nygaard 1970b; Waagstein 1988; Ellis *et al.* 2002). Late-stage emplacement of dykes and sills (for example, the Streymoy, Eysturoy and Fugloy-Svínoy sills) (Hald & Waagstein 1991) represent the final phase of growth of the FPLG.

Future Work

The thesis has applied the concept of facies architecture to the lava flows of the Faeroe Plateau Lava Group and has demonstrated that the architecture is related, in part, to the rate of effusion and the environment of eruption. However, a detailed study linking the compositions of the lavas to the architectures observed would aid in understanding the volcanic processes involved in their formation.

The change between the Middle and Upper basalt formations is not a sharp transition and the lava flows of the two formations are interbedded and detailed mapping of this boundary would help to understand the evolution from one style of volcanism to another. It may also help determine the direction in which the lavas travelled and in doing so, identify the area where the vent systems should be located. Also, mapping of the MBF-UBF boundary would further constrain the mass flow (volcaniclastic conglomerate) that has been identified from two localities, *ca.* 34 km apart, and may help determine the direction in which the flow travelled.

The identification of siderite spherules from ironstone beds of the Coal-bearing Formation have helped in understanding the evolution of the lake environment in which they formed. An investigation into their isotopic compositions can further confine their modes of formation and their lateral (catena) variations.

The thesis has demonstrated that geochemically analysing igneous material from ditch cuttings from offshore wells can help to correlate facies across a region. Therefore, igneous material from past and future wells can be geochemically analysed, not only to correlate facies, but also help date associated interlava lithologies.

The facies architectures of the lava flows and their interactions with volcaniclastic lithologies observed on the Faeroe Islands can help constrain environments of eruption and deposition in other Continental Flood Basalt provinces.

References

ABRAHAMSEN, N., SCHOENHARTING, G. & HEINESEN, M. 1984. Palaeomagnetism of the Vestmanna core and magnetic age and evolution of the Faeroe Islands. *In:* BERTHELSEN, O., NOE-NYGAARD, A. & RASMUSSEN, J. (eds) *The Deep Drilling Project 1980-1981 in the Faeroe Islands*. Føroya Fróðskaparfelag, Tórshavn, 93-108.

ANDERSEN, M.S. 1988. Late Cretaceous and early Tertiary extension and volcanism around the Faeroe Islands. *In:* MORTON, A.C. & PARSON, L.M. (eds) *Early Tertiary Volcanism and the Opening of the NE Atlantic*. Geological Society, London. Special Publications, **39**, 115-122.

ANDERSON, S.W., STOFAN, E.R., SMREKAR, S.E., GUEST, J.E. & WOOD, B. 1999. Pulsed inflation of pahoehoe lava flows: implications for flood basalt emplacement. *Earth and Planetary Science Letters*, **168**, 7-18.

ATKINSON, A., GRIFFIN, T.J. & STEPHENSON, P.J. 1975. A major lava tube system from Undara Volcano, North Queensland. *Bulletin Volcanologique*, **39**, 266-293.

AUBELE, J.C., CRUMPLER, L.S. & ELSTON, W. 1988. Vesicle zonation and vertical structure of basalt flows. *Journal of Volcanology and Geothermal Research*, **35**, 349-374.

BAAS-BECKING, L.G.M., KAPLAN, I.R. & MOORE, D. 1960. Limits of the natural environment in terms of pH and oxidation-reduction potentials. *Journal of Geology*, **68**, 243-284.

BAHK, J.J. & CHOUGH, S.K. 1996. An interplay of syn- and intereruption depositional processes: the lower part of the Jangki Group (Miocene), SE Korea. *Sedimentology*, **43**, 421-438.

BAKER, J.C., KASSAN, J. & HAMILTON, P.J. 1995. Early diagenetic siderite as an indicator of depositional environment in the Triassic Rewan Group, southern Bowen Basin, eastern Australia. *Sedimentology*, **43**, 77-88.

BASALTIC VOLCANISM STUDY PROJECT. 1981. *Basaltic Volcanism on the Terrestrial Planets*. Pergamon Press, New York.

BELL, B.R., WILLIAMSON, I.T., HEAD, F.E. & JOLLEY, D.W. 1996. On the origin of a reddened interflow bed within the Palaeocene lava field of north Skye. *Scottish Journal of Geology*, **32**, 117-126.

BERNER, R.A. 1981. New geochemical classification of sedimentary environments. *Journal of Sedimentary Petrology*, **51**, 359-365.

BERNER, R.A. & COCHRAN, M.F. 1998. Plant-induced weathering of Hawaiian basalts. *Journal of Sedimentary Research*, **68**, 723-726.

BESLY, B.M. & COLLINSON, J.D. 1991. Volcanic and tectonic controls of lacustrine and alluvial sedimentation in the Stephanian coal-bearing sequence of the Malpás-Sort Basin, Catalonian Pyrenees. *Sedimentology*, **38**, 3-26.

BESLY, B.M. & FIELDING, C.R. 1989. Palaeosols in Westphalian coal-bearing and red-bed sequences, central and northern England. *Palaeogeography, Palaeoclimatology, Palaeoecology*, **70**, 303-330.

BOLLINGBERG, H., BROOKS, C.K. & NOE-NYGAARD, A. 1975. Trace element variations in Faeroese basalts and their possible relationships to ocean floor spreading history. *Bulletin of the Geological Society of Denmark*, **24**, 55-60.

BOTT, M.H.P., SUNDERLAND, J., SMITH, P.J., CASTEN, U. & SAXOV, S. 1974. Evidence for continental crust beneath the Faeroe Islands. *Nature*, **248**, 202-204.

BOTT, M.H.P. & WATTS, A.B. 1971. Deep structure of the continental margin adjacent to the British Isles. *In:* DELANY, F.M. (ed.) *ICSU/SCOR Symposium on East Atlantic Continental Margins 1970*. Institute of Geological Sciences Report, **70/14**, 89-109.

BROOKS, C.K. 1976. The Fe_2O_3/FeO ratio of basalt analyses: an appeal for a standardized procedure. *Bulletin of the Geological Society of Denmark*, **25**, 117-120.

BROOKS, E.R., WOOD, M.M. & GARBUTT, P.L. 1982. Origin and metamorphism of peperite and associated rocks in the Devonian Elwell Formation, northern Sierra Nevada, California. *Geological Society of America Bulletin*, **93**, 1208-1231.

BROOKS, J. & GLENNIE, K.W. (eds). 1987. *Petroleum Geology of North West Europe: Proceedings of the 3rd Conference*. Graham & Trotman, London, **2**.

BUSBY-SPERA, C.J. & WHITE, J.D.L. 1987. Variation in peperite textures associated with differing host-sediment properties. *Bulletin of Volcanology*, **49**, 765-776.

CALDERONE, G.M., GRONVOLD, K. & OSKARSSON, N. 1990. The welded air-fall tuff layer at Krafla, northern Iceland: a composite eruption triggered by injection of basaltic magma. *Journal of Volcanology and Geothermal Research*, **44**, 303-314.

CALVARI, S. & PINKERTON, H. 1999. Lava tube morphology on Etna and evidence for lava flow emplacement mechanisms. *Journal of Volcanology and Geothermal Research*, **90**, 263-280.

CALVARI, S., TANNER, L.H. & GROPPELLI, G. 1998. Debris-avalanche deposits of the Milo Lahar sequence and the opening of the Velle del Bove on Etna volcano (Italy). *Journal of Volcanology and Geothermal Research*, **87**, 193-209.

CAMPBELL, L.M., CONAGHAN, P.J. & FLOOD, R.H. 2001. Flow-field and palaeogeographic reconstruction of volcanic activity in the Permian Gerringong Volcanic Complex, southern Sydney Basin, Australia. *Australian Journal of Earth Sciences*, **48**, 357-375.

CARR, P.F. & JONES, B.G. 2001. The influence of palaeoenvironment and lava flux on the emplacement of submarine, near-shore Late Permian basalt lavas, Sydney Basin (Australia). *Journal of Volcanology and Geothermal Research*, **112**, 247-266.

CAS, R.A.F., EDGAR, C., ALLEN, R.L., BULL, S., CLIFFORD, B.A., GIORDANO, G. & WRIGHT, J.V. 2001. Influence of magmatism and tectonics on sedimentation in an extensional lake basin: the Upper Devonian Bunga Beds, Boyd Volcanic Complex, south-eastern Australia. *In:* WHITE, J.D.L. & RIGGS, N.R. (eds) *Volcaniclastic*

Sedimentation in Lacustrine Settings. Special Publication of the International Association of Sedimentologists, **30**, 83-108.

CAS, R.A.F. & WRIGHT, J.V. 1987. *Volcanic Successions: Modern and Ancient*. Allen & Unwin, London.

CASHMAN, K., PINKERTON, H. & STEPHENSON, J. 1998. Introduction to special section: long lava flows. *Journal of Geophysical Research*, **103**(B11), 27281-27289.

CASHMAN, K.V. & KAUAHIKAUA, J.P. 1997. Reevaluation of vesicle distributions in basaltic lava flows. *Geology*, **25**, 419-422.

CASHMAN, K.V., THORNBER, C. & KAUAHIKAUA, J.P. 1999. Cooling and crystallization of lava in open channels, and the transition of pahoehoe lava to 'a'a. *Bulletin of Volcanology*, **61**, 306-323.

CHAMBERS, L.M. & FITTON, J.G. 2000. Geochemical transitions in the ancestral Iceland plume: evidence from the Isle of Mull Tertiary volcano, Scotland. *Journal of the Geological Society, London*, **157**, 261-263.

CHANG, L.L.Y. 1996. Siderite. *In:* CHANG, L.L.Y., HOWIE, R.A. & ZUSSMAN, J. (eds) *Non-Silicates: Sulphates, Carbonates, Phosphates, Halides: Rock-Forming Minerals*. 2nd Edition. The Geological Society, London, **5B**, 163-177.

CHOUBEY, V.D. 1973. Long-distance correlation of Deccan basalt flows, central India. *Geological Society of America Bulletin*, **84**, 2785-2790.

CLEMMENSEN, L.B. 1988. Aeolian morphology preserved by lava cover, the Precambrian Mussartût Member, Eriksford Formation, South Greenland. *Bulletin of the Geological Society of Denmark*, **37**, 105-116.

COLE, R.B. & RIDGWAY, K.D. 1993. The influence of volcanism on fluvial deposition systems in a Cenozoic strike-slip basin, Denali Fault System, Yukon Territory, Canada. *Journal of Sedimentary Petrology*, **63**, 152-166.

COLLINSON, J.D. 1996. Alluvial Sediments. *In:* READING, H.G. (ed.) *Sedimentary Environments: Processes, Facies and Stratigraphy*. 3rd Edition. Blackwell Science, Oxford, 37-82.

COUSSOT, P. & MEUNIER, M. 1996. Recognition, classification and mechanical description of debris flows. *Earth-Science Reviews*, **40**, 209-227.

COX, K.G., BELL, J.D. & PANKHURST, R.J. 1979. *The Interpretation of Igneous Rocks*. Allen & Unwin, London.

CROWN, D.A. & BALOGA, S.M. 1999. Pahoehoe toe dimensions, morphology, and branching relationships at Mauna Ulu, Kilauea Volcano, Hawai'i. *Bulletin of Volcanology*, **61**, 288-305.

DEAN, K., MCLACHLAN, K. & CHAMBERS, A. 1999. Rifting and the development of the Faeroe-Shetland Basin. *In:* FLEET, A.J. & BOLDY, S.A.R. (eds) *Petroleum Geology of Northwest Europe: Proceedings of the 5th Conference*. Geological Society, London, **1**, 533-544.

DEANS, T. 1934. The spherulitic ironstones of West Yorkshire. *Geological Magazine*, **71**, 49-65.

DEGRAFF, J.M. & AYDIN, A. 1987. Surface morphology of columnar joints and its significance to mechanics and direction of joint growth. *Geological Society of America Bulletin*, **99**, 605-617.

DONAIRE, T., SÁEZ, R. & PASCUAL, E. 2002. Rhyolitic globular peperites from the Aznalcóllar mining district (Iberian Pyrite Belt, Spain): physical and chemical controls. *Journal of Volcanology and Geothermal Research*, **114**, 119-128.

DOYLE, M.G. 2000. Clast shape and textural associations in peperite as a guide to hydromagmatic interactions: Upper Permian basaltic and basaltic andesite examples from Kiama, Australia. *Australian Journal of Earth Sciences*, **47**, 167-177.

DRAGONI, M., PIOMBO, A. & TALLARICO, A. 1995. A model for the formation of the lava tubes by roofing over a channel. *Journal of Geophysical Research*, **100**(B5), 8435-8447.

DUCHAUFOUR, P. 1998 (1997). *Handbook of Pedology: Soils, Vegetation, Environment. Trans:* SARMA, V.A.K. (ed.). A.A. Balkema, Rotterdam.

DURAISWAMI, R.A., BONDRE, N.R., DOLE, G., PHADNIS, V.M. & KALE, V.S. 2001. Tumuli and associated features from the western Deccan Volcanic Province, India. *Bulletin of Volcanology*, **63**, 435-442.

EASTON, R.M. & JOHNS, G.W. 1986. Volcanology and mineral exploration: the application of physical volcanology and facies studies. *Ontario Geological Survey Miscellaneous Paper*, **129**, 2-40.

ELLIS, D., BELL, B.R., JOLLEY, D.W. & O'CALLAGHAN, M. 2002. The stratigraphy, environment of eruption and age of the Faeroes Lava Group, NE Atlantic Ocean. *In:* JOLLEY, D.W. & BELL, B.R. (eds) *The North Atlantic Igneous Province: Stratigraphy, Tectonic, Volcanic and Magmatic Processes*. Geological Society, London. Special Publications, **197**, 253-269.

ERNST, R.E. & BUCHAN, K.L. 2001. Large mafic magmatic events through time and links to mantle-plume heads. *In:* ERNST, R.E. & BUCHAN, K.L. (eds) *Mantle Plumes: Their Identification Through Time*. Geological Society of America, Special Paper, **352**, 483-575.

FERNÁNDEZ-DÍAZ, L., PUTNIS, A., PRIETO, M. & PUTNIS, C.V. 1996. The role of magnesium in the crystallization of calcite and aragonite in a porous medium. *Journal of Sedimentary Research*, **66**, 482-491.

FINK, J.H. & FLETCHER, R.C. 1978. Ropy pahoehoe: surface folding of a viscous fluid. *Journal of Volcanology and Geothermal Research*, **4**, 151-170.

FISHER, R.V. 1961. Proposed classification of volcaniclastic sediments and rocks. *Geological Society of America Bulletin*, **72**, 1409-1414.

FISHER, R.V. 1966. Rocks composed of volcanic fragments and their classification. *Earth-Science Reviews*, **1**, 287-298.

FISHER, R.V. 1971. Features of coarse-grained, high-concentration fluids and their deposits. *Journal of Sedimentary Petrology*, **41**, 916-927.

FISHER, R.V. & SCHMINCKE, H.-U. 1984. *Pyroclastic Rocks*. Springer-Verlag, Berlin.

FISHER, R.V. & SMITH, G.A. 1991. Volcanism, tectonics and sedimentation. *In:* FISHER, R.V. & SMITH, G.A. (eds) *Sedimentation in Volcanic Settings*. SEPM (Society for Sedimentary Geology) Special Publication, Tulsa, Oklahoma, **45**, 1-5.

FITCH, F.J., HEARD, G.L. & MILLER, J.A. 1988. Basaltic magmatism of late Cretaceous and Palaeogene age recorded in wells NNE of the Shetlands. *In:* MORTON, A.C. & PARSON, L.M. (eds) *Early Tertiary Volcanism and the Opening of the NE Atlantic*. Geological Society, London. Special Publications, **39**, 253-262.

FLEET, A.J. & BOLDY, S.A.R. (eds). 1999. *Petroleum Geology of Northwest Europe: Proceedings of the 5th Conference*. Geological Society, London, **1**.

FREUNDT, A. & SCHMINCKE, H.-U. 1995. Eruption and emplacement of a basaltic welded ignimbrite during caldera formation on Grand Canaria. *Bulletin of Volcanology*, **56**, 640-659.

FURNES, H., FRIDLEIFSSON, I.B. & ATKINS, F.B. 1980. Subglacial volcanics - on the formation of acid hyaloclastites. *Journal of Volcanology and Geothermal Research*, **8**, 95-110.

GARIÉPY, C., LUDDEN, J. & BROOKS, C. 1983. Isotopic and trace element constraints on the genesis of the Faeroe lava pile. *Earth and Planetary Science Letters*, **63**, 257-272.

GIBB, F.G.F. & KANARIS-SOTIRIOU, R. 1988. The geochemistry and origin of the Faeroe-Shetland sill complex. *In:* MORTON, A.C. & PARSON, L.M. (eds) *Early Tertiary Volcanism and the Opening of the NE Atlantic*. Geological Society, London. Special Publications, **39**, 241-252.

GILLESPIE, M.R. & STYLES, M.T. 1999. *Classification of Igneous Rocks. BGS Rock Classification Scheme Research Report RR 99-06*. 2nd Edition. British Geological Survey, Nottingham, **1**.

GREELEY, R. 1976. Modes of emplacement of basaltic terrains and an analysis of mare volcanism in the Orientale Basin. *Geochimica et Cosmochimica Acta, Supplement*, **7**, 2747-2759.

GREELEY, R. 1977. Basaltic 'plains' volcanism. *In:* GREELEY, R. & KING, J.S. (eds) *Volcanism of the Eastern Snake River Plain, Idaho: A Comparative Planetary Geology Guidebook*. NASA, **CR-154621**, 23-44.

GREELEY, R. 1982. The Snake River Plain, Idaho: Representative of a new category of volcanism. *Journal of Geophysical Research*, **87**(B4), 2705-2712.

GREELEY, R. 1987. The role of lava tubes in Hawaiian volcanoes. *In:* DECKER, R.W., WRIGHT, T.L. & STAUFFER, P.H. (eds) *Volcanism in Hawaii*. United States Geological Survey Professional Paper, **1350**, 1589-1602.

GRIGOR'EV, D.P. 1965 (1961). *Ontogeny of Minerals*. *Trans:* BRENNER, Y. (ed.). IPST Ltd., Jerusalem, Israel.

HALD, N. & WAAGSTEIN, R. 1983. Silicic basalts from the Faeroe Islands: evidence of crustal contamination. *In:* BOTT, M.H.P., SAXOV, S., TALWANI, M. & THIEDE, J. (eds) *Structure and Development of the Greenland-Scotland Ridge*. Plenum Press, New York, 343-349.

HALD, N. & WAAGSTEIN, R. 1984. Lithology and chemistry of a 2-km sequence of Lower Tertiary tholeiitic lavas drilled on Suðuroy, Faeroe Islands (Lopra-1). *In:* BERTHELSEN, O., NOE-NYGAARD, A. & RASMUSSEN, J. (eds) *The Deep Drilling Project 1980-1981 in the Faeroe Islands*. Føroya Fróðskaparfelag, Tórshavn, 15-38.

HALD, N. & WAAGSTEIN, R. 1991. The dykes and sills of the early Tertiary Faeroe Island basalt plateau. *Transactions of the Royal Society of Edinburgh: Earth Sciences*, **82**, 373-388.

HANSON, R.E. & HARGROVE, U.S. 1999. Processes of magma/wet sediment interaction in a large-scale Jurassic andesitic peperite complex, northern Sierra Nevada, California. *Bulletin of Volcanology*, **60**, 610-626.

HANSON, R.E. & WILSON, T.J. 1993. Large-scale rhyolitic peperites (Jurassic, southern Chile). *Journal of Volcanology and Geothermal Research*, **54**, 247-264.

HAUGHTON, P.D.W. 1993. Simultaneous dispersal of volcaniclastic and non-volcanic sediment in fluvial basins: examples from the Lower Old Red Sandstone, east-central Scotland. *In:* MARZO, M. & PUIGDEFÁBREGAS, C. (eds) *Alluvial Sedimentation*. Special Publication of the International Association of Sedimentologists, **17**, 451-471.

HAY, R.L. & IIJIMA, A. 1968. Nature and origin of palagonite tuffs of the Honolulu group on Oahu, Hawaii. *In:* COATS, R.R., HAY, R.L. & ANDERSON, C.A. (eds) *Studies in Volcanology (Howell Williams Volume)*. Geological Society of America Memoir, **116**, 331-376.

HEALEY, J. 1963. Welded pyroclastic rock at Tongariro. *New Zealand Journal of Geology and Geophysics*, **6**, 712-714.

HINZ, K., ELDHOLM, O., BLOCK, M. & SKOGSEID, J. 1993. Evolution of North Atlantic volcanic continental margins. *In:* PARKER, J.R. (ed.) *Petroleum Geology of Northwest Europe: Proceedings of the 4th Conference*. Geological Society, London, **2**, 901-913.

HITCHEN, K. & RITCHIE, J.D. 1987. Geological review of the West of Shetland area. *In:* BROOKS, J. & GLENNIE, K.W. (eds) *Petroleum Geology of North West Europe: Proceedings of the 3rd Conference*. Graham & Trotman, London, **2**, 737-749.

HITCHEN, K. & RITCHIE, J.D. 1993. New K-Ar ages, and a provisional chronology, for the offshore part of the British Tertiary Igneous Province. *Scottish Journal of Geology*, **29**, 73-85.

HOLM, P.M., HALD, N. & WAAGSTEIN, R. 2001. Geochemical and Pb-Sr-Nd isotopic evidence for separate hot depleted and Iceland plume mantle sources for the Paleogene basalts of the Faroe Islands. *Chemical Geology*, **178**, 95-125.

HON, K., GANSECKI, C. & KAUAHIKAUA, J. 2003. The transition from 'a'ä to pähoehoe crust on flows emplaced during the Pu'u 'Ö'ö-Küpaianaha eruption. *In:* HELIKER, C.C., SWANSON, D.A. & TAKAHASHI, T.J. (eds) *The Pu'u 'Ö'ö-Küpaianaha Eruption of Kilauea Volcano, Hawai'i: The First 20 Years*. United States Geological Survey Professional Paper, **1676**, 89-103.

HON, K., KAUAHIKAUA, J., DENLINGER, R. & MACKAY, K. 1994. Emplacement and inflation of pahoehoe sheet flows: observations and measurements of active lava flows on Kilauea Volcano, Hawaii. *Geological Society of America Bulletin*, **106**, 351-370.

HOUNSLOW, M.W. 2001. The crystallographic fabric and texture of siderite in concretions: implications for siderite nucleation and growth processes. *Sedimentology*, **48**, 553-557.

JAMES, A.V.G. 1920. Factors producing columnar structure in lavas and its occurrence near Melbourne, Australia. *Journal of Geology*, **28**, 458-469.

JANDA, R.D., SCOTT, K.M., NOLAN, K.M. & MARTINSON, H.A. 1981. Lahar movement, effects, and deposits. *In:* LIPMAN, P.W. & MULLINEAUX, D.R. (eds) *The 1980 Eruptions of Mount St. Helens, Washington*. United States Geological Survey Professional Paper, **1250**, 461-478.

JENSEN, A. 1978. Compositional variations of the pyroxenes from three flows of the Faeroe Islands basalts. *Bulletin of the Geological Society of Denmark*, **27**(Special Issue), 63-78.

JENSEN, A. 1979. Mineralogical and geochemical variations across three basaltic lava flows from the Faeroe Islands. *Bulletin of the Geological Society of Denmark*, **28**, 95-114.

JENSEN, A. 1982. The distribution of Cu across three basaltic lava flows from the Faeroe Islands. *Bulletin of the Geological Society of Denmark*, **31**, 1-10.

JENSEN, A. 1985. Cupriferous pseudobrookite in a Tertiary basalt from the Faeroe Islands. *Bulletin of the Geological Society of Denmark*, **34**, 87-95.

JERRAM, D.A. 2002. The volcanology and facies architecture of flood basalts. *In:* MENZIES, M.A., KLEMPERER, S.L., EBINGER, C.J. & BAKER, J. (eds) *Volcanic Rifted Margins*. Geological Society of America, Special Paper, **362**, 119-132.

JERRAM, D.A., MOUNTNEY, N.P., HOLZFÖRSTER, F. & STOLLHOFEN, H. 1999. Internal stratigraphic relationships in the Etendeka Group in the Huab Basin, NW Namibia: Understanding the onset of flood volcanism. *Journal of Geodynamics*, **28**, 393-418.

JERRAM, D.A., MOUNTNEY, N.P., HOWELL, J.A., LONG, D. & STOLLHOFEN, H. 2000. Death of a sand sea: an active aeolian erg systematically buried by the Etendeka flood basalts of NW Namibia. *Journal of the Geological Society, London*, **157**, 513-516.

JERRAM, D.A. & STOLLHOFEN, H. 2002. Lava/sediment interaction in desert settings; are all peperite-like textures the result of magma-water interaction? *Journal of Volcanology and Geothermal Research*, **114**, 231-249.

JOLLEY, D.W. 1997. Palaeosurface palynofloras of the Skye lava field and the age of the British Tertiary volcanic province. *In:* WIDDOWSON, M. (ed.) *Palaeosurfaces: Recognition, Reconstruction and Palaeoenvironmental Interpretation*. Geological Society, London. Special Publications, **120**, 67-94.

JOLLEY, D.W. & BELL, B.R. 2002a. The evolution of the North Atlantic Igneous Province and the opening of the NE Atlantic rift. *In:* JOLLEY, D.W. & BELL, B.R. (eds) *The North Atlantic Igneous Province: Stratigraphy, Tectonic, Volcanic and Magmatic Processes*. Geological Society, London. Special Publications, **197**, 1-13.

JOLLEY, D.W. & BELL, B.R. 2002b. Genesis and age of the Erlend volcano, NE Atlantic Margin. *In:* JOLLEY, D.W. & BELL, B.R. (eds) *The North Atlantic Igneous Province: Stratigraphy, Tectonic, Volcanic and Magmatic Processes*. Geological Society, London. Special Publications, **197**, 95-109.

JONES, J.G. 1968. Pillow lava and pahoehoe. *Journal of Geology*, **76**, 485-488.

JONES, J.G. & NELSON, P.H.H. 1970. The flow of basalt lava from air into water — its structural expression and stratigraphic significance. *Geological Magazine*, **107**, 13-19.

KANARIS-SOTIRIOU, R., MORTON, A.C. & TAYLOR, P.N. 1993. Palaeogene peraluminous magmatism, crustal melting and continental break-up: the Erlend complex, Faeroe-Shetland Basin, NE Atlantic. *Journal of the Geological Society, London*, **150**, 903-914.

KANO, K., TAKEUCHI, K., YAMAMOTO, T. & HOSHIZUMI, H. 1991. Subaqueous rhyolite block lavas in the Miocene Ushikiri Formation, Shimane Peninsula, SW Japan. *Journal of Volcanology and Geothermal Research*, **46**, 241-253.

KANTOROWICZ, J.D. 1990. Lateral and vertical variations in pedogenesis and other early diagenetic phenomena, Middle Jurassic Ravenscar Group, Yorkshire. *Proceedings of the Yorkshire Geological Society*, **48**, 61-74.

KATAOKA, K. & NAKAJO, T. 2002. Volcaniclastic resedimentation in distal fluvial basins induced by large-volume explosive volcanism: the Ebisutoge-Fukuda tephra, Plio-Pleistocene boundary, central Japan. *Sedimentology*, **49**, 319-334.

KAUAHIKAUA, J., CASHMAN, K.V., MATTOX, T.N., HELIKER, C.C., HON, K.A., MANGAN, M.T. & THORNBER, C.R. 1998. Observations on basaltic lava streams in tubes from Kilauea Volcano, island of Hawai'i. *Journal of Geophysical Research*, **103**(B11), 27303-27323.

KENT, R.W., THOMSON, B.A., SKELHORN, R.R., KERR, A.C., NORRY, M.J. & WALSH, J.N. 1998. Emplacement of Hebridean Tertiary flood basalts: evidence from an inflated pahoehoe lava flow on Mull, Scotland. *Journal of the Geological Society, London*, **155**, 599-607.

KERR, A.C. 1999. The geochemical stratigraphy, field relations and temporal variation of the Mull-Morvern Tertiary lava succession, NW Scotland. *Transactions of the Royal Society of Edinburgh: Earth Sciences*, **86**, 37-47.

KESSLER, L.G. & BÉDARD, J.H. 2000. Epiclastic volcanic debrites-evidence of flow transformations between avalanche and debris flow processes, Middle Ordovician, Baie Verte Peninsula, Newfoundland, Canada. *Precambrian Research*, **101**, 135-161.

KESZTHELYI, L. 1995. A preliminary thermal budget for lava tubes on the Earth and planets. *Journal of Geophysical Research*, **100**(B10), 20411-20420.

KESZTHELYI, L. & SELF, S. 1998. Some physical requirements for the emplacement of long basaltic lava flows. *Journal of Geophysical Research*, **103**(B11), 27447-27464.

KIØRBOE, L. & PETERSEN, S.A. 1995. Seismic investigation of the Faeroe basalts and their substratum. *In:* SCRUTTON, R.A., STOKER, M.S., SHIMMIELD, G.B. & TUDHOPE, A.W. (eds) *The Tectonics, Sedimentation and Palaeoceanography of the North Atlantic Region*. Geological Society, London. Special Publications, **90**, 111-122.

KNOX, R.W.O'B., HOLLOWAY, S., KIRBY, G.A. & BAILEY, H.E. 1997. *Stratigraphic Nomenclature of the UK North West Margin. 2. Early Paleogene Lithostratigraphy and Sequence Stratigraphy*. British Geological Survey, Nottingham.

KOKELAAR, B.P. 1982. Fluidization of wet sediments during the emplacement and cooling of various igneous bodies. *Journal of the Geological Society, London*, **139**, 21-33.

KOKELAAR, B.P. 1986. Magma-water interactions in subaqueous and emergent basaltic volcanism. *Bulletin of Volcanology*, **48**, 275-289.

KOUL, S.L. & CHADDERTON, L.T. 1980. Fission track dating of zeolites of Faeroe Islands. *Mineralogical Journal*, **10**, 192-195.

KOUL, S.L., CHADDERTON, L.T. & BROOKS, C.K. 1983. East Greenland and the Faeroe Islands: a fission track study. *Matematisk-Fysiske Meddelelser Kongelige Danske Videnskabernes Selskab*, **40**(13), 1-37.

KRAUSKOPF, K.B. 1979. *Introduction to Geochemistry*. McGraw-Hill, New York.

LANDUYDT, C.J. 1990. Micromorphology of iron minerals from bog ores of the Belgian Campine area. *In:* DOUGLAS, L.A. (ed.) *Soil Micromorphology: A Basic and Applied Science, Developments in Soil Science*. Elsevier, Amsterdam, **19**, 289-294.

LARSEN, L.M., WAAGSTEIN, R., PEDERSEN, A.K. & STOREY, M. 1999. Trans-Atlantic correlation of the Palaeogene volcanic successions in the Faeroe Islands and East Greenland. *Journal of the Geological Society, London*, **156**, 1081-1095.

LAVIGNE, F., THOURET, J.C., VOIGHT, B., SUWA, H. & SUMARYONO, A. 2000. Lahars at Merapi volcano, Central Java: an overview. *Journal of Volcanology and Geothermal Research*, **100**, 423-456.

LE BAS, M.J., LE MAITRE, R.W., STRECKEISEN, A. & ZANETTIN, B. 1986. A chemical classification of volcanic rocks based on the total alkali silica diagram. *Journal of Petrology*, **27**, 745-750.

LECKIE, D., FOX, C. & TARNOCAI, C. 1989. Multiple paleosols of the late Albian Boulder Creek Formation, British Columbia, Canada. *Sedimentology*, **36**, 307-323.

LEVELL, B. & THOMPSON, M. 1999. Atlantic margin: Faeroe-Shetland. Introduction and review. *In:* FLEET, A.J. & BOLDY, S.A.R. (eds) *Petroleum Geology of Northwest Europe: Proceedings of the 5th Conference*. Geological Society, London, **1**, 531-532.

LIPMAN, P.W. & BANKS, N.G. 1987. Aa flow dynamics, Mauna Loa, 1984. *In:* DECKER, R.W., WRIGHT, T.L. & STAUFFER, P.H. (eds) *Volcanism in Hawaii*. United States Geological Survey Professional Paper, **1350**, 1527-1567.

LIRER, L., VINCI, A., ALBERICO, I., GIFUNI, T., BELLUCCI, F., PETROSINO, P. & TINTERRI, R. 2001. Occurrence of inter-eruption debris flow and hyperconcentrated flood-flow deposits on Vesuvio volcano, Italy. *Sedimentary Geology*, **139**, 151-167.

LONG, P.E. & WOOD, B.J. 1986. Structures, textures and cooling histories of Columbia River basalt flows. *Geological Society of America Bulletin*, **97**, 1144-1155.

LØVLIE, R. 1975. The oxidation state of some Tertiary rocks from the Faeroe Islands and its implication for palaeomagnetism. *Geophysical Journal of the Royal Astronomical Society*, **40**, 55-65.

LØVLIE, R. 1976. Post-baking alteration and partial remagnetization in five baked tuff layers from the Faeroe Islands. *Geophysical Journal of the Royal Astronomical Society*, **45**, 219-229.

LØVLIE, R. & KVINGEDAL, M. 1975. A palaeomagnetic discordance between a lava sequence and an associated interbasaltic horizon from the Faeroe Islands. *Geophysical Journal of the Royal Astronomical Society*, **40**, 45-54.

LOWE, D.R., WILLIAMS, S.N., LEIGH, H., CONNOR, C.B., GEMMELL, J.B. & STOIBER, R.E. 1986. Lahars initiated by the 13 November 1985 eruption of Nevado del Ruiz, Colombia. *Nature*, **324**, 51-53.

LUDVIGSON, G.A., GONZÁLEZ, L.A., METZGER, R.A., WITZKE, B.J., BRENNER, R.L., MURILLO, A.P. & WHITE, T.S. 1998. Meteoric sphaerosiderite lines and their use for paleohydrology and paleoclimatology. *Geology*, **26**, 1039-1042.

LUMSDEN, G.I. 1967. Intrusive coal at Douglas in Scotland. *Scottish Journal of Geology*, **3**, 235-241.

LUND, J. 1983. Biostratigraphy of interbasaltic coals from the Faeroe Islands. *In:* BOTT, M.H.P., SAXOV, S., TALWANI, M. & THIEDE, J. (eds) *Structure and Development of the Greenland-Scotland Ridge*. Plenum Press, New York, 417-423.

LUND, J. 1989. A late Paleocene non-marine microflora from the interbasaltic coals of the Faeroe Islands, North Atlantic. *Bulletin of the Geological Society of Denmark*, **37**, 181-203.

LYLE, P. 2000. The eruption environment of multi-tiered columnar basalt lava flows. *Journal of the Geological Society, London*, **157**, 715-722.

LYLE, P. & PRESTON, J. 1998. The influence of eruptive conditions on joint development in the Causeway Tholeiite Member of the Tertiary Antrim Lava Group, Northern Ireland. *Irish Journal of Earth Sciences*, **16**, 19-32.

MACDONALD, G.A. 1967. Forms and structures of extrusive basaltic rocks. *In:* HESS, H.H. & POLDERVAART, A. (eds) *The Poldervaart Treatise on Rocks of Basaltic Composition.* Interscience, New York, **1**, 1-61.

MACDONALD, G.A. 1972. *Volcanoes*. Prentice-Hall, Inc., Englewood Cliffs, New Jersey.

MACK, G.H., JAMES, W.C. & MONGER, H.C. 1993. Classification of paleosols. *Geological Society of America Bulletin*, **105**, 129-136.

MATHISEN, M.E. & MCPHERSON, J.G. 1991. Volcaniclastic deposits: implications for hydrocarbon exploration. *In:* FISHER, R.V. & SMITH, G.A. (eds) *Sedimentation in Volcanic Settings*. SEPM (Society for Sedimentary Geology) Special Publication, Tulsa, Oklahoma, **45**.

MCCLINTOCK, M.K. & WHITE, J.D.L. 2002. Granulation of weak rock as a precursor to peperite formation: coal peperite, Coombs Hills, Antarctica. *Journal of Volcanology and Geothermal Research*, **114**, 205-217.

MCPHIE, J. 1993. The Tennant Creek Porphyry revisited: A synsedimentary sill with peperite margins, Early Proterozoic, Northern Territory. *Australian Journal of Earth Sciences*, **40**, 545-558.

MCPHIE, J., DOYLE, M. & ALLEN, R. 1993. *Volcanic Textures: A Guide to the Interpretation of Textures in Volcanic Rocks*. Centre for Ore Deposit and Exploration Studies, University of Tasmania, Hobart, Tasmania, Australia.

MILLS, A.A. 1984. Pillow lavas and the Leidenfrost effect. *Journal of the Geological Society, London*, **141**, 183-186.

MINOURA, K., NAKAYA, S. & TAKEMURA, A. 1991. Origin of manganese carbonates in Jurassic red shale, central Japan. *Sedimentology*, **38**, 137-152.

MITCHELL, J.G. & EUWE, M.G. 1988. A model of single-stage concomitant potassium-argon exchange in acidic lavas from the Erlend Volcanic Complex, north of Shetland Islands. *Chemical Geology (Isotope Geoscience Section)*, **72**, 95-109.

MOORE, J.G. 1975. Mechanism of formation of pillow lava. *American Journal of Science*, **63**, 269-277.

MOORE, J.G., PHILLIPS, R.L., GRIGG, R.W., PETERSON, D.W. & SWANSON, D.A. 1973. Flow of lava into the sea, 1969-71, Kilauea volcano, Hawaii. *Geological Society of America Bulletin*, **84**, 537-546.

MOORE, S.E., FERRELL, R.E., JR. & AHARON, P. 1992. Diagenetic siderite and other ferroan carbonates in a modern subsiding marsh sequence. *Journal of Sedimentary Petrology*, **62**, 357-366.

MORTON, A.C., EVANS, D., HARLAND, R., KING, C. & RITCHIE, D.K. 1988. Volcanic ash in a cored borehole W of the Shetland Islands: evidence for Selandian (late Palaeocene) volcanism in the Faeroes region. *In:* MORTON, A.C. & PARSON, L.M.

(eds) *Early Tertiary Volcanism and the Opening of the NE Atlantic*. Geological Society, London. Special Publications, **39**, 263-269.

MOZLEY, P.S. 1989. Relation between depositional environment and the elemental composition of early diagenetic siderite. *Geology*, **17**, 704-706.

MUDGE, D.C. & RASHID, B. 1987. The geology of the Faeroe Basin area. *In:* BROOKS, J. & GLENNIE, K.W. (eds) *Petroleum Geology of North West Europe: Proceedings of the 3rd Conference*. Graham & Trotman, London, **2**, 751-763.

NAHON, D.B. 1991. *Introduction to the Petrology of Soils and Chemical Weathering*. John Wiley & Sons, Inc., New York.

NAKAYAMA, K. & YOSHIKAWA, S. 1997. Depositional processes of primary to reworked volcaniclastics on an alluvial plain; an example from the Lower Pliocene Ohta tephra bed of the Tokai Group, central Japan. *Sedimentary Geology*, **107**, 211-229.

NARANJO, J.L., SIGURDSSON, H., CAREY, S.N. & FRITZ, W.J. 1986. Eruption of Nevado del Ruiz volcano, Colombia, on 13 November 1985: tephra fall and lahars. *Science*, **233**, 941-963.

NAYLOR, P.H., BELL, B.R., JOLLEY, D.W., DURNALL, P. & FREDSTED, R. 1999. Palaeogene magmatism in the Faeroe-Shetland Basin: Influences on uplift and sedimentation. *In:* FLEET, A.J. & BOLDY, S.A.R. (eds) *Petroleum Geology of Northwest Europe: Proceedings of the 5th Conference*. Geological Society, London, **1**, 545-558.

NOE-NYGAARD, A. 1968. On extrusion forms in plateau basalts: Shield volcanoes of "scutulum" type. *Vísindafélag Íslendinga*, **Anniversary Volume**, 10-13.

NOE-NYGAARD, A. 1974. Cenozoic to recent volcanism in and around the North Atlantic Basin. *In:* NAIRN, A.E.M. & STEHLI, F.G. (eds) *The Ocean Basins and Margins: The North Atlantic*. Plenum Press, New York, **2**, 391-443.

NOMURA, S., KATO, K., KOMAKI, I., FUJIOKA, Y., SAITO, K. & YAMAOKA, I. 1999. Viscoelastic properties of coal in the thermoplastic phase. *Fuel*, **78**, 1583-1589.

ORTON, G.J. 1996. Volcanic Environments. *In:* READING, H.G. (ed.) *Sedimentary Environments: Processes, Facies and Stratigraphy*. 3rd Edition. Blackwell Science, Oxford, 485-567.

PALMER, B.A. & WALTON, A.W. 1990. Accumulation of volcaniclastic aprons in the Mount Dutton formation (Oligocene-Miocene) Marysvale volcanic field, Utah. *Geological Society of America Bulletin*, **102**, 734-748.

PARKER, J.R. (ed.) 1993. *Petroleum Geology of Northwest Europe: Proceedings of the 4th Conference*. Geological Society, London, **2**.

PARRA, M., DELMONT, P., DUMON, J.C., FERRAGNE, A. & PONS, J.C. 1987. Mineralogy and origin of Tertiary interbasaltic clays from the Faeroe Islands, northeastern Atlantic. *Clay Minerals*, **22**, 63-82.

PECK, D.L. 1978. *Cooling and Vesiculation of Alae lava lake, Hawaii*. United States Geological Survey Professional Paper, **935-B**.

PEDERSEN, G.K., LARSEN, L.M., PEDERSEN, A.K. & HJORTKJÆR, B.F. 1998. The syn-volcanic Naajaat lake, Paleocene of West Greenland. *Palaeogeography, Palaeoclimatology, Palaeoecology*, **140**, 271-287.

PETERSON, D.W., HOLCOMB, R.T., TILLING, R.I. & CHRISTIANSEN, R.L. 1994. Development of lava tubes in the light of observations at Mauna Ulu, Kilauea Volcano, Hawaii. *Bulletin of Volcanology*, **56**, 343-360.

PETERSON, D.W. & SWANSON, D.A. 1974. Observed formation of lava tubes during 1970-71 at Kilauea Volcano, Hawaii. *Studies in Speleology*, **2**, 209-222.

PETRUN, V.F. 1958. O mozaichnom stroenii kristallov kal'tsita (mosaic structure of calcite crystals). *Trudy Krivorozhskogo Gornorudnogo Instituta, Seriya Geologii i Mineralogii*, **2**, 33-43.

PICHLER, H. 1965. Acid hyaloclastites. *Bulletin Volcanologique*, **28**, 293-310.

PIERSON, T.C. & SCOTT, K.M. 1985. Downstream dilution of a lahar: transition from debris flow to hyperconcentrated streamflow. *Water Resources Research*, **21**, 1511-1524.

PLANKE, S. 2001. *Seismic volcanostratigraphy of Paleogene basalt complexes in the NE Atlantic. Conference*: Paleogene Stratigraphy, Tectonics and Petroleum Geology of North West Europe, The Geological Society, Burlington House, London.

PLANKE, S., SYMONDS, P.A., ALVESTAD, E. & SKOGSEID, J. 2000. Seismic volcanostrigraphy of large-scale basaltic extrusive complexes on rifted margins. *Journal of Geophysical Research*, **105**(B8), 19335-19351.

POLACCI, M., CASHMAN, K.V. & KAUAHIKAUA, J.P. 1999. Textural characterization of the pahoehoe-'a'a transition in Hawaiian basalt. *Bulletin of Volcanology*, **60**, 595-609.

POREBSKI, S.J. & GRADZINSKI, R. 1990. Lava-fed Gilbert-type delta in the Polonez Cove Formation (Lower Oligocene), King George Island, West Antarctica. *In:* COLELLA, A. & PRIOR, D. (eds) *Coarse-Grained Deltas*. Special Publication of the International Association of Sedimentologists, **10**, 335-351.

RASMUSSEN, J. & NOE-NYGAARD, A. 1969. *Beskrivelse til geologisk kort over Færøerne*. Danmarks Geologiske Undersøgelse, København, **1**.

RASMUSSEN, J. & NOE-NYGAARD, A. 1970a. *Geological Map of the Faeroe Islands: Pre-Quaternary*. Danmarks Geologiske Undersøgelse, København. Scale 1:200 000.

RASMUSSEN, J. & NOE-NYGAARD, A. 1970b (1969). *Geology of the Faeroe Islands. Trans:* HENDERSON, G. (ed.). Danmarks Geologiske Undersøgelse, København, **1**.

RASMUSSEN, J. & NOE-NYGAARD, A. 1990. *The Origin of the Faeroe Islands: In Text, Pictures and on Maps*. Danmarks Geologiske Undersøgelse, København.

RAWLINGS, D.J., WATKEYS, M.K. & SWEENEY, R.J. 1999. Peperitic upper margin of an invasive flow, Karoo flood basalt province, northern Lebombo. *South African Journal of Geology*, **102**, 377-383.

READING, H.G. (ed.) 1996. *Sedimentary Environments: Processes, Facies and Stratigraphy*. 3rd Edition. Blackwell Science, Oxford.

REIDEL, S.P. 1998. Emplacement of Columbia River flood basalt. *Journal of Geophysical Research*, **103**(B11), 27393-27410.

REIDEL, S.P. & TOLAN, T.L. 1992. Eruption and emplacement of flood basalt: an example from the large-volume Teepee Butte Member, Columbia River Basalt Group. *Geological Society of America Bulletin*, **104**, 1650-1671.

RETALLACK, G.J. 1981. Fossil soils: indicators of ancient terrestrial environments. *In:* NIKLAS, K.J. (ed.) *Paleobotany, Paleoecology, and Evolution*. Praeger Publishers, New York, **1**, 55-102.

RETALLACK, G.J. 1988. Field recognition of paleosols. *In:* REINHARDT, J. & SIGLEO, W.R. (eds) *Paleosols and Weathering Through Geologic Time: Techniques and Applications*. Geological Society of America, Special Paper, **216**, 1-20.

RETALLACK, G.J. 1994. A pedotype approach to latest Cretaceous and earliest Tertiary paleosols in eastern Montana. *Geological Society of America Bulletin*, **106**, 1377-1397.

RETALLACK, G.J. 1997. *A Colour Guide to Paleosols*. John Wiley & Sons Ltd., Chichester.

RETALLACK, G.J. 2001. *Soils of the Past: An Introduction to Paleopedology*. 2nd Edition. Blackwell Science Ltd., Oxford.

REUBI, O. & HERNANDEZ, J. 2000. Volcanic debris avalanche deposits of the upper Maronne valley (Cantal Volcano, France): evidence for contrasted formation and transport mechanisms. *Journal of Volcanology and Geothermal Research*, **102**, 271-286.

RICHARDSON, K.R., WHITE, R.S., ENGLAND, R.W. & FRUEHN, J. 1999. Crustal structure east of the Faeroe Islands: Mapping sub-basalt sediments using wide-angle seismic data. *Petroleum Geoscience*, **5**, 161-172.

RIDD, M.F. 1983. Aspects of the Tertiary geology of the Faeroe-Shetland Channel. *In:* BOTT, M.H.P., SAXOV, S., TALWANI, M. & THIEDE, J. (eds) *Structure and Development of the Greenland-Scotland Ridge*. Plenum Press, New York, 91-108.

RIISAGER, P., RIISAGER, J., ABRAHAMSEN, N. & WAAGSTEIN, R. 2002a. New paleomagnetic pole and magnetostratigraphy of Faroe Islands flood volcanics, North Atlantic Igneous Province. *Earth and Planetary Science Letters*, **201**, 261-276.

RIISAGER, P., RIISAGER, J., ABRAHAMSEN, N. & WAAGSTEIN, R. 2002b. Thellier palaeointensity experiments on Faroes flood basalts: technical aspects and geomagnetic implications. *Physics of the Earth and Planetary Interiors*, **131**, 91-100.

RITCHIE, J.D., GATLIFF, R.W. & RICHARDS, P.C. 1999. Early Tertiary magmatism in the offshore NW UK margin and surrounds. *In:* FLEET, A.J. & BOLDY, S.A.R. (eds) *Petroleum Geology of Northwest Europe: Proceedings of the 5th Conference*. Geological Society, London, **1**, 573-584.

RITCHIE, J.D. & HITCHEN, K. 1996. Early Paleogene offshore igneous activity to the northwest of the UK and its relationship to the North Atlantic Igneous Province. *In:* KNOX, R.W.O'B., CORFIELD, R.M. & DUNAWAY, R.E. (eds) *Correlation of the Early Paleogene in Northwest Europe*. Geological Society, London. Special Publications, **101**, 63-78.

ROBERTS, D.G. 1975. Marine geology of the Rockall Plateau and Trough. *Philosophical Transactions of the Royal Society of London*, **A278**, 447-509.

ROBERTS, D.G., BOTT, M.H.P. & URUSKI, C. 1983. Structure and origin of the Wyville-Thomson Ridge. *In:* BOTT, M.H.P., SAXOV, S., TALWANI, M. & THIEDE, J. (eds) *Structure and Development of the Greenland-Scotland Ridge*. Plenum Press, New York, 133-158.

ROCK-COLOR CHART COMMITTEE. 1995. *Rock-Color Chart*. The Geological Society of America, Boulder, Colorado.

RODOLFO, K.S. 1989. Origin and early evolution of lahar channel at Mabinit, Mayon Volcano, Philippines. *Geological Society of America Bulletin*, **101**, 414-426.

ROWLAND, S.K. & WALKER, G.P.L. 1990. Pahoehoe and aa in Hawaii: volumetric flow rate controls the lava structure. *Bulletin of Volcanology*, **52**, 615-628.

RUMPH, B., REAVES, C.M., ORANGE, V.G. & ROBINSON, D.L. 1993. Structuring and transfer zones in the Faeroe Basin. *In:* PARKER, J.R. (ed.) *Petroleum Geology of Northwest Europe: Proceedings of the 4th Conference*. Geological Society, London, **2**, 999-1009.

RUNKEL, A.C. 1990. Lateral and temporal changes in volcanogenic sedimentation; analysis of two Eocene sedimentary aprons, Big Band region, Texas. *Journal of Sedimentary Petrology*, **60**, 747-760.

RYAN, M.P. & SAMMIS, C.G. 1978. Cyclic fracture mechanisms in cooling basalts. *Geological Society of America Bulletin*, **89**, 1295-1308.

SABINE, P.A. 1971. Bentonitic beidellite-mudstone from the Faeroe Islands. *Clay Minerals*, **9**, 97-106.

SAEMUNDSSON, K. 1970. Interglacial lava flows in the lowlands of southern Iceland and the problem of two-tiered columnar jointing. *Jokull*, **20**, 62-77.

SAHAGIAN, D.L., ANDERSON, A.T. & WARD, B. 1989. Bubble coalescence in basalt flows: comparison of a numerical model with natural examples. *Bulletin of Volcanology*, **52**, 49-56.

SAKIMOTO, S.E.H. & ZUBER, M.T. 1998. Flow and convective cooling in lava tubes. *Journal of Geophysical Research*, **103**(B11), 27465-27487.

SAUNDERS, A.D., FITTON, J.G., KERR, A.C., NORRY, M.J. & KENT, R.W. 1997. The North Atlantic Igneous Province. *In:* MAHONEY, J.J. & COFFIN, M.L. (eds) *Large Igneous Provinces: Continental, Oceanic, and Planetary Flood Volcanism*. American Geophysical Union, Washington, Geophysical Monographs, **100**, 45-93.

SCHELLMANN, W. 1986. A new definition of laterite. *Geological Survey of India Memoir*, **120**, 1-7.

SCHERER, C.M.S. 2002. Preservation of aeolian genetic units by lava flows in the Lower Cretaceous of the Paraná Basin, southern Brazil. *Sedimentology*, **49**, 97-116.

SCHMID, R. 1981. Descriptive nomenclature and classification of pyroclastic deposits and fragments: recommendations of the IUGS Subcommission on the Systematics of Igneous Rocks. *Geology*, **9**, 41-43.

SCHMINCKE, H.-U. 1967. Fused tuff and pépérites in south-central Washington. *Geological Society of America Bulletin*, **78**, 319-330.

SCHNEIDER, J.-L. & FISHER, R.V. 1998. Transport and emplacement mechanisms of large volcanic debris avalanches: evidence from the northwest sector of Cantal Volcano (France). *Journal of Volcanology and Geothermal Research*, **83**, 141-165.

SELF, S., KESZTHELYI, L. & THORDARSON, T. 1998. The importance of pahoehoe. *Annual Review of Earth and Planetary Sciences*, **26**, 81-110.

SELF, S., THORDARSON, T. & KESZTHELYI, L. 1997. Emplacement of continental flood basalt lava flows. *In:* MAHONEY, J.J. & COFFIN, M.L. (eds) *Large Igneous Provinces: Continental, Oceanic, and Planetary Flood Volcanism*. American Geophysical Union, Washington, Geophysical Monographs, **100**, 381-410.

SELF, S., THORDARSON, T., KESZTHELYI, L., WALKER, G.P.L., HON, K., MURPHY, M.T., LONG, P. & FINNEMORE, S. 1996. A new model for the emplacement of Columbia River basalts as large, inflated pahoehoe lava flow fields. *Geophysical Research Letters*, **23**, 2689-2692.

SHARMA, P.V. 1994. Late Palaeocene geomagnetic polarity transition in the Vestmanna core of the Lower Basalt sequence on the Faeroe Islands. *Memoirs of the Geological Society of India*, **29**, 117-135.

SHAW, H.R. & SWANSON, D.A. 1970a. Eruption and flow rates of flood basalts. *In:* GILMOUR, E.H. & STRADLING, D. (eds) *Proceedings of the Second Columbia River Basalt Symposium*. Eastern Washington State College Press, Cheney, 271-299.

SHAW, H.R. & SWANSON, D.A. 1970b. Speculations on the fluid mechanical history of Yakima basalt flows. *In:* GILMOUR, E.H. & STRADLING, D. (eds) *Proceedings of the Second Columbia River Basalt Symposium*. Eastern Washington State College Press, Cheney, 330.

SINTON, C.W., HITCHEN, K. & DUNCAN, R.A. 1998. ^{40}Ar-^{39}Ar geochronology of silicic and basic volcanic rocks on the margins of the North Atlantic. *Geological Magazine*, **135**, 161-170.

SKILLING, I.P., WHITE, J.D.L. & MCPHIE, J. 2002. Peperite: a review of magma-sediment mingling. *Journal of Volcanology and Geothermal Research*, **114**, 1-17.

SMITH, G.A. 1986. Coarse-grained nonmarine volcaniclastic sediment: terminology and depositional process. *Geological Society of America Bulletin*, **97**, 1-10.

SMITH, G.A. 1987a. The influence of explosive volcanism on fluvial sedimentation: the Deschutes Formation (Neogene) in central Oregon. *Journal of Sedimentary Petrology*, **57**, 613-629.

SMITH, G.A. 1987b. Sedimentology of volcanism-induced aggradation in fluvial basins: examples from the Pacific Northwest, USA. *In:* ETHRIDGE, F.G., FLORES, R.M. & HARVEY, M.D. (eds) *Recent Developments in Fluvial Sedimentology*. Special Publication of the Society of Economic Palaeontologists and Mineralogists, Tulsa, Oklahoma, **39**, 217-228.

SMITH, G.A. 1988. Neogene synvolcanic and syntectonic sedimentation in central Washington. *Geological Society of America Bulletin*, **100**, 1479-1492.

SMITH, G.A. 1991. Facies sequences and geometries in continental volcaniclastic sequences. *In:* FISHER, R.V. & SMITH, G.A. (eds) *Sedimentation in Volcanic Settings*. SEPM (Society for Sedimentary Geology) Special Publication, Tulsa, Oklahoma, **45**, 109-121.

SMITH, G.A. & FRITZ, W.J. 1989. Volcanic influences on terrestrial sedimentation. *Geology*, **17**, 375-376.

SMITH, G.A. & LOWE, D.R. 1991. Lahars: volcano-hydrologic events and deposition in the debris flow - hyperconcentrated flow continuum. *In:* FISHER, R.V. & SMITH, G.A. (eds) *Sedimentation in Volcanic Settings*. SEPM (Society for Sedimentary Geology) Special Publication, Tulsa, Oklahoma, **45**, 59-87.

SMITH, G.A., MOORE, J.D. & MCINTOSH, W.C. 2002. Assessing roles of volcanism and basin subsidence in causing Oligocene-lower Miocene sedimentation in the Northern Rio Grande rift, New Mexico, U.S.A. *Journal of Sedimentary Research*, **72**, 836-848.

SMYTHE, D.K. 1983. Faeroe-Shetland Escarpment and continental margin north of the Faeroes. *In:* BOTT, M.H.P., SAXOV, S., TALWANI, M. & THIEDE, J. (eds) *Structure and Development of the Greenland-Scotland Ridge*. Plenum Press, New York, 109-119.

SOHN, Y.K., RHEE, C.W. & KIM, B.C. 1999. Debris flow and hyperconcentrated flood-flow deposits in an alluvial fan, northwestern part of the Cretaceous Yongdong Basin, Central Korea. *Journal of Geology*, **107**, 111-132.

SPARKS, R.S.J. & WRIGHT, J.V. 1979. Welded air-fall tuffs. *In:* CHAPIN, C.E. & ELSTON, W.E. (eds) *Ash Flow Tuffs*. Geological Society of America, Special Paper, **180**, 155-166.

SPENCER, E. 1925. On some occurrences of spherulitic siderite and other carbonates in sediments. *Quarterly Journal of the Geological Society, London*, **81**, 667-705.

SPRY, A. 1962. The origin of columnar jointing, particularly in basalt flows. *Journal of the Geological Society of Australia*, **8**, 191-216.

SQUIRE, R.J. & MCPHIE, J. 2002. Characteristics and origin of peperite involving coarse-grained host sediment. *Journal of Volcanology and Geothermal Research*, **114**, 45-61.

STACH, E., MACKOWSKY, M.T.H., TEICHMÜLLER, M., TAYLOR, G.H., CHANDRA, D. & TEICHMÜLLER, R. 1975. *Stach's Textbook of Coal Petrology*. Gebuder Borntraeger, Berlin.

STEEL, R.J. & AASHEIM, S.M. 1978. Alluvial sand deposition in a rapidly subsiding basin (Devonian, Norway). *In:* MIALL, A.D. (ed.) *Fluvial Sedimentology*. Memoir of the Canadian Society of Petroleum Geologists, Calgary, **5**, 385-412.

STEPHENSON, P.J., BURCH-JOHNSTON, A.T., STANTON, D. & WHITEHEAD, P.W. 1998. Three long lava flows in north Queensland. *Journal of Geophysical Research*, **103**(B11), 27359-27370.

STOKER, M.S., HITCHEN, K. & GRAHAM, C.C. 1993. Cretaceous and Tertiary igneous rocks. *The Geology of the Hebrides and West Shetland Shelves, and Adjacent Deep-water Areas: United Kingdom Offshore Regional Report*. HMSO, London, **2**, 68-79.

STOKER, M.S., MORTON, A.C., EVANS, D., HUGHES, M.J., HARLAND, R. & GRAHAM, D.K. 1988. Early Tertiary basalts and tuffaceous sandstones from the Hebrides Shelf and Wyville-Thomson Ridge, NE Atlantic. *In:* MORTON, A.C. & PARSON, L.M. (eds) *Early Tertiary Volcanism and the Opening of the NE Atlantic*. Geological Society, London. Special Publications, **39**, 271-282.

STOOPS, G. 1983. SEM and light microscopic observations of minerals in bog-ores of the Belgian Campine. *Geoderma*, **30**, 179-186.

SUBBARAO, K.V. & SUKHESWALA, R.N. (eds). 1981. *Deccan volcanism and related basalt provinces in other parts of the world*. Geological Society of India Memoir, **3**.

SUTHREN, R.J. 1985. Facies analysis of volcaniclastic sediments: a review. *In:* BRENCHLEY, P. & WILLIAMS, B.P.J. (eds) *Sedimentology: Recent Advances and Applied Aspects*. Geological Society, London. Special Publications, **18**, 123-146.

SUTHREN, R.J. & FURNES, H. 1980. Origin of some bedded welded tuffs. *Bulletin Volcanologique*, **43**, 61-71.

SWANSON, D.A. 1967. Yakima basalt of the Tieton River area, south central Washington. *Geological Society of America Bulletin*, **78**, 1077-1110.

SWANSON, D.A., WRIGHT, T.L. & HELZ, R.T. 1975. Linear vent systems and estimated rates of magma production and eruption for the Yakima basalt on the Columbia Plateau. *American Journal of Science*, **275**, 877-905.

TALBOT, M.R. & ALLEN, P.A. 1996. Lakes. *In:* READING, H.G. (ed.) *Sedimentary Environments: Processes, Facies and Stratigraphy*. 3rd Edition. Blackwell Science, Oxford, 83-124.

TARLING, D.H. 1970. Palaeomagnetic results from the Faeroe Islands. *In:* RUNCORN, S.K. (ed.) *Palaeogeophysics*. Academic Press, London, 193-208.

TEGNER, C., DUNCAN, R.A., BERNSTEIN, S., BROOKS, C.K., BIRD, D.K. & STOREY, M. 1998. ^{40}Ar-^{39}Ar geochronology of Tertiary mafic intrusions along the East Greenland rifted margin: relation to flood basalts and the Iceland hotspot track. *Earth and Planetary Science Letters*, **156**, 75-88.

THOMAS, L. 1992. *Handbook of Practical Coal Geology*. John Wiley, Chichester.

THORDARSON, T. & SELF, S. 1998. The Rosa Member, Columbia River Basalt Group: a gigantic pahoehoe lava flow field formed by endogenous processes? *Journal of Geophysical Research*, **103**(B11), 27411-27445.

TOMKEIEFF, S.I. 1940. The basalt lavas of the Giant's Causeway district of Northern Ireland. *Bulletin Volcanologique*, **6**, 89-146.

TUCKER, M.E. 1996a. *Sedimentary Petrology: An Introduction to the Origin of Sedimentary Rocks*. 2nd Edition. Blackwell Science, Oxford.

TUCKER, M.E. 1996b. *Sedimentary Rocks in the Field*. 2nd Edition. John Wiley & Sons Ltd., Chichester.

TURNER, J.D. & SCRUTTON, R.A. 1993. Subsidence patterns in western margin basins: evidence from the Faeroe-Shetland Basin. *In:* PARKER, J.R. (ed.) *Petroleum Geology of Northwest Europe: Proceedings of the 4th Conference*. Geological Society, London, **2**, 975-983.

VERRECCHIA, E.P., FREYTET, P., VERRECCHIA, K.E. & DUMONT, J.-L. 1995. Spherulites in calcrete laminar crusts: Biogenetic $CaCO_3$ precipitation as a major contributor to crust formation. *Journal of Sedimentary Research*, **A65**, 690-700.

WAAGSTEIN, R. 1977. *The Geology of the Faeroe Plateau*. PhD Thesis. University of Copenhagen.

WAAGSTEIN, R. 1988. Structure, composition and age of the Faeroe basalt plateau. *In:* MORTON, A.C. & PARSON, L.M. (eds) *Early Tertiary Volcanism and the Opening of the NE Atlantic*. Geological Society, London. Special Publications, **39**, 225-238.

WAAGSTEIN, R., GUISE, P. & REX, D. 2001. *Potassium-argon and argon-argon whole-rock dating of the Palaeocene lower basalt formation of the Faeroe Islands. Conference*: Paleogene Stratigraphy, Tectonics and Petroleum Geology of North West Europe, The Geological Society, Burlington House, London.

WAAGSTEIN, R., GUISE, P. & REX, D. 2002. K/Ar and $^{39}Ar/^{40}Ar$ whole-rock dating of zeolite facies metamorphosed flood basalts: the upper Paleocene basalts of the Faroe Islands, NE Atlantic. *In:* JOLLEY, D.W. & BELL, B.R. (eds) *The North Atlantic Igneous Province: Stratigraphy, Tectonic, Volcanic and Magmatic Processes*. Geological Society, London. Special Publications, **197**, 219-252.

WAAGSTEIN, R. & HALD, N. 1984. Structure and petrography of a 660 m lava sequence from the Vestmanna-1 drill hole, lower and middle basalt series, Faeroe Islands. *In:* BERTHELSEN, O., NOE-NYGAARD, A. & RASMUSSEN, J. (eds) *The Deep Drilling Project 1980-1981 in the Faeroe Islands*. Føroya Fróðskaparfelag, Tórshavn, 39-70.

WAAGSTEIN, R., HALD, N., JØRGENSEN, O., NIELSEN, P.H., NOE-NYGAARD, A., RASMUSSEN, J. & SCHÖNHARTING, G. 1984. Deep drilling on the Faeroe Islands. *Bulletin of the Geological Society of Denmark*, **32**, 133-138.

WALKER, B.H. & FRANCIS, E.H. 1986. High-level emplacement of an olivine-dolerite sill into Namurian sediments near Cardenden, Fife. *Transactions of the Royal Society of Edinburgh: Earth Sciences*, **77**, 295-307.

WALKER, F. & DAVIDSON, C.F. 1936. A contribution to the geology of the Faeroes. *Transactions of the Royal Society of Edinburgh*, **58**, 869-897.

WALKER, G.P.L. 1963. The Breiddalur central volcano, Eastern Iceland. *Quarterly Journal of the Geological Society, London*, **119**, 29-63.

WALKER, G.P.L. 1970. Compound and simple lava flows and flood basalts. *Bulletin Volcanologique*, **35**, 579-590.

WALKER, G.P.L. 1973. Lengths of lava flows. *Philosophical Transactions of the Royal Society of London*, **274**, 107-118.

WALKER, G.P.L. 1987. Pipe vesicles in Hawaiian basaltic lavas: their origin and potential as paleoslope indicators. *Geology*, **15**, 84-87.

WALKER, G.P.L. 1989. Spongy pahoehoe in Hawaii: a study of vesicle-distribution patterns in basalt and their significance. *Bulletin of Volcanology*, **51**, 199-209.

WALKER, G.P.L. 1991. Structure and origin by injection of lava under surface crust, of tumuli, "lava rises", "lava-rise pits", and "lava-inflation clefts" in Hawaii. *Bulletin of Volcanology*, **53**, 546-558.

WALKER, G.P.L. 1993. Basaltic-volcano systems. *In:* PRICHARD, H.M., ALABASTER, T., HARRIS, N.B.W. & NEARY, C.R. (eds) *Magmatic Processes and Plate Tectonics*. Geological Society, London. Special Publications, **76**, 3-38.

WALKER, G.P.L., CAÑÓN-TAPIA, E. & HERRERO-BERVERA, E. 1999. Origin of vesicle layering and double imbrication by endogenous growth in the Birkett basalt flow (Columbia river plateau). *Journal of Volcanology and Geothermal Research*, **88**, 15-28.

WATERS, A.C. 1961. Stratigraphic and lithologic variations in the Columbia River basalt. *American Journal of Science*, **259**, 583-611.

WENTWORTH, C.K. 1922. A scale of grade and class terms for clastic sediments. *Journal of Geology*, **30**, 377-392.

WENTWORTH, C.K. & MACDONALD, G.A. 1953. Structures and forms of basaltic rocks in Hawaii. *United States Geological Survey Bulletin*, **994**, 1-98.

WHITE, J.D.L., MCPHIE, J. & SKILLING, I. 2000. Peperite: a useful genetic term. *Bulletin of Volcanology*, **62**, 65-66.

WHITE, R.S., SMALLWOOD, J.R., FLIEDNER, M.M., BOSLAUGH, B., MARESH, J. & FRUEHN, J. 2003. Imaging and regional distribution of basalt flows in the Faeroe-Shetland Basin. *Geophysical Prospecting*, **51**, 215-231.

WIDDOWSON, M., WALSH, J.N. & SUBBARAO, K.V. 1997. The geochemistry of Indian bole horizons: palaeoenvironments implications of Deccan intravolcanic palaeosurfaces. *In:* WIDDOWSON, M. (ed.) *Palaeosurfaces: Recognition, Reconstruction and*

Palaeoenvironmental Interpretation. Geological Society, London. Special Publications, **120**, 269-281.

WILKINS, A., SUBBARAO, K.V., INGRAM, G. & WALSH, J.N. 1994. Weathering regimes within the Deccan basalts. *In:* SUBBARAO, K.V. (ed.) *Volcanism*. Wiley Eastern, 217-231.

WILLIAMS, H. & MCBIRNEY, A.R. 1979. *Volcanology*. Freeman, Cooper & Co., San Francisco.

WILLIAMSON, I.T. & BELL, B.R. 1994. The Palaeocene lava field of the west-central Skye, Scotland: stratigraphy, palaeogeography and structure. *Transactions of the Royal Society of Edinburgh: Earth Sciences*, **85**, 39-75.

WILMOTH, R.A. & WALKER, G.P.L. 1993. P-type and S-type pahoehoe: a study of vesicle distribution patterns in Hawaiian lava flows. *Journal of Volcanology and Geothermal Research*, **55**, 129-142.

WOHLETZ, K.H. 1983. Mechanisms of hydrovolcanic pyroclast formation: grain size scanning electron microscopy and experimental results. *Journal of Volcanology and Geothermal Research*, **17**, 31-63.

WOHLETZ, K.H. 2002. Water/magma interaction: some theory and experiments on peperite formation. *Journal of Volcanology and Geothermal Research*, **114**, 19-35.

WOLFF, J.A. & WRIGHT, J.V. 1981. Rheomorphism of welded tuffs. *Journal of Volcanology and Geothermal Research*, **10**, 13-34.

WOOD, D.A. 1979. Dynamic partial melting: its application to the petrogeneses of basalts erupted in Iceland, the Faeroe Islands, the Isle of Skye (Scotland) and the Troodos Massif (Cyprus). *Geochimica et Cosmochimica Acta*, **43**, 1031-1046.

WRIGHT, J.V. 1980. Stratigraphy and geology of the welded air-fall tuffs of Pantelleria, Italy. *Geologische Rundschau*, **69**, 263-291.

YARNOLD, J.C. 1993. Rock-avalanche characteristics in dry climates and the effect of flow into lakes: insights from mid-Tertiary sedimentary breccias near Artillery Peak, Arizona. *Geological Society of America Bulletin*, **105**, 345-360.

Appendix A: Chemical Compositions of Siderite Spherules

SUF.1.2a & SUF.1.2b, clay ironstone, Ulingatangi Section, Suðuroy, Faeroe Islands

AND

SUF.8.2a & SUF.8.2b, ironstone, Rokhagi Section, Suðuroy, Faeroe Islands

A.1 Chemical Compositions Expressed as Oxides

Sample SUF.1.2a

	1	2	3	4	5	6	7	8	9	10	11	12	13
FeO	60.61	59.78	59.69	59.65	58.74	58.51	58.15	56.52	55.76	54.69	54.73	52.40	50.57
MnO	0.15	0.12	0.23	0.45	0.74	0.76	0.87	1.91	2.60	3.00	3.91	5.83	5.63
MgO	0.00	0.03	0.04	0.09	0.07	0.07	0.06	0.05	0.11	0.07	0.10	0.10	0.09
CaO	0.62	0.45	0.63	1.45	1.57	1.35	0.71	1.46	1.66	1.25	1.02	2.10	1.61
ZnO	0.06	0.07	0.07	0.05	0.05	0.04	0.08	0.09	0.07	0.00	0.00	0.08	0.06
SiO_2	0.02	0.10	0.18	0.00	0.02	0.25	0.28	0.42	0.35	0.94	0.44	0.30	1.77
CO_2	37.78	37.26	37.55	38.09	37.81	37.83	37.24	37.67	37.74	37.81	37.50	37.96	38.47
Total	99.25	97.80	98.40	99.79	99.01	98.81	97.40	98.12	98.28	97.76	97.70	98.77	98.21

	14	15	16	17	18	19	20	21	22	23	24	25	26
FeO	49.78	50.60	50.25	49.72	48.94	49.10	48.78	48.46	49.00	48.97	49.37	48.41	49.25
MnO	7.83	7.29	7.83	7.99	8.11	7.59	7.59	7.27	6.67	6.48	8.03	8.31	7.13
MgO	0.12	0.08	0.07	0.08	0.07	0.08	0.08	0.10	0.09	0.08	0.06	0.08	0.10
CaO	2.87	2.00	2.43	2.29	2.43	2.14	2.11	1.91	1.69	1.62	2.45	2.92	2.01
ZnO	0.03	0.07	0.03	0.07	0.05	0.00	0.02	0.07	0.00	0.00	0.03	0.03	0.03
SiO_2	0.05	0.59	0.10	0.32	0.57	0.92	1.06	1.77	2.25	2.42	0.63	0.52	1.51
CO_2	37.83	38.08	37.79	37.80	37.86	37.91	37.90	38.44	38.88	38.93	38.15	37.98	38.52
Total	98.52	98.72	98.49	98.26	98.03	97.74	97.54	98.02	98.58	98.51	98.71	98.26	98.56

Results are given as weight percent
Chemical composition of siderite spherule SUF.1.2a, clay ironstone, Ulingatangi Section, Suðuroy, Faeroe Islands

Sample SUF.1.2a

	27	28	29	30	31	32	33	34	35	36	37	38	39
FeO	49.15	50.61	51.24	51.46	51.15	52.91	53.45	52.71	56.19	55.81	56.79	58.91	58.95
MnO	7.40	7.15	6.28	6.33	6.81	5.29	4.88	5.23	2.68	2.51	2.09	1.09	0.92
MgO	0.11	0.06	0.07	0.10	0.11	0.08	0.09	0.13	0.07	0.14	0.12	0.08	0.10
CaO	2.33	2.16	1.91	1.96	2.56	1.86	2.17	3.01	1.82	2.61	2.49	1.34	1.57
ZnO	0.02	0.05	0.09	0.06	0.05	0.01	0.00	0.05	0.03	0.15	0.03	0.05	0.00
SiO_2	0.88	0.28	0.82	0.56	0.08	0.52	0.19	0.03	0.01	0.00	0.01	0.03	0.01
CO_2	37.96	37.64	38.13	37.95	37.83	38.02	37.86	38.12	37.63	38.03	38.21	37.97	38.06
Total	97.85	97.94	98.55	98.43	98.58	98.69	98.64	99.30	98.44	99.26	99.74	99.46	99.62

	40	41	42	43	44	45	46	Average
FeO	59.49	58.99	60.26	60.20	60.02	60.12	60.50	54.33
MnO	0.66	0.56	0.32	0.24	0.16	0.09	0.10	4.02
MgO	0.08	0.13	0.05	0.09	0.07	0.05	0.05	0.08
CaO	1.51	1.80	1.03	1.07	0.61	0.48	0.27	1.72
ZnO	0.06	0.07	0.09	0.08	0.00	0.07	0.00	0.05
SiO_2	0.13	0.04	0.00	0.10	0.48	0.16	0.26	0.49
CO_2	38.35	38.15	38.03	38.16	38.13	37.60	37.78	37.97
Total	100.29	99.75	99.79	99.94	99.47	98.58	98.96	98.66

Results are given as weight percent
Chemical composition of siderite spherule SUF.1.2a, clay ironstone, Ulingatangi Section, Suðuroy, Faeroe Islands

Sample SUF.1.2b

	1	2	3	4	5	6	7	8	9	10	11	12	13
FeO	59.92	59.83	60.17	59.77	60.81	60.15	59.83	59.25	58.89	57.75	56.78	55.91	56.65
MnO	0.14	0.14	0.19	0.23	0.21	0.27	0.32	0.73	0.87	1.31	1.93	2.39	2.50
MgO	0.05	0.04	0.03	0.08	0.04	0.04	0.08	0.08	0.10	0.06	0.13	0.13	0.09
CaO	0.38	0.52	0.54	0.96	0.55	0.81	0.93	1.59	1.13	1.85	2.41	2.47	1.88
ZnO	0.05	0.01	0.03	0.05	0.00	0.09	0.04	0.00	0.09	0.05	0.08	0.09	0.04
SiO_2	0.32	0.52	0.03	0.09	0.00	0.02	0.02	0.02	0.03	0.07	0.02	0.01	0.00
CO_2	37.65	37.95	37.50	37.76	37.87	37.77	37.72	38.12	37.71	37.85	38.10	37.88	37.86
Total	98.50	98.99	98.49	98.94	99.48	99.14	98.93	99.79	98.82	98.94	99.46	98.88	99.04

	14	15	16	17	18	19	20	21	22	23	24	25	26
FeO	55.64	54.43	52.35	53.73	54.50	53.72	52.75	53.71	54.14	53.23	54.48	53.93	55.44
MnO	3.19	4.17	5.34	4.79	4.62	5.05	5.36	5.17	4.61	5.31	4.39	4.59	3.49
MgO	0.12	0.09	0.13	0.11	0.09	0.11	0.10	0.08	0.09	0.12	0.10	0.12	0.10
CaO	2.05	2.07	2.89	2.28	1.64	2.25	2.50	2.12	1.99	2.53	2.00	2.32	1.74
ZnO	0.00	0.11	0.00	0.04	0.05	0.06	0.08	0.01	0.00	0.10	0.00	0.06	0.07
SiO_2	0.02	0.07	0.00	0.08	0.10	0.07	0.02	0.01	0.14	0.01	0.14	0.03	0.06
CO_2	37.84	37.82	37.80	37.94	37.82	38.07	37.79	37.89	37.90	38.09	37.98	37.91	37.73
Total	98.86	98.76	98.52	98.97	98.82	99.34	98.60	98.99	98.88	99.39	99.09	98.96	98.63

Results are given as weight percent
Chemical composition of siderite spherule SUF.1.2b, clay ironstone, Ulingatangi Section, Suðuroy, Faeroe Islands

Sample SUF.1.2b

	27	28	29	30	31	32	33	34	35	36	37	38	39
FeO	55.50	55.83	55.41	56.39	57.45	58.21	58.66	58.82	59.07	59.04	59.24	60.32	60.57
MnO	3.29	2.59	2.25	2.11	1.82	1.25	0.90	0.59	0.46	0.45	0.29	0.15	0.12
MgO	0.11	0.09	0.13	0.12	0.11	0.09	0.10	0.11	0.10	0.13	0.08	0.04	0.06
CaO	2.05	1.71	1.68	1.86	1.73	1.56	1.53	1.37	1.57	1.62	0.99	0.56	0.52
ZnO	0.05	0.00	0.05	0.04	0.01	0.05	0.07	0.00	0.08	0.07	0.00	0.00	0.05
SiO_2	0.09	0.23	0.35	0.18	0.02	0.02	0.11	0.12	0.07	0.03	0.14	0.12	0.04
CO_2	37.92	37.59	37.34	37.73	37.84	37.82	38.01	37.77	37.96	37.94	37.54	37.71	37.74
Total	99.00	98.03	97.20	98.42	98.98	99.00	99.39	98.77	99.31	99.28	98.28	98.90	99.10

	40	Average
FeO	60.55	57.07
MnO	0.11	2.19
MgO	0.03	0.09
CaO	0.48	1.59
ZnO	0.03	0.04
SiO_2	0.03	0.09
CO_2	37.63	37.82
Total	98.86	98.89

Results are given as weight percent
Chemical composition of siderite spherule SUF.1.2b, clay ironstone, Ulingatangi Section, Suðuroy, Faeroe Islands

Sample SUF.8.2a

	1	2	3	4	5	6	7	8	9	10	11	12	13
FeO	58.87	60.12	59.96	59.61	58.81	60.14	59.05	58.85	59.85	59.95	59.61	59.00	58.67
MnO	1.50	0.58	0.59	0.95	0.91	0.27	0.20	0.37	0.11	0.07	0.06	0.11	0.15
MgO	0.02	0.00	0.02	0.02	0.00	0.02	0.01	0.06	0.00	0.01	0.04	0.04	0.07
CaO	0.52	0.48	0.77	0.80	1.00	0.90	1.71	1.31	1.11	1.56	1.74	2.07	1.32
ZnO	0.02	0.05	0.04	0.02	0.05	0.00	0.01	0.03	0.13	0.01	0.09	0.02	0.00
SiO_2	0.03	0.12	0.03	0.09	0.29	0.19	0.25	0.49	0.04	0.10	0.18	0.21	1.13
CO_2	37.48	37.77	37.79	37.89	37.83	38.00	38.02	38.11	37.75	38.16	38.28	38.20	38.81
Total	98.44	99.11	99.19	99.37	98.89	99.51	99.25	99.23	99.00	99.87	100.00	99.64	100.15

	14	15	16	17	18	19	20	21	22	23	24	25	26
FeO	58.86	58.48	58.26	58.24	58.32	57.90	58.11	58.38	58.22	58.20	58.36	57.34	57.17
MnO	0.14	0.11	0.17	0.19	0.18	0.22	0.21	0.25	0.27	0.37	0.46	0.55	0.57
MgO	0.04	0.02	0.00	0.00	0.02	0.02	0.04	0.02	0.05	0.03	0.01	0.03	0.03
CaO	2.41	1.77	2.45	2.01	2.20	2.24	2.27	1.64	1.86	2.22	2.02	2.63	2.02
ZnO	0.00	0.08	0.07	0.00	0.05	0.02	0.01	0.06	0.04	0.07	0.05	0.00	0.10
SiO_2	0.07	0.21	0.07	0.17	0.16	0.20	0.11	0.39	0.68	0.34	0.25	0.34	0.52
CO_2	38.17	37.66	37.85	37.62	37.86	37.69	37.73	37.84	38.37	38.19	38.03	38.07	37.80
Total	99.68	98.34	98.86	98.23	98.80	98.29	98.48	98.58	99.49	99.41	99.18	98.96	98.20

Results are given as weight percent

Chemical composition of siderite spherule SUF.8.2a, ironstone, Rokhagi Section, Suðuroy, Faeroe Islands

Sample SUF.8.2a

	27	28	29	30	31	32	33	34	35	36	37	38	39
FeO	57.62	56.33	57.27	58.19	58.97	58.49	57.94	58.09	57.90	58.65	58.82	58.64	59.14
MnO	0.58	0.67	0.58	0.56	0.43	0.39	0.28	0.28	0.21	0.18	0.12	0.14	0.11
MgO	0.02	0.02	0.04	0.03	0.00	0.02	0.00	0.04	0.05	0.03	0.05	0.01	0.04
CaO	2.32	2.75	1.87	2.39	1.81	2.26	2.30	2.73	1.95	2.25	2.11	2.19	1.67
ZnO	0.01	0.06	0.07	0.06	0.10	0.06	0.00	0.07	0.05	0.11	0.02	0.06	0.02
SiO_2	0.20	0.34	0.67	0.07	0.12	0.12	0.21	0.14	0.47	0.04	0.04	0.09	0.29
CO_2	37.80	37.65	37.97	38.03	38.05	38.08	37.77	38.18	37.91	37.97	37.89	37.91	38.10
Total	98.54	97.83	98.46	99.31	99.49	99.41	98.49	99.52	98.54	99.24	99.06	99.04	99.37

	40	41	42	43	44	45	46	47	48	49	50	Average
FeO	58.82	58.44	59.51	58.62	59.40	59.52	59.44	59.22	58.77	59.44	58.86	58.69
MnO	0.12	0.09	0.13	0.40	0.19	0.31	0.66	0.94	1.02	0.51	0.96	0.39
MgO	0.04	0.07	0.01	0.05	0.02	0.01	0.03	0.02	0.03	0.06	0.02	0.03
CaO	1.81	1.75	1.32	1.13	1.08	0.89	0.79	0.71	0.48	0.40	0.32	1.65
ZnO	0.00	0.05	0.00	0.01	0.08	0.01	0.00	0.05	0.01	0.00	0.02	0.04
SiO_2	0.18	0.10	0.06	0.36	0.35	0.21	0.13	0.06	0.35	0.71	0.66	0.25
CO_2	37.84	37.48	37.68	37.63	37.93	37.66	37.66	37.55	37.57	38.15	37.91	37.91
Total	98.82	97.99	98.71	98.19	99.05	98.59	98.70	98.54	98.23	99.27	98.75	98.95

Results are given as weight percent
Chemical composition of siderite spherule SUF.8.2a, ironstone, Rokhagi Section, Suðuroy, Faeroe Islands

Sample SUF.8.2b

	1	2	3	4	5	6	7	8	9	10	11	12	13
FeO	59.63	60.25	60.08	58.70	59.10	59.44	59.18	58.11	58.72	59.72	59.20	59.27	58.67
MnO	0.87	0.70	0.55	1.28	0.86	0.67	0.28	0.42	0.44	0.18	0.06	0.13	0.13
MgO	0.03	0.04	0.02	0.01	0.04	0.03	0.02	0.09	0.05	0.01	0.05	0.04	0.02
CaO	0.44	0.35	0.42	0.95	0.84	0.57	1.31	1.22	1.54	1.25	1.49	1.57	1.35
ZnO	0.04	0.00	0.02	0.00	0.00	0.02	0.08	0.00	0.05	0.01	0.01	0.04	0.08
SiO_2	0.24	0.06	0.07	0.12	0.35	0.35	0.06	1.15	0.20	0.04	0.22	0.25	0.59
CO_2	37.82	37.75	37.62	37.69	37.95	37.84	37.61	38.60	37.83	37.75	37.87	38.05	38.01
Total	99.07	99.15	98.78	98.75	99.13	98.93	98.54	99.59	98.84	98.95	98.91	99.35	98.84

	14	15	16	17	18	19	20	21	22	23	24	25	26
FeO	58.75	58.82	57.96	57.60	58.24	58.14	57.21	57.74	57.42	57.97	57.87	57.64	57.97
MnO	0.14	0.16	0.17	0.24	0.21	0.21	0.27	0.30	0.41	0.31	0.40	0.29	0.27
MgO	0.04	0.04	0.03	0.02	0.01	0.03	0.04	0.02	0.05	0.02	0.06	0.06	0.01
CaO	1.82	1.77	1.80	2.31	2.74	2.16	2.07	2.15	2.95	1.72	1.72	1.92	1.55
ZnO	0.07	0.02	0.00	0.09	0.05	0.07	0.00	0.00	0.07	0.00	0.08	0.01	0.03
SiO_2	0.22	0.35	0.61	0.65	0.05	0.33	0.78	0.31	0.09	0.52	0.32	0.62	0.67
CO_2	37.92	38.10	37.95	38.28	38.07	38.01	38.03	37.73	37.98	37.84	37.64	37.98	37.91
Total	98.96	99.27	98.52	99.19	99.38	98.95	98.40	98.25	98.98	98.38	98.10	98.52	98.40

Results are given as weight percent
Chemical composition of siderite spherule SUF.8.2b, ironstone, Rokhagi Section, Suðuroy, Faeroe Islands

Sample SUF.8.2b

	27	28	29	30	31	32	33	34	35	36	37	38	39
FeO	56.81	56.87	57.35	57.13	58.00	57.37	58.63	57.87	58.16	58.43	57.43	57.72	58.56
MnO	0.33	0.32	0.50	0.42	0.30	0.24	0.16	0.28	0.19	0.15	0.38	0.19	0.15
MgO	0.16	0.02	0.02	0.05	0.03	0.02	0.07	0.07	0.04	0.01	0.13	0.08	0.05
CaO	1.51	1.60	2.48	1.81	1.34	1.67	1.18	1.12	1.28	1.40	1.26	1.08	1.36
ZnO	0.00	0.10	0.00	0.07	0.00	0.00	0.01	0.02	0.09	0.02	0.04	0.05	0.00
SiO_2	1.79	0.86	0.17	0.78	0.78	0.41	0.74	0.79	0.71	0.41	1.84	1.04	0.61
CO_2	38.99	37.64	37.66	37.92	37.96	37.22	38.10	37.75	37.88	37.61	39.26	37.96	38.00
Total	99.58	97.42	98.17	98.20	98.41	96.93	98.89	97.89	98.35	98.04	100.32	98.12	98.75

	40	41	42	43	44	45	46	47	48	49	50	Average
FeO	58.64	59.44	59.13	59.10	58.14	59.45	58.64	59.19	59.63	60.08	59.32	58.49
MnO	0.16	0.08	0.08	0.15	0.47	0.28	0.79	0.99	0.75	0.47	1.12	0.38
MgO	0.04	0.03	0.03	0.00	0.05	0.05	0.09	0.08	0.03	0.00	0.02	0.04
CaO	2.40	1.31	1.93	1.19	1.15	1.16	0.64	0.67	0.36	0.36	0.41	1.41
ZnO	0.00	0.00	0.02	0.01	0.00	0.01	0.03	0.08	0.00	0.05	0.00	0.03
SiO_2	0.12	0.18	0.08	0.38	0.81	0.24	0.74	0.33	0.15	0.29	0.29	0.48
CO_2	38.12	37.79	37.95	37.81	38.06	37.91	38.12	38.03	37.53	37.84	37.80	37.93
Total	99.48	98.82	99.22	98.65	98.68	99.08	99.05	99.37	98.45	99.08	98.95	98.76

Results are given as weight percent
Chemical composition of siderite spherule SUF.8.2b, ironstone, Rokhagi Section, Suðuroy, Faeroe Islands

Summary of samples SUF.1.2 & SUF.8.2

	Average compositions for Sample SUF.1.2			Average compositions for Sample SUF.8.2			Differences between Samples SUF.1.2 & SUF.8.2
	SUF.1.2a	SUF.1.2b	Overall	SUF.8.2a	SUF.8.2b	Overall	
FeO	54.33	57.07	55.61	58.69	58.49	58.59	-2.98
MnO	4.02	2.19	3.17	0.39	0.38	0.38	2.79
MgO	0.08	0.09	0.09	0.03	0.04	0.03	0.05
CaO	1.72	1.59	1.66	1.65	1.41	1.53	0.13
ZnO	0.05	0.04	0.04	0.04	0.03	0.03	0.01
SiO_2	0.49	0.09	0.30	0.25	0.48	0.36	-0.06
CO_2	37.97	37.82	37.90	37.91	37.93	37.92	-0.02
Total	98.66	98.89	98.77	98.95	98.76	98.85	-0.08

	SUF.1.2a			SUF.1.2b			SUF.8.2a			SUF.8.2b		
	Max	Min	Range	Max	Min	Range	Max	Min	Range	Max	Min	Range
FeO	60.61	48.41	12.20	60.81	52.35	8.46	60.14	56.33	3.81	60.25	56.81	3.44
MnO	8.31	0.09	8.22	5.36	0.11	5.25	1.50	0.06	1.44	1.28	0.06	1.22
MgO	0.14	0.00	0.14	0.13	0.03	0.11	0.07	0.00	0.07	0.16	0.00	0.16
CaO	3.01	0.27	2.75	2.89	0.38	2.51	2.75	0.32	2.42	2.95	0.35	2.61
ZnO	0.15	0.00	0.15	0.11	0.00	0.11	0.13	0.00	0.13	0.10	0.00	0.10
SiO_2	2.42	0.00	2.42	0.52	0.00	0.52	1.13	0.03	1.10	1.84	0.04	1.80
CO_2	38.93	37.24	1.69	38.12	37.34	0.78	38.81	37.48	1.32	39.26	37.22	2.03

Results are given as weight percent

A.2 Chemical Compositions Expressed as Elements

Sample SUF.1.2a

	1	2	3	4	5	6	7	8	9	10	11	12	13
Fe	47.11	46.47	46.40	46.37	45.66	45.48	45.20	43.93	43.34	42.51	42.54	40.73	39.31
Mn	0.12	0.09	0.18	0.35	0.58	0.59	0.68	1.48	2.01	2.32	3.03	4.52	4.36
Mg	0.00	0.02	0.02	0.05	0.04	0.04	0.04	0.03	0.07	0.04	0.06	0.06	0.05
Ca	0.45	0.32	0.45	1.03	1.12	0.97	0.50	1.04	1.18	0.89	0.73	1.50	1.15
Zn	0.05	0.05	0.06	0.04	0.04	0.03	0.07	0.07	0.06	0.00	0.00	0.06	0.05
Si	0.01	0.04	0.08	0.00	0.01	0.11	0.13	0.20	0.16	0.44	0.20	0.14	0.83
CO_3	51.52	50.80	51.20	51.94	51.56	51.59	50.78	51.37	51.46	51.55	51.14	51.76	52.45
Total	99.25	97.80	98.40	99.79	99.01	98.81	97.40	98.12	98.28	97.76	97.70	98.77	98.21

	14	15	16	17	18	19	20	21	22	23	24	25	26
Fe	38.70	39.33	39.06	38.64	38.04	38.16	37.92	37.67	38.09	38.06	38.37	37.63	38.28
Mn	6.06	5.64	6.06	6.19	6.28	5.88	5.88	5.63	5.17	5.02	6.22	6.43	5.52
Mg	0.07	0.05	0.04	0.05	0.04	0.05	0.05	0.06	0.06	0.05	0.03	0.05	0.06
Ca	2.05	1.43	1.73	1.64	1.74	1.53	1.50	1.37	1.20	1.16	1.75	2.09	1.44
Zn	0.02	0.06	0.02	0.05	0.04	0.00	0.01	0.05	0.00	0.00	0.02	0.03	0.03
Si	0.02	0.28	0.05	0.15	0.27	0.43	0.50	0.83	1.05	1.13	0.29	0.25	0.71
CO_3	51.59	51.93	51.52	51.54	51.63	51.69	51.68	52.41	53.01	53.08	52.02	51.79	52.52
Total	98.52	98.72	98.49	98.26	98.03	97.74	97.54	98.02	98.58	98.51	98.71	98.26	98.56

Results are given as weight percent
Chemical composition of siderite spherule SUF.1.2a, clay ironstone, Ulingatangi Section, Suðuroy, Faeroe Islands

Sample SUF.1.2a

	27	28	29	30	31	32	33	34	35	36	37	38	39
Fe	38.20	39.34	39.83	40.00	39.76	41.13	41.54	40.97	43.68	43.38	44.14	45.79	45.82
Mn	5.73	5.54	4.87	4.90	5.27	4.10	3.78	4.05	2.08	1.94	1.62	0.84	0.71
Mg	0.07	0.03	0.04	0.06	0.07	0.05	0.05	0.08	0.04	0.08	0.07	0.05	0.06
Ca	1.67	1.54	1.37	1.40	1.83	1.33	1.55	2.15	1.30	1.87	1.78	0.96	1.12
Zn	0.02	0.04	0.07	0.05	0.04	0.01	0.00	0.04	0.03	0.12	0.02	0.04	0.00
Si	0.41	0.13	0.39	0.26	0.04	0.24	0.09	0.01	0.01	0.00	0.00	0.01	0.01
CO_3	51.75	51.32	51.99	51.75	51.58	51.84	51.62	51.98	51.31	51.86	52.10	51.77	51.89
Total	97.85	97.94	98.55	98.43	98.58	98.69	98.64	99.30	98.44	99.26	99.74	99.46	99.62

	40	41	42	43	44	45	46	Average
Fe	46.24	45.85	46.84	46.79	46.65	46.73	47.03	42.23
Mn	0.51	0.43	0.25	0.19	0.12	0.07	0.08	3.12
Mg	0.05	0.08	0.03	0.06	0.04	0.03	0.03	0.05
Ca	1.08	1.29	0.74	0.76	0.44	0.34	0.19	1.23
Zn	0.05	0.06	0.07	0.06	0.00	0.06	0.00	0.04
Si	0.06	0.02	0.00	0.05	0.23	0.07	0.12	0.23
CO_3	52.30	52.02	51.86	52.03	51.99	51.27	51.51	51.77
Total	100.29	99.75	99.79	99.94	99.47	98.58	98.96	98.66

Results are given as weight percent
Chemical composition of siderite spherule SUF.1.2a, clay ironstone, Ulingatangi Section, Suðuroy, Faeroe Islands

Sample SUF.1.2b

	1	2	3	4	5	6	7	8	9	10	11	12	13
Fe	46.58	46.50	46.77	46.46	47.27	46.75	46.51	46.05	45.77	44.89	44.13	43.46	44.04
Mn	0.11	0.11	0.14	0.18	0.17	0.21	0.25	0.57	0.68	1.01	1.50	1.85	1.94
Mg	0.03	0.02	0.02	0.05	0.02	0.02	0.05	0.05	0.06	0.04	0.08	0.08	0.06
Ca	0.27	0.37	0.38	0.68	0.39	0.58	0.66	1.14	0.81	1.32	1.72	1.76	1.35
Zn	0.04	0.01	0.03	0.04	0.00	0.07	0.03	0.00	0.07	0.04	0.06	0.07	0.03
Si	0.15	0.24	0.01	0.04	0.00	0.01	0.01	0.01	0.02	0.03	0.01	0.00	0.00
CO_3	51.33	51.74	51.13	51.49	51.63	51.50	51.43	51.97	51.41	51.60	51.95	51.65	51.63
Total	98.50	98.99	98.49	98.94	99.48	99.14	98.93	99.79	98.82	98.94	99.46	98.88	99.04

	14	15	16	17	18	19	20	21	22	23	24	25	26
Fe	43.24	42.31	40.69	41.77	42.36	41.76	41.00	41.75	42.08	41.37	42.35	41.92	43.09
Mn	2.47	3.23	4.14	3.71	3.58	3.91	4.15	4.00	3.57	4.11	3.40	3.56	2.70
Mg	0.08	0.05	0.08	0.07	0.05	0.07	0.06	0.05	0.05	0.07	0.06	0.07	0.06
Ca	1.46	1.48	2.06	1.63	1.17	1.61	1.79	1.52	1.42	1.81	1.43	1.66	1.24
Zn	0.00	0.09	0.00	0.04	0.04	0.05	0.06	0.01	0.00	0.08	0.00	0.05	0.06
Si	0.01	0.03	0.00	0.04	0.05	0.03	0.01	0.01	0.07	0.00	0.06	0.01	0.03
CO_3	51.59	51.56	51.54	51.73	51.56	51.91	51.53	51.66	51.68	51.94	51.79	51.69	51.44
Total	98.86	98.76	98.52	98.97	98.82	99.34	98.60	98.99	98.88	99.39	99.09	98.96	98.63

Results are given as weight percent
Chemical composition of siderite spherule SUF.1.2b, clay ironstone, Ulingatangi Section, Suðuroy, Faeroe Islands

Sample SUF.1.2b

	27	28	29	30	31	32	33	34	35	36	37	38	39
Fe	43.14	43.40	43.07	43.83	44.66	45.25	45.60	45.72	45.92	45.89	46.05	46.88	47.08
Mn	2.55	2.00	1.74	1.64	1.41	0.97	0.70	0.46	0.36	0.35	0.23	0.12	0.09
Mg	0.07	0.05	0.08	0.07	0.06	0.05	0.06	0.06	0.06	0.08	0.05	0.03	0.04
Ca	1.46	1.22	1.20	1.33	1.24	1.12	1.09	0.98	1.12	1.16	0.70	0.40	0.37
Zn	0.04	0.00	0.04	0.03	0.01	0.04	0.06	0.00	0.07	0.05	0.00	0.00	0.04
Si	0.04	0.11	0.16	0.08	0.01	0.01	0.05	0.05	0.03	0.01	0.07	0.05	0.02
CO_3	51.70	51.25	50.91	51.44	51.59	51.57	51.83	51.50	51.76	51.73	51.19	51.42	51.46
Total	99.00	98.03	97.20	98.42	98.98	99.00	99.39	98.77	99.31	99.28	98.28	98.90	99.10

	40	Average
Fe	47.06	44.36
Mn	0.09	1.70
Mg	0.02	0.05
Ca	0.34	1.14
Zn	0.02	0.03
Si	0.02	0.04
CO_3	51.31	51.57
Total	98.86	98.89

Results are given as weight percent
Chemical composition of siderite spherule SUF.1.2b, clay ironstone, Ulingatangi Section, Suðuroy, Faeroe Islands

Sample SUF.8.2a

	1	2	3	4	5	6	7	8	9	10	11	12	13
Fe	45.76	46.73	46.61	46.33	45.71	46.75	45.90	45.74	46.52	46.60	46.33	45.86	45.60
Mn	1.16	0.45	0.46	0.73	0.71	0.21	0.16	0.29	0.09	0.06	0.05	0.08	0.11
Mg	0.01	0.00	0.01	0.01	0.00	0.01	0.00	0.04	0.00	0.01	0.03	0.03	0.04
Ca	0.37	0.34	0.55	0.57	0.71	0.64	1.22	0.93	0.80	1.12	1.25	1.48	0.95
Zn	0.01	0.04	0.03	0.02	0.04	0.00	0.01	0.02	0.11	0.01	0.07	0.01	0.00
Si	0.01	0.05	0.01	0.04	0.13	0.09	0.12	0.23	0.02	0.04	0.08	0.10	0.53
CO_3	51.11	51.49	51.52	51.67	51.58	51.82	51.84	51.97	51.47	52.03	52.20	52.08	52.91
Total	98.44	99.11	99.19	99.37	98.89	99.51	99.25	99.23	99.00	99.87	100.00	99.64	100.15

	14	15	16	17	18	19	20	21	22	23	24	25	26
Fe	45.75	45.46	45.29	45.27	45.33	45.01	45.17	45.38	45.25	45.24	45.36	44.57	44.44
Mn	0.11	0.08	0.13	0.15	0.14	0.17	0.17	0.20	0.21	0.28	0.35	0.43	0.44
Mg	0.02	0.01	0.00	0.00	0.01	0.01	0.02	0.01	0.03	0.02	0.01	0.02	0.02
Ca	1.72	1.26	1.75	1.43	1.58	1.60	1.62	1.17	1.33	1.58	1.44	1.88	1.44
Zn	0.00	0.07	0.06	0.00	0.04	0.01	0.01	0.05	0.03	0.05	0.04	0.00	0.08
Si	0.03	0.10	0.03	0.08	0.07	0.09	0.05	0.18	0.32	0.16	0.12	0.16	0.24
CO_3	52.05	51.36	51.61	51.30	51.62	51.39	51.44	51.59	52.31	52.08	51.85	51.90	51.55
Total	99.68	98.34	98.86	98.23	98.80	98.29	98.48	98.58	99.49	99.41	99.18	98.96	98.20

Results are given as weight percent
Chemical composition of siderite spherule SUF.8.2a, ironstone, Rokhagi Section, Suðuroy, Faeroe Islands

Sample SUF.8.2a

	27	28	29	30	31	32	33	34	35	36	37	38	39
Fe	44.79	43.78	44.52	45.23	45.84	45.46	45.03	45.15	45.01	45.59	45.72	45.58	45.97
Mn	0.45	0.52	0.45	0.43	0.33	0.30	0.21	0.21	0.16	0.14	0.09	0.11	0.09
Mg	0.01	0.01	0.02	0.02	0.00	0.01	0.00	0.02	0.03	0.02	0.03	0.01	0.03
Ca	1.66	1.96	1.33	1.70	1.30	1.61	1.64	1.95	1.39	1.61	1.51	1.57	1.19
Zn	0.01	0.05	0.06	0.05	0.08	0.05	0.00	0.06	0.04	0.09	0.02	0.05	0.02
Si	0.09	0.16	0.31	0.03	0.06	0.05	0.10	0.06	0.22	0.02	0.02	0.04	0.14
CO_3	51.54	51.33	51.77	51.85	51.89	51.92	51.51	52.06	51.69	51.77	51.67	51.69	51.94
Total	98.54	97.83	98.46	99.31	99.49	99.41	98.49	99.52	98.54	99.24	99.06	99.04	99.37

	40	41	42	43	44	45	46	47	48	49	50	Average
Fe	45.72	45.43	46.26	45.56	46.17	46.26	46.20	46.03	45.68	46.20	45.75	45.62
Mn	0.09	0.07	0.10	0.31	0.15	0.24	0.51	0.73	0.79	0.40	0.74	0.30
Mg	0.03	0.04	0.00	0.03	0.01	0.00	0.02	0.01	0.02	0.04	0.01	0.02
Ca	1.30	1.25	0.94	0.80	0.77	0.64	0.56	0.51	0.34	0.29	0.23	1.18
Zn	0.00	0.04	0.00	0.01	0.06	0.00	0.00	0.04	0.01	0.00	0.02	0.03
Si	0.08	0.05	0.03	0.17	0.17	0.10	0.06	0.03	0.16	0.33	0.31	0.12
CO_3	51.60	51.11	51.37	51.31	51.72	51.35	51.35	51.20	51.22	52.02	51.69	51.69
Total	98.82	97.99	98.71	98.19	99.05	98.59	98.70	98.54	98.23	99.27	98.75	98.95

Results are given as weight percent
Chemical composition of siderite spherule SUF.8.2a, ironstone, Rokhagi Section, Suðuroy, Faeroe Islands

Sample SUF.8.2b

	1	2	3	4	5	6	7	8	9	10	11	12	13
Fe	46.35	46.83	46.70	45.62	45.94	46.20	46.00	45.17	45.64	46.42	46.02	46.07	45.60
Mn	0.67	0.54	0.43	0.99	0.66	0.52	0.21	0.33	0.34	0.14	0.05	0.10	0.10
Mg	0.02	0.02	0.01	0.01	0.02	0.02	0.01	0.05	0.03	0.00	0.03	0.02	0.01
Ca	0.31	0.25	0.30	0.68	0.60	0.40	0.93	0.87	1.10	0.89	1.06	1.12	0.96
Zn	0.03	0.00	0.02	0.00	0.00	0.01	0.07	0.00	0.04	0.00	0.01	0.04	0.06
Si	0.11	0.03	0.03	0.05	0.16	0.17	0.03	0.54	0.09	0.02	0.10	0.12	0.28
CO_3	51.57	51.48	51.29	51.39	51.75	51.60	51.28	52.63	51.59	51.47	51.64	51.89	51.82
Total	99.07	99.15	98.78	98.75	99.13	98.93	98.54	99.59	98.84	98.95	98.91	99.35	98.84

	14	15	16	17	18	19	20	21	22	23	24	25	26
Fe	45.67	45.72	45.05	44.77	45.27	45.19	44.47	44.88	44.63	45.06	44.99	44.81	45.06
Mn	0.10	0.12	0.13	0.19	0.17	0.16	0.21	0.23	0.32	0.24	0.31	0.22	0.21
Mg	0.02	0.03	0.02	0.01	0.01	0.02	0.02	0.02	0.03	0.01	0.04	0.04	0.01
Ca	1.30	1.27	1.29	1.65	1.96	1.54	1.48	1.53	2.11	1.23	1.23	1.37	1.11
Zn	0.06	0.02	0.00	0.07	0.04	0.06	0.00	0.00	0.06	0.00	0.07	0.01	0.02
Si	0.10	0.16	0.28	0.30	0.02	0.16	0.36	0.15	0.04	0.24	0.15	0.29	0.31
CO_3	51.70	51.95	51.75	52.19	51.91	51.82	51.85	51.44	51.79	51.60	51.32	51.79	51.69
Total	98.96	99.27	98.52	99.19	99.38	98.95	98.40	98.25	98.98	98.38	98.10	98.52	98.40

Results are given as weight percent
Chemical composition of siderite spherule SUF.8.2b, ironstone, Rokhagi Section, Suðuroy, Faeroe Islands

Sample SUF.8.2b

	27	28	29	30	31	32	33	34	35	36	37	38	39
Fe	44.15	44.20	44.58	44.41	45.08	44.60	45.57	44.98	45.21	45.42	44.64	44.86	45.52
Mn	0.25	0.25	0.39	0.33	0.23	0.19	0.12	0.22	0.14	0.12	0.29	0.15	0.11
Mg	0.10	0.02	0.01	0.03	0.02	0.01	0.04	0.04	0.02	0.01	0.08	0.05	0.03
Ca	1.08	1.14	1.77	1.30	0.96	1.19	0.85	0.80	0.92	1.00	0.90	0.77	0.98
Zn	0.00	0.08	0.00	0.06	0.00	0.00	0.01	0.02	0.07	0.01	0.03	0.04	0.00
Si	0.84	0.40	0.08	0.36	0.37	0.19	0.34	0.37	0.33	0.19	0.86	0.48	0.29
CO_3	53.16	51.32	51.34	51.71	51.75	50.76	51.96	51.47	51.66	51.29	53.53	51.76	51.81
Total	99.58	97.42	98.17	98.20	98.41	96.93	98.89	97.89	98.35	98.04	100.32	98.12	98.75

	40	41	42	43	44	45	46	47	48	49	50	Average
Fe	45.58	46.20	45.96	45.94	45.19	46.21	45.58	46.01	46.35	46.70	46.11	45.46
Mn	0.13	0.06	0.06	0.11	0.36	0.22	0.62	0.77	0.58	0.36	0.87	0.29
Mg	0.02	0.02	0.02	0.00	0.03	0.03	0.05	0.05	0.02	0.00	0.01	0.02
Ca	1.72	0.94	1.38	0.85	0.82	0.83	0.46	0.48	0.25	0.25	0.29	1.01
Zn	0.00	0.00	0.02	0.01	0.00	0.00	0.02	0.07	0.00	0.04	0.00	0.02
Si	0.05	0.09	0.04	0.18	0.38	0.11	0.34	0.16	0.07	0.14	0.13	0.22
CO_3	51.98	51.52	51.74	51.55	51.90	51.69	51.97	51.85	51.17	51.59	51.53	51.72
Total	99.48	98.82	99.22	98.65	98.68	99.08	99.05	99.37	98.45	99.08	98.95	98.76

Results are given as weight percent
Chemical composition of siderite spherule SUF.8.2b, ironstone, Rokhagi Section, Suðuroy, Faeroe Islands

Summary of samples SUF.1.2 & SUF.8.2

	Average compositions for Sample SUF.1.2			Average compositions for Sample SUF.8.2			Differences between Samples SUF.1.2 & SUF.8.2
	SUF.1.2a	SUF.1.2b	Overall	SUF.8.2a	SUF.8.2b	Overall	
Fe	42.23	44.36	43.22	45.62	45.46	45.54	-2.32
Mn	3.12	1.70	2.46	0.30	0.29	0.30	2.16
Mg	0.05	0.05	0.05	0.02	0.02	0.02	0.03
Ca	1.23	1.14	1.19	1.18	1.01	1.09	0.10
Zn	0.04	0.03	0.04	0.03	0.02	0.03	0.01
Si	0.23	0.04	0.14	0.12	0.22	0.17	-0.03
CO_3	51.77	51.57	51.67	51.69	51.72	51.71	-0.03
Total	98.66	98.89	98.77	98.95	98.76	98.85	-0.08

	SUF.1.2a			SUF.1.2b			SUF.8.2a			SUF.8.2b		
	Max	Min	Range	Max	Min	Range	Max	Min	Range	Max	Min	Range
Fe	47.11	37.63	9.48	47.27	40.69	6.58	46.75	43.78	2.96	46.83	44.15	2.68
Mn	6.43	0.07	6.36	4.15	0.09	4.06	1.16	0.05	1.11	0.99	0.05	0.95
Mg	0.08	0.00	0.08	0.08	0.02	0.07	0.04	0.00	0.04	0.10	0.00	0.10
Ca	2.15	0.19	1.96	2.06	0.27	1.80	1.96	0.23	1.73	2.11	0.25	1.86
Zn	0.12	0.00	0.12	0.09	0.00	0.09	0.11	0.00	0.11	0.08	0.00	0.08
Si	1.13	0.00	1.13	0.24	0.00	0.24	0.53	0.01	0.51	0.86	0.02	0.84
CO_3	53.08	50.78	2.30	51.97	50.91	1.07	52.91	51.11	1.80	53.53	50.76	2.77

Results are given as weight percent

A.3 Chemical Compositions Expressed as Carbonates

Sample SUF.1.2a

	1	2	3	4	5	6	7	8	9	10	11	12	13
$FeCO_3$	97.74	96.40	96.27	96.20	94.73	94.35	93.78	91.14	89.92	88.19	88.25	84.51	81.56
$MnCO_3$	0.25	0.19	0.38	0.73	1.21	1.23	1.42	3.09	4.21	4.86	6.34	9.45	9.13
$MgCO_3$	0.00	0.06	0.08	0.18	0.14	0.15	0.12	0.10	0.23	0.15	0.21	0.20	0.18
$CaCO_3$	1.11	0.81	1.12	2.58	2.81	2.42	1.26	2.60	2.96	2.23	1.82	3.74	2.88
$ZnCO_3$	0.10	0.10	0.11	0.08	0.08	0.06	0.13	0.13	0.11	0.00	0.00	0.12	0.09
$Si(CO_3)_2$	0.06	0.24	0.44	0.01	0.04	0.61	0.69	1.04	0.86	2.32	1.07	0.75	4.37
Total	99.25	97.80	98.40	99.79	99.01	98.81	97.40	98.12	98.28	97.76	97.70	98.77	98.21

	14	15	16	17	18	19	20	21	22	23	24	25	26
$FeCO_3$	80.29	81.61	81.04	80.18	78.93	79.18	78.67	78.15	79.02	78.97	79.61	78.07	79.43
$MnCO_3$	12.69	11.81	12.68	12.94	13.14	12.30	12.30	11.78	10.81	10.50	13.02	13.46	11.56
$MgCO_3$	0.25	0.18	0.14	0.16	0.14	0.17	0.17	0.21	0.19	0.18	0.12	0.16	0.21
$CaCO_3$	5.13	3.56	4.33	4.09	4.34	3.82	3.76	3.41	3.01	2.89	4.37	5.22	3.59
$ZnCO_3$	0.04	0.11	0.04	0.10	0.08	0.01	0.03	0.10	0.00	0.00	0.04	0.05	0.05
$Si(CO_3)_2$	0.12	1.46	0.25	0.79	1.41	2.28	2.62	4.37	5.54	5.97	1.55	1.29	3.73
Total	98.52	98.72	98.49	98.26	98.03	97.74	97.54	98.02	98.58	98.51	98.71	98.26	98.56

Results are given as weight percent

Chemical composition of siderite spherule SUF.1.2a, clay ironstone, Ulingatangi Section, Suðuroy, Faeroe Islands

Sample SUF.1.2a

	27	28	29	30	31	32	33	34	35	36	37	38	39
$FeCO_3$	79.26	81.62	82.63	82.99	82.48	85.33	86.19	85.00	90.61	90.00	91.58	94.99	95.07
$MnCO_3$	11.99	11.58	10.18	10.26	11.04	8.58	7.90	8.47	4.34	4.07	3.39	1.77	1.49
$MgCO_3$	0.23	0.12	0.15	0.21	0.23	0.16	0.19	0.28	0.14	0.29	0.25	0.17	0.22
$CaCO_3$	4.17	3.85	3.42	3.51	4.56	3.32	3.88	5.38	3.25	4.66	4.45	2.39	2.80
$ZnCO_3$	0.03	0.07	0.14	0.09	0.07	0.02	0.00	0.08	0.05	0.24	0.05	0.07	0.01
$Si(CO_3)_2$	2.18	0.69	2.03	1.37	0.20	1.29	0.48	0.08	0.04	0.00	0.03	0.07	0.03
Total	97.85	97.94	98.55	98.43	98.58	98.69	98.64	99.30	98.44	99.26	99.74	99.46	99.62

	40	41	42	43	44	45	46	Average
$FeCO_3$	95.94	95.12	97.18	97.08	96.79	96.95	97.57	87.62
$MnCO_3$	1.07	0.91	0.52	0.39	0.26	0.14	0.17	6.52
$MgCO_3$	0.16	0.28	0.10	0.19	0.14	0.11	0.10	0.17
$CaCO_3$	2.70	3.22	1.84	1.90	1.09	0.86	0.47	3.08
$ZnCO_3$	0.10	0.12	0.14	0.12	0.00	0.12	0.00	0.07
$Si(CO_3)_2$	0.33	0.10	0.00	0.25	1.19	0.39	0.65	1.20
Total	100.29	99.75	99.79	99.94	99.47	98.58	98.96	98.66

Results are given as weight percent

Chemical composition of siderite spherule SUF.1.2a, clay ironstone, Ulingatangi Section, Suðuroy, Faeroe Islands

Sample SUF.1.2b

	1	2	3	4	5	6	7	8	9	10	11	12	13
$FeCO_3$	96.63	96.48	97.04	96.39	98.07	97.00	96.49	95.55	94.97	93.12	91.56	90.17	91.36
$MnCO_3$	0.23	0.22	0.30	0.38	0.35	0.44	0.52	1.18	1.41	2.12	3.13	3.88	4.05
$MgCO_3$	0.11	0.09	0.06	0.17	0.08	0.08	0.16	0.16	0.20	0.13	0.28	0.28	0.20
$CaCO_3$	0.67	0.92	0.96	1.71	0.98	1.45	1.66	2.84	2.02	3.30	4.30	4.40	3.36
$ZnCO_3$	0.08	0.02	0.05	0.07	0.00	0.13	0.06	0.00	0.13	0.08	0.12	0.13	0.06
$Si(CO_3)_2$	0.79	1.27	0.08	0.22	0.00	0.04	0.05	0.06	0.08	0.18	0.06	0.03	0.00
Total	98.50	98.99	98.49	98.94	99.48	99.14	98.93	99.79	98.82	98.94	99.46	98.88	99.04

	14	15	16	17	18	19	20	21	22	23	24	25	26
$FeCO_3$	89.72	87.78	84.42	86.65	87.89	86.63	85.07	86.62	87.31	85.84	87.86	86.97	89.40
$MnCO_3$	5.17	6.76	8.66	7.77	7.49	8.19	8.68	8.38	7.47	8.61	7.11	7.44	5.66
$MgCO_3$	0.26	0.19	0.28	0.23	0.18	0.23	0.22	0.17	0.19	0.25	0.21	0.25	0.20
$CaCO_3$	3.66	3.70	5.16	4.07	2.93	4.02	4.46	3.78	3.56	4.52	3.56	4.15	3.10
$ZnCO_3$	0.00	0.17	0.00	0.07	0.08	0.10	0.12	0.01	0.01	0.16	0.00	0.09	0.12
$Si(CO_3)_2$	0.05	0.16	0.00	0.19	0.25	0.16	0.06	0.03	0.35	0.02	0.34	0.07	0.15
Total	98.86	98.76	98.52	98.97	98.82	99.34	98.60	98.99	98.88	99.39	99.09	98.96	98.63

Results are given as weight percent
Chemical composition of siderite spherule SUF.1.2b, clay ironstone, Ulingatangi Section, Suðuroy, Faeroe Islands

Sample SUF.1.2b

	27	28	29	30	31	32	33	34	35	36	37	38	39
$FeCO_3$	89.49	90.04	89.36	90.93	92.65	93.87	94.60	94.85	95.26	95.22	95.53	97.27	97.68
$MnCO_3$	5.33	4.19	3.64	3.42	2.94	2.03	1.47	0.96	0.75	0.74	0.48	0.25	0.19
$MgCO_3$	0.23	0.19	0.27	0.25	0.22	0.18	0.22	0.22	0.20	0.26	0.16	0.09	0.13
$CaCO_3$	3.65	3.05	2.99	3.31	3.09	2.79	2.72	2.45	2.81	2.90	1.76	1.01	0.93
$ZnCO_3$	0.08	0.00	0.08	0.06	0.02	0.07	0.11	0.00	0.13	0.10	0.00	0.01	0.07
$Si(CO_3)_2$	0.21	0.58	0.85	0.44	0.06	0.06	0.28	0.29	0.16	0.07	0.36	0.29	0.10
Total	99.00	98.03	97.20	98.42	98.98	99.00	99.39	98.77	99.31	99.28	98.28	98.90	99.10

	40	Average
$FeCO_3$	97.64	92.03
$MnCO_3$	0.18	3.55
$MgCO_3$	0.05	0.19
$CaCO_3$	0.86	2.84
$ZnCO_3$	0.04	0.07
$Si(CO_3)_2$	0.08	0.21
Total	98.86	98.89

Results are given as weight percent
Chemical composition of siderite spherule SUF.1.2b, clay ironstone, Ulingatangi Section, Suðuroy, Faeroe Islands

Sample SUF.8.2a

	1	2	3	4	5	6	7	8	9	10	11	12	13
$FeCO_3$	94.93	96.96	96.70	96.12	94.84	96.99	95.22	94.91	96.52	96.67	96.12	95.14	94.61
$MnCO_3$	2.43	0.94	0.95	1.54	1.48	0.43	0.33	0.60	0.18	0.12	0.10	0.17	0.24
$MgCO_3$	0.05	0.00	0.04	0.04	0.00	0.04	0.02	0.13	0.00	0.03	0.09	0.09	0.15
$CaCO_3$	0.93	0.86	1.38	1.42	1.78	1.60	3.05	2.33	1.99	2.79	3.11	3.69	2.36
$ZnCO_3$	0.03	0.07	0.06	0.03	0.08	0.00	0.02	0.05	0.20	0.02	0.13	0.03	0.00
$Si(CO_3)_2$	0.07	0.28	0.07	0.22	0.71	0.46	0.61	1.21	0.10	0.24	0.44	0.52	2.78
Total	98.44	99.11	99.19	99.37	98.89	99.51	99.25	99.23	99.00	99.87	100.00	99.64	100.15

	14	15	16	17	18	19	20	21	22	23	24	25	26
$FeCO_3$	94.92	94.31	93.95	93.93	94.05	93.38	93.71	94.14	93.89	93.85	94.11	92.47	92.19
$MnCO_3$	0.22	0.17	0.27	0.30	0.30	0.35	0.35	0.41	0.44	0.59	0.74	0.89	0.92
$MgCO_3$	0.08	0.05	0.00	0.00	0.04	0.05	0.08	0.04	0.10	0.07	0.03	0.07	0.06
$CaCO_3$	4.29	3.15	4.37	3.58	3.93	4.00	4.05	2.93	3.33	3.96	3.61	4.70	3.60
$ZnCO_3$	0.00	0.13	0.11	0.00	0.08	0.03	0.01	0.09	0.06	0.10	0.08	0.00	0.15
$Si(CO_3)_2$	0.16	0.52	0.16	0.42	0.38	0.49	0.28	0.97	1.68	0.84	0.61	0.83	1.28
Total	99.68	98.34	98.86	98.23	98.80	98.29	98.48	98.58	99.49	99.41	99.18	98.96	98.20

Results are given as weight percent
Chemical composition of siderite spherule SUF.8.2a, ironstone, Rokhagi Section, Suðuroy, Faeroe Islands

Sample SUF.8.2a

	27	28	29	30	31	32	33	34	35	36	37	38	39
$FeCO_3$	92.92	90.84	92.36	93.83	95.10	94.32	93.43	93.67	93.38	94.58	94.86	94.56	95.37
$MnCO_3$	0.93	1.09	0.94	0.90	0.70	0.64	0.45	0.45	0.34	0.29	0.19	0.22	0.18
$MgCO_3$	0.04	0.05	0.08	0.06	0.01	0.05	0.00	0.08	0.10	0.06	0.11	0.02	0.09
$CaCO_3$	4.14	4.90	3.33	4.26	3.24	4.03	4.10	4.88	3.48	4.02	3.76	3.92	2.98
$ZnCO_3$	0.02	0.10	0.11	0.10	0.15	0.10	0.00	0.11	0.08	0.17	0.03	0.10	0.04
$Si(CO_3)_2$	0.48	0.85	1.65	0.17	0.30	0.29	0.51	0.33	1.17	0.10	0.11	0.22	0.72
Total	98.54	97.83	98.46	99.31	99.49	99.41	98.49	99.52	98.54	99.24	99.06	99.04	99.37

	40	41	42	43	44	45	46	47	48	49	50	Average
$FeCO_3$	94.86	94.25	95.97	94.53	95.79	95.99	95.85	95.50	94.78	95.85	94.91	94.64
$MnCO_3$	0.19	0.15	0.22	0.65	0.30	0.49	1.07	1.52	1.65	0.83	1.55	0.63
$MgCO_3$	0.09	0.14	0.01	0.10	0.04	0.01	0.06	0.04	0.06	0.13	0.05	0.06
$CaCO_3$	3.24	3.12	2.35	2.01	1.92	1.59	1.41	1.27	0.85	0.72	0.58	2.94
$ZnCO_3$	0.00	0.08	0.00	0.01	0.12	0.01	0.00	0.08	0.02	0.00	0.03	0.06
$Si(CO_3)_2$	0.45	0.25	0.16	0.89	0.87	0.51	0.31	0.14	0.87	1.74	1.62	0.62
Total	98.82	97.99	98.71	98.19	99.05	98.59	98.70	98.54	98.23	99.27	98.75	98.95

Results are given as weight percent
Chemical composition of siderite spherule SUF.8.2a, ironstone, Rokhagi Section, Suðuroy, Faeroe Islands

Sample SUF.8.2b

	1	2	3	4	5	6	7	8	9	10	11	12	13
$FeCO_3$	96.17	97.16	96.89	94.66	95.31	95.85	95.44	93.72	94.70	96.32	95.47	95.59	94.61
$MnCO_3$	1.41	1.13	0.89	2.08	1.39	1.09	0.45	0.68	0.72	0.29	0.10	0.21	0.21
$MgCO_3$	0.06	0.09	0.03	0.03	0.09	0.07	0.03	0.18	0.11	0.01	0.11	0.08	0.03
$CaCO_3$	0.78	0.62	0.76	1.69	1.49	1.01	2.33	2.18	2.76	2.22	2.65	2.80	2.41
$ZnCO_3$	0.06	0.00	0.03	0.00	0.00	0.03	0.13	0.00	0.07	0.01	0.01	0.07	0.12
$Si(CO_3)_2$	0.59	0.16	0.17	0.29	0.86	0.87	0.15	2.83	0.48	0.11	0.55	0.61	1.46
Total	99.07	99.15	98.78	98.75	99.13	98.93	98.54	99.59	98.84	98.95	98.91	99.35	98.84

	14	15	16	17	18	19	20	21	22	23	24	25	26
$FeCO_3$	94.75	94.86	93.47	92.89	93.93	93.76	92.26	93.11	92.60	93.48	93.33	92.96	93.48
$MnCO_3$	0.22	0.26	0.28	0.39	0.35	0.34	0.43	0.48	0.66	0.50	0.65	0.47	0.43
$MgCO_3$	0.08	0.09	0.07	0.05	0.02	0.07	0.09	0.05	0.11	0.05	0.13	0.13	0.03
$CaCO_3$	3.25	3.16	3.21	4.12	4.89	3.85	3.70	3.83	5.27	3.07	3.07	3.42	2.76
$ZnCO_3$	0.11	0.03	0.00	0.14	0.07	0.12	0.00	0.00	0.11	0.00	0.13	0.02	0.04
$Si(CO_3)_2$	0.55	0.87	1.49	1.60	0.11	0.82	1.92	0.77	0.23	1.28	0.79	1.52	1.65
Total	98.96	99.27	98.52	99.19	99.38	98.95	98.40	98.25	98.98	98.38	98.10	98.52	98.40

Results are given as weight percent
Chemical composition of siderite spherule SUF.8.2b, ironstone, Rokhagi Section, Suðuroy, Faeroe Islands

Sample SUF.8.2b

	27	28	29	30	31	32	33	34	35	36	37	38	39
$FeCO_3$	91.61	91.71	92.49	92.13	93.53	92.52	94.55	93.32	93.79	94.23	92.61	93.08	94.44
$MnCO_3$	0.53	0.52	0.81	0.69	0.48	0.39	0.25	0.45	0.30	0.25	0.61	0.31	0.24
$MgCO_3$	0.34	0.05	0.03	0.11	0.07	0.04	0.14	0.14	0.08	0.03	0.26	0.17	0.11
$CaCO_3$	2.70	2.86	4.43	3.24	2.40	2.97	2.11	1.99	2.29	2.50	2.24	1.93	2.44
$ZnCO_3$	0.00	0.16	0.01	0.11	0.01	0.00	0.01	0.03	0.13	0.03	0.06	0.08	0.01
$Si(CO_3)_2$	4.41	2.12	0.41	1.92	1.93	1.01	1.82	1.96	1.75	1.01	4.54	2.56	1.51
Total	99.58	97.42	98.17	98.20	98.41	96.93	98.89	97.89	98.35	98.04	100.32	98.12	98.75

	40	41	42	43	44	45	46	47	48	49	50	Average
$FeCO_3$	94.56	95.85	95.36	95.31	93.76	95.87	94.57	95.46	96.17	96.89	95.65	94.32
$MnCO_3$	0.26	0.12	0.13	0.24	0.76	0.45	1.29	1.60	1.22	0.76	1.81	0.61
$MgCO_3$	0.07	0.06	0.06	0.00	0.11	0.11	0.19	0.16	0.06	0.00	0.04	0.09
$CaCO_3$	4.29	2.34	3.45	2.13	2.04	2.06	1.15	1.20	0.64	0.63	0.73	2.52
$ZnCO_3$	0.00	0.00	0.04	0.02	0.00	0.01	0.04	0.13	0.00	0.08	0.00	0.05
$Si(CO_3)_2$	0.29	0.45	0.19	0.95	2.01	0.58	1.81	0.82	0.37	0.72	0.70	1.17
Total	99.48	98.82	99.22	98.65	98.68	99.08	99.05	99.37	98.45	99.08	98.95	98.76

Results are given as weight percent
Chemical composition of siderite spherule SUF.8.2b, ironstone, Rokhagi Section, Suðuroy, Faeroe Islands

Summary of samples SUF.1.2 & SUF.8.2

	Average compositions for Sample SUF.1.2			Average compositions for Sample SUF.8.2			Differences between Samples SUF.1.2 & SUF.8.2
	SUF.1.2a	SUF.1.2b	Overall	SUF.8.2a	SUF.8.2b	Overall	
$FeCO_3$	87.62	92.03	89.67	94.64	94.32	94.48	-4.81
$MnCO_3$	6.52	3.55	5.14	0.63	0.61	0.62	4.52
$MgCO_3$	0.17	0.19	0.18	0.06	0.09	0.07	0.11
$CaCO_3$	3.08	2.84	2.97	2.94	2.52	2.73	0.24
$ZnCO_3$	0.07	0.07	0.07	0.06	0.05	0.05	0.02
$Si(CO_3)_2$	1.20	0.21	0.74	0.62	1.17	0.90	-0.15
Total	98.66	98.89	98.77	98.95	98.76	98.85	-0.08

	SUF.1.2a			SUF.1.2b			SUF.8.2a			SUF.8.2b		
	Max	Min	Range	Max	Min	Range	Max	Min	Range	Max	Min	Range
$FeCO_3$	97.74	78.07	19.67	98.07	84.42	13.64	96.99	90.84	6.15	97.16	91.61	5.55
$MnCO_3$	13.46	0.14	13.32	8.68	0.18	8.50	2.43	0.10	2.33	2.08	0.10	1.98
$MgCO_3$	0.29	0.00	0.29	0.28	0.05	0.23	0.15	0.00	0.15	0.34	0.00	0.34
$CaCO_3$	5.38	0.47	4.91	5.16	0.67	4.49	4.90	0.58	4.32	5.27	0.62	4.65
$ZnCO_3$	0.24	0.00	0.24	0.17	0.00	0.17	0.20	0.00	0.20	0.16	0.00	0.16
$Si(CO_3)_2$	5.97	0.00	5.97	1.27	0.00	1.27	2.78	0.07	2.71	4.54	0.11	4.43

Results are given as weight percent

Appendix B: Geochemical Calculations

To determine total iron (FeO^T) ferric iron (Fe_2O_3) needs to be converted to ferrous iron (FeO); this is done in the following equation:

$$FeO = Fe_2O_3 \times 0.89981$$

Therefore:

$$FeO^T = FeO + (Fe_2O_3 \times 0.89981)$$

For calculating Mg # FeO^T needs to be adjusted using the fixed oxidation ratio of 0.15 (Brooks 1976); this is expressed as follows:

$$\frac{Fe_2O_3}{FeO} = 0.15$$

To obtain adjusted iron a conversion factor (CF) needs to be obtained by using the following equation:

$$\frac{FeO^T}{CF} = \mathrm{FeO}$$

Therefore:

$$\frac{FeO^T}{FeO} = CF$$

$$\frac{FeO + (Fe_2O_3 \times 0.89981)}{FeO} = CF$$

$$\frac{FeO}{FeO} + \frac{Fe_2O_3 \times 0.89981}{FeO} = CF$$

$$1 + \left(\left(\frac{Fe_2O_3}{FeO}\right) \times 0.89981\right) = CF$$

$$1 + (0.15 \times 0.89981) = CF$$

$$1 + 0.1349715 = CF$$

$$1.1349715 = CF$$

$$\frac{FeO^T}{1.135} = Adjusted\ FeO$$

The adjusted FeO using the conversion factor of 1.135 is used to obtain atomic Mg # in the following equation:

$$Mg\ \# = 100 \times \frac{Mg}{Mg + Fe^2}$$

Where:

$$Mg = \frac{MgO}{40.32}$$

$$Fe^2 = \frac{Adjusted\ FeO}{71.85}$$

This gives the following equation:

$$Mg\ \# = \frac{\left(\frac{MgO}{40.32}\right)}{\left(\frac{MgO}{40.32}\right) + \left(\frac{FeO^T/1.135}{71.85}\right)}$$

This can be simplified using the following equations:

$$Mg\ \# = \frac{\left(\frac{MgO}{40.32}\right)}{\left(\frac{MgO}{40.32}\right) + \left(\frac{FeO^T}{1.135} \times \frac{1}{71.85}\right)}$$

$$Mg\ \# = \frac{\left(\frac{MgO}{40.32}\right)}{\left(\frac{MgO}{40.32}\right) + \left(\frac{FeO^T}{81.55}\right)}$$

$$Mg\ \# = \frac{\left(\frac{MgO}{40.32} \times 40.32\right)}{\left(\frac{MgO}{40.32} \times 40.32\right) + \left(\frac{FeO^T}{81.55} \times 40.32\right)}$$

$$Mg\ \# = \frac{\left(\frac{40.32 \times MgO}{40.32}\right)}{\left(\frac{40.32 \times MgO}{40.32}\right) + \left(\frac{40.32 \times FeO^T}{81.55}\right)}$$

$$Mg\ \# = \frac{MgO}{MgO + (0.4944 \times FeO^T)}$$

Even though this equation manipulates oxide values, the Mg # is given as an atomic value. This equation is used in Larsen *et al.* (1999) (L.M. Larsen *pers. comm.*).

Appendix C: Sample List

C.1 Lower Basalt Formation

Sample #	Lithology	Location	Geology
SUF.7.1	Aphyric Basalt	Disused quarry, *ca.* 1 km SW of Hvalba, Suðuroy, Faeroe Islands	Uppermost lava flow of the LBF
SUF.9.1	Volcaniclastic Conglomerate	Coastal section, *ca.* 1 km E of Froðba, Suðuroy, Faeroe Islands	Interlava sequence inbetween the Kúlugjógv and Skarvatangi lava flows
SUF.9.2	Volcaniclastic Siltstone		
SUF.10.1	Argillite	Roadside cutting, *ca.* 500 m E of the southern entrance to the road tunnel at Liðarhagi, Suðuroy, Faeroe Islands	Interlava lithology inbetween two tabular lava flows of the LBF
SUF.11.1	Volcaniclastic Siltstone	Coastal section, Hvalbiareiði Bay, *ca.* 1.5 km SW of Hvalba, Suðuroy, Faeroe Islands	Interlava sequence below the Hvalbiarciði Lava Flow

C.2 Coal-bearing Formation

Sample #	Lithology	Location	Geology
SUF.1.1	Unit 2: Volcaniclastic Sandstone	Ulingatangi Section, *ca.* 300 m N of Ulingatangi, *ca.* 1.2 km E of Froðba, Suðuroy, Faeroe Islands	Interlava sequence inbetween the LBF and MBF
SUF.1.2	Unit 3: Clay Ironstone		
SUF.1.3	Unit 6: Organic-rich Mudstone		
SUF.1.4	Devitrified Basaltic Tuff		
SUF.1.5	Clay Ironstone Concretion from Unit 6		
SUF.6.1	Fine to Medium grained Basaltic Sandstone	Grímsfjall Section, *ca.* 1.5 km W of Hvalba, Suðuroy, Faeroe Islands	Interlava sequence inbetween the LBF and MBF
SUF.6.2	Fine to Medium Grained Basaltic Sandstone		
SUF.6.3	Coarse Sand to Granule Grade Basaltic Sandstone		
SUF.8.2	Ironstone	Rokhagi mine, E side of Rokhagi valley, *ca.* 3.5 km SE of Hvalba, Suðuroy, Faeroe Islands	Collected from the mine waste

C.3 Volcaniclastic Sandstone Formation

Sample #	Lithology	Location	Geology
SUF.2.1	Tuffaceous Sandstone	Coastal section N of Stapin, Hvannhagi-Lónin Traverse, *ca.* 2.5 km N of Tvøroyri, Suðuroy, Faeroe Islands	Raft contained within doleritic sills
SUF.3.1	Dolerite	Wave cut platform S of Stapin, Hvannhagi-Lónin Traverse, *ca.* 2.5 km N of Tvøroyri, Suðuroy, Faeroe Islands	Sill
SUF.3.2	Agglomerate		Stapin Vent sequence from the uppermost section of the LBF
SUF.4.1	Unit 6: Volcaniclastic Conglomerate	Section III, Dysjarnar Traverse, *ca.* 200 m E of Dysjarnar, Hvannhagi-Lónin Traverse, *ca.* 2.5 km N of Tvøroyri, Suðuroy, Faeroe Islands	Volcaniclastic sequence inbetween doleritic sills and the MBF
SUF.4.2	Unit 5: Olivine-phyric Welded Tuff		
SUF.4.3	Unit 2: Olivine-phyric Tuff		
SUF.5.1	Unit 4: Volcaniclastic Sandstone	Section II, Dysjarnar Traverse, *ca.* 360 m E of Dysjarnar, Hvannhagi-Lónin Traverse, *ca.* 2.5 km N of Tvøroyri, Suðuroy, Faeroe Islands	Volcaniclastic sequence inbetween doleritic sills and the MBF
SUF.5.2	Unit 3: Volcaniclastic Mudstone		
SUF.5.3	Unit 3: Volcaniclastic Sandstone		
SUF.5.4	Unit 2: Olivine-phyric Tuff		
SUF.12.1	Shale	Wave cut platform S of Stapin, Hvannhagi-Lónin Traverse, *ca.* 2.5 km N of Tvøroyri, Suðuroy, Faeroe Islands	Sedimentary sequence overlying the Stapin Vent
SUF.12.2	Coal		
SUF.13.1	Unit 9: Volcaniclastic Sandstone	Section B, Svalbarðaá-Myllá Traverse, *ca.* 500 m N of Trongisvágur, Suðuroy, Faeroe Islands	Volcaniclastic sequence inbetween doleritic sills and the MBF
SUF.13.2	Unit 8: Volcaniclastic Conglomerate		
SUF.13.3	Unit 7: Olivine-phyric Tuff		
SUF.13.4			
SUF.13.5	Unit 5: Volcaniclastic Sandstone		

Sample #	Lithology	Location	Geology
SUF.13.6	Unit 3: Interbedded Volcaniclastic Siltstones and Sandstones	Section B, Svalbarðaá-Myllá Traverse, *ca.* 500 m N of Trongisvágur, Suðuroy, Faeroe Islands	Volcaniclastic sequence inbetween doleritic sills and the MBF
SUF.13.7	Unit 1: Olivine-phyric Tuff		
SUF.14.1	Unit 7: Olivine-phyric Tuff	Section C, Svalbarðaá-Myllá Traverse, *ca.* 500 m N of Trongisvágur, Suðuroy, Faeroe Islands	Volcaniclastic sequence inbetween doleritic sills and the MBF
SUF.14.2	Unit 1: Olivine-phyric Tuff		
SUF.16.1	Olivine-phyric Tuff	Reyðibarmur Section, *ca.* 1.6 km NE of Hvalba, Suðuroy, Faeroe Islands	Volcaniclastic sequence inbetween a peperite sequence and the MBF
SUF.18.1	Unit 2: Tuffaceous Sandstone	Hvannagjógv Section, *ca.* 2.5 km WNW of Trongisvágur, Suðuroy, Faeroe Islands	Volcaniclastic sequence intercalated with MBF lava flows
SUF.18.2	Unit 1: Tuffaceous Sandstone		

C.4 Middle Basalt Formation

Sample #	Lithology	Location	Geology
EYF.1.1	Unit 1: Volcaniclastic Sandstone	Eiði Section, roadside cutting, *ca.* 300 m E of Eiði, Eysturoy, Faeroe Islands	Interlava sequence inbetween MBF lava flow units
EYF.1.2	Unit 2: Volcaniclastic Sandstone		
EYF.2.3	Volcaniclastic Sandstone	Roadside cutting at Hvílingarsteinur, *ca.* 1.6 km SW of Slættaratindur and *ca.* 300 m NE of Eiðisvatn, Eysturoy, Faeroe Islands	Interlava sequence inbetween MBF lava flow units
EYF.3.2	Volcaniclastic Sandstone	Disused quarry, *ca.* 600 m N of Svínáir, Eysturoy, Faeroe Islands	Interlava sequence inbetween MBF lava flow units
STF.2.1	Unit 1: Volcaniclastic Sandstone	Ærgisá Section, *ca.* 2.5 km N of Leynar, Streymoy, Faeroe Islands	20 m section through the MBF
STF.2.2	Unit 2: Volcaniclastic Sandstone		
STF.2.3	Unit 3: Volcaniclastic Sandstone		

Sample #	Lithology	Location	Geology
STF.2.4	Unit 4: Volcaniclastic Sandstone	Ærgisá Section, *ca.* 2.5 km N of Leynar, Streymoy, Faeroe Islands	20 m section through the MBF
STF.3.1	Volcaniclastic Sandstone with leaf imprint	í Bugum Section, roadside cutting, *ca.* 2 km ESE of Hósvík, Streymoy, Faeroe Islands	Interlava sequence inbetween MBF lava flow units
STF.3.2	Volcaniclastic Sandstone		
STF.4.1	Volcaniclastic Sandstone	Klivarnar Section, roadside cutting, SE side of Leynavatn, *ca.* 1 km NNE of Leynar, Streymoy, Faeroe Islands	Interlava sequence inbetween MBF lava flow units
VAF.1.2	Volcaniclastic Sandstone	Cliff exposure, Stórabrugv, 17 km SE of Oyragjógv, Vágar, Faeroe Islands	Interlava sequence inbetween MBF lava flow units
VIF.1.1	Unit 2a: Volcaniclastic Sandstone	Viðareiði Section, coastal exposure, Viðoy, Faeroe Islands	Middle sedimentary package inbetween MBF lava flow units
VIF.1.2	Unit 2b: Volcaniclastic Conglomerate		
VIF.1.3	Unit 3: Volcaniclastic Siltstone		Upper sedimentary package inbetween MBF lava flow units
VIF.5.1	Aphyric Basalt	Disused quarry at Selgjógv, *ca.* 3.5 km NW of Hvannasund, Viðoy, Faeroe Islands	Middle Basalt Formation lava flow units
VIF.5.2	Plagioclase-phyric Basalt		

C.5 Upper Basalt Formation

Sample #	Lithology	Location	Geology
BOF.1.1	Unit 1: Volcaniclastic Sandstone	Hálgafelli Section, *ca.* 200 m SE of Hálgafelli, *ca.* 420-430 above sea level, *ca.* 1 km SW of Klaksvík, Borðoy, Faeroe Islands	Interlava sequence inbetween tabular and agglutinated lava flows of the UBF
BOF.1.2	Unit 3: Volcaniclastic Sandstone		
BOF.1.3	Basalt		Agglutinated lava flow
BOF.1.4	Unit 5: Volcaniclastic Siltstone		Interlava sequence inbetween agglutinated and tabular lava flows of the UBF
BOF.1.5	Unit 2: Volcaniclastic Siltstone		Interlava sequence inbetween tabular and agglutinated lava flows of the UBF
FUF.1.1	Unit 1: Volcaniclastic Sandstone	Kirkja Section, *ca.* 50 m E of Kirkja harbour, Fugloy, Faeroe Islands	Interlava sequence inbetween two tabular lava flows of the UBF

Sample #	Lithology	Location	Geology
FUF.1.2	Unit 2: Volcaniclastic Sandstone	Kirkja Section, *ca.* 50 m E of Kirkja harbour, Fugloy, Faeroe Islands	Interlava sequence inbetween two tabular lava flows of the UBF
FUF.1.3	Unit 3: Volcaniclastic Sandstone		
KUF.1.1	Unit 1: Volcaniclastic Sandstone	Kunoy Section, *ca.* 500 m above sea level, *ca.* 800 m S of Middagsfjall, *ca.* 1.5 km NE of Kunoy, Kunoy, Faeroe Islands	Interlava lithology inbetween two tabular lava flows of the UBF
KUF.1.2	Unit 2: Volcaniclastic Sandstone	Kunoy Section, *ca.* 520 m above sea level, *ca.* 800 m S of Middagsfjall, *ca.* 1.5 km NE of Kunoy, Kunoy, Faeroe Islands	Interlava lithology inbetween two tabular lava flows of the UBF
KUF.1.3	Unit 3: Volcaniclastic Sandstone	Kunoy Section, *ca.* 600 m above sea level, *ca.* 800 m S of Middagsfjall, *ca.* 1.5 km NE of Kunoy, Kunoy, Faeroe Islands	Interlava lithology inbetween two tabular lava flows of the UBF
KUF.1.4	Unit 4: Volcaniclastic Sandstone	Kunoy Section, *ca.* 730 m above sea level, *ca.* 800 m S of Middagsfjall, *ca.* 1.5 km NE of Kunoy, Kunoy, Faeroe Islands	Interlava lithology inbetween two tabular lava flows of the UBF
KUF.1.5	Unit 5: Volcaniclastic Sandstone	Kunoy Section, *ca.* 780 m above sea level, *ca.* 800 m S of Middagsfjall, *ca.* 1.5 km NE of Kunoy, Kunoy, Faeroe Islands	Interlava lithology inbetween two tabular lava flows of the UBF
SAF.1.1	Unit 1: Volcaniclastic Sandstone	Lítlavatn Section, roadside cutting between Sandur and Skálavík, *ca.* 400 m N of Lítlavatn, Sandoy, Faeroe Islands	Interlava sequence inbetween two tabular lava flows of the UBF
SAF.1.2	Unit 2: Volcaniclastic Sandstone		
SAF.1.3	Unit 3: Volcaniclastic Sandstone		
STF.1.1	Basalt	Sneis Section, plateau region *ca.* 60-100 m below Sneis, *ca.* 6 km ENE of Vestmanna, Streymoy, Faeroe Islands	Sill
STF.1.5	Unit 2: Volcaniclastic Conglomerate		Sedimentary sequence inbetween the MBF and UBF.
STF.1.6	Unit 1: Volcaniclastic Sandstone	Sneis Section, *ca.* 800 m NW of Sneis, *ca.* 6 km ENE of Vestmanna, Streymoy, Faeroe Islands	
STF.1.7	Unit 3: Volcaniclastic Sandstone	Sneis Section, *ca.* 400 m NW of Sneis, *ca.* 6 km ENE of Vestmanna, Streymoy, Faeroe Islands	

Sample #	Lithology	Location	Geology
STF.1.9	Unit 2: Volcaniclastic Conglomerate	Sneis Section, plateau region *ca.* 60-100 m below Sneis, *ca.* 6 km ENE of Vestmanna, Streymoy, Faeroe Islands	Sedimentary sequence inbetween the MBF and UBF.
STF.1.11	Unit 2: Reddened Volcaniclastic Conglomerate		
STF.6.1	Unit 2: Volcaniclastic Sandstone	Argir Section, *ca.* 600 m E of Itróttavøllur, *ca.* 1 km W of Argir, Streymoy, Faeroe Islands	Interlava sequence inbetween two tabular lava flows of the UBF
STF.6.2	Unit 3: Volcaniclastic Siltstone		
STF.6.3	Unit 4: Volcaniclastic Sandstone		
STF.6.4	Unit 1: Volcaniclastic Sandstone		
VIF.2.1	Volcaniclastic Sandstone	Gjógvin Stóra Section, *ca.* 100-150 m above sea level, *ca.* 5 km SE of Viðareiði, Viðoy, Faeroe Islands	25 m section through the lower section of the UBF
VIF.2.2	Volcaniclastic Conglomerate		
VIF.3.5	Aphyric Basalt	N side of Malinsfjall, *ca.* 1.5 km S of Viðareiði, Viðoy, Faeroe Islands	Upper Basalt Formation tabular lava flow
VIF.4.1	Pyroclastic Breccia	Húsið millum Gjáir, *ca.* 250 m S of Gjógvin Stóra, W side of Viðvík, *ca.* 5 km SE of Viðareiði, Viðoy, Faeroe Islands	Gas streaming vent juxtaposed against the uppermost MBF lava flow units

C.6 Faeroe-Shetland Basin

Well 214/4-1 61° 57' 54'' N, 002° 14' 01'' W			
Run #	**Sidewall Core #**	**Depth in ft (m)**	**Lithology**
3a	13	12,787 (3,897)	Unit 6b: Quartz Wacke
	12	12,793 (3,899)	Unit 6a: Quartz Wacke
	11	12,802 (3,902)	Unit 5b: Lithic Greywacke
	9	12,830 (3,911)	Unit 5a: Lithic Greywacke
	7	12,880 (3,926)	Unit 4e: Lithic Greywacke
	5	12,916 (3,937)	Unit 4d: Lithic Greywacke
	4	12,933 (3,942)	Unit 4c: Quartz Wacke
	3	12,941 (3,944)	Unit 4b: Lithic Greywacke
	1	12,979 (3,956)	Unit 4a: Siltstone
3b	44	13,212 (4,027)	Unit 2: Siltstone
	42	13,280 (4,048)	Unit 1: Hyaloclastite
	41	13,320 (4,060)	
	40	13,360 (4,072)	
	39	13,400 (4,084)	

Well 214/4-1 61° 57' 54'' N, 002° 14' 01'' W			
Run #	**Sidewall Core #**	**Depth in ft (m)**	**Lithology**
Run 3b	38	13,430 (4,093)	Unit 1: Hyaloclastite
	37	13,460 (4,103)	
	36	13,500 (4,115)	
	35	13,550 (4,130)	
	34	13,580 (4,139)	
	33	13,600 (4,145)	
	32	13,630 (4,154)	
	31	13,660 (4,164)	
	30	13,680 (4,170)	
	29	13,700 (4,176)	
	28	13,720 (4,182)	
	27	13,740 (4,188)	
	25	13,780 (4,200)	
	23	13,820 (4,212)	
	22	13,840 (4,218)	
	21	13,860 (4,225)	
	20	13,880 (4,231)	Calcite Vein
	19	13,890 (4,234)	Unit 1: Hyaloclastite
	18	13,900 (4,237)	
	17	13,920 (4,243)	
	16	13,940 (4,249)	
	15	13,960 (4,255)	
	14	13,980 (4,261)	
	13	14,000 (4,267)	
	12	14,020 (4,273)	
	11	14,040 (4,279)	
	7	14,120 (4,304)	
	6	14,140 (4,310)	
	5	14,160 (4,316)	
	4	14,180 (4,322)	
	3	14,200 (4,328)	
	1	14,240 (4,340)	

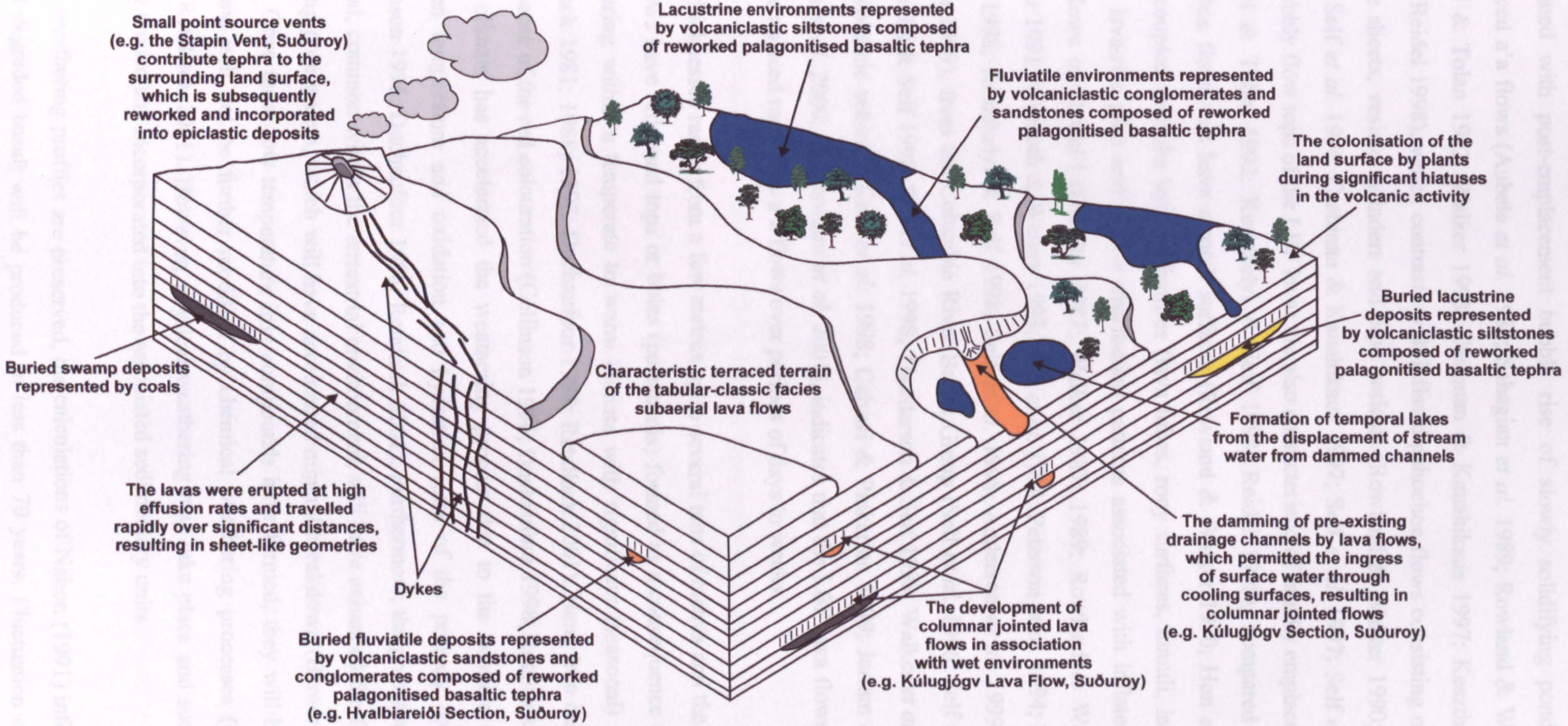

Fig. 3.24. Schematic palaeogeographical block diagram for the Lower Basalt Formation with the main elements highlighted. Length of each horizontal dimension of the figure is very approximately 1-2 km.